Main Group Element-Based Heterocyclic Cations:
Studies on the Stereochemistry and Reactivity of
Intramolecularly Stabilized Silylium and Siloxysilylium Ions

Dissertation

zur Erlangung des

DOKTORGRADES DER NATURWISSENSCHAFTEN

(DR. RER. NAT.)

der Fakultät Chemie und Pharmazie

der Universität Regensburg

vorgelegt von

Nicolò Fontana

aus Verbania (Italien)

im Jahr 2022

This work was supervised by Dr. Jonathan O. Bauer and submitted for approval on the 02.02.2022 to the offices of the faculty.

Date of the oral examination 14.04.2022

Members of the commission:

Prof. Dr. Patrick Nürnberger (Vorsitzender)

Prof. Dr. Manfred Scheer (Erstgutachter)

Prof. Dr. Nikolaus Korber (Zweitgutachter)

Prof. Dr. Frank-Michael Matysik (Prüfer)

Universität Regensburg

Statutory declaration

I hereby declare in lieu of oath that I have prepared the present work without undue help from third parties and without using any aids other than those specified; the data and concepts taken directly or indirectly from other sources are marked with a reference to the literature.

Nicolò Fontana

This thesis was elaborated within the period from February 2018 to December 2021 in the Institute of Inorganic Chemistry at the University of Regensburg under the supervision of Dr. Jonathan O. Bauer.

List of publications:

Easy Access to Enantiomerically Pure Heterocyclic Silicon-Chiral Phosphonium Cations and the Matched/Mismatched Case of Dihydrogen Release.
N. Fontana, N. A. Espinosa-Jalapa, M. Seidl, J. O. Bauer.
Chem. Eur. J. **2021**, 27, 2649-2653.

Functional Group Variation in *tert*-Butyldiphenylsilanes (TBDPS): Syntheses, Reactivities, and Effects on the Intermolecular Interaction Pattern in the Molecular Crystalline State.
J. O. Bauer, N. A. Espinosa-Jalapa, N. Fontana, T. Götz, A. Falk.
Eur. J. Inorg. Chem. **2021**, 2636-2642.

Hidden Silylium Type Reactivity of a Siloxane-Based Phosphonium-Hydroborate Ion Pair.
N. Fontana, N. A. Espinosa-Jalapa, M. Seidl, J. O. Bauer.
Chem. Commun., *Chem. Commun.*, **2022**, 58, 2144.

Dedicated to Anna,
my Love, my Pride,
my Great Scientist.

"I wish it need not have happened in my time," said Frodo.

"So do I," said Gandalf, "and so do all who live to see such times.

But that is not for them to decide. All we have to decide is what to do with the time that is given us."

J.R.R. Tolkien

Preface

Some of the presented results have already been published during the preparation of this thesis (*vide supra*). The corresponding citations and license numbers are given at the beginning of the respective chapters.

Each chapter includes a list of authors. At the beginning of each chapter the individual contribution of each author is described.

To ensure uniform design of this work, all chapters are subdivided into the following sections:
- Introduction
- Results and Discussion
- Conclusion
- References
- Synthesis and characterization
- Quantum Chemical Calculations
- X-ray Crystallographic Details

Furthermore, all chapters have their own numeration of compounds. The depicted molecular structures may differ slightly in their style. A general introduction together with the objectives of this thesis are given at the beginning. In addition, a comprehensive conclusion of this work is presented at the end of this thesis.

Abbreviations

Ar	Aryl
BAr^F_4	tetrakis(3,5-bis(trifluoromethyl)phenyl)borate
BCF	tris(pentafluorophenyl)borane
Bn	Benzyl (C_7H_7)
Bu	Butyl
Ch	Chalcogen (Element of group XVI)
DFT	Density functional theory
Et	Ethyl
Exc	Excess
FBN	*p*-fluorobenzonitrile
h	Hour(s)
*i*Pr	*Iso* propyl
Me	Methyl
Mes	Mesityl, 2,4,6-trimethylphenyl
min	Minute(s)
mol	Mole(s)
Nu	Nucleophile
Pemp	Pentamethylphenyl
Ph	Phenyl
RT	Room temperature
s	Second(s)
*t*Bu	*Tert* butyl
THF	Tetrahydrofuran
TMEDA	N,N,N',N'-Tetramethylethylenediamine
Tol	4-Methylphenyl
XRD	X-ray diffraction

Table of Content:

1 Introduction

During the years, silicon chemistry has been thoroughly studied from both the academia and the industry. The massive interest around this topic resides in the manifold of different species that can be prepared together with the wide range of properties such species possess. From the small monomeric silanes to the linear and cage-like (*e.g.* silsequioxanes) silicone polymers, these compounds have been stimulating the imagination of chemists all over the world posing new challenges and fueling an unstoppable curiosity.[1,2] Among the different fields this chemistry is involved in, this work will mainly focus on the description of compounds from a molecular perspective, starting from silanes and expanding up to disiloxanes. In particular, the synthesis and characterization of novel silylium ions (molecules featuring a positively charged silicon atom) is herein reported.[3,4]

1.1   The beginning in silylium ion chemistry

Silylium ions are molecules that feature a positively charged silicon atom in the formal oxidation state (IV). These species have been thoroughly studied by modern chemists and are still in the spotlight due to their extremely potent and versatile reactivity.[4] The high natural abundance of silicon (27.7% in the earth's crust), combined with both the enhanced Lewis acidity and accessible precursors for preparing silylium ions, define this species as promising catalysts for highly desirable transition-metals free processes. From Lewis acid catalysis to Diels Alder, hydrodefluorination reactions and small molecule activation, silylium ions have also been applied to a manifold of appealing chemical transformations proving more and more to be valuable alternatives to classic catalytic systems. Since the isolation of the first carbocation ([Ph$_3$C]$^+$) in 1901[5] and due to the fact that silicon and carbon both belong to group XIV in the periodic table, chemists have tried to predict whether silylium ions could simply be described as the heavier analogues in regards of their chemical properties, reactivity and bonding situation. Although by considering the periodic properties of these two elements (*e.g.* electronegativity, size, polarizability, *etc.*) every parameter points in the direction of a potentially higher stabilization of the cationic charge for the heavier congener, this comparison finds experimental relevance only when systems in the gas phase are considered. On the contrary, in the condensed phase both the difference in electronegativity between carbon and silicon as well as the bigger size of the latter, result in the destabilization of the positive charge and in an enhanced tendency for the silicon atom to coordinate σ-, π- and n- donors adopting a tetrahedral conformation. This specific set of electronic and steric properties gives silylium ions a peculiar reactivity, unprecedented to elements of group XIV, allowing them to react promptly with any electron rich species such as nucleophiles, solvents or even counter anions. In fact, while carbocations could already be isolated and characterized in the beginning of the 20th century,[5] the search for a silylium ion without any stabilizing interaction, and therefore featuring a perfect trigonal planar

1901	First report on $[Ph_3C]^+$
1975	First attempts to synthesize silylium ions $R_3SiOClO_3$
1993	Isolation of stabilized silylium ions $[Et_3Si(tol)]^+[B(C_6F_5)_4]^-$, $[i\text{-}Pr_3Si]^+[HCB_{11}H_5Br_6]^-$
1996	Application of silylium ions in hydrosilylation
1997	Isolation of the first free silylium ion $[Mes_3Si]^+[B(C_6F_5)_4]^-$
2002	X-ray Characterization of the first free silylium ion $[Mes_3Si]^+[HCB_{11}Me_5Br_6]^-$
2005	Application of silylium ions in Lewis acid catalysis and C-F bond activation
2019	Isolation of $[SiH_3]^+[HCB_{11}H_5Br_6]^-$

Figure 1 Landmarks in the chemistry of silylium ions.

conformation in contrast to the distorted tetrahedron obtained after stabilization (named for simplicity "free" *vs.* "stabilized" silylium ions respectively), continued until one century later. Starting from the seminal attempts of Corey *et al.*,[6] chemists had to tune the reaction conditions excluding any possible threat to the stability of the newly formed silylium ion. Handling these species using flame-dried glassware, distilled solvents and in general excluding the presence of any nucleophilic species in the reaction environment allowed for the detection and isolation of the first examples of positively charged silicon-based molecules in the condensed phase. Although with the diffusion of the Schlenk techniques the former two concepts became routine procedures, the latter gave new impulse to the research of weakly coordinating anions. In this regards, a major role was played by the use of more stable halogenated borates (*e.g.* $[B(C_6F_5)_4]^-$, $[B_{12}Cl_{12}]^{2-}$), aluminates (*e.g.* $[Al(OC(CF_3)_3)_4]^-$) and carboranes (*e.g.* $[HCB_{11}H_5Br_6]^-$) instead of the commonly used anions (*e.g.* perchlorate, BAr^F_4), achieving an overall stabilization of the system and preventing a direct quenching of the reactive center.[7] Another important step forward in isolating and characterizing silylium ions was accomplished by using less nucleophilic solvents like benzene, toluene and, later on, difluoro- or dichlorobenzene. This led to the formation of Lewis adducts in contrast with the complete halogen abstraction or nucleophilic attack observed in CH_2Cl_2 and CH_3CN solutions at room temperature. By adopting these new protocols, the groups of Lambert and Reed published the first isolated silylium ions in 1993.[8] Although the authors claimed the presence of no intermolecular stabilization, following studies disproved these theories showing a major stabilizing contribution coming from the solvent or the counteranion. Roughly ten years later, in 2002, Lambert *et al.* reported the first crystal structure of a free silylium ion in which neither intra- nor intermolecular interaction was detected.[8h] By cleverly starting from tri-

Figure 2 Crystal structure of the first free silylium ion $[Mes_3Si]^+$.

mesitylsilane, full steric shielding around the cationic center was established preventing any possible interaction *via* steric repulsion of the *ortho* methyl groups. At first, such comprehensive and multidirectional steric hindrance resulted in the failure of the classical hydride abstraction protocol since not even the strong Lewis acidic reagent ($[Ph_3C]^+$) could approach the hydridic center. However, by using a very elegant strategy later denominated "allyl leaving approach", the authors were able to finally synthesize $[Mes_3Si]^+$ *via* a substituent rearrangement induced by means of another silylium ion ($[Et_3Si \cdot (C_6H_6)]^+[B(C_6F_5)_4]^-$).[8h] The electrophilic attack on the terminal allylic carbon, which takes place on a remote position with regard to the high steric bulk of the mesityl groups, generates an unstable carbocation that rapidly releases allyltriethylsilane together with the desired trimesitylsilylium ion. The crystal structure of the latter ultimately proved the presence of a perfectly trigonal planar silylium ion in which the propeller-like conformation of the mesityl groups fully occupies the space around the cationic center granting the kinetic stabilization required to prevent any interaction with electron donors (Figure 2). This outstanding result demonstrated once again the difference between a free and a stabilized silylium ion paving the way to a manifold of different species, processes and applications. While for free silylium ions some of these were discovered soon after, the potential and versatility of these acids were both further explored by tuning the reactivity of the silicon center *via* coordination of inter- or intramolecular Lewis bases (a process called for simplicity "taming" or "stabilization" of silylium ions). In fact, by adjusting the extent of the electron density coming from the basic counterpart, together with a fine design of the substitution motif on the silicon (or the molecular scaffold in general), new possibilities in controlling and directing the reactivity of these compounds opened up (selected examples are presented in figure 3).

2006 Müller *et al.*   **2011** Oestreich *et al.*   **2020** Müller *et al.*   **2020** Landais *et al.*
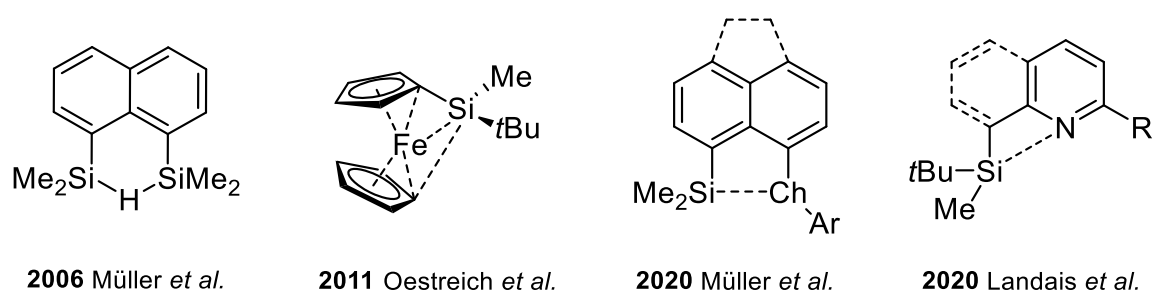
Figure 3 Selected examples of intramolecularly stabilized silylium ions from Müller,[9] Oestreich[10] and Landais.[11]

These strategies to tune the reactivity of silylium ions have given new impulse to the research in this field bringing up new challenges and enlarging the chemical toolbox for generating and handling silylium ions. In the following sections, a quick overview of the synthesis, characterization and possible applications of these cationic species will be presented.

1.2 Synthetic strategies towards silylium ions

1.2.1 Silicon-hydride abstraction and substituents redistribution

The most commonly employed method to synthesize silylium ions is based on the heterolytic cleavage of a silicon-hydrogen bond by means of a Lewis acidic reagent. This protocol, often named "Bartlett-Condon-Schneider reaction" (BCS), "Corey reaction" or, more generally, "hydride abstraction reaction" takes advantage of the high polarization of the silicon hydrogen bond.[6,12] In fact, while for the lighter congeners the difference in electronegativity is almost negligible leading to apolar hydrocarbons, hydrogen atoms directly connected to silicon centers are better described as "silicon hydrides" to emphasize the partially negative charged nature of hydrogen atoms attached to silicon (η_{Si} = 1.9 *vs.* η_C = 2.4 in Pauli's electronegativity scale). This formal charge separation finds confirmation in the high susceptibility towards Lewis acids that can actively induce the cleavage of this bond, generating silylium ions together with the acid's conjugate base. The driving force for this reaction resides obviously in the aforementioned polarization (*vide supra*) as well as in the increased stability acquired by breaking a weaker silicon-hydrogen in favor of the formation of a stronger E-H bond in the product (Figure 4). For this reason, together with its simplicity in pairing it with different weakly coordinating anions, the trytilium carbocation ([Ph$_3$C]$^+$) is by far the most widely reported reagent for this type of transformations, featuring short reaction times paired with a good chemoselectivity.[4]
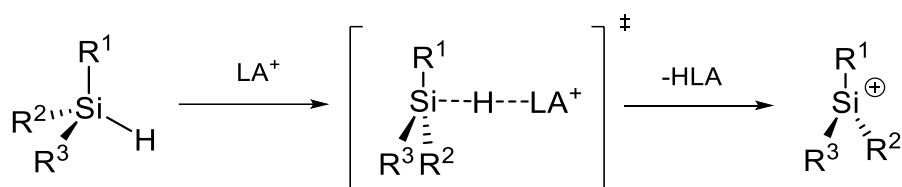
Figure 4 Mechanism involved in the hydride abstraction reaction using a Lewis acid.

As mentioned in the previous section, the greatest challenge in performing these transformations lies in the intrinsic instability of the desired products. However, the use of [Ph$_3$C]$^+$, as well as other main group based Lewis acids (*e.g.* BCF), together with aromatic solvents and stable weakly coordinating anions, provided solid protocols for obtaining silylium ions from a manifold of different substrates, remaining the most widely used approach to these transformations. Interestingly, by further applying this protocol to sterically hindered silanes, a new type of reactivity opened up. While going unnoticed during the first attempts of hydride abstraction on homoleptic bulky silanes (*e.g.* Mes$_3$SiH), by performing the Corey reaction on heteroleptic substrates, different chemoselectivity towards various combinations of differently substituted silylium ion and silanes were obtained. In particular, this phenomenon was observed with bulky aryl rings and small linear aliphatic chains showing a relevant correlation between the counter anion employed ([B(C$_6$F$_5$)$_4$]$^-$ or [HCB$_{11}$H$_5$Br$_6$]$^-$) and the different outcome of the reaction.[13] The possibility to tune this redistribution of the different residues might

allow an alternative reaction path to synthesize and isolate sterically hindered free silylium ions avoiding the design for brilliant but demanding solutions like the "allyl leaving approach" (Figure 5).
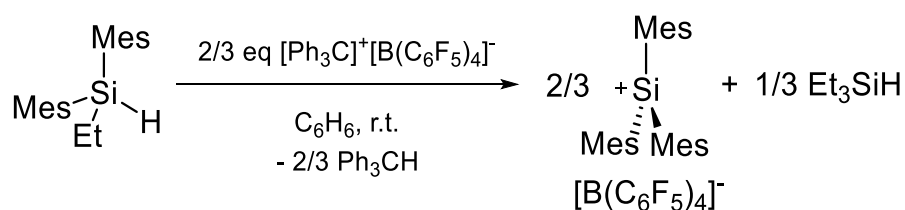
Figure 5 Example of a substituent redistribution reaction. The steric cover provided by the two mesityl groups is not enough to prevent a scrambling of the substituents during the reaction. The result is the formation of a tris aryl silylium ion and the respective tris alkyl silane.

1.2.2   Silicon-carbon and Silicon-silicon cleavage

With fewer applications than the previous approach but still worth mentioning due to both its use in the synthesis of the first stable silylium ion and its recent developments, the heterolytic cleavage of a silicon-carbon bond offers an alternative way to obtain cationic silicon species. Although featuring an overall lesser efficiency compared to the hydride abstraction reaction, this synthetic approach becomes valuable when bulky substituents would prevent the acid from accessing the nucleus adjacent to the silicon center. In this regard, the most famous case is undoubtedly the "allyl leaving approach" (*vide supra*) from Lambert *et al.*[8i] in which the attack of the reagent induced a spontaneous cleavage of the remote silicon-carbon bond (Figure 6).
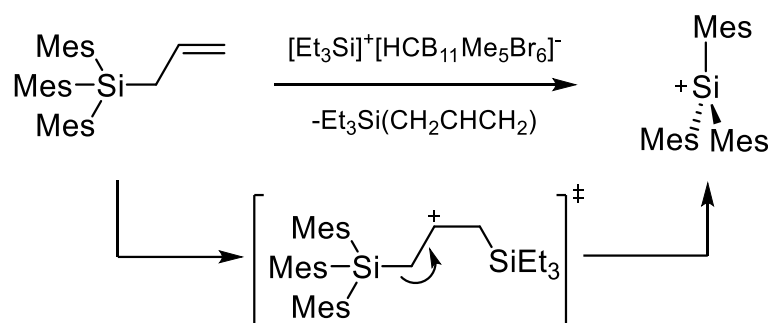
Figure 6 Mechanism for the allyl leaving approach.

This strategy, although solving brilliantly the aforementioned problem, failed in finding wide applications for the synthesis of silylium ions mainly because of the higher bond strength of the silicon-carbon in comparison to silicon-hydrogen bonds. In fact, harsher reagents and reaction conditions are generally required to break such bonds reducing both chemoselectivity and tolerance towards different functional groups. In recent years, the research of Oestreich *et al.* have shed light on new possible applications for this approach. By taming the known degradation reaction called "protodesilylation" which often takes place on phenyl-substituted silylium ions, primary and secondary

silanes were reacted affording the characterization of $RSiH_2^+$ and SiH_3^+ in the solid phase for the first time. After every attempt involving a classical hydride transfer failed due to the increase in electrophilicity of the silicon center related to the removal of electron donor substituents (usually alkylic groups), the authors treated secondary and primary phenylsilanes with a strong proton source ($[C_6H_6\cdot H]^+[CHB_{11}H_5Br_6]^-$) inducing the protonation of the *ipso*-carbon and the consequent cleavage of the silicon-carbon bond.[14] Moreover, this class of reagents were also proved to induce the release of dihydrogen from silanes instead of benzene when no phenyl ring was present (Figure 7). Although showing once again how this approach could brilliantly solve a major challenge, a wide range of applications is yet to be discovered. Similar conditions have been used in the synthesis of silylium ions starting from disilanes. This methodology, however, presented the exact same limitations of the synthesis *via* carbon-carbon activation (*vide supra*) and at the time this introduction is written, only a few examples can be found in the literature.[15]
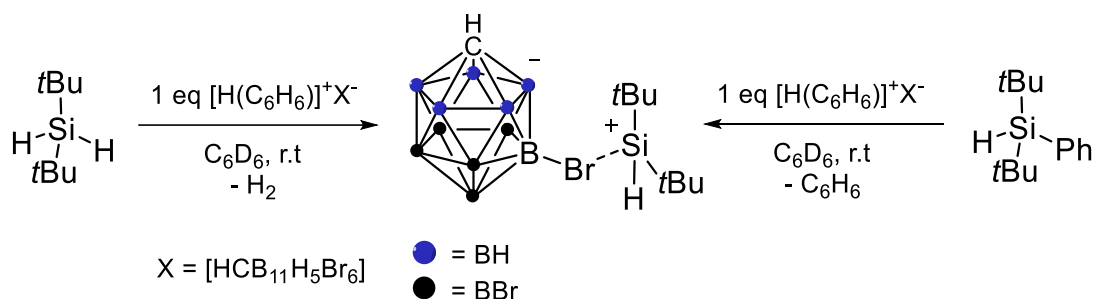
Figure 7 Dihydrogen release *vs.* protodesilylation using a strong acid with a weakly coordinating anion.

1.2.3   Other methods

As seen so far, silylium ions can be synthesized using different approaches. However, a few less general reactions are also worth mentioning even though a thorough investigation exceeds the scope of this dissertation. Among these, the heterolytic cleavage of silicon-halogen, or silicon-oxygen, bonds is surely one of the most interesting since this approach became quickly the method of choice in the synthesis of carbocations. Sadly, this direct analogy between the chemistry of carbon and silicon has proved, once again, misleading. In fact, several factors including the increased strength of the interaction between silicon and these functional groups in comparison with its lighter congener, and the higher affinity of the newly formed silylium ion towards the leaving group, doomed this approach in its applications. Nonetheless, three different classes of reagents have been investigated providing interesting results: the "magic acid" ($HSO_3F\cdot SbF_5$),[16] strong Lewis acids (*e.g.* silylium ions)[17] and silver salts of weakly coordinating anions (*e.g.* $Ag^+[Al(OR^F)_4]^-$)[18] (Figure 8). As expected, the use of strong fluoride-containing Brønsted acids on alkoxysilanes led to the respective fluorosilanes *via* cleavage of the silicon-oxygen bond and subsequent fluoride abstraction. The

achievement of a complete halide abstraction using strong Lewis acids proved to be restricted only to highly intramolecularly stabilized substrates (*e.g.* the synthesis of silaimidazolium salts).
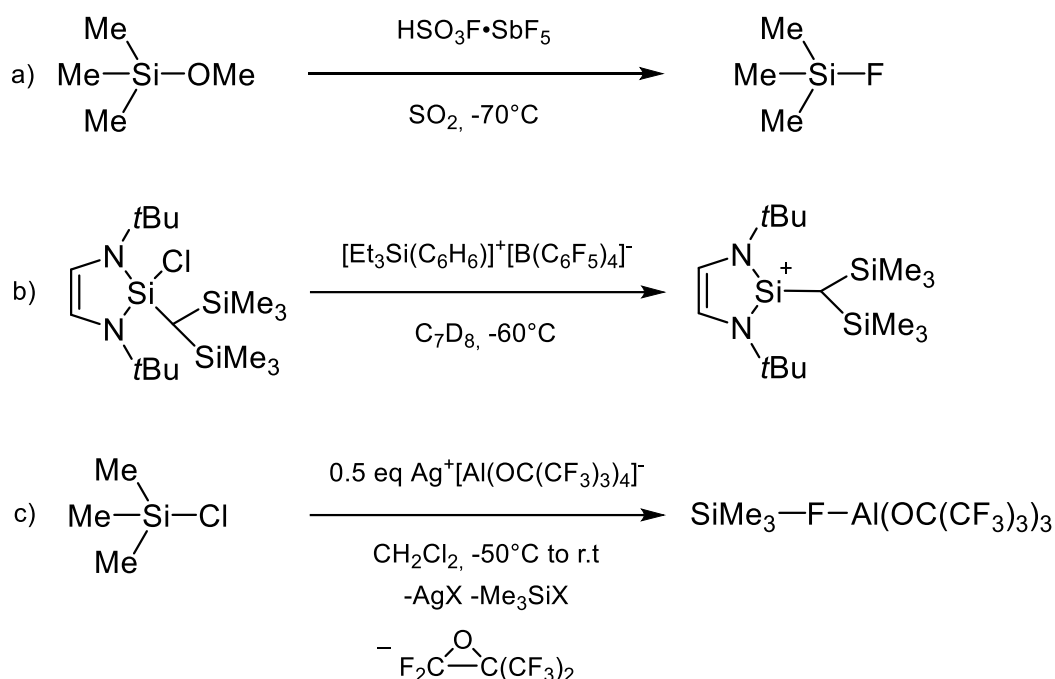
Figure 8 Selected attempts for the synthesis of silylium ions using magic acid (a)[16], highly stabilized substrates (b)[17] and using silver salts (c)[18] respectively.

The most interesting result, however, came from the attempts in achieving a classic metathesis reaction using silver salts. While halide abstraction was achieved starting from different silyl halides (Cl, Br, I), the aluminum based counter anion proved non-innocent by coordinating immediately the newly formed silylium ion into a donor-acceptor complex. Further studies on this reaction also demonstrated how the reactions proceed *via* formation of a bissilylated halonium ion after precipitation of the silver halide. A subsequent rearrangement in the coordination sphere of the metal center resulted in zwitterionic species with a high degree of stabilization. Other feasible routes to obtain silylium ions start from low coordinative silicon species (silylenes and silyl radicals) but, as mentioned above, their use is considered exotic and their explanation is referred to the original contributions.[19]

1.3   Characterization of silylium ions

With the development of new approaches and protocols for the synthesis of silylium ions, two analytic techniques became predominant for their routine characterization: ^{29}Si NMR and single-crystal X-ray diffraction analysis. Although the generation of an electronic deficit in the molecule can be detected in most cases thanks to its effects on the neighboring nuclei (*e.g.* in the ^{1}H NMR), only these two techniques provide a precise assessment of the bonding and coordination properties of

the silicon center in these molecules. While single-crystal X-ray diffraction, together with CP-MAS NMR, gives insights into their nature in the solid phase, silicon NMR has quickly become the method of choice for their characterization in the liquid media. Especially with the latter technique, the outstanding repercussions deriving from a change in the coordination motif around the silicon center have been guiding researchers in the field towards the characterization of stabilized, as well as free, silylium ions. In fact, depending on the stabilization provided by the substituents, the anionic counterpart and the solvent, the ^{29}Si chemical shift (δ) for this type of molecules can vary from very high field (δ= -27.6 ppm for $[SiH_3]^+[HCB_{11}H_5Br_6]^-$)[14] to extreme low field spanning a range of several hundred ppm (δ= 315.7 ppm for an aromatic cationic homoleptic silicon cycle).[19g] In estimating possible values for the $\delta(^{29}Si)$ of silylium ions, the general rules on the effect of electron donating and electron withdrawing neighboring substituents still apply reliably (a few examples are reported in figure 9). Thus, a higher field chemical shift is to be expected for ions substituted with three alkylic- compared to three arylic- residues. It must be noted, however, that an increase in the bulkiness of such substituents could prevent the coordination of lone pair donor moieties resulting in a considerable shift towards lower fields (see free silylium ions). Regarding the effects of the reaction environment, the possibility for the cationic center to get stabilized by coordination of electron donating media affects strongly the electron density around it. In the case of aromatic solvents, for example, a moderate shift (~10–20 ppm) towards higher fields is to be expected. On the other hand, as seen in the previous sections, coordination of counter anions can partially compensate the electron deficit at the silicon center providing a crucial contribution to the estimation of the ^{29}Si chemical shift. In recent years, the application of theoretical methods and calculations is supporting these qualitative estimations with much more precise data. While a thorough explanation of the employed methods exceeds by far the purpose of this work, it is important mentioning that the application of such techniques allows for a better understanding of the experimentally obtained analytical data and to estimate the properties of unknown species.[20]
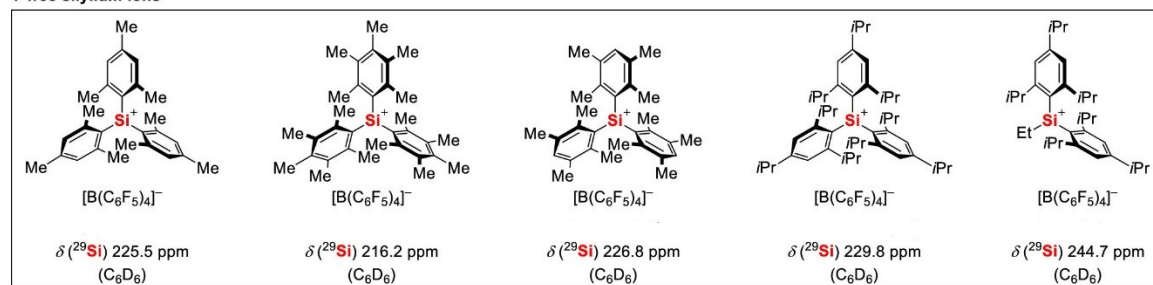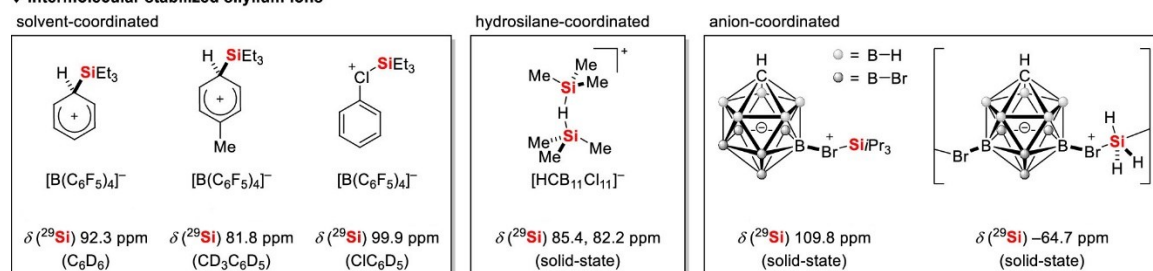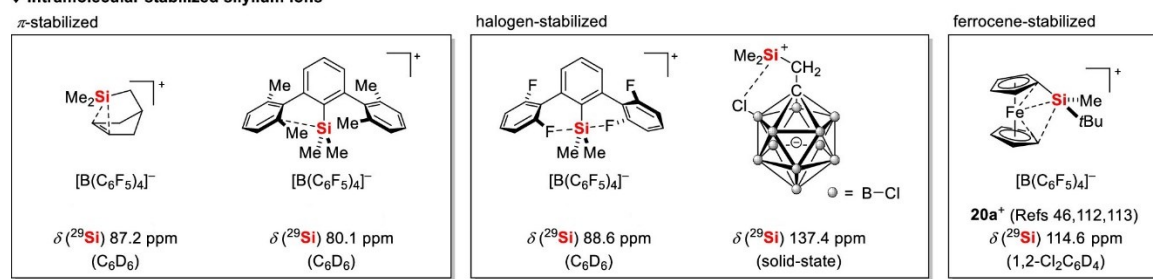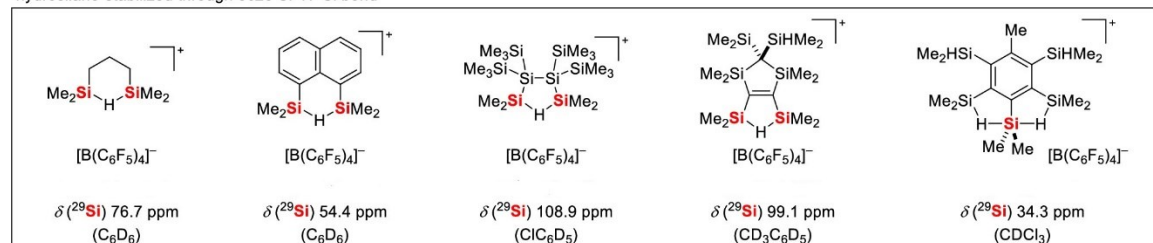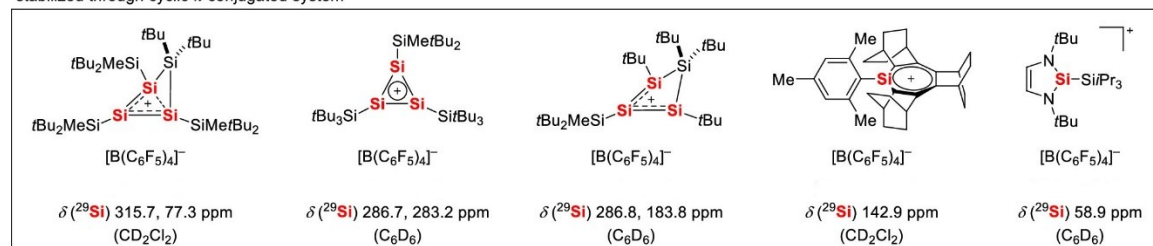
Figure 9 Examples of ^{29}Si NMR chemical shifts for silylium ions as summarized by Oestreich *et al.*[4]

Together with silicon NMR and quantum chemical methods, X-ray crystallography serves as one of the most valuable analytics in defining precisely the geometry, connections and electronic distribution for silylium ions in the solid phase. Historically, this technique was also fundamental in settling the debate on whether or not the first two isolated silylium ions exhibited stabilizing interactions ([Et$_3$Si(toluene)]$^+$[B(C$_6$F$_5$)$_4$]$^-$ and [*i*-Pr$_3$Si]$^+$[CB$_{11}$H$_6$Br$_6$]$^-$).[8a-g] Thanks to single crystal X-ray diffraction

9

FBN
$\delta(^{19}F) = -103.4$ ppm
$^1J(CF) = 255.7$ Hz

FBN-BCF adduct
$\delta(^{19}F) = -92.5$ ppm
$^1J(CF) = 268.0$ Hz
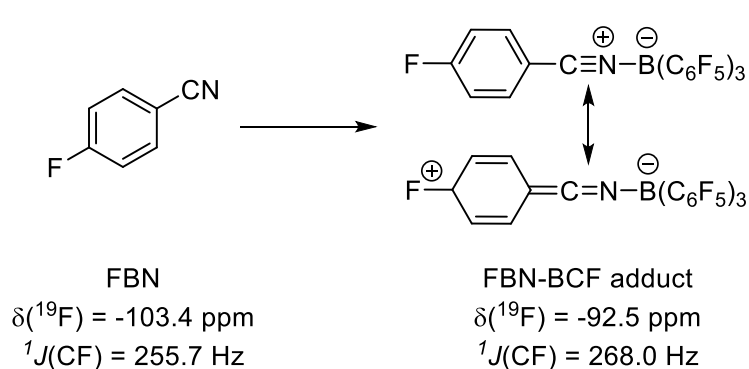
Figure 10 Coordination of FBN to a Lewis Acid (BCF) and related chemical shift values of the two forms.

analysis of free silylium ions in the solid phase (Mes_3Si^+ and later on $Pemp_3Si^+$), the distinction between free and stabilized cations was fully exploited. In fact, together with the previously described low field shift in the ^{29}Si NMR ($\sim\delta(^{29}Si) = 220$ ppm), the differences in the geometry around the silicon center (pyramidalized for the aliphatic *vs.* trigonal planar for the aromatics) paved the way to a more precise classification and consequent estimation of the properties for these molecules. The great interest in these species and their chemistry has led to the synthesis and characterization of many examples from which a selection is depicted in figure 9. The latest contribution in investigating and categorizing the properties of silylium ions has come from Müller *et al.* in 2019.[21] In the last decade, great interest has developed around intramolecularly stabilized silylium ions and a plethora of new examples featuring strong, as well as weak, stabilization effects have been prepared. However, as pointed out by the authors, a reliable method to describe precisely the Lewis acidity of these molecules has yet to be developed. Protocols like the Gutmann-Beckett, Hilt or the Childs methods which are based on evaluating the difference in chemical shift of sensitive nuclei before and after coordination of a Lewis base to the investigated acid, have been applied to silylium ions with disappointing results. In fact, while the latter uses crotonaldehyde (not suitable for interacting with cationic silicon species) the other two are based on evaluating the $\delta(^{31}P)$ of $OPEt_3$ and the $\delta(^2H)$ of deuterated pyridine respectively. Unfortunately, both of these reagents were also found not suitable for this task since they bind too strongly to the silicon center therefore disrupting the stabilizing interaction of the intramolecular base and preventing its estimation. To overcome this challenge and introduce a reliable method to describe the acidity of these species, the authors have proposed a new scale employing *p*-fluorobenzonitrile (FBN) as chemical probe. With its electron donating cyano group, this molecule can easily interact with Lewis acidic reagents inducing a mesomeric rearrangement in the electron density to the nitrilium ylide form. The result of this coordination is an indirect shift of the signal related to the fluorine in *para* position toward lower fields as well as an increase in the value of the carbon-fluorine coupling constant ($\delta(^{19}F) = -103.4$, $^1J_{(C-F)} = 255.7$ Hz for FBN *vs* $\delta(^{19}F) = -92.5$, $^1J_{(C-F)} = 268.0$ Hz for the nitrilium yilide). By simply recording NMR spectra of samples containing differently substituted silylium ions together with FBN, the authors managed to create a comprehensive and reliable scale to highlight the Lewis acidity of these moieties. Moreover, the availability and compatibility of the probe, as well as the easiness in preparing and analyzing the samples, provided a solid method for this class of compounds.
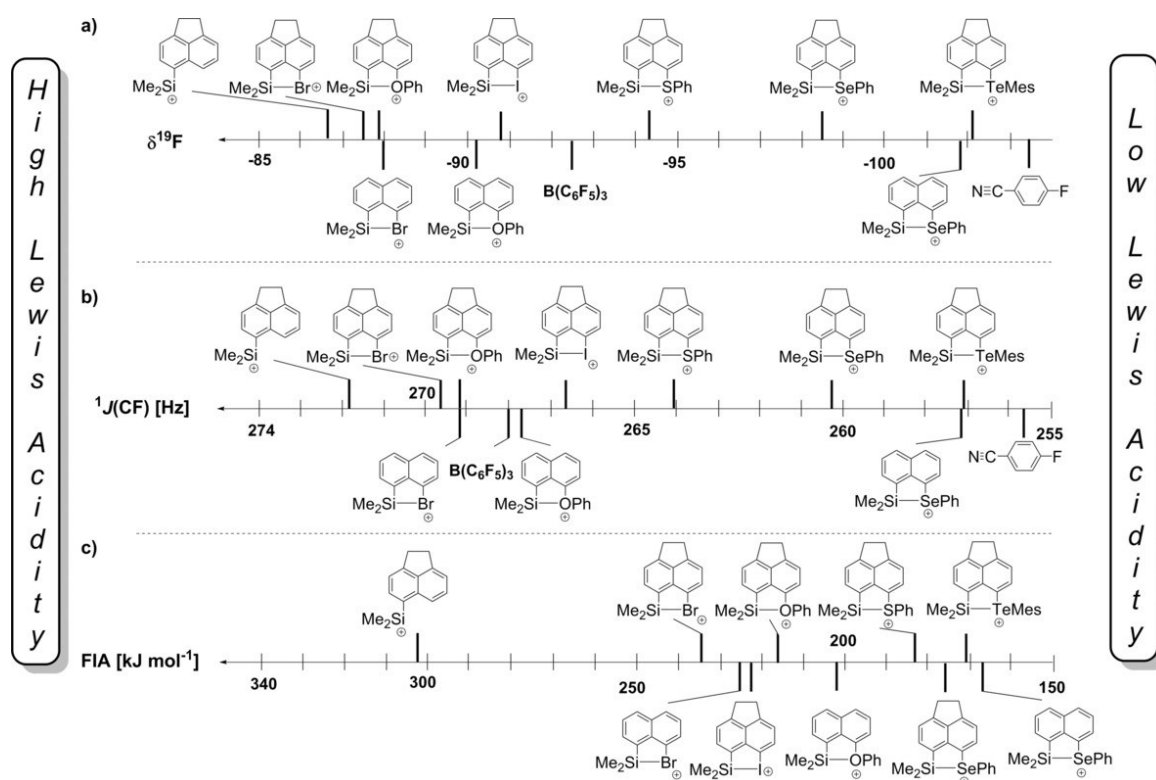
Figure 11 Different Lewis acidity scales for silylium ions reported by Müller *et al.* by considering the $\delta(^{19}F)$ and the $^{1}J(CF)$ of these ions after coordination with FBN (**a** and **b** respectively) or *via in silico* estimation (**c**).

1.4   Synthetic and catalytic applications of silylium ions

When it comes to applications, understanding the extreme electrophilicity of silylium ions is essential.[22] As already described (*vide supra*), the electron deficiency at the silicon center makes them suitable for reactions with almost any nucleophile. Although in the beginning such reactivity proved too challenging and the reaction conditions needed refining, with the introduction of intramolecular stabilizing groups, the use of silylium ions as silylation reagents as well as catalysts have received great interest.[23] In the following paragraphs a few examples of applications will be reported although a thorough overview of the latest advances in this field was recently reported by Klare, Müller, Oestreich *et al.*[4] and exceeds by far the purpose of this contribution.

1.4.1   Activation of carbon-fluorine bonds

One of the most efficient and outstanding demonstration of possible applications in the chemistry of silylium ions is the activation of C-F bonds. Weather to achieve hydrodefluorination or simple fluoride abstraction followed by further functionalization, these reactions provide an elegant way to activate fairly inert functional groups. In fact, the disposal of fluoro alkanes, which have found wide
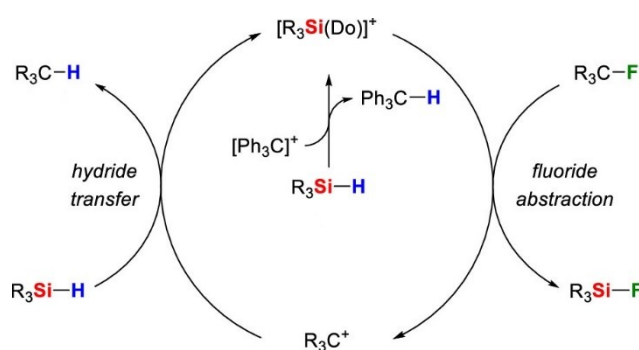
Figure 12 General mechanism for the hydrodefluorination reaction.

use due to their peculiar stability and physical properties, represents still a big challenge. With the groundbreaking work of Ozerov *et al.*[24] aliphatic CF$_3$ groups were selectively transformed into CH$_3$ in short times and with very high turnover numbers. For this transformation, a fairly simple mechanism was proposed starting with the formation of the silylium ion *via* classical hydride transfer. The newly formed cationic silicon would then attack the carbon fluoride bond and, by fully abstracting the halide and generating a carbocation, induce the abstraction of the silicon hydride to regenerate the silylium catalyst while releasing the hydrogenated alkane. Together with the obviously enhanced electrophilicity of the *in situ* formed silylium ion, an important contribution to the driving force of this reaction resides in the breaking of the relatively weaker C-F and Si-H bonds to form the stronger C-H and Si-F bonds (100 kcal·mol^{-1} *vs.* 108 kcal·mol^{-1} for carbon and 90 kcal·mol^{-1} *vs.* 159 kcal·mol^{-1} for silicon). Interestingly, these species were demonstrated to react selectively only with C(sp^3)-F bonds allowing for the use of halogenated aromatic solvents and exploiting an orthogonal reactivity to that of many transition metal complexes. It must be noted, however, that perfluorinated borate counteranions (*e.g.* [B(C$_6$F$_5$)$_4$]$^-$) were found to slowly degrade in the reaction conditions limiting the turnover numbers. To overcome this challenge, the more stable perhalogenated-*closo*-carboranes were used leading to an increase of the overall reaction efficiency (*e.g.* [HCB$_{11}$H$_5$Cl$_6$]$^-$ with a TON = 880 after 1 h).[24] After a few years from the original contribution, the substrate scope for the hydrodefluorination of C(sp^3)-F bonds using silylium ions included almost any kind of substrate. However, applications involving the activation of C(sp^2)-F bonds remained scarce until the discoveries of the Siegel group.[25] Based on their previous studies on the stabilization of phenyl cations, [25a] the authors performed a very elegant intramolecular Friedel-Craft arylation triggered by a fluoride abstraction and propelled by a protodesilylation reaction leading to the synthesis of fluoroanthene.[25b] More in detail, a catalytic amount of *closo*-carborane stabilized silylium ion was used to abstract a fluoride from 1-(2-fluorophenyl)naphthalene inducing an electrophilic attack from the neighboring naphthyl group resulting in
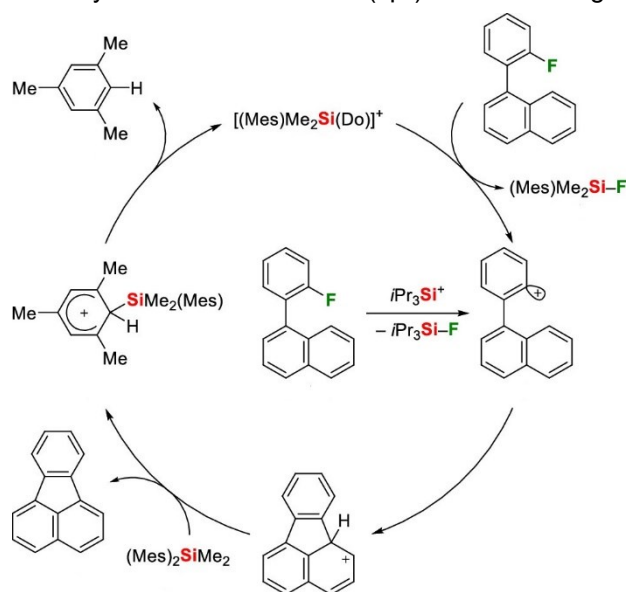
Figure 13 Mechanism for the silylium catalysed Friedel-Craft cyclization discovered by Siegel *et al.*

the formation of the inner five membered ring. Subsequently, interaction of the transient cationic fluoroanthene with a molecule of sacrificial silane (in this case dimethyldimesitylsilane) allows for the rearomatization of the substrate *via* release of a mesitylene molecule, finally regenerating the catalytic species. This type of reaction has been tested on different substrate but the scope was demonstrated to be restricted to intramolecular electrophilic attacks. At the same time the elegance and simplicity of this example have been inspiring the forthcoming research to investigate for more applications.

1.4.2   Lewis acid catalyzed reactions
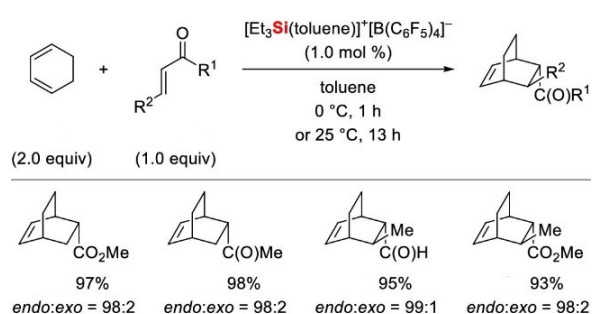
Figure 15 Silylium ion catalysed Diels Alder reactions by Sawamura *et al.*[26]

A plethora of different applications for silylium ions have been researched in last thirty years. Although reagents, scope and experimental conditions can vary, in most of them an initial coordination of the cationic silicon center to the substrate has been proposed. In fact, while the extent of such acidity is exploited by the manifold of electron rich substrates that these molecules are able to bind to, the different nature of the species that subsequently attacks the activated intermediate, allows for a wide range of applications. In the field of Diels-Alder reactions, the contributions coming from the groups of Sawamura[26] (Figure 15) and Oestreich[27] (Figure 14) have demonstrated how silylium ions can play a major role in these transformations affecting reaction times, yields and regioselectivities. Moreover, by activating the dienophilic counterpart (usually methyl acrylate), this catalysts have succeeded in converting very inert substrates like 1,3-cyclohexadiene, 2,3-dimethyl-1,4-butadiene and others, for which every previous attempt failed. Another important application based on the acidity of silylium ions lies in the activation of small molecules. With the use of stoichiometric amounts of tritylium ions to perform *in situ* the hydride transfer reaction from R_3SiH, CO_2 can be transformed into acetic acid and methanol after hydrolysis.[23a] To further enhance this reactivity, triaryl silylium ions can be combined with bulky electron donating phosphines to obtain frustrated Lewis pairs. [13,28] This

Figure 14 Silylium ion catalysed Diels Alder reactions by Oestreich *et al.*[27]

highly reactive species are able to activate both dihydrogen and CO_2 even making the isolation of stable silylacylphosphonium salts possible. Although very promising, no reversible activation of small molecules using this kind of systems has been achieved yet.

Examples of different reactions involving silylium ions are also reported for:

❖ Mukayiama condensation[29]

❖ Hydrosilylation[30]

❖ Polymerization reactions[31]

❖ C-C and C-Si bond formation[32]

1.5   Stereogenicity at silicon and chiral memory

Similarly to carbon, the ability of silicon to create four bonds leading to a tetrahedral geometry allows for the synthesis of chiral silanes and, potentially, silicon-based chiral polymers. Although relatively in its infancy, this field has received great impulse in recent times envisioning the possibility to obtain well defined chiral reagents and catalysts. In particular, with the development of new catalytic applications for silylium ions, the interest in making these processes stereoselective has grown even more. While achieving a high control on the final configuration of silicon stereocenters was partially facilitated by the massive amount of data gathered in the field of organic stereochemistry, the possibility to apply this knowledge to the chemistry of silylium ions to develop stereoselective catalytic processes is still a great challenge. In fact, the valence reduction related with the generation of the catalytically active species, implies a flattening of the three remaining ligands toward a trigonal planar geometry and intrinsically enables racemization processes. As discussed in the sections before, the use of free silylium ions in catalysis has found severe limitations due to synthetic procedures and difficulties in handling. On the other hand, inter- or intramolecularly stabilized ions not only proved easier to work with, but they also demonstrated both a higher stability and compatibility towards different functionalities. While in the case of fully trigonal planar silylium ions, highly specific ligands would be required in order to influence the stereochemical environment around the substrate and to prevent strong donors from attacking the silicon atom, the use of stabilizing groups allows for a fine tuning of both the electronic and steric properties of the silicon

Figure 16 Stereochemical investigation on the anchimeric stabilization provided by an oxygen-based residue to a silicon stereocentre featuring a chiral backbone.

center. Among the different strategies introduced, the use of neighboring electron donating functional groups (anchimerically assisted stabilization) has attracted wide interest. In particular, the

possibility to use such groups to stabilize the ionic species in a stereoselective fashion thus preventing possible racemization paths and subsequently reobtaining the starting material in the same configuration, has been described as "chiral memory".[33] Although this definition is widely used in different types of chemistry (*e.g.* supramolecular chemistry), it could easily mislead the reader by attributing the retention (or inversion) of the absolute configuration at a stereogenic silicon center to some sort of intrinsic property of the species instead of a high stereoselectivity throughout the transformations involved. However, the simplicity with which this definition provides a simple and quick

Figure 17 Stereochemical investigation on the chiral memory of different silanes using nitrogen and sulphur-based donors.

way to describe a series of stereoselective transformations has raised large consent by the scientific community and this definition can now be found abundantly in the recent literature. Therefore, it is important for the reader not to forget that this is an oversimplification and the proper way to describe this phenomenon is simply based on exploiting the very stereoselective reaction mechanisms that lead to the preservation of the stereochemical identity throughout the whole process. For example, in the synthesis of pyridine or quinoline stabilized silylium ions reported by Landais *et al.,*[11] the anchimerically assisting group facilitates the hydride abstraction by coordinating the silicon atom from backside, and by hindering one of the two possible directions for the nucleophilic attack. More in detail, the authors reported that the reaction of a highly enantiomerically enriched mixture of quinoline stabilized ion (>95:5) at 0°C with $[Ph_3C]^+[B(C_6F_5)_4]^-$ followed by hydride addition using *n*-Bu₄NBH₄, afforded the starting quinolinium with full retention of configuration (>95:5) following an inversion-inversion mechanism. So far, nitrogen[11], oxygen[33a], sulfur[34] and other Lewis basic elements have been studied with interesting results, opening the way for a thorough investigation on this promising transformations both in the solid phase as well as in solution.

1.6   Reference

[1]   a) I. Khan, S. A. Awan, M. Rizwan, S. Ali, M. J. Hassan, M. Brestic, X. Zhang, L. Huang, *Ecotoxicol. Environ. Saf.* **2021**, *222*, 112510; b) E. Koch, D. Clement, *Prop. Explos. Pyrotech.* **2007**, *32*, No. 3, 205-212; c) C. Marschner, T. Don Tilley, *Dalton Trans.* **2017**, *46*, 8699-8700; d) Z. Wu, X. Zhang, X. Jin, T. Li, J. Ge, Z. Li, *J. Nanomater.* Volume **2021**, Article ID 6650131, 17 pages, **2021**. https://doi.org/10.1155/2021/6650131; e) D. Lumen, S. Wang, E. Mäkilä, S. Imlimthan, M. Sarparanta, A. Correia, C. Westerveld Haug, J. Hirvonen, H. A. Santos, A. J. Airaksinen, W. Filtvedt, J. Salonen, *Eur. J. Pharm. Biopharm*. **2021**, *158*, 254-265; f) R Dekker, N Usechak, M Först, A Driessen, *J. Phys. D: Appl. Phys.* **2007**, *40*, R249-R271; g) Apelian, D. (**2009**). "Aluminum Cast Alloys: Enabling Tools for Improved Performance". Wheeling, Illinois: North American Die Casting Association. Archived from the original on 2012-01-06; h) R. J. Clark, M. Aghajamali, C. M. Gonzalez, L. Hadidi, M. Amirul Islam, M. Javadi, M. Hosnay Mobarok, T. K. Purkait, C. Jay T. Robidillo, R. Sinelnikov, A. N. Thiessen, J. Washington, H. Yu, J. G. C. Veinot, *Chem. Mater.* **2017**, *29*, 80-89.

[2]   a) S. Ganachaud, S. Boileau, B. Boury (Eds.), *Silicon Based Polymers: Advances in Synthesis and Supramolecular Organization*, Springer, Netherlands, **2008**; b) U. Schubert, N. Hüsing, *Synthesis of Inorganic Materials* (4th Ed.), Wiley-VCH, Weinheim, Germany, **2019**.

[3]   For a comprehensive overlook see: a) V. Y. Lee, A. Sekiguchi, *Organosilicon Compounds Theory and Experiment (Synthesis)*, **2017**, Pages 197-230, Elsevier, Tsukuba, Japan; b) T. Müller, *Silylium Ions.* In: D. Scheschkewitz (eds) *Functional Molecular Silicon Compounds I. Structure and Bonding*, **2013**, vol *155*. Springer, Cham. https://doi.org/10.1007/430_2013_132.

[4]   For related reviews see: a) H. F. T. Klare, M. Oestreich, *Dalton Trans.* **2010**, *39*, 9176-9184; b) H. F. T. Klare, L. Albers, L. Süsse, S. Keess, T. Müller, M. Oestreich, *Chem. Rev.* **2021**, *121*, 5889-5985.

[5]   G. A. Olah, G. K. Surya Prakash, *Carbocation Chemistry*, Edited by George A. Olah and G. K. Surya Prakash, ISBN 0-471-28490-4 Copyright # 2004 John Wiley & Sons, Inc.

[6]   J. Y. Corey, *J. Am. Chem. Soc.* **1975**, *97*, 3237-3238.

[7]   a) A. G. Massey, A. J. Park, *J. Organometal. Chem.* **1964**, 2, 245-250; b) S. H. Strauss, *Chem. Rev.* **1993**, *93*, 927-942; c) C. A. Reed, *Acc. Chem. Res.* **1998**, *31*, 133-139; d) I. Krossing, I. Raabe, *Angew. Chem. Int. Ed.* **2004**, *43*, 2066-2090; e) I. M. Riddlestone, A. Kraft, J. Schaefer, I. Krossing, *Angew. Chem. Int. Ed.* **2018**, *57*, 13982-14024.

[8]   a) J. B. Lambert, S. Zhang, *J. Chem. Soc.*, *Chem. Commun.* **1993**, 383-384; b) J. B. Lambert, S. Zhang, S. M. Ciro, *Organometallics* **1994**, *13*, 2430-2443. c) J. B. Lambert, S. Zhang, C. L. Stern, J. C. Huffman, *Science* **1993**, *260*, 1917-1918; d) Z. Xie, D. J. Liston, T. Jelinek, V. Mitro, R. Bau, C. A. Reed, *J. Chem. Soc.*, *Chem. Commun.* **1993**, 384-386; e) Z. Xie, R. Bau, A. Benesi, C. A. Reed, *Organometallics* **1995**, *14*, 3933-3941; f) Z. Xie, J. Manning, R.W. Reed, R. Mathur, P. D. W. Boyd, A. Benesi, C. A. Reed, *J. Am. Chem. Soc.* **1996**, *118*, 2922-2928; g) C. A. Reed, Z. Xie, R. Bau, A. Benesi, *Science* **1993**, *262*, 402-404; h) K. C. Kim, C. A. Reed, D. W. Elliott, L. J. Mueller, F. Tham, L. Lin, J. B. Lambert, *Science* **2002**, *297*, 825-827; j) P. P. Gaspar, *Science* **2002**, *297*, 785-786.

[9]   a) R. Panisch, M. Bolte, T. Müller, *J. Am. Chem. Soc.* **2006**, *128*, 9676-9682; b) S. Kenzler, S. Rathjen, A. Merk, M. Schmidtmann, T. Müller, *Chem. Eur. J.* **2019**, *25*, 15123-15130; c) S. Kenzler, S. Rathjen, K. Reger, M. S. Werdemann, M. Wernke, P. Tholen, C. Girschik, M. Schmidtmann, Y. Landais, T. Müller, *Chem. Eur. J.* **2020**, *26*, 16441-16449; d) A. Merk, L. Behrmann, N. Kordts, K. Görtemaker, M. Schmidtmann, T. Müller, *Chem. Eur. J.* **2021**, *27*, 3496-3503.

[10] K. Müther, R. Fröhlich, C. Mück-Lichtenfeld, S. Grimme, M. Oestreich, *J. Am. Chem. Soc.* **2011**, *133*, 12442-12444.

[11] A. Fernandes, C. Laye, S. Pramanik, D. Palmeira, Ö. Ö. Pekel, S. Massip, M. Schmidtmann, T. Müller, F. Robert, Y. Landais, *J. Am. Chem. Soc.* **2020**, *142*, 564.

[12] P.D. Bartlett, F. E. Condon, A. Schneider, *J. Am. Chem. Soc.* **1944**, *66*, 1531-1539.

[13] a) A. Schäfer, M. Reißmann, A. Schäfer, W. Saak, D. Haase, T. Müller, *Angew. Chem. Int. Ed.* **2011**, *50*, 12636; *Angew. Chem.* **2011**, *123*, 12845; b) A. Schäfer, M. Reißmann, S. Jung, A. Schäfer, W. Saak, E. Brendler, T. Müller, *Organometallics* **2013**, *32*, 4713-4722.

[14] Q. Wu, E. Irran, R. Müller, M. Kaupp, H. F. T. Klare, M. Oestreich, *Science* **2019**, *365*, 168-172.

[15] a) M. Okano, K. Mochida, *Chem. Lett.* **1991**, *20*, 819-822; b) M. Ichinohe, H. Fukui, A. Sekiguchi, *Chem. Lett.* **2000**, *29*, 600-601.

[16] G. A. Olah, D. H. O'Brien, C. Y. Lui, *J. Am. Chem. Soc.* **1969**, *91*, 701-706.

[17] S. Ishida, T. Nishinaga, R. West, K. Komatsu, *Chem. Commun.* **2005**, 778-780.

[18] a) A Budanow, M. Bolte, M. Wagner, H. W. Lerner, *Eur. J. Inorg. Chem.* **2015**, 2524-2527; b) A. Budanow, T. Sinke, J. Tillmann, M. Bolte, M. Wagner, H. W. Lerner, *Organometallics* **2012**, *31*, 7298-7301.

[19] a) A. Schäfer, A. Schäfer, T. Müller, *Dalton Trans.* **2010**, *39*, 9296-9303; b) P. Jutzi, E. A. Bunte, *Angew. Chem., Int. Ed. Engl.* **1992**, *31*, 1605-1607; c) T. Müller, P. Jutzi, T. Kühler, *Organometallics* **2001**, *20*, 5619-5628; d) P. P. Power, *Chem. Rev.* **2003**, *103*, 789-810; e) V. Y. Lee, A. Sekiguchi, *Eur. J. Inorg. Chem.* **2005**, 1209-1222. f) A. Sekiguchi, T. Matsuno, M. Ichinohe, *J. Am. Chem.Soc.* **2001**, *123*, 12436-12437; g) A. Sekiguchi, T. Matsuno, M. Ichinohe, *J. Am. Chem. Soc.* **2000**, *122*, 11250-11251; h) A. Sekiguchi, T. Fukawa, M. Nakamoto, V. Y. Lee, M. Ichinohe, *J. Am. Chem. Soc.* **2002**, *124*, 9865-9869.

[20] C. H. Ottosson, D. Cremer, *Organometallics* **1996**, *15*, 5495-5501.

[21] S. Künzler, S. Rathjen, A. Merk, M. Schmidtmann, T. Müller, *Chem. Eur. J.* **2019**, *25*, 15123.

[22] H. Großekappenberg, M. Reißmann, M. Schmidtmann, T. Müller, *Organometallics* **2015**, *34*, 4952-4958.

[23] a) A. Schulz, A. Villinger, *Angew. Chem., Int. Ed.* **2012**, *51*, 4526-4528; b) T. Stahl, H. F. T. Klare, M. Oestreich, *ACS Catal.* **2013**, *3*, 1578-1587.

[24] a) V. J. Scott, R. Çelenligil-Çetin, O. V. Ozerov, *J. Am. Chem. Soc.* **2005**, *127*, 2852-2853; b) C. Douvris, O. V. Ozerov, *Science* **2008**, *321*, 1188-1190; c) C. Douvris, C. M. Nagaraja, C.-H. Chen, B. M. Foxman, O. V. Ozerov, *J. Am. Chem. Soc.* **2010**, *132*, 4946-4953.

[25] a) S. Duttwyler, C. Douvris, N. L. P. Fackler, F. S. Tham, C. A. Reed, K. K. Baldridge, J. S. Siegel, *Angew. Chem., Int. Ed.*, **2010**, *49*, 7519-7522; b) O. Allemann, S. Duttwyler, P. Romanato, K. K. Baldridge, J. S. Siegel, *Science* **2011**, *332*, 574-577.

[26] a) K. Hara, R. Akiyama, M. Sawamura, *Org. Lett.* **2005**, *7*, 5621-5623.

[27] a) H. F. T. Klare, K. Bergander, M. Oestreich, *Angew. Chem., Int. Ed.* **2009**, *48*, 9077-9079; *Angew. Chem.* **2009**, *121*, 9241; b) R. K. Schmidt, K. Müther, C. Mück-Lichtenfeld, S. Grimme, M. Oestreich, *J. Am. Chem. Soc.* **2012**, *134*, 4421-4428.

[28] a) M. Reißmann, A. Schäfer, S. Jung, T. Müller, *Organometallics* **2013**, *32*, 6736-6744; b) A. Schäfer, M. Reißmann, A. Schäfer, M. Schmidtmann, T. Müller, *Chem. Eur. J.* **2014**, *20*, 9381-9386.

[29] A. D. Dilman, S. L. Ioffe, *Chem. Rev.* **2003**, *103*, 733-772.

[30] K. Müther, M. Oestreich, *Chem. Commun.* **2011**, *47*, 334-336.

[31] M. Hong, J. Chen, E. Y. X. Chen, *Chem. Rev.* **2018**, *118*, 10551-10616.

[32] a) S. Popov, B. Shao, A. L. Bagdasarian, T. R. Benton, L. Zou, Z. Yang, K. N. Houk, H. M. Nelson, *Science* **2018**, *361*, 381-387. b) Q. Wu, A. Roy, E. Irran, Z. W. Qu, S. Grimme, H. F. T. Klare, M. Oestreich, *Angew. Chem., Int. Ed.* **2019**, *58*, 17307-17311.

[33]   a) P. Ducos, V. Liautard, F. Robert, Y. Landais, *Chem. Eur. J.* **2015**, *21*, 11573; b) S. Künzler, S. Rathjen, K. Rüger, M. S. Würdemann, M. Wernke, P. N. Kumar, C. Laye, F. Robert, Y. Landais, *Eur. J. Org. Chem.* **2021**, 3613-3621.

[34]   N. Fontana, N. A. Espinosa-Jalapa, M. Seidl, J. O. Bauer, *Chem. Eur. J.* **2021**, *27*, 2649

2 Research Objectives

As already described in chapter one, the study of silylium ions is currently a hot topic in the field of silicon chemistry and a plethora of useful applications for these molecules have already been discovered. In this work, we further exploit the potential of these species by introducing for the first time an anchimerically stabilized silylium ion featuring a siloxane backbone. The properties of the Si–O–Si bond (*e.g.* bond angle, electronic situation, flexibility) have been thoroughly studied providing valuable insight into structure and bonding of a fundamentally important bonding motif, which is present in silicates, silanolates, and siloxanes. At the same time, the robustness and general availability of these compounds make them promising candidates for future catalytic applications. However, in order to find applications in catalysis, the extreme electrophilicity of silylium ions (and of siloxysilylium ions as well) requires well-balanced taming. Thus, our research objective was to combine siloxane and phosphorus chemistry by introducing a phosphine sulfide functionality as stabilizing group. The use of an internal Lewis base to tame the electrophilicity of the silicon-based cationic center is unprecedented and enhances the stability of these species enormously, allowing in-depth model studies on the stereochemistry and reactivity of this new type of heterocyclic cations. For this purpose, the first investigations focus on simplified systems obtained by designing a silane moiety that features both the internal phosphine sulfide Lewis base and a reactive Si–H bond connected to the same silicon atom. Through the use of Si-centered chirality as stereochemical probe, valuable information about the mechanism and stereochemical stability of anchimerically stabilized silylium ions can be obtained. The comparison between this new type of main group element-based heterocyclic silylium ions and its disiloxane congeners provide further insights on the nature of the Si–O–Si bond and its possible applications to directly tame the reactivity of siloxysilylium ions.

Therefore, the objective of this work can be summarized as follows:

- ❖ Synthesis and characterization of novel functionalized silanes and siloxanes using state of the art techniques.
- ❖ Development of a reliable synthetic way to obtain and isolate the respective silylium and siloxysilylium ions.
- ❖ Investigations into the mechanism of the hydride abstraction reaction including chiral memory studies.
- ❖ Investigation on the reactivity and the possible applications of new main group element-based heterocyclic cations in hydrodefluorination reactions and the activation of small molecules.
- ❖ In dept analysis of these brand-new species *via* quantum calculation methods.

Preface

A synthetic version of the following chapter has already been published.

The article is reprinted with permission of Wiley-VCH. License Number: 5186400637946.

"Easy Access to Enantiomerically Pure Heterocyclic Silicon-Chiral Phosphonium Cations and the Matched/Mismatched Case of Dihydrogen Release"

Authors

N. Fontana, N. A. Espinosa-Jalapa, M. Seidl, J. O. Bauer, *Chem. Eur. J.* **2021**, *27*, 2649.

Author contribution

All the reported synthesis and characterizations (multinuclear NMR, MS, EA) in this work were performed by N. Fontana except for compounds **4a** and **4b** which were prepared and isolated for the first time by Dr. N. A. Espinosa-Jalapa. Characterizations in the solid phase (single-crystal X-ray diffraction) were performed by N. Fontana and the structures were refined by Dr. M. Seidl (Research group of Prof. M. Scheer) who also prepared the data for the SI. DFT calculations on the matched-mismatched case were performed by Dr. J. O. Bauer. Samples for chiral HPLC-UV were prepared by N. Fontana and measured either by Dr. M. Zabka or V. Scheidler (Research group of Prof. R. Gschwind). The obtained data were then analyzed and reported by N. Fontana. The supporting information were prepared by N. Fontana and revised by both Dr. N. A. Espinosa-Jalapa and Dr. J. O. Bauer. The original manuscript was prepared by N. Fontana and revised by Dr. J. O. Bauer.

Acknowledgements

3 Easy Access to Enantiomerically Pure Heterocyclic Silicon-Chiral Phosphonium Cations and the Matched/Mismatched Case of Dihydrogen Release

Abstract: *Phosphonium ions are widely used in preparative organic synthesis and catalysis. The provision of new types of cations that contain both functional and chiral information is a major synthetic challenge and can open up new horizons in asymmetric cation-directed and Lewis acid catalysis. We discovered an efficient methodology towards new Si-chiral four-membered CPSSi* heterocyclic cations. Three synthetic approaches are presented. The stereochemical sequence of anchimerically assisted cation formation with $B(C_6F_5)_3$ and subsequent hydride addition was fully elucidated and proceeds with excellent preservation of the chiral information at the stereogenic silicon atom. Also the mechanism of dihydrogen release from a protonated hydrosilane was studied in detail by the help of Si-centerd chirality as stereochemical probe. Chemoselectivity switch (dihydrogen release vs. protodesilylation) can easily be achieved through slight modifications of the solvent. A matched/mismatched case was identified and the intermolecularity of this reaction supported by spectroscopic, kinetic, deuterium labelling experiments, and quantum chemical calculations.*

3.1 Introduction

In recent years, numerous inspiring examples of phosphorus-containing cations with promising applications in synthesis and catalysis have been reported.[1,2] Chiral quaternary phosphonium ions have proven to be important synthetic targets for applications in asymmetric ion-pairing catalysis.[3,4] Studies on silyl phosphonium ions have gained great interest in view of modulating structure and reactivity of frustrated Lewis pairs (FLPs).[5] Functionalized chiral cationic phosphorus compounds are interesting synthetic targets not only for a use in counterion-directed asymmetric catalysis; in case of an additionally present Lewis acidic center, new activation modes can open up. Due to their exceptionally strong Lewis acidity,[6] silylium ions have emerged as versatile reagents.[7,8] However, well-balanced inter- or intramolecular electronic stabilization of the electron-deficient silicon center by a Lewis base is generally required to tame such reactive species for broad synthetic utilizations.[9] Pioneering work on applications of cationic silicon-based Lewis acids has been done by Müller, Oestreich, Ozerov, and others during the last two decades.[9-15] Silylium ions have been employed as powerful highly electrophilic Lewis acid catalysts,[9] e.g. for demanding low-temperature Diels-Alder reactions,[10] hydrodefluorinations,[11] and C–C bond-forming reactions,[12] and used in frustrated Lewis pair combinations for the activation of dihydrogen,[5b,13] carbon dioxide,[5b,d,14] and carbon monoxide.[15] Neutral, frustrated silicon/phosphorus Lewis pairs with highly electrophilic silicon atoms were reported by Mitzel et al.[16] The strongly electron-withdrawing perfluorinated ethyl groups[17] in $(C_2F_5)_3SiCH_2P(tBu)_2$ led to the activation of CO_2 and SO_2 while forming a higher-coordinate silicon center.[16a] Quite recently, the same group also reported a zwitterionic four-membered heterocycle with a pentacoordinate silicon center (Figure 18, **a**).[16b]

a)
zwitterionic,
higher-coordinate *Si*

Mitzel, **2019**

b)
Si-chiral
silylium ion

Robert and Landais, **2020**

c)
Silyl-substituted
carbenoids

Gessner, **2016**

d)
Si-chiral
phosphonium ion

This work
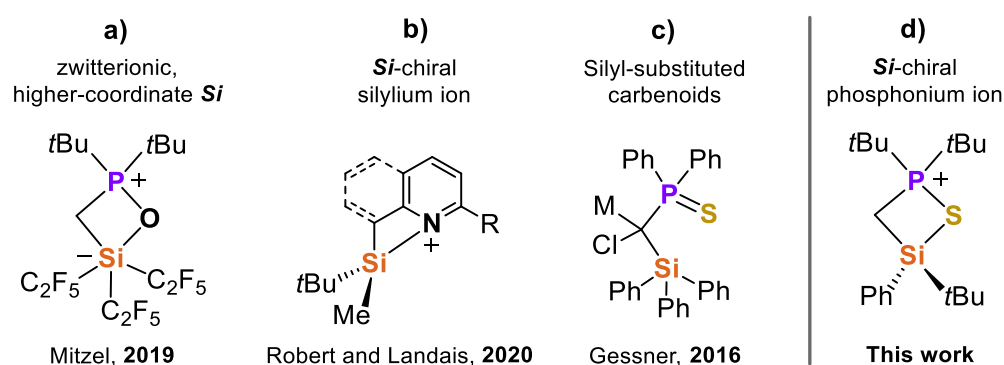
Figure 18 a) Zwitterionic heterocycle with a pentacoordinate highly Lewis acidic silicon center. b) Chiral memory studies in silyl pyridinium and quinolinium cations. c) Silyl-substituted metal carbenoids. d) Si-chiral heterocyclic silyl phosphonium sulfide reported herein.

Compounds with asymmetrically substituted silicon atoms have found use as stereochemical probes,[18] and many intriguing strategies for their stereoselective synthesis have been reported over the past few years.[19,20] However, the synthesis of Lewis base-stabilized silylium ions with silicon-centered chirality is challenging and the understanding of chiral memory in *Si*-stereogenic silylium ions is still in its infancy.[21] Very recently, Robert, Landais, and co-workers thoroughly investigated the chiral memory in highly strained four-membered silyl pyridinium and quinolinium rings stabilized through intramolecular N–Si-interaction (Figure 18, **b**).[21b] Silyl-substituted phosphine sulfides have recently been used for generating alkali metal carbenoids (Figure 18, **c**),[22] but the stereochemical implications of a P=S moiety on the stabilization of silylium ions have not yet been reported. Eventually, we got inspired by the idea to disclose a new class of small cationic heterocyclic rings having a Lewis acidic, chiral, and configurationally stable silicon atom for potential use in asymmetric cation-directed or Lewis acid-catalyzed reactions (Figure 18, **d**). Herein, we report on a convenient route toward small and configurationally stable, highly enantiomerically enriched silicon-chiral phosphonium sulfide cations that have a [P–S–Si]$^+$ motif (Figure 18, **d**). The neighboring group participation of the P=S moiety led to complete conservation of the chiral information at the stereogenic silicon atom during *S*-silyl phosphonium cation formation/hydride addition. Furthermore, a synthetic approach toward the cationic species *via* dihydrogen release or protodesilylation starting from protonated intermediates was discovered. Experimental, computational, and stereochemical findings revealed a hitherto unknown intermolecular process for generating stabilized silylium ion-like species.

3.2 Results and discussion

3.2.1 Synthesis of silyl phosphine sulfides and their cations

Sulfur-stabilized silyl cations have already proven to be relevant species in synthetically valuable reactions and the nature of this interaction has gained great interest.[11f,21c,23] However, detailed structural information on this type of interaction is still lacking. We therefore chose a phosphine sulfide-functionalized hydrosilane (**1**) as attractive starting system and performed our initial investigations with racemic compounds (Scheme 1). (*rac*)-**1** was readily synthesized by reaction of *t*Bu-PhHSiCl with LiCH$_2$P(S)(*t*Bu)$_2$ *via* nucleophilic substitution. Hydride abstraction from (*rac*)-**1**, assisted by intramolecular attack of the P=S group at the silicon atom, was achieved using B(C$_6$F$_5$)$_3$, which was Lewis acidic enough to irreversibly form the *S*-silylated phosphonium hydroborate (*rac*)-**2a** (Scheme 1, route **a**).[24] Alternatively, we opened up a route toward ion pair (*rac*)-**2b** (with the weakly coordinating borate [B(C$_6$F$_5$)$_4$]$^-$ as counterion) through Brønsted acid-promoted dehydrogenation,[25] and we were fortunate to be able to isolate and crystallize a protonated intermediate [(*rac*)-**3**] before the release of dihydrogen at 150°C under neat conditions (Scheme 1, route **b**).
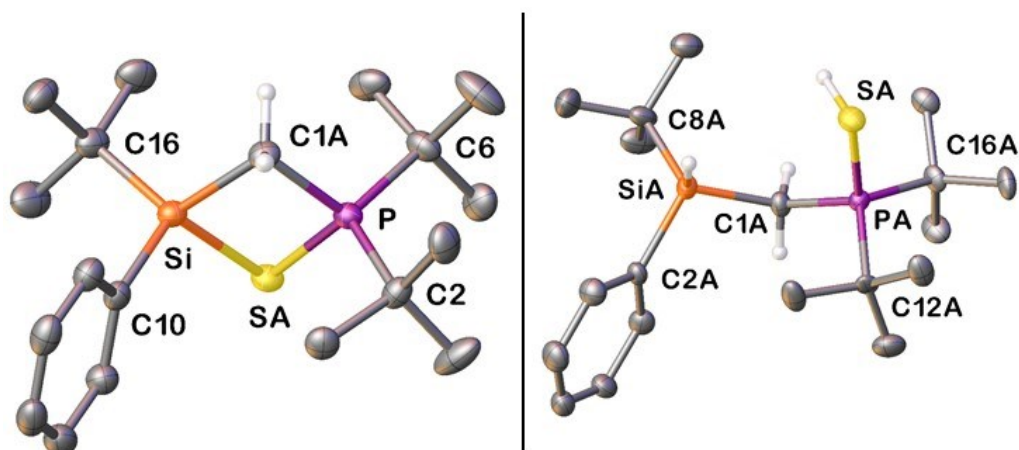
Figure 19 Molecular structures of (*rac*)-**2a** (left) and (*rac*)-**3** (right) in the crystal (displacement ellipsoids set at the 50 % probability level, counteranions and hydrogen atoms, except for the CH$_2$ and SH groups are omitted for clarity).

Compounds (*rac*)-**1**, (*rac*)-**2a**, and (*rac*)-**3** were characterized by single-crystal X-ray diffraction analysis (Figure 19; for details on (*rac*)-**1**, see the SI). (*rac*)-**2a** crystallized from pentane in the space group $P\bar{1}$. The cation of (*rac*)-**2a** forms an almost planar four-membered highly strained CPSSi heterocycle [sum of angles: 358.8(4)°] with the P–S distance of 2.0755(6) Å being elongated only by 0.11 Å compared to the same bond in the starting compound (*rac*)-**1** [1.9693(4) Å].[26] The P–S bond length of 2.0815(16) Å in the sulfur-protonated ion pair (*rac*)-**3** (space group $P2_1/c$) does not differ significantly from that in (*rac*)-**2a**.
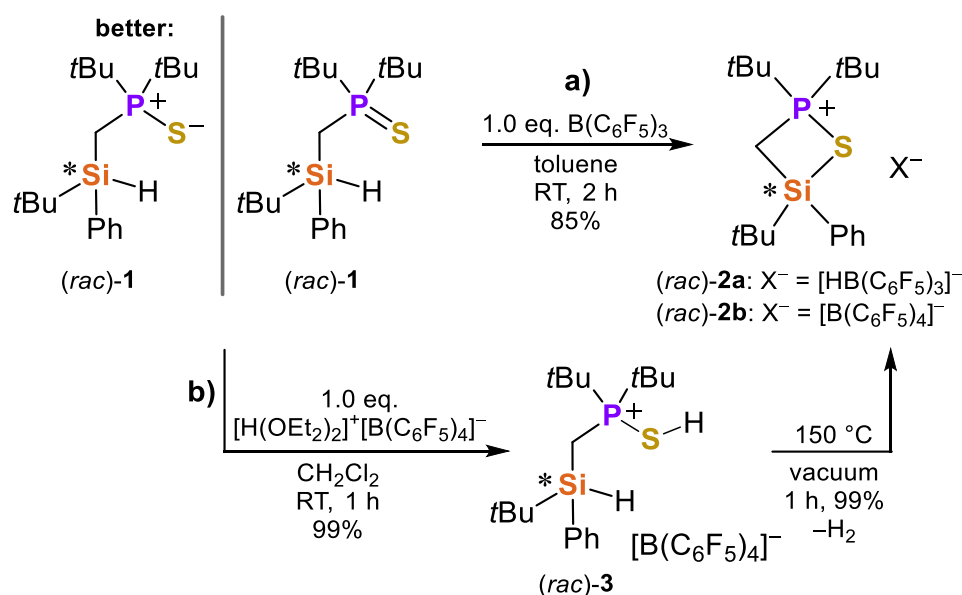
Scheme 1 Synthesis of racemic heterocyclic S-silyl phosphonium sulfides [(*rac*)-**2**] starting from hydrosilane (*rac*)-**1** either *via* hydride abstraction using $B(C_6F_5)_3$ (route **a**) or *via* protonation followed by liberation of dihydrogen from intermediate (*rac*)-**3** (route **b**).

The relative unaffected nature of the P–S bond when comparing all three compounds is also reflected by the almost identical ^{31}P NMR chemical shifts of (*rac*)-**2a** [δ (^{31}P) = 89.0 ppm] and (*rac*)-**3** [δ (^{31}P) = 88.6 ppm], which are only slightly downfield-shifted with respect to (*rac*)-**1** [δ (^{31}P) = 76.8 ppm]. In general, the spectroscopic data are quite the same for the cations in both compounds (*rac*)-**2a/b**, thus indicating that the $[HB(C_6F_5)_3]^-$ counterion in (*rac*)-**2a** is not being coordinated *via* a Si···H···B interaction in solution.[27] An interaction with the solvent CD_2Cl_2 can also be safely excluded.[10b] ^{29}Si NMR spectroscopy of compounds (*rac*)-**2a** and **b** in CD_2Cl_2 shows a signal at δ = 13.7 and 13.6 ppm, respectively. We were indeed surprised about this relatively small downfield-shift with respect to (*rac*)-**1** [δ (^{29}Si) = –2.0 ppm]. Since the ^{29}Si NMR chemical shift turned out to be a powerful diagnostic tool for estimating the Lewis acidity of silicon centers,[10b] However, ^{19}F and ^{13}C NMR spectroscopy of the adduct obtained by reacting (*rac*)-**2a** with FBN using the protocol developed by Müller *et al.* (see section 1.3),[23f] confirmed the low Lewis acidity of this compound (see the SI). Considering these results, we came to the conclusion that the P=S moiety enables a significant electronic stabilization of the cationic silicon center resulting in a strong S–Si interaction and a high level of rigidity. This agrees well with a strong electrovalent nature of the P=S bond in (*rac*)-**1** and should therefore be better formulated as a zwitterionic P^+–S^- bond with hyperconjugative multiple bond character (Scheme 1).[28] This is in line with the natural bond orbital (NBO) analysis of compound **1** and the cations of compounds **2** and **3**, performed on the M062X/6-31+G(d) level of theory (for details on the NBO calculations, see the SI).

3.2.2 Synthesis of silyl phosphine selenides and their cations

To better understand the stabilizing effect of the chalcogen, a modification of (*rac*)-**1** featuring an NMR active element was synthesized ((*rac*)-**1-Se**). In order to obtain this compound, and foreseeing the possibility to extend this study to both the lighter and heavier chalcogen derivatives (P=O, P=Te), a different synthetic approach was used preparing the P(III) functionalized silane backbone and subsequently oxidizing it with the respective element (*e.g.* red selenium). Efficiency and reliability of this approach were further confirmed by the possibility to obtain (*rac*)-**1** *via* oxidation of the phosphorus center with sulfur. Similarly to the respective sulfide, reaction of (*rac*)-**1-Se** with B(C_6F_5)$_3$ afforded the cationic species (*rac*)-**2a-Se** which could be fully characterized both in the solid state and in solution (Figure 20). Single crystal X-ray diffraction analysis describes compound (*rac*)-**2a-Se** as an almost planar rhomboidal four membered ring (Si–C–P angle 97.18(14)°, Si–Se–P angle 74.818(19)°) in which the substituents at both phosphorus and silicon are pointing out from the ring plane. As expected, the bond distance for the Si–Se interaction is in the range of a single bond (2.3416(6) Å) while the P–Se bond is elongated in comparison to the neutral precursor (2.126(6) Å *vs.* 2.2204(5) Å). In CD_2Cl_2, as reported for (*rac*)-**2a**, all the NMR sensitive nuclei involved in the stabilization of the silicon center (^{29}Si, ^{31}P) are downfield shifted. In this case, however, smaller shifts were detected for the phosphorus and silicon nuclei in the selenium derivative in comparison to the ones in the sulfur compound ($^{Se}\Delta\delta$(^{29}Si)= 8.9 ppm *vs.* $^{S}\Delta\delta$(^{29}Si)= 15.7 ppm and $^{Se}\Delta\delta$(^{31}P)= 3.6 ppm *vs.* $^{S}\Delta\delta$(^{31}P)= 11.9 ppm).
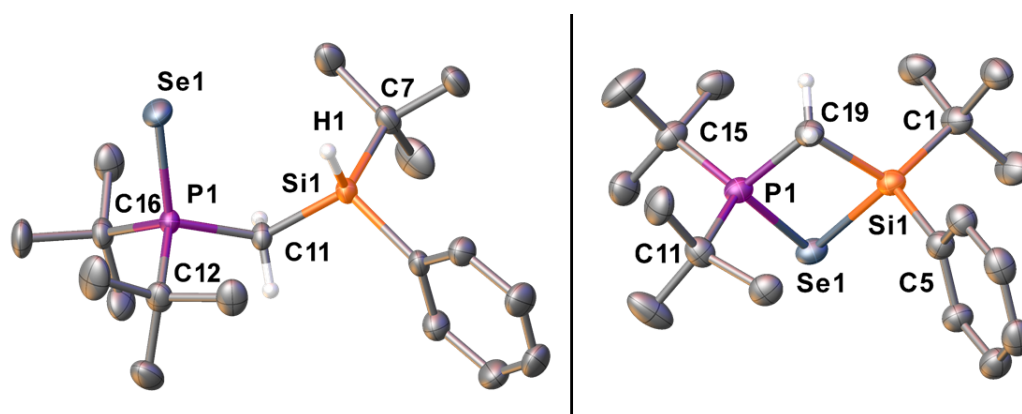
Figure 20 Molecular structures of (*rac*)-**1-Se** (left) and (*rac*)-**2a-Se** (right) in the crystal (displacement ellipsoids set at the 50 % probability level, counteranions and hydrogen atoms, except for the CH_2 and SiH groups are omitted for clarity).

Further proof for the enhanced strength of the interaction between silicon and selenium was obtained by both the chemical shift and the coupling constant of the ^{77}Se signal. With its remarkable shift towards lower field (almost 250 ppm compared to its precursor) and a marked decrease in the $^1J_{Se-P}$ (approx. 300 Hz compared to its precursor), this spectrum describes this compound as a dialkyl selenide (R_2Se) more than as a phosphorous-selenide (P=Se or $^+$P–Se$^-$). Moreover, the

small shifts for the signals in both silicon and phosphorus NMRs (8 and 3 ppm respectively) point in the direction of a more localized charge on the chalcogen atom and a stronger stabilization of the silylium ion (distorted tetrahedron C–Si–Se angle 90.15(9)°).

3.2.3   Synthesis of enantiomerically enriched silanes

The next step was to examine this type of [P–S–Si]⁺ interaction within the strained CPSSi* heterocyclic cation more closely with regard to its stereochemical behavior. For this purpose we first had to provide highly enantiomerically enriched hydrosilanes (Scheme 2). (*rac*)-**1** was converted to diastereomers **4a**,**b** by Lewis acid-catalyzed dehydrogenative Si–O coupling with (+)-menthol, followed by fractional crystallization of the two diastereomers, each of them being isolated in diastereomerically pure form.
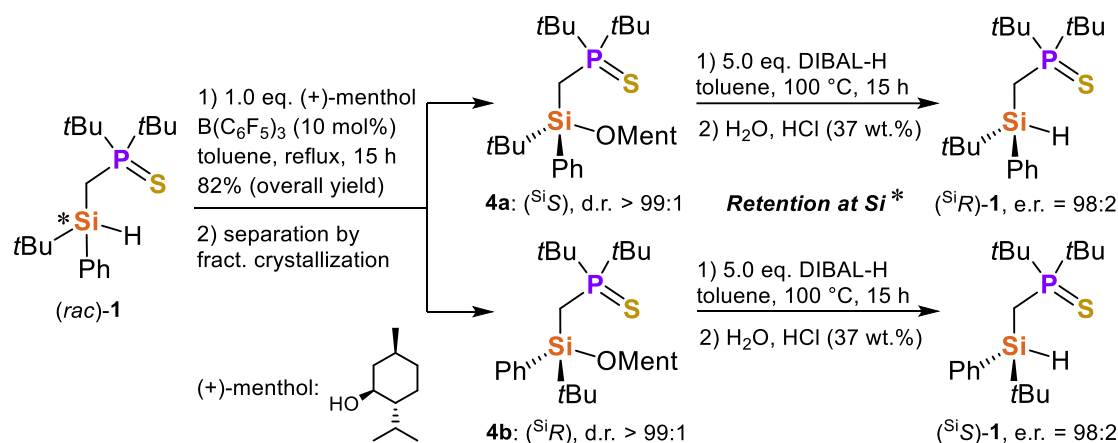
Scheme 2 Synthesis of highly enantiomerically enriched hydrosilanes (ˢⁱR)-**1** and (ˢⁱS)-**1** *via* catalytic dehydrogenative Si–O coupling of (*rac*)-**1** and (+)-menthol, separation of diastereomers **4a**,**b** by fractional crystallization, followed by stereospecific Si-O cleavage using DIBAL-H.

The absolute configurations of menthoxysilanes **4a** (ˢⁱS) and **4b** (ˢⁱR) were determined by single-crystal X-ray diffraction analysis. Reaction of **4a**,**b** with DIBAL-H resulted in stereospecific Si–O cleavage with retention at the silicon atom.[29] Hydrosilanes (ˢⁱR)-**1** and (ˢⁱS)-**1**, respectively, were obtained in excellent enantiomeric ratios of e.r. = 98:2 in each case, measured by chiral HPLC. Recrystallization of (ˢⁱR)-**1** (e.r. = 98:2) gave optically pure single-crystals (e.r. > 99:1), suitable for X-ray diffraction analysis and determination of the absolute configuration at the silicon stereocenter (for details concerning X-ray crystallography, see the SI). Encouraged by these results, we have decided to expand our investigation in a different direction trying to open up a new synthetic way with the opposite overall stereochemical outcome. While the above-mentioned cleavage using DIBAL-H afforded the product exclusively with retention of configuration at the silicon stereocenter, introducing a two-step synthesis featuring two opposite stereoselective mechanisms (*e.g.* inversion-retention or *vice versa*) would significantly increase the versatility of the whole process. Treatment

of compound **4a** with two equivalents of BF$_3$•OEt$_2$ at low temperature afforded a selective release of the chiral auxiliary to yield the respective fluorosilane ((^{Si}R)-**6**) in excellent yields. Based on the high stereoselectivity observed for this transformation (e.r. >90:10), the proposed mechanism includes the activation of the silyl ether by the Lewis acidic reagent followed by a subsequent nucleophilic attack at the silicon center by a fluoride anion in a S$_N$2 fashion. Crystals of compound **6** suitable for X-ray analysis were obtained but, even after several attempts, the isolation of enantiomerically pure crystalline material eluded us. However, absolute configuration could be established indirectly by comparison with the HPLC data related to hydrosilanes (^{Si}R)-**1** and (^{Si}S)-**1**. Interestingly, by further reacting (^{Si}R)-**6** with LiAlH$_4$ at low temperature, (^{Si}R)-**1** was reobtained in good enantiomeric ratio and without any loss of enantiomeric enrichment from the previous step (e.r. >90:10). Although our primary goal for this synthetic path was not reached (the mechanism led again to an overall retention of configuration at the stereogenic center *via* double inversion), we were delighted in discovering an efficient and stereoselective alternative for the synthesis of (^{Si}R)-**1** using common reagents and affording the products in high yields (Scheme 3).
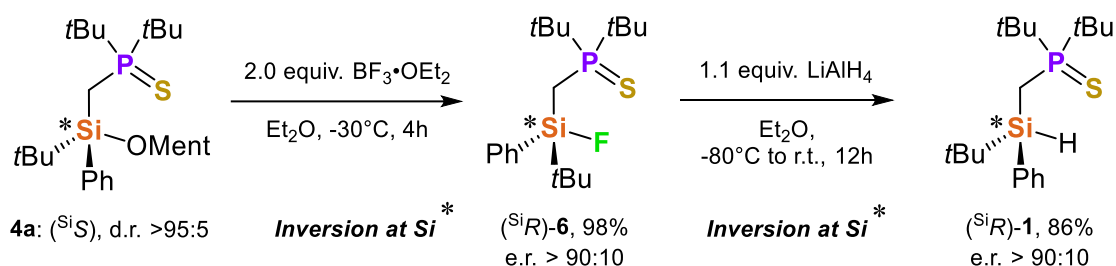
Scheme 3 Alternative synthesis of (^{Si}R)-**1** *via* fluorosilane (^{Si}R)-**4a** and subsequent reduction using LiAlH$_4$.

3.2.4   Configurational stability and chiral memory

In order to further investigate the applicability of this new type of cation as a potential chiral auxiliary, information on the configurational stability of the silicon atom is essential. Hydrosilane (^{Si}R)-**1** (e.r. = 98:2) was used to elucidate the stereochemical course and chiral memory during the sequence of cation formation and subsequent hydride addition (Scheme 3). Reaction of (^{Si}R)-**1** with B(C$_6$F$_5$)$_3$ in toluene at −80 °C immediately led to phase separation indicating the formation of *S*-silyl phosphonium hydroborate **2a**. It is important to note that the ion pair formed was stirred for one day at room temperature prior to isolation. **2a** was then converted back into the hydrosilane **1** with NaBHEt$_3$, for which an enantiomeric ratio of e.r. = 97:3 was determined by chiral HPLC. An overall retention of configuration at silicon was identified over two steps. Since it is obvious that the hydride abstraction takes place with the anchimeric assistance[30] of the P=S moiety, we can with great certainty assume a stereochemical course with double inversion[18d,21b] at the silicon center passing through a silyl phosphonium cation with ^{Si}R-configuration. The overall process [(^{Si}R)-**1** → (^{Si}R)-**2a** → (^{Si}R)-**1**] thus proceeds with excellent preservation of the stereochemical identity. The isolable *S*-

silyl phosphonium hydroborate (^{Si}R)-**2a** shows exceptional configurational stability, which, in comparison to the silyl pyridinium and quinolinium systems,[21b] remains unaffected even for one day at room temperature. This further supports a strong [P–S–Si]$^+$ interaction, which prevents ring opening and racemization of the *Si*-stereogenic center very efficiently.
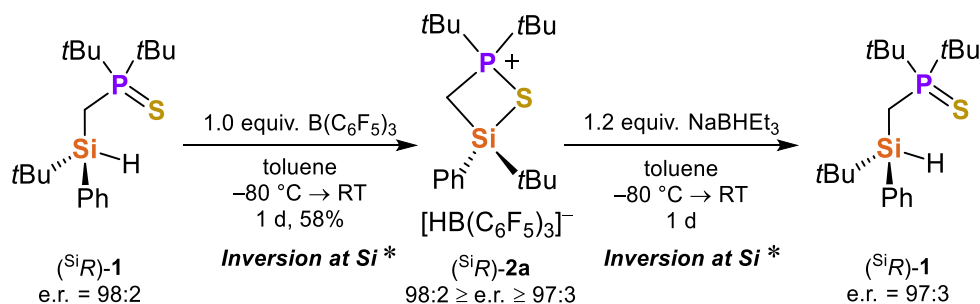
Scheme 4. Elucidation of chiral memory in the stereochemical process of anchimerically assisted cation formation [(^{Si}R)-**1** → (^{Si}R)-**2a**] and subsequent hydride addition [(^{Si}R)-**2a** → (^{Si}R)-**1**].

3.2.5 The matched/mismatched case of dihydrogen release

These results prompted us to take a closer look at route **b** of Scheme 1 from a mechanistic point of view by using the chiral information on silicon as stereochemical probe. When we performed the dehydrogenation reaction at 150°C starting from neat (^{Si}R)-**3** (e.r. = 98:2), a complete loss of configurational identity at the stereogenic silicon center occurred (see the SI). Instead, what caught our particular interest was the fact that a diethyl ether-containing solution of the racemic phosphonium borate (*rac*)-**3** in CD$_2$Cl$_2$ was slowly converted to (*rac*)-**2b** with liberation of dihydrogen even at room temperature, which was unambiguously proven by the characteristic ^{1}H NMR signals of the heterocyclic cation and H$_2$ (δ = 4.61 ppm). Interestingly, when using highly enantiomerically enriched (^{Si}R)-**3** (e.r. = 98:2), no reaction was observed even after four days.[31] NMR monitoring of the reaction progress of previously isolated (*rac*)-**3** and highly enantiomerically enriched (^{Si}R)-**3** (e.r. = 98:2), followed by a thorough kinetic analysis, showed a decrease of the reaction rate of dihydrogen release by 65% when using (^{Si}R)-**3** instead of (*rac*)-**3**. Based on these results, we proposed an intermolecular mechanism in which two cations of **3** must be involved for the release of dihydrogen, which in the case of chiral molecules would inevitably lead to matched or mismatched transition state combinations (Scheme 4, top). The intermolecularity is also supported by the fact that the rate of the reaction from (*rac*)-**3** to (*rac*)-**2b** was slowed down by 80% when the initial concentration of (*rac*)-**3** was decreased from 0.2 M to 0.1 M. A deuterium labeling experiment gave additional support of the intermolecularity of the reaction (see the SI).
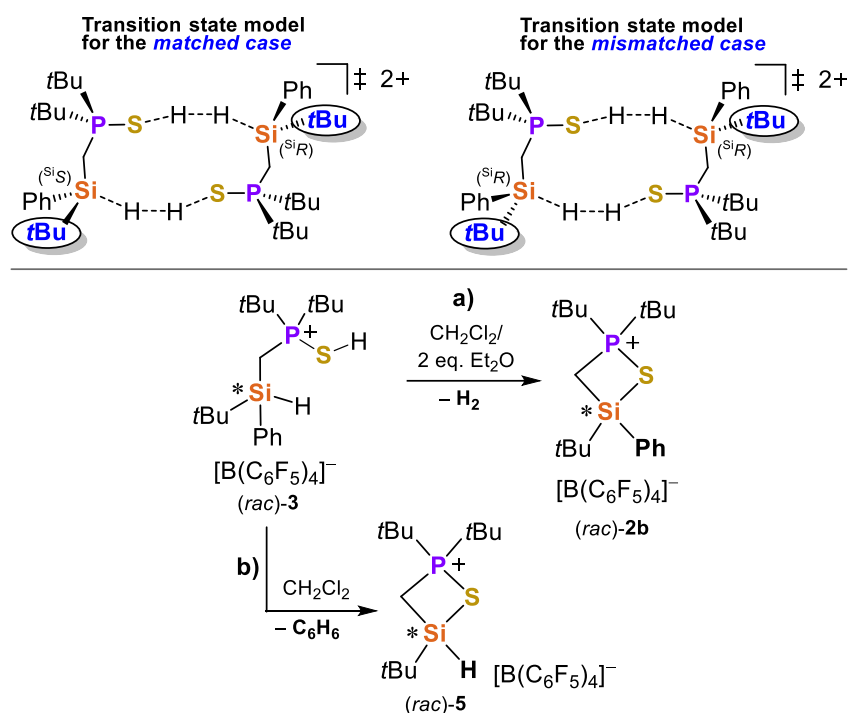
Scheme 5. Transition state models for the matched/mismatched case of intermolecular dehydrogenation (top). Chemoselectivity switch (dihydrogen release, path a); protodesilylation, path b) by changing the solvent (bottom).

DFT calculations [M062X/6-31+G(d)] on intermolecularly stabilized, eight-membered intermediates after hydrogen elimination gave a simplified but plausible estimate (ΔH = +28 kJ mol^{-1}) of the energy difference between a centrosymmetric (matched) and an asymmetric (mismatched) case, which should also be reflected in the energy of the transition state combinations (see the SI). During our mechanistic studies on compound **3**, a second reaction pathway was observed that could be useful for alternative synthetic approaches to generate functionalized silylium ions (Scheme 4, bottom). In the absence of diethyl ether, a switch from dihydrogen release to protodesilylation was identified leading chemoselectively to the hydrosilyl phosphonium borate **5**, which is an interesting species for future reactivity studies. In a similar kinetic study, a matched/mismatched case could also be proven for the protodesilylation (lowering of the reaction rate by 90% when using (^{Si}R)-**3** instead of (*rac*)-**3**) (for details, see the SI).

3.3 Conclusions

In conclusion, our findings shed light on fundamental questions regarding the configurational stability of chiral, Lewis acidic silicon centers in silyl phosphonium sulfide and selenide cations. Dehydrogenative cation formation from a protonated intermediate was achieved and an intermolecular mechanism with two molecules involved was unambiguously identified by combining various experimental, stereochemical, and quantum chemical methods. Chemoselectivity switch between dihydrogen release and protodesilylation was shown. The *Si*-chiral heterocyclic silyl phosphonium sulphides and selenides described herein represent a new class of chiral, functionalized cations that might enable future use in asymmetric synthesis and catalysis. Modulating the Lewis acidity of the *Si*-stereogenic center by varying the strength of the P–S–Si interaction and increasing the degree of functionality by changing the substituents are just two of the adjusting screws that are being addressed in our ongoing studies. A major advantage of our cation type is the ability to easily functionalize the phosphoryl group over a wide range and also to incorporate phosphorus-centered chirality[32] in the molecular design.

3.4 References

[1]   For reviews, see: a) C. A. Dyker, N. Burford, *Chem. Asian J.* **2008**, *3*, 28; b) Highlight: K.-O. Feldmann, J. J. Weigand, *Angew. Chem. Int. Ed.* **2012**, *51*, 6566; *Angew. Chem.* **2012**, *124*, 6670; c) M. H. Holthausen, J. J. Weigand, *Chem. Soc. Rev.* **2014**, *43*, 6639.

[2]   For selected examples, see: a) M. T. Reetz, G. Lohmer, R. Schwickardi, *Angew. Chem. Int. Ed.* **1998**, *37*, 481; *Angew. Chem.* **1998**, *110*, 492; b) M. Asay, S. Inoue, M. Driess, *Angew. Chem. Int. Ed.* **2011**, *50*, 9589; *Angew. Chem.* **2011**, *123*, 9763; c) C. Marquardt, C. Thoms, A. Stauber, G. Balázs, M. Bodensteiner, M. Scheer, *Angew. Chem. Int. Ed.* **2014**, *53*, 3727; *Angew. Chem.* **2014**, *126*, 3801; d) Z. Deng, J.-H. Lin, J.-C. Xiao, *Nat. Commun.* **2016**, *7*, 10337; e) L. Dütsch, M. Fleischmann, S. Welsch, G. Balázs, W. Kremer, M. Scheer, *Angew. Chem. Int. Ed.* **2018**, *57*, 3256; *Angew. Chem.* **2018**, *130*, 3311; f) F. Buß, C. Mück-Lichtenfeld, P. Mehlmann, F. Dielmann, *Angew. Chem. Int. Ed.* **2018**, *57*, 4951; *Angew. Chem.* **2018**, *130*, 5045; g) T. Scherpf, C. Schwarz, L. T. Scharf, J.-A. Zur, A. Helbig, V. H. Gessner, *Angew. Chem. Int. Ed.* **2018**, *57*, 12859; *Angew. Chem.* **2018**, *130*, 13041; h) U. Lennert, P. B. Arockiam, V. Streitferdt, D. J. Scott, C. Rödl, R. M. Gschwind, R. Wolf, *Nat. Catal.* **2019**, *2*, 1101; i) C. Taube, K. Schwedtmann, M. Noikham, E. Somsook, F. Hennersdorf, R. Wolf, J. J. Weigand, *Angew. Chem. Int. Ed.* **2020**, *59*, 3585; *Angew. Chem.* **2020**, *132*, 3613; j) P. B. Arockiam, U. Lennert, C. Graf, R. Rothfelder, D. J. Scott, T. G. Fischer, K. Zeitler, R. Wolf, *Chem. Eur. J.* **2020**, DOI: 10.1002/chem.202002646.

[3]   For a review, see: K. Brak, E. N. Jacobsen, *Angew. Chem. Int. Ed.* **2013**, *52*, 534; *Angew. Chem.* **2013**, *125*, 558.

[4]   For selected examples, see: a) D. Uraguchi, S. Sakaki, T. Ooi, *J. Am. Chem. Soc.* **2007**, *129*, 12392; b) R. He, X. Wang, T. Hashimoto, K. Maruoka, *Angew. Chem. Int. Ed.* **2008**, *47*, 9466; *Angew. Chem.* **2008**, *120*, 9608; c) D. Uraguchi, Y. Ueki, T. Ooi, *J. Am. Chem. Soc.* **2008**, *130*, 14088; d) R. He, C. Ding, K. Maruoka, *Angew. Chem. Int. Ed.* **2009**, *48*, 4559; *Angew. Chem.* **2009**, *121*, 4629; e) D. Uraguchi, Y.

Asai, T. Ooi, *Angew. Chem. Int. Ed.* **2009**, *48*, 733; *Angew. Chem.* **2009**, *121*, 747; f) D. Uraguchi, T. Ito, T. Ooi, *J. Am. Chem. Soc.* **2009**, *131*, 3836; g) D. Uraguchi, Y. Ueki, T. Ooi, *Science* **2009**, *326*, 120.

[5] a) D. Chen, V. Leich, F. Pan, J. Klankermayer, *Chem. Eur. J.* **2012**, *18*, 5184; b) M. Reißmann, A. Schäfer, S. Jung, T. Müller, *Organometallics* **2013**, *32*, 6736; c) M. Reißmann, A. Schäfer, R. Panisch, M. Schmidtmann, M. Bolte, *Inorg. Chem.* **2015**, *54*, 2393; d) S. A. Weicker, D. W. Stephan, *Chem. Eur. J.* **2015**, *21*, 13027; e) A. Merk, H. Großekappenberg, M. Schmidtmann, M.-P. Luecke, C. Lorent, M. Driess, M. Oestreich, H. F. T. Klare, T. Müller, *Angew. Chem. Int. Ed.* **2018**, *57*, 15267; *Angew. Chem.* **2018**, *130*, 15487.

[6] H. Großekappenberg, M. Reißmann, M. Schmidtmann, T. Müller, *Organometallics* **2015**, *34*, 4952.

[7] For general reviews on silylium ion chemistry, see: a) T. Müller in *Science of Synthesis Knowledge Updates 2013/3* (Ed.: M. Oestreich), Thieme, Stuttgart, **2013**, pp. 1-42; b) T. Müller in *Functional Molecular Silicon Compounds I* (Ed.: D. Scheschkewitz), Springer, Cham, **2014**, pp. 107-162; c) V. Ya. Lee, A. Sekiguchi in *Organosilicon Chemistry*, *Vol. 1* (Ed.: V. Ya. Lee), Academic Press, London, Oxford, San Diego, Cambridge, **2017**, pp. 197-230; d) V. Y. Lee, *Russ. Chem. Rev.* **2019**, *88*, 351.

[8] For seminal contributions in generating silylium ions, see: a) J. Y. Corey, *J. Am. Chem. Soc.* **1975**, *97*, 3237; b) J. B. Lambert, S. Zhang, C. L. Stern, J. C. Huffman, *Science* **1993**, *260*, 1917; c) C. A. Reed, Z. Xie, R. Bau, A. Benesi, *Science* **1993**, *262*, 402; d) Z. Xie, J. Manning, R. W. Reed, R. Mathur, P. D. W. Boyd, A. Benesi, C. A. Reed, *J. Am. Chem. Soc.* **1996**, *118*, 2922; e) J. B. Lambert, Y. Zhao, *Angew. Chem. Int. Ed. Engl.* **1997**, *36*, 400; *Angew. Chem.* **1997**, *109*, 389; f) M. J. MacLachlan, S. C. Bourke, A. J. Lough, I. Manners, *J. Am. Chem. Soc.* **2000**, *122*, 2126; g) T. Müller, *Angew. Chem. Int. Ed.* **2001**, *40*, 3033; *Angew. Chem.* **2001**, *113*, 3123; h) P. P. Gaspar, *Science* **2002**, *297*, 785; i) K.-C. Kim, C. A. Reed, D. W. Elliott, L. J. Mueller, F. Tham, L. Lin, J. B. Lambert, *Science* **2002**, *297*, 825; j) S. Duttwyler, Q.-Q. Do, A. Linden, K. K. Baldridge, J. S. Siegel, *Angew. Chem. Int. Ed.* **2008**, *47*, 1719; *Angew. Chem.* **2008**, *120*, 1743; k) K. Müther, R. Fröhlich, C. Mück-Lichtenfeld, S. Grimme, M. Oestreich, *J. Am. Chem. Soc.* **2011**, *133*, 12442; l) R. Ramírez-Contreras, N. Bhuvanesh, J. Zhou, O. V. Ozerov, *Angew. Chem. Int. Ed.* **2013**, *52*, 10313; *Angew. Chem.* **2013**, *125*, 10503; m) N. Kramer, H. Wadepohl, L. Greb, *Chem. Commun.* **2019**, *55*, 7764; n) Q. Wu, E. Irran, R. Müller, M. Kaupp, H. F. T. Klare, M. Oestreich, *Science,* **2019**, *365*, 168; o) Q. Wu, A. Roy, G. Wang, E. Irran, H. F. T. Klare, M. Oestreich, *Angew. Chem. Int. Ed.* **2020**, *59*, 10523; *Angew. Chem.* **2020**, *132*, 10609.

[9] For reviews on applications of silylium ions, see: a) H. F. T. Klare, M. Oestreich, *Dalton Trans.* **2010**, *39*, 9176; b) P. Shaykhutdinova, S. Keess, M. Oestreich in *Organosilicon Chemistry: Novel Approaches and Reactions* (Eds.: T. Hiyama, M. Oestreich), Wiley-VCH, Weinheim, **2020**, pp. 131-170; c) J. S. Siegel, *Nat. Rev. Chem.* **2020**, *4*, 4-5; d) J. C. L. Walker, H. F. T. Klare, M. Oestreich, *Nat. Rev. Chem.* **2020**, *4*, 54.

[10] a) K. Hara, R. Akiyama, M. Sawamura, *Org. Lett.* **2005**, *7*, 5621; b) H. F. T. Klare, K. Bergander, M. Oestreich, *Angew. Chem. Int. Ed.* **2009**, *48*, 9077; *Angew. Chem.* **2009**, *121*, 9241; c) R. K. Schmidt, K. Müther, C. Mück-Lichtenfeld, S. Grimme, M. Oestreich, *J. Am. Chem. Soc.* **2012**, *134*, 4421.

[11] a) V. J. Scott, R. Çelenligil-Çetin, O. V. Ozerov, *J. Am. Chem. Soc.* **2005**, *127*, 2852; b) R. Panisch, M. Bolte, T. Müller, *J. Am. Chem. Soc.* **2006**, *128*, 9676; c) C. Douvris, O. V. Ozerov, *Science* **2008**, *321*, 1188; d) Highlight: G. Meier, T. Braun, *Angew. Chem. Int. Ed.* **2009**, *48*, 1546; *Angew. Chem.* **2009**, *121*, 1575; e) C. Douvris, C. M. Nagaraja, C.-H. Chen, B. M. Foxman, O. V. Ozerov, *J. Am. Chem. Soc.* **2010**, *132*, 4946; f) T. Stahl, H. F. T. Klare, M. Oestreich, *J. Am. Chem. Soc.* **2013**, *135*, 1248.

[12] a) N. Lühmann, R. Panisch, T. Müller, *Appl. Organomet. Chem.* **2010**, *24*, 533; b) O. Allemann, S. Duttwyler, P. Romanato, K. K. Baldridge, J. S. Siegel, *Science* **2011**, *332*, 574.

[13] a) A. Schäfer, M. Reißmann, A. Schäfer, W. Saak, D. Haase, T. Müller, *Angew. Chem. Int. Ed.* **2011**, *50*, 12636; *Angew. Chem.* **2011**, *123*, 12845; b) A. Schäfer, M. Reißmann, A. Schäfer, M. Schmidtmann, T. Müller, *Chem. Eur. J.* **2014**, *20*, 9381.

[14] a) Berkefeld, W. E. Piers, M. Parvez, *J. Am. Chem. Soc.* **2010**, *132*, 10660; b) A. Schäfer, W. Saak, D. Haase, T. Müller, *Angew. Chem. Int. Ed.* **2012**, *51*, 2981; *Angew. Chem.* **2012**, *124*, 3035; c) M. Konno, M. Chiba, K. Nemoto, T. Hattori, *Chem. Lett.* **2012**, *41*, 913; d) M. F. Silva Valverde, E. Theuergarten, T. Bannenberg, M. Freytag, P. G. Jones, M. Tamm, *Dalton Trans.* **2015**, *44*, 9400.

[15] a) M. Devillard, B. de Bruin, M. A. Siegler, J. I. van der Vlugt, *Chem. Eur. J.* **2017**, *23*, 13628; b) L. Omann, Z.-W. Qu, E. Irran, H. F. T. Klare, S. Grimme, M. Oestreich, *Angew. Chem. Int. Ed.* **2018**, *57*, 8301; *Angew. Chem.* **2018**, *130*, 8433.

[16] a) B. Waerder, M. Pieper, L. A. Körte, T. A. Kinder, A. Mix, B. Neumann, H.-G. Stammler, N. W. Mitzel, *Angew. Chem. Int. Ed.* **2015**, *54*, 13416; *Angew. Chem.* **2015**, *127*, 13614; b) T. A. Kinder, R. Pior, S. Blomeyer, B. Neumann, H.-G. Stammler, N. W. Mitzel, *Chem. Eur. J.* **2019**, *25*, 5899; c) T. A. Kinder, S. Blomeyer, M. Franke, F. Depenbrock, B. Neumann, H.-G. Stammler, N. W. Mitzel, *Eur. J. Inorg. Chem.* **2019**, 3933.

[17] S. Steinhauer, H.-G. Stammler, B. Neumann, N. Ignat`ev, B. Hoge, *Angew. Chem. Int. Ed.* **2014**, *53*, 562; *Angew. Chem.* **2014**, *126*, 573.

[18] For selected examples, see: a) M. Oestreich, S. Rendler, *Angew. Chem. Int. Ed.* **2005**, *44*, 1661; *Angew. Chem.* **2005**, *117*, 1688; b) A. Nakazaki, T. Nakai, K. Tomooka, *Angew. Chem. Int. Ed.* **2006**, *45*, 2235; *Angew. Chem.* **2006**, *118*, 2293; c) S. Rendler, M. Oestreich, C. P. Butts, G. C. Lloyd-Jones, *J. Am. Chem. Soc.* **2007**, *129*, 502; d) S. Rendler, M. Oestreich, *Angew. Chem. Int. Ed.* **2008**, *47*, 5997; *Angew. Chem.* **2008**, *120*, 6086; e) T. Fallon, M. Oestreich, *Angew. Chem. Int. Ed.* **2015**, *54*, 12488; *Angew. Chem.* **2015**, *127*, 12666; f) S. G. Koller, J. O. Bauer, C. Strohmann, *Angew. Chem. Int. Ed.* **2017**, *56*, 7991; *Angew. Chem.* **2017**, *129*, 8102.

[19] For reviews, see: a) M. Oestreich, *Synlett* **2007**, 1629; b) L.-W. Xu, L. Li, G.-Q. Lai, J.-X. Jiang, *Chem. Soc. Rev.* **2011**, *40*, 1777; c) Highlight: L.-W. Xu, *Angew. Chem. Int. Ed.* **2012**, *51*, 12932; *Angew. Chem.* **2012**, *124*, 13106; d) R. Shintani, *Asian J. Org. Chem.* **2015**, *4*, 510; e) J. O. Bauer, C. Strohmann, *Eur. J. Inorg. Chem.* **2016**, 2868; f) Y.-M. Cui, Y. Lin, L.-W. Xu, *Coord. Chem. Rev.* **2017**, *330*, 37; g) L.-W. Xu in *Organosilicon Chemistry*, *Vol. 1* (Ed.: V. Ya. Lee), Academic Press, London, Oxford, San Diego, Cambridge, **2017**, pp. 145-194; h) R. Shintani, *Synlett* **2018**, *29*, 388; i) K. Igawa, K. Tomooka in *Organosilicon Chemistry: Novel Approaches and Reactions* (Eds.: T. Hiyama, M. Oestreich), Wiley-VCH, Weinheim, **2020**, pp. 495-532.

[20] For some recent contributions, see: a) J. O. Bauer, C. Strohmann, *Angew. Chem. Int. Ed.* **2014**, *53*, 720; *Angew. Chem.* **2014**, *126*, 738; b) J. O. Bauer, C. Strohmann, *Angew. Chem. Int. Ed.* **2014**, *53*, 8167; *Angew. Chem.* **2014**, *126*, 8306; c) J. O. Bauer, C. Strohmann, *J. Am. Chem. Soc.* **2015**, *137*, 4304; d) K. Igawa, D. Yoshihiro, Y. Abe, K. Tomooka, *Angew. Chem. Int. Ed.* **2016**, *55*, 5814; *Angew. Chem.* **2016**, *128*, 5908; e) J. R. Jagannathan, J. C. Fettinger, J. T. Shaw, A. K. Franz, *J. Am. Chem. Soc.* **2020**, *142*, 11674; f) D. Mu, W. Yuan, S. Chen, N. Wang, B. Yang, L. You, B. Zu, P. Yu, C. He, *J. Am. Chem. Soc.* **2020**, *142*, 13459.

[21] a) P. Ducos, V. Liautard, F. Robert, Y. Landais, *Chem. Eur. J.* **2015**, *21*, 11573; b) A. Fernandes, C. Laye, S. Pramanik, D. Palmeira, Ö. Ö. Pekel, S. Massip, M. Schmidtmann, T. Müller, F. Robert, Y. Landais, *J.*

Am. Chem. Soc. **2020**, *142*, 564; c) S. Künzler, S. Rathjen, K. Rüger, M. S. Würdemann, M. Wernke, P. Tholen, C. Girschik, M. Schmidtmann, Y. Landais, T. Müller, *Chem. Eur. J.* **2020**, DOI: 10.1002/chem.202002977.

[22] S. Molitor, V. H. Gessner, *Angew. Chem. Int. Ed.* **2016**, *55*, 7712; *Angew. Chem.* **2016**, *128*, 7843.

[23] a) U.-H. Berlekamp, P. Jutzi, A. Mix, B. Neumann, H.-G. Stammler, W. W. Schoeller, *Angew. Chem. Int. Ed.* **1999**, *38*, 2048; *Angew. Chem.* **1999**, *111*, 2071; b) G. K. S. Prakash, C. Bae, Q. Wang, G. Rasul, G. A. Olah, *J. Org. Chem.* **2000**, *65*, 7646; c) H. F. T. Klare, M. Oestreich, J.-i. Ito, H. Nishiyama, Y. Ohki, K. Tatsumi, *J. Am. Chem. Soc.* **2011**, *133*, 3312; d) C. D. F. Königs, H. F. T. Klare, M. Oestreich, *Angew. Chem. Int. Ed.* **2013**, *52*, 10076; *Angew. Chem.* **2013**, *125*, 10260; e) V. H. G. Rohde, P. Pommerening, H. F. T. Klare, M. Oestreich, *Organometallics* **2014**, *33*, 3618; f) S. Künzler, S. Rathjen, A. Merk, M. Schmidtmann, T. Müller, *Chem. Eur. J.* **2019**, *25*, 15123; g) A. Denhof, M. Olaru, E. Lork, S. Mebs, L. Chęcińska, J. Beckmann, *Eur. J. Inorg. Chem.* **2020**, 4093.

[24] For an intermolecular P=O silylation, see: P. Felgenhauer, R. Labbow, A. Schulz, A. Villinger, *Inorg. Chem.* **2018**, *57*, 9348.

[25] Q.-A. Chen, H. F. T. Klare, M. Oestreich, *J. Am. Chem. Soc.* **2016**, *138*, 7868.

[26] For a detailed study of bonding parameters in phosphine sulfides, see: T. Cantat, I. Ricard, P. Le Floch, N. Mézailles, *Organometallics* **2006**, *25*, 4965.

[27] A. Y. Houghton, J. Hurmalainen, A. Mansikkamäki, W. E. Piers, H. M. Tuononen, *Nat. Chem.* **2014**, *6*, 983.

[28] For a review on bonding in heavier main group element compounds, see: W. Kutzelnigg, *Angew. Chem. Int. Ed. Engl.* **1984**, *23*, 272; *Angew. Chem.* **1984**, *96*, 262; for studies concerning the concept of hypervalency on sulfur centers, see: a) D. Leusser, J. Henn, N. Kocher, B. Engels, D. Stalke, *J. Am. Chem. Soc.* **2004**, *126*, 1781; b) M. S. Schmøkel, S. Cenedese, J. Overgaard, M. R. V. Jørgensen, Y.-S. Chen, C. Gatti, D. Stalke, B. B. Iversen, *Inorg. Chem.* **2012**, *51*, 8607.

[29] M. Oestreich, G. Auer, M. Keller, *Eur. J. Org. Chem.* **2005**, 184.

[30] B. Capon, *Q. Rev., Chem. Soc.* **1964**, *18*, 45.

[31] (*rac*)-**3** and (^Si^*R*)-**3** were prepared *in situ* from compound **1** and [H(Et$_2$O)$_2$][B(C$_6$F$_5$)$_4$].

[32] a) K. M. Pietrusiewicz, M. Zabłocka, *Chem. Rev.* **1994**, *94*, 1375; b) Z. S. Han, N. Goyal, M. A. Herbage, J. D. Sieber, B. Qu, Y. Xu, Z. Li, J. T. Reeves, J.-N. Desrosiers, S. Ma, N. Grinberg, H. Lee, H. P. R. Mangunuru, Y. Zhan, D. Krishnamurthy, B. Z. Lu, J. J. Song, G. Wang, C. H. Senanayake, *J. Am. Chem. Soc.* **2013**, *135*, 2474.

3.5 Synthesis and Characterizations

3.5.1 General Remarks

All experiments were performed in an inert atmosphere of purified nitrogen using standard Schlenk techniques or an MBraun Unilab 1200/780 glovebox. Glassware was heated at 140 °C prior to use. Diethyl ether (Et$_2$O), dichloromethane (DCM), hexane, pentane, tetrahydrofuran (THF), and toluene were dried and degassed with an MBraun SP800 solvent purification system. *n*-Butyllithium (2.5 M or 1.6 M solution in hexane, Merck KGaA), dichlorophenylsilane (97 %, Merck KGaA), di-*tert*-butylmethylphosphine (97%, Merck KGaA), *tert*-butyllithium (1.9 M solution in pentane, Merck KGaA), sulfur (99%, Merck KGaA), (+)-menthol (97%, Merck KGaA), hydrogen chloride (2.0 M solution in diethyl ether, Merck KGaA), bromopentafluorobenzene (99%, Fluorochem), boron trichloride (1.0 M solution in hexane fractions, Merck KGaA), *tert*-butyltrichlorosilane (99%, Merck KGaA), sodium triethylborohydride (1.0 M solution in toluene, Merck KGaA), and sodium borotetradeuteride (Merck KGaA, 90%, 98% atom %), 4-fluorobenzonitrile (99%, Merck KGaA) were used without any further purification. Tris-pentafluoro-phenyl-borane,[1] [H(OEt$_2$)$_2$][B(C$_6$F$_5$)$_4$],[2] [D(OEt$_2$)$_2$][B(C$_6$F$_5$)$_4$],[2] (di-*tert*-butylphosphaneyl)methyllithium,[3] lithium mentholate,[4] and di-*tert*-butylmethylthiophosphane[5] were synthesized following reported procedures. (Di-*tert*-butylphosphorothioyl)methyllithium was freshly prepared *via* deprotonation of di-*tert*-butylmethylphosphane with either *n*-butyllithium or *tert*-butyllithium. C$_6$D$_6$ and CD$_2$Cl$_2$ used for NMR spectroscopy were dried over Na/K amalgam and CaH$_2$ respectively. NMR spectra were either recorded using a Bruker Avance 400 (400.13 MHz) or a Bruker Avance III HD 400 (400.13 MHz) at 25 °C. Chemical shifts (*δ*) are reported in parts per million (ppm). ^{1}H and ^{13}C{^{1}H} NMR spectra are referenced to tetramethylsilane (SiMe$_4$, *δ* = 0.0 ppm) as external standard, with the deuterium signal of the solvent serving as internal lock and the residual solvent signal as an additional reference. ^{11}B{^{1}H}, ^{19}F{^{1}H}, ^{29}Si{^{1}H}, and ^{31}P{^{1}H} NMR spectra are referenced to BF$_3$•OEt$_2$, CFCl$_3$, SiMe$_4$ and H$_3$PO$_4$, respectively. For the assignment of the multiplicities, the following abbreviations are used: s = singlet, d = doublet, t = triplet m = multiplet. For simplicity, multiplets of order higher than one are described approximating them to the closest first-order type. High-resolution mass spectrometry was carried out on a Jeol AccuTOF GCX and an Agilent Q-TOF 6540 UHD spectrometer. Elemental analyses were performed on a Vario MICRO cube apparatus. Evaluation of the enantiomeric ratios was assessed using an Agilent Infinity 1260 HPLC mounting a Chiralpak IC column.

3.5.2 Synthesis of (*rac*)-(*t*Bu)₂P(S)CH₂Si(H)Ph*t*Bu ((*rac*)-1)
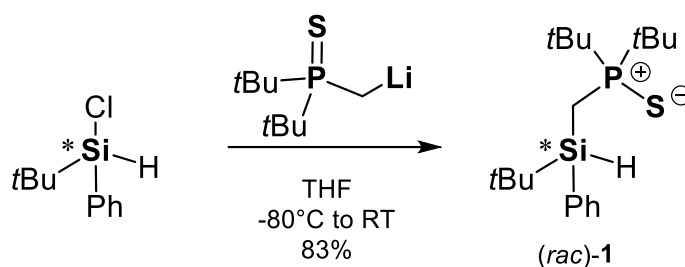
tert-Butylchloro(phenyl)silane (1.16 g, 5.85 mmol, 1.0 equiv.) was added *via* syringe to a solution of (di-*tert*-butylphosphorothioyl)methyllithium (1.13 g, 5.85 mmol, 1.0 equiv.) in THF (10 ml) at -80°C. The reaction mixture was allowed to slowly warm up to room temperature and kept stirring for 15 h. Following, all volatiles were removed in vacuum and the residue was extracted with pentane (10 ml). The suspension was filtered off *via* suction filtration and the remaining solids were washed with pentane (3 x 5 ml). The filtrates were collected and all volatiles were removed in vacuum yielding a pale beige solid. The crude residue was dissolved in the minimum amount possible of pentane (~2 ml) and crystallized at -35°C affording (*rac*)-1 (1.7 g, 4.86 mmol, 83%) as colourless single-crystalline needles, suitable for single-crystal X-ray diffraction analysis.

¹H NMR (400.13 MHz, C₆D₆, 298 K): δ =1.00 [s, 9H, SiC(CH_3)₃], 1.06 [d, $^3J_{\text{P-H}}$= 14.8 Hz, 9H, PC(CH_3)₃], 1.22 [d, $^3J_{\text{P-H}}$= 14.8 Hz, 9H, PC(CH_3)₃], 1.49-1.43 [m, 2H, SiCH_2P], 4.91 [m, 1H, SiH], 7.19-7.15 [m, 3H, H_{Ph}], 7.56-1.54 [m, 2H, H_{Ph}]. **¹³C{¹H} NMR** (100.61 MHz, C₆D₆, 298 K): δ = 5.0 [d, $^1J_{\text{C-P}}$ = 32.6 Hz, SiCH_2P], 17.6 [d, $^3J_{\text{C-P}}$ = 3.7 Hz, SiCH_2(CH₃)₃], 27.6 [d, $^2J_{\text{C-P}}$ = 9.2 Hz, PCH₂(CH_3)₃], 29.1 [s, SiCH₂(CH_3)₃], 38.2 [d, $^1J_{\text{C-P}}$ = 42.4 Hz, PCH_2(CH₃)₃], 38.8 [d, $^1J_{\text{C-P}}$ = 42.4 Hz, PCH_2(CH₃)₃], 128.1 [s, C$_{meta}$], 129.7 [s, C$_{para}$], 135.2 [s, $^3J_{\text{C-P}}$ = 1.4 Hz, C$_{ipso}$], 135.7 [s, C$_{ortho}$]. **²⁹Si{¹H} NMR** (79.49 MHz, C₆D₆, 298 K): δ = -2.0 [d, $^2J_{\text{Si-P}}$= 7.5 Hz, SiCH₂P]. **³¹P{¹H} NMR** (162.04 MHz, C₆D₆, 298 K): δ = 77.1. **CHN Analysis** C₁₉H₃₅PSSi: calculated: C 64.36%, H 9.95%; found C 64.43%, H 9.79%. **HR-MS (ESI+)**, calcd. m/z for C₁₉H₃₆PSSi⁺ [M+H]⁺: 355,2044; found: 355.2043.
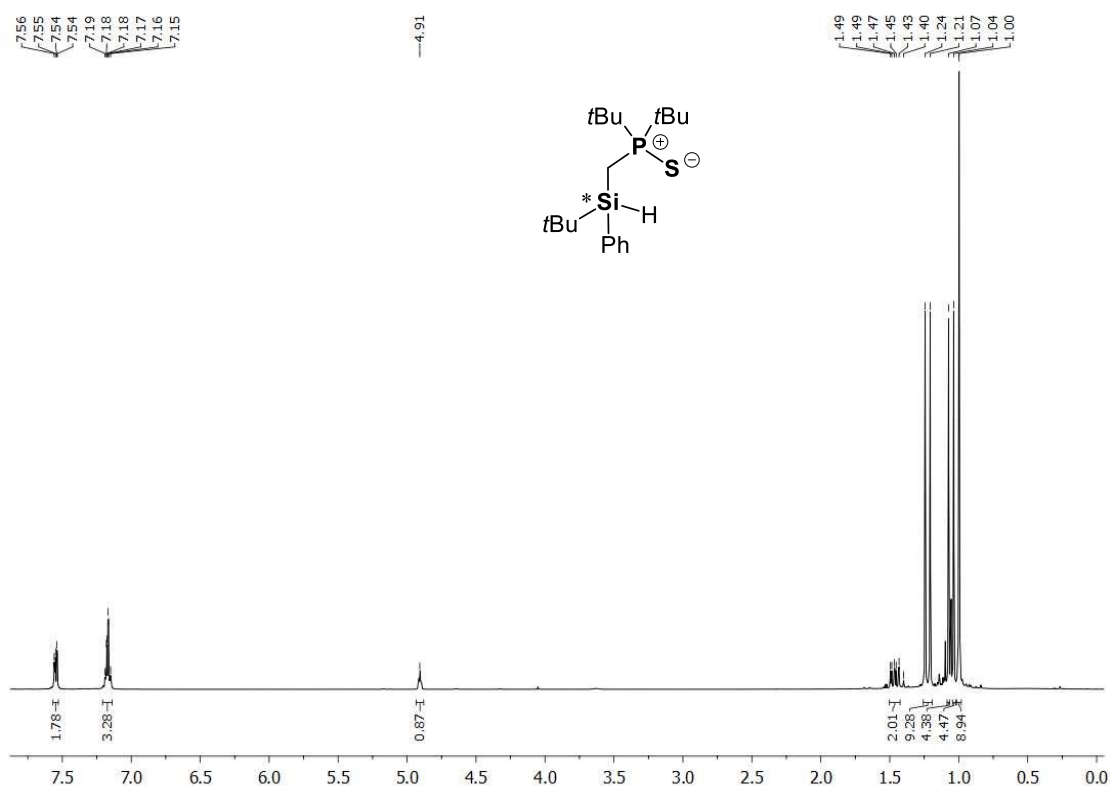
Figure S21. ^{1}H NMR spectrum (C$_6$D$_6$, 298 K) of compound (*rac*)-**1**.
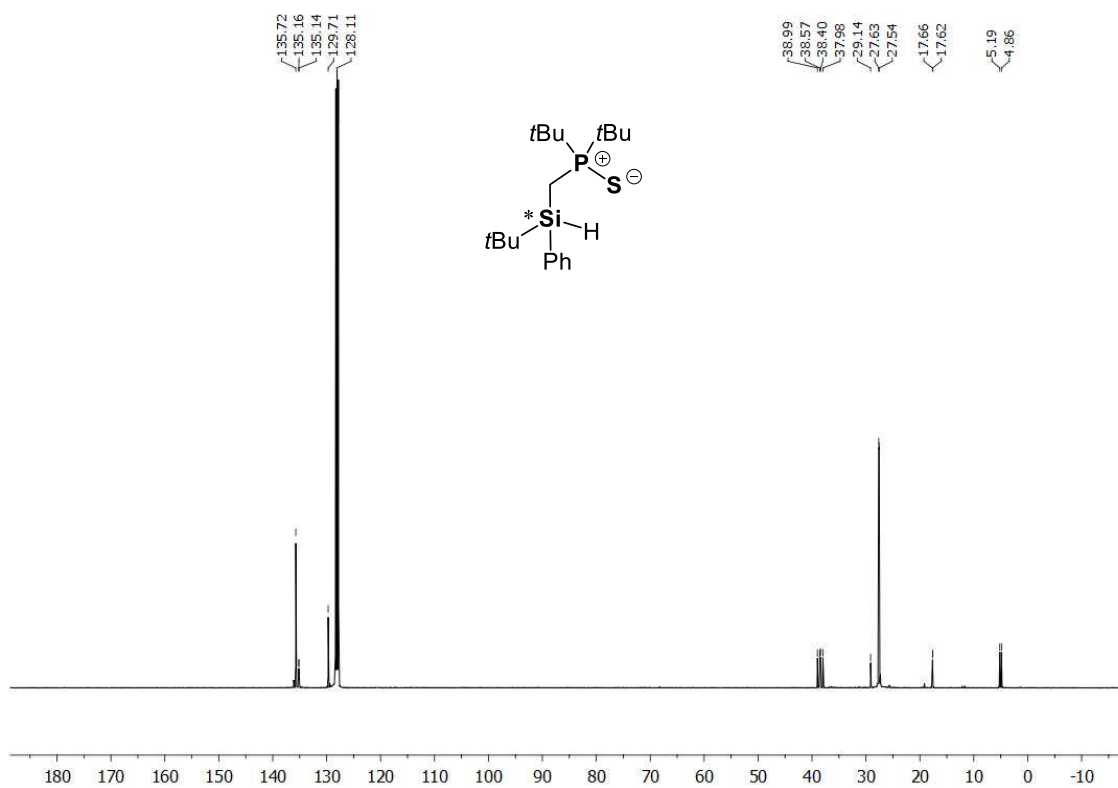
Figure S22. ^{13}C{^{1}H} NMR spectrum (C$_6$D$_6$, 298 K) of compound (*rac*)-**1**.
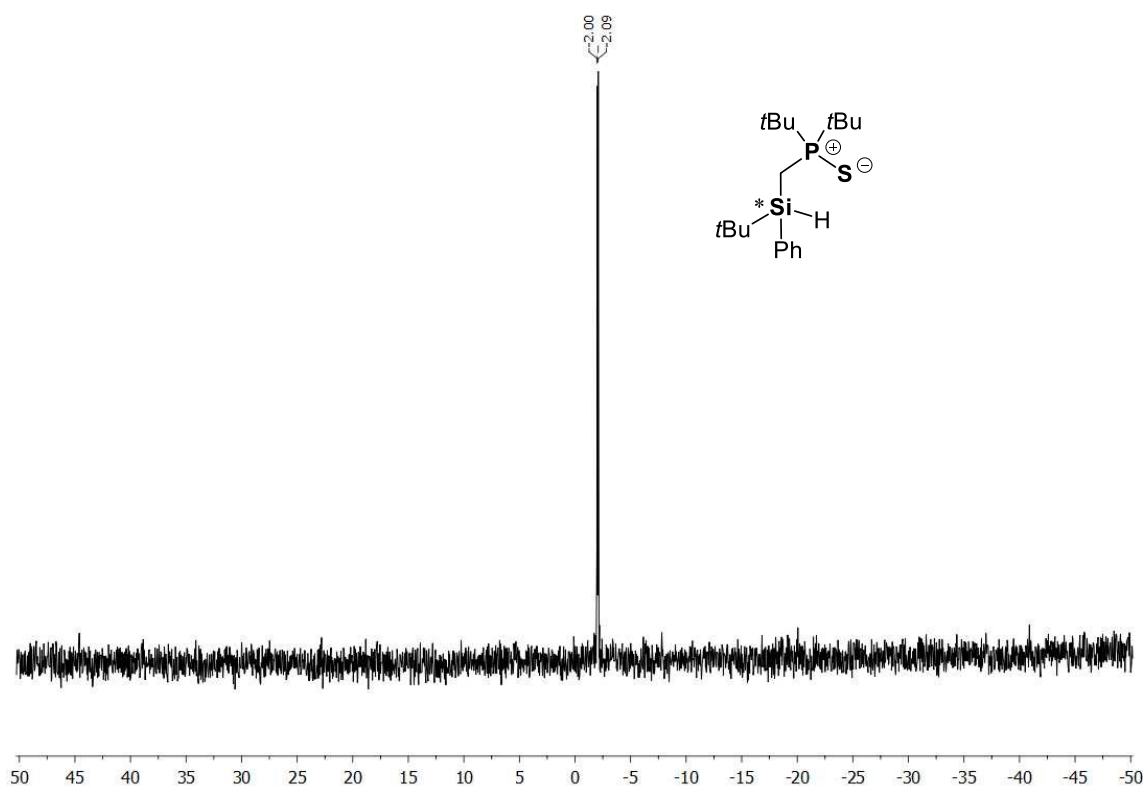
Figure S23. ^{29}Si{^{1}H} NMR spectrum (C$_6$D$_6$, 298 K) of compound (*rac*)-**1**.
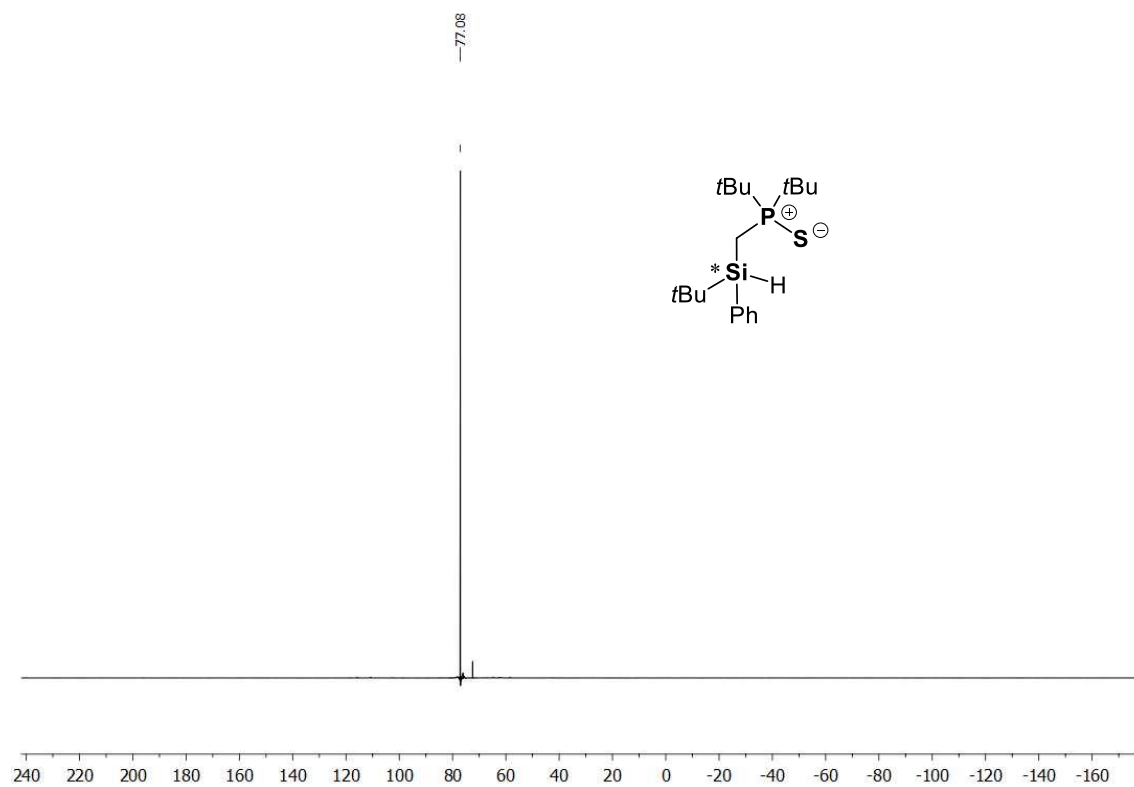
Figure S24. ^{31}P{^{1}H} NMR spectrum (C$_6$D$_6$, 298 K) of compound (*rac*)-**1**.

3.5.3 Synthesis of (rac)-[(tBu)₂P(S)CH₂Si(H)PhtBu][HB(C₆F₅)₃] ((rac)-2a)

(rac)-**1** → (rac)-**2a**

Reaction conditions: 1.0 eq. B(C₆F₅)₃, toluene, RT, 2 h, 85%
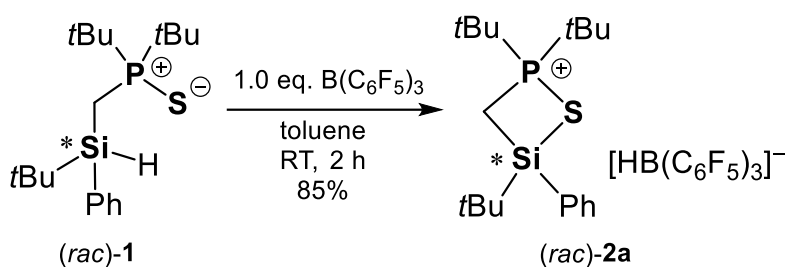
Inside a glovebox, an oven dried Schlenk flask was charged with compound (rac)-**1** (200 mg, 0.56 mmol, 1.0 equiv.) and tris(pentafluorophenyl)borane (289 mg, 0.56 mmol, 1.0 equiv.). Toluene (2 ml) was added, and the solution was stirred for two hours at room temperature. The resulting biphasic solution was fully dried and the residue was washed with pentane (2 x 5 ml), yielding pure (rac)-**2a** as a white solid (415 mg, 0.48 mmol, 85%). In an independent experiment, colourless crystals, suitable for single-crystal X-ray diffraction analysis were obtained by pentane vapor diffusion into the toluene biphasic solution containing (rac)-**2a**.

¹H NMR (400.30 MHz, CD₂Cl₂, 298 K): δ = 1.10 [s, 9H SiC(CH₃)₃], 1.22 [d, $^3J_{P-H}$= 18.8 Hz, 9H, PC(CH₃)₃], 1.56 [d, $^3J_{P-H}$= 18.8 Hz, 9H, PC(CH₃)₃], 5.06 [ddd(ABX), J₁= 12.8 Hz, J₂= 16.6 Hz, J₃= 103,0 Hz, 2H, SiCH₂P], 7.49-7.62 [m, 5H, HPh]. **¹¹B{¹H} NMR** (128.43 MHz, CD₂Cl₂, 298 K): δ = -25.3 [bs] **¹³C{¹H} NMR** (100.66 MHz, CD₂Cl₂, 298 K): δ = 7.1 [d, $^1J_{C-P}$ = 21.1 Hz, SiCH₂P], 22.8 [s, SiC(CH₃)₃], 25.1 [s, SiC(CH₃)₃], 26.6 [d, $^2J_{C-P}$ = 16.6 Hz, PC(CH₃)₃], 26.6 [d, $^2J_{C-P}$ = 16.5 Hz, PC(CH₃)₃], 40.1 [d, $^1J_{C-P}$ = 22.4 Hz, PC(CH₃)₃], 41.4 [d, $^1J_{C-P}$ = 20.3 Hz, PC(CH₃)₃], 127.7 [s, CPh], 129.2 [s, CPh], 129.4 [s, CPh], 132.3 [s, CPh], 133.7 [bs, CAr-borate], 134.7 [s, CAr-borate], 137.1 [bd, $^1J_{C-F}$ = 250 Hz, CAr-borate], 148.6 [bd, $^1J_{C-F}$ = 235.7 Hz, CAr-borate]. **¹⁹F{¹H} NMR** (376.66 MHz, CD₂Cl₂, 298 K): δ = -166.8 [bs, 6F], -163.8 [bs, 3F], -134.2 [bs, 6F]. **²⁹Si{¹H} NMR** (79.49 MHz, CD₂Cl₂, 298 K): δ = 13.7 [d, $^2J_{Si-P}$= 14.7 Hz, SiCH₂P]. **³¹P{¹H} NMR** (162.04 MHz, CD₂Cl₂, 298 K): δ = 89.0. **CHN Analysis** C₃₇H₃₅BF₁₅PSSi: calculated: C 51.28%, H 4.07%; S 3.70%; [(C₃₇H₃₅BF₁₅PSSi)0.7•H₂O] calculated C 50.52%, H 4.17%; S 3.64% found C 50.05%, H 4.27%, S 3.97%. **HR-MS (ESI)**, calcd. m/z for C₁₉H₃₆OPSSi⁺ [Cation+H₂O]⁺, C₁₈HBF₁₅⁻ [Anion⁻]: 371.1994, 512.9931; found: 371.1992, 512.9951.

The Lewis acidity of this compound was tested using FBN as probe. Solid (rac)-**2a** (30 mg, 0.035 mmol, 1.0 equiv.) was loaded into a Young-type NMR tube and dissolved into a CD₂Cl₂ solution (0.5 ml) containing FBN (4.2 mg, 0.035 mmol, 1.0 equiv.). The reagents were allowed to react for 2 hours before measuring the spectra. The low Lewis acidity of this compound was demonstrated by the following results:

¹³C{¹H} NMR (100.66 MHz, CD₂Cl₂, 298 K): δ = 165.9 [d, $^1J_{C-F}$ = 256.8 Hz].
¹⁹F{¹H} NMR (376.66 MHz, CD₂Cl₂, 298 K): δ = -102.36 [bs].
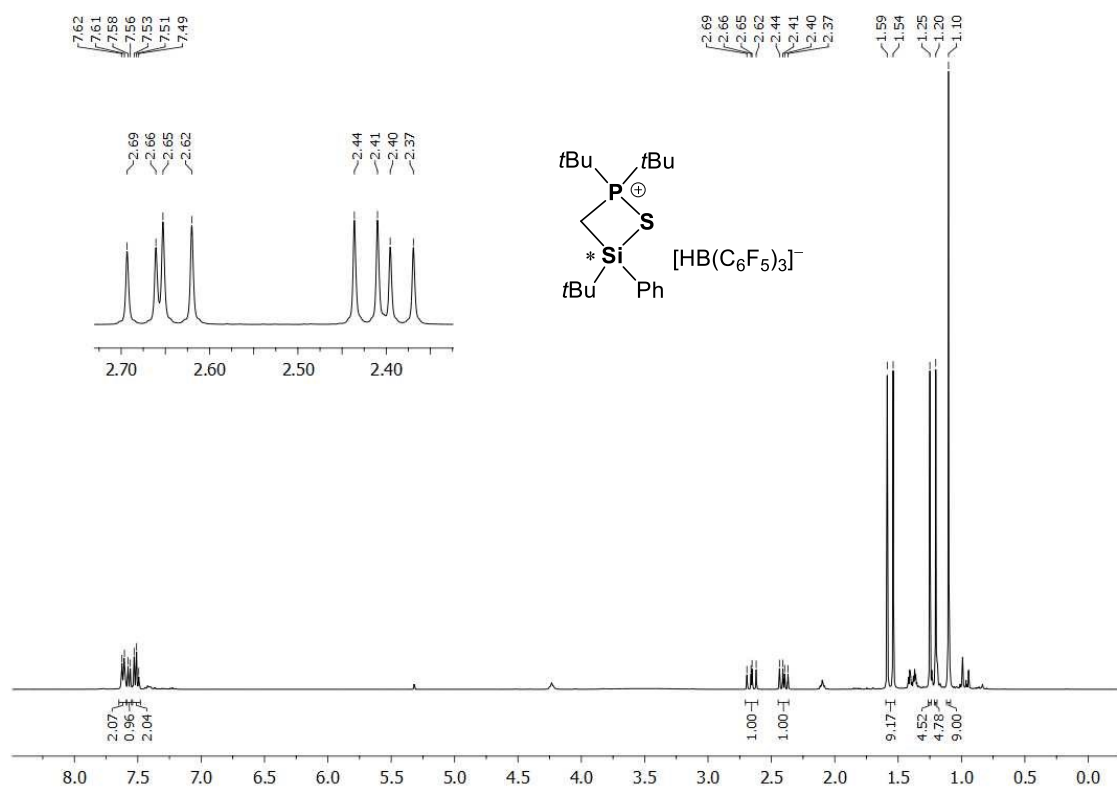
Figure S25. ^{1}H NMR (CD$_2$Cl$_2$, 298 K) of compound (*rac*)-**2a**.
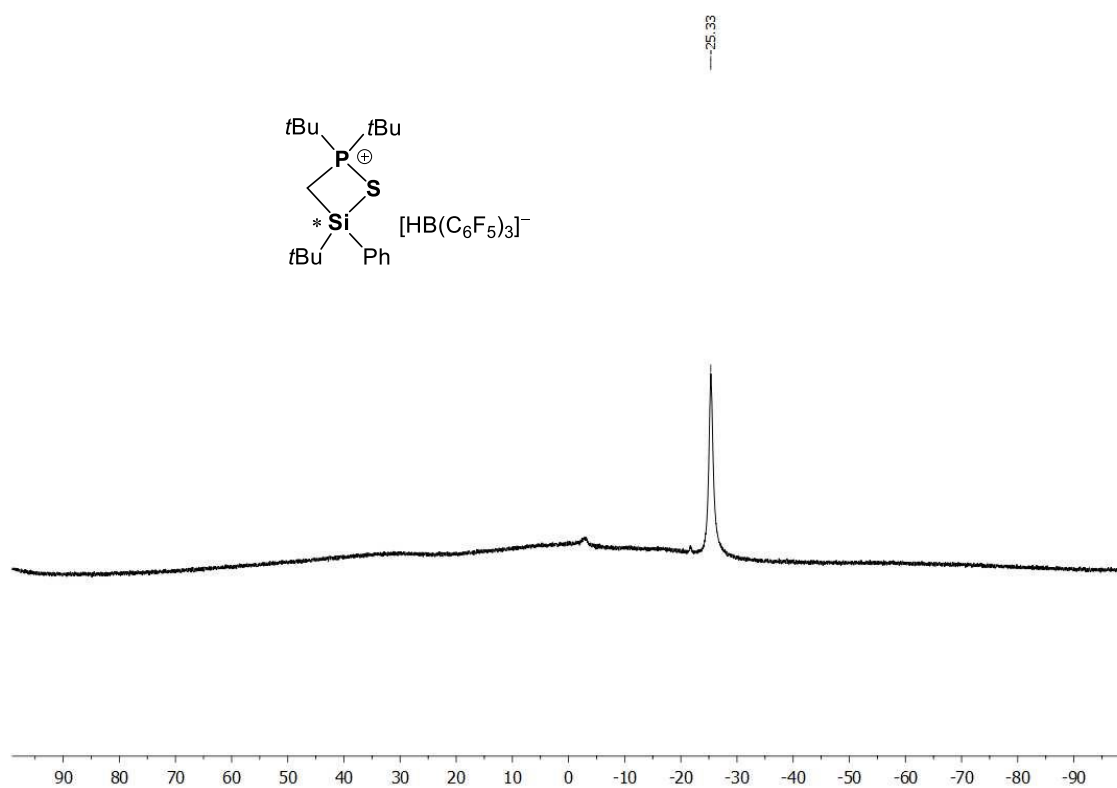
Figure S26. ^{11}B{^{1}H} NMR (CD$_2$Cl$_2$, 298 K) of compound (*rac*)-**2a**.
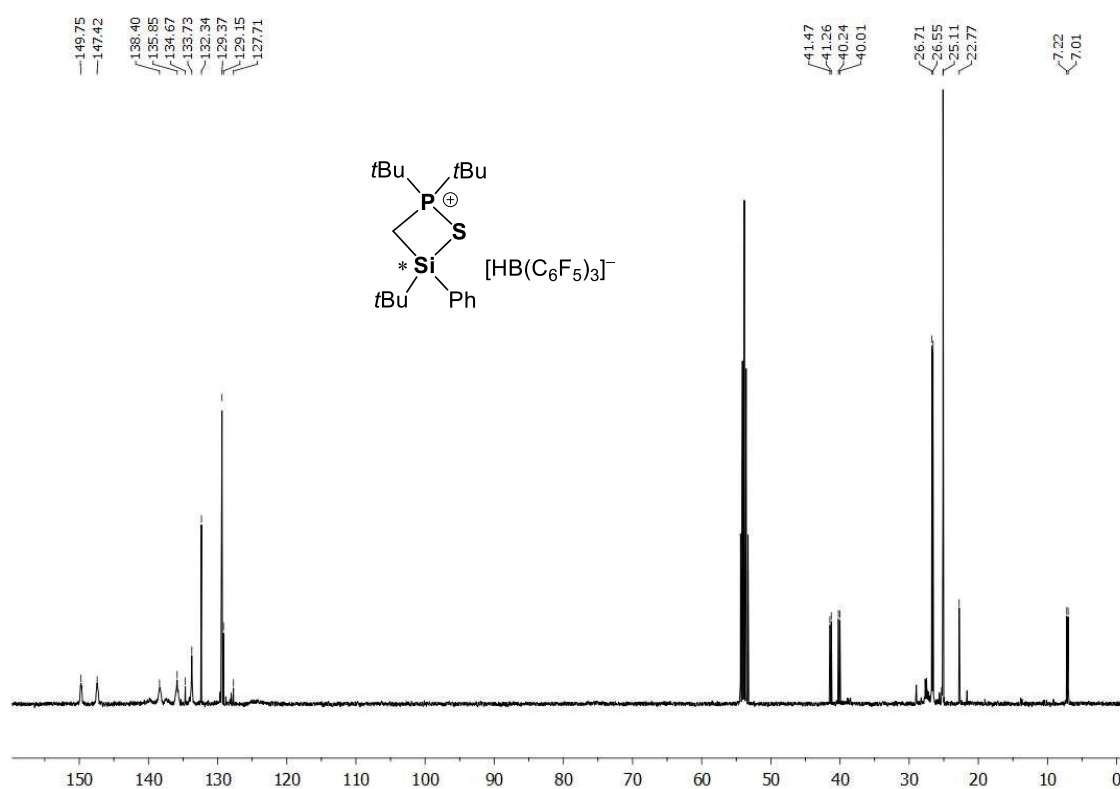
Figure S27. $^{13}C\{^1H\}$ NMR (CD$_2$Cl$_2$, 298 K) of compound (*rac*)-**2a**.
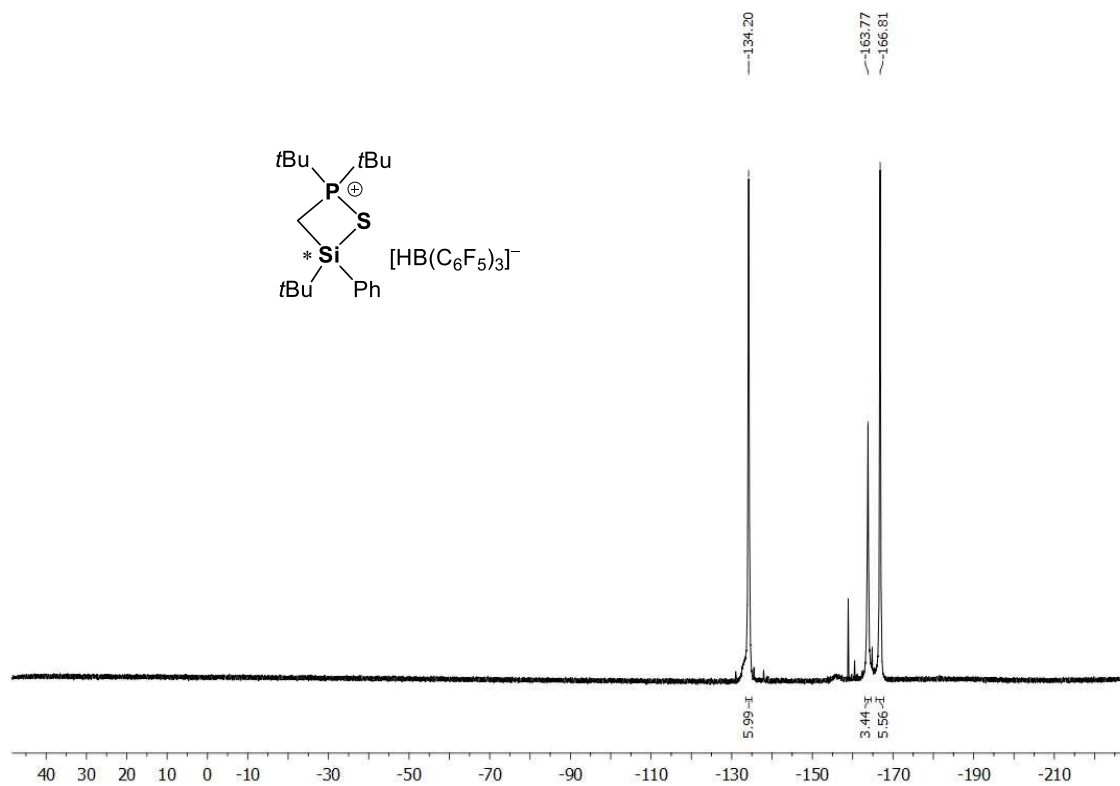
Figure S28. $^{19}F\{^1H\}$ NMR (CD$_2$Cl$_2$, 298 K) of compound (*rac*)-**2a**.
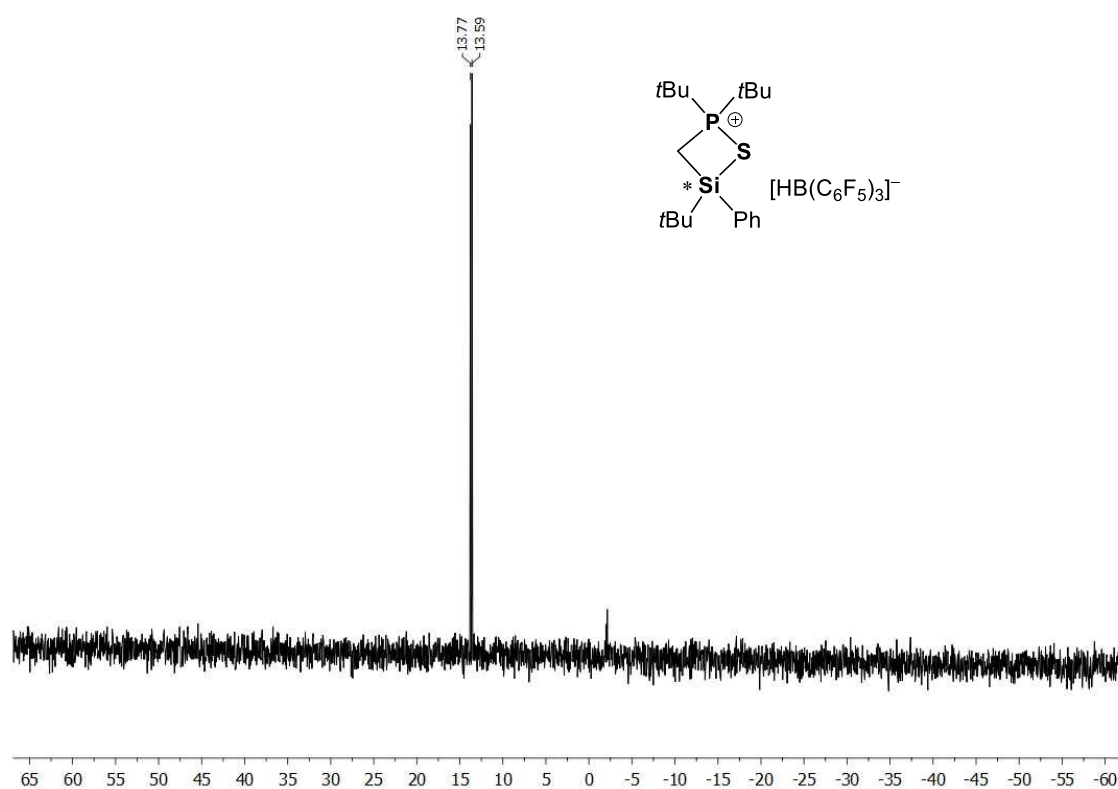
Figure S29. ^{29}Si{^{1}H} NMR (CD$_2$Cl$_2$, 298 K) of compound (*rac*)-**2a**.
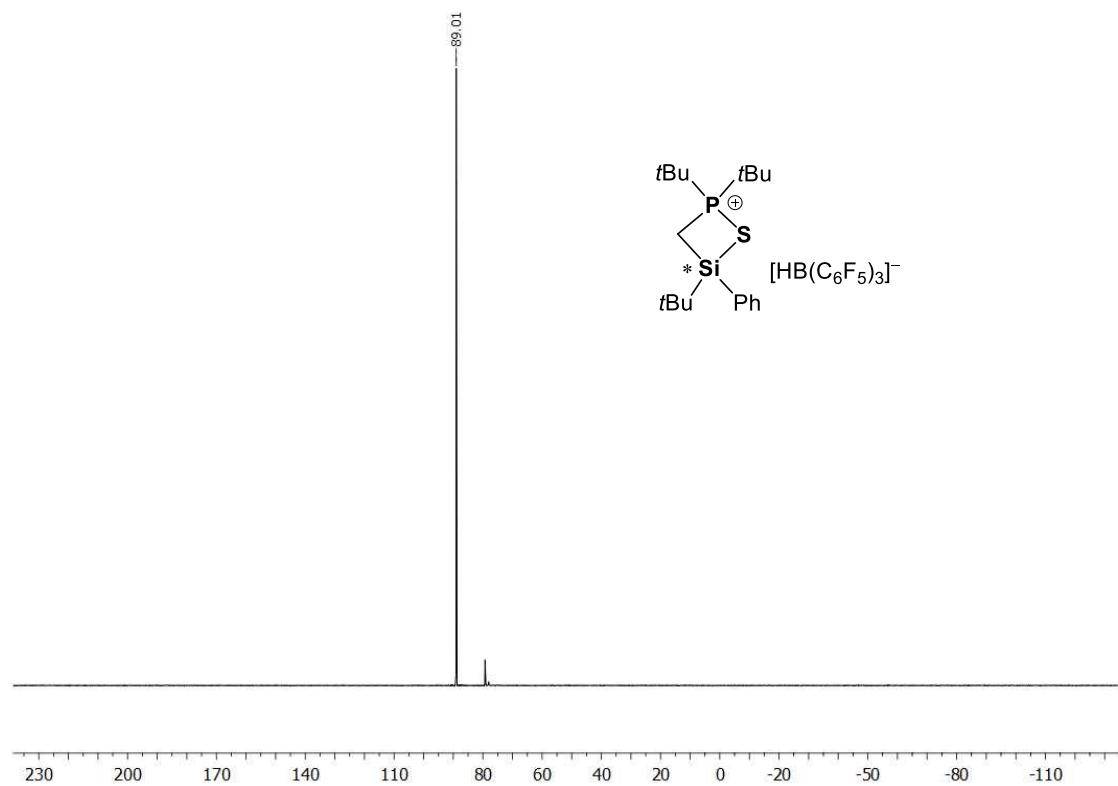
Figure S30. ^{31}P{^{1}H} NMR (CD$_2$Cl$_2$, 298 K) of compound (*rac*)-**2a**.

41

3.5.4 Synthesis of (*rac*)-[(*t*Bu)$_2$P(SH)CH$_2$Si(H)Ph*t*Bu][B(C$_6$F$_5$)$_4$] ((*rac*)-3)
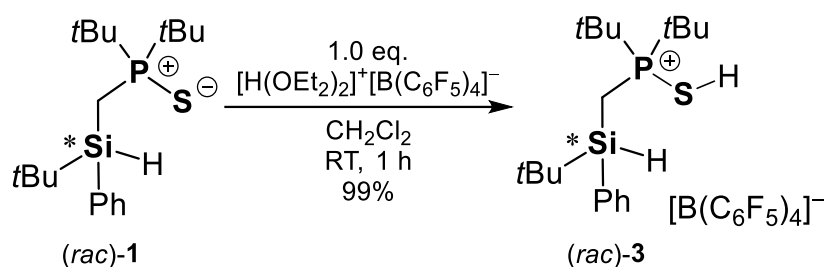
In a glovebox, an oven dried Schlenk flask was loaded with (*rac*)-**1** (171.25 mg, 0.48 mmol, 1.0 equiv.) and [H(OEt$_2$)$_2$][B(C$_6$F$_5$)$_4$] (400 mg, 0. 48 mmol, 1.0 equiv.). Dichloromethane (5 ml) was added and the solution was stirred for 20 minutes at room temperature. The solution was concentrated down to ~ 1 ml volume and compound (*rac*)-**3** precipitated while adding pentane (~10 ml) under vigorous stirring. Following, all the solids were left to sediment and the mother-liquor discarded. The remaining colourless solids were washed with pentane (2 x 5 ml), decanted and dried, affording (*rac*)-**3** (495 mg, 0.48 mmol, >99%) as a colourless solid. Crystals, suitable for single-crystal X-ray diffraction analysis were obtained by slow evaporation of a solution of compound (*rac*)-**3** in dichloromethane under inert gas.

Note: The compound was also obtained following the same procedure but using diethyl ether as solvent.

^{1}H NMR (400.32 MHz, CD$_2$Cl$_2$, 298 K): δ = 1.05 [s, 9H, SiC(C*H*$_3$)$_3$], 1.35 [d, $^3J_{\text{P-H}}$= 18.1 Hz, 9H, PC(C*H*$_3$)$_3$], 1.51 [d, $^3J_{\text{P-H}}$= 17.9 Hz, 9H, PC(C*H*$_3$)$_3$], 1.77-1.82 [m, 2H, SiC*H*$_2$P], 4.51 [m, 1H, Si*H*], 7.46-7.50 [m, 2H, *H*$_{\text{Ph}}$], 7.54-7.56 [m, 1H, *H*$_{\text{Ph}}$], 7.57-7.61 [m, 2H, *H*$_{\text{Ph}}$]. **^{11}B{^{1}H} NMR** (128.43 MHz, CD$_2$Cl$_2$, 298 K): δ = 16.9. **^{13}C{^{1}H} NMR** (100.66 MHz, CD$_2$Cl$_2$, 298 K): δ = 1.0 [d, $^1J_{\text{C-P}}$ = 28.8 Hz, SiCH$_2$P], 18.2 [d, $^3J_{\text{C-P}}$ = 5.2 Hz, SiC(CH$_3$)$_3$], 26.6 [s, SiC(CH$_3$)$_3$], 26.8 [s, PC(CH$_3$)$_3$], 27.2 [s, PC(CH$_3$)$_3$], 39.6 [d, $^1J_{\text{C-P}}$ = 10.4 Hz, PC(CH$_3$)$_3$], 39.9 [d, $^1J_{\text{C-P}}$ = 11.4 Hz, PC(CH$_3$)$_3$], 129.4 [s, *H*$_{\text{Ph}}$], 130.6 [s, *H*$_{\text{Ph}}$], 131.9 [s, *H*$_{\text{Ph}}$], 135.7 [s, *H*$_{\text{Ph}}$], 136.3 [s, *ipso*-C$_{\text{Ar-borate}}$], 136.3 [bd, $^1J_{\text{C-F}}$= 247 Hz, *meta*-C$_{\text{Ar-borate}}$], 138.7 [bd, $^1J_{\text{C-F}}$= 245.6 Hz, *para*-C$_{\text{Ar-borate}}$], 148.7 [bd, $^1J_{\text{C-F}}$= 239.9 Hz, *ortho*-C$_{\text{Ar-borate}}$]. **^{19}F{^{1}H} NMR** (376.66 MHz, CD$_2$Cl$_2$, 298 K): δ = -167.3 [bt, $^3J_{\text{F-F}}$ = 18.1, 8F, *meta*-F$_{\text{Ar-borate}}$], -163.5 [t, $^3J_{\text{F-F}}$= 20.5 Hz 4F, *para*-F$_{\text{Ar-borate}}$], -132.8 [bs, 8F, *ortho*-F$_{\text{Ar-borate}}$]. **^{29}Si{^{1}H} NMR** (79.49 MHz, CD$_2$Cl$_2$, 298 K): δ = -2.6 [d, $^2J_{\text{Si-P}}$= 9.4 Hz]. **^{31}P{^{1}H} NMR** (162.04 MHz, CD$_2$Cl$_2$, 298 K): δ = 88.6. **CHN Analysis** C$_{43}$H$_{36}$BF$_{20}$PSSi: calculated: C 49.92%, H 3.51%, S 3.10%; found: C 50.00%, H 3.92%, S 2.30%. **HR-MS (ESI)**, calcd. m/z for C$_{19}$H$_{36}$PSSi$^+$ [Cation]$^+$, C$_{24}$BF$_{20}^-$ [Anion$^-$]: 355.2044, 678.9774; found: 355.2052, 678.9848.
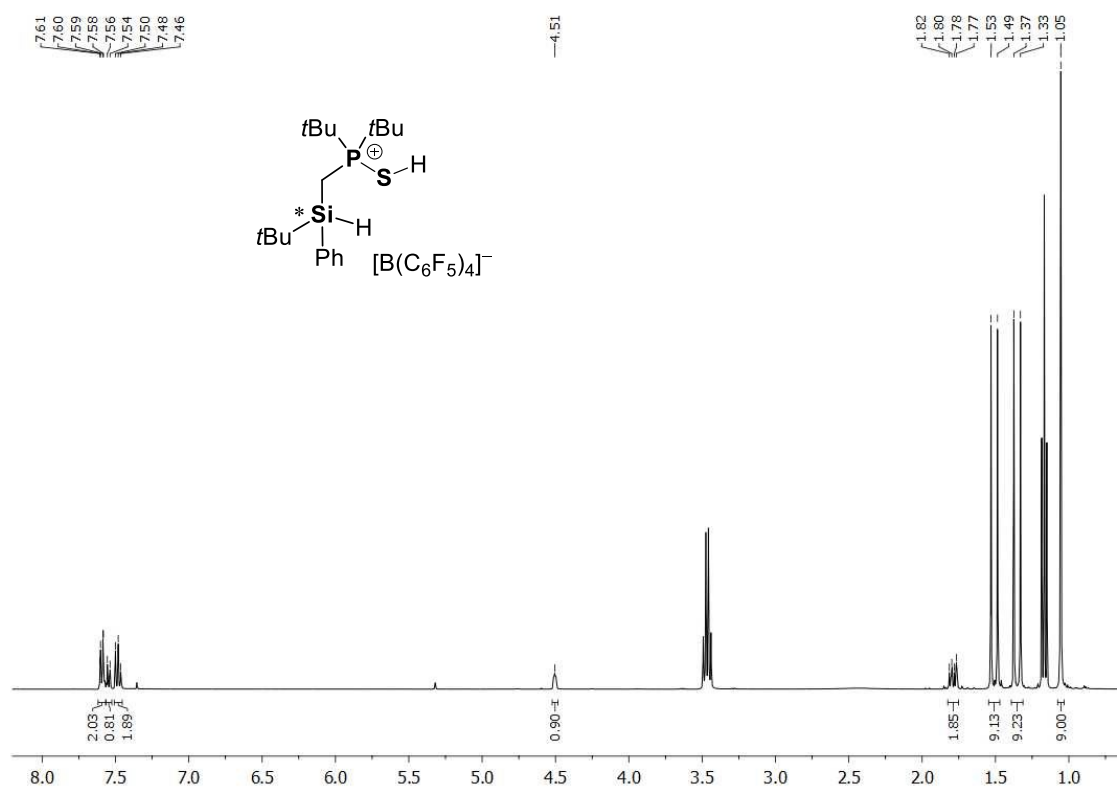
Figure S31. ^{1}H NMR (CD$_2$Cl$_2$, 298 K) of compound (*rac*)-**3.** Signals of diethyl ether are due to its use as solvent.
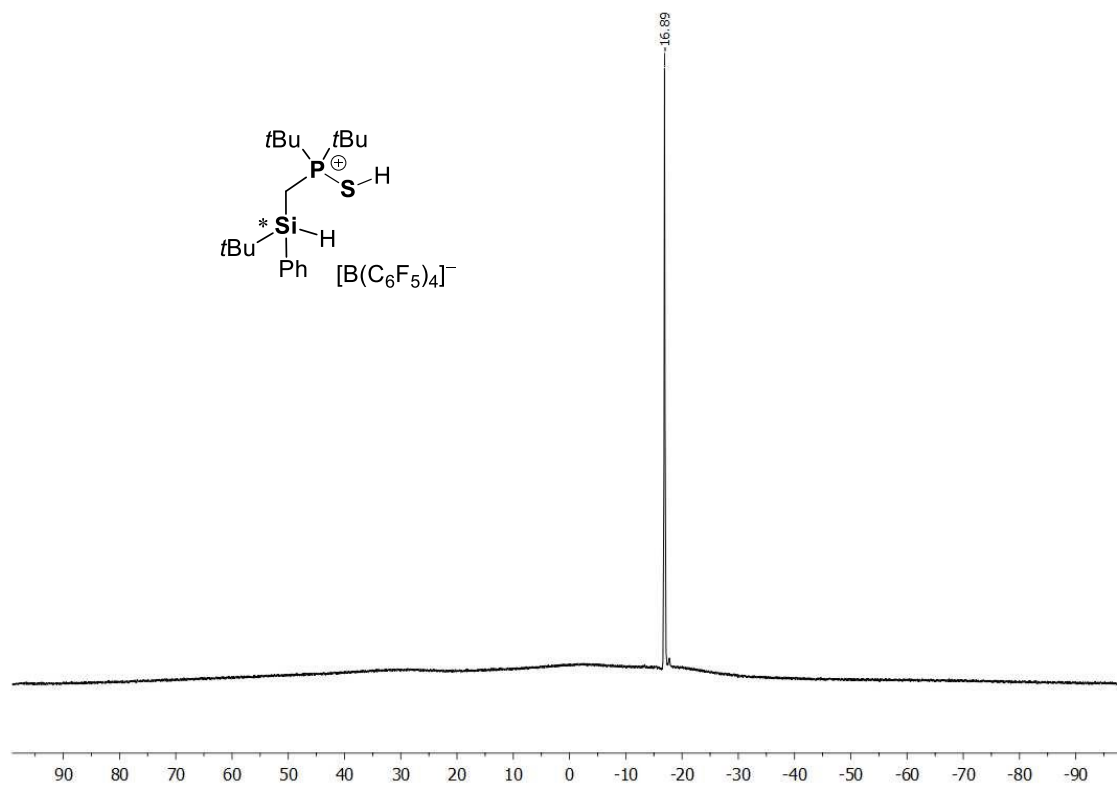
Figure S32. ^{11}B{^{1}H} NMR (CD$_2$Cl$_2$, 298 K) of compound (*rac*)-**3**.
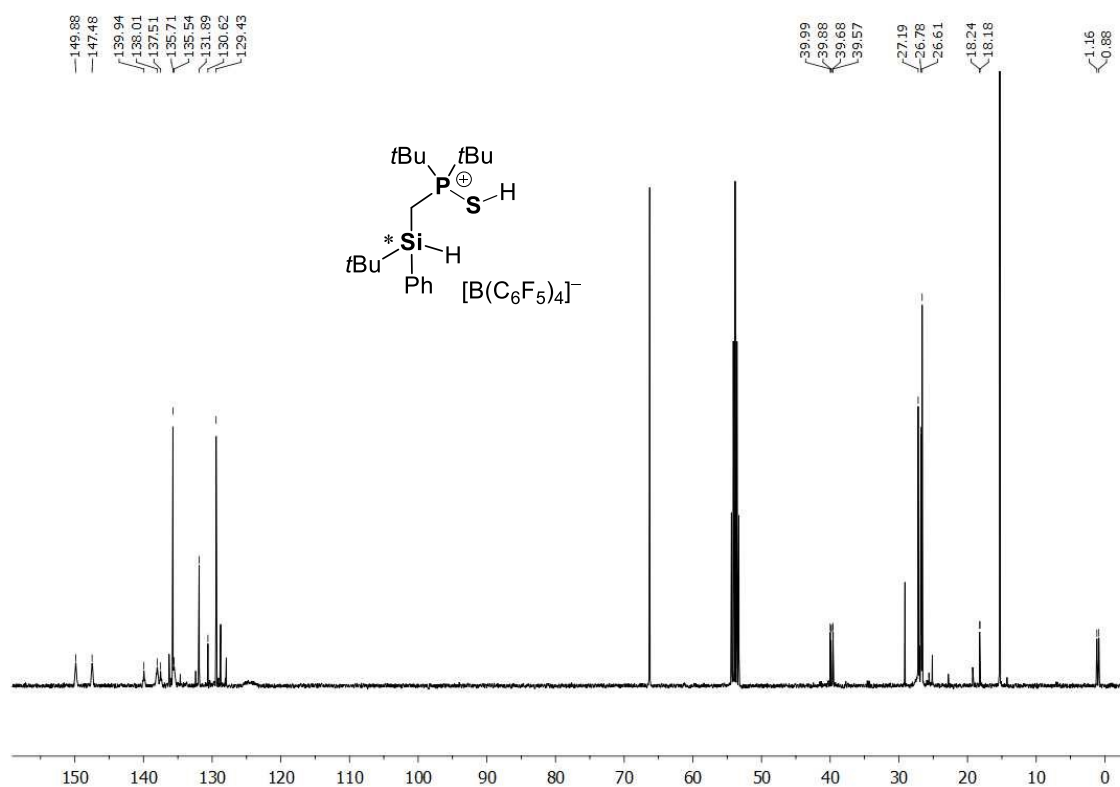
Figure S33. $^{13}C\{^1H\}$ NMR (CD$_2$Cl$_2$, 298 K) of compound (*rac*)-**3**. Signals of diethyl ether are due to its use as solvent.
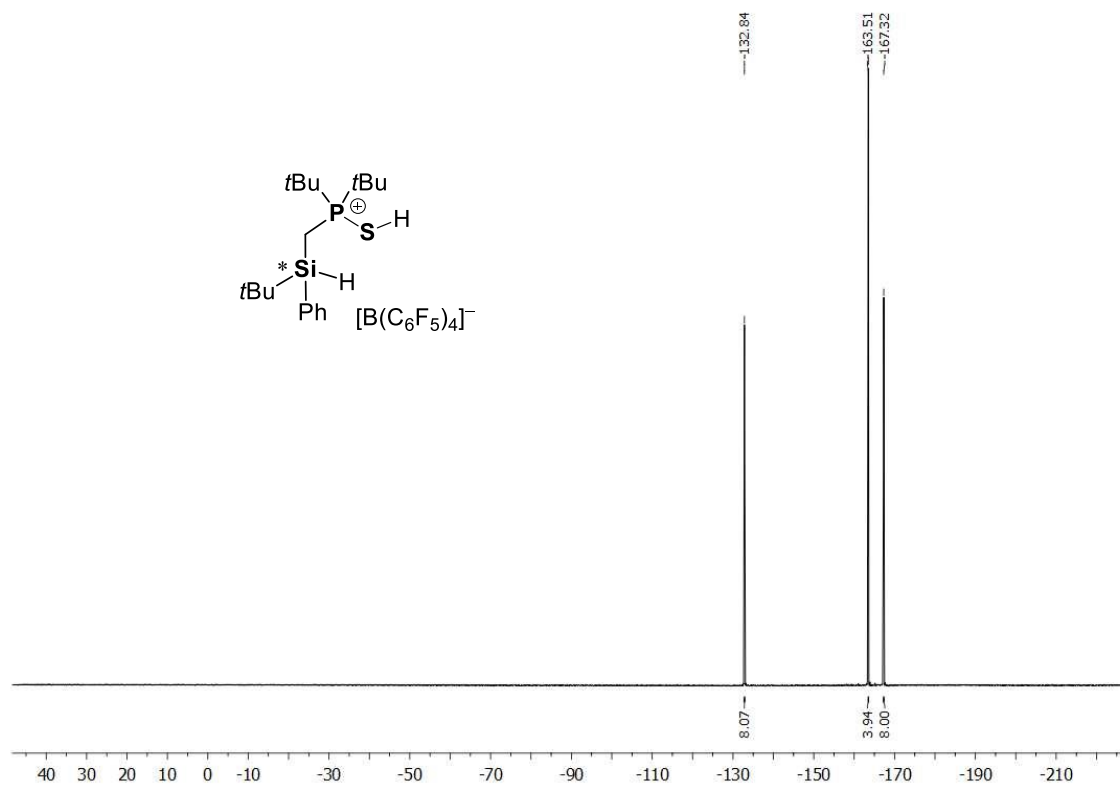
Figure S34. $^{19}F\{^1H\}$ NMR (CD$_2$Cl$_2$, 298 K) of compound (*rac*)-**3**.
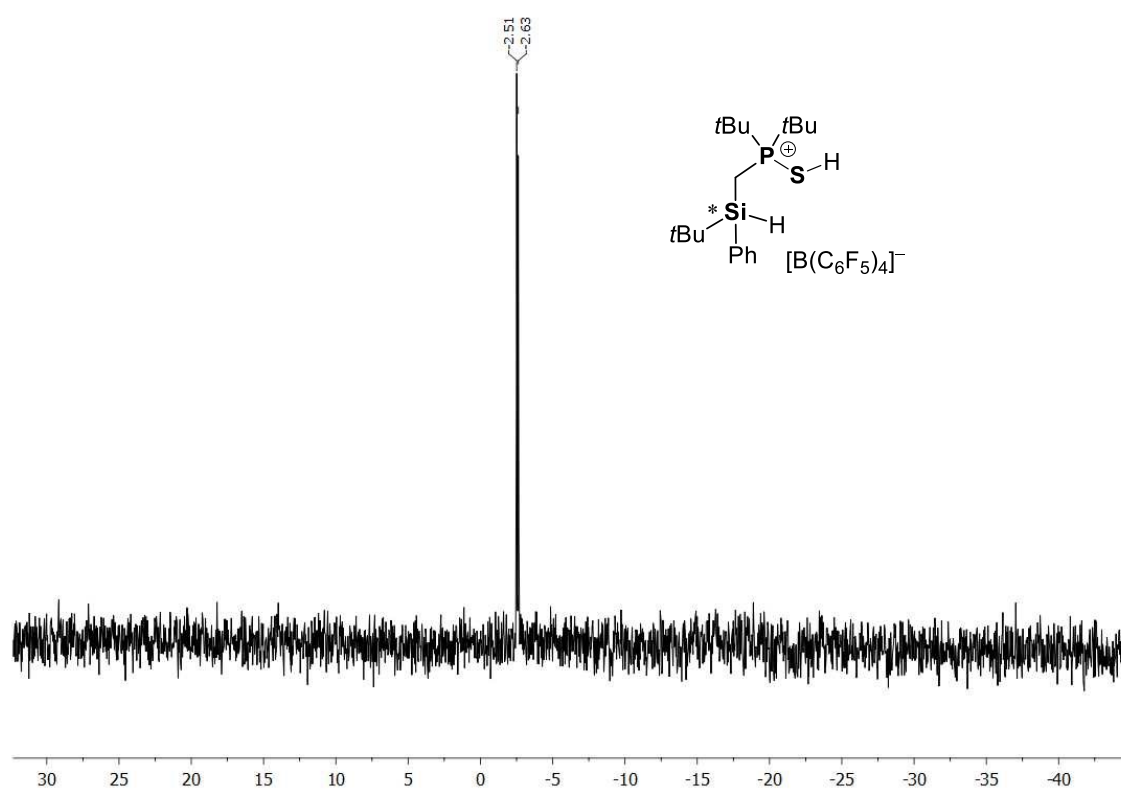
Figure S35. $^{29}Si\{^1H\}$ NMR (CD$_2$Cl$_2$, 298 K) of compound (*rac*)-**3**.
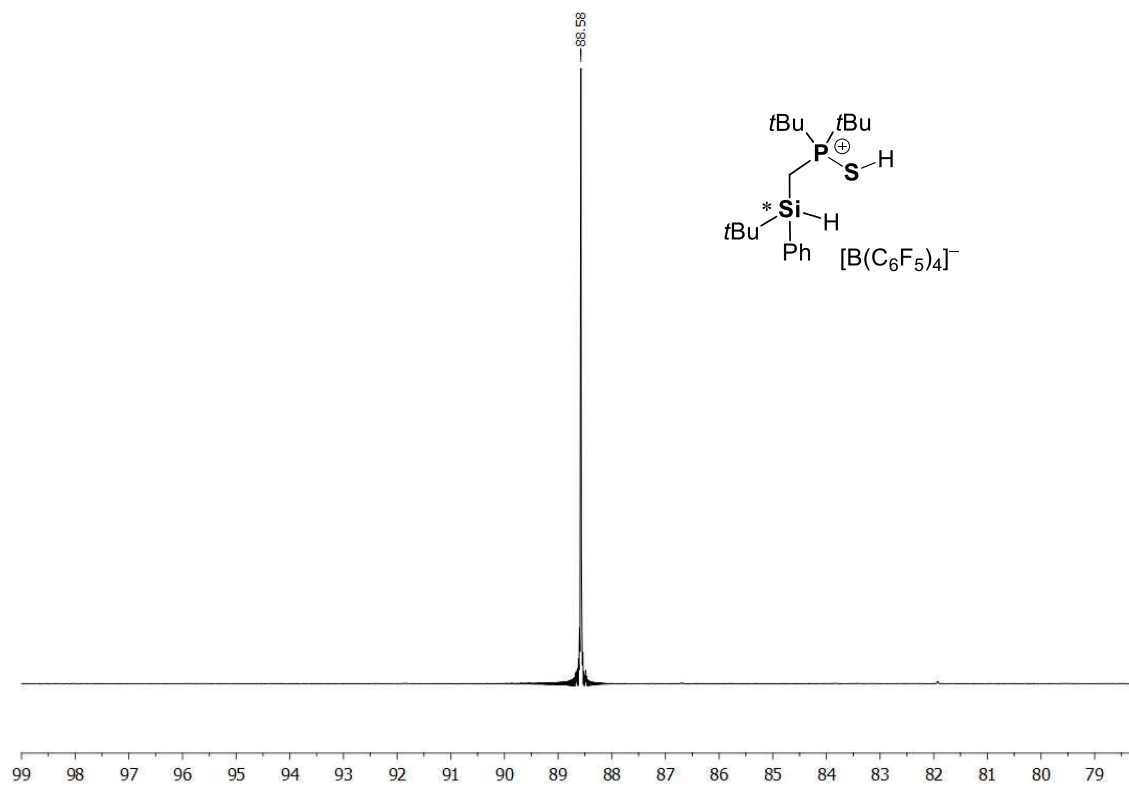
Figure S36. $^{31}P\{^1H\}$ NMR (CD$_2$Cl$_2$, 298 K) of compound (*rac*)-**3**.

45

3.5.5 Synthesis of (*rac*)-[(*t*Bu)$_2$P(S)CH$_2$SiPh*t*Bu][B(C$_6$F$_5$)$_4$] ((*rac*)-2b)
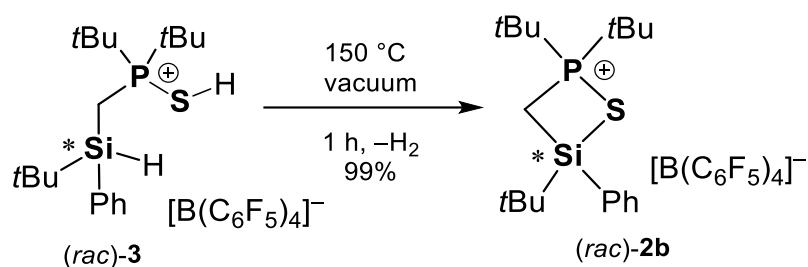
In an oven dried Schlenk flask, compound (*rac*)-**3** (495 mg, 0.48 mmol, 1.0 equiv.) was heated up to 150°C while applying vacuum. During this time, the solid melted and gently started bubbling. After one hour the bubbling ceased rendering a yellowish oil. This residue was then washed with pentane (3 x 5 ml) and dried affording pure (*rac*)-**2b** (494 mg, 0.48 mmol, >99%) as a colourless solid.

^{1}H NMR (400.30 MHz, CD$_2$Cl$_2$, 298 K): δ = 1.11 [s, 9H, SiC(CH_3)$_3$], 1.22 [d, $^3J_{P\text{-}H}$= 18.6 Hz, 9H, PC(CH_3)$_3$], 1.56 [d, $^3J_{P\text{-}H}$= 18.8 Hz, 9H, PC(CH_3)$_3$], 2.46 [ddd(ABX), J$_1$= 12.78 Hz, J$_2$= 16.10 Hz, J$_3$= 110.45 Hz, 2H, SiCH_2P], 7.51-7.54 [m, 2H, H_{Ph}], 7.57-7.61 [m, 3H, H_{Ph}]. **^{11}B{^{1}H} NMR** (128.43 MHz, CD$_2$Cl$_2$, 298 K): δ = 16.9. **^{13}C{^{1}H} NMR** (100.61 MHz, CD$_2$Cl$_2$, 298 K): δ = 7.1 [d, $^1J_{C\text{-}P}$ = 21.3 Hz, SiCH$_2$P], 22.8, 25.2 [s, SiC(CH$_3$)$_3$], 26.6 [d, $^2J_{C\text{-}P}$ = 2.3 Hz, PC(CH$_3$)$_3$], 26.8 [d, $^2J_{C\text{-}P}$ = 2.1 Hz, PC(CH_3)$_3$], 27.3, 27.7 [d, $^3J_{C\text{-}P}$ = 10.0 Hz, SiC(CH$_3$)$_3$], 40.2 [d, $^1J_{C\text{-}P}$ = 22.4, PC(CH$_3$)$_3$], 41.4 [d, $^1J_{C\text{-}P}$ = 19.9, PC(CH$_3$)$_3$], 128.7 [s, C$_{Ph}$], 129.4 [s, C$_{Ph}$], 132.4 [s, C$_{Ph}$], 133.7 [s, *ipso*-C$_{Ar\text{-}borate}$], 135.7 [s, C$_{Ph}$], 136.8 [dd, $^1J_{C\text{-}F}$ = 246.0 Hz, *meta*-C$_{Ar\text{-}borate}$], 138.7 [dd, $^1J_{C\text{-}F}$ = 243.5 Hz, *para*-C$_{Ar\text{-}borate}$], 148.6 [dd, $^1J_{C\text{-}F}$ = 242.4 Hz, *ortho*-C$_{Ar\text{-}borate}$]. **^{19}F{^{1}H} NMR** (376.66 MHz, CD$_2$Cl$_2$, 298 K): δ = -167.2 [bt, $^3J_{F\text{-}F}$ = 18.0 Hz, 8F, *meta*-F$_{Ar\text{-}borate}$], -163.4 [t, $^3J_{F\text{-}F}$= 19.9 Hz, 4F, *para*-F$_{Ar\text{-}borate}$], -132.8 [bs, 8F, *ortho*-F$_{Ar\text{-}borate}$]. **^{29}Si{^{1}H} NMR** (79.49 MHz, CD$_2$Cl$_2$, 298 K): δ = 13.6 [d, $^2J_{Si\text{-}P}$= 14.9 Hz]. **^{31}P{^{1}H} NMR** (162.04 MHz, CD$_2$Cl$_2$, 298 K): δ = 88.9. **CHN Analysis** C$_{43}$H$_{34}$BF$_{20}$PSSi: calculated: C 50.01%, H 3.32%; S 2.72% found C 49.15 %, H 3.74%, S 3.21%. **HR-MS (ESI)**, calcd. m/z for C$_{19}$H$_{36}$OPSSi$^+$ [Cation]$^+$, C$_{24}$BF$_{20}^-$ [Anion$^-$]: 371.1994, 678.9774; found: 371.1995, 678.9801.
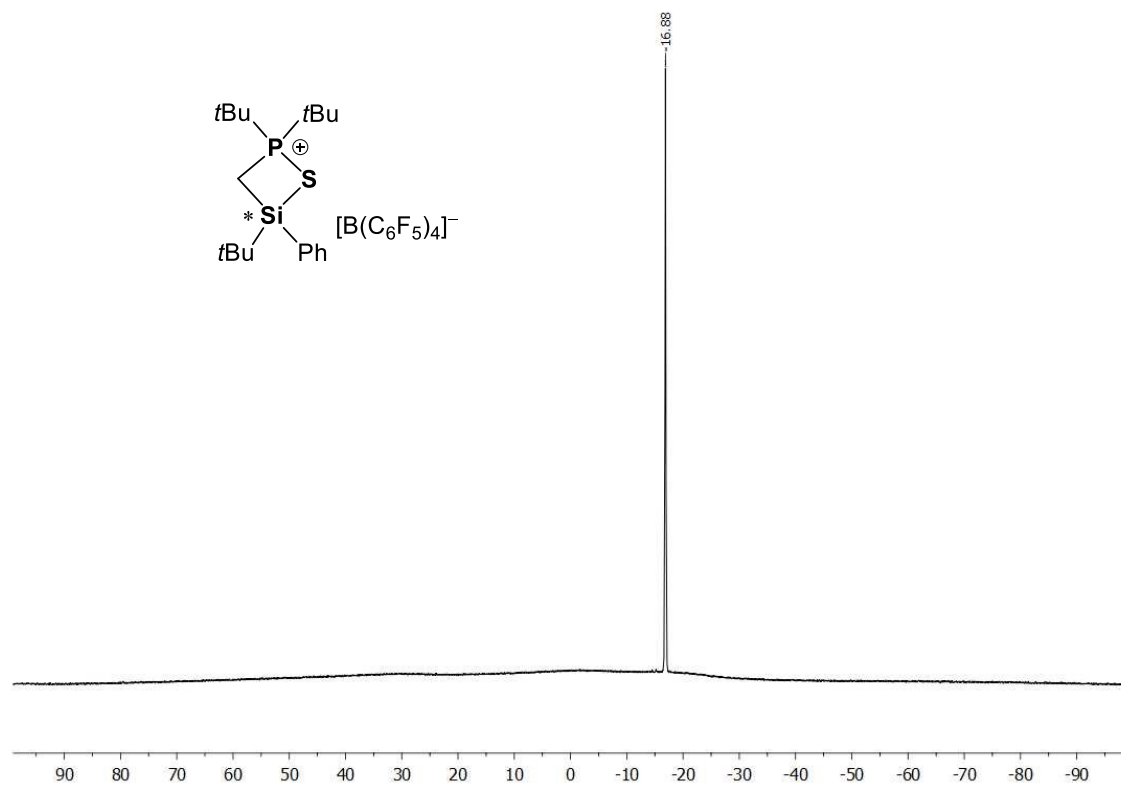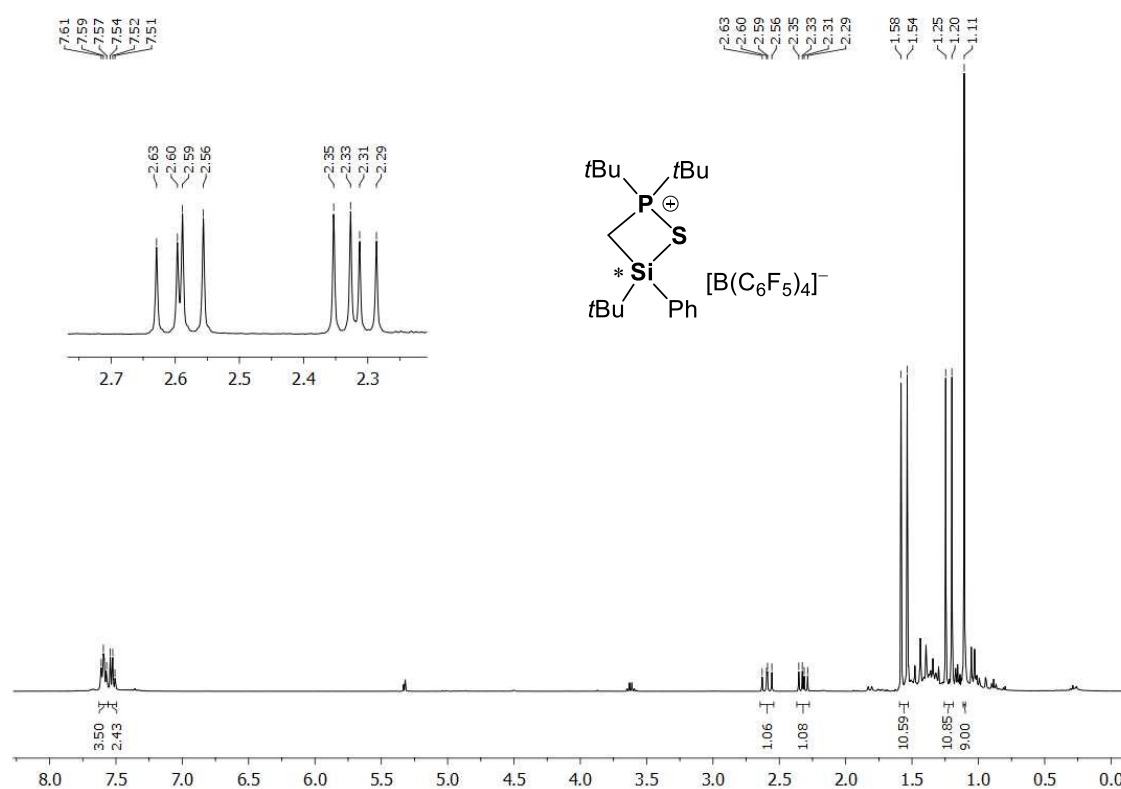
Figure S37. ^{1}H NMR (CD$_2$Cl$_2$, 298 K) of compound (*rac*)-**2b**.

Figure S38. ^{11}B{^{1}H} NMR (CD$_2$Cl$_2$, 298 K) of compound (*rac*)-**2b**.
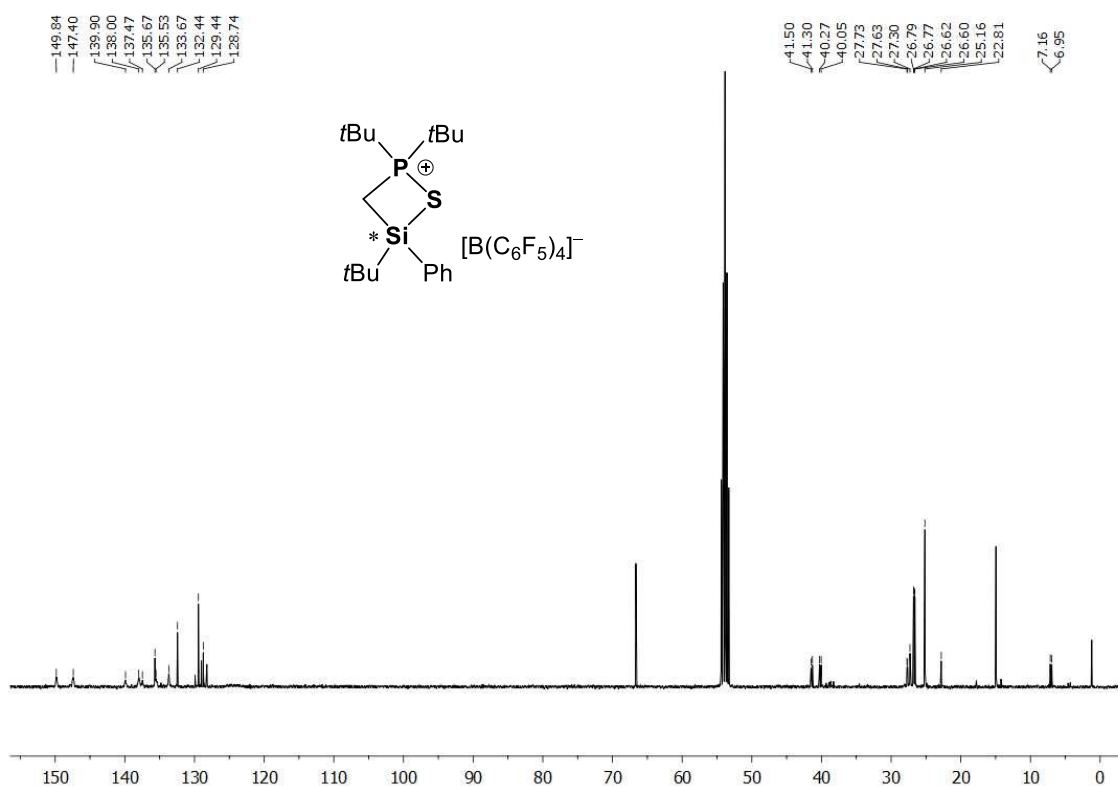
Figure S39. $^{13}C\{^1H\}$ NMR (CD$_2$Cl$_2$, 298 K) of compound (*rac*)-**2b**.
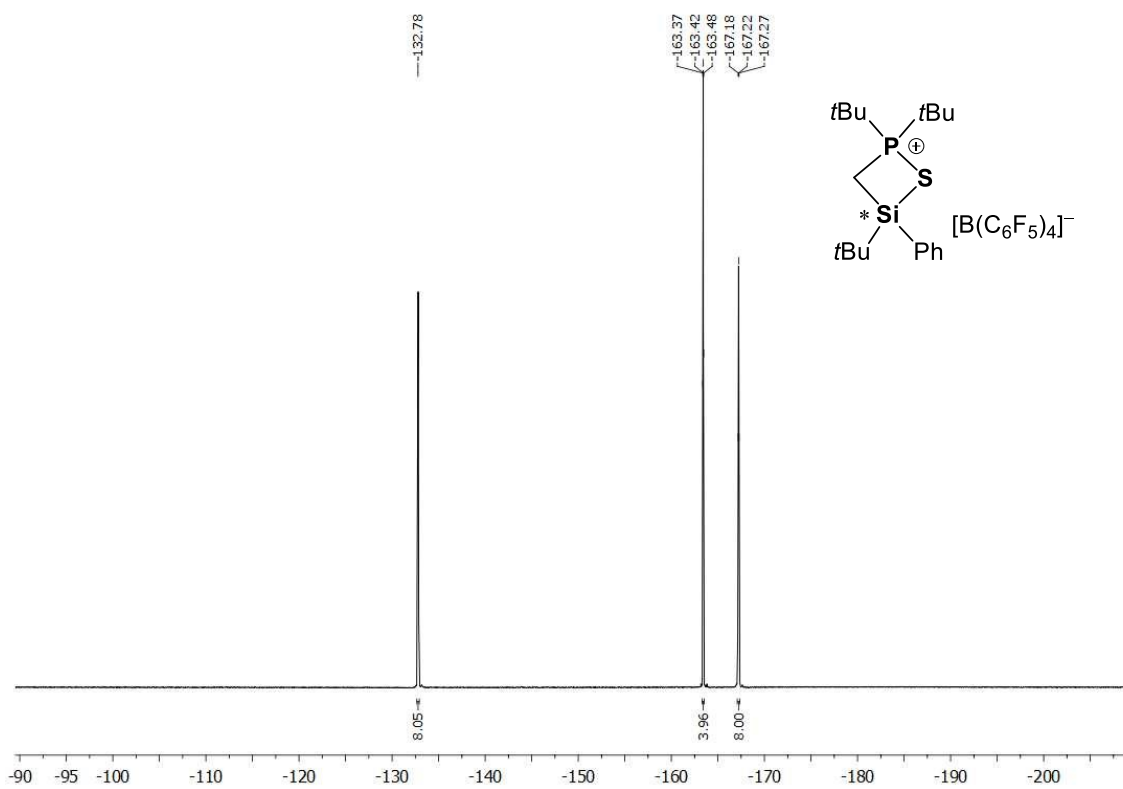
Figure S40. $^{19}F\{^1H\}$ NMR (CD$_2$Cl$_2$, 298 K) of compound (*rac*)-**2b**.
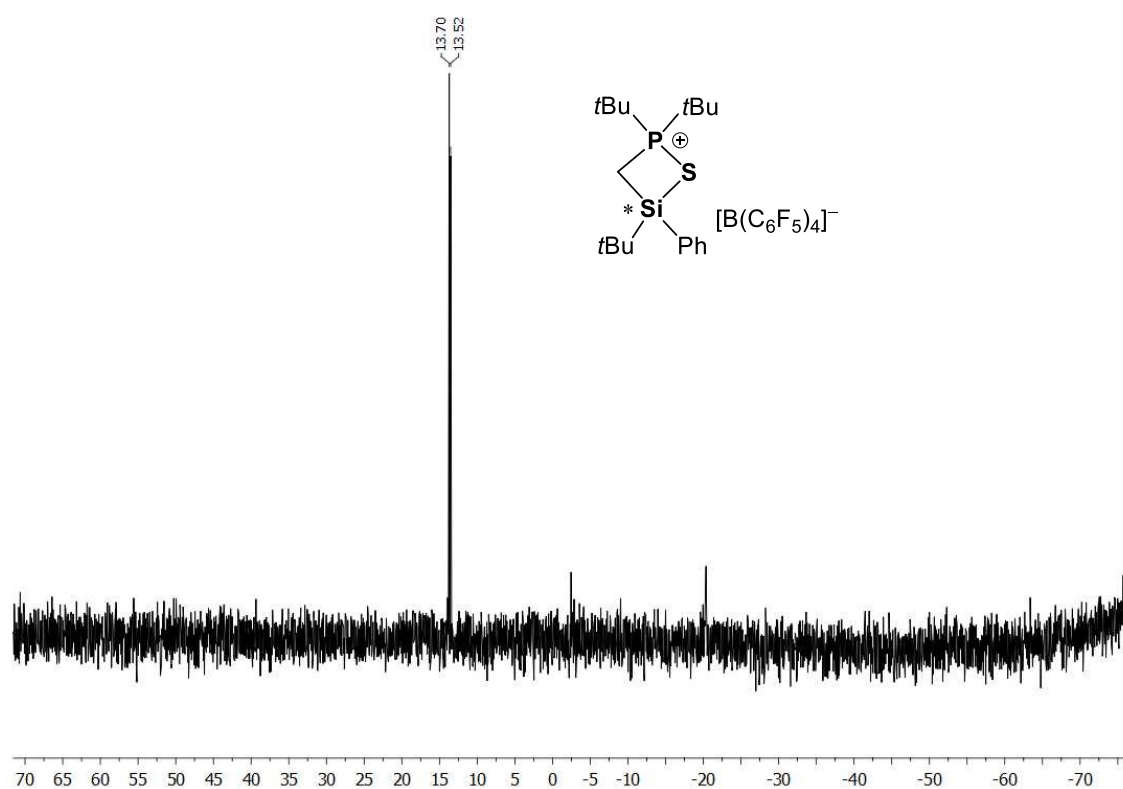
Figure S41. $^{29}Si\{^1H\}$ NMR (CD$_2$Cl$_2$, 298 K) of compound (*rac*)-**2b**.
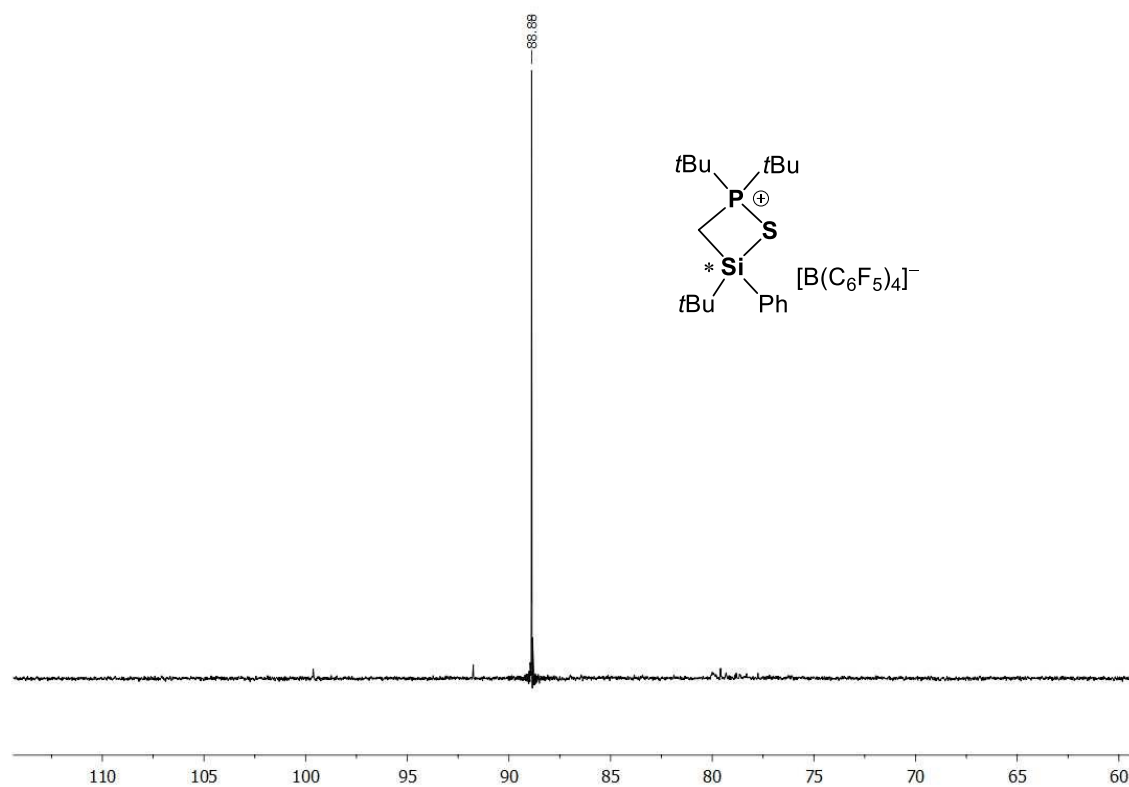
Figure S42. $^{31}P\{^1H\}$ NMR (CD$_2$Cl$_2$, 298 K) of compound (*rac*)-**2b**.

49

3.5.6   Synthesis of tBu_2PCH_2Li
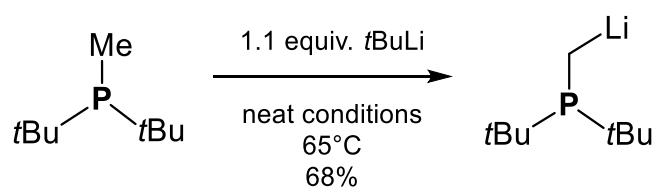
tBu_2PCH_2Li was synthesized according to a slightly modified procedure by Lerner *et al.*[3] In a glove-box, a Schlenk flask was loaded with pure di-*tert*-butylmethylphosphine (2.0 g, 12.5 mmol, 1.0 equiv.). After connecting the flask to a Schlenk line, *tert*-butyllithium (7.3 ml of a 1.9 M solution in pentane, 13.8 mmol, 1.1 equiv.) was added carefully. The resulting clear solution was stirred for 15 min at room temperature. Afterwards, a distillation bridge with a receiving Schlenk flask was con-nected and the Schlenk containing the mixture was gradually heated up to 65°C while gently stirring. The system was allowed to react under these conditions for 16 h during which the solvent was slowly distilled off and the oily residue turned into a pale-yellow solid. The distillation bridge with the receiving Schlenk flask was removed while flowing nitrogen from both ends to prevent possible flames. The solid was washed with dry pentane (3 x 5 ml) and carefully dried in vacuum giving pure tBu_2PCH_2Li as a white solid (1.41 g, 8.5 mmol, 68%). Spectroscopic data were in accordance with those reported in the literature.[3]

3.5.7 Synthesis of (*rac*)-(*t*Bu)₂PCH₂Si(H)Ph*t*Bu
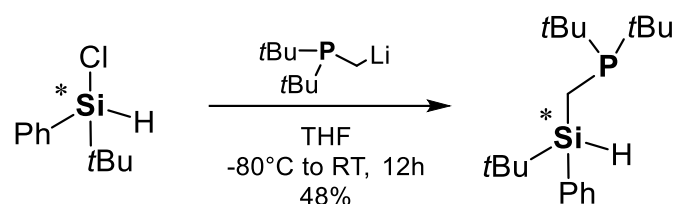
In an oven dried Schlenk flask, to a cold suspension (-80°C) of ((di-*tert*-butylphosphaneyl)methyl)lithium (1.01 g, 6.1 mmol, 1.0 equiv.) in THF (10 ml), *tert*-butylchloro(phenyl) silane (1.21 g, 6.1 mmol, 1.0 equiv.) was added *via* syringe. The mixture was stirred overnight without further cooling. The solvent was replaced with pentane. The salts were removed *via* suction filtration and washed three times with pentane. The crude mixture was purified *via* Kugelrohr distillation (85°C oven temperature, $1*10^{-3}$ mbar) affording the desired product as a colourless oil (0.935 g, 2.90 mmol, 48%).

¹H NMR (400.30 MHz, CD$_2$Cl$_2$, 298 K): δ =0.97 [s, 9H, SiC(C*H*$_3$)$_3$], 1.02 [d, $^3J_{\text{P-H}}$= 10.7 Hz, 9H, PC(C*H*$_3$)$_3$], 1.14 [d, $^3J_{\text{P-H}}$= 10.7 Hz, 9H, PC(C*H*$_3$)$_3$], 4.22 [m, 1H, Si*H*], 7.32-7.40 [m, 3H, *H*$_{ar}$], 7.55-7.57 [m, 2H, *H*$_{ar}$]. **¹³C{¹H} NMR** (100.66 MHz, CD$_2$Cl$_2$, 298 K): δ = -0.8 [d, $^1J_{\text{C-P}}$= 42.9 Hz, SiCH$_2$P], 18.1 [d, $^3J_{\text{C-P}}$= 6 Hz, Si*C*(CH$_3$)$_3$], 27.4 [s, SiC(*C*H$_3$)$_3$], 29.6 [d, $^2J_{\text{C-P}}$= 14.1 Hz, PC(*C*H$_3$)$_3$], 29.8 [d, $^2J_{\text{C-P}}$= 13.9 Hz, PC(*C*H$_3$)$_3$], 32.0 [d, $^1J_{\text{C-P}}$= 25.3 Hz, P*C*(CH$_3$)$_3$], 32.3 [d, $^3J_{\text{C-P}}$= 24.5 Hz, P*C*(CH$_3$)$_3$], 127.93 135.2 [s, C$_{meta}$], 129.61 [s, C$_{para}$], 135.2 [d, $^3J_{\text{C-P}}$= 2.7 Hz, C$_{ipso}$], 136.0 [s, C$_{ortho}$]. **²⁹Si{¹H} NMR** (79.49 MHz, CD$_2$Cl$_2$, 298 K): δ = 4.8 [d, $^2J_{\text{Si-P}}$= 22.5 Hz]. **³¹P{¹H} NMR** (162.04 MHz, CD$_2$Cl$_2$, 298 K): δ = 21.7. **CHN Analysis:** C$_{19}$H$_{35}$PSi: calculated: C 69.09, H 10.55; found C 70.75, H 10.94 [C$_{19}$H$_{35}$PSi(CH$_2$Cl$_2$)$_{0.125}$]. **HR-MS (ESI)**, calcd. m/z for C$_{19}$H$_{36}$PSi$^+$ [M+H]$^+$: 323.23; found: 323.2308.
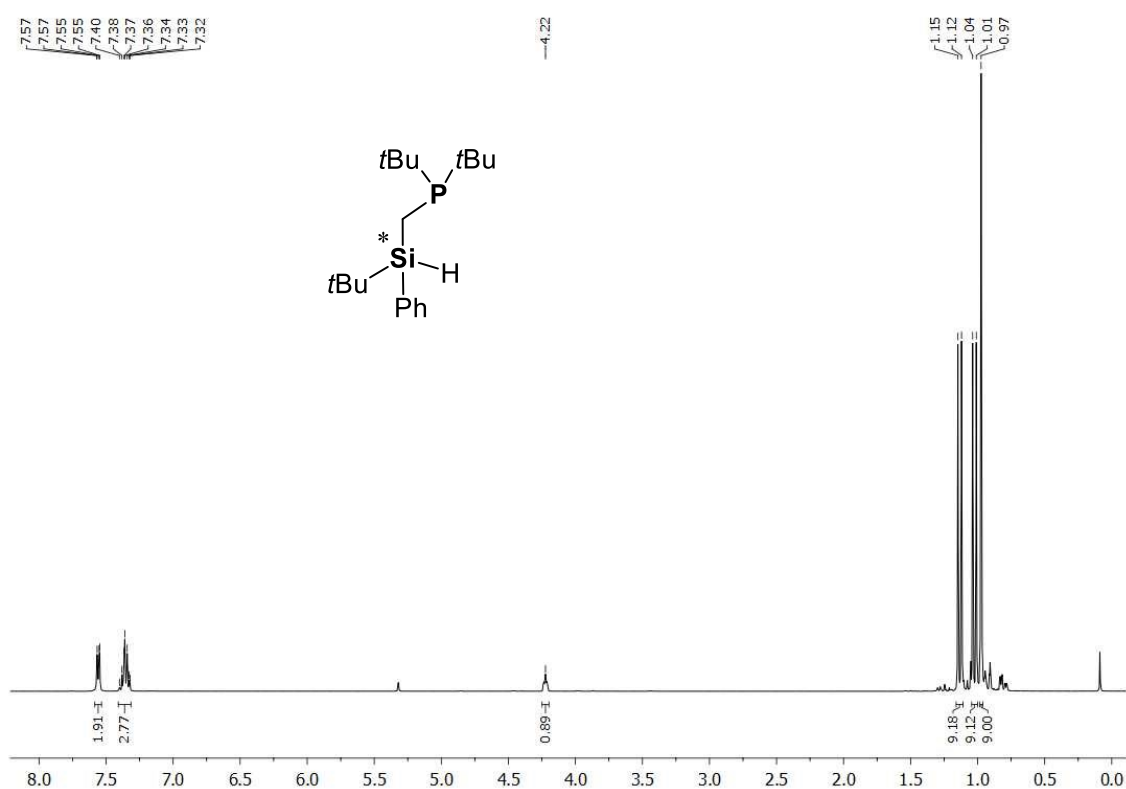
Figure S43. ^{1}H NMR spectrum (CD$_2$Cl$_2$, 298 K) of (*rac*)-(tBu)$_2$PCH$_2$Si(H)PhtBu.
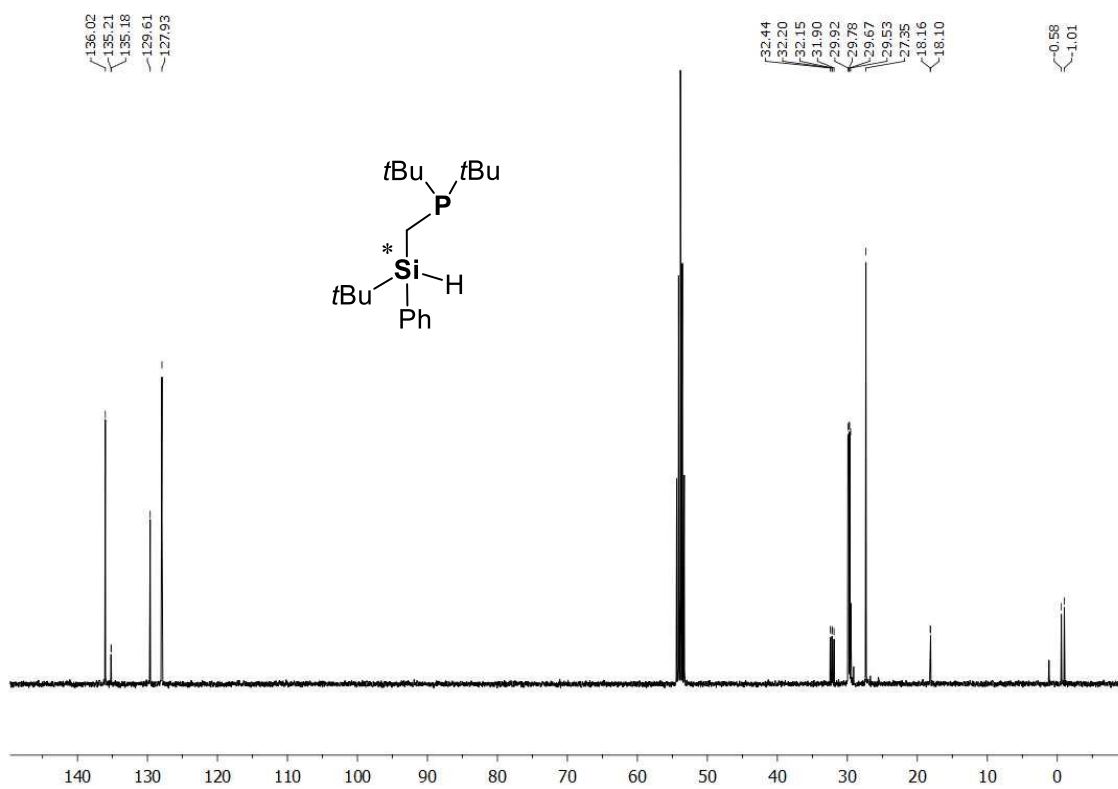
Figure S44. ^{13}C{^{1}H} NMR spectrum (CD$_2$Cl$_2$, 298 K) of (*rac*)-(tBu)$_2$PCH$_2$Si(H)PhtBu.
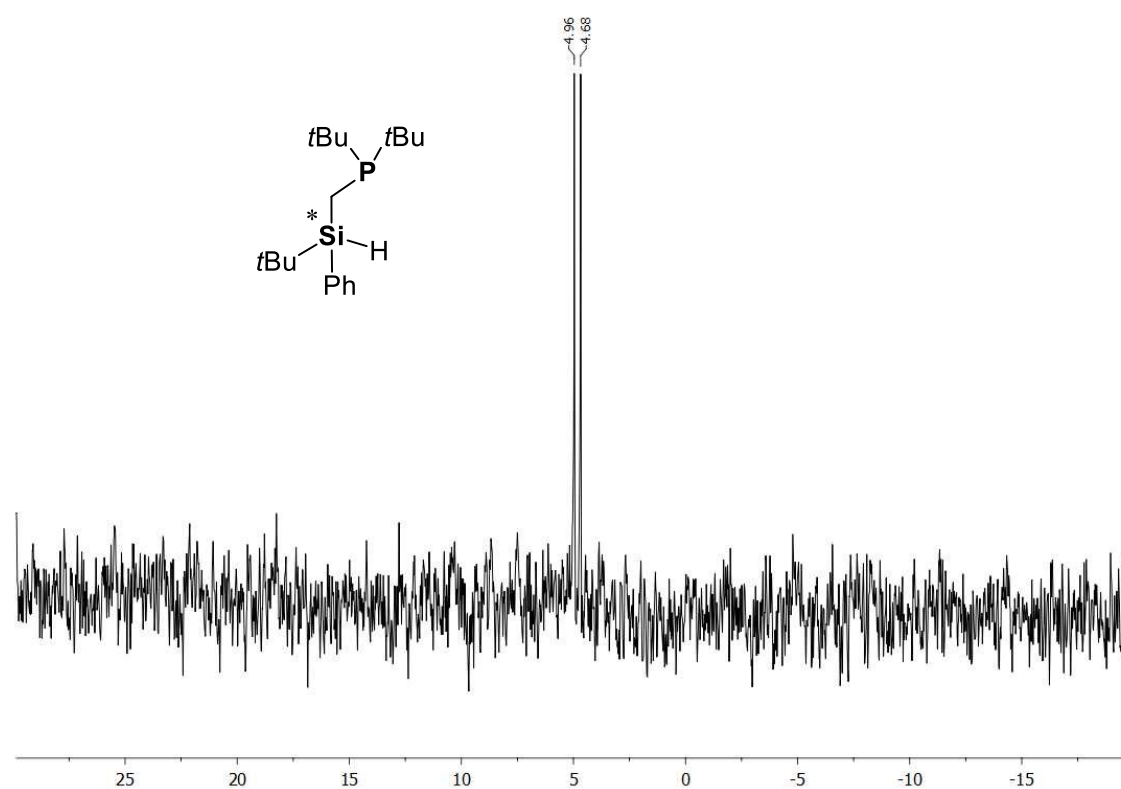
Figure S45. $^{29}Si\{^1H\}$ NMR spectrum (CD$_2$Cl$_2$, 298 K) of (*rac*)-(*t*Bu)$_2$PCH$_2$Si(H)Ph*t*Bu.
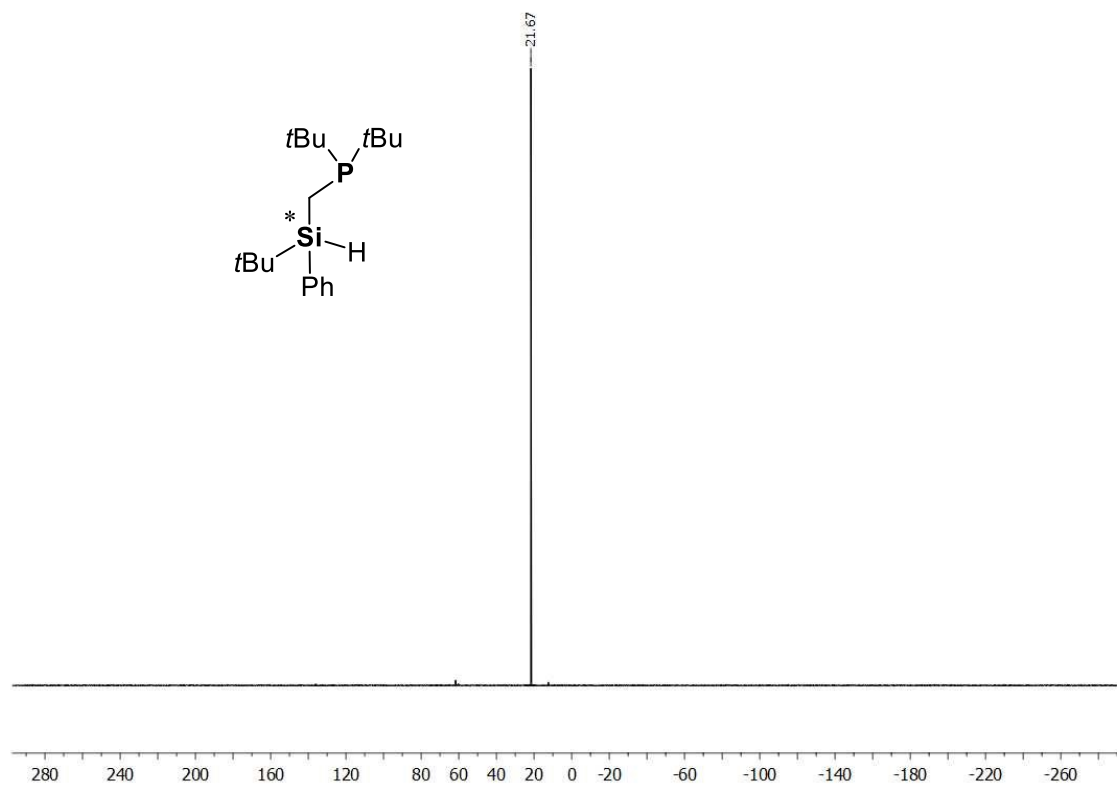
Figure S46. $^{31}P\{^1H\}$- NMR spectrum (CD$_2$Cl$_2$, 298 K) of (*rac*)-(*t*Bu)$_2$PCH$_2$Si(H)Ph*t*Bu.

3.5.8 Synthesis of (*rac*)-(*t*Bu)₂P(Se)CH₂Si(H)Ph*t*Bu ((*rac*)-1-Se)

(*rac*)-**1-Se**
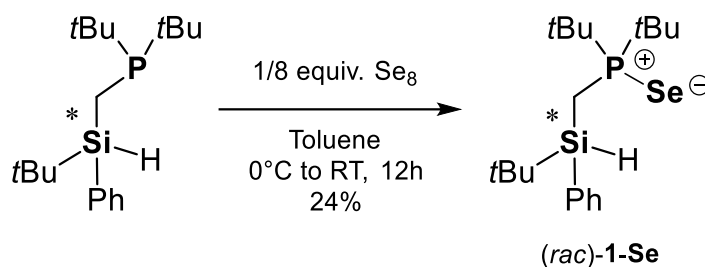
In an oven dried Schlenk flask, red selenium (90 mg, 1.1 mmol, 1.0 equiv.) was suspended in toluene (5 ml) and cooled down to 0°C. Afterwards, di-*tert*-butyl((*tert*-butyl(phenyl)silyl)methyl)phosphane (358.8 mg, 1.1 mmol, 1.0 equiv.) was added *via* syringe and the suspension was stirred without further cooling for 12 hours. The volatiles were removed in vacuum and the residue was extracted with pentane (3x5 ml). Drying this solution afforded a white solid which was purified *via* crystallization from cold pentane to give the desired silane (*rac*)-**1-Se** (108 mg, 0.27 mmol, 24%). The crystals proved suitable for X-ray diffraction.

¹H NMR (400.30 MHz, CD₂Cl₂, 298 K): δ =0.96 [s, 9H, SiC(CH_3)₃], 1.21 [d, $^3J_{P-H}$= 15.4 Hz, 9H, PC(CH_3)₃], 1.39 [d, $^3J_{P-H}$= 15.1 Hz, 9H, PC(CH_3)₃], 1.68 [ddd(ABX), J_1= 4.4 Hz, J_2= 14.2 Hz, J_3= 54.1 Hz, 2H, SiCH_2P], 4.56 [m with satellites, $^3J_{H-P}$= 3.9 Hz, $^4J_{H-Se}$= 104.5 Hz, 1H, SiH], 7.33-7.42 [m, 3H, H_{ar}], 7.56-7.58 [m, 2H, H_{ar}]. **¹³C{¹H} NMR** (100.66 MHz, CD₂Cl₂, 298 K): δ = 4.2 [d, $^1J_{C-P}$= 26.3 Hz, SiCH₂P], 17.8 [d, $^3J_{C-P}$= 4.5 Hz, SiC(CH₃)₃], 27.4 [s, SiC(CH₃)₃], 28.0 [dd, $^2J_{C-P}$= 1.8 Hz, $^2J_{C-P}$= 5.8 Hz, PC(CH₃)₃], 37.8 [d, $^1J_{C-P}$= 34.1 Hz, PC(CH₃)₃], 38.5 [d, $^3J_{C-P}$= 34.1 Hz, PC(CH₃)₃], 128.1 [s, C$_{Ar}$] 129.8 [s, C$_{Ar}$], 134.8 [s, C$_{Ar}$], 135.8 [d, C$_{Ar}$]. **²⁹Si{¹H} NMR** (79.49 MHz, CD₂Cl₂, 298 K): δ = -1.7 [d, $^2J_{Si-P}$= 6.6 Hz]. **³¹P{¹H} NMR** (162.04 MHz, CD₂Cl₂, 298 K): δ = 74.2 [s with satellites, $^1J_{P-Se}$= 348.5 Hz]. **⁷⁷Se{¹H} NMR** (76.31 MHz, CD₂Cl₂, 298 K): δ = -388.3 [d, $^1J_{Se-P}$ = 695.7 Hz]. **CHN Analysis:** C₁₉H₃₅PSeSi: calculated: C 56.84%, H 8.79%; found C 56.39%, H 8.35%. **HR-MS (ESI)**, calcd. m/z for C₁₉H₃₆PSeSi⁺ [M+H]⁺: 403.1489; found: 403.1492.
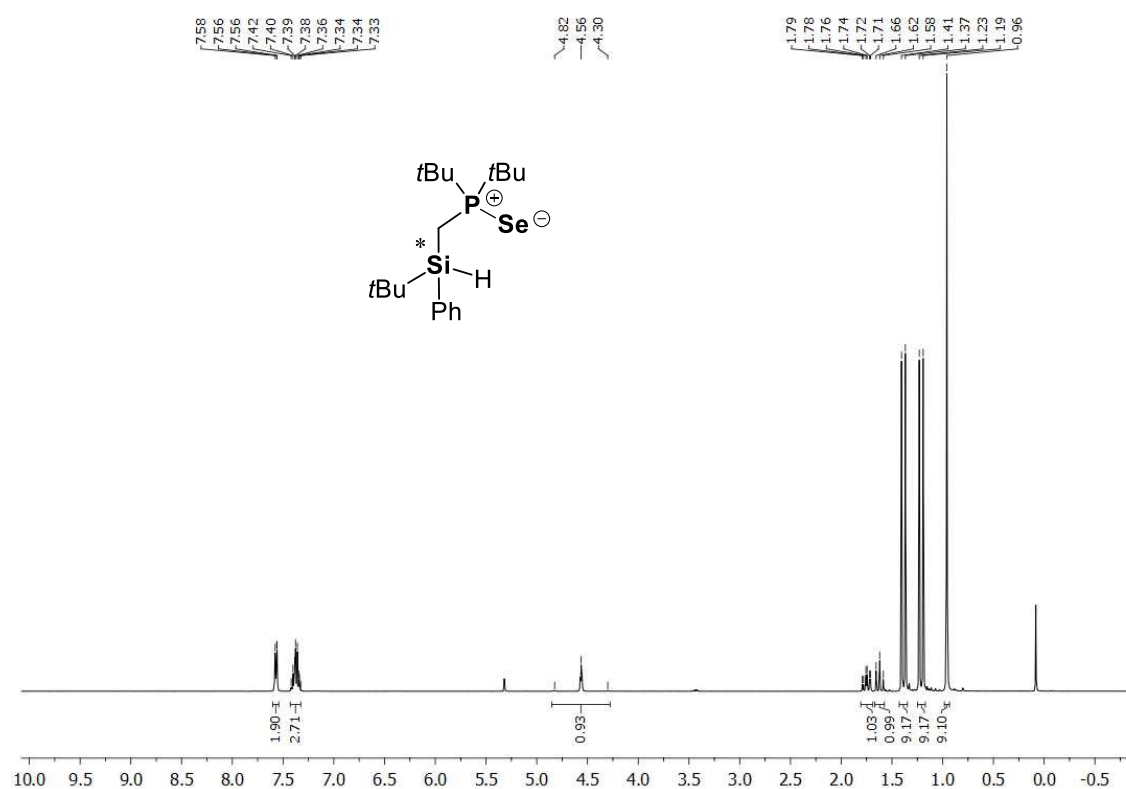
Figure S47. ^{1}H- NMR spectrum (CD$_2$Cl$_2$, 298 K) of compound (*rac*)-**1-Se**.
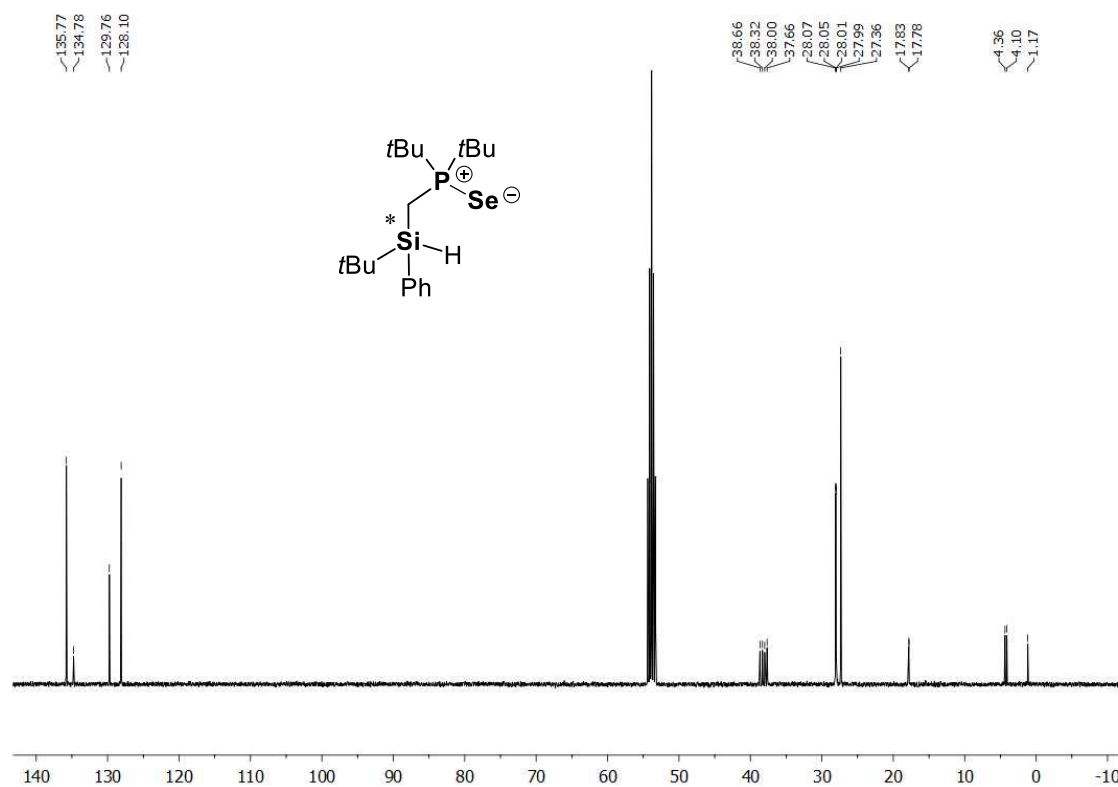
Figure S48. ^{13}C{^{1}H}- NMR spectrum (CD$_2$Cl$_2$, 298 K) of compound (*rac*)-**1-Se**.
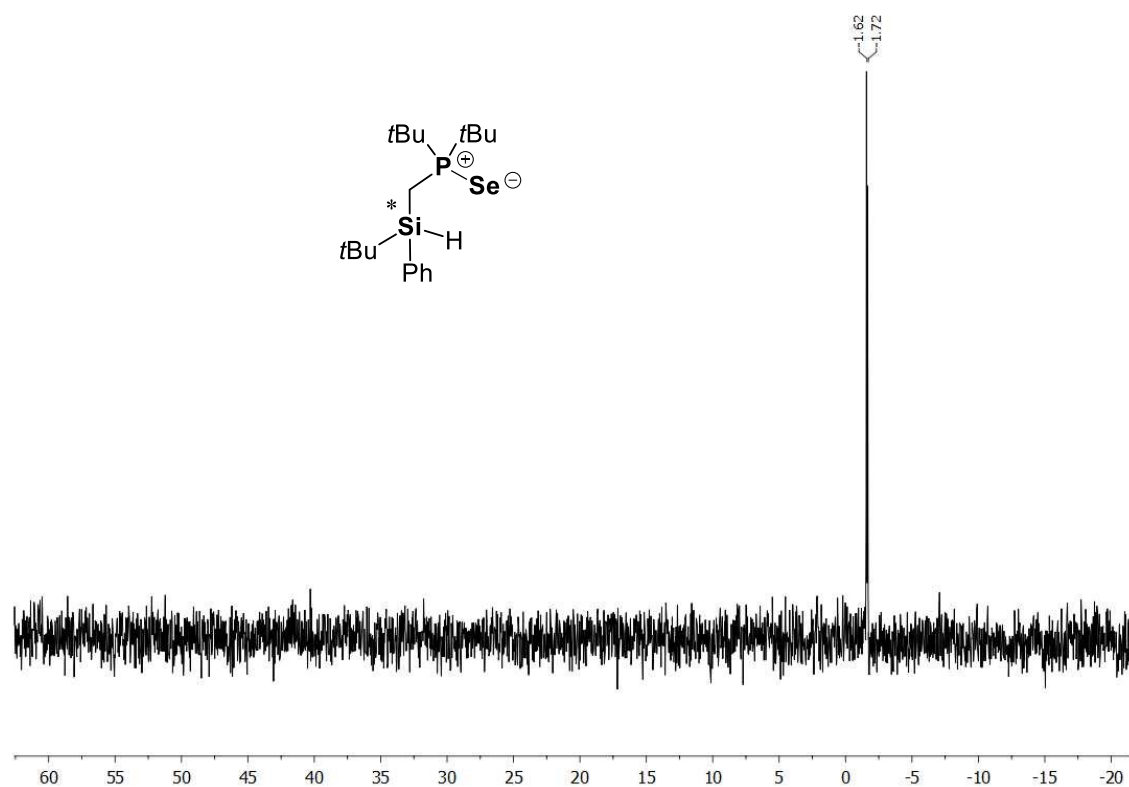
Figure S49. ^{29}Si{^{1}H}- NMR spectrum (CD$_2$Cl$_2$, 298 K) of compound (*rac*)-**1-Se**.
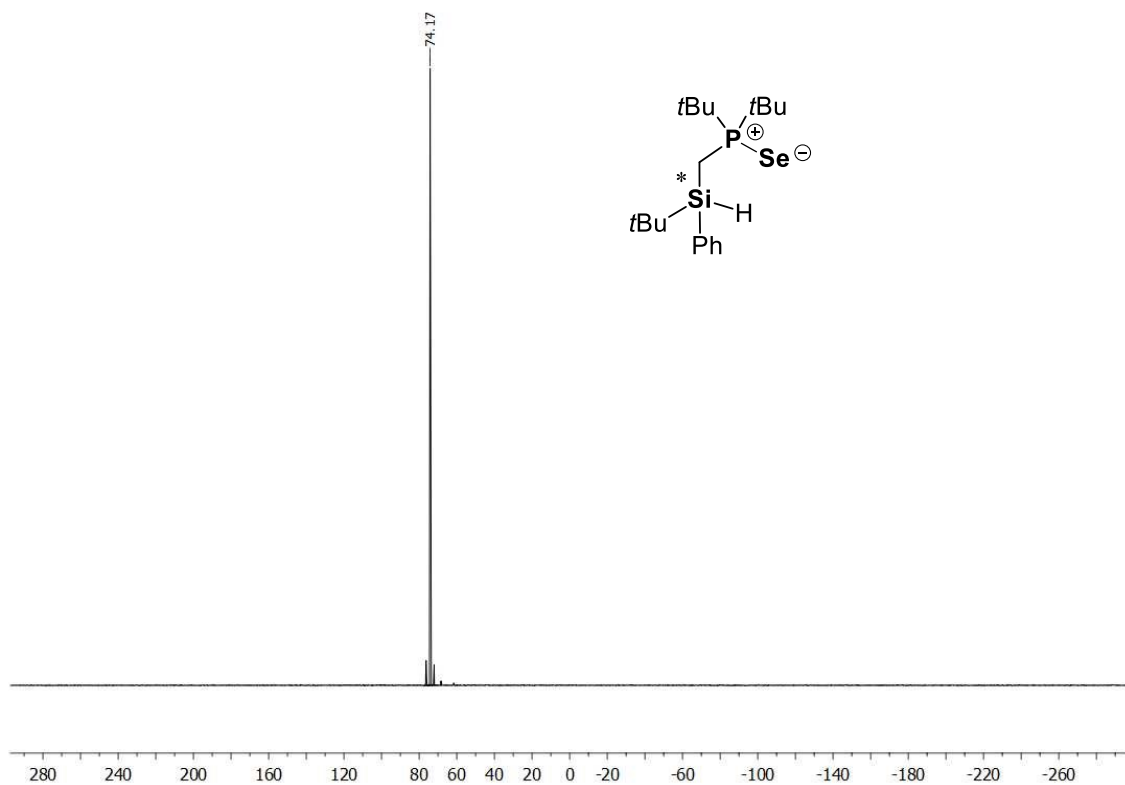
Figure S50. ^{31}P{^{1}H}- NMR spectrum (CD$_2$Cl$_2$, 298 K) of compound (*rac*)-**1-Se**.
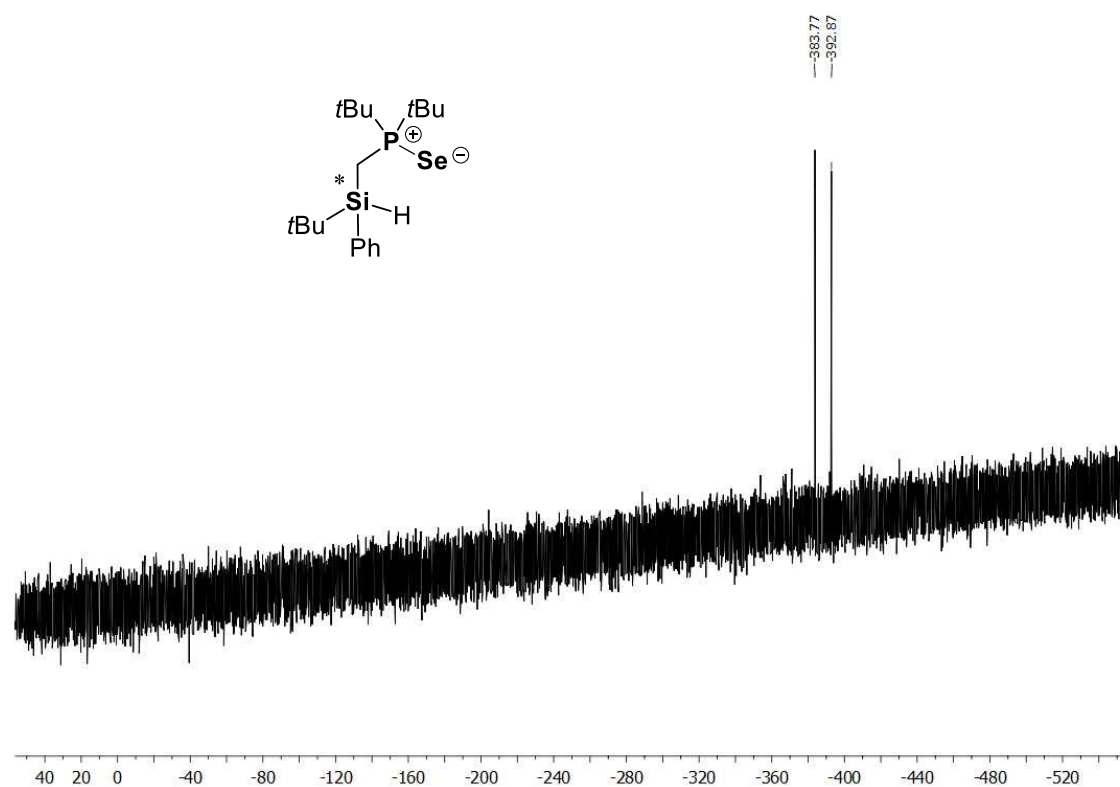
Figure S51. ^{77}Se{^{1}H}- NMR spectrum (CD$_2$Cl$_2$, 298 K) of compound (*rac*)-**1-Se**.

3.5.9 Synthesis of (*rac*)-[(*t*Bu)₂P(Se)CH₂Si(H)Ph*t*Bu][HB(C₆F₅)₃] ((rac)-2a-Se)

(*rac*)-**1-Se**   (*rac*)-**2a-Se**
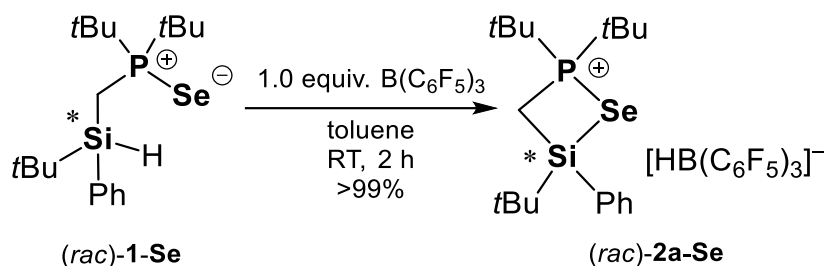
Inside a glovebox, an oven dried Schlenk flask was charged with di-*tert*-butyl(((*tert*-butyl(phenyl)silyl)methyl)phosphine selenide (48 mg, 0.12 mmol, 1.0 equiv.) and tris(pentafluorophenyl)borane (61 mg, 0.12 mmol, 1.0 equiv.). Toluene (2 ml) was added, and the solution was stirred for two hours at room temperature. The resulting biphasic solution was fully dried and the residue washed with pentane (2 x 5 ml), yielding the desired product (*rac*)-**2a-Se** as a white solid (112 mg, 0.12 mmol, >99%). In an independent experiment, colourless crystals, suitable for single-crystal X-ray diffraction analysis were obtained by pentane vapor diffusion into the toluene biphasic reaction solution.

¹H NMR (400.30 MHz, CD₂Cl₂, 298 K): δ = 1.09 [s, 9H SiC(CH_3)₃], 1.22 [d, $^3J_{\text{P-H}}$= 19.0 Hz, 9H, PC(CH_3)₃], 1.55 [d, $^3J_{\text{P-H}}$= 19.1 Hz, 9H, PC(CH_3)₃], 2.7 [ddd(ABX), J_1= 13.3 Hz, J_2= 16.0 Hz, J_3= 29.0 Hz, 2H, SiCH_2P], 3.62 [bq, $^1J_{\text{B-H}}$=81.0 Hz, 1H, BH] 7.49-7.52 [m, 2H, H_{Ph}], 7.56-7.57 [m, 1H, H_{Ph}], 7.61-7.63 [m, 2H, H_{Ph}]. **¹¹B{¹H} NMR** (128.43 MHz, CD₂Cl₂, 298 K): δ = -25.6 [bs] **¹³C{¹H} NMR** (100.66 MHz, CD₂Cl₂, 298 K): δ = 8.5 [d, $^1J_{\text{C-P}}$ = 19.2 Hz, SiCH₂P], 22.2 [s, SiC(CH₃)₃], 25.2 [s, SiC(CH_3)₃], 26.8 [d, $^2J_{\text{C-P}}$ = 2.3 Hz, PC(CH₃)₃], 27.0 [d, $^2J_{\text{C-P}}$ = 2.3 Hz, PC(CH_3)₃], 39.7 [d, $^1J_{\text{C-P}}$ = 17.7 Hz, PC(CH₃)₃], 41.1 [d, $^1J_{\text{C-P}}$ = 15.4 Hz, PC(CH₃)₃], 128.4 [s, C_{Ph}], 129.3 [s, C_{Ph}], 132.3 [s, C_{Ph}], 134.0 [s, C_{Ph}], 137.1 [bd, $^1J_{\text{C-F}}$ = 244.6 Hz, C$_{\text{Ar-borate}}$], 148.6 [bd, $^1J_{\text{C-F}}$ = 229.1 Hz, C$_{\text{Ar-borate}}$]. **¹⁹F{¹H} NMR** (376.66 MHz, CD₂Cl₂, 298 K): δ = -167.3 [bs, 6F], -164.5 [bs, 3F], -133.7 [bs, 6F]. **²⁹Si{¹H} NMR** (79.49 MHz, CD₂Cl₂, 298 K): δ = 7.2 [d, $^2J_{\text{Si-P}}$= 14.2 Hz, SiCH₂P]. **³¹P{¹H} NMR** (162.04 MHz, CD₂Cl₂, 298 K): δ = 77.8 [s]. **⁷⁷Se{¹H} NMR** (76.31 MHz, CD₂Cl₂, 298 K): δ = -139.1 [d, $^1J_{\text{Se-P}}$ = 306.4 Hz]. **HR-MS (FD-MS)**, calcd. m/z for C₁₉H₃₆OPSSi⁺ [Cation⁺], C₁₈HBF₁₅⁻ [Anion⁻]: 401.1333, 512.9931; found: 818.2512 [C₃₈H₆₈OP₂Se₂Si₂] the compound hydrolyzed during the measurement.
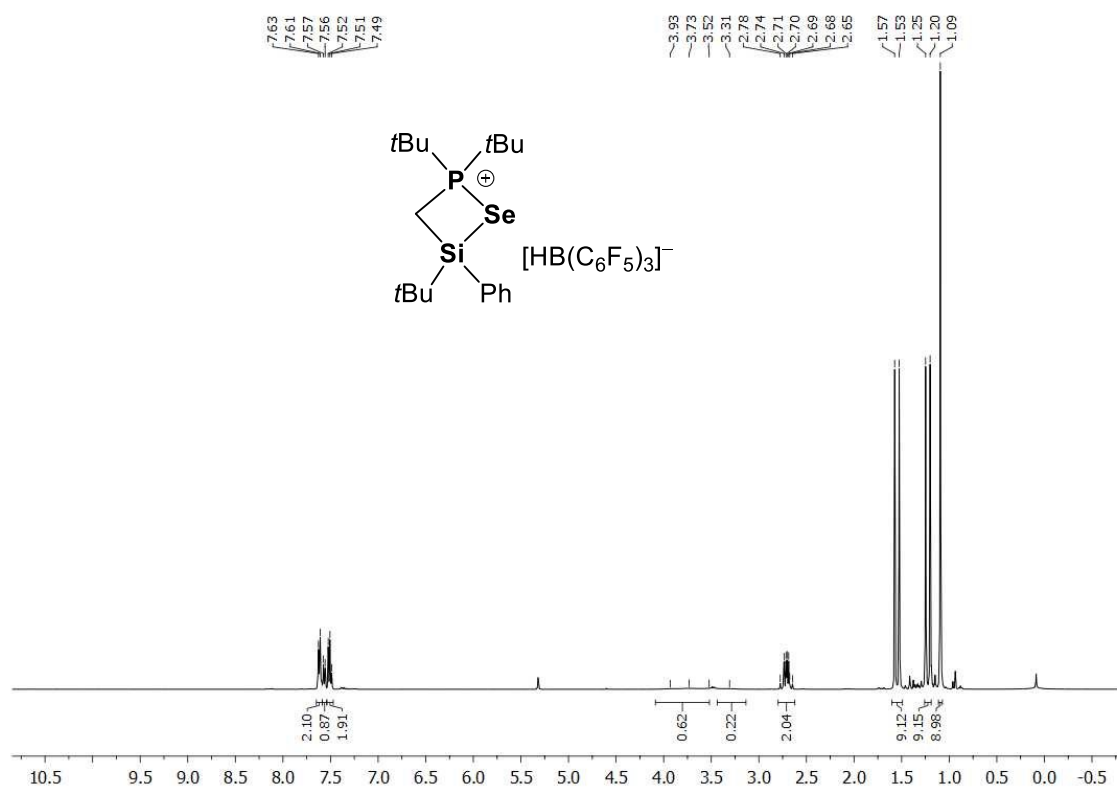
Figure S52. ^{1}H NMR spectrum (CD$_2$Cl$_2$, 298 K) of compound (*rac*)-**2a-Se**.
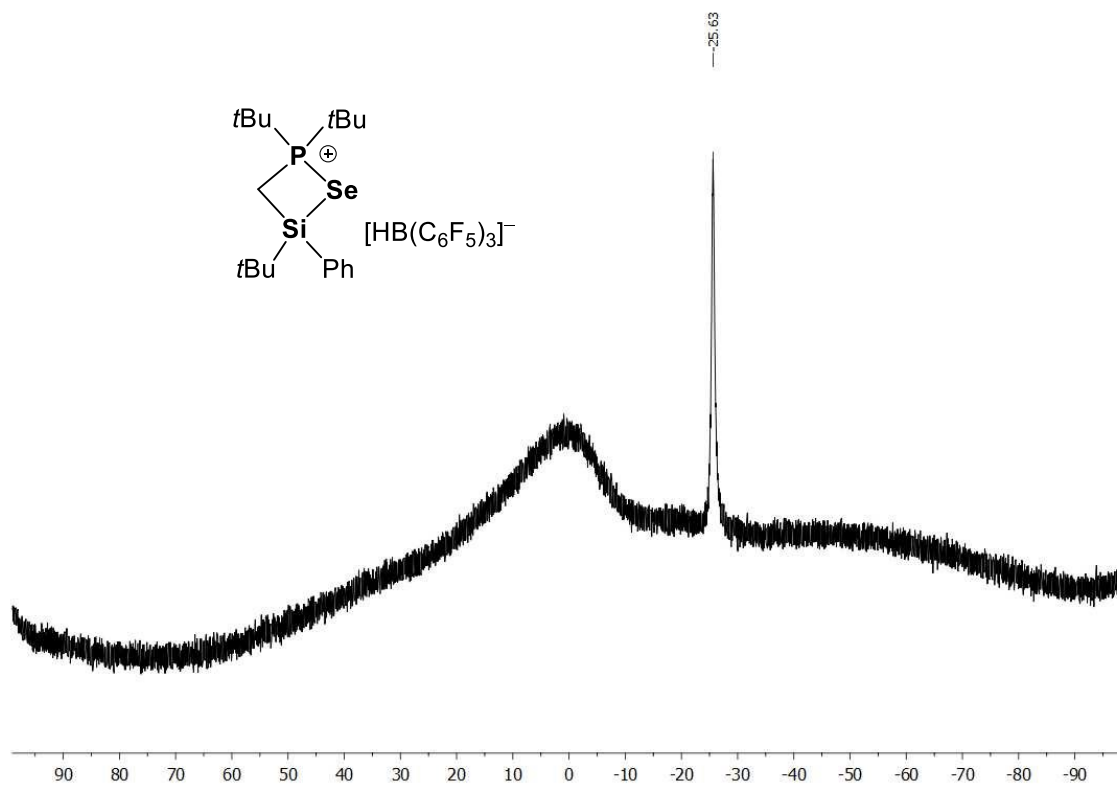
Figure S53. ^{11}B{^{1}H} NMR spectrum (CD$_2$Cl$_2$, 298 K) of compound (*rac*)-**2a-Se**.

59
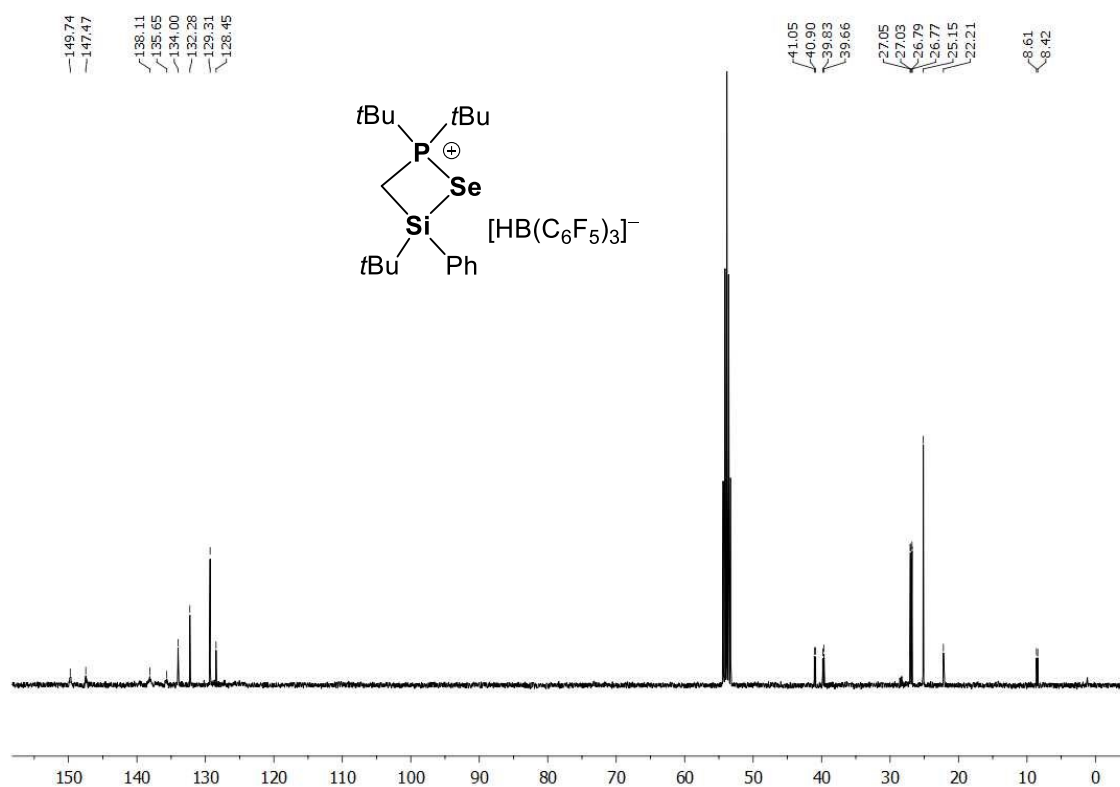
Figure S54. ^{13}C{^{1}H} NMR spectrum (CD$_2$Cl$_2$, 298 K) of compound (*rac*)-**2a-Se**.
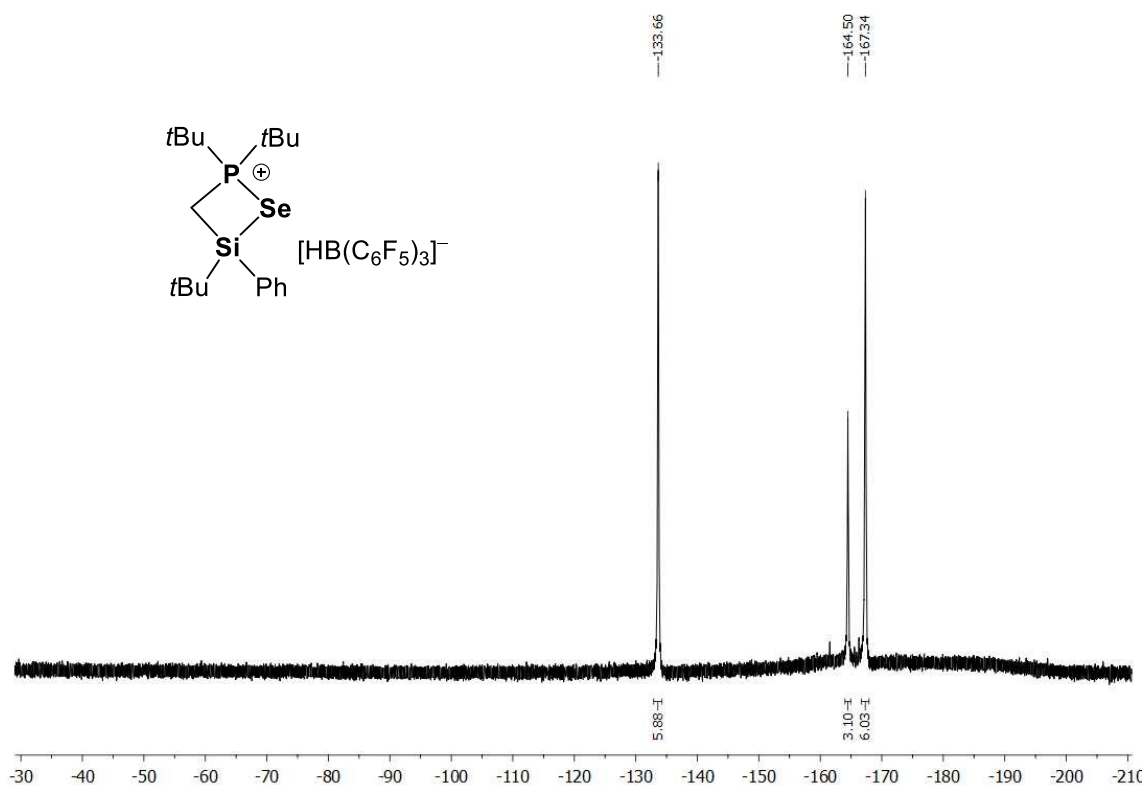
Figure S55. ^{19}F{^{1}H} NMR spectrum (CD$_2$Cl$_2$, 298 K) of compound (*rac*)-**2a-Se**.
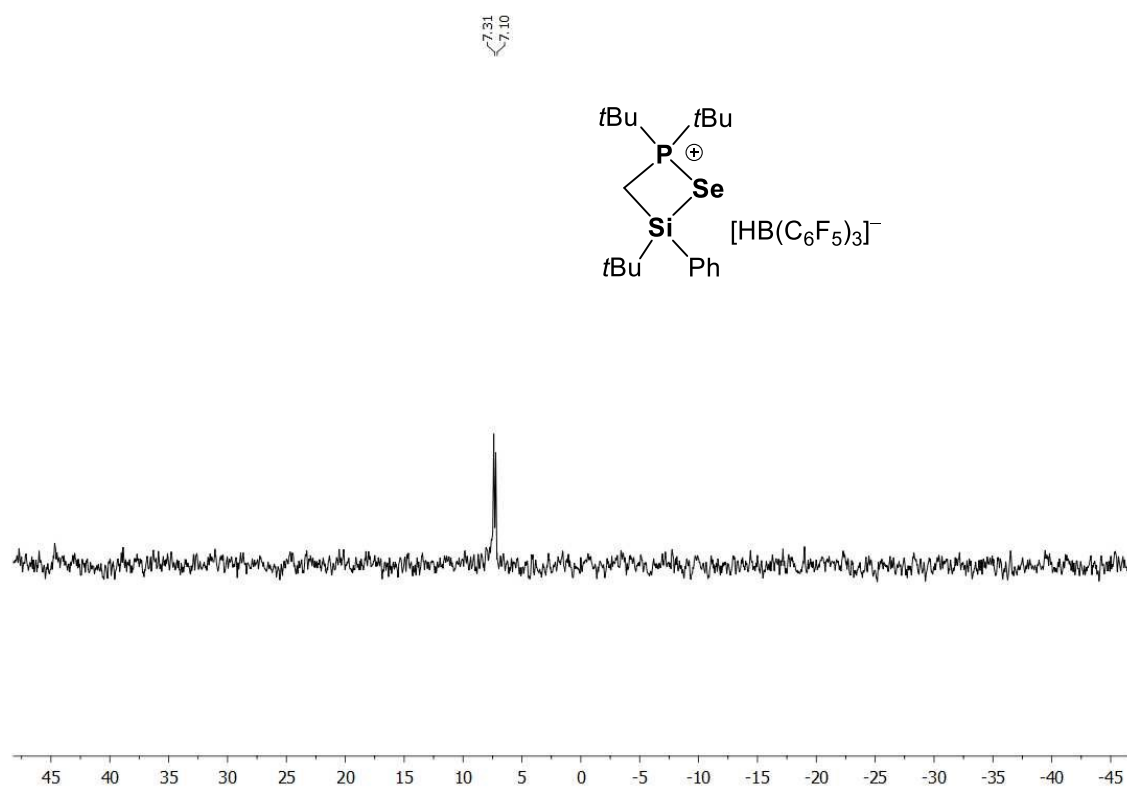
Figure S56. ^{29}Si{^{1}H} NMR spectrum (CD$_2$Cl$_2$, 298 K) of compound (*rac*)-**2a-Se**.
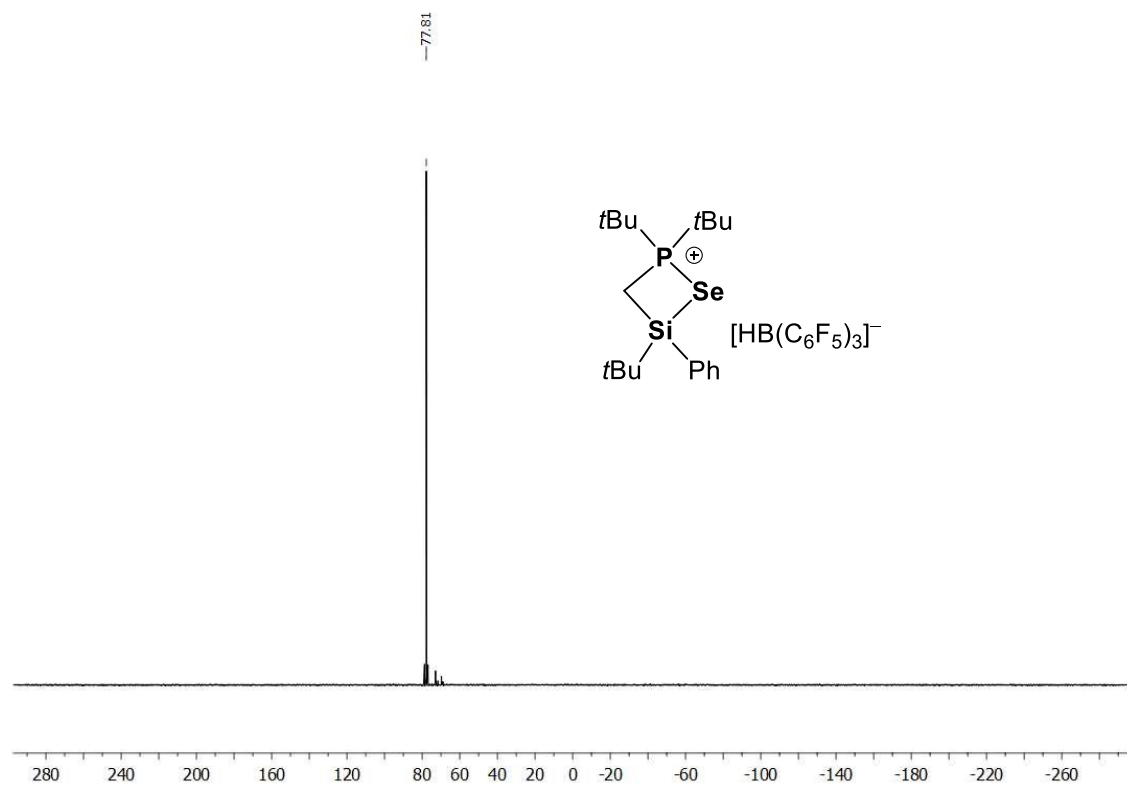
Figure S57. ^{31}P{^{1}H} NMR spectrum (CD$_2$Cl$_2$, 298 K) of compound (*rac*)-**2a-Se**.
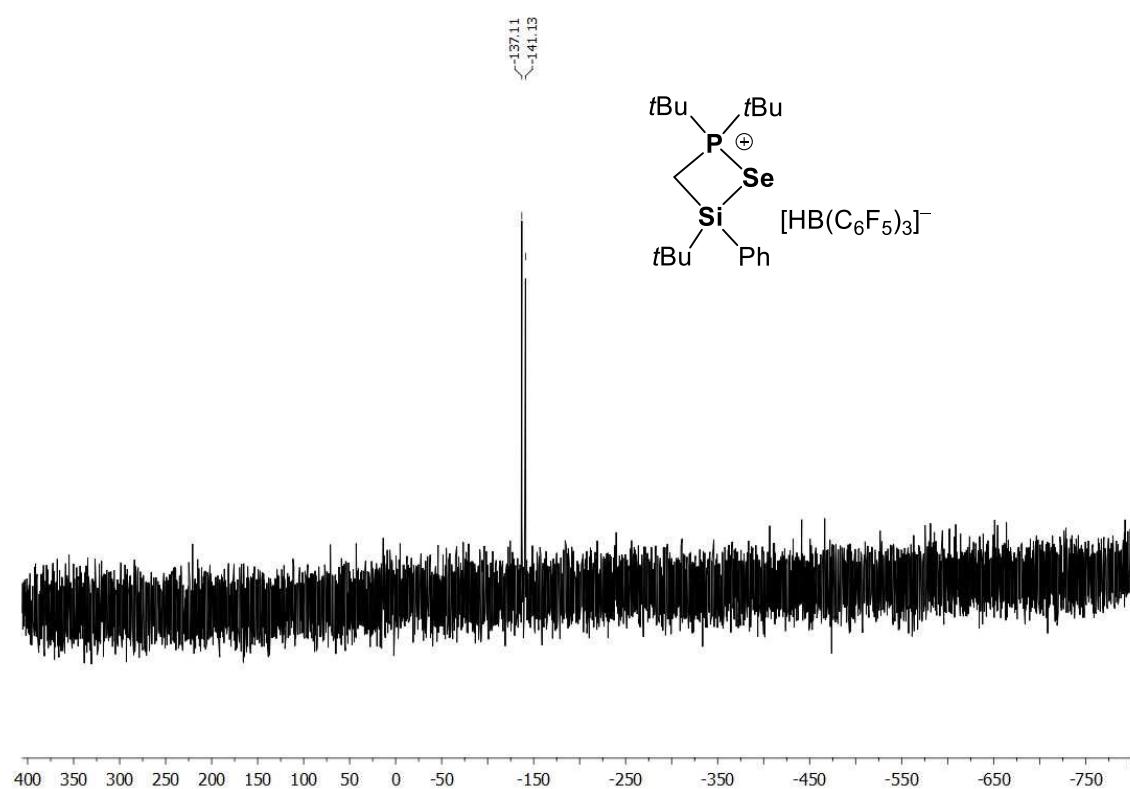
Figure S58. $^{77}Se\{^1H\}$ NMR spectrum (CD$_2$Cl$_2$, 298 K) of compound (*rac*)-**2a-Se**.

3.5.10 Investigation of the stereochemical course
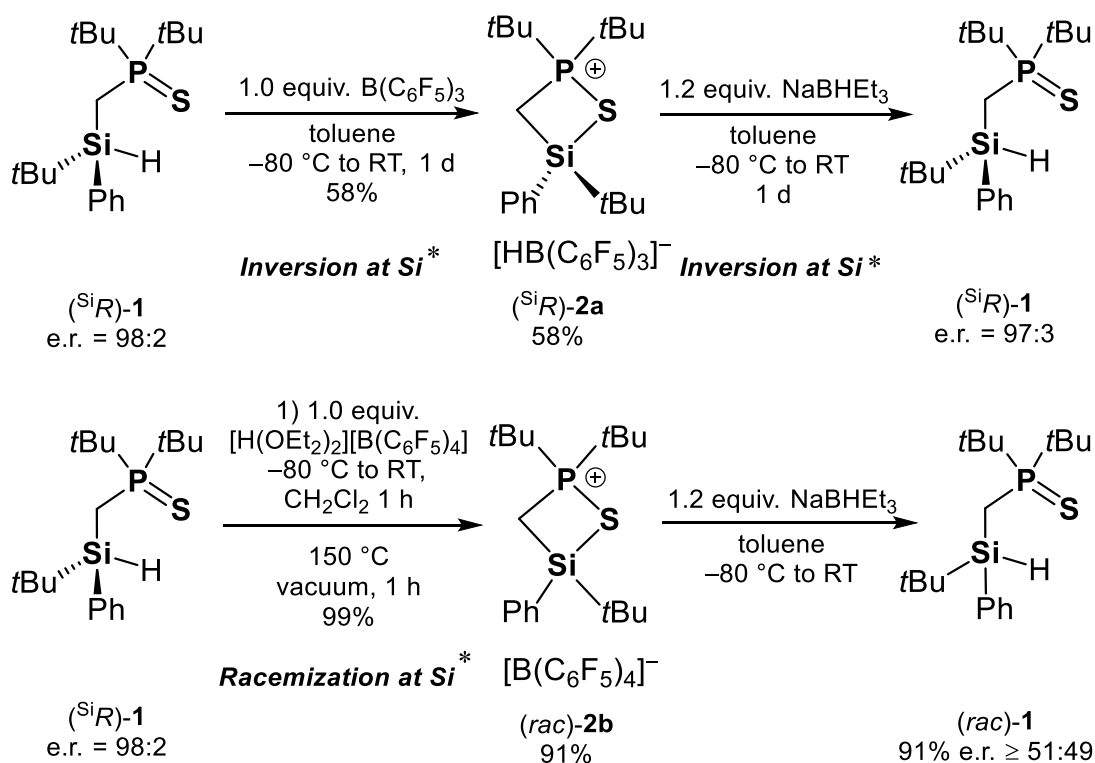
Investigation of the stereochemical course of silyl phosphonium ion formation *via* hydride abstraction followed by hydride addition:

An oven dried Schlenk was brought into a glovebox and loaded with (^{Si}R)-**1** (115 mg, 0.32 mmol, 1.0 equiv.) and tris(pentafluorophenyl)borane (166 mg, 0.32 mmol, 1.0 equiv.). The Schlenk flask containing the solids was taken out of the glovebox, connected to a Schlenk line and toluene was added (10 mL) at -80°C. The reaction mixture was allowed to slowly warm up to room temperature and kept stirring for one day. The clear beige solution was then concentrated down to ~ 1 ml and pentane (15 ml) was added under vigorous stirring. Immediate separation of a colourless oil was observed. The supernatant layer was removed by means of PTFE tube and the sticky oil was further washed with pentane (2 x 5 ml). The washed residue was dried in vacuum affording pure silyl phosphonium ion (^{Si}R)-**2a** (163 mg, 0.186 mmol, 58%) as a viscous beige oil. Compound (^{Si}R)-**2a** was dissolved in toluene (5 ml) and cooled down to -80°C. NaBHEt₃ (0.22 ml of a 1.0 M solution in toluene, 1.2 equiv.) was added *via* syringe and the mixture was allowed to slowly warm up to room temperature and kept stirring for another day. Following, all volatiles were removed in vacuum and the residue was extracted with pentane (3 x 5 ml). The combined pentane extracts were collected, dried under vacuum and the residue was subjected to HPLC analysis confirming the formation of highly enantiomerically enriched silane (^{Si}R)-**1** (er 97:3).

HPLC-UV (Hexane/Isopropanol 99:1, flow of 0.9 mL⁻¹, 10µl injected, 215 nm, 20°C): retention time, area, area %: 8.37 min, 8054.39, 97.6% [(^{Si}R)-**1**]; 14.07 min, 194.75, 2.4% [(^{Si}S)-**1**].
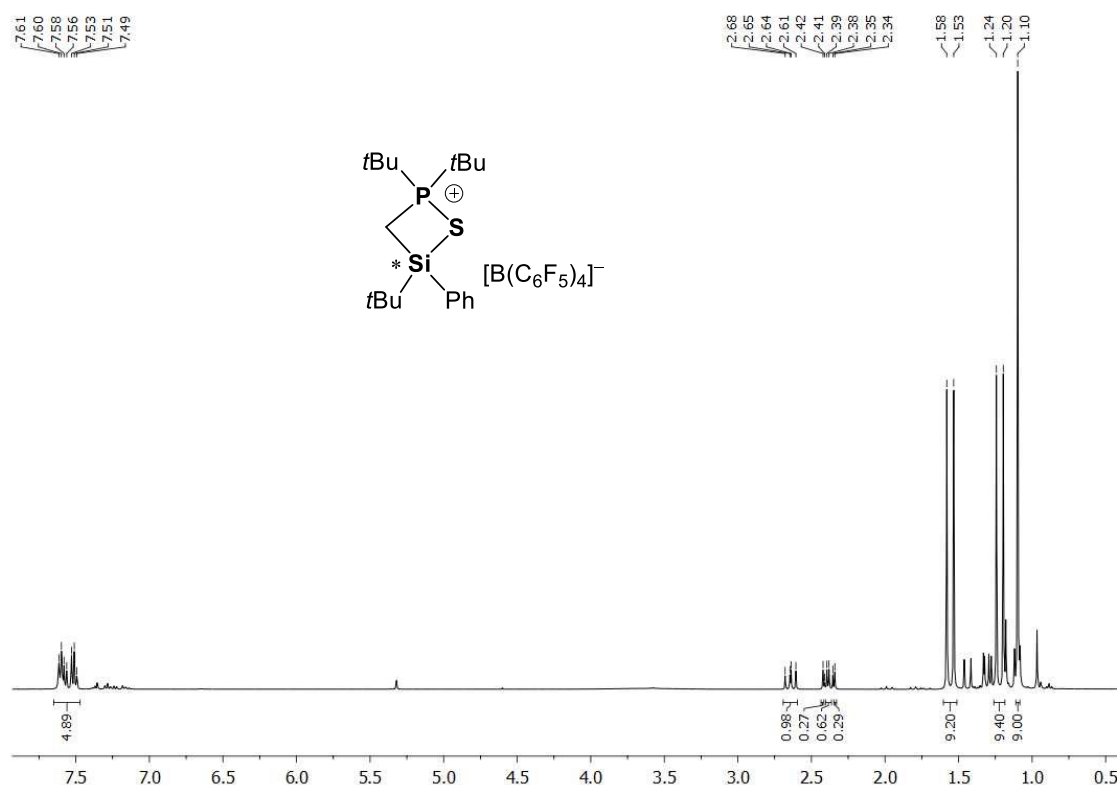
Figure S59. ^{1}H NMR (CD$_2$Cl$_2$, 298 K) of compound (^{Si}R)-**2a**.

Investigation of the stereochemical course of silyl phosphonium ion formation *via* dihydrogen release followed by hydride addition:

An oven dried Schlenk was brought into a glovebox and loaded with (^{Si}R)-**1** (100 mg, 0.28 mmol, 1 equiv.) and [H(OEt$_2$)$_2$][B(C$_6$F$_5$)$_4$] (233.6 mg, 0.28 mmol, 1 equiv.). The Schlenk flask containing the solids was taken out of the glovebox, connected to a Schlenk line and diethyl ether was added (10 ml) at -80°C. The reaction mixture was allowed to slowly warm up to room temperature and kept stirring for 1 h. Then, all volatiles were gently removed in vacuum rendering a foamy solid which was heated up to 150°C in vacuum for two hours turning into an oily residue. After cooling down to room temperature, the residue was dissolved in dichloromethane (2 ml) and precipitated by addition of pentane (15 ml) under vigorous stirring. The white precipitate was washed with pentane (2 x 5 ml) and dried in vacuum yielding (*rac*)-**2b** (263.3 mg, 0.255 mmol, 91%) as a viscous beige oil. Compound (*rac*)-**2b** was dissolved in toluene (5 ml) and cooled down to -80°C. NaBHEt$_3$ (0.31 ml of a 1.0 M solution in toluene, 1.2 equiv.) was added *via* syringe and the mixture was allowed to slowly warm up to room temperature and kept stirring for 15 h. Following, all volatiles were removed in vacuum and the residue extracted with pentane (3 x 5 ml). The combined pentane extracts were collected, dried in vacuum and the residue subjected to HPLC analysis confirming the formation of silane (*rac*)-**1**.

HPLC-UV (Hexane/Isopropanol 99:1, flow of 0.9 mL^{-1}, 10 μl injected, 215 nm, 20°C): retention time, area, area %: 7.99 min, 4290.87, 50.6% [(^{Si}R)-**1**]; 11.26 min, 4190.13, 49.4% [(^{Si}S)-**1**].
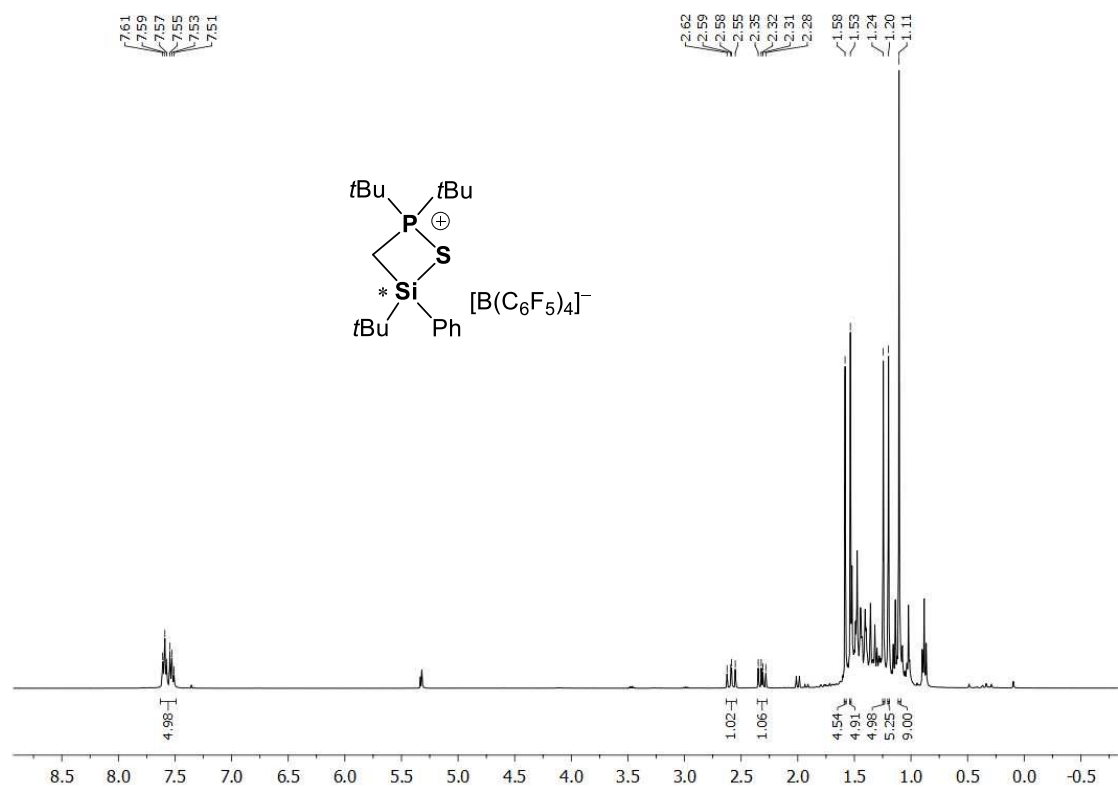
Figure S60. ^{1}H NMR (CD$_2$Cl$_2$, 298 K) of compound (*rac*)-**2b** obtained from (^{Si}R)-**1**.

3.5.11 Synthesis of (^{Si}S)- and (^{Si}R)-(tBu)$_2$P(S)CH$_2$SiPhtBu(OC$_{10}$H$_{20}$) (4a, 4b)

4a: (^{Si}S), 39%
d.r. > 99:1

4b: (^{Si}R), 35%,
d.r. > 99:1
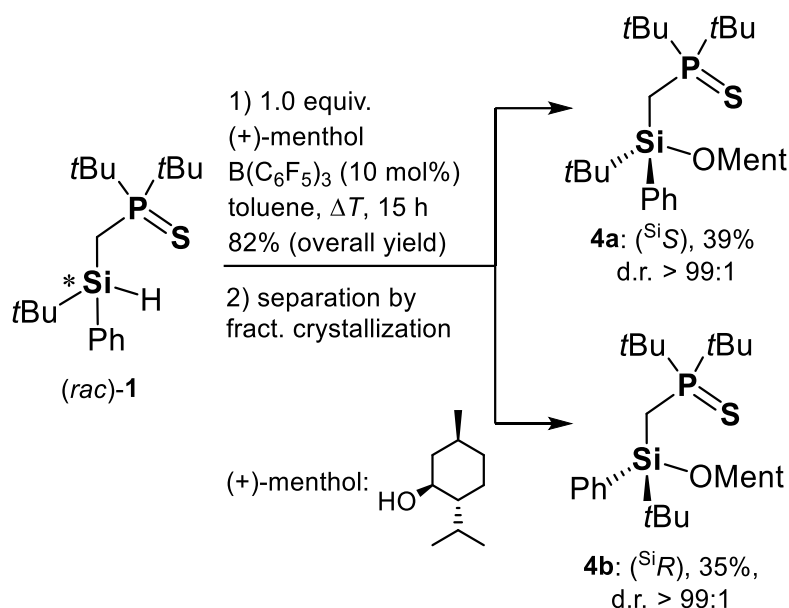
In a glovebox, an oven dried Schlenk tube was loaded with silane (*rac*)-**1** (3.54 g, 10 mmol, 1.0 equiv.), tris(pentafluorophenyl)borane (512 mg, 1 mmol, 10 mol%) and toluene (~ 30 mL). Following, (+)-menthol (1.56 g, 10 mmol, 1.0 equiv.) was added as a solution in toluene (10 mL) to the previous mixture at room temperature. The Schlenk tube was taken out of the glovebox and heated to reflux under nitrogen atmosphere for 15 hours. The reaction mixture was then cooled down to room temperature and an aliquot of the crude mixture analyzed by NMR. Full conversion of the starting material and formation of the desired products **4a** and **4b** was confirmed by ^{1}H and ^{31}P{^{1}H} NMR (d.r. 52:48). Following, all volatiles from the reaction mixture were removed in vacuum yielding a brownish oily residue. Purification of the crude was performed *via* Kugelrohr distillation (200°C oven temperature, 1.2 x 10^{-2} mbar) yielding **4a** and **4b** together as an oily white solid (4.17 g, 8.2 mmol, 82%, d.r. 52:48). Highly enriched fractions of **4a** and **4b** were obtained by fractional crystallization as described as follows. The pure distilled mixture of **4a** and **4b** (4.17 g, 8.2 mmol) was fully dissolved in the minimum amount of pentane (~40 mL) at room temperature and the clear solution was stored in a fridge (~0°C). Colourless clear crystals deposited already after 10 hours but the mixture was left undisturbed to crystalize for three days at this temperature. The mother-liquor was removed *via* suction filtration and the remaining colourless crystalline material was washed with cold pentane (~3 ml, 0°C). Diastereoisomer **4a** was isolated as colourless crystals, highly enriched as confirmed by NMR spectroscopy (580 mg, 1.0 mmol, d.r. <99:1). These crystals were also suitable for single-crystal X-ray diffraction. The mother-liquor and the pentane washing were collected, dried and the isolated colourless solid recrystallized from a concentrated pentane solution at 0°C, yielding diastereoisomer **4b** as colourless crystals suitable for single-crystal X-ray diffraction analysis and highly enriched as confirmed by NMR spectroscopy (650 mg, 1.3 mmol, d.r. >99:1). This process was repeated two more times yielding batches of the two diastereoisomers alternatively (Overall

separation yielded **4a**: 1.92 g, 3.88 mmol, 39%, **4b**: 1.74 g, 3.52 mmol, 35%). The absolute configurations of the two species were univocally assigned by X-ray diffraction analysis.

4a

^{1}H NMR (400.13 MHz, C_6D_6, 298 K): δ = 0.81 [d, $^3J_{H\text{-}H}$= 5.9 Hz, 3H, CHCH_3], 0.87 [d, $^3J_{H\text{-}H}$= 7.0 Hz, 3H, CH(CH_3)$_2$], 0.93-.097 [m, 1H, CHCH$_3$], 1.02 [d, $^3J_{H\text{-}H}$= 7.0 Hz, 3H, CH(CH_3)$_2$], 1.22 [d, $^3J_{H\text{-}P}$= 6.1 Hz, 9H, PC(CH_3)$_3$], 1.22 [s, 9H, SiC(CH_3)$_3$], 1.26 [d, $^3J_{H\text{-}P}$= 6.1 Hz, 9H, PC(CH_3)$_3$], 1.37-1.47 [m, 1H, CH_{Ment}], 1.53-1.62 [m, 2H, C$H_{2\text{Ment}}$], 1.73-1.85 [m, 2H, C$H_{2\text{Ment}}$], 2.19-2.23 [m, 1H, CH_{Ment}], 2.62-2.73 [m, 1H CHH_{Ment}], 2.59-2.67 [m, CHH$_{\text{Ment}}$], 4.02-4.08 [m, 1H, OCH], 7.19-7.24 [m, 1H, H_{Ph}], 7.27-7.31 [m, 2H, H_{Ph}], 8.28-8.30 [m, 2H, H_{Ph}]. **^{13}C{^{1}H} NMR** (100.61 MHz, C_6D_6, 298 K): δ = 9.4 [d, $^1J_{C\text{-}P}$= 36.1 Hz, SiCH_2P], 16.4, 20.9 [d, $^3J_{C\text{-}P}$= 2.7 Hz, SiC(CH$_3$)$_3$], 21.8, 22.5, 23.2, 25.3, 27.5, 27.9 [d, $^2J_{C\text{-}P}$= 1.5 Hz, P(C(CH_3)$_3$)$_2$], 28.1 [d, $^2J_{C\text{-}P}$= 1.7 Hz, P(C(CH_3)$_3$)$_2$], 32.0, 34.8, 38.7 [d, $^1J_{C\text{-}P}$= 35.2 Hz, P(C(CH$_3$)$_3$)$_2$], 39.1 [d, $^1J_{C\text{-}P}$= 34.8 Hz, P(C(CH$_3$)$_3$)$_2$], 46.4, 51.2, 75.1, 127.4 [s, C$_{Ph}$], 129.9 [s, C$_{Ph}$], 135.9 [s, C$_{Ph}$], 136.8 [s, C$_{Ph}$]. **^{29}Si NMR** (79.49 MHz, C_6D_6, 298 K): δ = -5.6 [d, $^2J_{Si\text{-}P}$= 7.5 Hz]. **^{31}P{^{1}H} NMR** (161.98 MHz, C_6D_6, 298 K): δ = 75.2. **CHN Analysis** $C_{29}H_{53}$OPSSi: calculated: C 68.45%, H 10.50%; found C 68.47%, H 10.50%. **HR-MS (ESI)**, calcd. m/z for $C_{29}H_{54}$OPSSi [M+H]$^+$: 509.3397; found: 509.3389.

4b

^{1}H NMR (400.13 MHz, C_6D_6, 298 K): δ = 0.84 [d, $^3J_{H\text{-}H}$= 6.1 Hz, 3H, CHCH_3], 0.89 [d, $^3J_{H\text{-}H}$= 6.9 Hz, 3H, CH(CH_3)$_2$], 1.01 [d, $^3J_{H\text{-}H}$= 7.2 Hz, 3H, CH(CH_3)$_2$], 1.20 [d, $^3J_{H\text{-}P}$= 13.8 Hz, 9H, PC(CH_3)$_3$], 1.22 [s, 9H, SiC(CH_3)$_3$], 1.26 [d, $^3J_{H\text{-}P}$= 14.7 Hz, 9H, PC(CH_3)$_3$], 1.31-1.35 [m, 2H, CH_{Ment}], 1.38-1.44 [m, 1H, CH_{Ment}], 1.54-1.61 [m, 2H, CH_{Ment}], 1.67-1.79 [m, 2H, CH_{Ment}], 2.28-2.31 [m, 1H, CH_{Ment}], 2.59-2.67 [m, 1H, CH_{Ment}], 4.12-4.18 [m, 1H, CH_{Ment}], 7.20-7.25 [m, 1H, H_{Ph}], 7.28-7.32 [m, 2H, H_{Ph}], 8.19-8.21 [m, 2H, H_{Ph}]. **^{13}C{^{1}H} NMR** (100.61 MHz, C_6D_6, 298 K): δ = 9.8 [d, $^1J_{C\text{-}P}$= 35.6 Hz, SiCH_2P], 16.5, 21.1 [d, $^3J_{C\text{-}P}$= 3.6 Hz, SiC(CH$_3$)$_3$], 21.8, 22.5, 23.2, 25.4, 27.8, 27.9 [d, $^2J_{C\text{-}P}$= 1.6 Hz, P(C(CH_3)$_3$)$_2$], 28.1 [d, $^2J_{C\text{-}P}$= 1.6 Hz, P(C(CH_3)$_3$)$_2$], 32.0, 34.8, 38.6 [d, $^1J_{C\text{-}P}$= 5.1 Hz, P(C(CH$_3$)$_3$)$_2$], 39.0 [d, $^1J_{C\text{-}P}$= 4.6 Hz, P(C(CH$_3$)$_3$)$_2$], 46.2, 51.2, 75.5, 127.5 [s, C$_{Ph}$], 129.8 [s, C$_{Ph}$], 136.0 [s, C$_{Ph}$], 136.5 [s, C$_{Ph}$]. **^{29}Si NMR** (79.49 MHz, C_6D_6, 298 K): δ = -6.4 [d, $^2J_{Si\text{-}P}$= 8.5 Hz]. **^{31}P{^{1}H} NMR** (161.98 MHz, C_6D_6, 298 K): δ = 75.4. **CHN Analysis** $C_{29}H_{53}$OPSSi: calculated: C 68.45%, H 10.50%; found C 68.64%, H 10.47%. **HR-MS (ESI)**, calcd. m/z for $C_{29}H_{54}$OPSSi [M+H]$^+$: 509.3397; found: 509.3389.
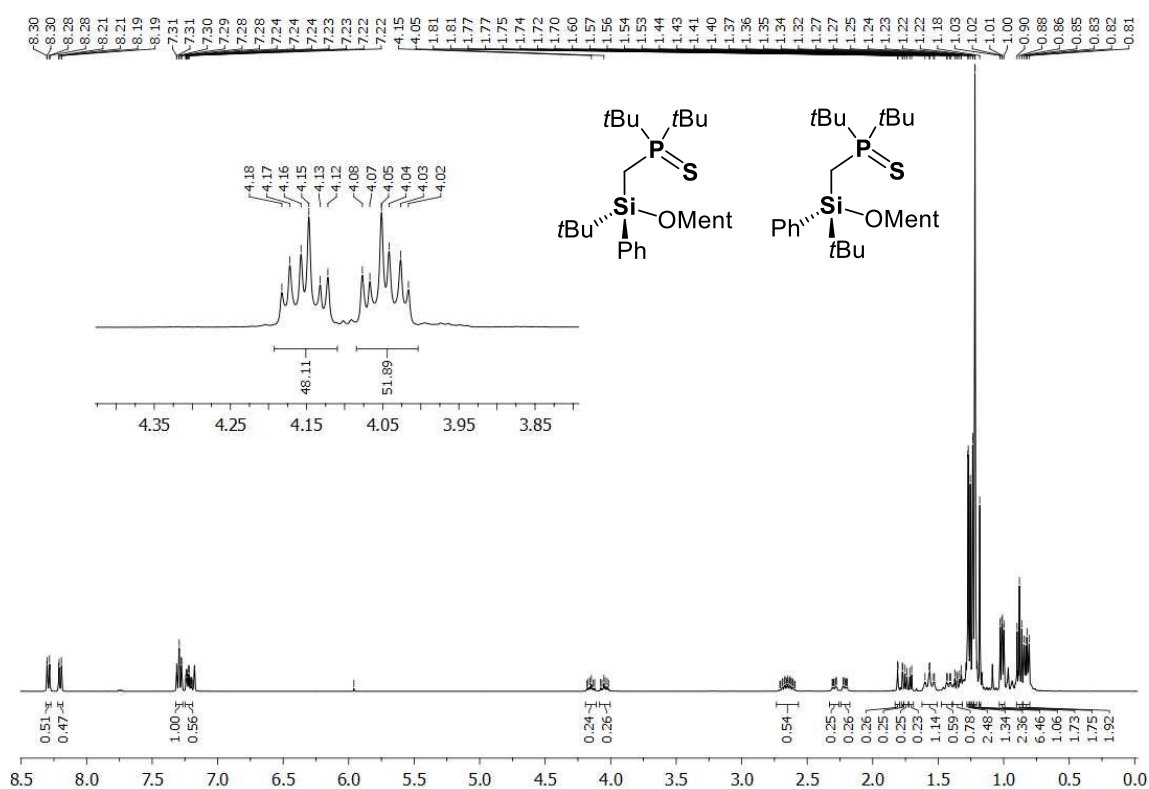
Figure S61. ^{1}H NMR (C$_6$D$_6$, 298 K) of the mixture containing **4a** and **4b**. Expansion highlight the signals related to the protons in geminal position with respect to the oxygen. The integration is normalized to one hundred to show the diastereomeric ratio.
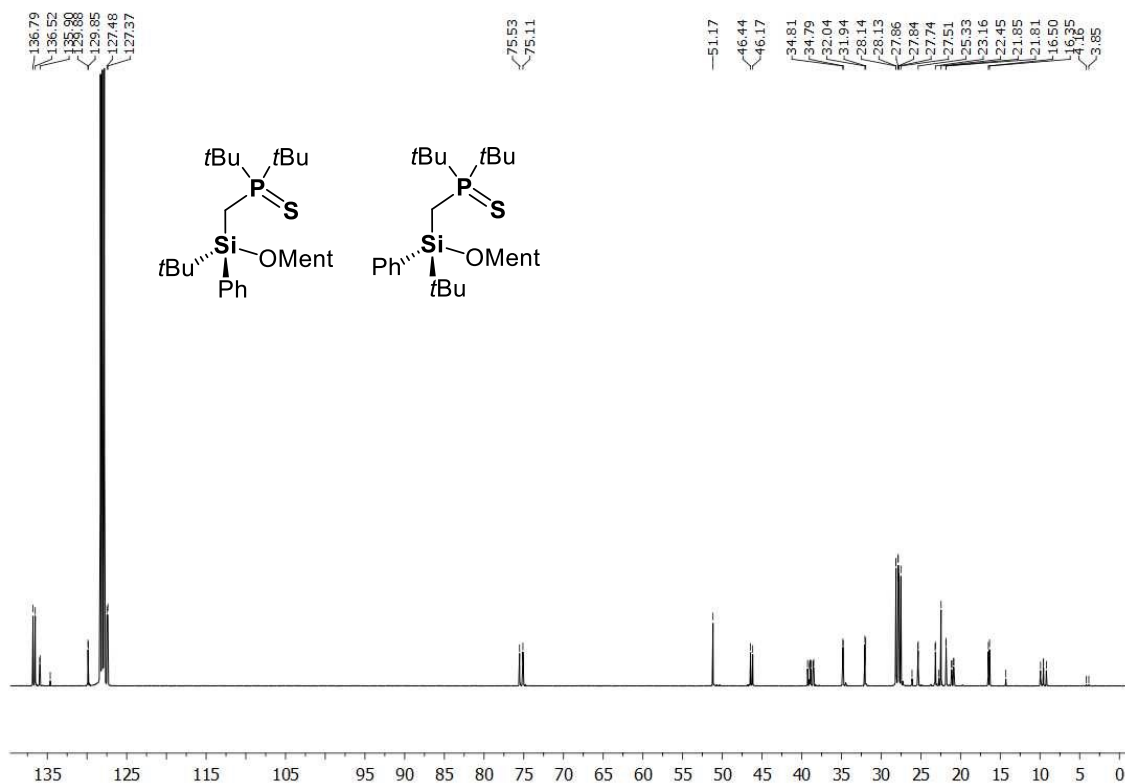
Figure S62. ^{13}C{^{1}H} NMR (C$_6$D$_6$, 298 K) of the mixture containing **4a** and **4b**.
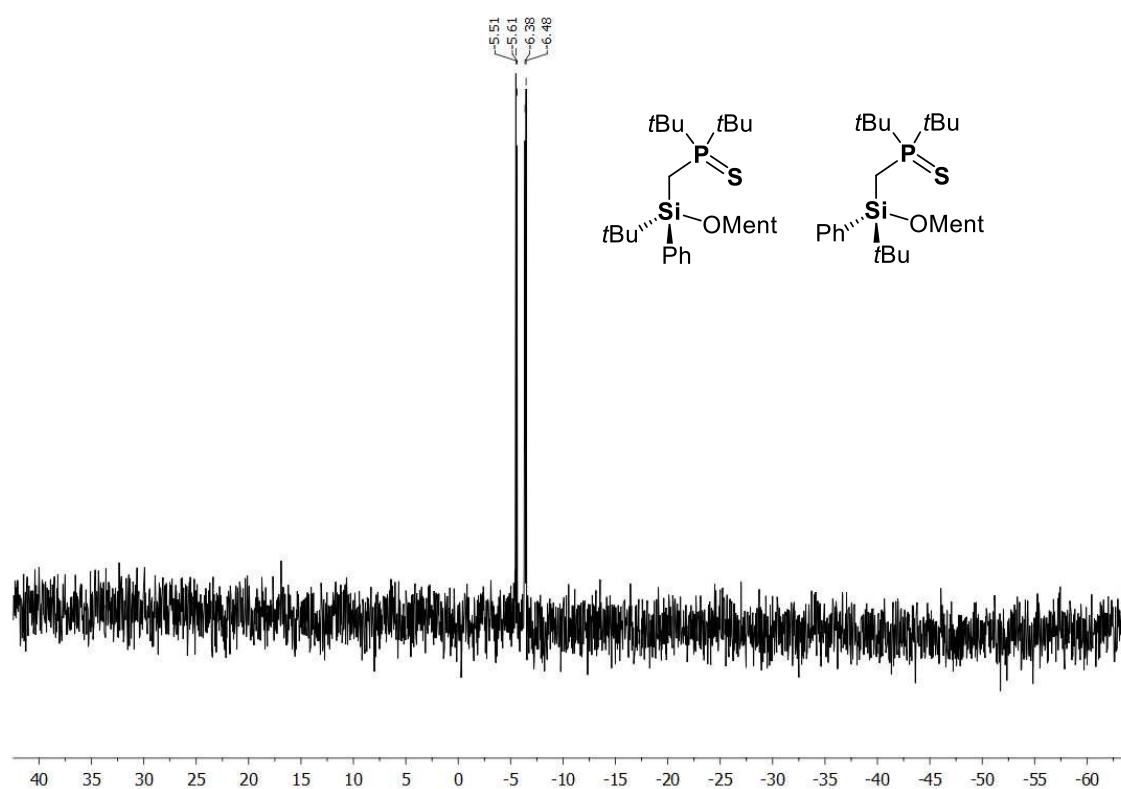
Figure S63. ^{29}Si{^{1}H} NMR (C$_6$D$_6$, 298 K) of the mixture containing **4a** and **4b**.
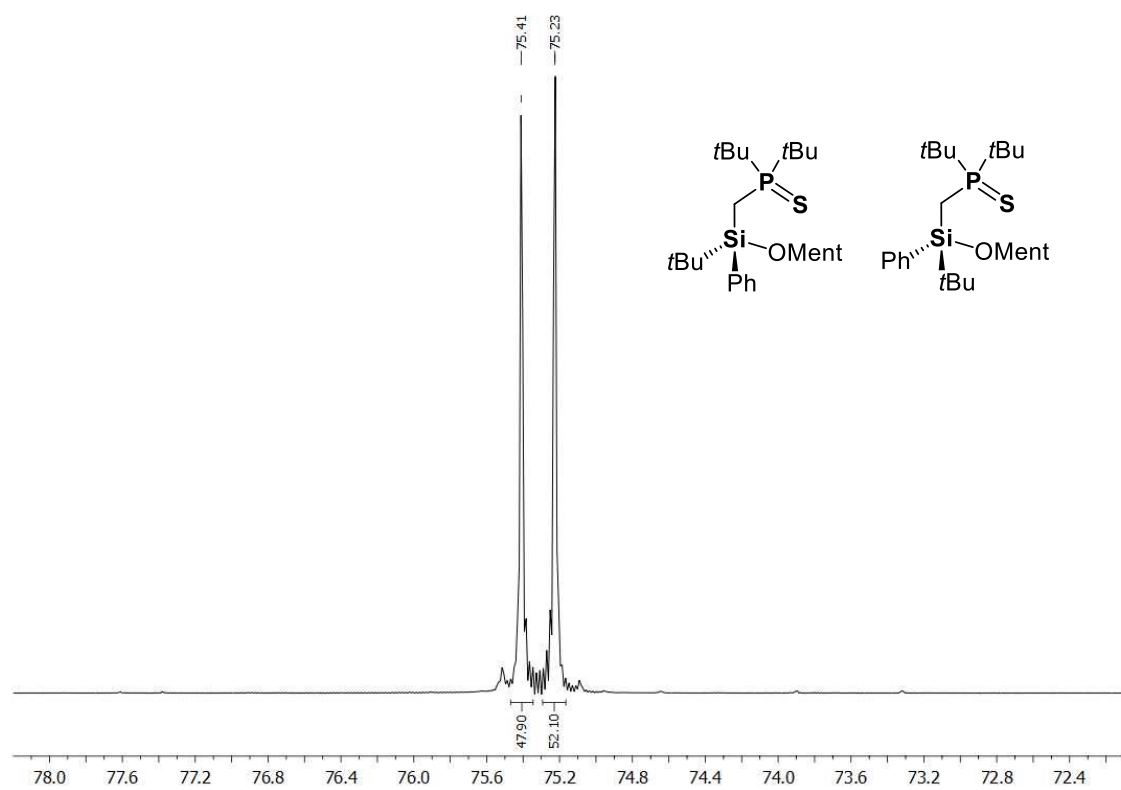
Figure S64. ^{31}P{^{1}H} NMR (C$_6$D$_6$, 298 K) of the mixture containing **4a** and **4b**.
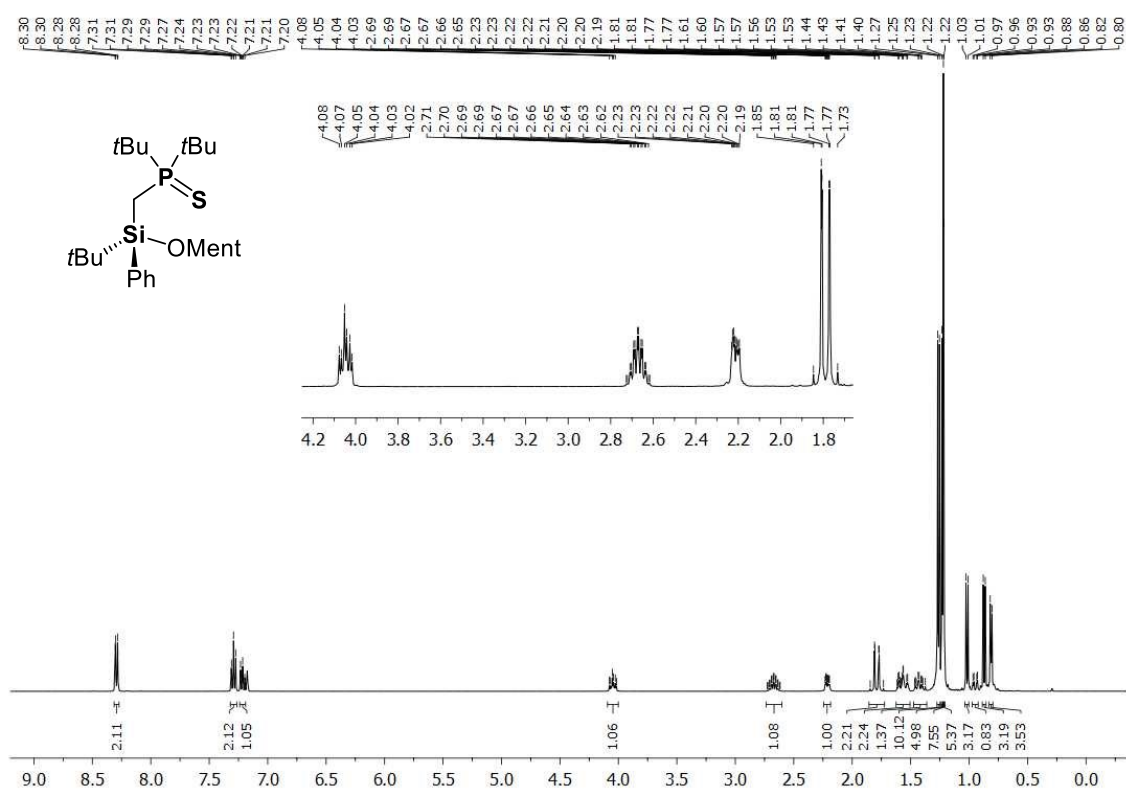
Figure S65. ^{1}H NMR (C$_6$D$_6$, 298 K) of compound **4a**.
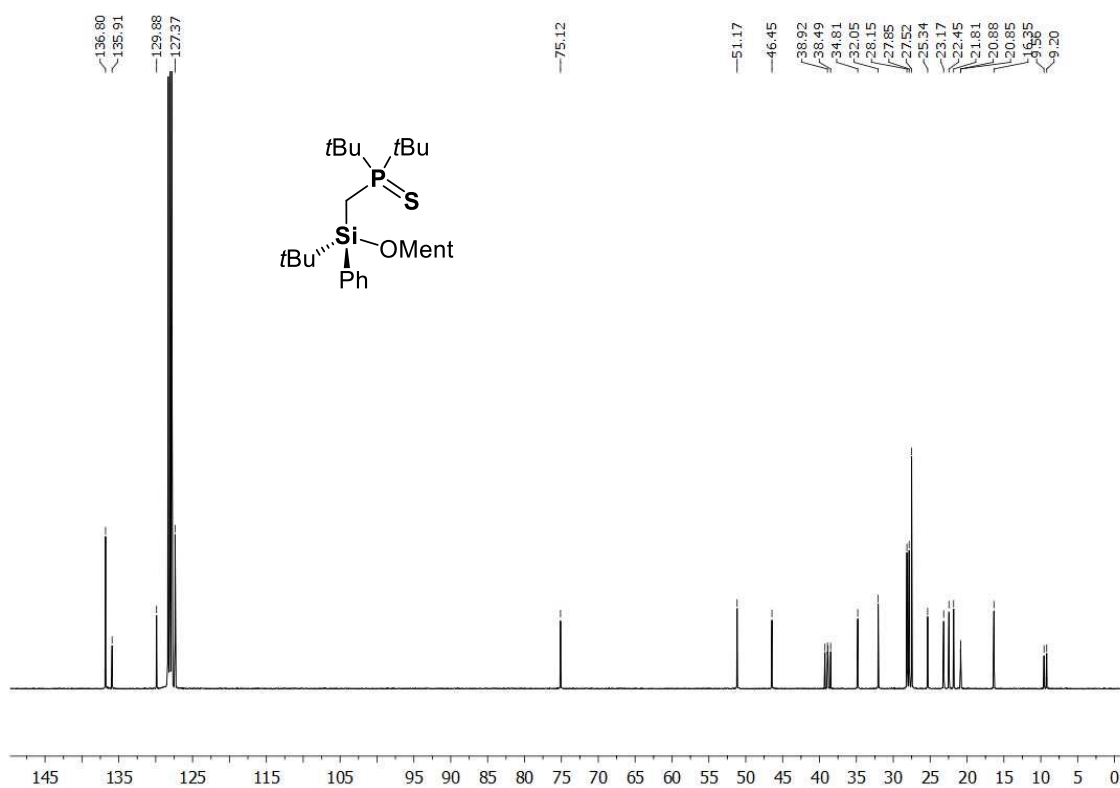
Figure S66. ^{13}C{^{1}H} NMR (C$_6$D$_6$, 298 K) of compound **4a**.
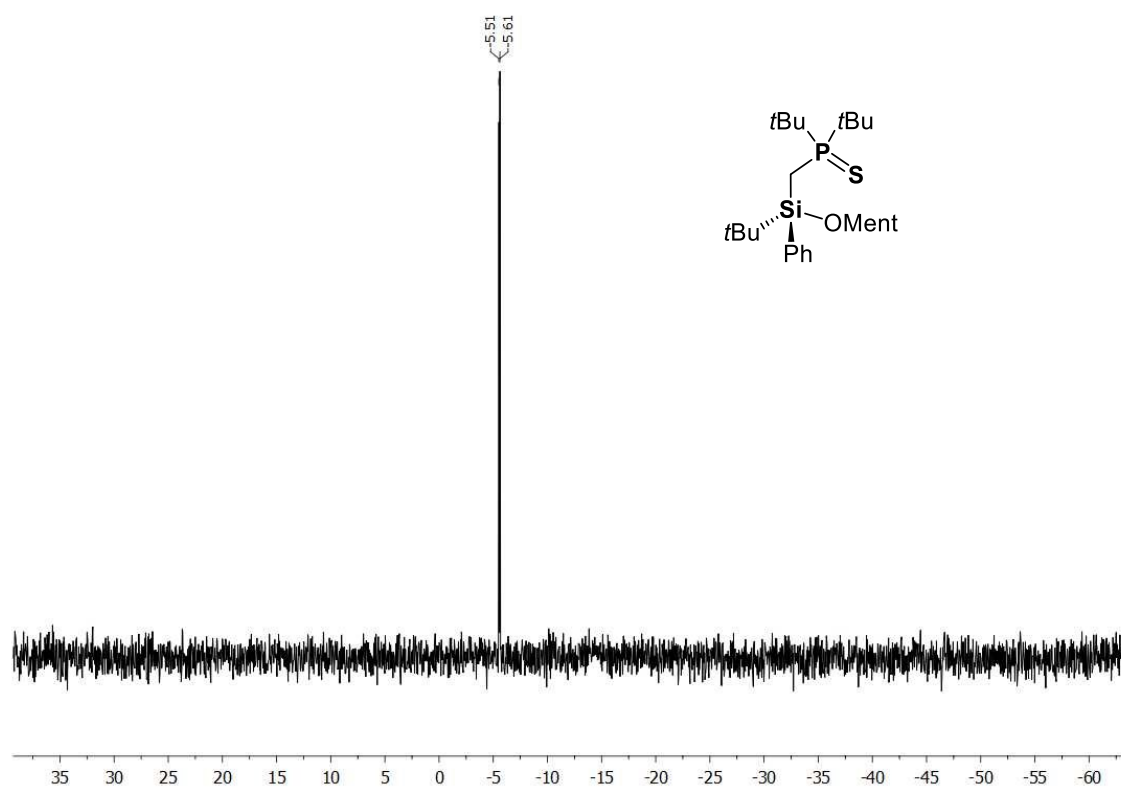
Figure S67. ^{29}Si{^{1}H} NMR (C$_6$D$_6$, 298 K) of compound **4a**.
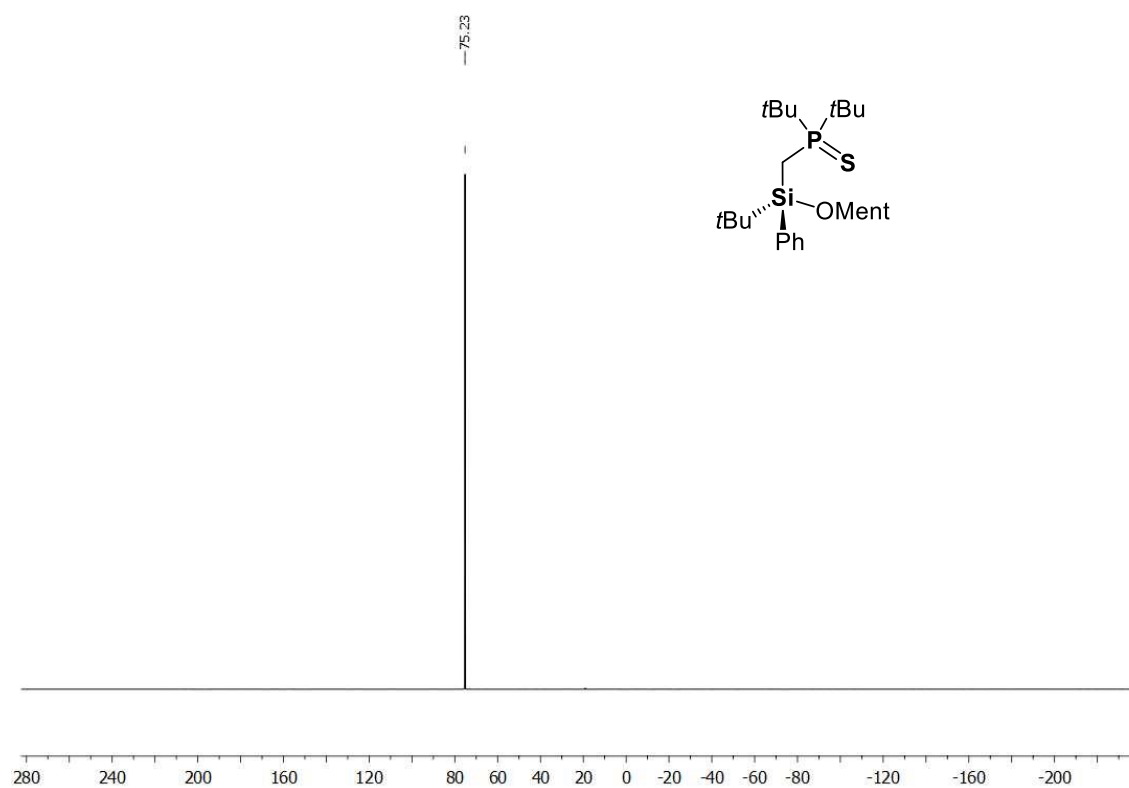
Figure S68. ^{31}P{^{1}H} NMR (C$_6$D$_6$, 298 K) of compound **4a**.
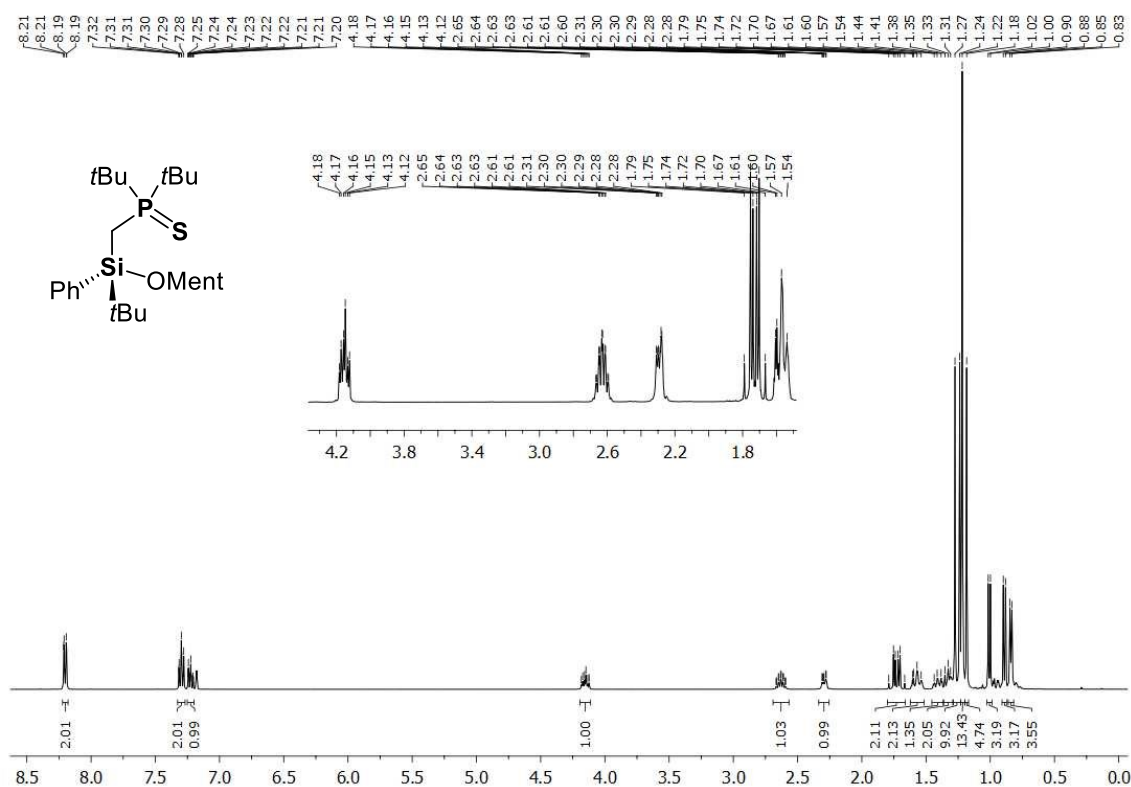
Figure S69. ^{1}H NMR (C$_6$D$_6$, 298 K) of compound **4b**.
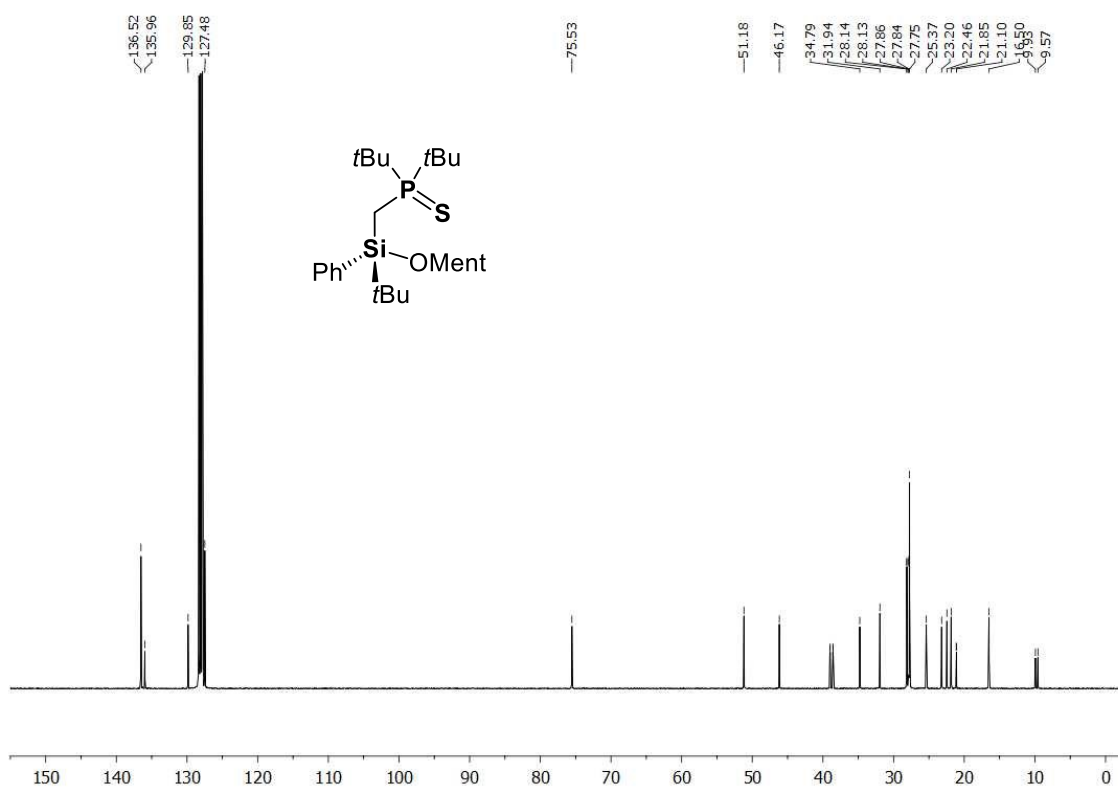
Figure S70. ^{13}C{^{1}H} NMR (C$_6$D$_6$, 298 K) of compound **4b**.
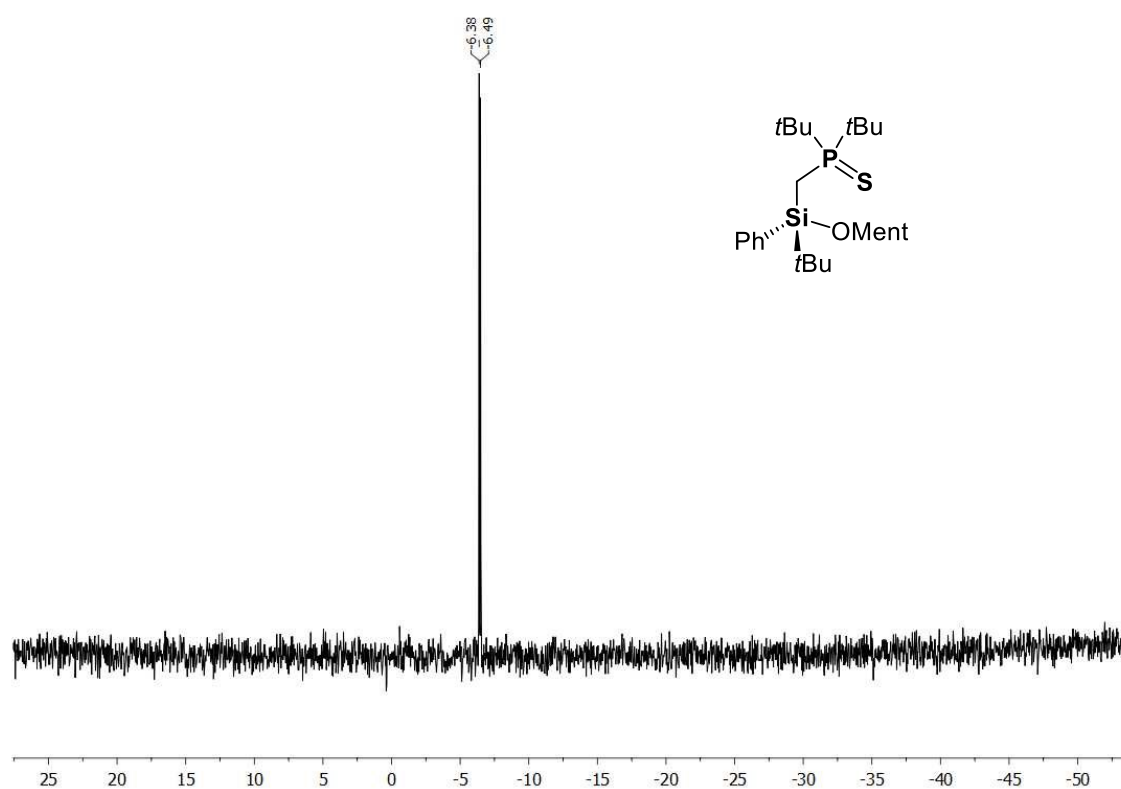
Figure S71. ^{29}Si{^{1}H} NMR (C$_6$D$_6$, 298 K) of compound **4b**.
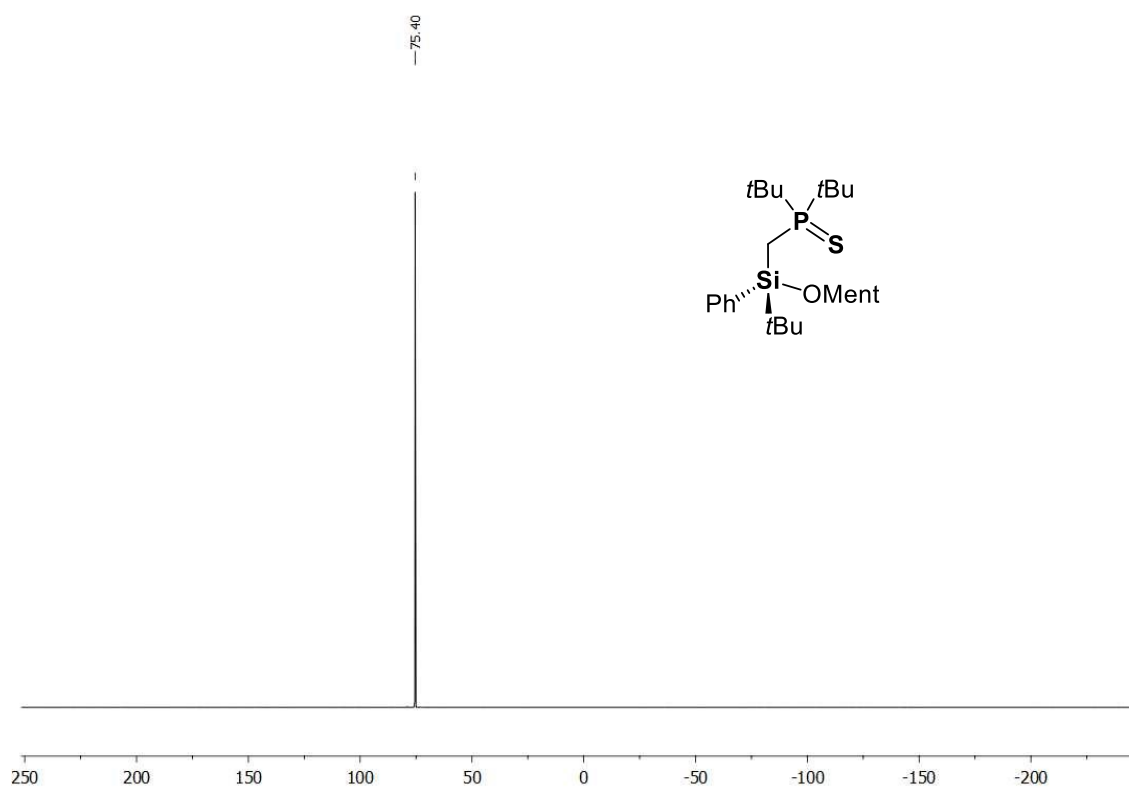
Figure S72. ^{31}P{^{1}H} NMR (C$_6$D$_6$, 298 K) of compound **4b**.

3.5.12 Synthesis of (^{Si}R)-(tBu)$_2$P(S)CH$_2$Si(H)PhtBu ((^{Si}R)-1)

4a: (^{Si}S), d.r. > 99:1   **Retention at Si** *   (^{Si}R)-**1**, 35%
e.r. = 98:2
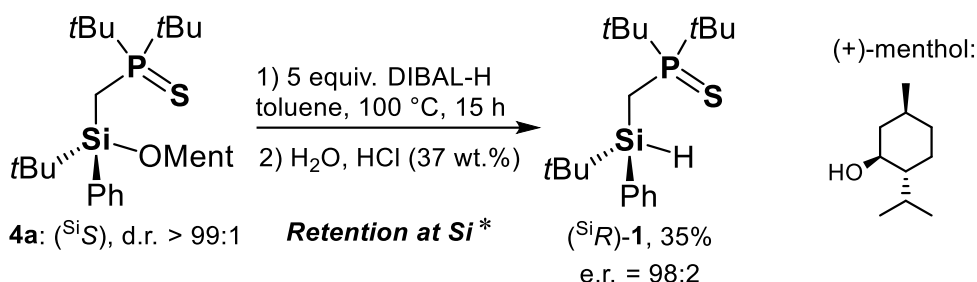
In a glovebox, compound **4a** (650 mg, 1.28 mmol, 1.0 equiv., d.r. > 99:1) was treated with a toluene solution of DIBAL-H (6.4 ml of a 1.0 M solution, 5.0 equiv.) at room temperature. The Schlenk flask containing the cloudy mixture was taken out of the glovebox and connected to a Schlenk line. The mixture was diluted to double its volume with toluene (6.4 ml) and warmed up to 100°C for 15 hours. Subsequently, the solution was cooled down to 0°C and carefully quenched with distilled water (10 mL) followed by concentrated HCl (37 wt.%, 0.8 ml) under vigorous stirring. The organic phase was removed by means of PTFE tubing and the aqueous phase was extracted with pentane (3 x 15 mL). The combined organic layers were collected, dried over MgSO$_4$ and all volatiles were removed in vacuum rendering a white solid. The crude product was fully dissolved in the minimum amount possible of pentane and precipitated by cooling down to -80°C. The mother-liquor was removed *via* suction filtration, the white precipitate washed with cold pentane (3 x 3 mL at -80°C) and dried in vacuum, affording the highly enantiomerically enriched silane (^{Si}R)-**1** as a white powder (157 mg, 35%, e.r. 98:2). Crystals suitable for X-ray diffraction analysis were obtained by slowly cooling down a pentane solution of (^{Si}R)-**1** to -35°C. The absolute configuration at silicon of (^{Si}R)-**1** was unequivocally determined by X-ray crystallographic analysis. The enantiomeric ratio of compound (^{Si}R)-**1** was determined by chiral HPLC.

HPLC-UV (Hexane/Isopropanol 99:1, flow of 0.9 mL^{-1}, 10 µl injected, 215 nm, 20°C): retention time = 8-12 min.
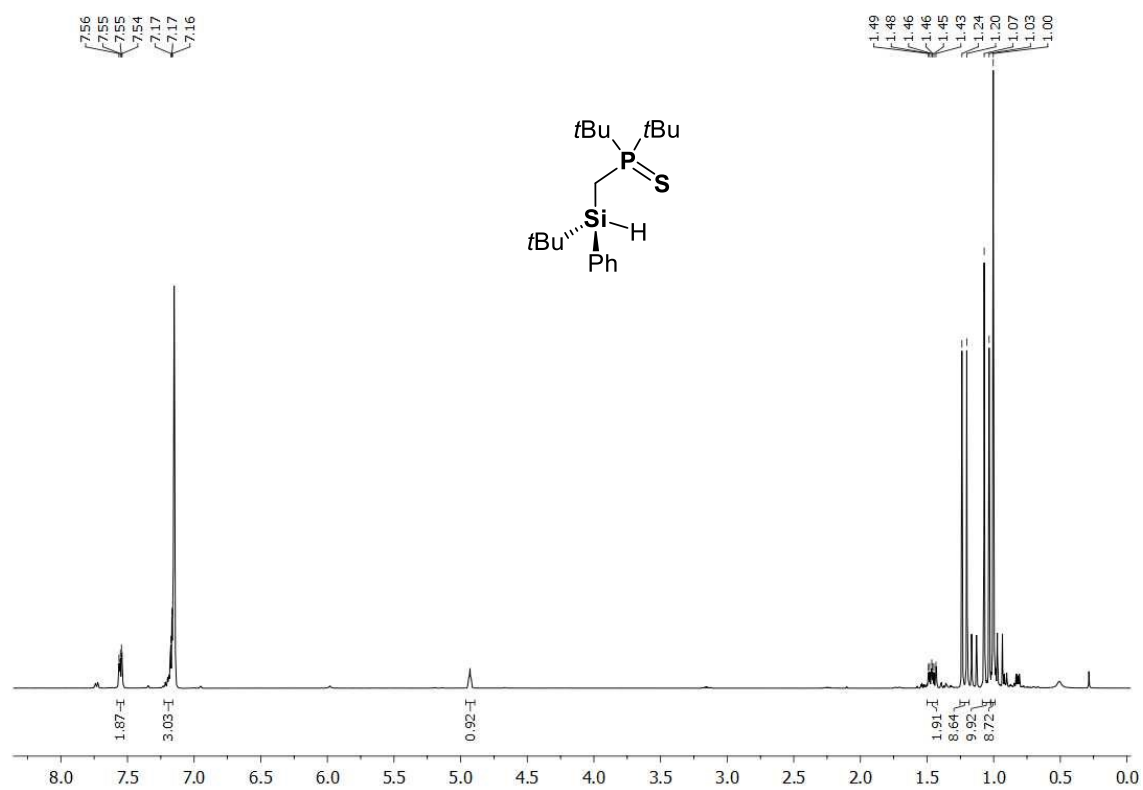
Figure S73. ^{1}H NMR (CD$_2$Cl$_2$, 298 K) of compound (^{Si}R)-**1**. Data are in accordance with (*rac*)-**1**.

3.5.13 Synthesis of (^{Si}S)-(tBu)$_2$P(S)CH$_2$Si(H)PhtBu ((^{Si}S)-1)

4b: (^{Si}R), d.r. > 99:1   *Retention at Si* *   (^{Si}S)-**1**, 62%
                                                              e.r. = 98:2
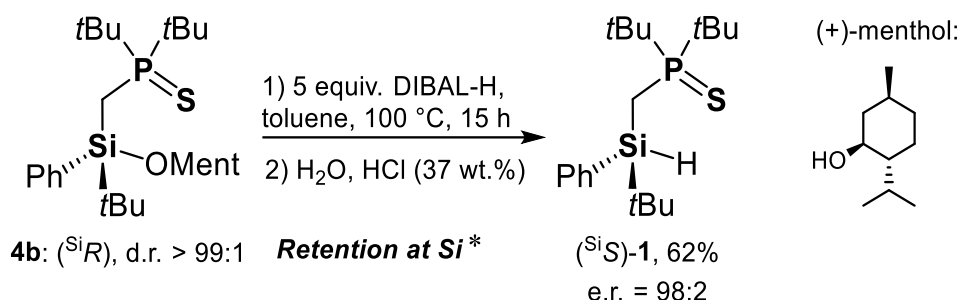
In a glovebox, compound **4b** (1.2 g, 2.36 mmol, d.r. >99:1, 1.0 equiv.) was treated with a toluene solution of DIBAL-H (12 ml of a 1.0 M solution, 5.0 equiv.) at room temperature. The Schlenk flask containing the cloudy mixture was taken out of the glovebox and connected to a Schlenk line. The mixture was diluted to double its volume with toluene (12 ml) and warmed up to 100°C for 15 hours. Subsequently, the solution was cooled down to 0°C and carefully quenched with distilled water (20 mL) followed by concentrated HCl (37 wt.%, 1.5 ml) under vigorous stirring. The organic phase was removed by means of PTFE tubing and the aqueous phase was extracted with pentane (3 x 20 mL). The combined organic layers were collected, dried over MgSO$_4$ and all volatiles were removed in vacuum rendering a white solid. The crude product was fully dissolved in the minimum amount of pentane and precipitated by cooling down to -80°C. The mother-liquor was removed *via* suction filtration, the white precipitate washed with cold pentane (3 x 5 mL at -80°C) and dried in vacuum, affording highly enantiomerically enriched silane (^{Si}S)-**1** as a white powder (521 mg, 62%, e.r. 98:2). **HPLC-UV** (Hexane/Isopropanol 99:1, flow of 0.9 mL^{-1}, 10 μl injected, 215 nm, 20°C): retention time = 14-17 min
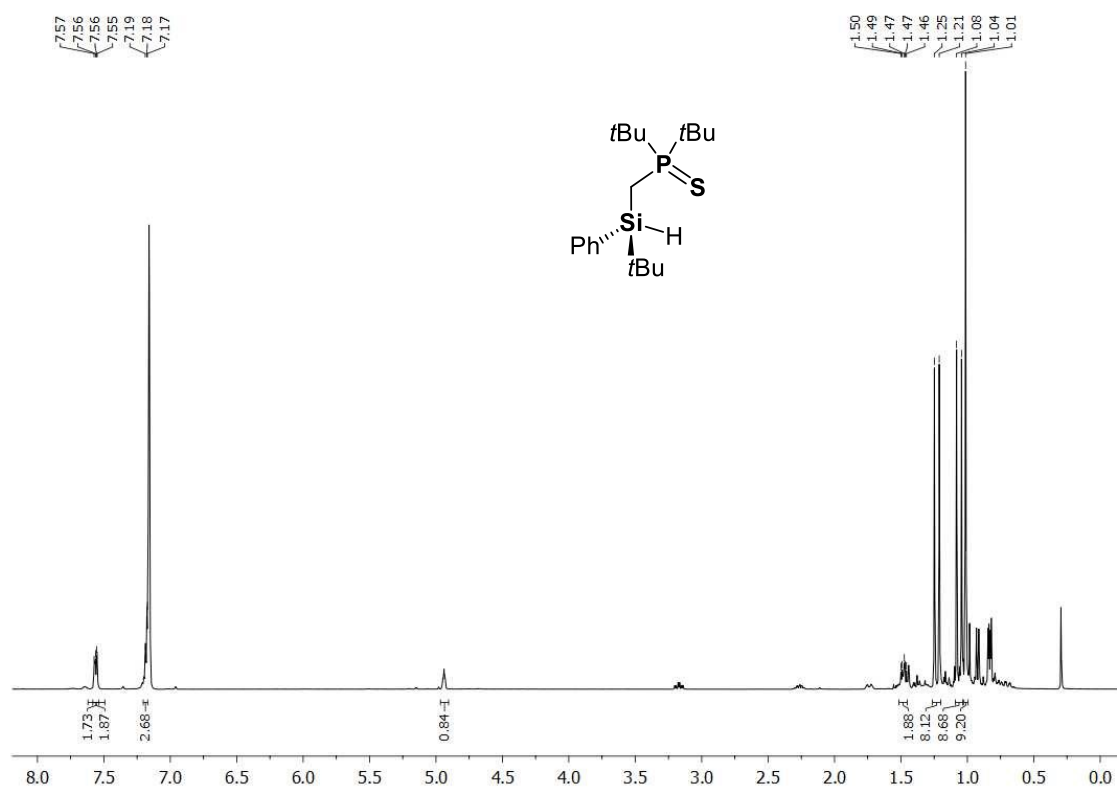
Figure S74. ^{1}H NMR (CD$_2$Cl$_2$, 298 K) of compound (^{Si}S)-**1**. Data are in accordance with (*rac*)-**1**.

3.5.14 Synthesis of (^{Si}R)-(*t*Bu)$_2$P(S)CH$_2$Si(F)Ph*t*Bu
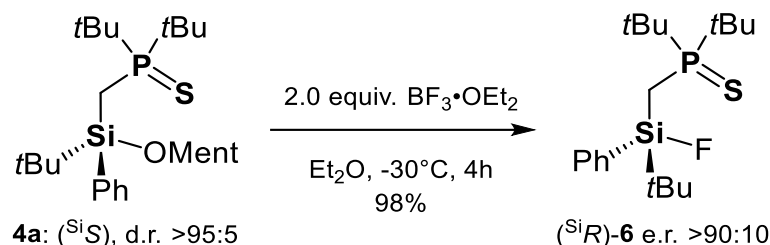
An oven dried Schlenk flask was charged with the (^{Si}S)-menthoxysilane (500 mg, 0.98 mmol, 1.0 eq. d.r. >95%). The compound was dissolved in ether (20 ml) and cooled down to -30°C. BF$_3$•OEt$_2$ (280 mg, 1.96 mmol, 2.0 eq.) was added *via* syringe. The solution was stirred at this temperature for four hours and afterwards dried in vacuum maintaining the temperature under -30°C. The crude mixture was purified by precipitation from cold pentane (-80°C) affording compound (^{Si}R)-**6** as a colourless powder (357 mg, 0.96 mmol, 98%, e.r. >90%). Crystals suitable for X-ray diffraction were grown from cold pentane. Only racemic crystals were obtained. Alternatively, a crude mixture obtained using 360 mg of (^{Si}S)-menthoxysilane and 1 g of BF$_3$•OEt$_2$ was purified *via* Kugelrohr sublimation (80-100°C oven temperature, 2.0*10^{-3} mbar). The racemized product was isolated as colourless crystals from cold pentane (145 mg, 0.40 mmol, 55%).

¹H NMR (400.30 MHz, CD₂Cl₂, 298 K): δ = 0.98 [s, 9H, SiC(CH_3)₃], 1.26 [d, $^3J_{P\text{-}H}$= 15.1 Hz, 9H, PC(CH_3)₃], 1.32 [d, $^3J_{P\text{-}H}$= 15.2 Hz, 9H, PC(CH_3)₃], 1.73 [dddd(ABXY), J= 11.18 Hz, J_2= 14.70 Hz, J_3= 29.05 Hz, J_4= 72.15 Hz, 2H, SiCH_2P], , 7.37-7.41 [m, 2H, H$_{Ph}$], 7.43-7.46 [m, 1H, H$_{Ph}$], 7.59-7.62 [m, 2H, H$_{Ph}$]. **¹³C{¹H} NMR** (100.61 MHz, CD₂Cl₂, 298 K): δ = 7.5 [dd, $^2J_{C\text{-}F}$= 10.6 Hz, $^1J_{C\text{-}P}$= 33.5 Hz, SiCH₂P], 19.6 [dd, $^3J_{C\text{-}P}$= 3.8 Hz, $^2J_{C\text{-}F}$= 14.1 Hz, SiC(CH₃)₃], 25.9 [s, SiC(CH_3)₃], 27.6 [dd, $^5J_{C\text{-}F}$= 1.8 Hz, $^2J_{C\text{-}P}$= 9.1 Hz, PC(CH_3)₃], 38.7 [dd, $^4J_{C\text{-}F}$= 13.8 Hz, $^1J_{C\text{-}P}$= 42.7 Hz, PC(CH₃)₃], 128.0 [d, meta-C$_{Ar}$], 130.4 [s, para-C$_{Ar}$], 133.4 [d, $^3J_{C\text{-}F}$= 14.1 Hz, ortho-C$_{Ar}$], 134.4 [d, $^1J_{C\text{-}F}$= 3.1 Hz, ipso-C$_{Ar}$]. **¹⁹F{¹H} NMR** (376.66 MHz, CD₂Cl₂, 298 K): δ = -175.2 [d, $^3J_{F\text{-}P}$= 299 Hz]. **²⁹Si NMR** (79.49 MHz, CD₂Cl₂, 298 K): δ = 10.0 [dd, $^1J_{Si\text{-}F}$= 300.0 Hz, $^2J_{Si\text{-}P}$= 9.4 Hz]. **³¹P NMR** (162.04 MHz, CD₂Cl₂, 298 K): δ = 75.9 [m, $^3J_{P\text{-}H}$= 15.1 Hz]. **CHN Analysis** C₁₉H₃₄FPSSi: calculated C 61.25%, H 9.20%, S 8.60%; found C 60.99%, H 8.97%, S 7.54%. **HR-MS (ESI)**, calcd. m/z for C₁₉H₃₄FPSSi [M+H]⁺:372.19; found: 373.1952.
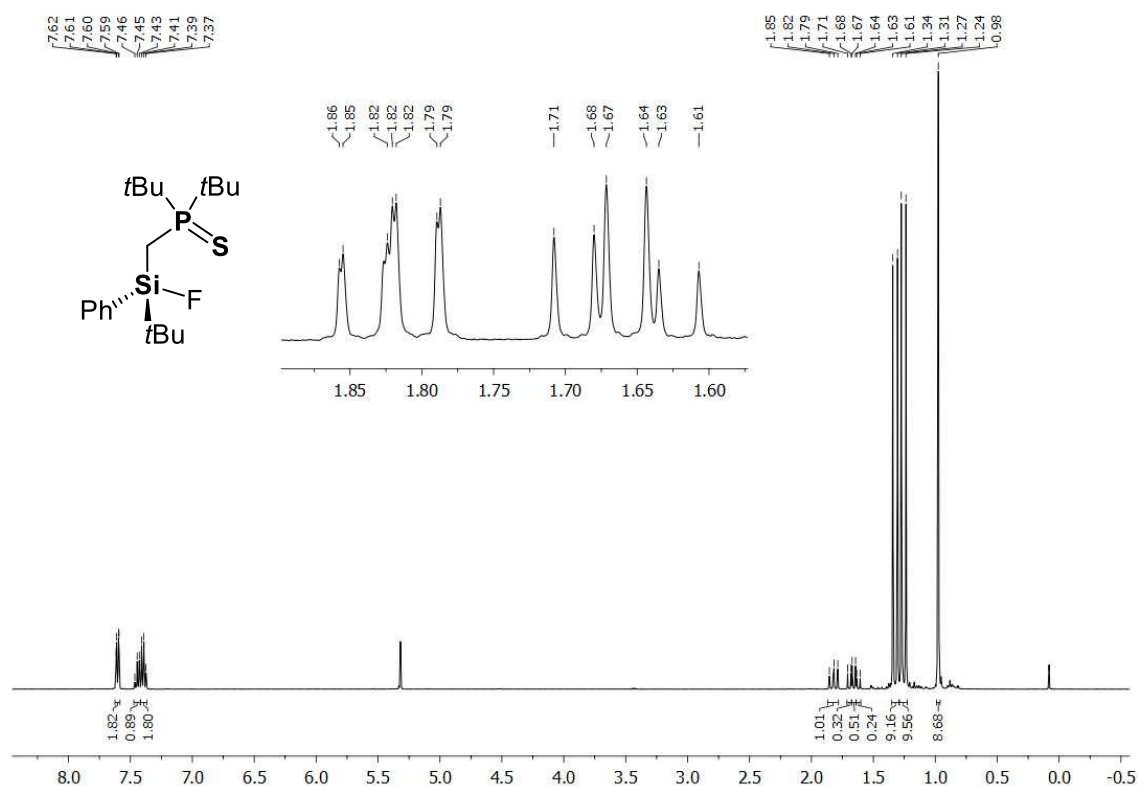
Figure S75. ¹H NMR (CD₂Cl₂, 298 K) of compound (^{Si}R)-**6**.
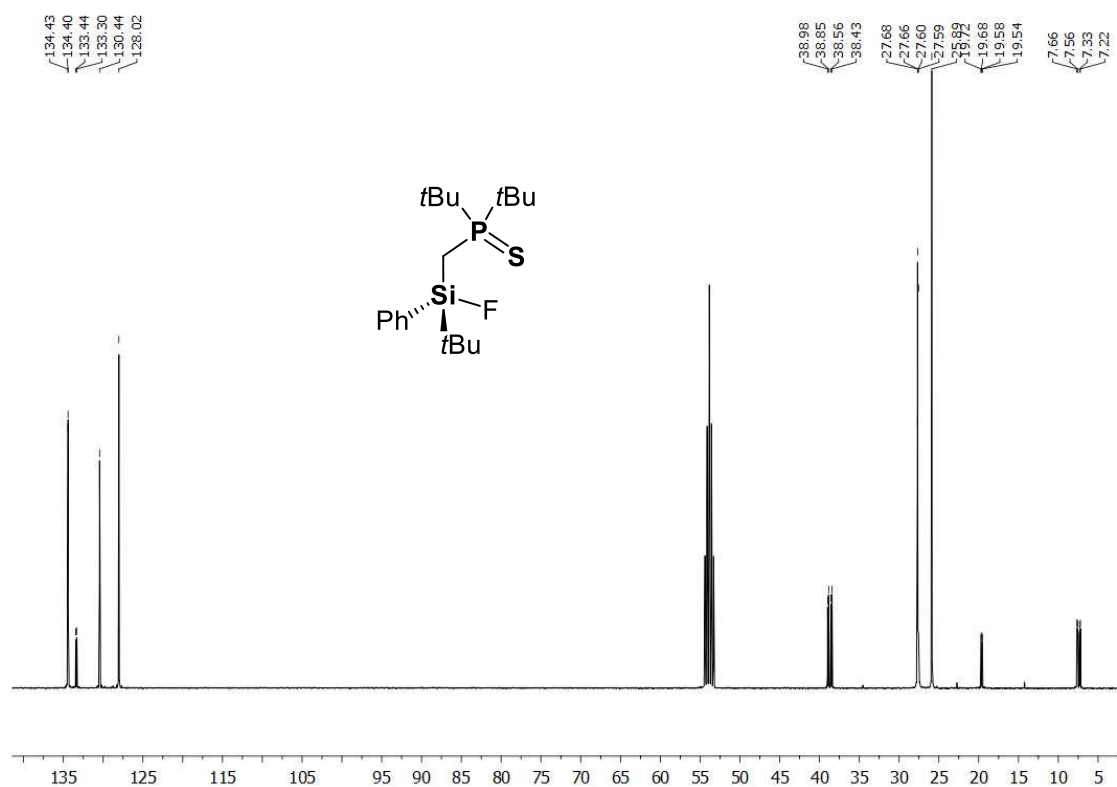
Figure S76. $^{13}C\{^1H\}$ NMR (CD$_2$Cl$_2$, 298 K) of compound (^{Si}R)-**6**.
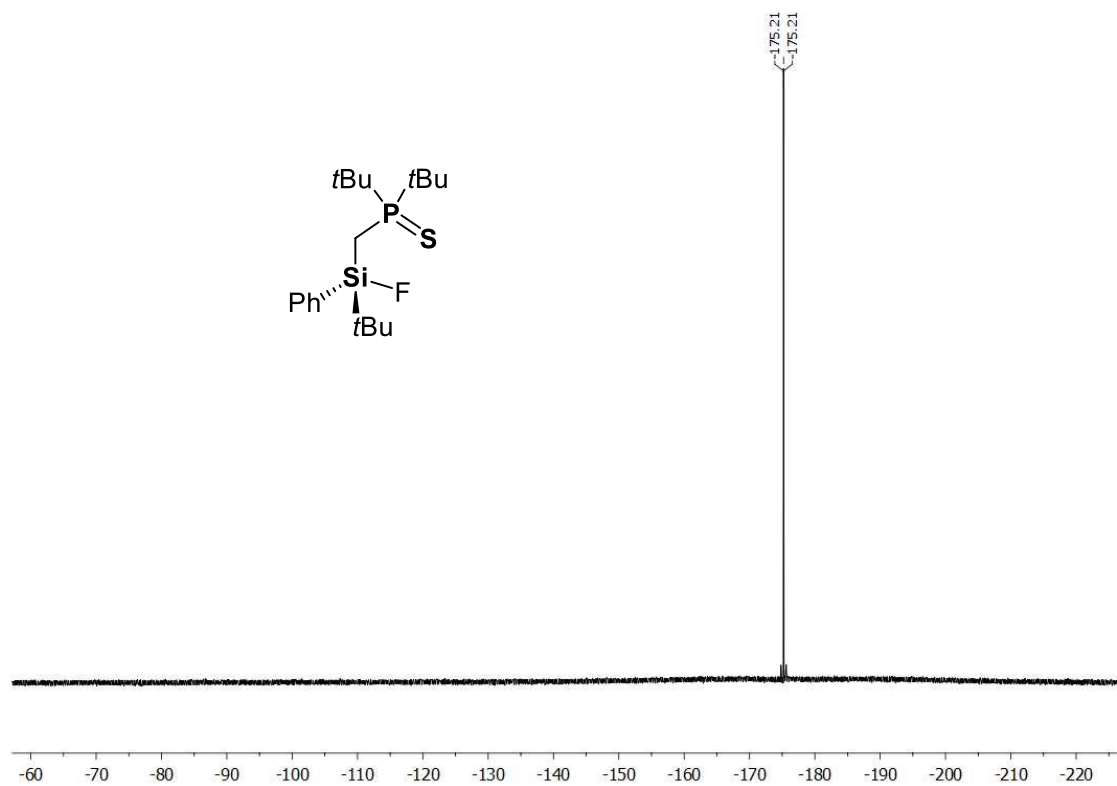
Figure S77. $^{19}F\{^1H\}$ NMR (CD$_2$Cl$_2$, 298 K) of compound (^{Si}R)-**6**.
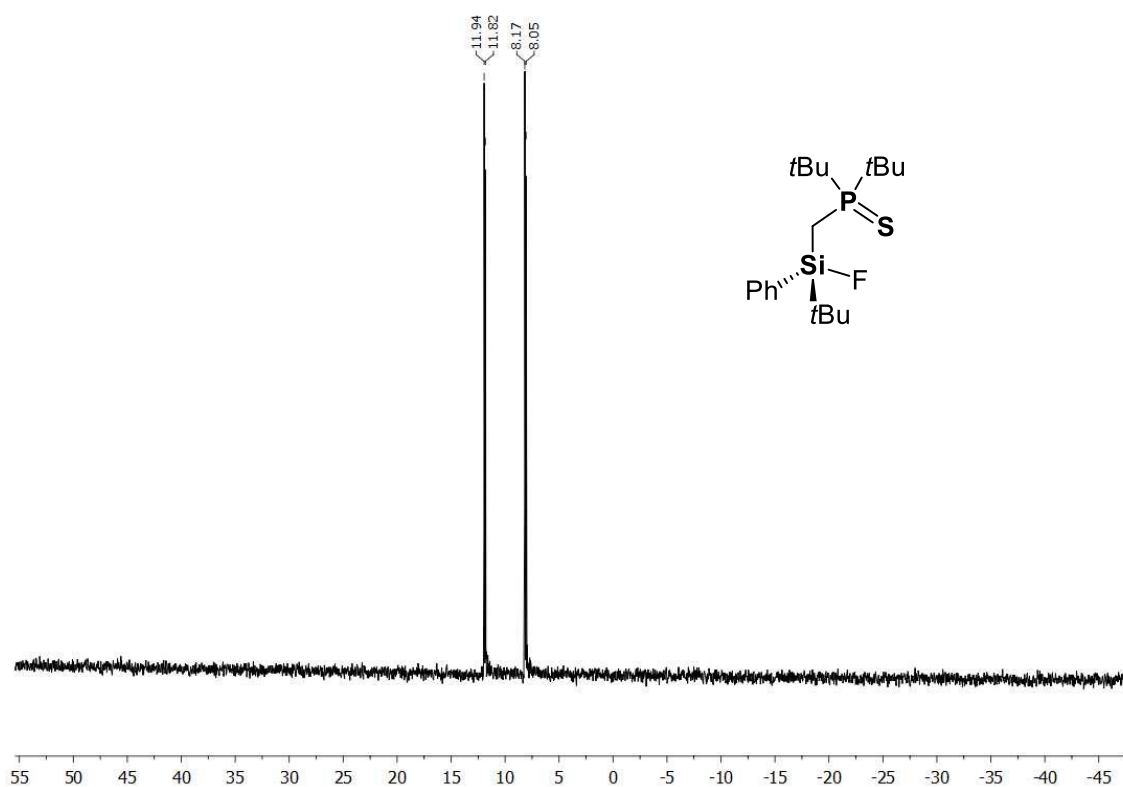
Figure S78. ^{29}Si {^{1}H} NMR (CD$_2$Cl$_2$, 298 K) of compound (^{Si}R)-**6**.
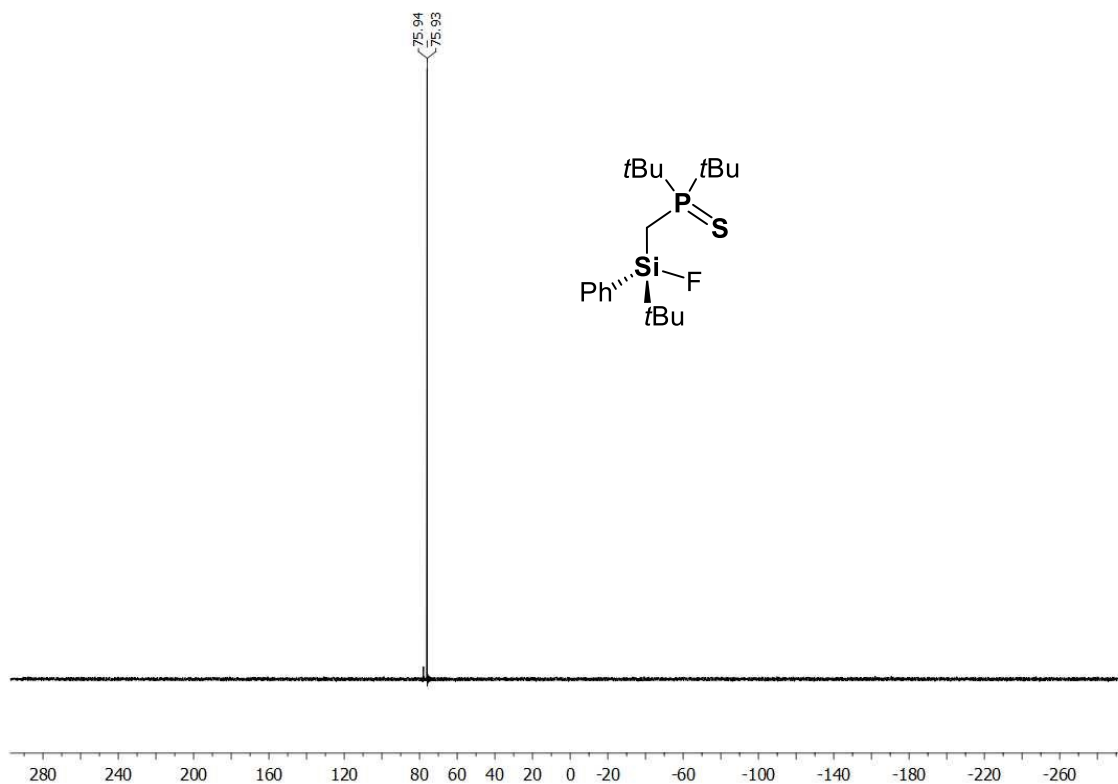
Figure S79. ^{31}P{^{1}H} NMR (CD$_2$Cl$_2$, 298 K) of compound (^{Si}R)-**6**.

3.5.15   Synthesis of (^{Si}R)-(^tBu)$_2$P(S)CH$_2$Si(H)Ph^{t}Bu

(^{Si}R)-**6**, e.r. >90:10 → (^{Si}R)-**1**, e.r. >90:10

1.1 equiv. LiAlH$_4$
Et$_2$O

-80°C to RT, 12h
86%

An oven dried Schlenk flask was charged with the (^{Si}R)-**6** (180 mg, 0.48 mmol, 1.0 equiv. e.r. >90%) and LiAlH$_4$ (20 mg, 0.53 mmol, 1.1 equiv.). The compounds were suspended in ether (10 ml) after cooling down the flask to -80°C. The mixture was stirred at this temperature for four hours and afterwards dried in vacuum. The residue was extracted three times with pentane (10 ml). The crude mixture was purified by precipitation from cold pentane (-80°C) affording compound (^{Si}R)-**1** as a colourless powder (147 mg, 0.42 mmol, 86%, e.r. >90%). Analytics were in accordance to the ones reported previously.

^{1}H NMR (400.13 MHz, C$_6$D$_6$, 298 K): δ =1.00 [s, 9H, SiC(CH_3)$_3$], 1.06 [d, $^3J_{P-H}$= 14.8 Hz, 9H, PC(CH_3)$_3$], 1.22 [d, $^3J_{P-H}$= 14.8 Hz, 9H, PC(CH_3)$_3$], 1.49-1.43 [m, 2H, SiCH_2P], 4.91 [m, 1H, SiH], 7.19-7.15 [m, 3H, H_{Ph}], 7.56-1.54 [m, 2H, H_{Ph}].

Chromatogram of (^{Si}R)-**1** from (^{Si}R)-**6**
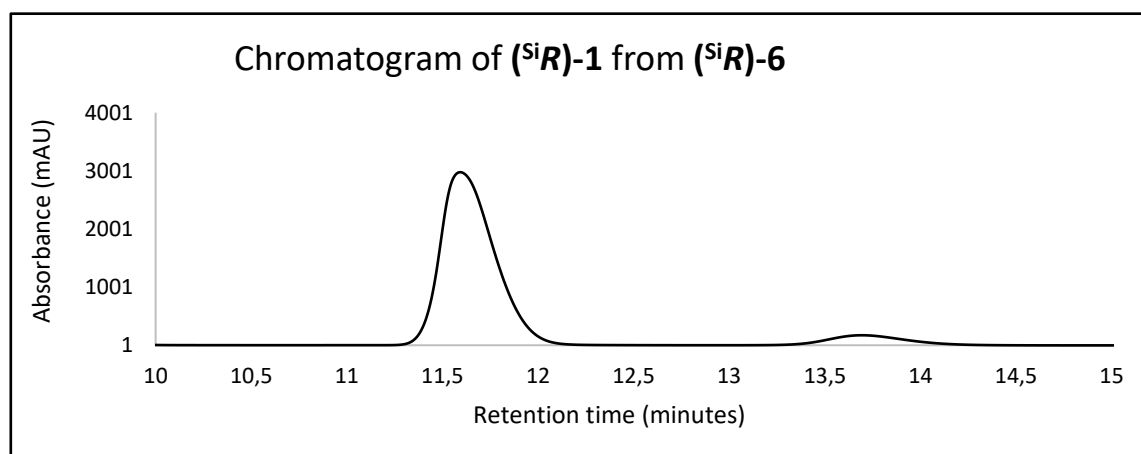
Retention time (Min)	Area	Area %
11.6	146476.58	92.2
13.7	12438.05	7.8

3.5.16 Synthesis of (*rac*)-(*t*Bu)$_2$P(S)CH$_2$Si(D)Ph*t*Bu ((*rac*)-1-*d*)

(*rac*)-**1**   1) 1.0 equiv. [H(OEt$_2$)$_2$][B(C$_6$F$_5$)$_4$] CH$_2$Cl$_2$, RT, 1 h   2) 150 °C, vacuum, 2 h   3) 1.0 equiv. NaBD$_4$, Et$_2$O RT, 15h   22%   (*rac*)-**1**-*d*
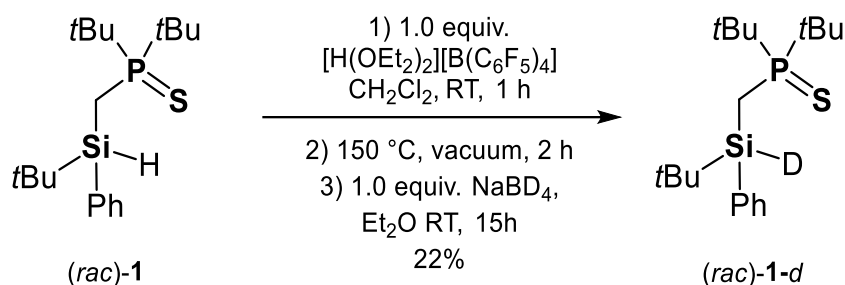
In an oven dried Schlenk flask, compound (*rac*)-**1** (500 mg, 1.41 mmol, 1.0 equiv.) and [H(OEt$_2$)$_2$][B(C$_6$F$_5$)$_4$] (1.17 g, 1.41 mmol, 1.0 equiv.) were dissolved in dichloromethane (10 ml) at room temperature and stirred for one hour. Following, the solvent was gently removed in vacuum rendering a foamy solid. This residue was heated up to 150°C in vacuum for two hours during which small bubbles developed. After cooling down the viscous solid, washings with pentane (3 x 10 mL) were performed to remove the traces of starting material. The residue was then dried, dissolved in diethyl ether (10 mL) and added to a suspension of NaBD$_4$ (1 eq, 59 mg, 1,41 mmol, 1.0 equiv.) in the same solvent (5 mL) at room temperature. The mixture was stirred for 15 hours and then dried in vacuum. The residue was extracted with pentane (3 x 10 mL) rendering a white solid which was further purified *via* Kugelrohr distillation (130°C, 1*10^{-3} mbar). Compound (*rac*)-**1**-*d* was isolated as a white microcrystalline solid (110 mg, 0.31 mmol, 22%).

¹H NMR (400.13 MHz, CD$_2$Cl$_2$, 298 K): δ =0.81 [s, 9H, SiC(C*H*$_3$)$_3$], 0.87 [d, $^3J_{P-H}$= 14.9 Hz, 9H, PC(C*H*$_3$)$_3$], 1.04 [d, $^3J_{P-H}$= 14.6 Hz, 9H, PC(C*H*$_3$)$_3$], 1.25-1.30 [m, 2H, SiC*H*$_2$P], 6.98 [m, 3H, *H*$_{ar}$], 7.36 [m, 2H, *H*$_{ar}$]. **²H NMR** (61.42 MHz, CH$_2$Cl$_2$, 298 K): δ =4.57 [bs, Si*D*]. **¹³C{¹H} NMR** (100.61 MHz, CD$_2$Cl$_2$, 298 K): δ = 5.0 [d, $^1J_{C-P}$= 32.2 Hz, Si*C*H$_2$P], 17.6 [d, $^3J_{C-P}$= 3.7 Hz, Si*C*(CH$_3$)$_3$], 27.5 [s, SiC(*C*H$_3$)$_3$], 27.63 [bs, PC(*C*H$_3$)$_3$], 38.2 [d, $^1J_{C-P}$= 42.3 Hz, P*C*(CH$_3$)$_3$], 38.8 [d, $^1J_{C-P}$= 42.3 Hz, P*C*(CH$_3$)$_3$], 128.1 [s, C$_{meta}$], 129.7 [s, C$_{para}$], 135.1 [s C$_{ipso}$], 135.7 [s, C$_{ortho}$]. **²⁹Si{¹H} NMR** (79.49 MHz, CD$_2$Cl$_2$, 298 K): δ = 5.1 [dt, $^1J_{Si-D}$= 32.5 Hz, $^2J_{Si-P}$= 6.8 Hz]. **³¹P{¹H} NMR** (161.98 MHz, CD$_2$Cl$_2$, 298 K): δ = 75.2.
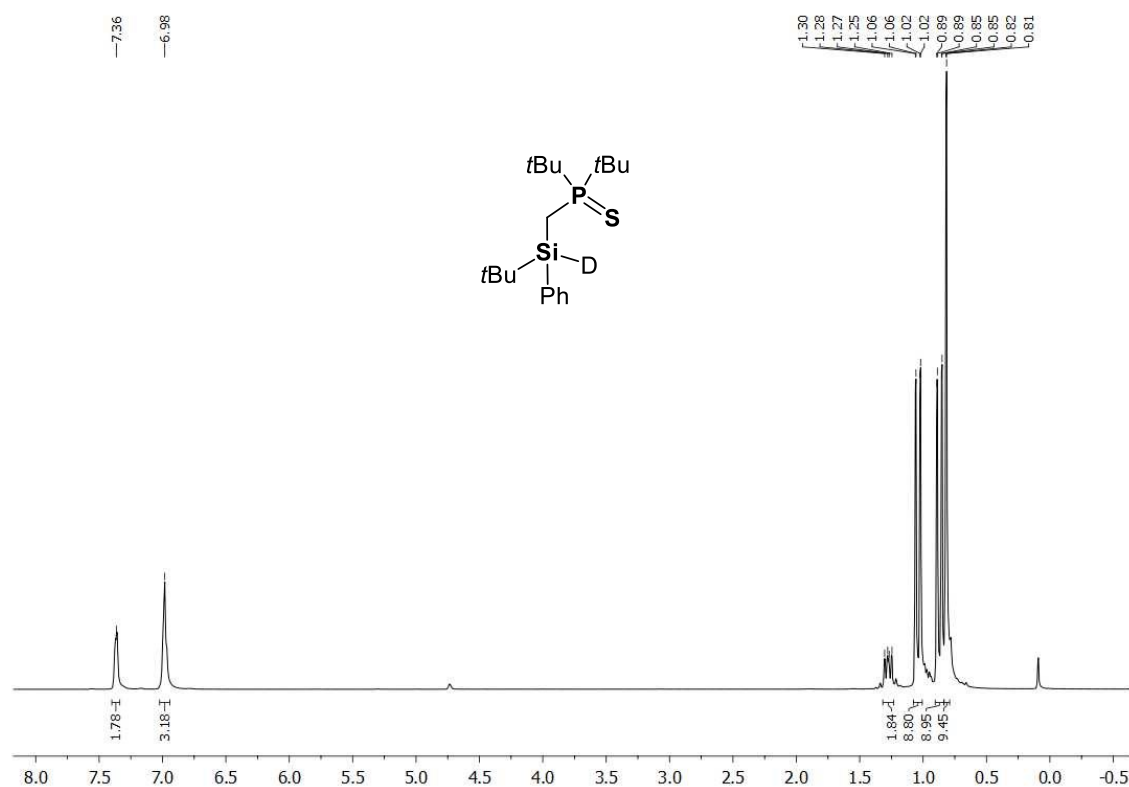
Figure S80. ^{1}H NMR (CD$_2$Cl$_2$, 298 K) of compound (*rac*)-**1**-*d*.
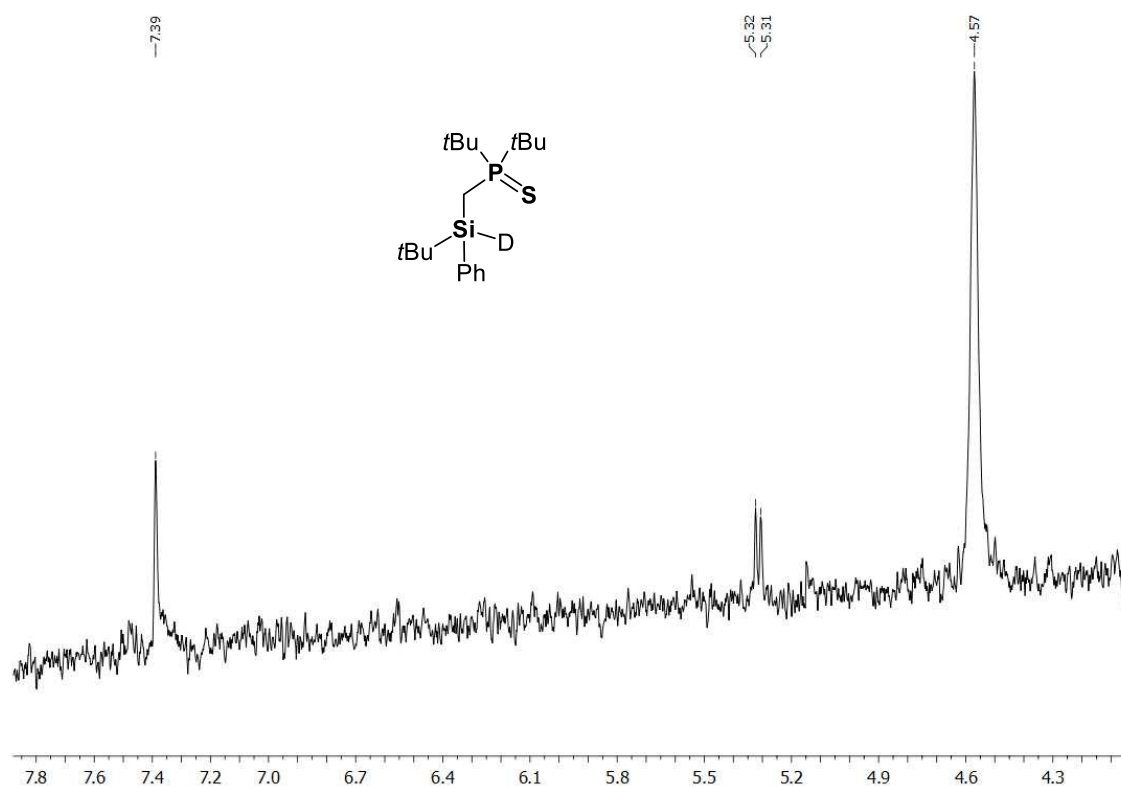
Figure S81. ^{2}H NMR (CH$_2$Cl$_2$, 298 K) of compound (*rac*)-**1**-*d* (CD$_2$Cl$_2$ and C$_6$D$_6$ were used as internal references).
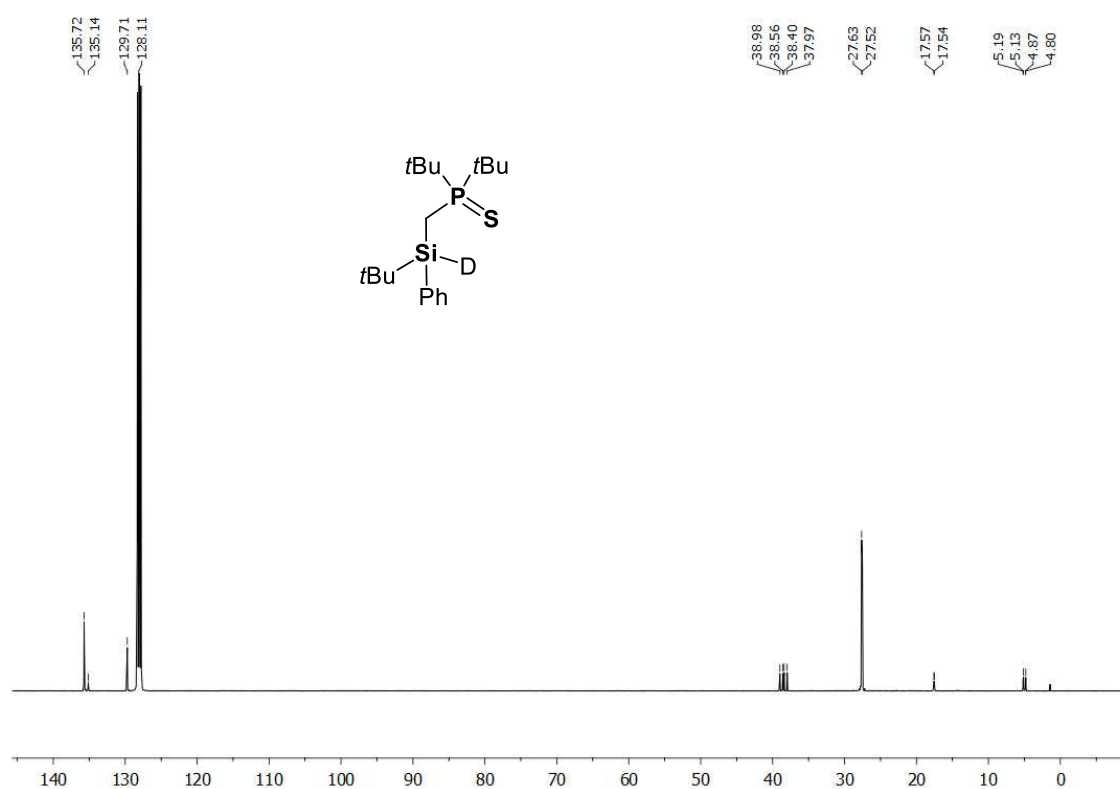
Figure S82. $^{13}C\{^1H\}$ NMR (CD$_2$Cl$_2$, 298 K) of compound (*rac*)-**1**-*d*.
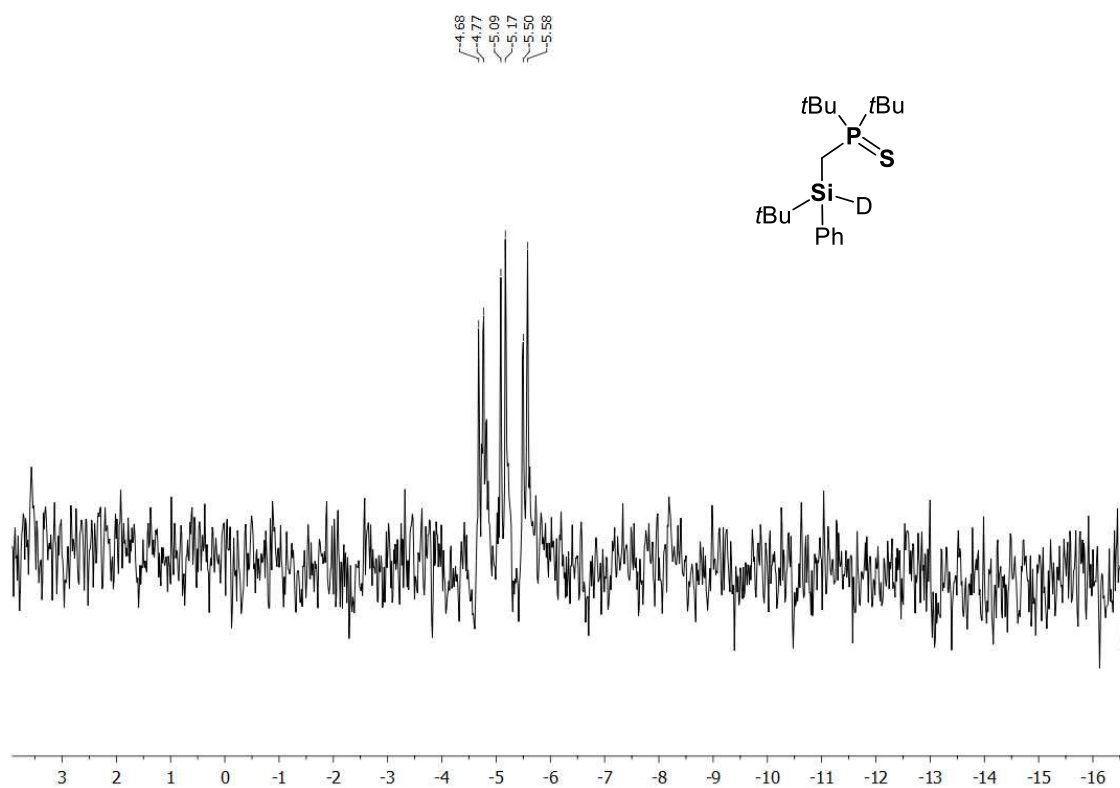
Figure S83. $^{29}Si\{^1H\}$ NMR (CD$_2$Cl$_2$, 298 K) of compound (*rac*)-**1**-*d*.
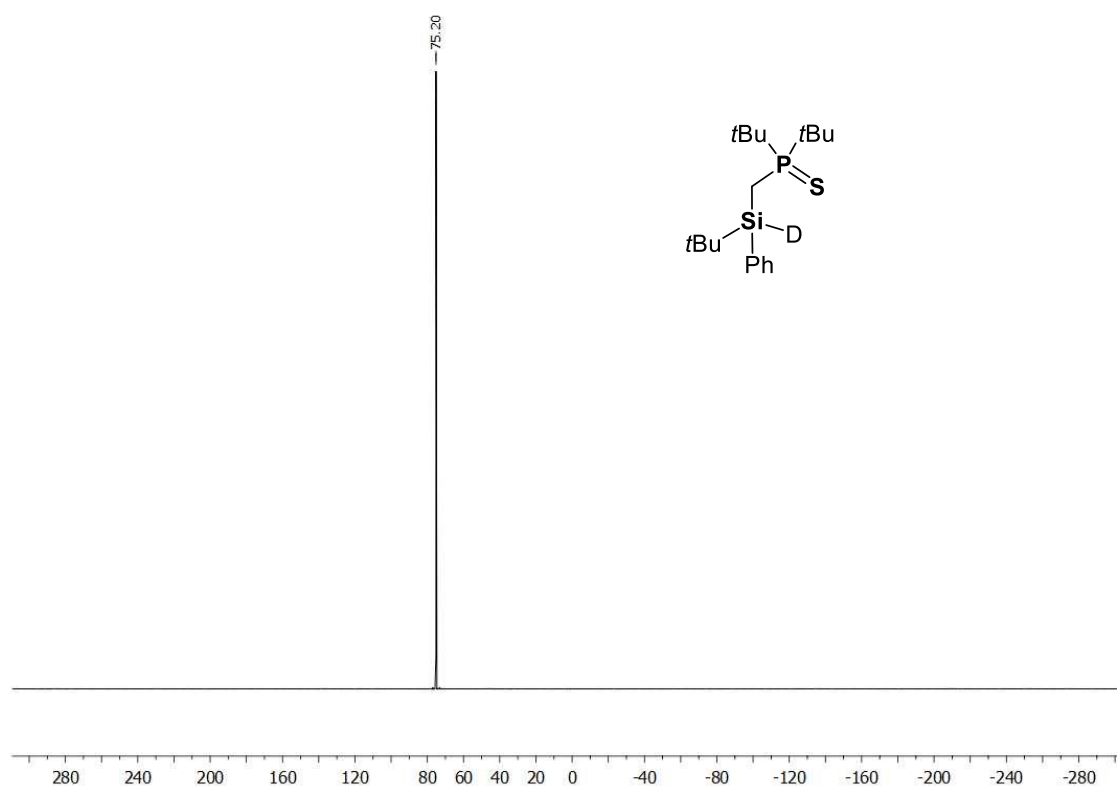
Figure S84. $^{31}P\{^1H\}$ NMR (CD$_2$Cl$_2$, 298 K) of compound (*rac*)-**1**-*d*.

3.5.17   Synthesis of (*rac*)-[(*t*Bu)₂P(SD)CH₂Si(D)Ph*t*Bu][B(C₆F₅)₄] ((*rac*)-3-*d₂*)
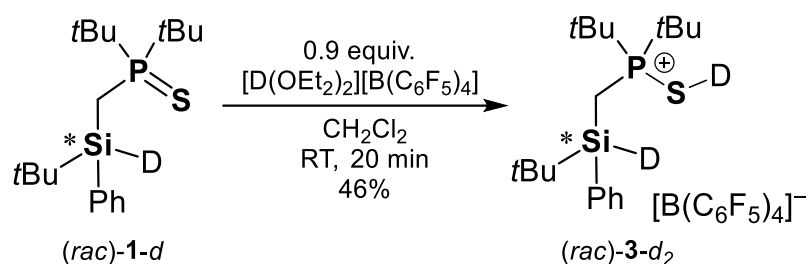
In a glovebox, an oven dried Schlenk flask was charged with (*rac*)-**1**-*d* (50 mg, 0.14 mmol, 1.0 equiv.) and [D(OEt₂)₂][B(C₆F₅)₄] (105 mg, 0.13 mmol, 0.9 equiv.). The Schlenk flask containing the solids was taken out of the glovebox, connected to a Schlenk line and dichloromethane (5 ml) was added at room temperature. After stirring for 20 minutes, the solvent was removed in vacuum and the residue washed with pentane (2 x 5 ml). The remaining white solid was dried in vacuum yielding pure (*rac*)-**3**-*d₂* (67 mg, 0.065 mmol, 46%) as a colourless solid.

¹H NMR (400.32 MHz, CD₂Cl₂, 298 K): δ = 0.98 [s, 9H, SiC(C*H₃*)₃], 1.23 [d, $^3J_{\text{P-H}}$= 15.6 Hz, 9H, PC(C*H₃*)₃], 1.39 [d, $^3J_{\text{P-H}}$= 15.4 Hz, 9H, PC(C*H₃*)₃], 1.54-1.70 [m, 2H, SiC*H₂*P], 7.36-7.45 [m, 3H, *H*ar], 7.57-7.59 [m, 2H, *H*ar]. **²H NMR** (61.42 MHz, CH₂Cl₂, 298 K): δ = 4.59 **¹¹B{¹H} NMR** (128.43 MHz, CD₂Cl₂, 298 K): δ = 16.9. **¹³C{¹H} NMR** (100.66 MHz, CD₂Cl₂, 298 K): δ = 3.8 [d, $^1J_{\text{C-P}}$ = 32.4 Hz, SiC*H₂*P], 17.8 [d, $^3J_{\text{C-P}}$ = 4.4 Hz, SiC(CH₃)₃], 27.2 [s, SiC (*CH₃*)₃], 27.5 [d, $^2J_{\text{C-P}}$ = 1.4 Hz, PC(*CH₃*)₃], 27.6 [d, $^2J_{\text{C-P}}$ = 1.4 Hz, PC(*CH₃*)₃], 38.6 [d, $^1J_{\text{C-P}}$ = 39.9 Hz, P*C*(CH₃)₃], 39.2 [d, $^1J_{\text{C-P}}$ = 40.2 Hz, P*C*(CH₃)₃], 130.2, 134.05, 135.7, 139.0 [bd, $^1J_{\text{C-F}}$= 190.6 Hz, *para*-*C*Ar-borate], 148.6 [bd, $^1J_{\text{C-F}}$= 241.3 Hz, *ortho*-*C*Ar-borate]. **¹⁹F{¹H} NMR** (376.66 MHz, CD₂Cl₂, 298 K): δ = -167.4 [bt, $^3J_{\text{F-F}}$ = 17.1, 8F, *meta*-*F*Ar-borate], -163.6 [t, $^3J_{\text{F-F}}$= 20.4 Hz 4F, *para*-*F*Ar-borate], -132.9 [bs, 8F, *ortho*-*F*Ar-borate]. **²⁹Si{¹H} NMR** (79.49 MHz, CD₂Cl₂, 298 K): δ = -2.89 [dt, $^1J_{\text{Si-D}}$= 32.2 Hz $^2J_{\text{Si-P}}$= 7.1 Hz]. **³¹P{¹H} NMR** (162.04 MHz, CD₂Cl₂, 298 K): δ = 80.2.
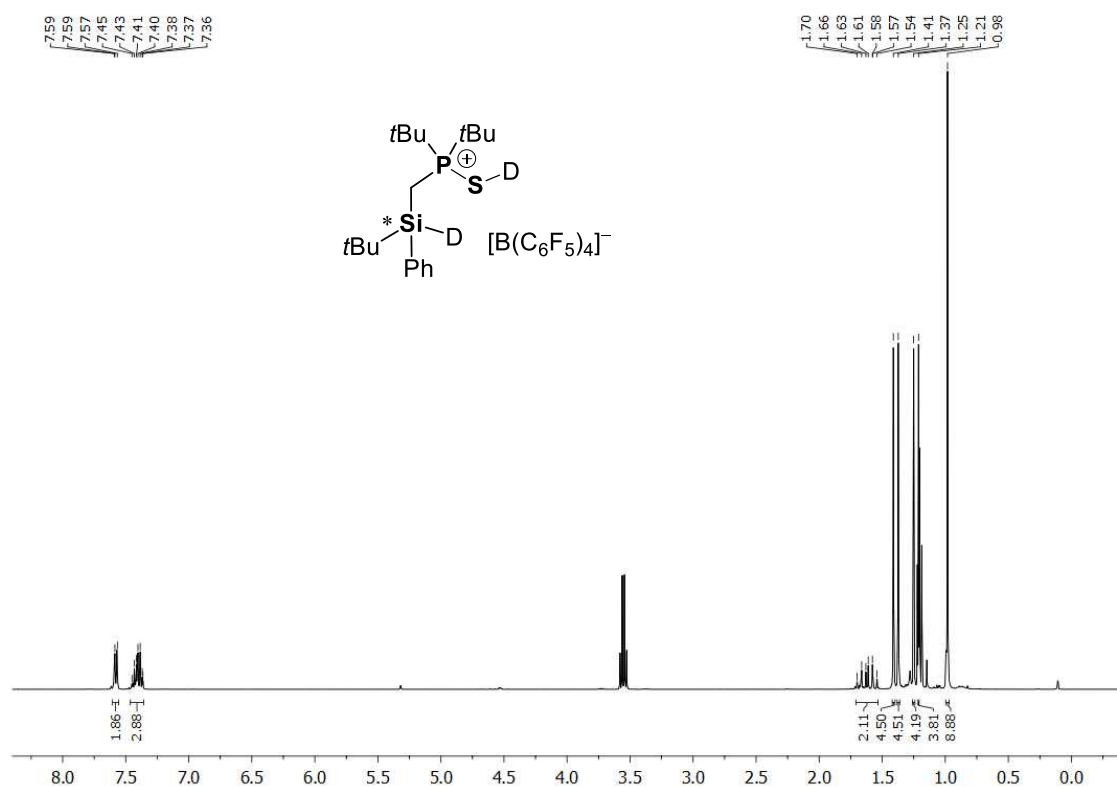
Figure S85. ^{1}H NMR (CD$_2$Cl$_2$, 298 K) of compound (*rac*)-**3**-*d*$_2$. Signals of diethyl ether are due to the use of the etherate reagent.
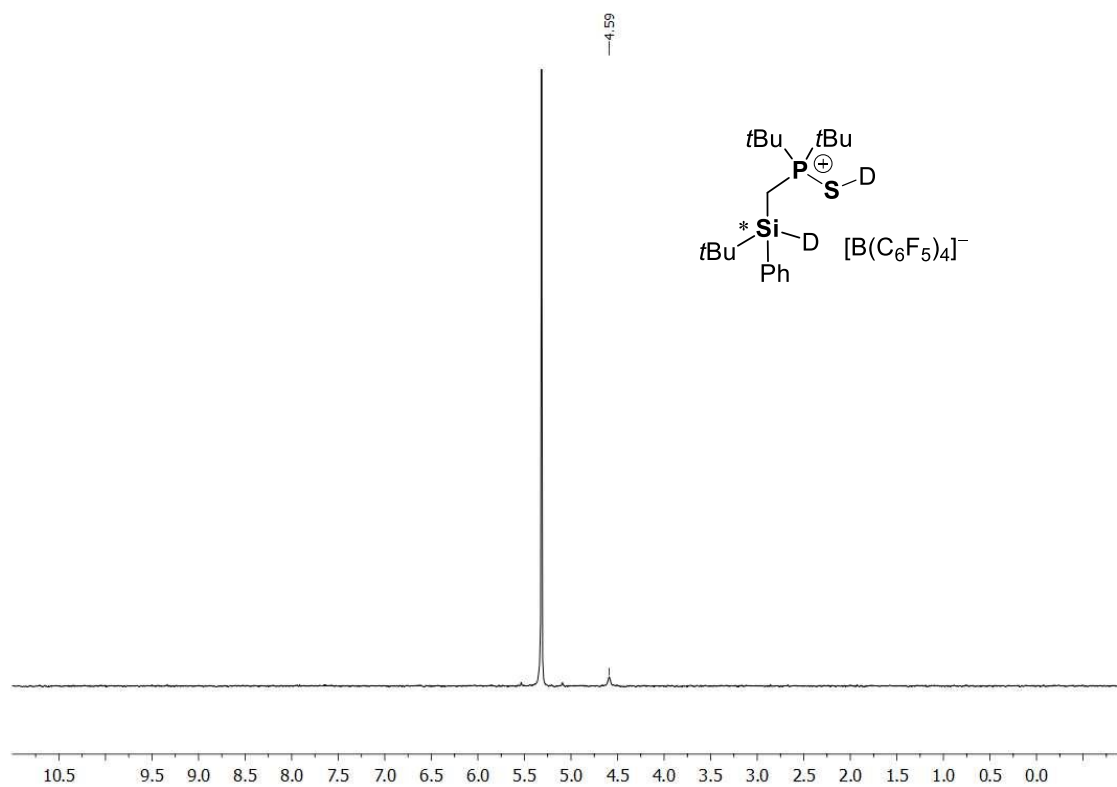
Figure S86. ^{2}H NMR (CH$_2$Cl$_2$, 298 K) of compound (*rac*)-**3**-*d*$_2$ using CD$_2$Cl$_2$ as internal standard.
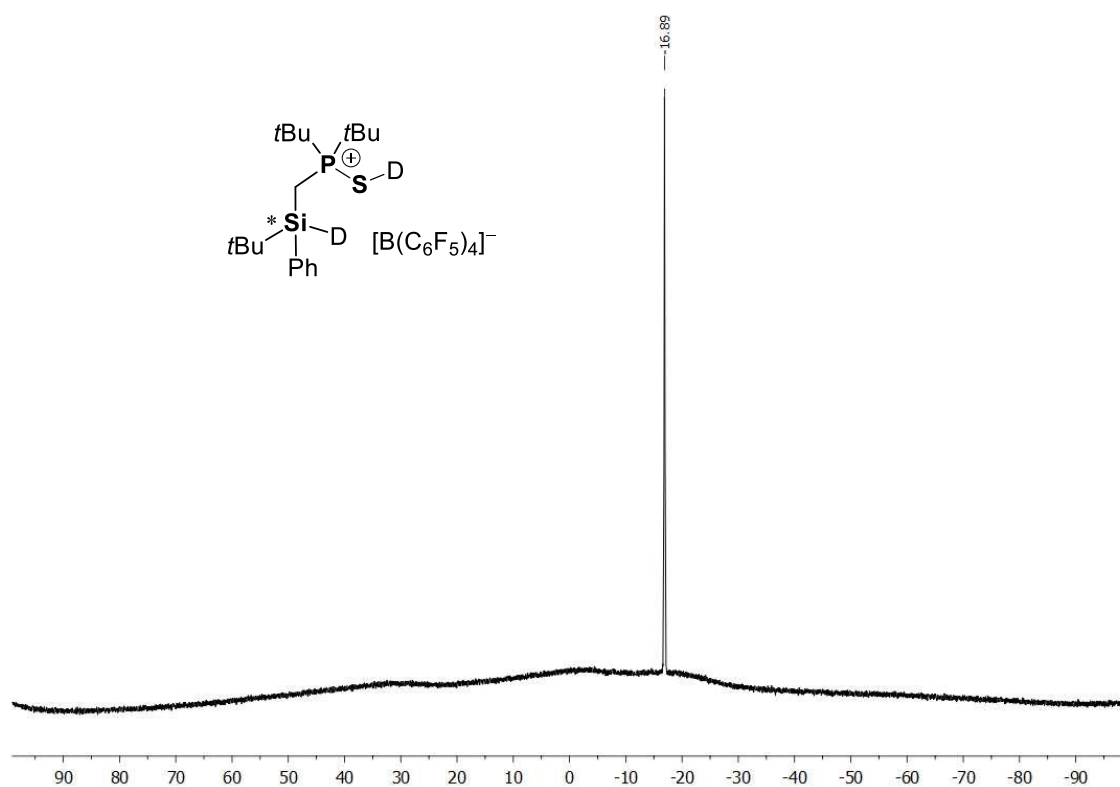
Figure S87. $^{11}B\{^1H\}$ NMR (CD$_2$Cl$_2$, 298 K) of compound (*rac*)-**3**-*d$_2$*.
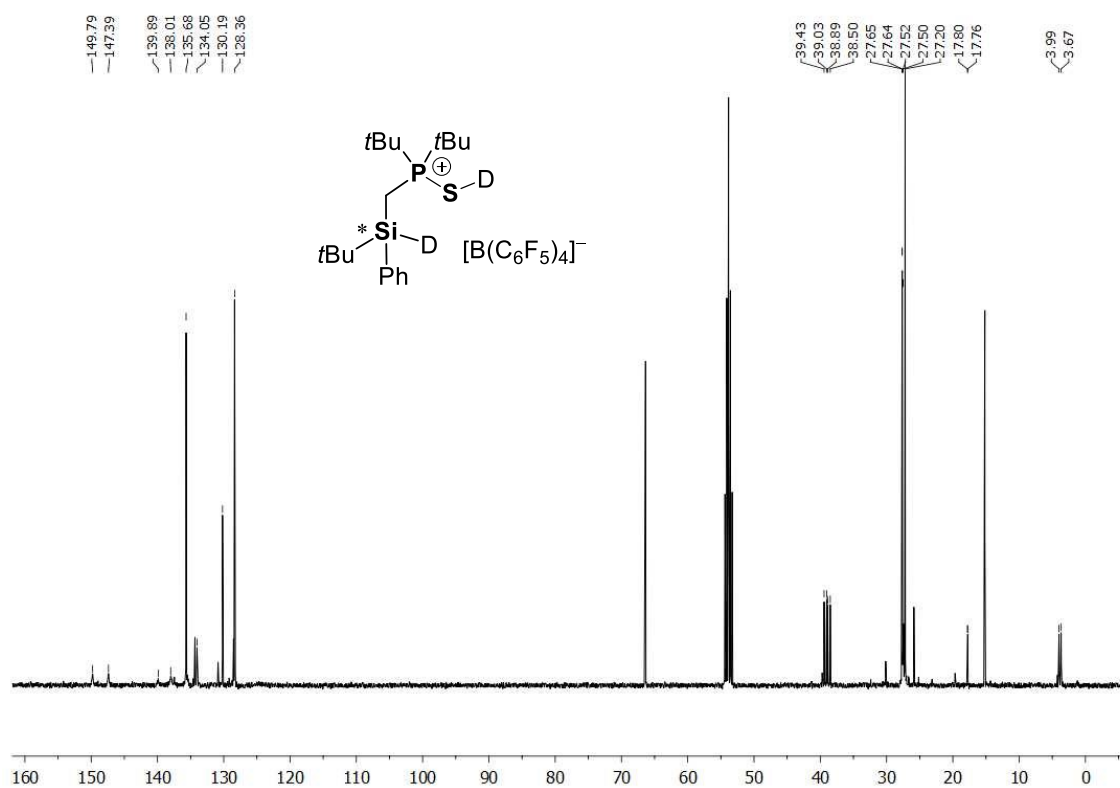
Figure S88. $^{13}C\{^1H\}$ NMR (CD$_2$Cl$_2$, 298 K) of compound (*rac*)-**3**-*d$_2$*.
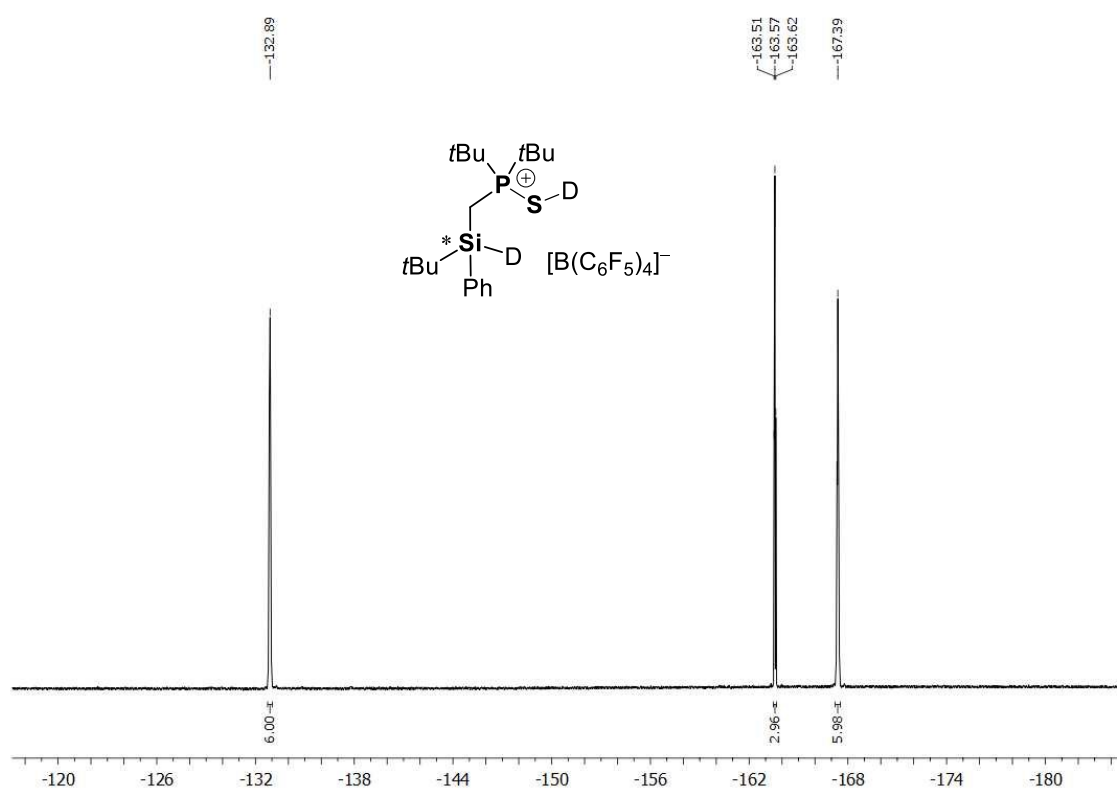
Figure S89. $^{19}F\{^1H\}$ NMR (CD$_2$Cl$_2$, 298 K) of compound (*rac*)-**3-d_2**.
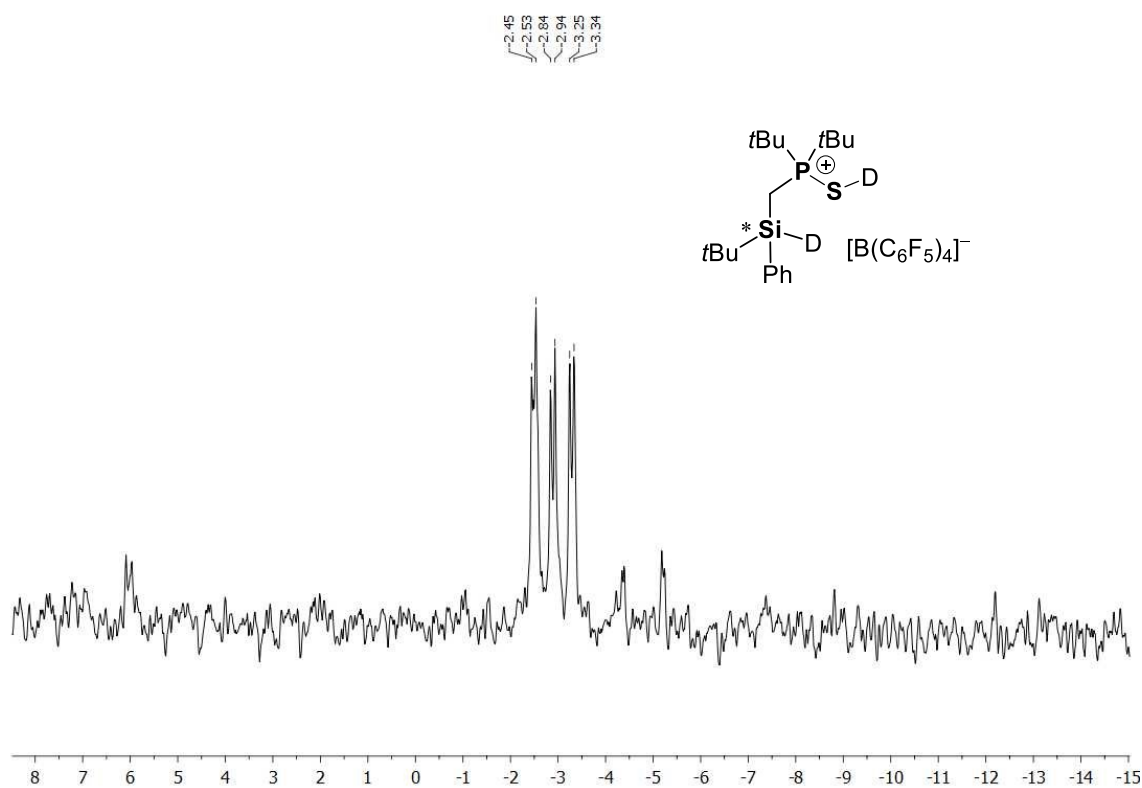
Figure S90. $^{29}Si\{^1H\}$ NMR (CD$_2$Cl$_2$, 298 K) of compound (*rac*)-**3-d_2**.
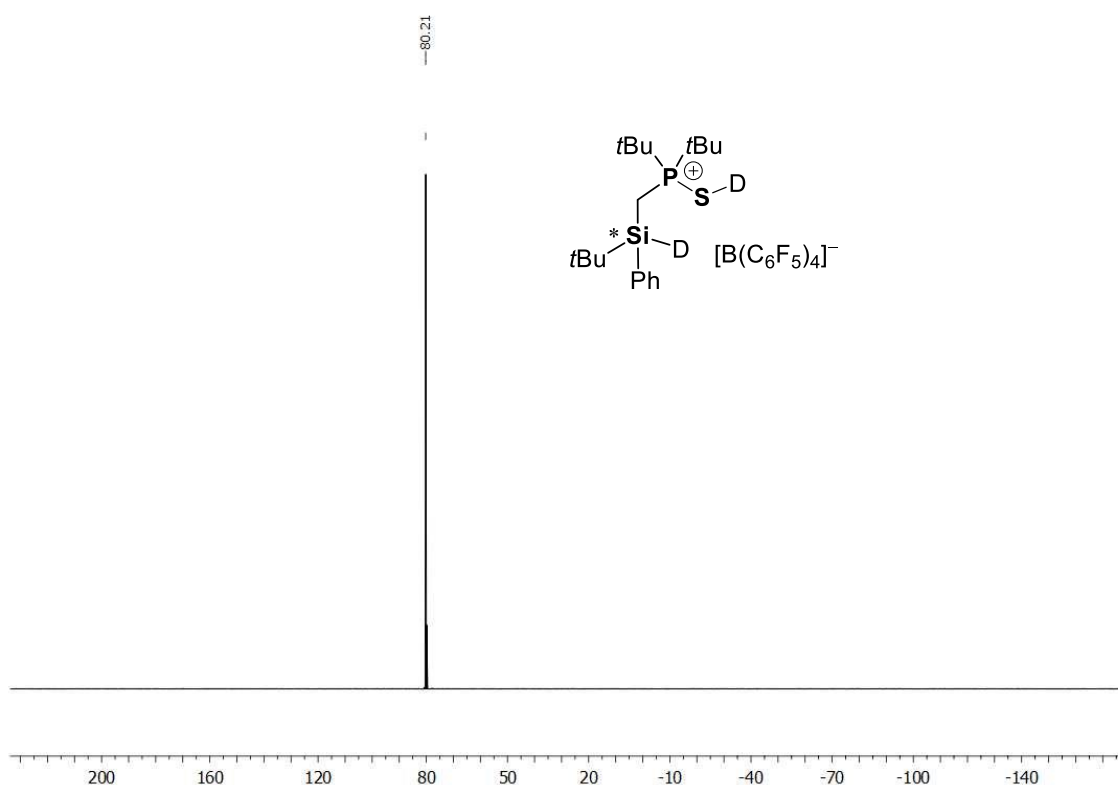
Figure S91. ^{31}P{^{1}H} NMR (CD$_2$Cl$_2$, 298 K) of compound (*rac*)-**3**-*d$_2$*.

3.5.18 Deuterium labeling experiment on compound (*rac*)-3
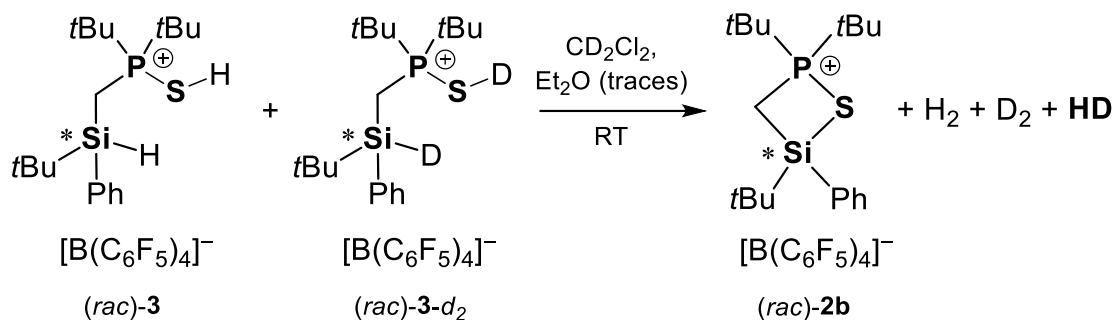
Into a high-pressure Young NMR tube, freshly precipitated compounds (*rac*)-**3** and (*rac*)-**3**-*d$_2$* (37 mg, 0.036 mmol, 1.0 equiv. each, Et$_2$O/pentane) were dissolved in CD$_2$Cl$_2$. The tube was immediately sealed and shaken vigorously. The solution was left to react one day at room temperature and then ^{1}H NMR spectra of the 1:1 mixture of (*rac*)-**3** and double deuterated (*rac*)-**3**-*d$_2$* were recorded during the following 15 days. Reduction in the intensities of the signals related to the silicon hydride (m, 4.51 ppm) and the methylene protons (m, 1.82-1.77 ppm) belonging to the starting compounds was observed. After one day, signals corresponding to dihydrogen (s, 4.60 ppm) and hydrogen deuteride (HD) (pseudo-triplet, 4.56, $J_{\text{H-D}}$= 43 Hz) could already be observed. After four weeks, the

90

NMR tube was shaken again and the sample recorded giving a clearer picture of the gasses released during the reaction (end of the experiment, figure S53). The formation of HD supports the hypothesis that two molecules are involved in the dehydrogenation reaction.
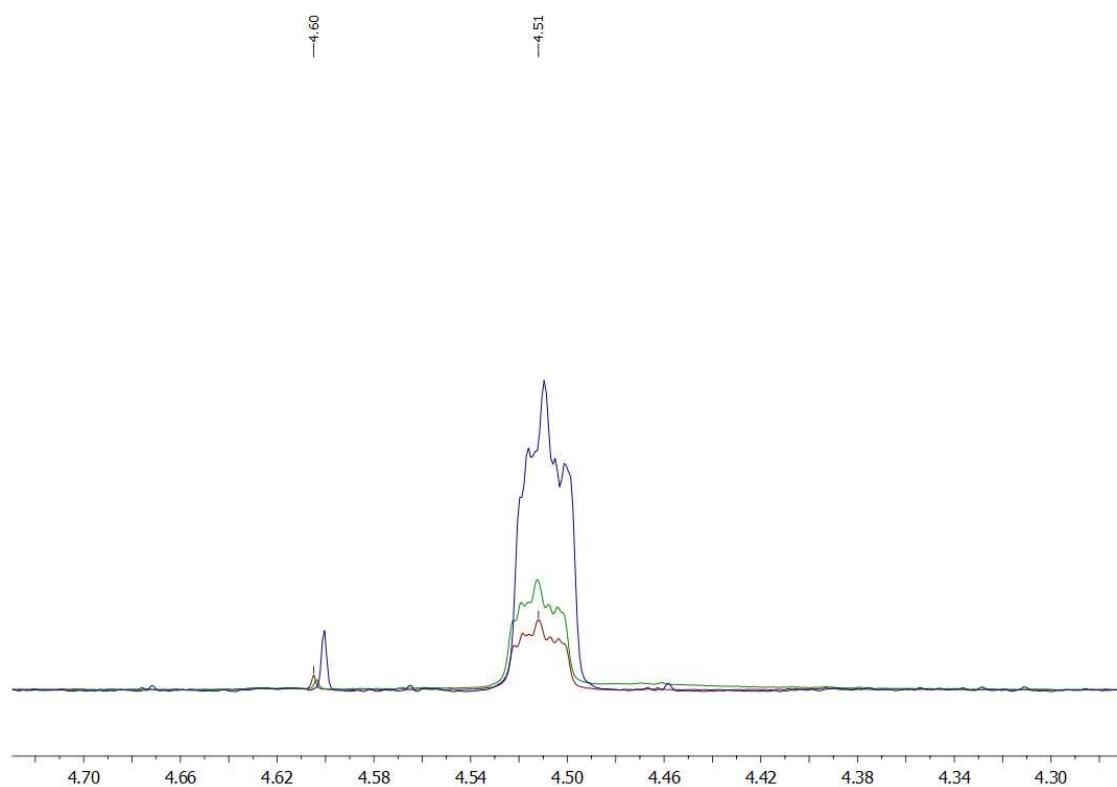
Figure S92. ^{1}H NMR spectrum (CD$_2$Cl$_2$, 298 K) highlighting the decrease of the silicon-hydride signal for fifteen days. Only the spectra recorded after four hours (dark blue), six- (green) and eleven days (red) are shown for clarity.
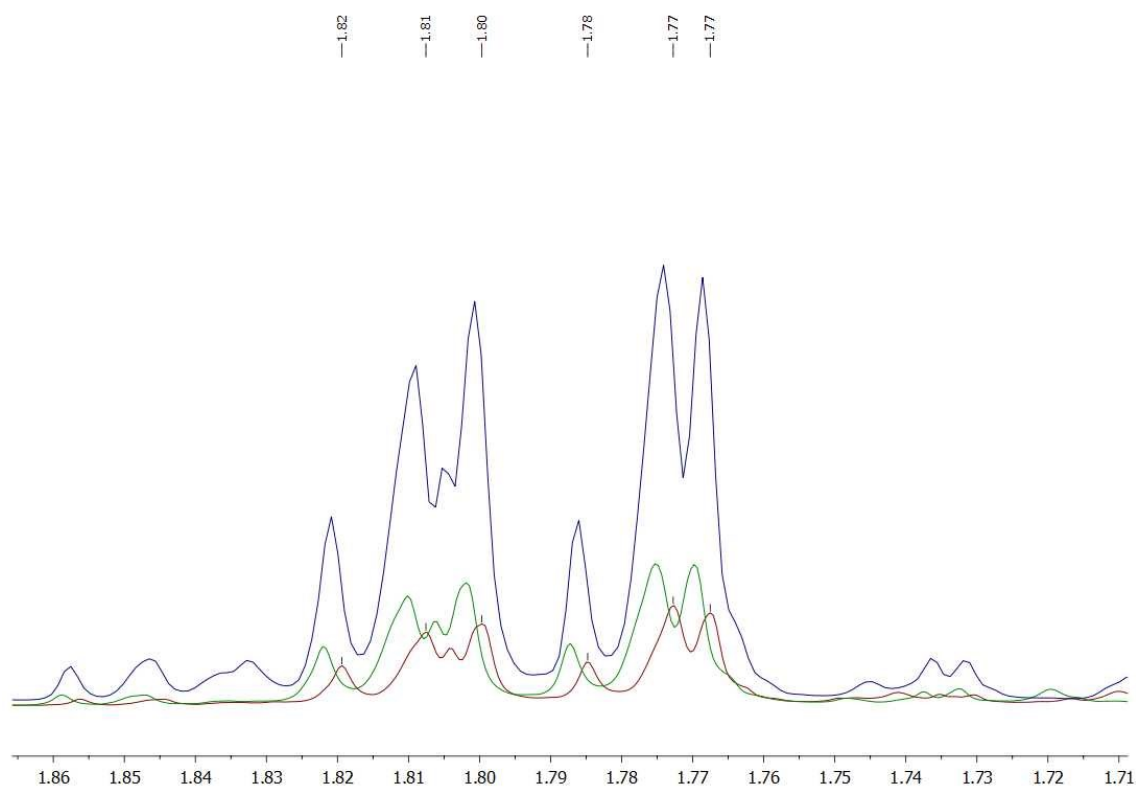
Figure S93. ^{1}H NMR spectrum (CD$_2$Cl$_2$, 298 K) highlighting the decrease of the methylene protons signal for fifteen days. Only three spectra, recorded after four hours (dark blue), six- (green) and eleven days (red) are shown for clarity.
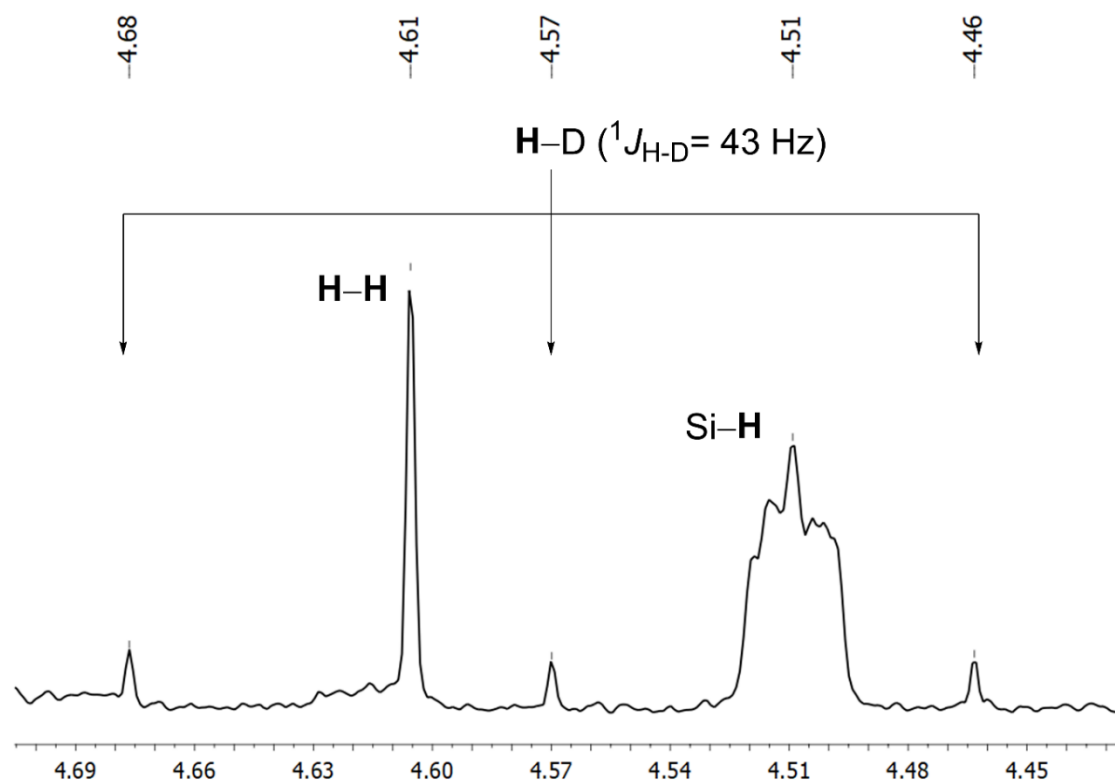
Figure S94. ^{1}H NMR spectrum (CD$_2$Cl$_2$, 298 K) of the experiment highlighting the formation of dihydrogen and hydrogen deuteride after four weeks (end of the experiment).

3.5.19   Study on the matched/mismatched case
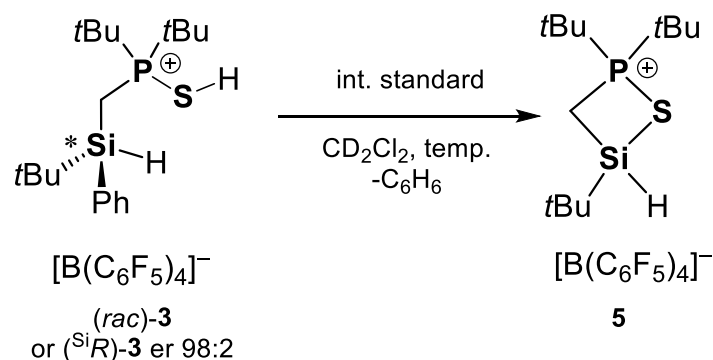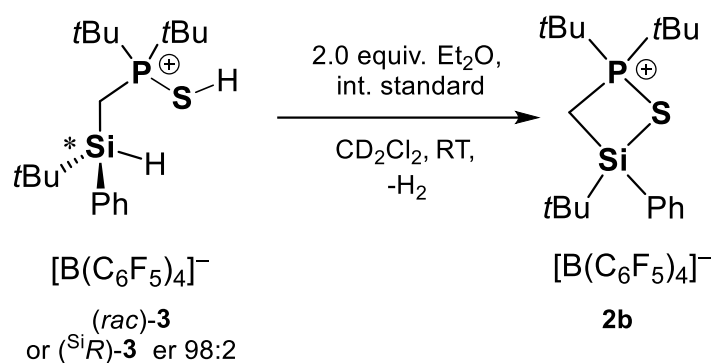
Experiment 1: racemic compound

In an oven dried Schlenk flask, compound (*rac*)-**1** (590 mg, 0.565 mmol, 1.0 equiv.) and [H(OEt₂)₂][B(C₆F₅)₄] (1.38 g, 0.565 mmol, 1.0 equiv.) were dissolved in dichloromethane (50 ml) at room temperature and stirred for 4 days. An aliquot was collected directly into a Young NMR tube using a PTFE tube. Subsequently, all volatiles were removed, the sample was dissolved in CD₂Cl₂ (0.4 ml) and NMR spectra were recorded showing the formation of compound **2b** (approx. 66% conversion).

Experiment 2: highly enantiomerically enriched compound

In an oven dried Schlenk flask, compound (^{Si}S)-**1** (50 mg, 0.141 mmol, 1.0 equiv. er 98:2) and [H(OEt₂)₂][B(C₆F₅)₄] (117 mg, 0.141 mmol, 1.0 equiv.) were dissolved in dichloromethane (10 ml) at room temperature and stirred for 4 days. An aliquot was collected directly into a Young NMR tube using a PTFE tube. Subsequently, all volatiles were removed, the sample was dissolved in CD₂Cl₂ (0.4 ml) and NMR spectra were recorded showing only the formation of compound **3**.
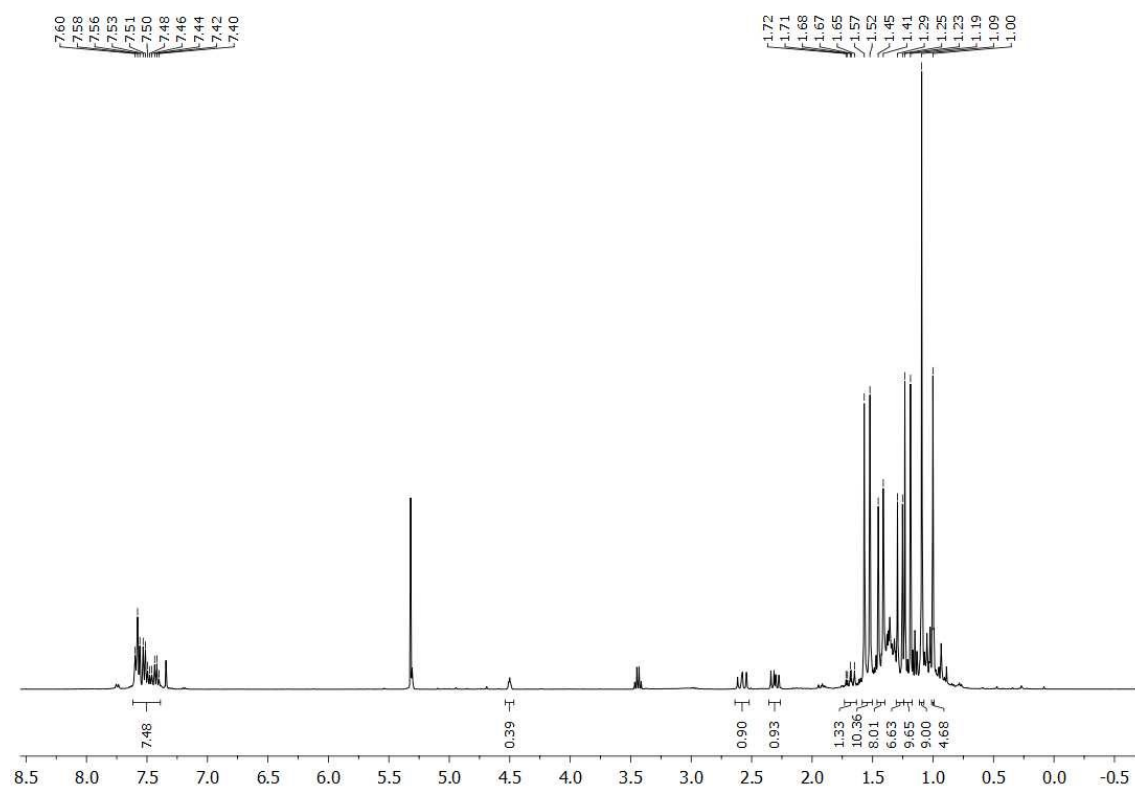
Figure S95. ^{1}H NMR spectrum (CD$_2$Cl$_2$, 298 K) of (*rac*)-**3** recorded after four days (experiment 1).
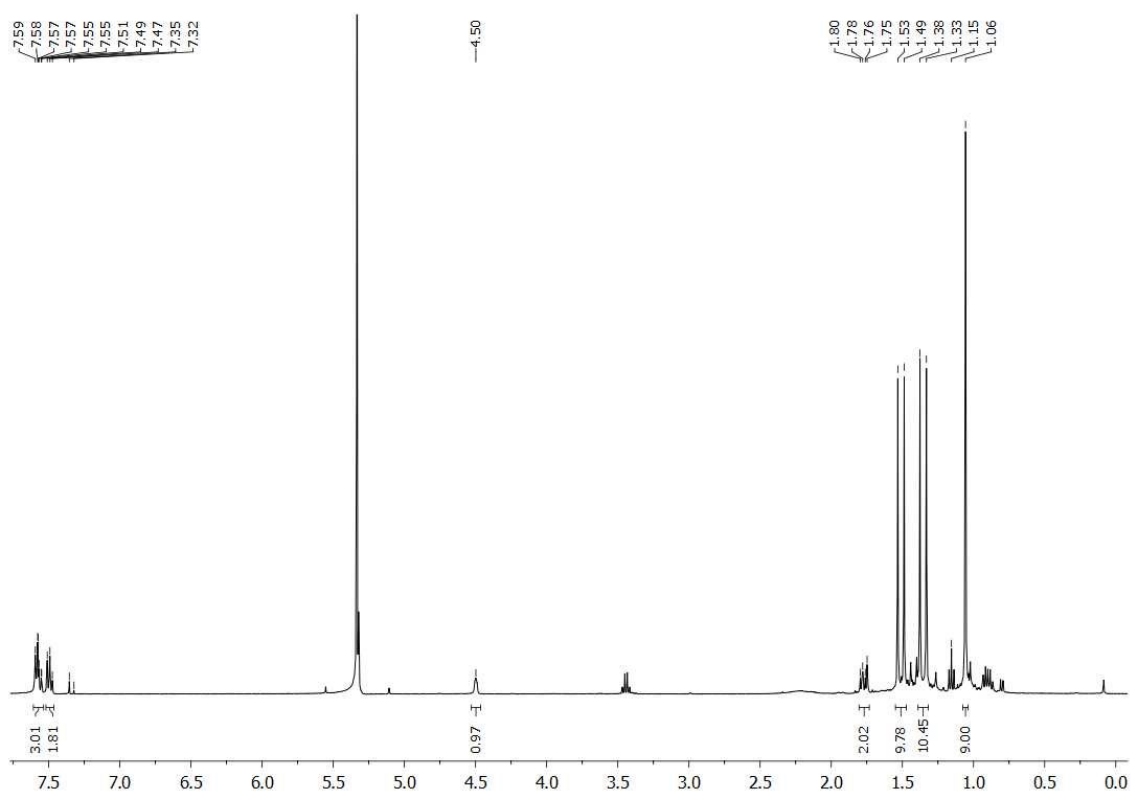
Figure S96. ^{1}H NMR spectrum (CD$_2$Cl$_2$, 298 K) of (^{Si}S)-**3** recorded after four days (experiment 2).

General remarks on the investigation:

The observations in experiments 1 and 2 prompted us to further investigate the mechanism of this reaction.

As better elucidated by the following tables, the formation of the four-membered ring happens reliably but with rates dependent on the stereochemical composition of the substrate. Moreover, a comparison between two different concentrations supported the hypothesis of an intermolecular mechanism (see previous section). During this study, a different reactivity was discovered. Depending whether diethyl ether is present or not, compound **3** spontaneously tends to give compounds **2b** or **5** respectively. In order to differentiate between the two possible ring-closing reactions, during the first phase of this study two equivalents of diethyl ether were added in order to prevent the formation of compound **5**. On the contrary, in the second phase, diethyl ether free conditions were kept to selectively give compound **5**. Although isolation and crystallization of pure compound **5** failed so far, NMR evidence of its formation was obtained throughout the whole study. Interestingly, our findings showed that the protodesilylation reaction leading to the formation of compound **5** became unneglectable only when diethyl ether is not present. This might be related to a stabilizing effect of such solvent over the proposed transition state for the dihydrogen release reaction.

General procedure for the experiment in the presence of ether:

In a glovebox, a Young NMR tube was loaded with the solid substrate (80 mg, 0.085 mmol, 1 equiv. for the 0.2 M samples and 40 mg, 0.042 mmol, 1 equiv. for the 0.1 M). The tube was sealed, brought out of the glovebox and connected to a Schlenk line. Maintaining the system in inert atmosphere, CD_2Cl_2 (0.4 ml), Et_2O (0.17 mmol, 17 µl, 2 equiv.) and an internal standard (CH_2ClBr, 0.17 mmol, 17 µl, 2 equiv.) were added *via* syringe. The tube was immediately sealed and shaken. NMRs were recorded over the next days after vigorously shaking the sample (see table S1). Between measures, the sample was kept in the same room of the measuring instrument to assure a constant temperature of 298 K throughout the whole experiment.

General procedure for the experiment in the absence of ether:

In a glovebox, a Young NMR tube was loaded with the solid substrate (80 mg, 0.085 mmol, 1 equiv.). The tube was sealed, brought out of the box and connected to a Schlenk line. Maintaining the system in inert atmosphere, CD_2Cl_2 (0.4 ml) and an internal standard (CH_2ClBr, 0.17 mmol, 17 µl, 2 equiv.) were added *via* syringe. The tube was immediately sealed and shaken. NMR spectra were recorded over the next days after vigorously shaking the sample (see table S2). After approximately six days, the samples were heated up to 60°C using an oil bath allowing them to reach completion (table S2, entries 3 and 4).

Entry	Experiment specifics and reaction rates	Time (min)	Substrate Concentration (mol L^{-1})	Conversion %
1	Racemic mixture 0.2 M Presence of ether Estimated reaction rate -2*10^{-5} mol L^{-1} min^{-1}	692	2.10E-01	1
		1779	1.93E-01	9
		5161	1.38E-01	35
		7195	1.02E-01	52
		8426	8.39E-02	60.4
		9691	6.85E-02	67.66
		10694	5.84E-02	72.4
		11212	5.45E-02	74.25
		12010	4.92E-02	76.76
		13637	3.87E-02	81.73
		14084	3.67E-02	82.69
		15862	2.80E-02	86.8
		19542	1.74E-02	91.76
2	Racemic mixture 0.1 M Presence of ether Estimated reaction rate -4*10^{-6} mol L^{-1} min^{-1} (slowed down by 80% compared to entry 1)	1226	1.06E-01	0
		2397	1.05E-01	1
		5712	9.53E-02	10
		6860	9.00E-02	15
		8257	8.44E-02	20.25
		9508	7.88E-02	25.6
		10742	7.41E-02	30
		11445	7.09E-02	33
		11930	6.85E-02	35.32
		12731	6.32E-02	40.33
		14359	5.64E-02	46.7
		14804	5.47E-02	48.3
		16646	4.87E-02	54.01
		20283	3.56E-02	66.35
3	(^{Si}R)-**3** (er. 98:2) 0.2 M Presence of ether Estimated reaction rate -7*10^{-6} mol L^{-1} min^{-1} (slowed down by 65% compared to entry 1)	1226	1.06E-01	0
		2397	1.05E-01	1
		5712	9.53E-02	10
		6860	9.00E-02	15
		8257	8.44E-02	20.25
		9508	7.88E-02	25.6
		10742	7.41E-02	30
		11445	7.09E-02	33
		11930	6.85E-02	35.32
		12731	6.32E-02	40.33

		14359	5.64E-02	46.7
		14804	5.47E-02	48.3
		16646	4.87E-02	54.01
		20283	3.56E-02	66.35

Table S1 Substrate concentrations and conversions recorded at different times in the presence of diethyl ether. Reaction rates have been estimated using a linear approximation. CH_2ClBr (10 µl) was used as an additional internal standard
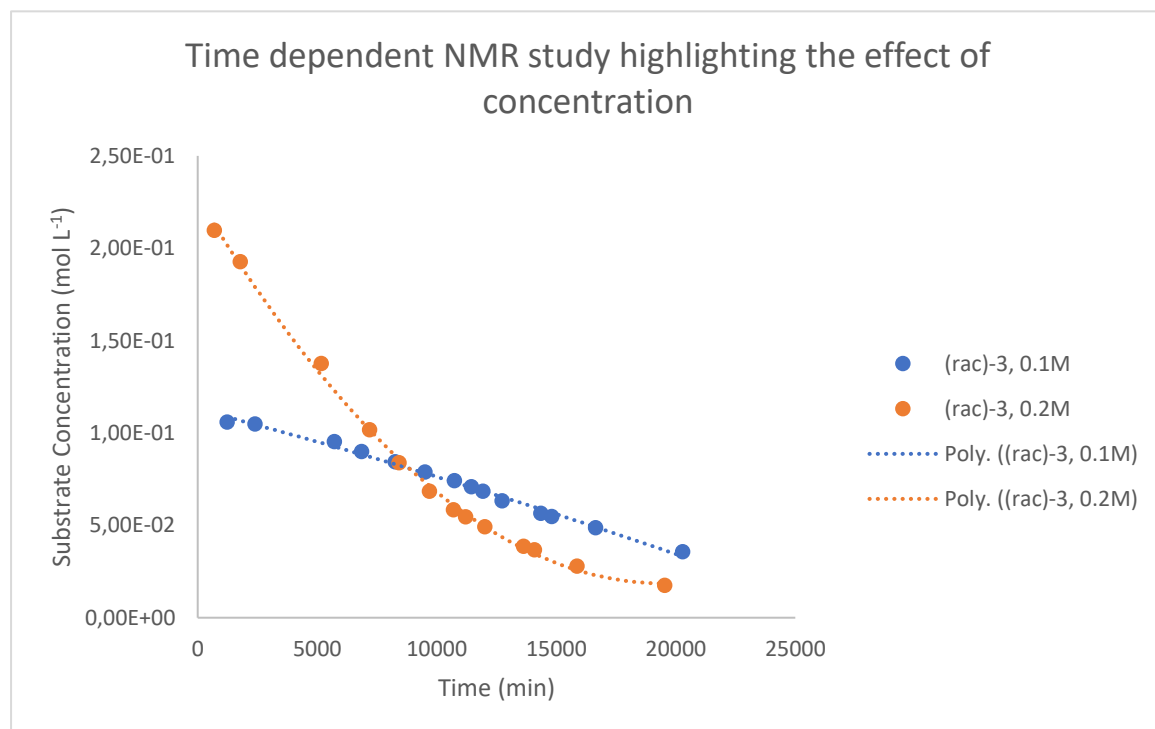
Figure S97 Trends for the spontaneous conversion of compound (*rac*)-**3** into the relative four-membered cycle **2b** in the presence of diethyl ether using two different initial concentrations: 0.2 M [Table S1, entry 1, orange] and 0.1 M [Table S1, entry 2, blue].
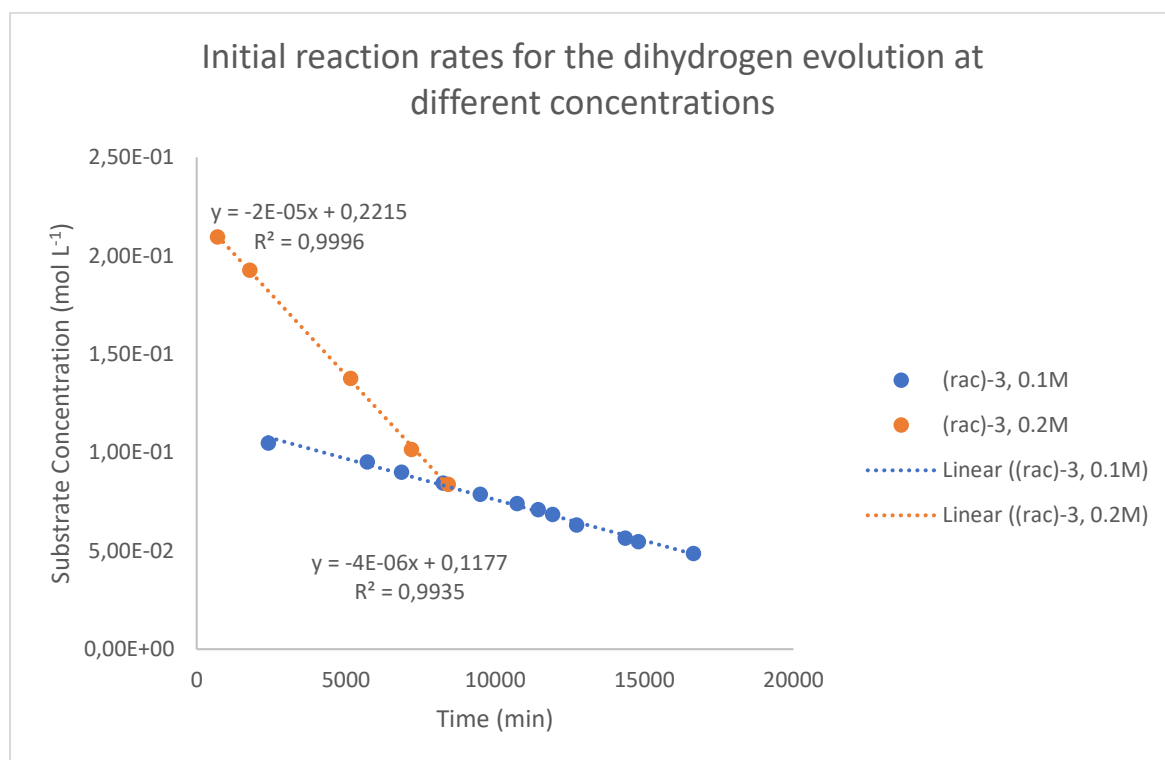
Figure S98 Initial reaction rates for the conversion of compound (*rac*)-**3** into the four-membered cycle **2b** in the presence of diethyl ether using two different initial concentrations of the substrate: 0.2 M [Table S1, entry 1, orange] and 0.1 M [Table S1, entry 2, blue]. The two slopes indicate a slower rate for the least concentrated sample with a difference equal to almost one order of magnitude (80% reduction).
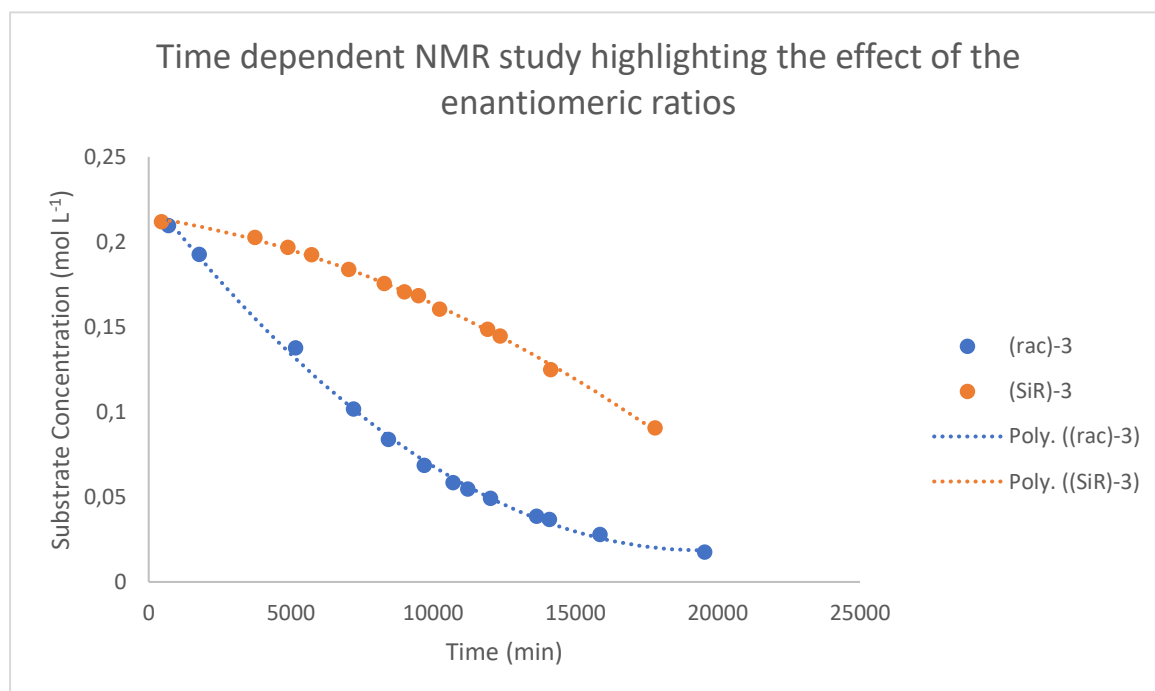
Figure S99 Trends for the spontaneous conversion of compounds (*rac*)-**3** [Table S1, entry 1, blue] and (^{Si}R)-**3** [Table S1, entry 3, orange] into the four-membered cycle **2b** in the presence of diethyl ether, showed with an order two approximation.
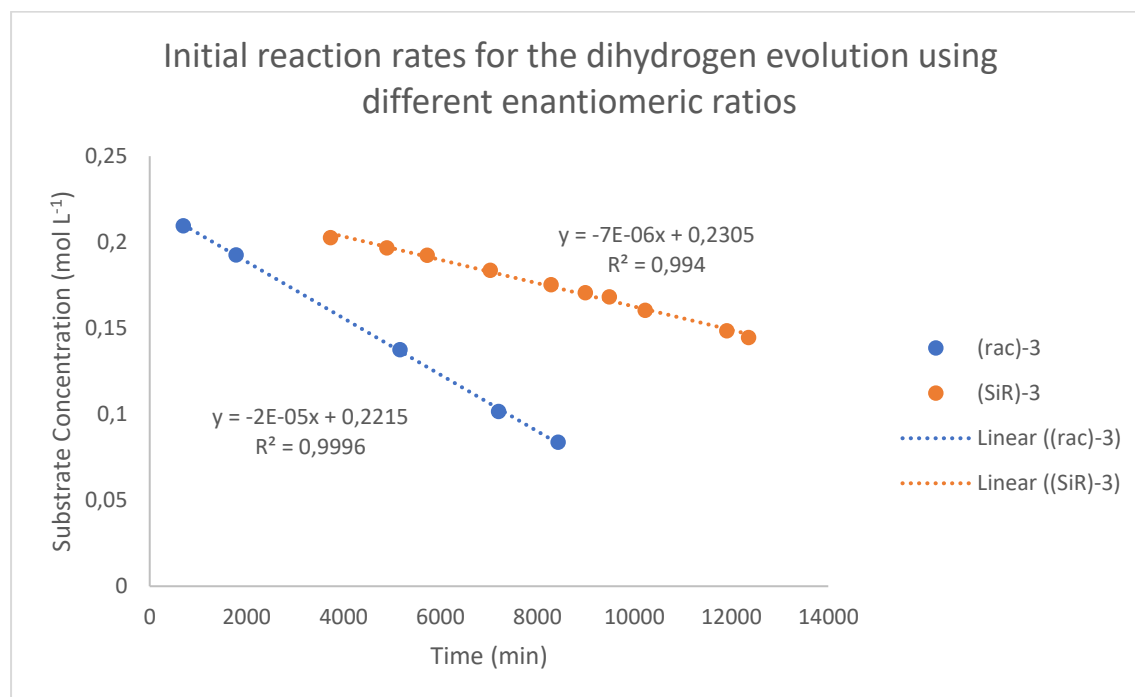
Figure S100 Initial reaction rates for the spontaneous conversion of compounds (*rac*)-**3** [Table S1, entry 1, blue] and (^{Si}R)-**3** [Table S1, entry 3, orange] into the four-membered cycle **2b** in the presence of diethyl ether. The graph clearly shows a higher reaction rate for the racemic sample. By using a highly enantiomerically enriched sample the reaction rate decreases by 65%.
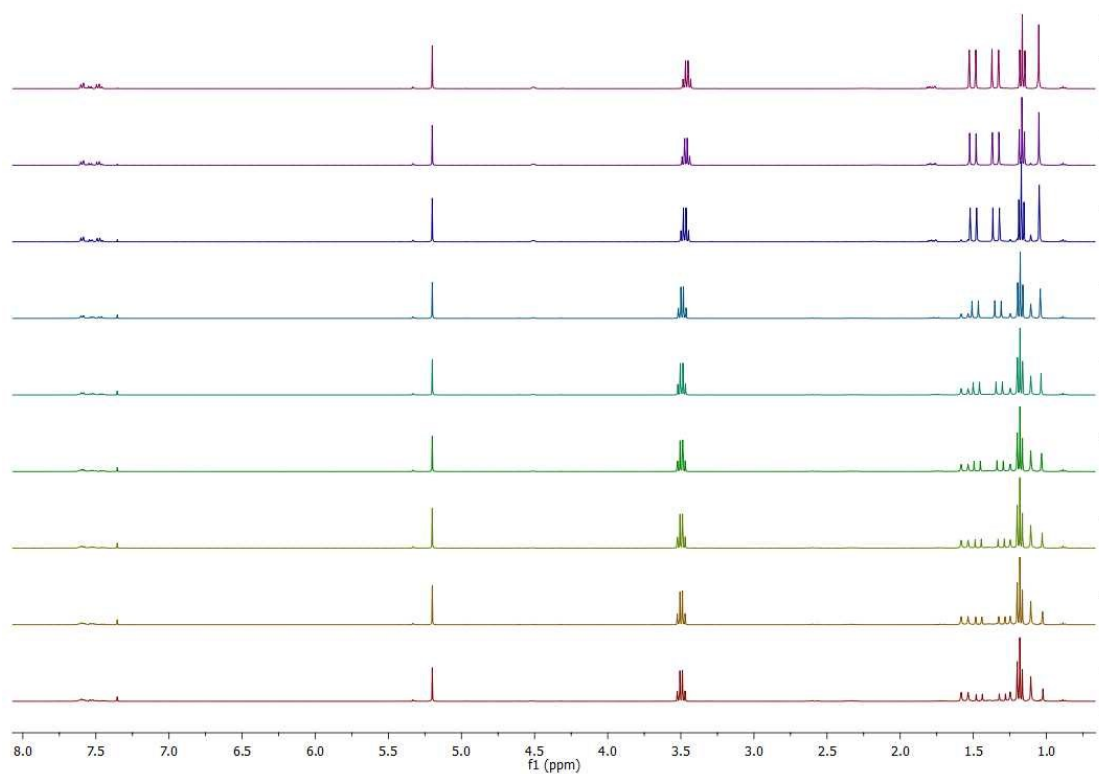
Figure S101. Time dependent ^{1}H NMR spectra (CD$_2$Cl$_2$, 298 K) of entry 1 [(*rac*)-**3**, 0.2M] as reported in table S1.
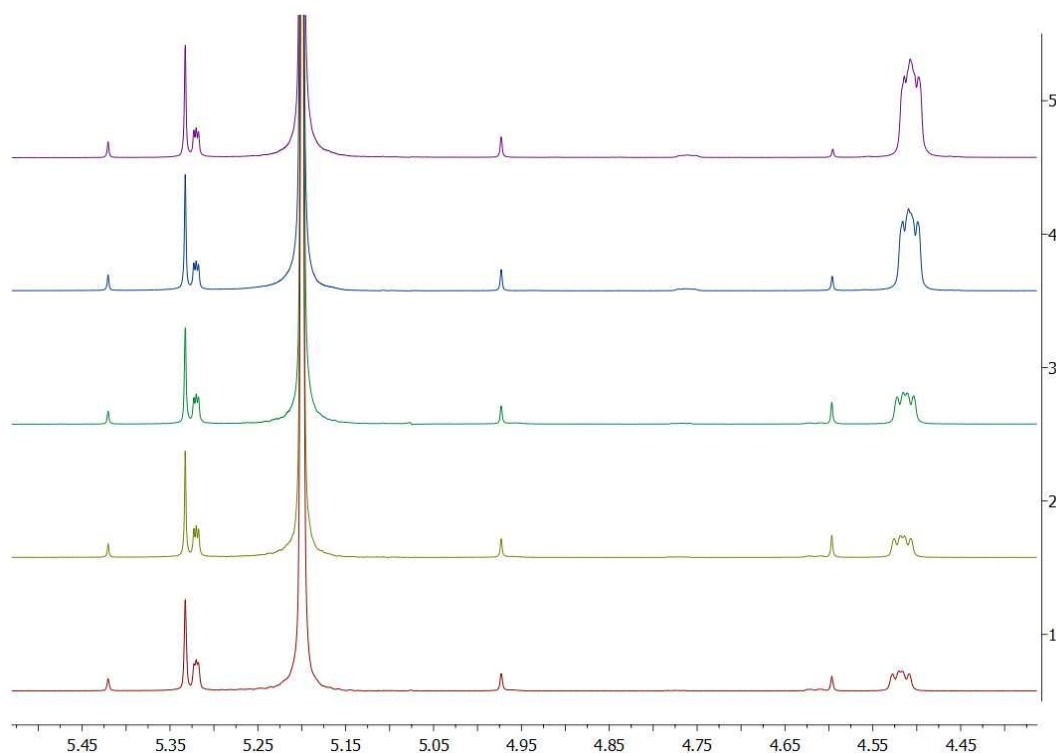
Figure S102. Expansion of the silicon hydride region in the time dependent ^{1}H NMR spectra (CD$_2$Cl$_2$, 298 K) of entry 1 [(*rac*)-**3**, 0.2M] as reported in table S1. Only spectra recorded at 0, 1, 52, 67.7 and 72.4% conversion (from top to bottom) are shown for clarity.
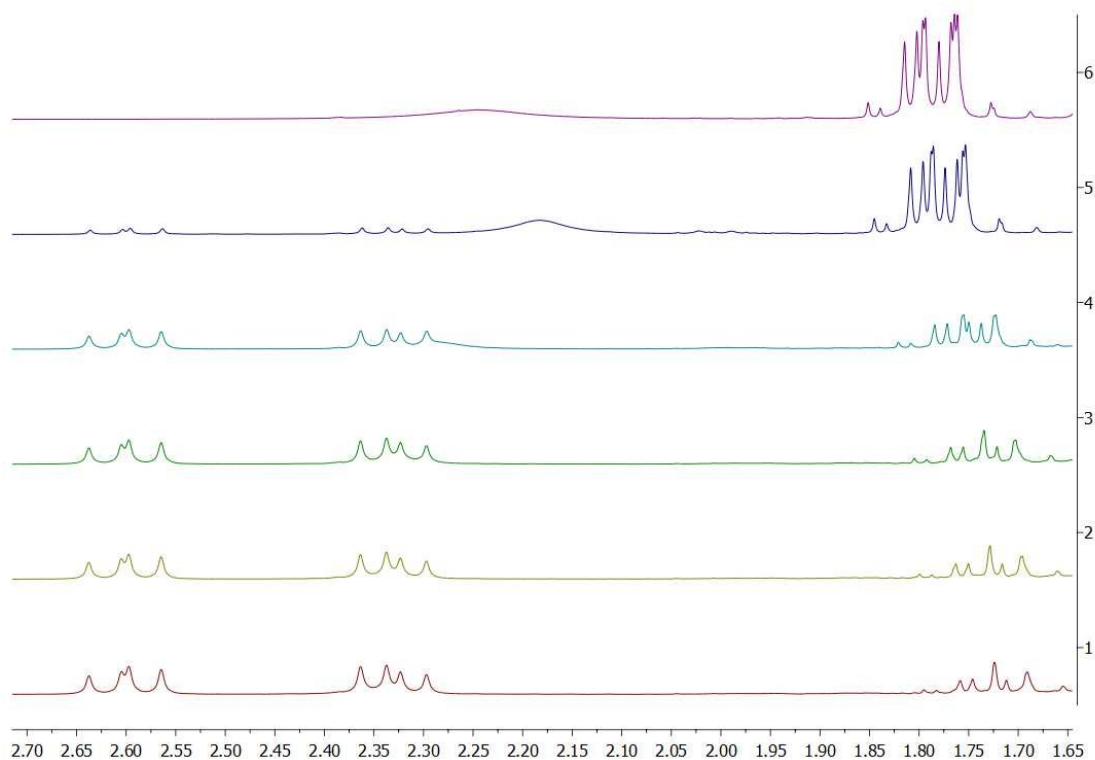
Figure S103. Expansion of the methylene region in the time dependent ^{1}H NMR spectra (CD$_2$Cl$_2$, 298 K) of entry 1 [(*rac*)-**3**, 0.2M] as reported in table S1. Only spectra recorded at 0, 1, 52, 67.7 and 72.4% conversion (from top to bottom) are shown for clarity.
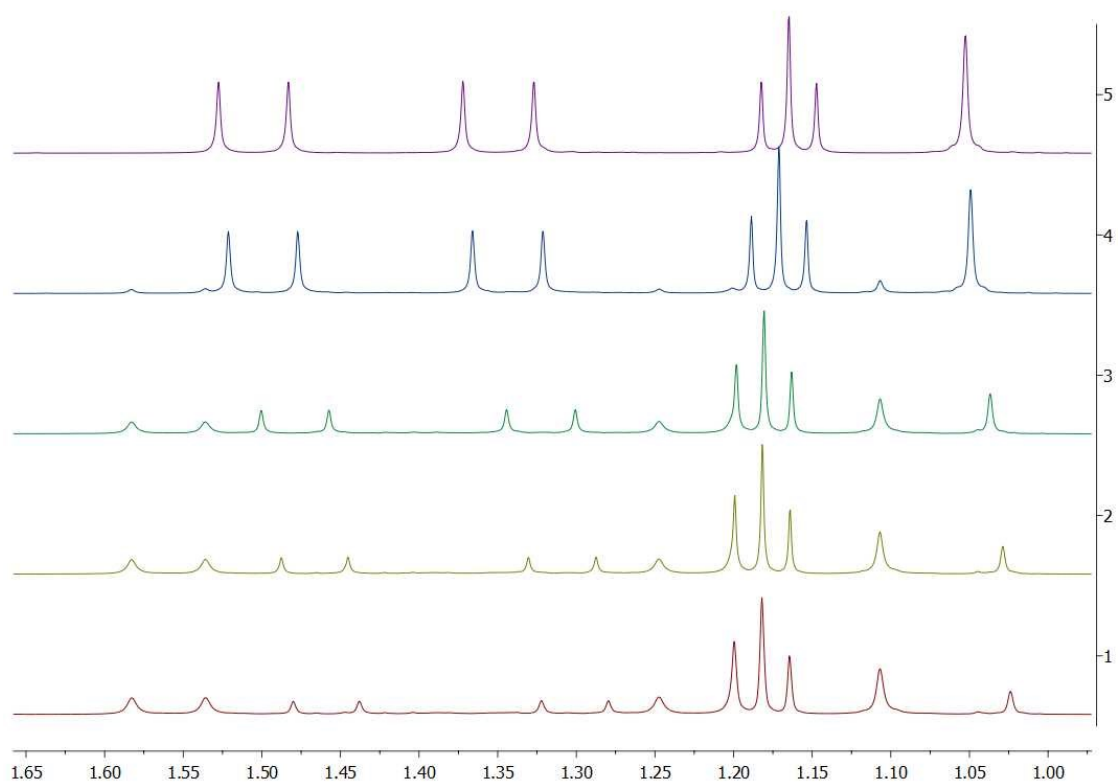
Figure S104. Expansion of the aliphatic region in the time dependent ^1H NMR spectra (CD$_2$Cl$_2$, 298 K) of entry 1 [(*rac*)-**3**, 0.2M] as reported in table S1. Only spectra recorded at 0, 1, 52, 67.7 and 72.4% conversion (from top to bottom) are shown for clarity.
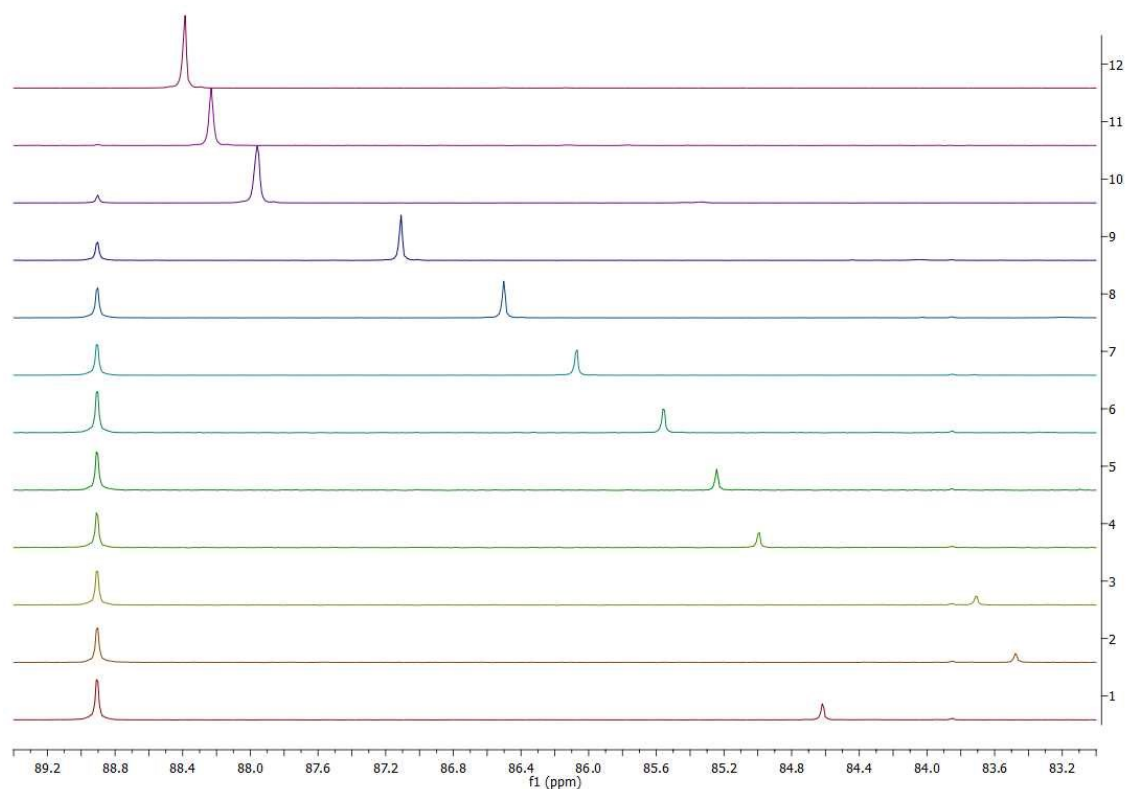
Figure S105. Time dependent $^3P\{^1H\}$ NMR spectra (CD$_2$Cl$_2$, 298 K) of entry 1 [(*rac*)-**3**, 0.2M] as reported in table S1.
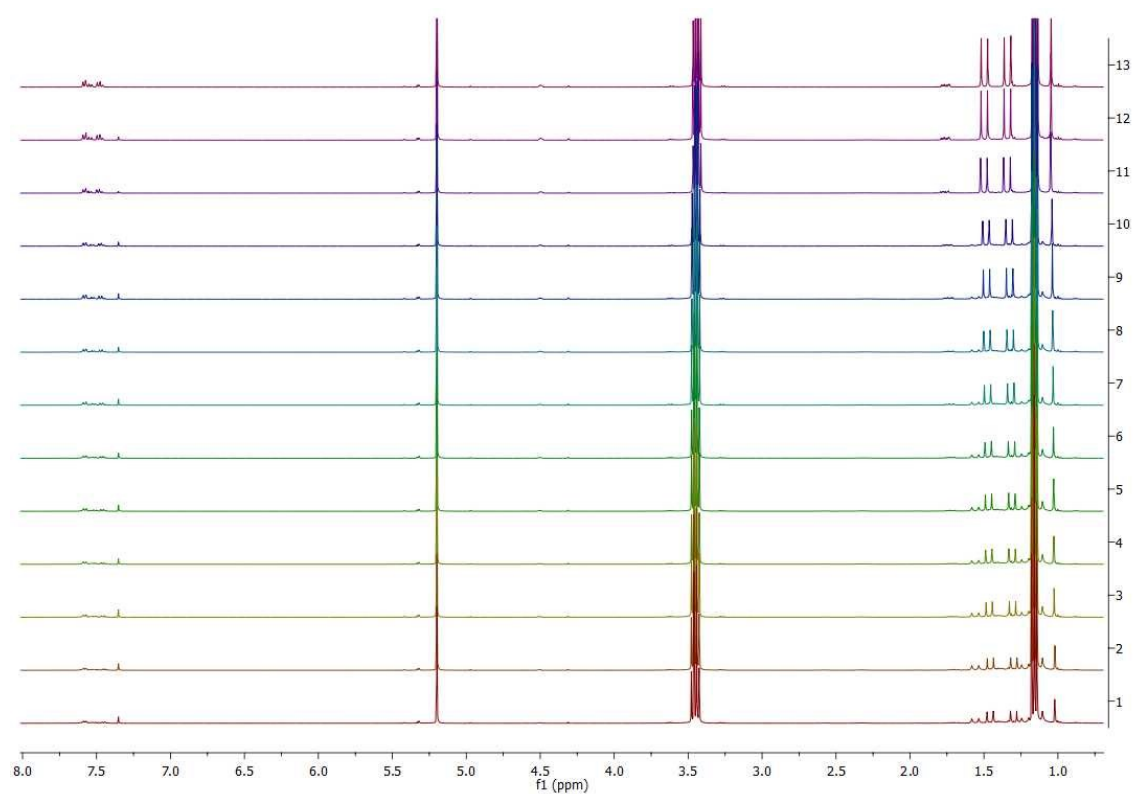
Figure S106. Time dependent ^{1}H NMR spectra (CD$_2$Cl$_2$, 298 K) of entry 2 [(*rac*)-**3**, 0.1M] as reported in table S1.
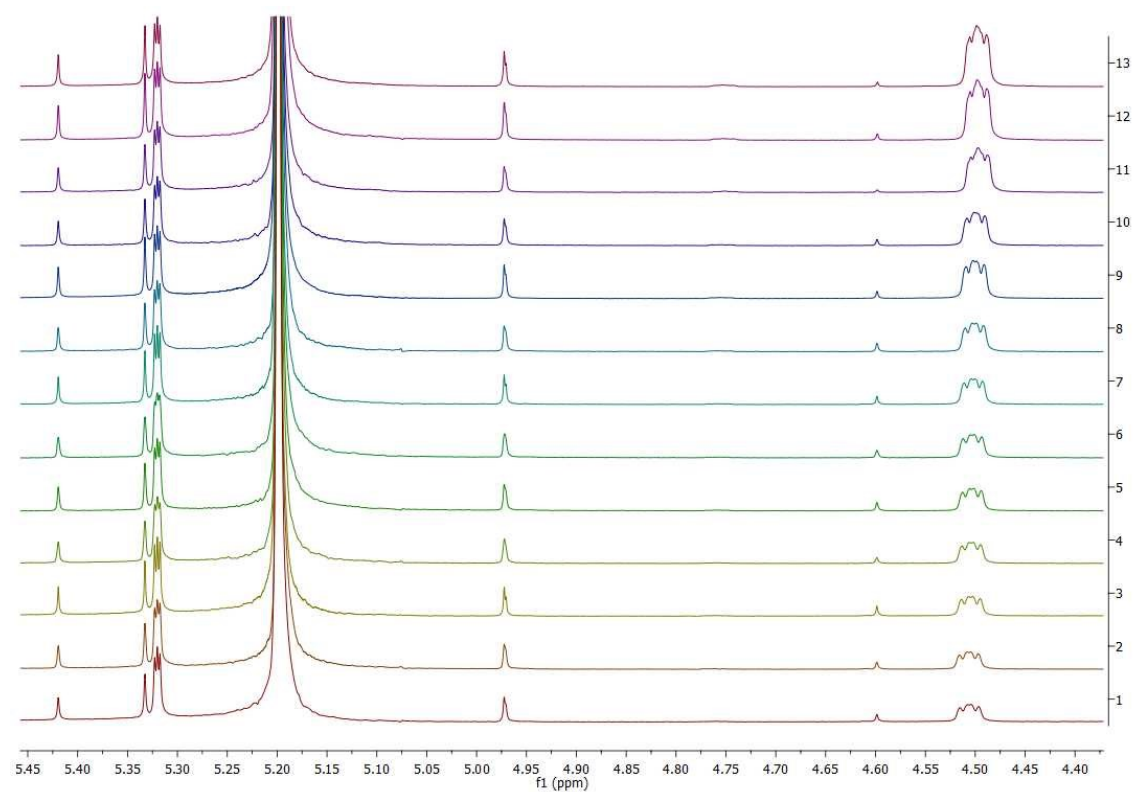
Figure S107. Expansion of the silicon hydride region in the time dependent ^{1}H NMR spectra (CD$_2$Cl$_2$, 298 K) of entry 2 [(*rac*)-**3**, 0.1M] as reported in table S1.
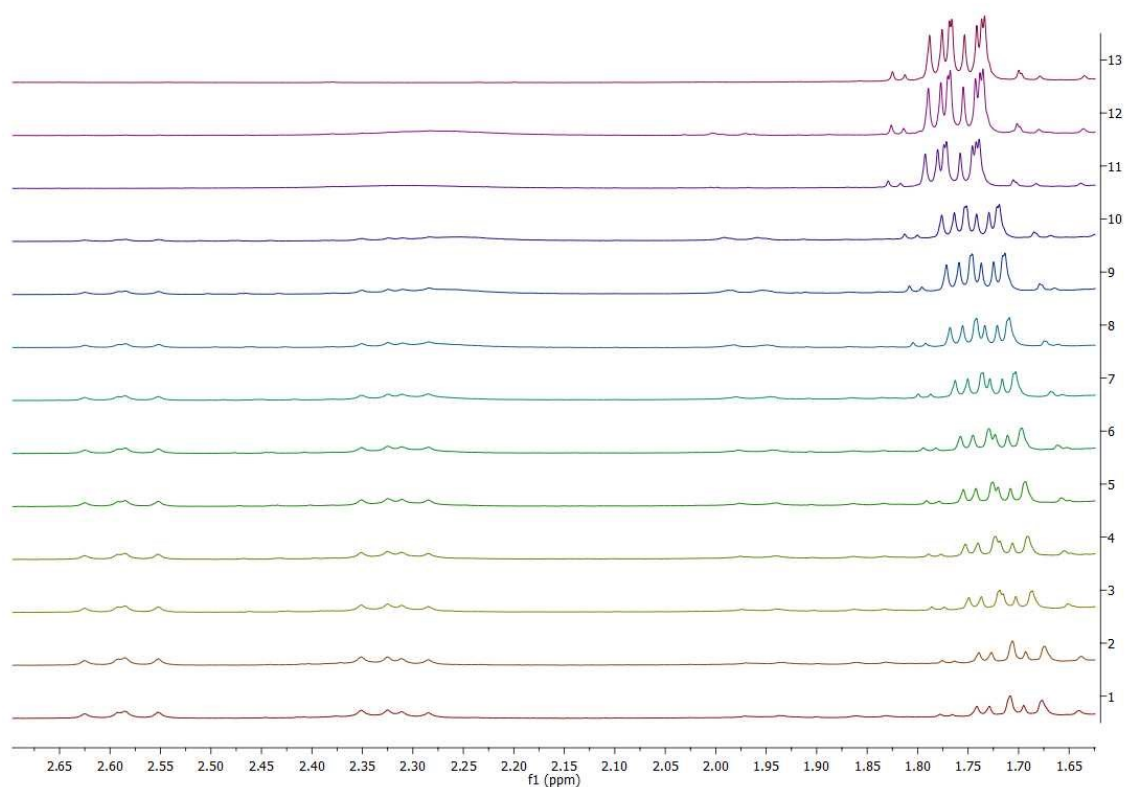
Figure S108. Expansion of the methylene region in time dependent ^{1}H NMR spectra (CD$_2$Cl$_2$, 298 K) of entry 2 [(*rac*)-**3**, 0.1M] as reported in table S1.
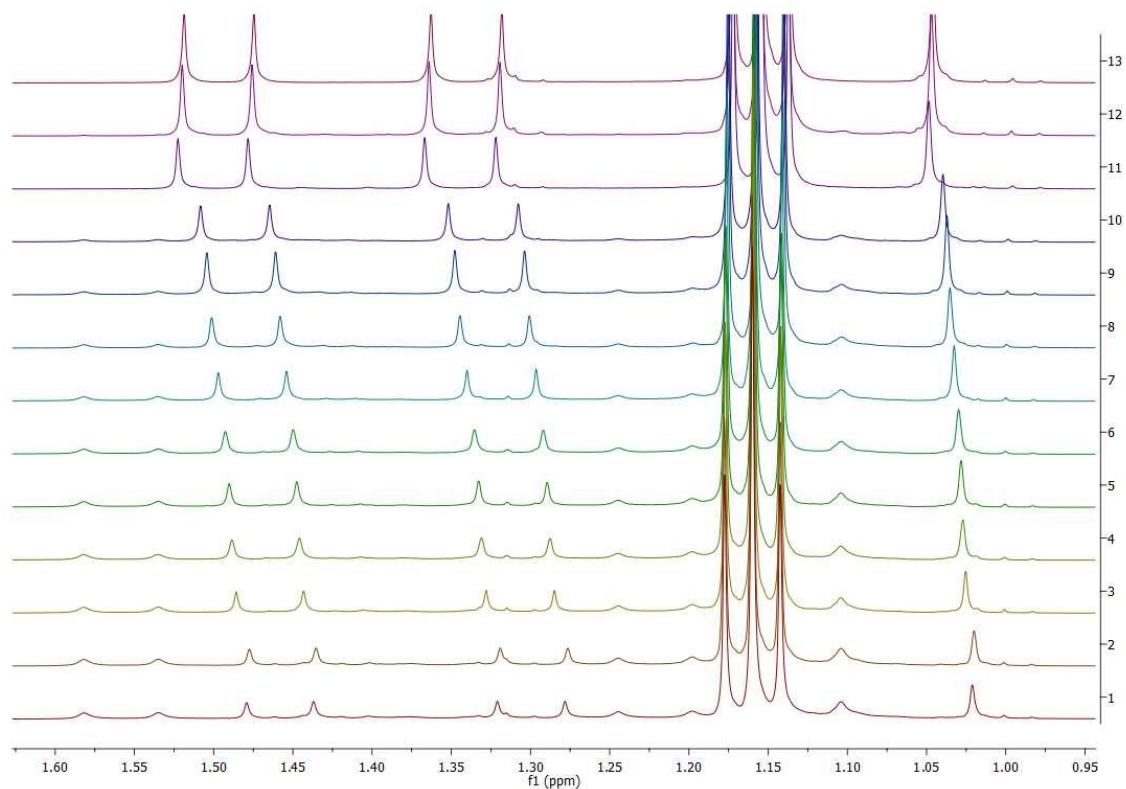
Figure S109. Expansion of the aliphatic region in time dependent ^{1}H NMR spectra (CD$_2$Cl$_2$, 298 K) of entry 2 [(*rac*)-**3**, 0.1M] as reported in table S1.
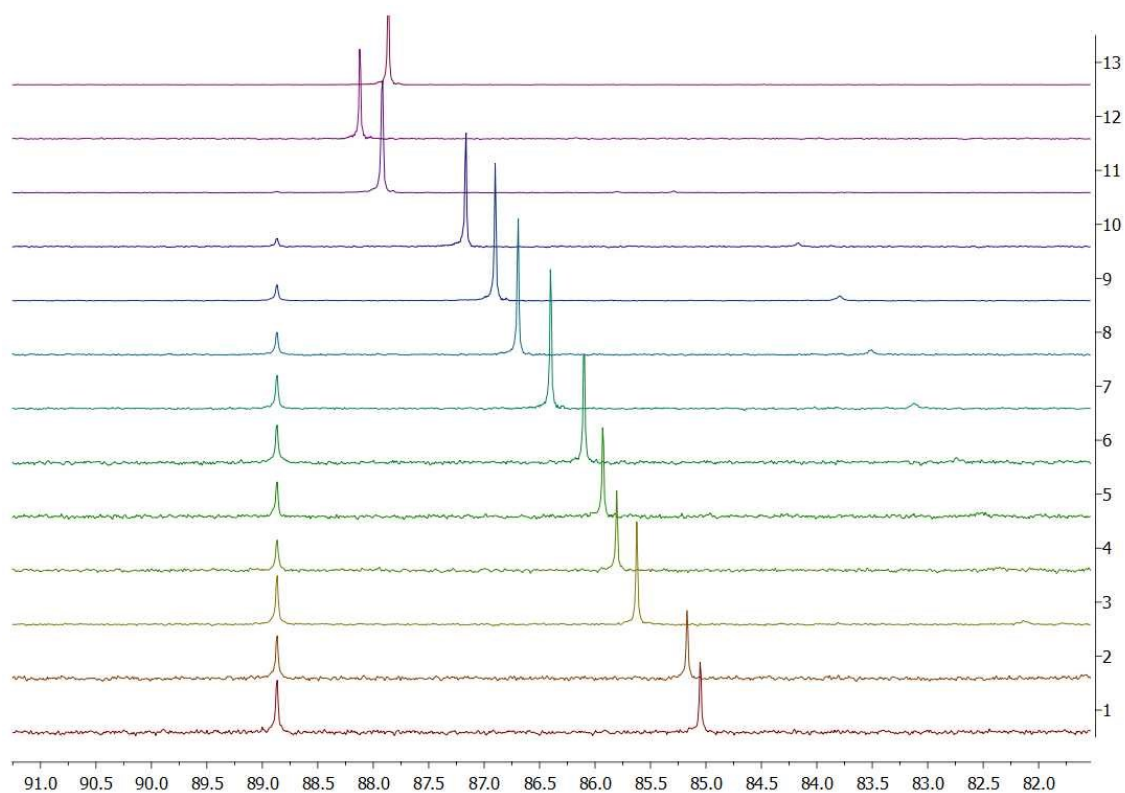
Figure S110. Time dependent $^{31}P\{^1H\}$ NMR spectra (CD$_2$Cl$_2$, 298 K) of entry 2 [(*rac*)-**3**, 0.1M] as reported in table S1.
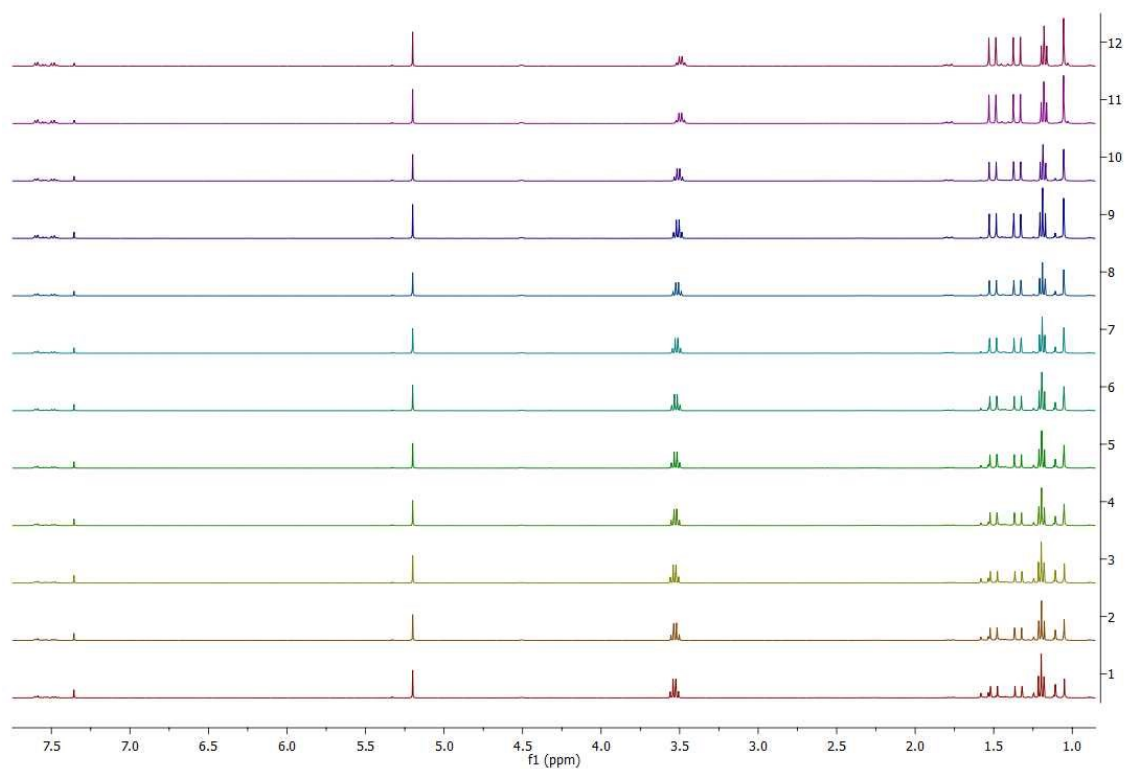
Figure S111. Time dependent ^1H NMR spectra (CD$_2$Cl$_2$, 298 K) of entry 3 [(^{Si}R)-**3**, 0.2M] as reported in table S1.
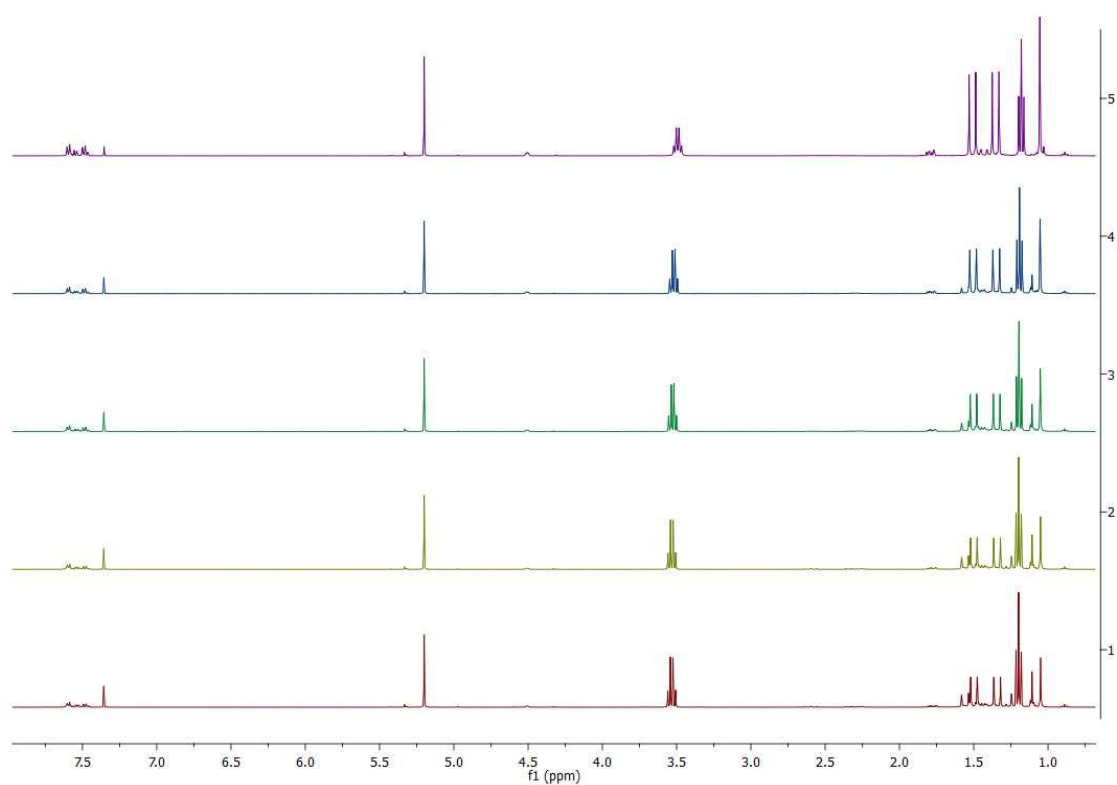
Figure S112. Time dependent ^{1}H NMR spectra (CD$_2$Cl$_2$, 298 K) of entry 3 [(^{Si}R)-**3**, 0.2M] as reported in table S1. Only spectra recorded at 0, 13, 20, 24 and 31% conversion are shown for clarity.
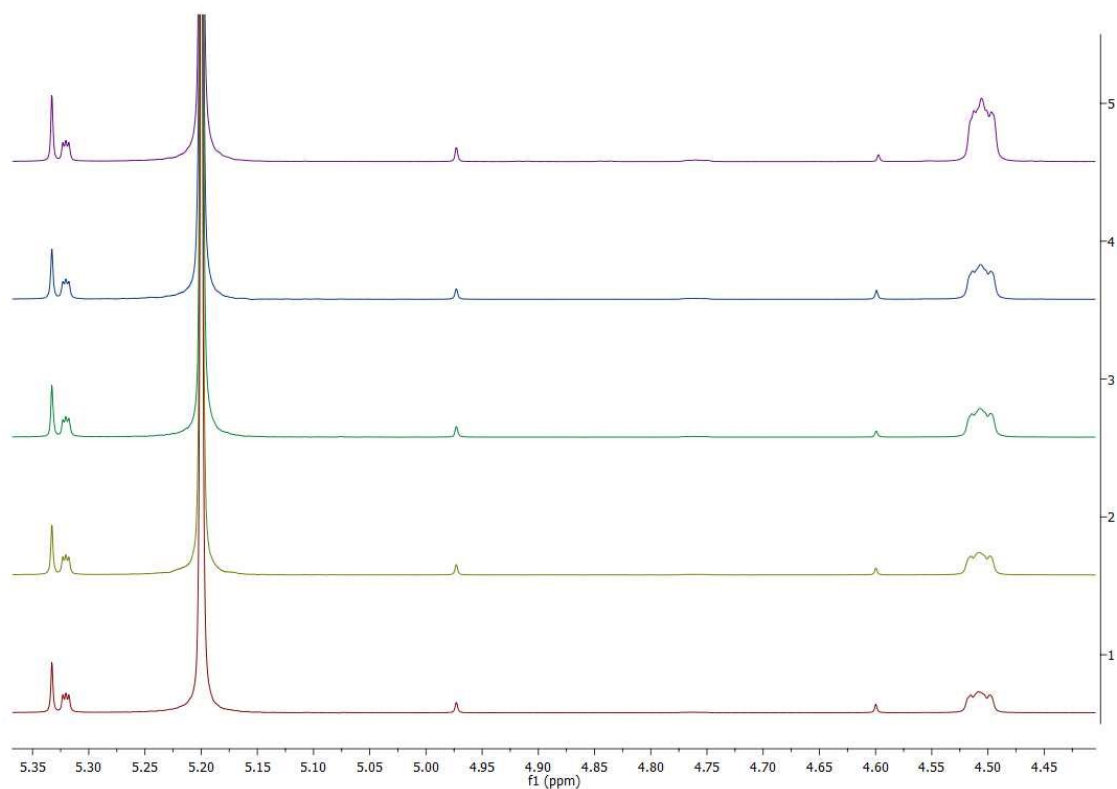
Figure S113. Expansion of the silicon hydride region in the time dependent ^{1}H NMR spectra (CD$_2$Cl$_2$, 298 K) of entry 3 [(^{Si}R)-**3**, 0.2M] as reported in table S1. Only spectra recorded at 0, 13, 20, 24 and 31% conversion are shown for clarity.
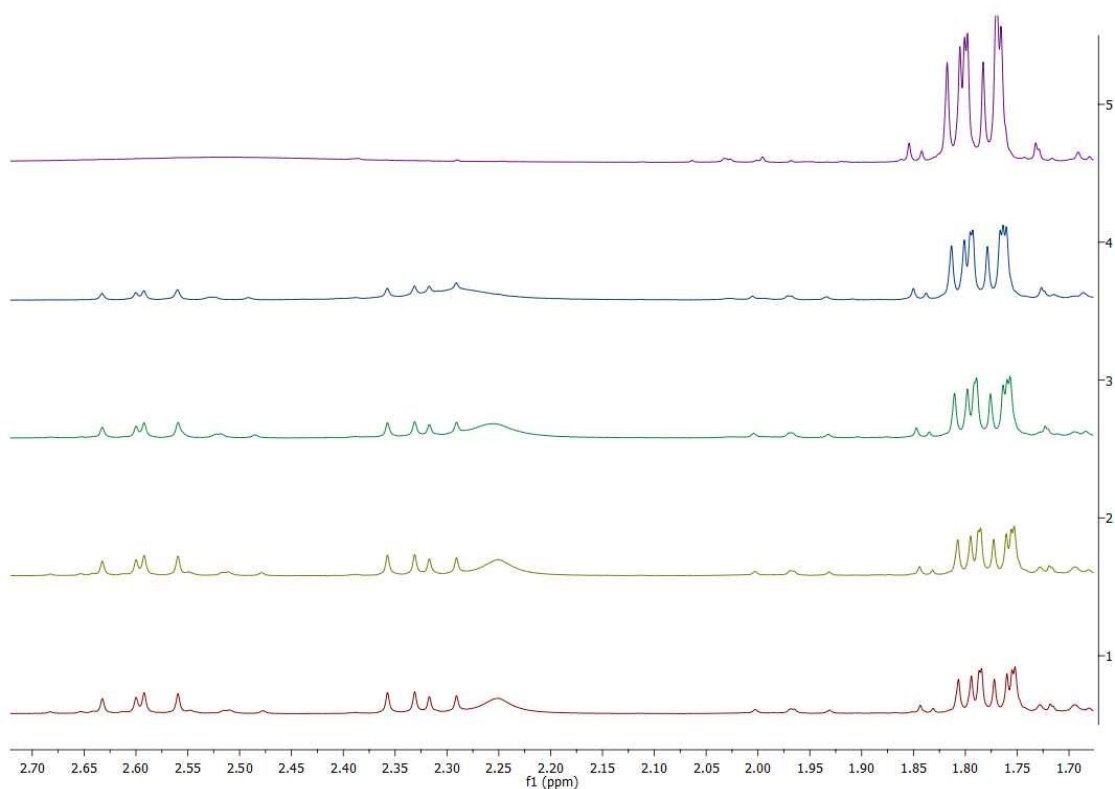
Figure S114. Expansion of the methylene region in the time dependent ^{1}H NMR spectra (CD$_2$Cl$_2$, 298 K) of entry 3 [(^{Si}R)-**3**, 0.2M] as reported in table S1. Only spectra recorded at 0, 13, 20, 24 and 31% conversion are shown for clarity.
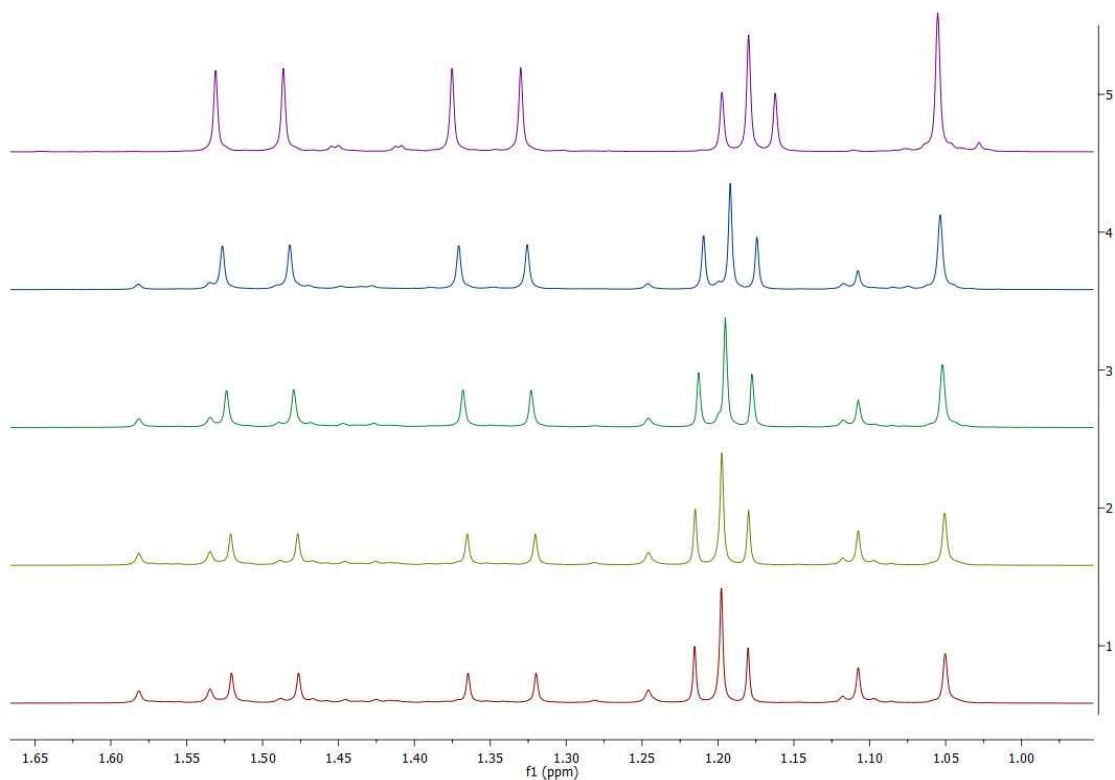
Figure S115. Expansion of the aliphatic region in the time dependent ^{1}H NMR spectra (CD$_2$Cl$_2$, 298 K) of entry 3 [(^{Si}R)-**3**, 0.2M] as reported in table S1. Only spectra recorded at 0, 13, 20, 24 and 31% conversion are shown for clarity.
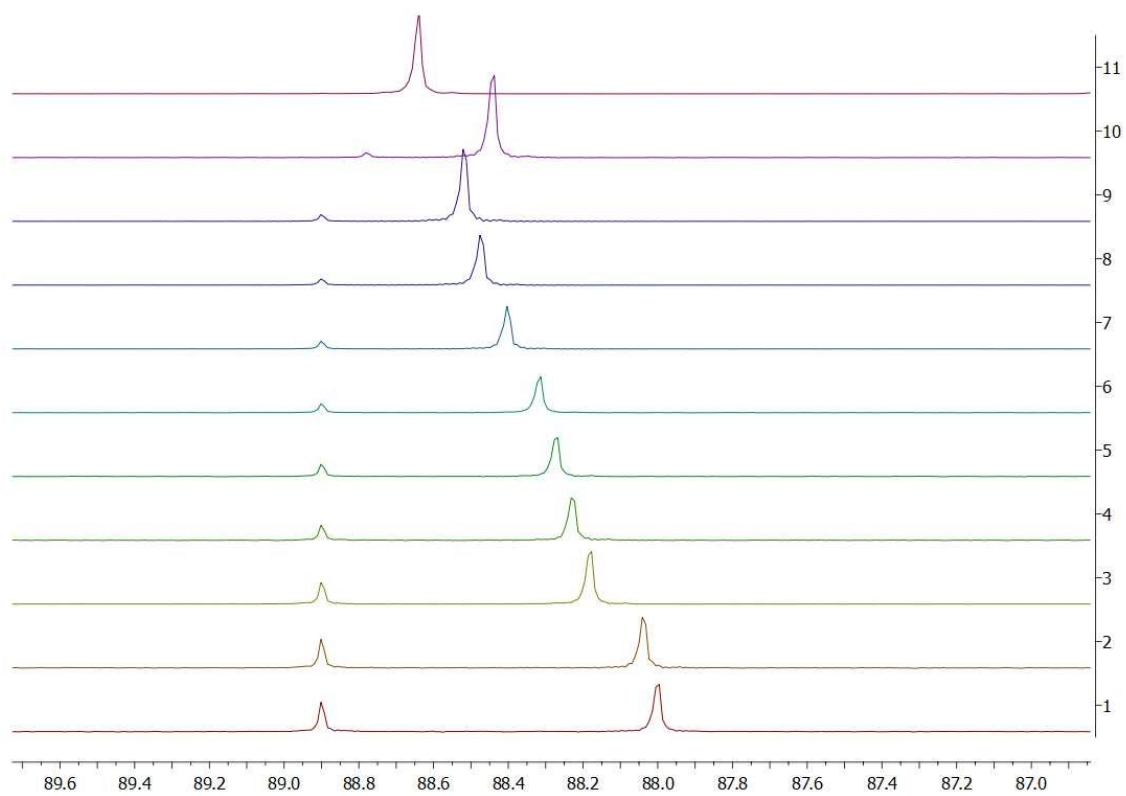
Figure S116. Time dependent $^{31}P\{^1H\}$ NMR spectra (CD$_2$Cl$_2$, 298 K) of entry 3 [(^{Si}R)-**3**, 0.2M] as reported in table S1.

Entry	Experiment specifics and reaction rates	Time (min)	Substrate Concentration (mol L^{-1})	Conversion %
1	Racemic mixture 0.2 M Absence of ether Estimated reaction rate -3*10^{-6} mol L^{-1} min^{-}	704	2.12E-01	0
		1778	2.10E-01	1
		5214	1.99E-01	6.09
		7186	1.91E-01	9.72
		8519	1.86E-01	12.36
		9672	1.82E-01	14.12
		10375	1.78E-01	16.04
		10944	1.76E-01	16.9
		11682	1.71E-01	19.43
		13369	1.67E-01	21.33
		13816	1.64E-01	22.73
2	(^{Si}R)-3 (er. 98:2) 0.2 M Absence of ether Estimated reaction rate -3*10^{-7} mol L^{-1} min^{-1} (slowed down by 90% compared to entry 1)	648	2.12E-01	0
		1711	2.11E-01	0.38
		5158	2.10E-01	0.73
		7151	2.10E-01	1.02
		8464	2.09E-01	1.27
		9637	2.08E-01	1.87
		10340	2.07E-01	2.46
		10867	2.05E-01	2.97
		11606	2.02E-01	4.48
		13294	1.97E-01	6.82
		13740	1.95E-01	8.05
3	Racemic mixture 0.2 M heating Absence of ether Estimated reaction rate (RT) -4*10^{-6} mol L^{-1} min^{-1} Estimated reaction rate (60°C) -4*10^{-5} mol L^{-1} min^{-1}	1127	2.09E-01	1.32
		2559	2.03E-01	4.18
		6402	1.88E-01	11.02
		7446	1.82E-01	13.89
		8302	1.78E-01	16.16
		9202	1.75E-01	17.18
		11056 [a]	1.29E-01	39.23
		12571 [a]	5.00E-02	76.37
		14019 [a]	9.95E-03	95.3
4	(^{Si}R)-3 (er. 98:2) 0.2 M heating Absence of ether Estimated reaction rate (RT) -7*10^{-7} min^{-1} (slowed down by 82% compared to entry 3)	1081	2.12E-01	0.1
		2514	2.11E-01	0.32
		6345	2.09E-01	1.09
		7387	2.08E-01	1.77
		8302	2.07E-01	2.28
		9202 [a]	2.05E-01	3.08

Estimated reaction rate (60°C) $-5*10^{-5}$ mol L^{-1} min^{-1}	11048 [a]	1.58E-01	25.23
	12570 [a]	6.06E-02	71.36

Table S2 Substrate concentrations and conversions recorded at different times in the absence of diethyl ether. Different enantiomeric ratios of the substrate are reported. Reaction rates have been estimated using a linear approximation. CH$_2$ClBr (10 µl) was used as an additional internal standard. a) Sealed NMR tube was heated to 60°C in an oil bath for approximately 50 hours.
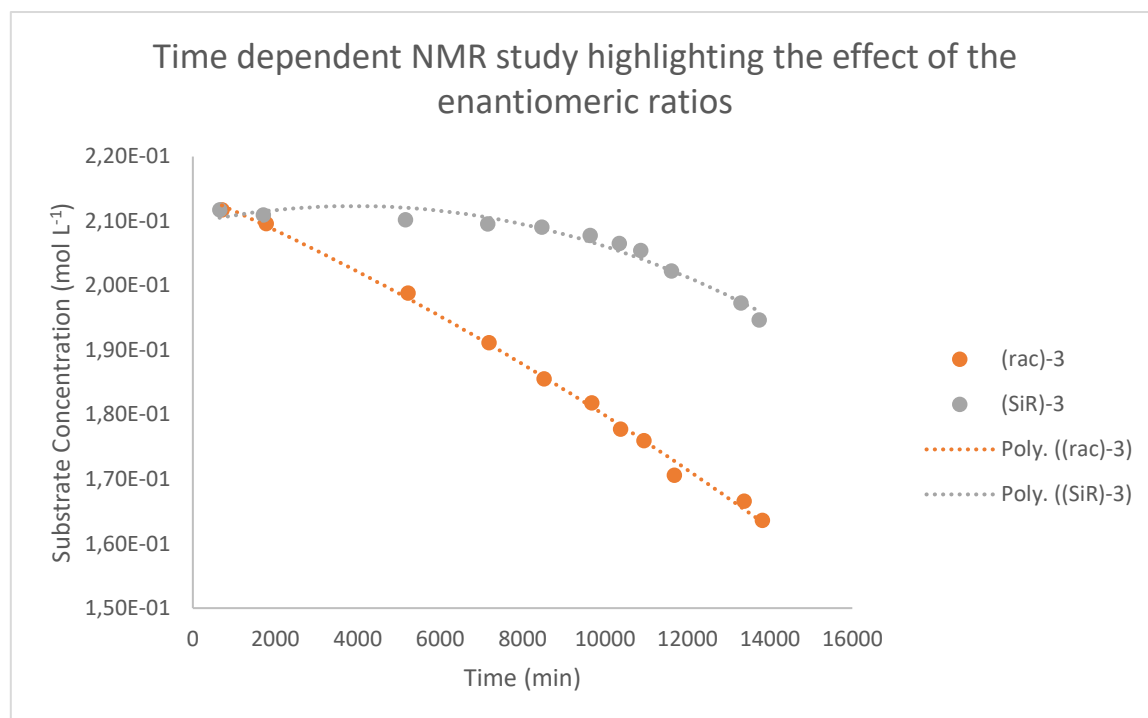
Figure S117 Trends for the conversion of compounds (*rac*)-**3** [Table S2, entry 1, orange] and (^{Si}R)-**3** [Table S2, entry 2, grey] into the four-membered cycle **5** in the absence of diethyl ether expressed with an order two approximation. The different slopes indicate a higher reaction rate for the racemic mixture.
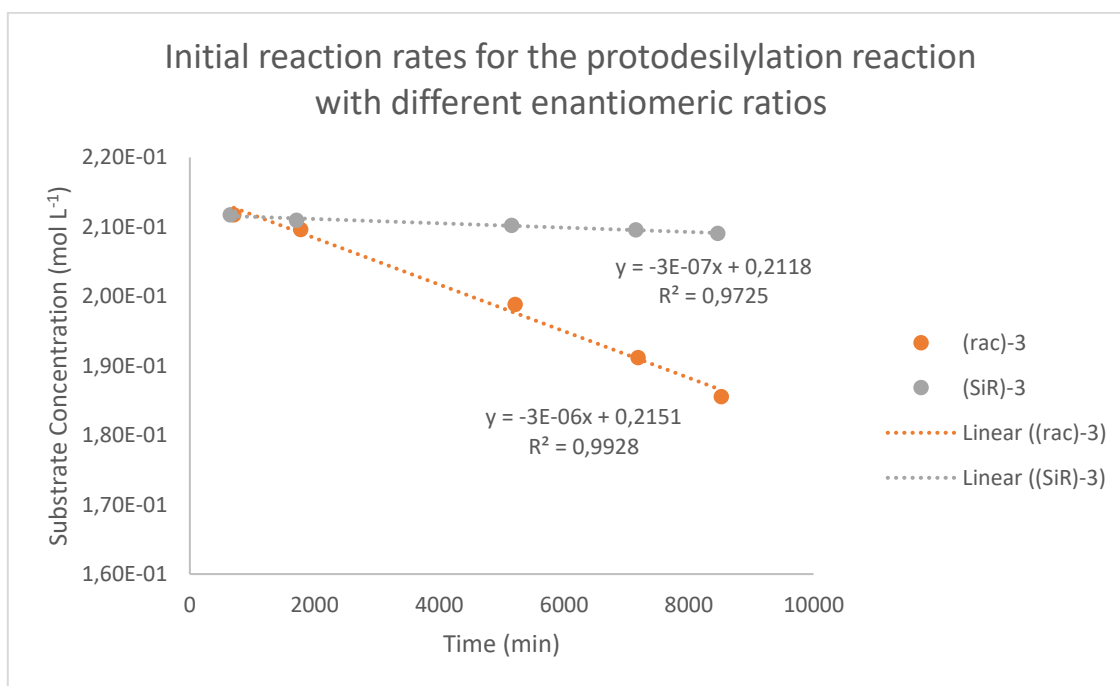
Figure S118 Initial reaction rates, expressed with a linear approximation, for the conversion of compounds (*rac*)-**3** [Table S2, entry, orange] and (*SiR*)-**3** [Table S2, entry, grey] into the four-membered cycle **5** in the absence of diethyl ether. A reaction rate higher by one order of magnitude is recorded for the racemic mixture. For the enantiomerically pure sample, a rate decrease of 90% is obtained.
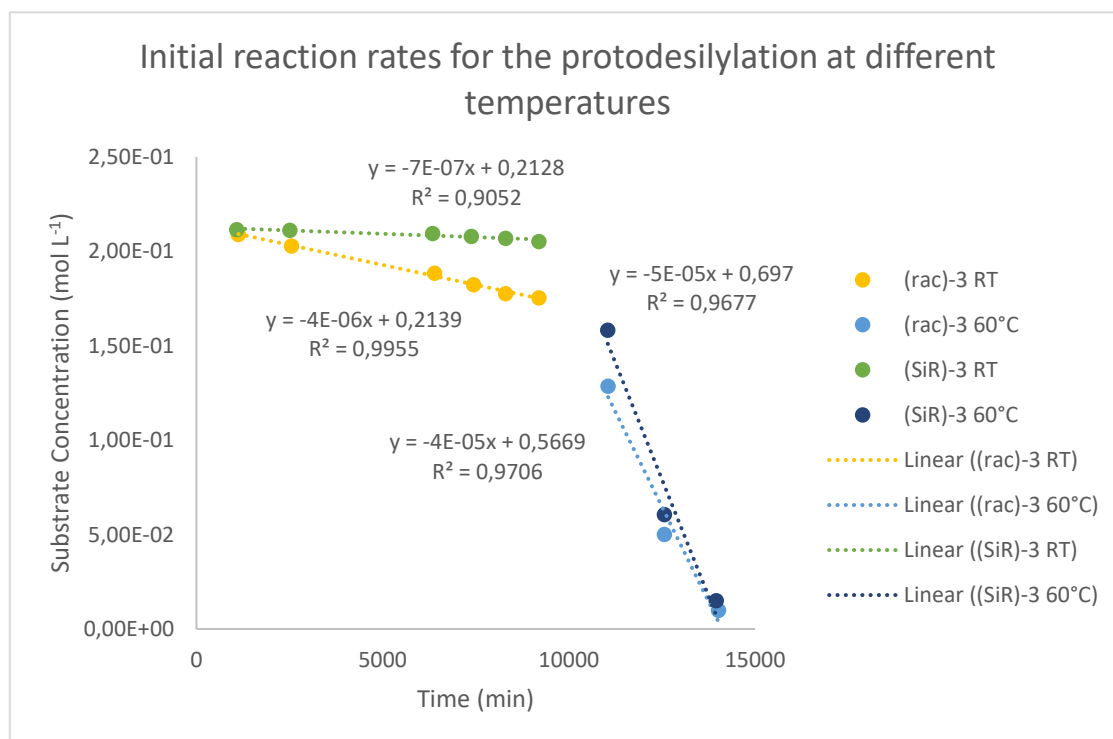
Figure S119 Initial reaction rates, expressed with a linear approximation, for the conversion of compound (*rac*)-**3** [Table S2, entry 3, RT yellow, 60°C light blue] and (*SiR*)-**3** [Table S2, entry 4, RT green, 60°C dark blue], into the four-membered cycle **5** in the absence of diethyl ether. The enantiomerically pure sample reacts 82% slower than the racemic mixture at room temperature.

NMR analysis of compound 5:

^{1}H NMR (400.30 MHz, CD$_2$Cl$_2$, 298 K): δ = 0.88 [s, 9H, SiC(CH_3)$_3$], 1.50 [dd, $^3J_{P-H}$= 18.8 Hz, 9H, PC(CH_3)$_3$], 1. [d, $^3J_{P-H}$= 18.6 Hz, 9H, PC(CH_3)$_3$], 2.18-2.37 [m, 2H, SiCH_2P], 5.01 [bs, 1H, SiH]. **^{11}B{^{1}H} NMR** (128.43 MHz, CD$_2$Cl$_2$, 298 K): δ = 16.9. **^{13}C{^{1}H} NMR** (100.66 MHz, CD$_2$Cl$_2$, 298 K): δ = 5.4 [d, $^1J_{C-P}$ = 22.3 Hz, SiCH$_2$P], 21.2 [s, SiC(CH$_3$)$_3$], 24.4 [s, SiC(CH$_3$)$_3$], 26.2 [d, $^2J_{C-P}$ = 2.0 Hz, PC(CH$_3$)$_3$], 26.2 [d, $^2J_{C-P}$ = 2.2 Hz, PC(CH$_3$)$_3$], 40.0 [d, $^1J_{C-P}$ = 23.3 Hz, PC(CH$_3$)$_3$], 41.3 [d, $^1J_{C-P}$ = 19.4 Hz, PC(CH$_3$)$_3$], 129.7 [s,*ipso*-C$_{Ar-borate}$], 136.8 [bd, $^1J_{C-F}$= 245.9 Hz, *meta*-C$_{Ar-borate}$], 138.6 [bd, $^1J_{C-F}$= 244.9 Hz, *para*-C$_{Ar-borate}$], 148.6 [bd, $^1J_{C-F}$= 242.1 Hz, *ortho*-C$_{Ar-borate}$]. **^{19}F{^{1}H} NMR** (376.66 MHz, CD$_2$Cl$_2$, 298 K): δ = -167.4 [bt, $^3J_{F-F}$ = 17.1, 8F, *meta*-F$_{Ar-borate}$], -163.4 [t, $^3J_{F-F}$= 20.2 Hz 4F, *para*-F$_{Ar-borate}$], -132.9 [bs, 8F, *ortho*-F$_{Ar-borate}$]. **^{31}P{^{1}H} NMR** (162.04 MHz, CD$_2$Cl$_2$, 298 K): δ = 91.7.
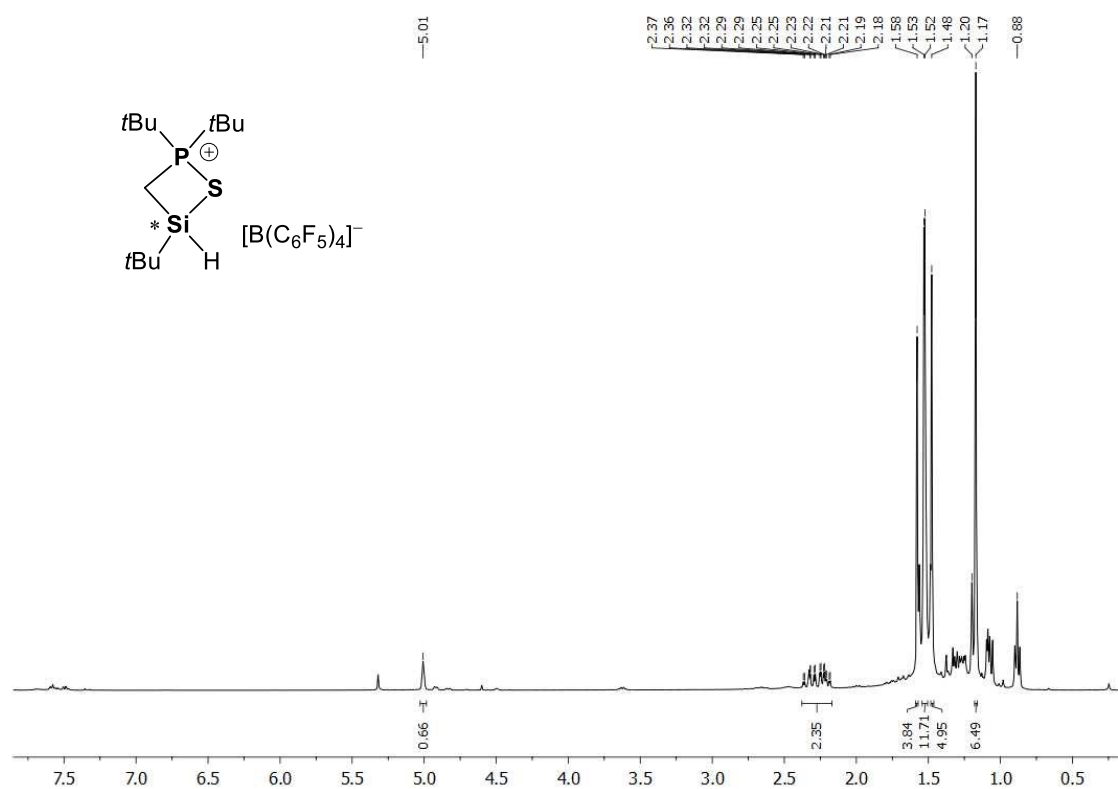
Figure S120. ^{1}H NMR (CD$_2$Cl$_2$, 298 K) of compound **5**.

—16.91
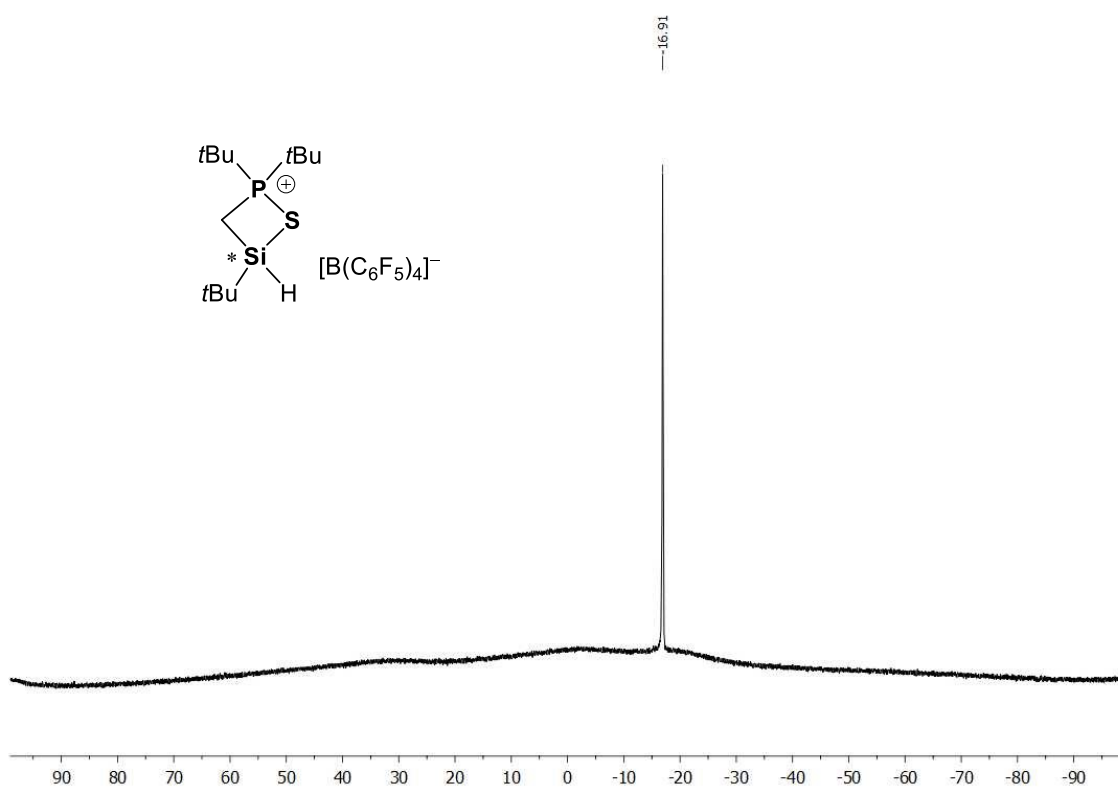
Figure S121. ^{11}B{^{1}H} NMR (CD$_2$Cl$_2$, 298 K) of compound **5**.
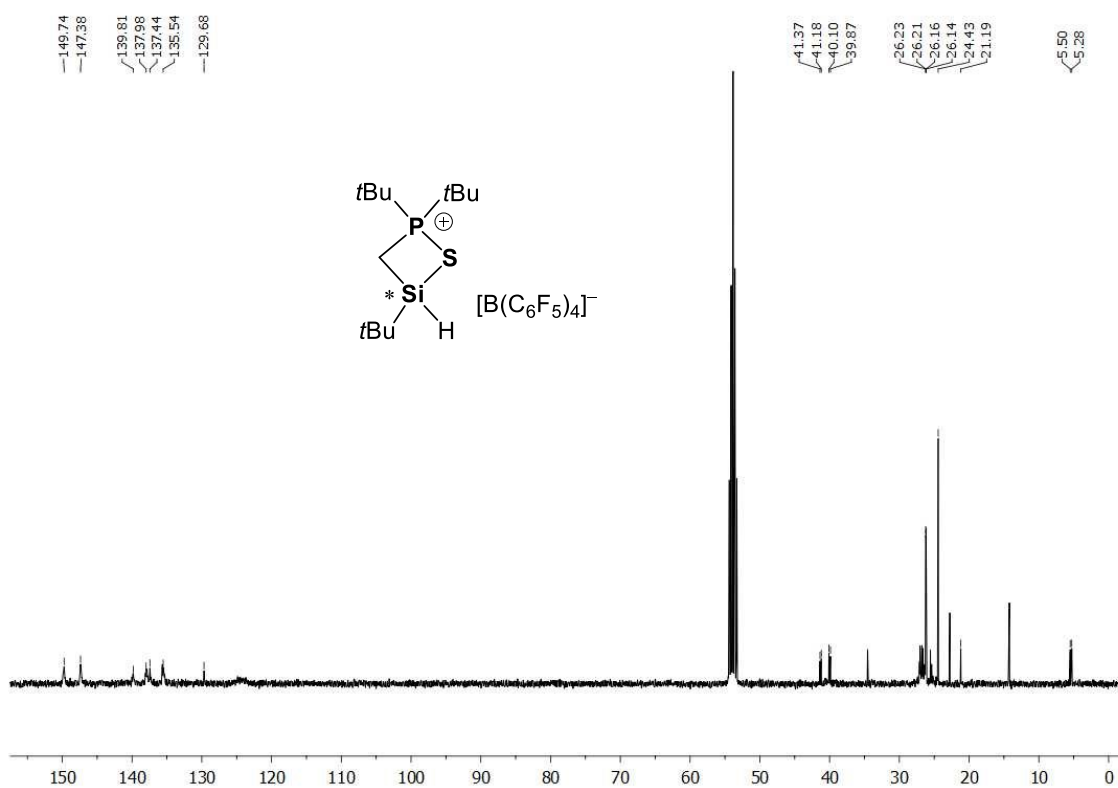
Figure S122. ^{13}C{^{1}H} NMR (CD$_2$Cl$_2$, 298 K) of compound **5**.
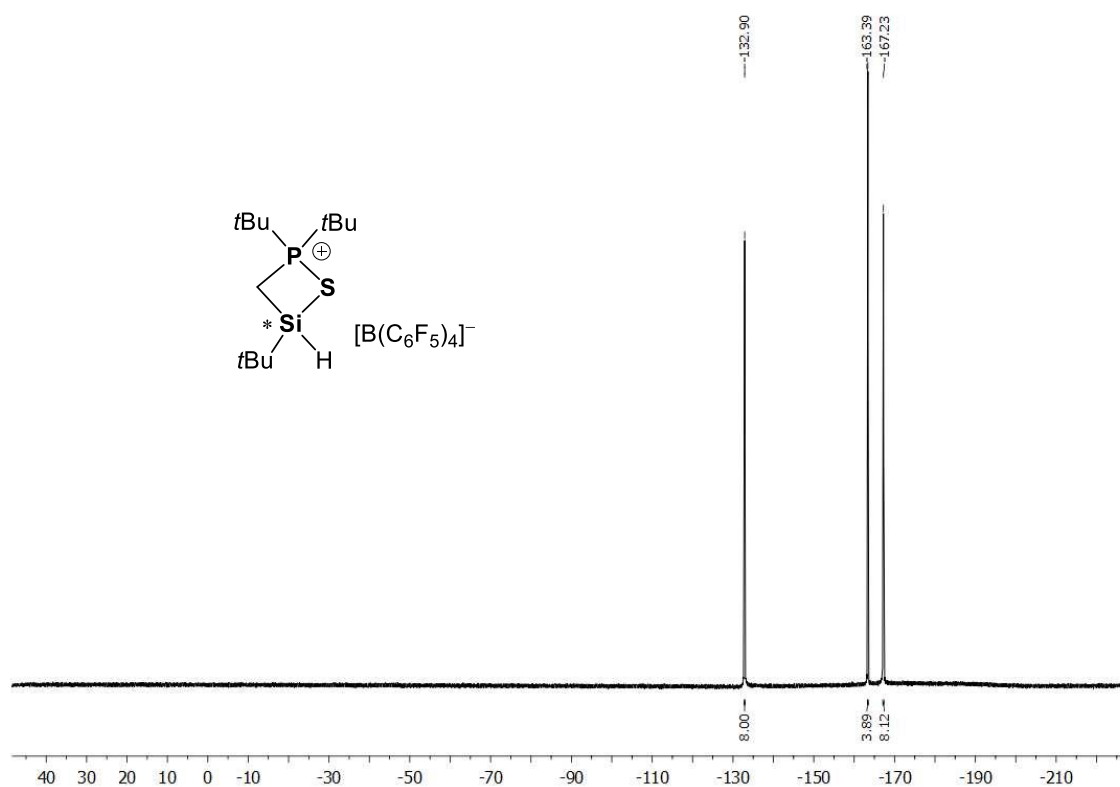
Figure S123. ^{19}F{^{1}H} NMR (CD$_2$Cl$_2$, 298 K) of compound **5**.
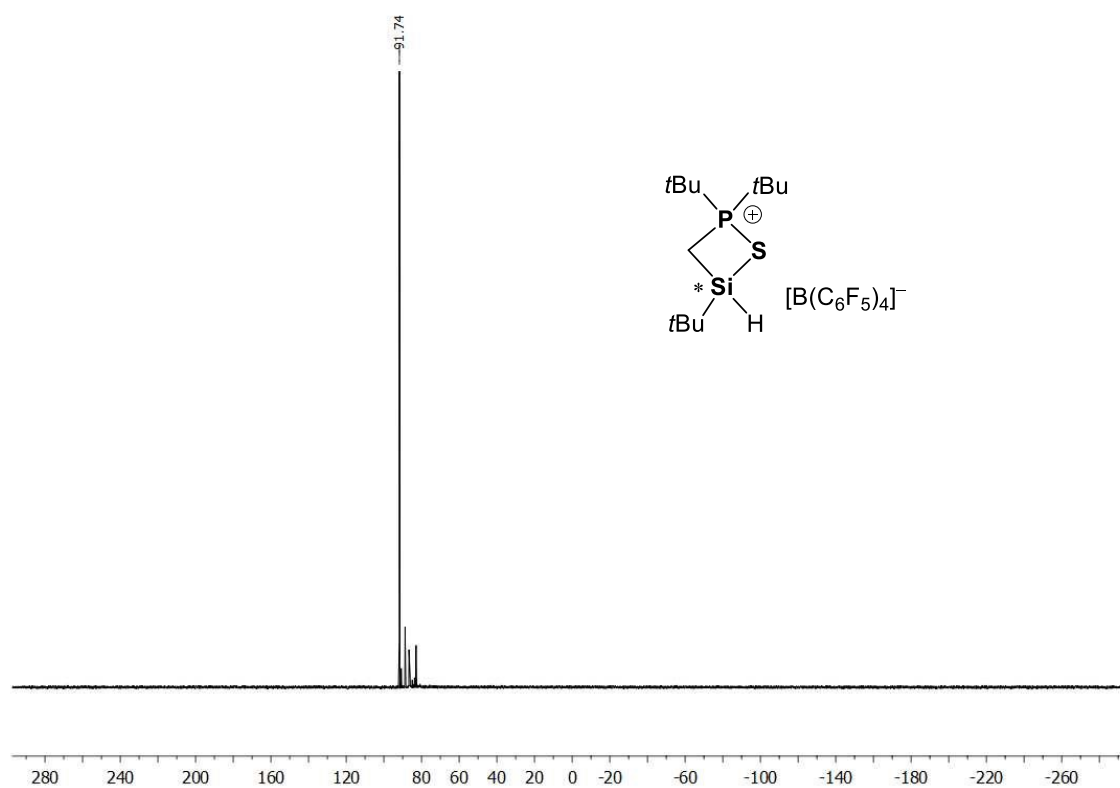
Figure S124. ^{31}P{^{1}H} NMR (CD$_2$Cl$_2$, 298 K) of compound **5**.

113
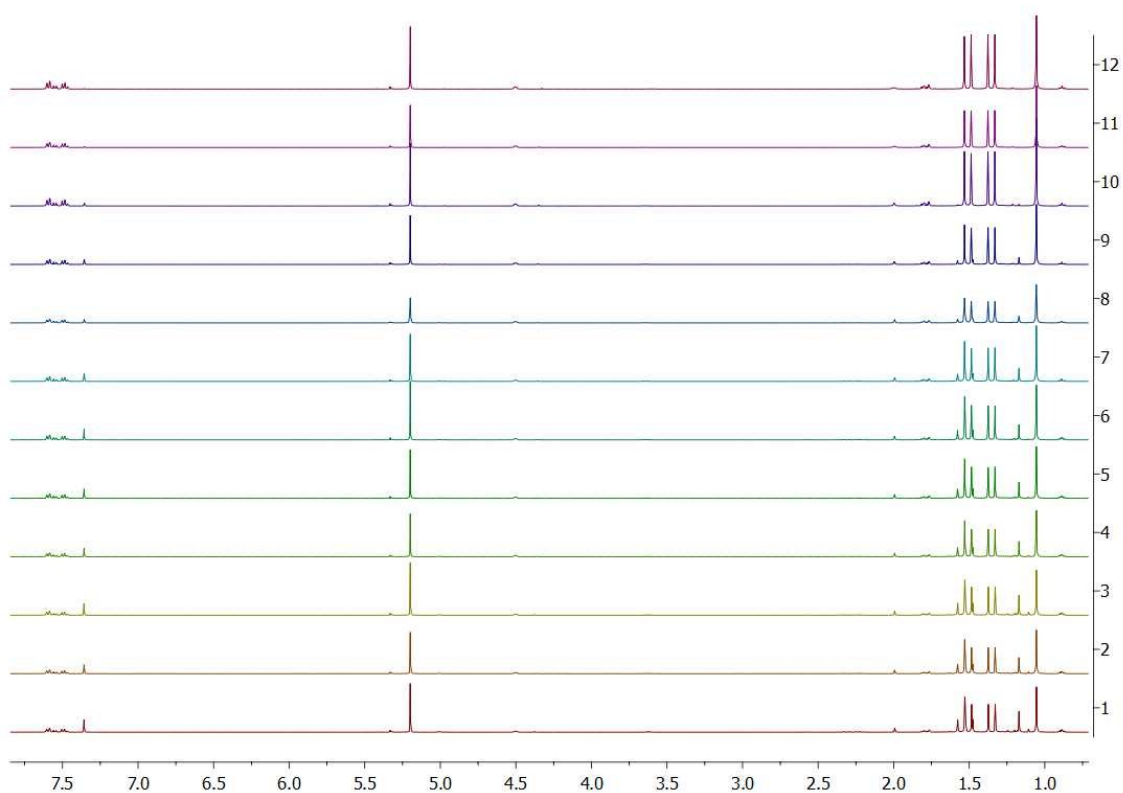
Figure S125. Time dependent ^1H NMR spectra (CD$_2$Cl$_2$, 298 K) of entry 1 [(*rac*)-**3**, 0.2M] as reported in table S2.
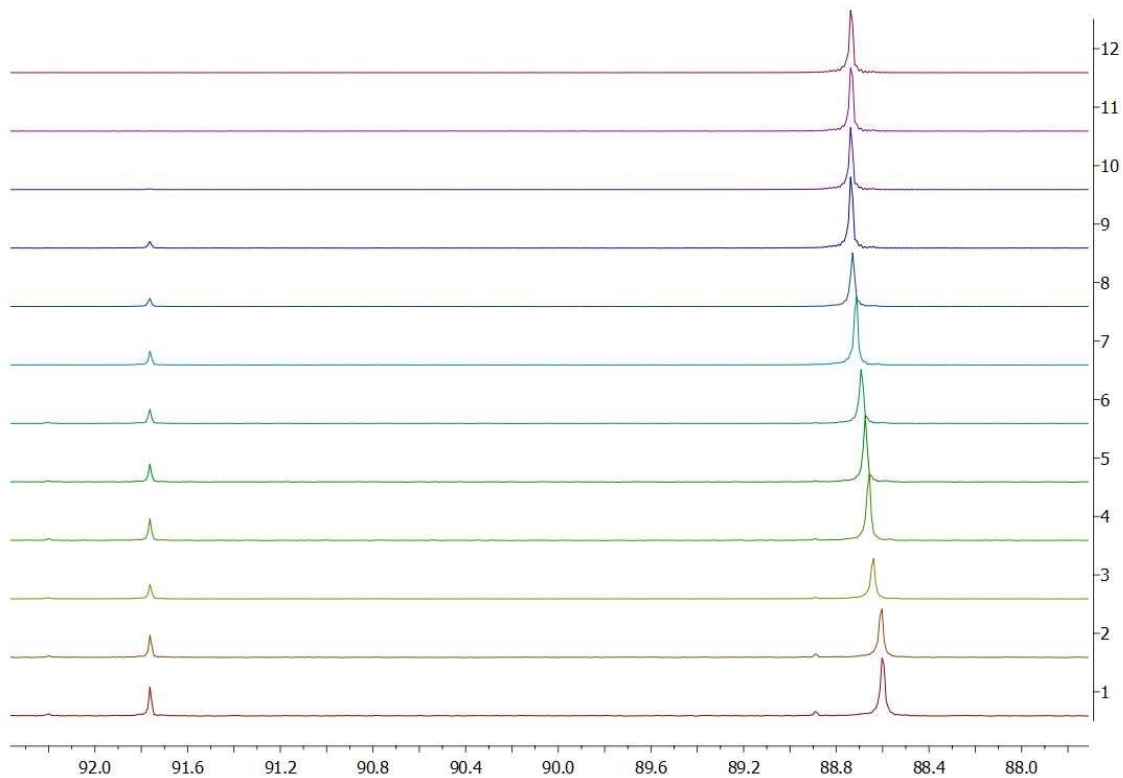
Figure S126. Time dependent $^{31}P\{^1H\}$ NMR spectra (CD$_2$Cl$_2$, 298 K) of entry 1 [(*rac*)-**3**, 0.2M] as reported in table S2.
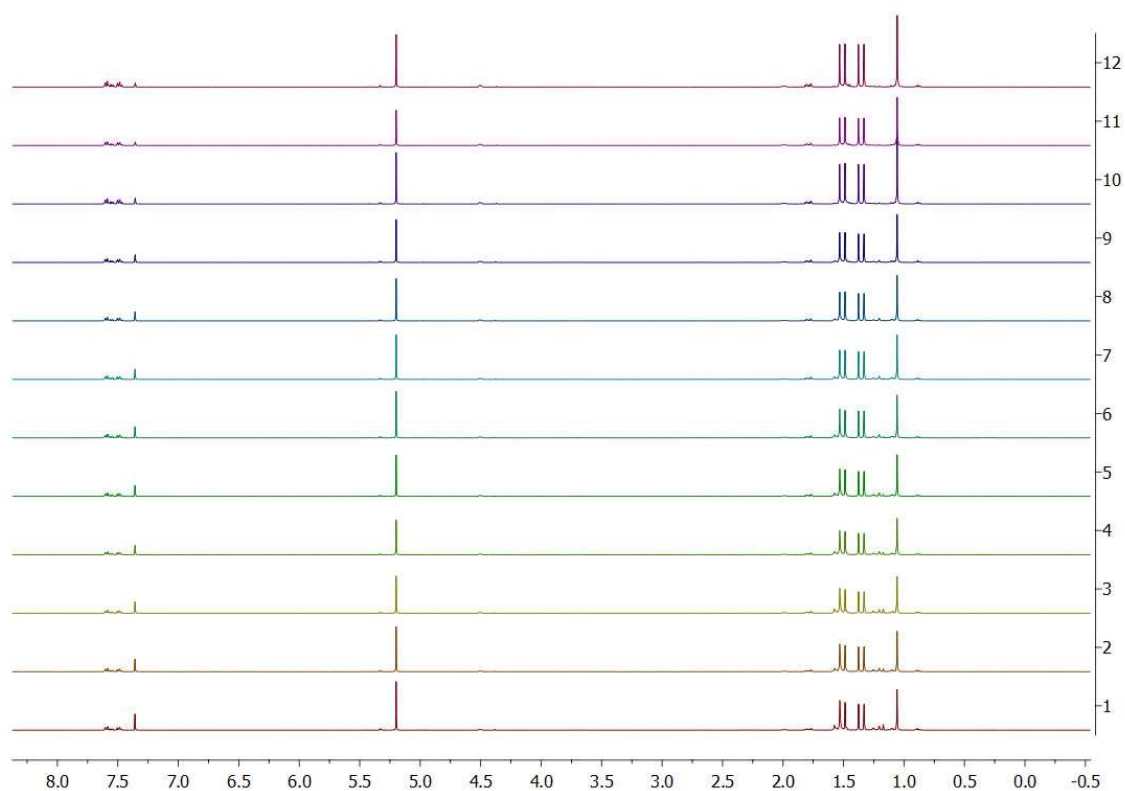
Figure S127. Time dependent ^{1}H NMR spectra (CD$_2$Cl$_2$, 298 K) of entry 2 [(^{Si}R)-**3**, 0.2M] as reported in table S2.
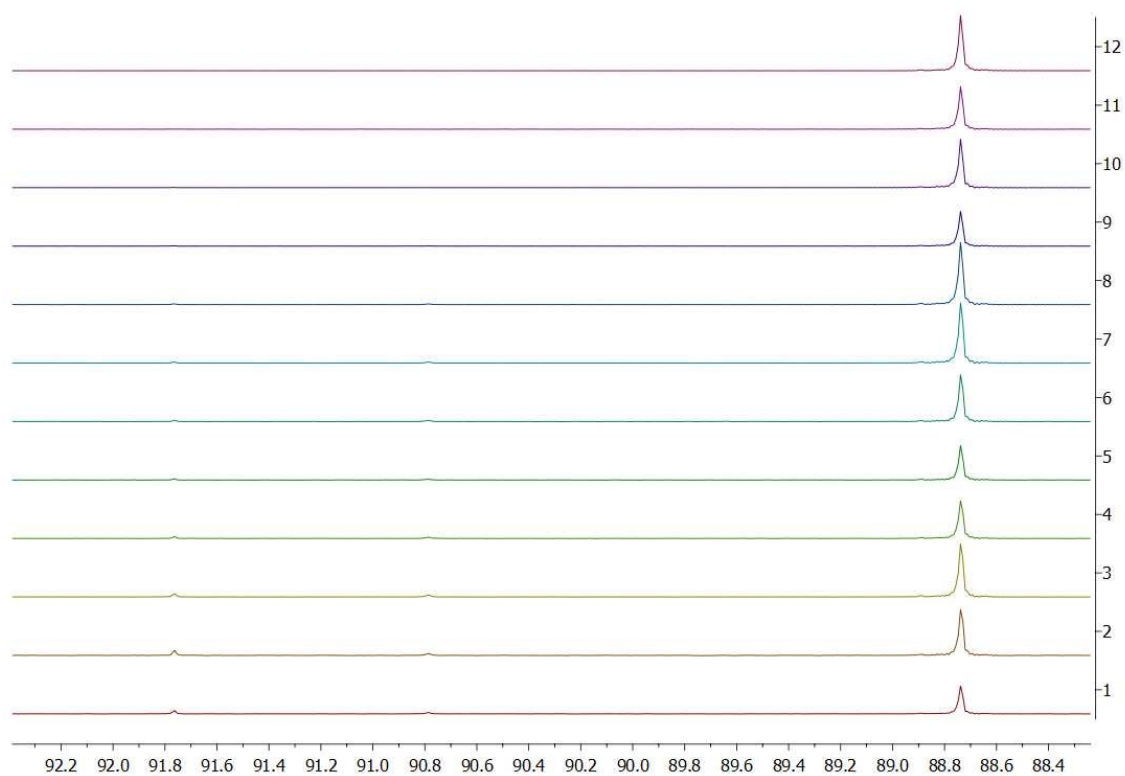
Figure S128. Time dependent ^{31}P{^{1}H} NMR spectra (CD$_2$Cl$_2$, 298 K) of entry 2 [(^{Si}R)-**3**, 0.2M] as reported in table S2.
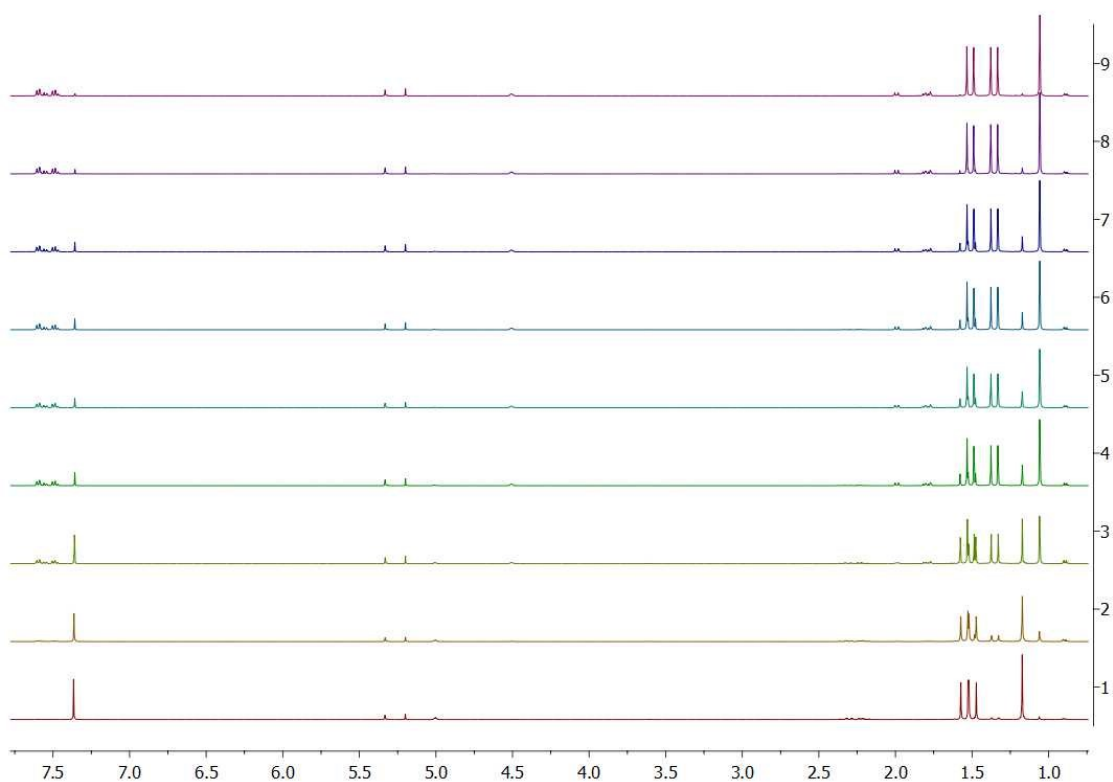
Figure S129. Time dependent ^{1}H NMR spectra (CD$_2$Cl$_2$, 298 K) of entry 3 [(*rac*)-**3**, 0.2M] as reported in table S2.
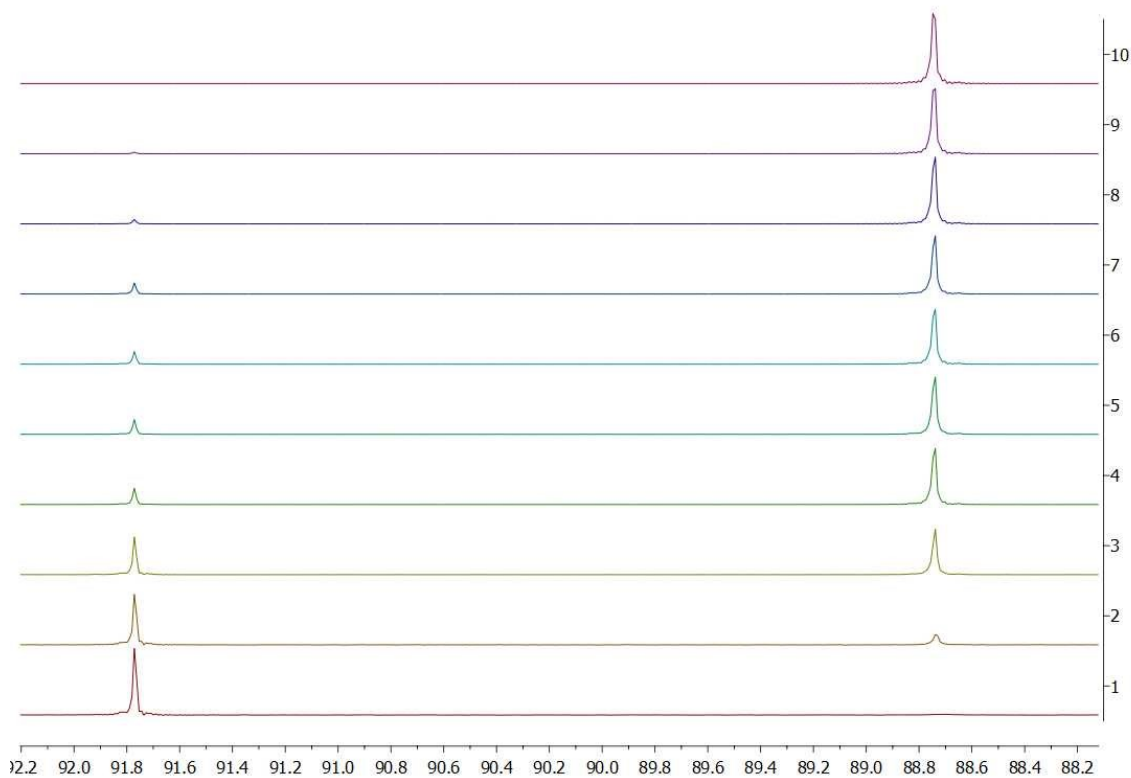
Figure S130. Time dependent ^{31}P{^{1}H} NMR spectra (CD$_2$Cl$_2$, 298 K) of entry 3 [(*rac*)-**3**, 0.2M] as reported in table S2.
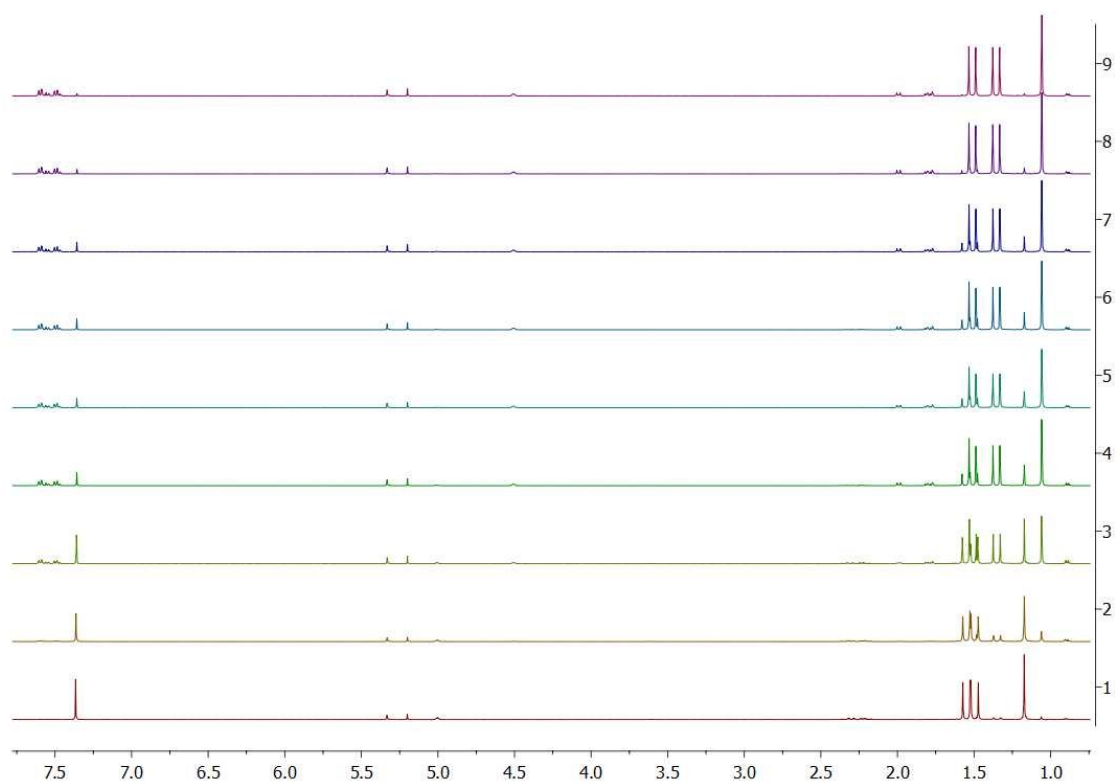
Figure S131. Time dependent ^{1}H NMR spectra (CD$_2$Cl$_2$, 298 K) of entry 4 [(^{Si}R)-**3**, 0.2M] as reported in table S2.
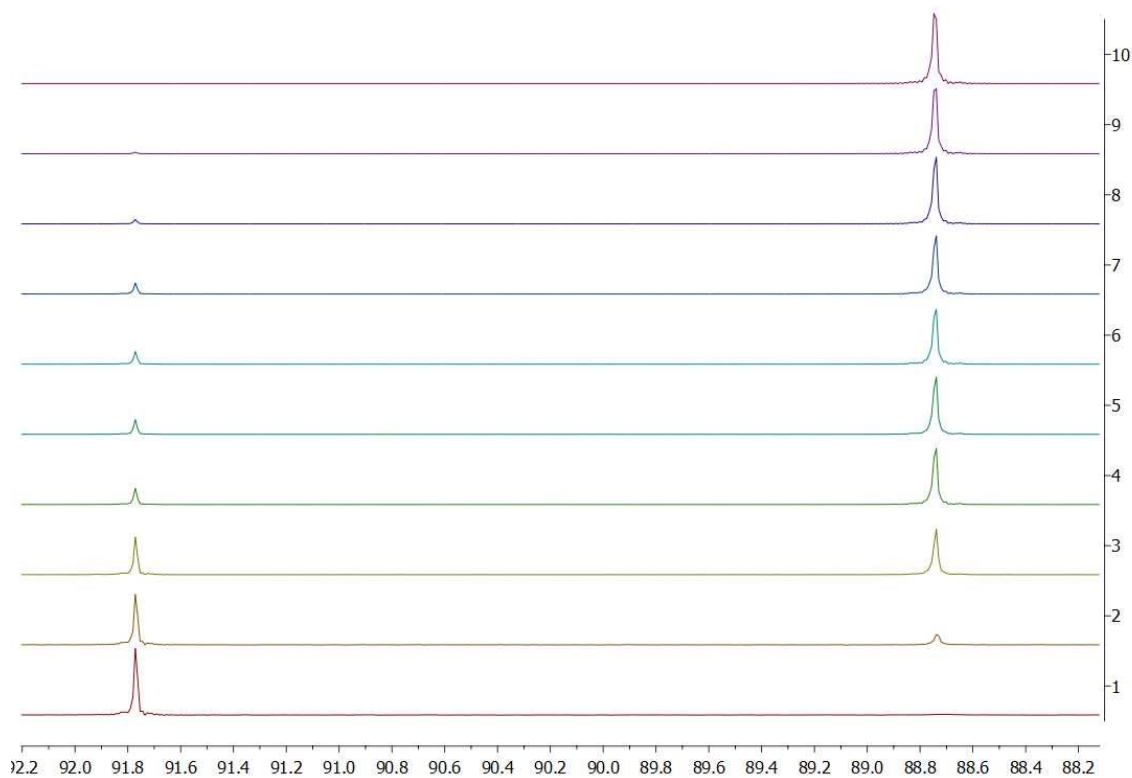
Figure S132. Time dependent ^{31}P{^{1}H} NMR spectra (CD$_2$Cl$_2$, 298 K) of entry 4 [(^{Si}R)-**3**, 0.2M] as reported in table S2.

3.5.20 HPLC Analysis and Enantiomeric Ratios

The chromatograms below have been recorded from pentane solutions of the reported compounds using the following conditions: Hexane/Isopropanol 99:1, flow of 0.9 mL^{-1}, 10 µl injected, 215 nm, 20°C for the hydrosilanes; Hexane/Isopropanol 98:2, flow of 0.9 mL^{-1}, 10 µl injected, 215 nm, 20°C for the fluorosilane.

Chromatogram of silane (*rac*)-**1**
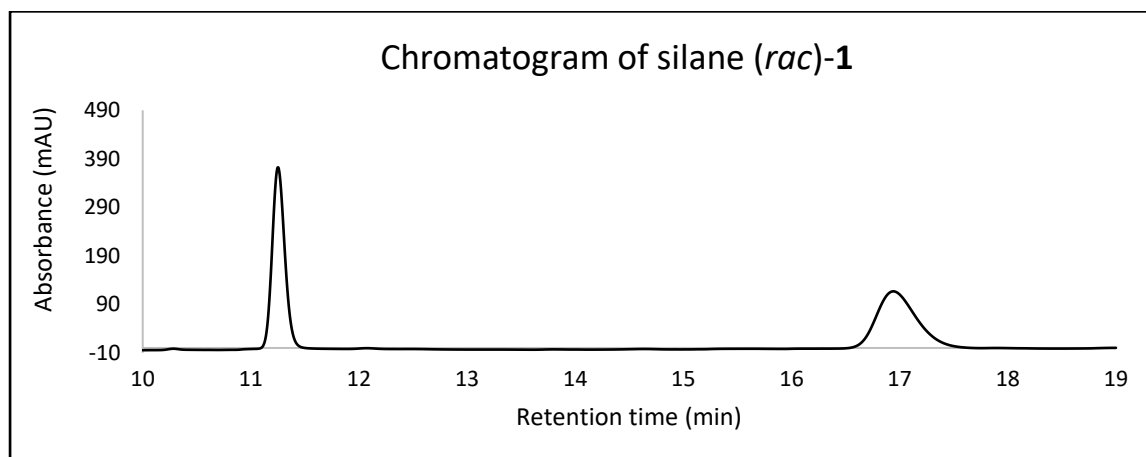
Retention time (Min)	Area	Area %
11.25	7513.65	50.3
16.94	7421.53	49.7

Chromatogram of silane (^{Si}S)-**1**
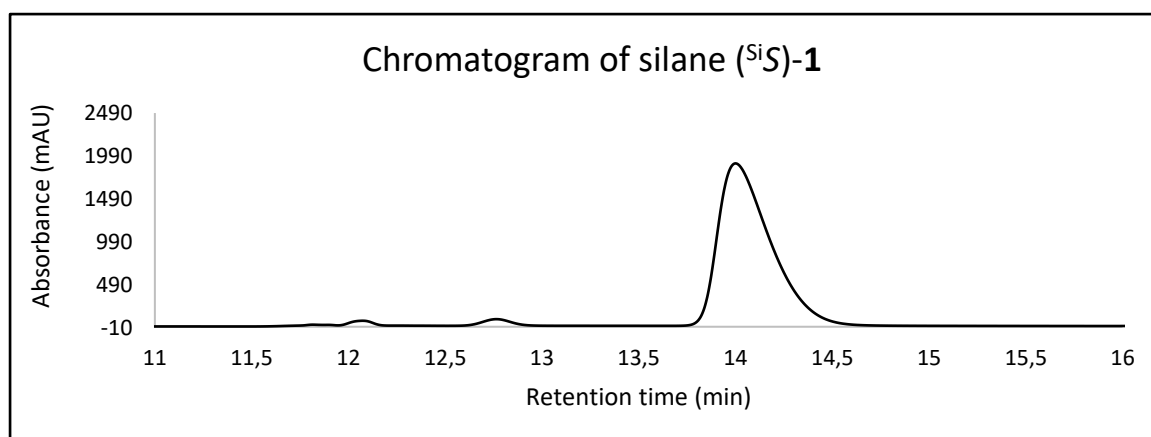
Retention time (Min)	Area	Area %
12.09	1671.59	1.8
14.02	92263.05	98.2

Chromatogram of silane (^{Si}R)-**1**
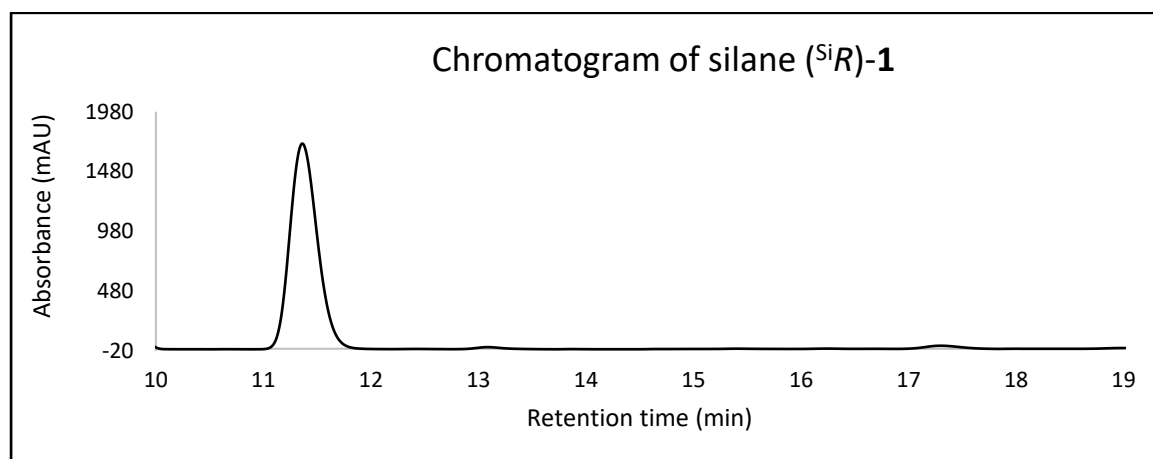
Retention time (Min)	Area	Area %
11.38	75572.27	98.2
17.34	1352.71	1.8

Chromatogram of silane (^{Si}S)-**1** after distillation
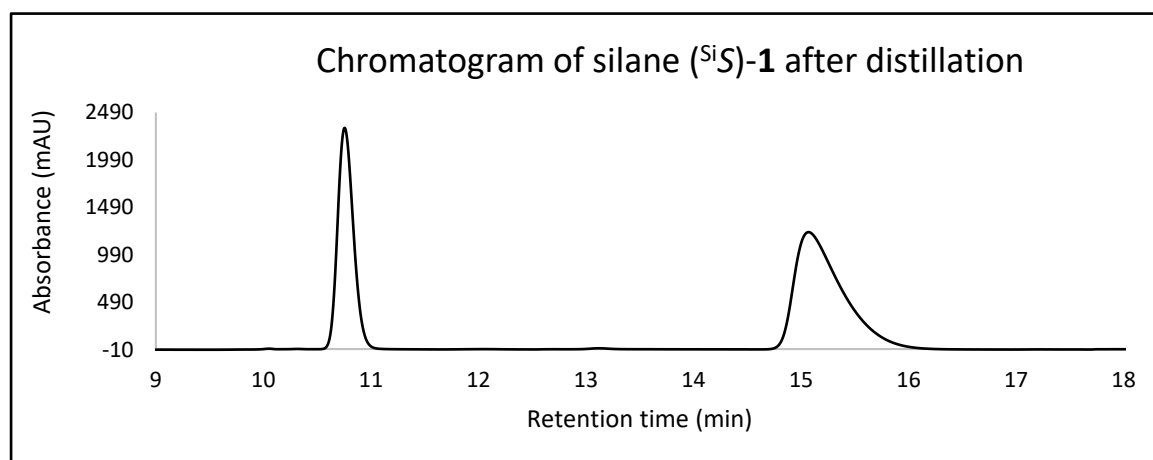
Retention time (Min)	Area	Area %
10.76	59545.25	38.7
15.1	94321.74	61.3

Chromatogram of silane (^{Si}R)-**1** after treatment with BCF and NaBHEt$_3$
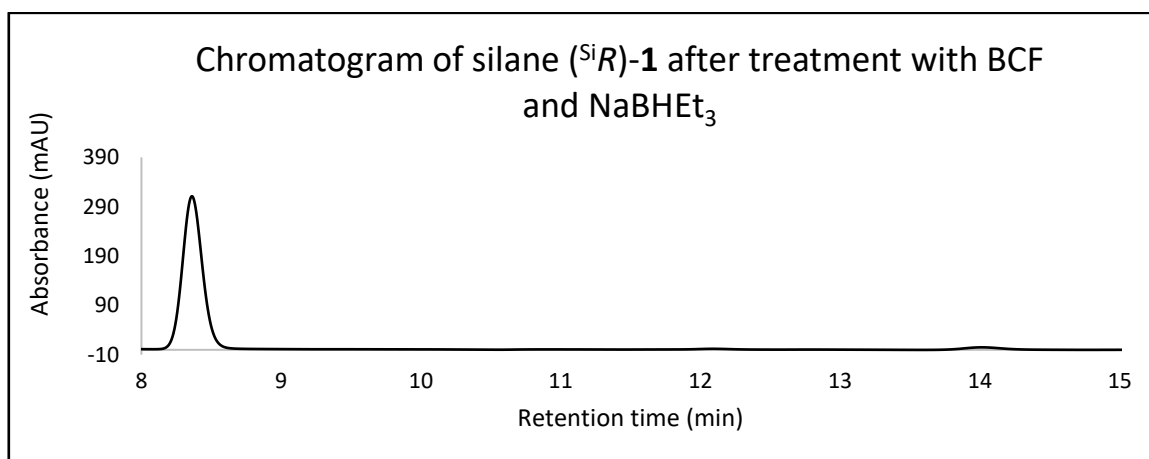
Retention time (Min)	Area	Area %
8.37	8054.39	97.6
14.07	194.75	2.4

Chromatogram of silane (^{Si}R)-**1** after protonation, dehydrogenation and treatment with NaBHEt$_3$
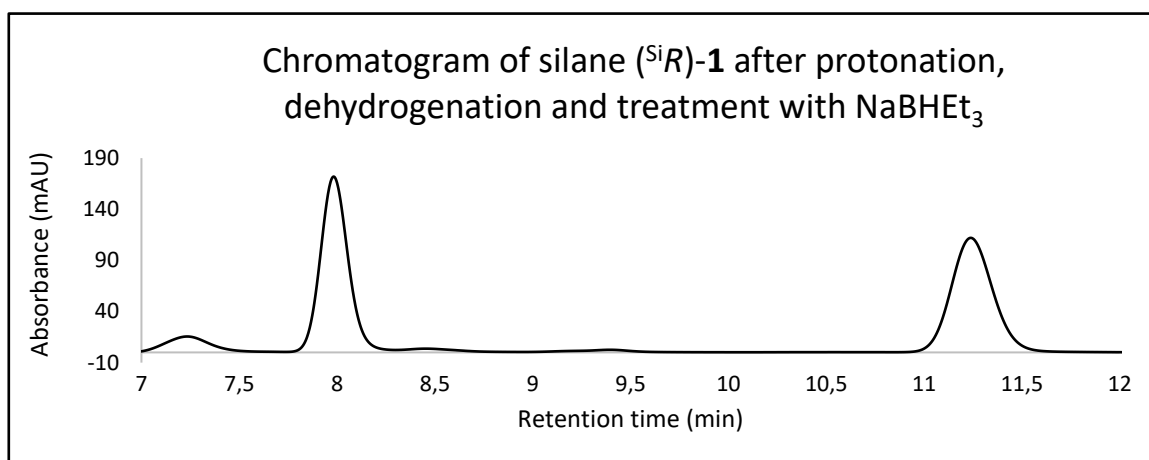
Retention time (Min)	Area	Area %
7.99	4290.87	50.6
11.26	4190.13	49.4

Chromatogram of (^{Si}R)-fluorosilane
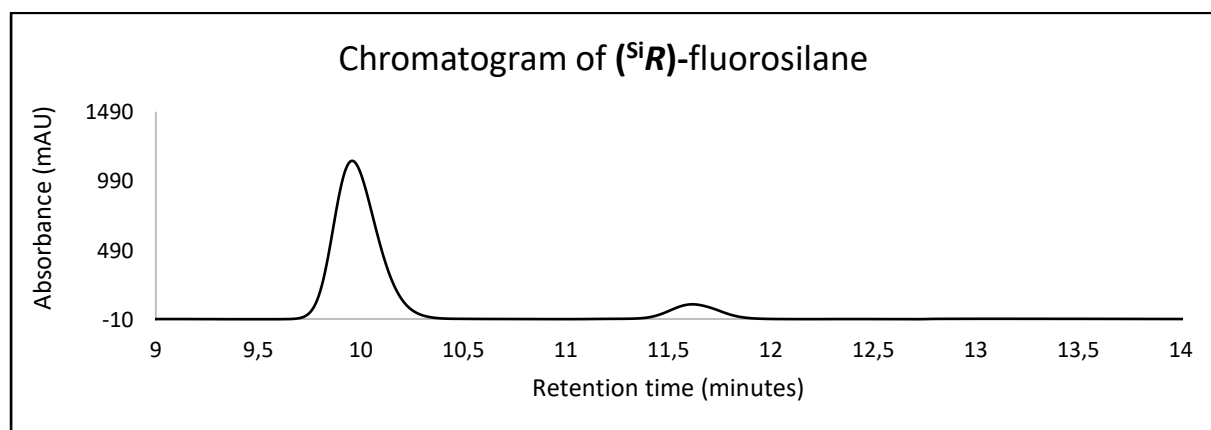
Retention time (Min)	Area	Area %
9.97	42758.79	90.5
11.62	4471.72	9.5

3.6   Quantum Chemical Calculations

Optimization and additional harmonic vibrational frequency analyses were performed with the software package Gaussian 09 (Revision E.01) on the M062X/6-31+G(d) level of theory without symmetry restrictions.[6] The GJF input files were created with the program GaussView 5.0. For the ground state structures, vibrational frequency analysis showed no imaginary frequency in the harmonical approximation. The relative enthalpies (ΔH) were indicated on the basis of the calculated zero-point-corrected energies (ZPE). Natural bond orbital (NBO) analysis has been performed on the M062X/6-31+G(d) level of theory. Bond ionicities (i_{AB}) of A–B bonds have been calculated according to the following equation: $i_{AB} = |c_A|^2 - |c_B|^2$ (with c_A and c_B being NBO polarization coefficients). The total (SCF) and zero-point-corrected (ZPE) energies of the calculated systems can be found in Table S3. Bond ionicities (i_{AB}) and natural atomic charges (Q_A) at atoms A can be found in Table S4. Figure S133 shows the model system to estimate the energetic difference in the matched/mismatched case. The calculated standard orientations of the optimized structures can be found in Tables S5–S9. The Hartree units were converted as follows:[7] 1 Hartree = 2625.4995 kJ·mol^{-1}, 1 cal = 4.184 J

Table S3 Total (SCF) and zero-point-corrected (ZPE) energies of the optimized structures.

Optimized structure	Method/Basis	SCF [Hartree]	ZPE [Hartree]
1	M062X/6-31+G(d)	−1773.74518474	−1773.240490
2-Cation	M062X/6-31+G(d)	−1772.95547382	−1772.458784
3-Cation	M062X/6-31+G(d)	−1774.11603987	−1773.602744
Matched	M062X/6-31+G(d)	−3545.83144127	−3544.834403
Mismatched	M062X/6-31+G(d)	−3545.82147117	−3544.823730

Table S4 Bond ionicities (i_{AB}) and natural atomic charges (Q_A).

Property	1	2-Cation	3-Cation
i_{CP}	0.261	0.214	0.211
i_{PS}	0.010	0.118	0.116
i_{SSi}	—	0.487	—
i_{SiC}	0.517	0.547	0.552
Q_C	−1.346	−1.341	−1.339
Q_P	1.441	1.513	1.526
Q_S	−0.598	−0.381	−0.203
Q_{Si}	1.601	1.821	1.599

Details on the NBO calculations: The phosphine sulfide unit in **1** shows a high concentration of the natural atomic charge (Q) on phosphorus (1.441) and sulfur (–0.598), but only an extremely low degree of ionicity (i_{PS} = 0.010) within the P–S σ-bond in accordance with a zwitterionic P^+–S^- formulation. The charge of the phosphorus center is only marginally affected when either the cyclic cation **2** (Q_P = 1.513) or the *S*-protonated species **3** (Q_P = 1.526) is formed, whereas the negative charge of the sulfur atom is noticeably reduced in both cationic species, either interacting with a silyl-cationic center (**2**: Q_S = –0.381) or with a proton (**3**: Q_S = –0.203). The heterocyclic cation of compound **2** has a significantly increased positive charge on the silicon atom (Q_{Si} = 1.821) compared to **1** (1.601) and **3** (1.599), thus leading to an increase of silicon electrophilicity. The S–Si bond within the cationic heterocycle has a considerably polar character (i_{SSi} = 0.487) (Table S4).

Details on the calculations regarding the matched/mismatched case:
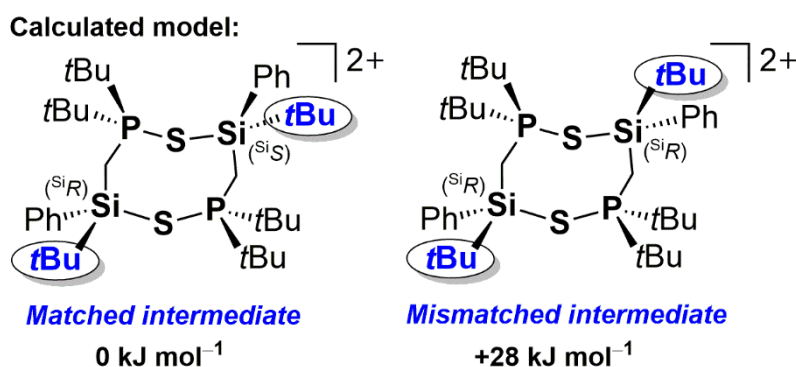
Figure S133 Intermolecularly stabilized, eight-membered intermediates as simplified models to estimate the energetic difference in the matched/mismatched case [M062X/6-31+G(d)].

Table S5 Standard orientation of 1 [M062X/6-31+G(d)].

Atomic symbol	x	y	z
Si	1.27293100	0.91902400	–0.30723700
C	–0.29849200	0.54382100	0.70152100
C	2.37456700	–0.60212700	–0.27715400
P	–1.65514700	–0.31345300	–0.19254400
S	–1.02590900	–1.33670000	–1.76474500
C	–2.83140200	1.06688000	–0.71349900
C	–2.41248400	–1.44280600	1.11586300
C	–3.55239300	1.72932600	0.46594900
C	–3.86488500	0.53095500	–1.71380700
C	–1.97590800	2.12138700	–1.43491000
C	–3.78224200	–1.94977400	0.64883900
C	–1.46648400	–2.64734600	1.25431400
C	–2.54530600	–0.76967100	2.49036200
C	2.63330300	–1.30047300	0.91170700
C	3.47470400	–2.41182800	0.93171200
C	4.07755500	–2.84673400	–0.24727300
C	3.83358200	–2.16777400	–1.44002500

C	2.98956700	–1.05864800	–1.45119300
H	0.02894700	–0.12919600	1.50362300
H	–0.68608100	1.44383300	1.19530400
H	–4.10258300	2.60227100	0.09276000
H	–2.86203200	2.08544500	1.23931800
H	–4.28117900	1.05851400	0.92969900
H	–4.47136400	1.37274200	–2.07048000
H	–3.37548700	0.06439900	–2.57281200
H	–4.54154700	–0.20093100	–1.26590800
H	–1.27665200	2.62461600	–0.75814900
H	–1.41036800	1.67773000	–2.26045600
H	–2.64225900	2.88871100	–1.84781500
H	–4.10176900	–2.76741600	1.30692200
H	–4.54914500	–1.16983300	0.69929900
H	–3.73602800	–2.33761900	–0.37449400
H	–1.82753300	–3.28109600	2.07396900
H	–0.43714400	–2.34886900	1.48700500
H	–1.43667800	–3.23674800	0.33518000
H	–3.17522400	0.12160500	2.47690800
H	–3.00608500	–1.48705000	3.18098700
H	–1.57332700	–0.49516800	2.91194600
H	2.17211900	–0.98145800	1.84646200
H	3.65717300	–2.93833300	1.86460600
H	4.72964100	–3.71558600	–0.23744800
H	4.29261600	–2.50862100	–2.36395800
H	2.79036200	–0.55211400	–2.39346500
H	0.98766700	1.28483300	–1.71459100
C	2.15366600	2.40353000	0.50435300
C	1.27322900	3.65519500	0.38136400
H	1.02730800	3.88038100	–0.66392700
H	0.33175600	3.55629700	0.93772600
H	1.79939100	4.52882000	0.79261600
C	3.47549600	2.64547200	–0.23933400
H	4.00015400	3.51006000	0.19215200
H	4.14351200	1.77895100	–0.16837900
H	3.30902700	2.85695300	–1.30301500
C	2.45092000	2.13520500	1.98520000
H	3.12904300	1.28321700	2.11202300
H	2.93588700	3.01169900	2.43874300
H	1.53662900	1.93407400	2.55909900

Table S6 Standard orientation of 2-Cation [M062X/6-31+G(d)].

Atomic symbol	x	y	z
Si	0.94244300	0.79530100	0.06425800
C	–0.41182700	0.30541300	1.33677600
C	2.31483300	–0.45657400	0.02298600
P	–1.59073300	–0.26702200	0.06681500

S	–0.50352500	0.41366300	–1.58302600
C	–3.22729700	0.63394300	0.10328600
C	–1.68063300	–2.13326500	0.09585400
C	–4.15906200	0.02118100	1.15804500
C	–3.87271900	0.58020900	–1.29087300
C	–2.95361500	2.10350400	0.45803500
C	–2.64622600	–2.62177700	–0.99208700
C	–0.27437000	–2.68642800	–0.18729600
C	–2.13184600	–2.62439900	1.48222800
C	2.79925200	–0.97956500	–1.18435400
C	3.84859600	–1.89588100	–1.19147200
C	4.42594100	–2.30270300	0.01104300
C	3.95823600	–1.78943700	1.22049400
C	2.91016600	–0.87135300	1.22468900
H	–0.12470100	–0.49112100	2.02837300
H	–0.81190100	1.14851100	1.90671200
H	–5.03120400	0.67649300	1.25889800
H	–3.68738400	–0.05111800	2.14473200
H	–4.52577400	–0.96531200	0.86349400
H	–4.82492100	1.11958400	–1.23997900
H	–3.25213100	1.07600400	–2.04342300
H	–4.08962700	–0.43570300	–1.62667200
H	–2.61629300	2.23102500	1.49125200
H	–2.22882500	2.56282400	–0.21966200
H	–3.89570100	2.65272800	0.35599700
H	–2.57659800	–3.71352600	–1.04608600
H	–3.68673300	–2.37262600	–0.76695600
H	–2.38674300	–2.22722500	–1.98108500
H	–0.34118400	–3.77974800	–0.17396300
H	0.45881200	–2.39506800	0.57233500
H	0.10357000	–2.38265600	–1.16713100
H	–3.15863200	–2.34936700	1.72474000
H	–2.08001900	–3.71868600	1.47597300
H	–1.47467400	–2.27759300	2.28609900
H	2.34853400	–0.68212400	–2.13026000
H	4.21464900	–2.29354100	–2.13317500
H	5.24233000	–3.01872500	0.00574600
H	4.40885300	–2.10363300	2.15716300
H	2.55921500	–0.47975200	2.17934500
C	1.54757000	2.57637600	0.10372500
C	0.39865600	3.58908500	0.12272900
H	–0.21509400	3.52498000	–0.78279900
H	–0.25187500	3.46468700	0.99732300
H	0.81008000	4.60529400	0.16943400
C	2.42306500	2.80630500	–1.13959900
H	2.82683100	3.82653500	–1.11753500
H	3.27280000	2.11550600	–1.17856000

H	1.85004100	2.70452600	–2.07003000
C	2.40091500	2.73089400	1.37651800
H	3.26670200	2.05952900	1.37701700
H	2.78204700	3.75838400	1.43369100
H	1.82093000	2.55025200	2.29119100

Table S7 Standard orientation of 3-Cation [M062X/6-31+G(d)].

Atomic symbol	x	y	z
Si	1.40544400	0.97737300	–0.31403900
C	–0.23937700	0.77391500	0.67543800
C	2.24739000	–0.69515000	–0.28368200
P	–1.63027900	–0.13709700	–0.04295700
S	–1.00433600	–1.45321300	–1.54929500
C	–2.73575300	1.05683400	–0.95830000
C	–2.43042600	–1.13651400	1.31784600
C	–3.55734100	1.88161700	0.04405400
C	–3.67510800	0.31002700	–1.91935300
C	–1.83353600	1.99646400	–1.77679400
C	–3.75676000	–1.74057900	0.84056000
C	–1.46125300	–2.27549600	1.68091800
C	–2.65981900	–0.25316800	2.55656200
C	2.34705200	–1.46254000	0.88931100
C	2.96692700	–2.71158100	0.88406700
C	3.50452800	–3.21461400	–0.30044700
C	3.42564900	–2.46506200	–1.47412600
C	2.80230500	–1.21839300	–1.46322800
H	0.02971100	0.26693300	1.61001300
H	–0.62954600	1.75902200	0.96511900
H	–4.07282100	2.67094900	–0.51355500
H	–2.93768600	2.37375100	0.80193000
H	–4.32288300	1.28337400	0.54522900
H	–4.32326700	1.05341800	–2.39630300
H	–3.12892900	–0.20044900	–2.71833400
H	–4.32009600	–0.41313300	–1.41642700
H	–1.20728700	2.63528500	–1.14566200
H	–1.19117800	1.45088800	–2.47408700
H	–2.48351000	2.65317200	–2.36509600
H	–4.11172500	–2.43660100	1.60850100
H	–4.53303400	–0.98252800	0.70440200
H	–3.63936500	–2.30789600	–0.08886300
H	–1.85071500	–2.78058500	2.57117200
H	–0.45250100	–1.92094300	1.92226600
H	–1.38817800	–3.01868400	0.88213600
H	–3.33560400	0.58312500	2.36704900
H	–3.12215800	–0.87677200	3.32950000
H	–1.72696500	0.13897100	2.97209400
H	1.94979500	–1.08370000	1.83105300

H	3.03663300	–3.28750000	1.80229300
H	3.98890900	–4.18650700	–0.30728900
H	3.84911500	–2.85146500	–2.39637300
H	2.74107900	–0.64893100	–2.38896900
H	1.10017500	1.31593700	–1.72494600
C	2.39244400	2.36750000	0.49977600
C	1.63721700	3.69599000	0.34204000
H	1.43445600	3.93108000	–0.70985700
H	0.68392900	3.70117800	0.88642500
H	2.23934300	4.51804000	0.75066800
C	3.74513900	2.45848600	–0.22678900
H	4.34453400	3.27000500	0.20592000
H	4.32241300	1.53188100	–0.12932100
H	3.62287500	2.67470300	–1.29509600
C	2.63037700	2.07544000	1.98783400
H	3.18902100	1.14386400	2.13641200
H	3.22115400	2.88486100	2.43629500
H	1.69168600	2.01205800	2.55398000
H	0.08205100	–1.89121100	–0.87680800

Table S8 Standard orientation of Matched [M062X/6-31+G(d)].

Atomic symbol	x	y	z
Si	2.05866600	–0.10448100	1.00742700
C	1.02415100	–1.69757400	0.75249300
C	3.63787200	0.05917600	0.03386300
P	0.11206900	–2.52190400	–0.59725900
S	–1.21845200	–1.29470100	–1.60385800
C	–0.78770800	–3.94238100	0.25419500
C	1.25478900	–3.04737700	–1.99116700
C	0.14346000	–4.63250200	1.26896200
C	–1.28424900	–4.95861700	–0.78253500
C	–1.99951300	–3.37879000	1.00641500
C	0.50049100	–3.67824000	–3.17697000
C	1.95271600	–1.78377400	–2.52325200
C	2.27589600	–4.06025200	–1.44772000
C	4.41032500	–1.08574200	–0.22212300
C	5.68138600	–0.98761500	–0.78164300
C	6.20705500	0.26621100	–1.09221100
C	5.46508000	1.41603000	–0.82672000
C	4.19541600	1.31143700	–0.26210600
H	1.72030400	–2.47857000	1.09651200
H	0.27506600	–1.63280400	1.55703600
H	–0.37415700	–5.52523400	1.63630000
H	0.34861300	–4.00059600	2.13860500
H	1.09255800	–4.96494400	0.84056400
H	–1.96881500	–5.64761900	–0.27656400
H	–1.83816400	–4.48453200	–1.59998300

H	–0.47012800	–5.55834000	–1.19594600
H	–1.73409500	–2.61037500	1.74040800
H	–2.74695000	–2.96993800	0.32019300
H	–2.46754100	–4.20413200	1.55442600
H	1.22555300	–3.78465500	–3.99155600
H	0.10591200	–4.67057400	–2.96463400
H	–0.31024700	–3.04378900	–3.54528100
H	2.76685600	–2.09825700	–3.18560100
H	2.39362600	–1.16069900	–1.74483600
H	1.25996500	–1.17620000	–3.11127300
H	1.81409800	–5.02629400	–1.22615000
H	3.03039500	–4.23187900	–2.22284400
H	2.80266100	–3.71298100	–0.55396400
H	4.02638000	–2.07496800	0.02043200
H	6.26228900	–1.88540300	–0.97030000
H	7.19770000	0.34756200	–1.52885800
H	5.88022600	2.39475100	–1.04793700
H	3.64131600	2.21865100	–0.03307900
C	2.48978800	–0.13070300	2.87543000
C	1.25756600	–0.12867200	3.79000000
H	0.67260300	0.79275700	3.69069500
H	0.59479900	–0.98416100	3.60699100
H	1.58479000	–0.19657800	4.83501100
C	3.37851100	1.08120400	3.21203700
H	3.65886300	1.03471300	4.27149700
H	4.30403500	1.08630300	2.62698900
H	2.86485500	2.03596800	3.05311000
C	3.30452900	–1.41282800	3.14616100
H	4.19559400	–1.48668000	2.51309700
H	3.65202800	–1.39509800	4.18653900
H	2.70839500	–2.32675100	3.03123900
Si	–2.58663200	0.11696700	–0.52658800
C	–1.74654400	1.75983800	–1.02832300
C	–4.09756600	0.02349700	–1.69504600
H	–1.51543800	1.55037000	–2.07789700
H	–2.55238400	2.50732800	–1.05643000
P	–0.29973600	2.68546700	–0.42494700
C	–0.98042100	4.14147500	0.55278400
C	0.70360300	3.10414100	–1.95151300
S	0.90275000	1.79847700	1.03989400
C	–2.01196400	3.58816400	1.55174300
C	–1.66055100	5.13142000	–0.40878800
C	0.11865600	4.88052100	1.33331700
C	–0.18571300	3.67120300	–3.07434600
C	1.79772000	4.12303400	–1.60652500
C	1.32386900	1.78611600	–2.44005700
H	0.92369800	5.24542900	0.69245000

H	–0.34544300	5.75222600	1.80718800
H	0.55073500	4.26495800	2.12496700
H	–0.93051600	5.69465600	–0.99613000
H	–2.38077500	4.66553500	–1.08949700
H	–2.21522800	5.85514100	0.19795100
H	2.49852400	4.17263100	–2.44690000
H	1.38451200	5.12587800	–1.46529700
H	2.36582600	3.84879100	–0.71308700
H	1.86087700	1.98419600	–3.37457800
H	2.04468400	1.37512700	–1.72866400
H	0.56366200	1.02486200	–2.65256400
H	0.47208400	3.90399000	–3.91906300
H	–0.92700600	2.95467000	–3.43998800
H	–0.69578500	4.59468100	–2.79922300
H	–2.87128000	3.10973200	1.06972900
H	–1.56650800	2.87909500	2.25563400
H	–2.39637000	4.43285500	2.13349000
C	–2.93066500	–0.21431800	1.27521400
C	–2.00263900	0.07742100	2.28813600
C	–4.14907300	–0.80488800	1.65697900
C	–2.27930700	–0.20288700	3.62503300
H	–1.05193600	0.53713200	2.03843300
C	–4.42641700	–1.09250100	2.99123900
H	–4.90314100	–1.05323300	0.91911500
C	–3.49193100	–0.79161700	3.97990800
H	–1.55122500	0.04282300	4.39288000
H	–5.37656000	–1.54571400	3.25714500
H	–3.71008400	–1.00829000	5.02123900
C	–4.63633100	–1.41409300	–1.82769900
C	–3.72294200	0.50626800	–3.11134800
C	–5.19587100	0.96157300	–1.15179100
H	–3.91495400	–2.06765000	–2.32962300
H	–4.89794900	–1.87924000	–0.87335000
H	–5.54683300	–1.39851100	–2.43879000
H	–3.49530600	1.57758100	–3.14424200
H	–2.87850800	–0.04626900	–3.54252900
H	–4.58012300	0.34658500	–3.77632600
H	–4.84679100	1.99733800	–1.05014100
H	–6.03285500	0.97878900	–1.86079500
H	–5.59407400	0.64903400	–0.18335000

Table S9 Standard orientation of Mismatched [M062X/6-31+G(d)].

Atomic symbol	x	y	z
Si	–2.49113700	–0.70846400	–0.63234800
C	–1.32020000	–2.21569200	–0.81593100
C	–3.59173900	–0.78364900	0.86762100
P	0.40828800	–2.46002400	–0.31017400

S	1.43944500	–0.96063900	–1.34973300
C	0.99663800	–4.03028600	–1.16437400
C	0.48697400	–2.51100900	1.55529000
C	0.35573300	–5.26431800	–0.50844100
C	2.52968200	–4.12838900	–1.09537700
C	0.56697600	–3.98146800	–2.64241800
C	1.78523400	–3.12794600	2.08474300
C	0.35023900	–1.07206700	2.05609900
C	–0.72480000	–3.30991200	2.07035400
C	–4.01040300	–2.02355900	1.37972600
C	–4.98795500	–2.09969200	2.36991000
C	–5.57345200	–0.93427400	2.86124000
C	–5.19458000	0.30462800	2.34488400
C	–4.22055000	0.37419800	1.35289200
H	–1.88747700	–3.08880600	–0.46065300
H	–1.27383300	–2.32102800	–1.90617800
H	0.63650200	–6.14000000	–1.10358800
H	–0.73898300	–5.22006400	–0.50474900
H	0.71157900	–5.43846800	0.50979600
H	2.82502600	–5.07316600	–1.56414300
H	3.01116200	–3.31785700	–1.64943000
H	2.91429200	–4.13719300	–0.07321900
H	–0.51318600	–4.10609200	–2.76657100
H	0.88783600	–3.06650600	–3.15088600
H	1.04638600	–4.82235400	–3.15447900
H	1.80277000	–2.98037400	3.17079900
H	1.84124600	–4.20366900	1.90114000
H	2.67356400	–2.64264400	1.67713800
H	0.08490000	–1.09681100	3.11953200
H	–0.44815200	–0.53304100	1.53409200
H	1.29185900	–0.52607500	1.95963900
H	–0.82181100	–4.30584400	1.63279600
H	–0.58978000	–3.44183400	3.14970600
H	–1.65568500	–2.75767200	1.92718700
H	–3.59865600	–2.95431100	0.99357300
H	–5.30018300	–3.06796900	2.74894900
H	–6.33615600	–0.99383300	3.63166800
H	–5.66799600	1.21328000	2.70489900
H	–3.95783100	1.34445000	0.93742400
C	–3.53124900	–0.71880400	–2.23492700
C	–2.69391900	–0.50687200	–3.50567100
H	–2.27416300	0.50243600	–3.56252500
H	–1.86555400	–1.22078300	–3.60208900
H	–3.33589200	–0.64602200	–4.38424600
C	–4.63403300	0.34966600	–2.16066800
H	–5.24864700	0.29452400	–3.06746200
H	–5.29796500	0.19455500	–1.30359800

H	–4.22540800	1.36490600	–2.10329400
C	–4.20056300	–2.10913500	–2.29547400
H	–4.80588300	–2.32194800	–1.40669600
H	–4.87612800	–2.13682900	–3.15920300
H	–3.47879600	–2.92387100	–2.43315100
Si	2.50048000	0.70668700	–0.36361700
C	1.33300600	2.00691000	0.46025800
C	3.57996200	1.29737500	–1.82652600
C	3.59094900	0.11065400	1.03857400
C	3.78352100	0.85700900	2.21283800
C	4.34471600	–1.06465800	0.87762300
C	4.68026000	0.43710800	3.19538200
H	3.24903400	1.79085100	2.37755300
C	5.24457400	–1.48553900	1.85262500
H	4.22810600	–1.66549700	–0.02289500
C	5.40987500	–0.73636700	3.01749400
H	4.81500000	1.03144500	4.09410700
H	5.81849100	–2.39559700	1.70314500
H	6.11197500	–1.06163400	3.77919900
C	4.80394800	0.36686700	–1.95106800
C	2.87619300	1.28881300	–3.19558500
C	4.10872900	2.69829800	–1.45520200
H	4.62300500	2.69398800	–0.48511300
H	4.84497300	3.01339300	–2.20481000
H	3.33407700	3.47128200	–1.42556200
H	1.87953400	1.73026100	–3.19566400
H	3.48851600	1.84412800	–3.91689700
H	2.77989600	0.26619600	–3.57583100
H	5.45328200	0.40072500	–1.07219900
H	4.51477000	–0.67471000	–2.13540100
H	5.39574700	0.69371000	–2.81495600
H	1.27486200	1.64597900	1.49383100
H	1.93835500	2.92639500	0.51716100
P	–0.37355600	2.59525800	0.14063900
C	–0.34312900	4.06077300	–1.05230700
C	–1.05929000	3.04179600	1.83704800
S	–1.56722900	1.29303700	–0.97350200
C	0.46342900	3.63199800	–2.28210200
C	0.34433600	5.26846100	–0.39466400
C	–1.74932300	4.46935400	–1.52516500
C	–0.05454400	3.91129800	2.61958600
C	–2.38417500	3.80225300	1.68454100
C	–1.27887300	1.75760700	2.64661200
H	–2.40694000	4.78925700	–0.71764600
H	–1.62172700	5.32324800	–2.19963900
H	–2.24337300	3.67533100	–2.08897600
H	–0.29530000	5.75572500	0.34441600

H	1.30876400	5.03000200	0.06741000
H	0.54088500	6.00355100	−1.18235900
H	−2.86648700	3.85036700	2.66654400
H	−2.22437800	4.83105700	1.35247100
H	−3.07856400	3.31560000	0.99293900
H	−1.77232600	2.03226700	3.58560000
H	−1.92251500	1.03305200	2.14295400
H	−0.33209600	1.27960300	2.91433400
H	−0.49240700	4.09547300	3.60712500
H	0.90308100	3.40851600	2.78508200
H	0.13176900	4.88308900	2.16423800
H	1.49854700	3.40057800	−2.02982900
H	0.01390100	2.77463700	−2.79095500
H	0.48016300	4.46805700	−2.98986500

3.7   X-Ray Crystallographic Details

The crystals were selected and measured on a GV50 diffractometer equipped with a TitanS2 detector ((*rac*)-**1**, (Si*R*)-**1**, (*rac*)-**2a**, (*rac*)-**2b**, **4a**, (*rac*)-**1-Se**, (*rac*)-**2a-Se**), on a SuperNova diffractometer equipped with an Atlas detector (**4b**) or on an Xcalibur, AtlasS2, Gemini ultra diffractometer ((*rac*)-**6**). The crystals were kept at T = 123(1) K ((*rac*)-**1**, (Si*R*)-**1**, (*rac*)-**2a**, **4a**, **4b,** (*rac*)-**1-Se**, (*rac*)-**2a-Se**, (*rac*)-**6**) or 90(1) K ((*rac*)-**2b**) during data collection. Data collection and reduction were performed with **CrysAlisPro** [Version 1.171.39.46 ((*rac*)-1-**Se**), Version 1.171.41.54a ((*rac*)-**1**, (*rac*)-**2a**, (*rac*)-**2b**, **4a**, **4b**, (*rac*)-**6**), Version 1.171.41.76a (Si*R*)-**1**, Version 1.171.41.89a ((*rac*)-**2a-Se**)].[8] For the compounds (*rac*)-**1**, (Si*R*)-**1**, (*rac*)-**2a**, (*rac*)-**2b**, **4a**, **4b,** (*rac*)-**1-Se**, (*rac*)-**2a-Se** and (*rac*)-**6** a numerical absorption correction based on gaussian integration over a multifaceted crystal model and an empirical absorption correction using spherical harmonics as implemented in SCALE3 ABSPACK was applied. Using **Olex2**,[9] the structures were solved with **ShelXT**[10] and a least-square refinement on F^2 was carried out with **ShelXL**[11] for all structures. All non-hydrogen atoms were refined anisotropically. Hydrogen atoms at the carbon atoms were located in idealized positions and refined isotropically according to the riding model. Figures were created with **Olex2**.[9]

Compound (*rac*)-1: The asymmetric unit contains one molecule of (*t*Bu)$_2$P(S)CH$_2$Si(H)Ph *t*Bu. The hydrogen atom on the Si atom was located from the difference Fourier map and refined without restraints.

Compound (Si*R*)-1: The asymmetric unit contains one molecule of (*t*Bu)$_2$P(S)CH$_2$Si(H)Ph *t*Bu. The Hydrogen atom at the Si atom is partly substituted by an OH group (83:17). To describe the disorder the Si-H bond length was restrained with the DFIX restraint to 1.4 Å.

Compound (*rac*)-1-Se: The asymmetric unit contains one molecule of (*t*Bu)$_2$P(Se)CH$_2$Si(H)Ph *t*Bu.

Compound (*rac*)-2a: The asymmetric unit contains one molecule of [(*t*Bu)$_2$P(S)CH$_2$SiPh*t*Bu]$^+$ and one molecule of the anion [(C$_6$F$_5$)$_3$BH]$^-$. The CH$_2$ group and the S atom of the four-membered cycle PSSi(CH$_2$) are disordered and superpose each other in the ratio of 94:6. The restraints SIMU and

SADI were applied to model this disorder. The hydrogen atom at the boron atom was located in an idealized position.

Compound (*rac*)-2a-Se: The asymmetric unit contains one molecule of $[(t\text{Bu})_2\text{P(Se)CH}_2\text{SiPh}t\text{Bu}]^+$ and one molecule of the anion $[(\text{C}_6\text{F}_5)_3\text{BH}]^-$. The CH_2 group and the Se atom of the four-membered cycle $\text{PSSi(CH}_2)$ are disordered and superpose each other in the ratio of 95:5. The restraints SIMU, SADI and DFIX were applied to model this disorder. The hydrogen atom at the boron atom was located in an idealized position.

Compound (*rac*)-3: The asymmetric unit contains one molecule of $[(t\text{Bu})_2\text{P(SH)CH}_2\text{Si(H)Ph}t\text{Bu}]^+$ and one molecule of the anion $[(\text{C}_6\text{F}_5)_4\text{B}]^-$. The whole molecule $[(t\text{Bu})_2\text{P(SH)CH}_2\text{Si(H)Ph}t\text{Bu}]^+$ shows a disorder over two positions (75:25). The restraints SADI, ISOR and SIMU were applied to model this disorder. The hydrogen atoms on the Si and S atoms were located from the difference Fourier map. Only for the S-H distances a restraint (SADI) was applied.

Compound 4a: The asymmetric unit contains one molecule of $(t\text{Bu})_2\text{P(S)CH}_2\text{SiPh}t\text{Bu}$ $(\text{OC}_{10}\text{H}_{20})$.

Compound 4b: The asymmetric unit contains one molecule of $(t\text{Bu})_2\text{P(S)CH}_2\text{SiPh}t\text{Bu}$ $(\text{OC}_{10}\text{H}_{20})$.

Compound 6: The asymmetric unit contains one molecule of $(t\text{Bu})_2\text{P(S)CH}_2\text{Si(F)Ph}t\text{Bu}$. The Si and F atom are disordered over two position (97:3). The modelling of the disorder did not require the use of any restrains.

CCDC-2044276 ((*rac*)-**1**), CCDC-2044277 ((*rac*)-**2a**), CCDC-2044278 ((*rac*)-**3**), CCDC-2044279 (($^{\text{Si}}R$)-**1**), CCDC-2044280 (**4a**), and CCDC-2044281 (**4b**) contain the supplementary crystallographic data for this paper. These data can be obtained free of charge at www.ccdc.cam.ac.uk/conts/retrieving.html (or from the Cambridge Crystallographic Data Center, 12 Union Road, Cambridge CB2 1EZ, UK; Fax: + 44-1223-336-033; e-mail: deposit@ccdc.cam.ac.uk).

Table S10 Crystallographic data for compounds (*rac*)-**1**, (^{Si}R)-**1**, and (*rac*)-**1-Se**.

Compound	(*rac*)-**1**	(^{Si}R)-**1**	(*rac*)-**1-Se**
Data set (internal naming)	**nf_357_dist_2a**	**nf_550_finally**	**nf_388_measure_abs**
Formula	$C_{19}H_{35}PSSi$	$C_{19}H_{35}O_{0.17}PSSi$	$C_{19}H_{35}PSeSi$
$D_{calc.}$ / g · cm^{-3}	1.107	1.104	1.238
m/mm^{-1}	1.865	2.531	3.543
Formula Weight	354.59	357.31	401.49
Colour	clear colourless	clear colourless	clear colourless
Shape	block	needle	block
Size/mm^3	0.55×0.12×0.10	0.40×0.03×0.02	0.33×0.06×0.03
T/K	122.99(10)	122.98(13)	122.99(10)
Crystal System	monoclinic	orthorhombic	monoclinic
Flack Parameter		-0.011(14)	
Hooft Parameter		-0.005(12)	
Space Group	$P2_1/c$	$P2_12_12$	$P2_1/c$
a/Å	10.39600(10)	18.9787(6)	10.3720(2)
b/Å	15.6691(2)	17.5252(7)	15.5409(3)
c/Å	13.3770(2)	6.4642(2)	13.7454(2)
α/°	90	90	90
β/°	102.5930(10)	90	103.546(2)
γ/°	90	90	90
V/Å^3	2126.64(5)	2150.03(13)	2153.99(7)
Z	4	4	4
Z'	1	1	1
Wavelength/Å	1.39222	1.54184	1.54184
Radiation type	Cu K$_\beta$	Cu K$_\alpha$	Cu K$_\square$
Q_{min}/°	3.934	3.433	4.364
Q_{max}/°	73.930	73.605	73.483
Measured Refl.	30433	6888	9702
Independent Refl.	5782	4095	4237
Reflections with I > 2(I)	5495	3923	3663
R_{int}	0.0240	0.0227	0.0305
Parameters	212	220	212
Restraints	0	1	0
Largest Peak	0.470	0.240	0.612
Deepest Hole	-0.386	-0.267	-0.368
GooF	1.053	1.046	1.039
wR_2 (all data)	0.0984	0.0732	0.0830
wR_2	0.0972	0.0717	0.0788
R_1 (all data)	0.0380	0.0312	0.0404
R_1	0.0364	0.0290	0.0327

Table S11 Crystallographic data for compounds, (*rac*)-**2a**, (*rac*)-**2a**, (*rac*)-**3**.

Compound	(*rac*)-**2a**	(*rac*)-**2a-Se**	(*rac*)-**3**
Data set (internal naming)	nf_526	nf_434_box_2_exp_abs	nf_433
Formula	$C_{37}H_{35}BF_{15}PSSi$	$C_{37}H_{35}BF_{15}PSeSi$	$C_{43}H_{36}BF_{20}PSSi$
$D_{calc.}$ / g · cm^{-3}	1.526	1.606	1.571
m/mm^{-1}	2.405	2.167	2.352
Formula Weight	866.58	913.48	1034.65
Colour	colourless	clear colourless	clear colourless
Shape	block	block	block
Size/mm^3	0.74×0.30×0.21	0.39×0.11×0.07	0.14×0.08×0.05
T/K	123.01(10)	123.00(10)	89.9(4)
Crystal System	triclinic	triclinic	monoclinic
Space Group	P-1	P-1	$P2_1/c$
a/Å	11.5017(2)	11.4288(4)	14.9231(2)
b/Å	13.3522(2)	13.4171(4)	16.3721(3)
c/Å	14.1961(2)	14.2558(4)	18.3876(3)
α/°	97.5640(10)	98.249(3)	90
β/°	104.1100(10)	103.401(3)	103.238(2)
γ/°	112.789(2)	113.040(3)	90
V/Å^3	1885.98(6)	1888.71(11)	4373.12(13)
Z	2	2	4
Z'	1	1	1
Wavelength/Å	1.54184	1.39222	1.54184
Radiation type	Cu K$_\alpha$	Cu K	Cu K$_\alpha$
Q_{min}/°	3.318	2.981	3.659
Q_{max}/°	73.866	69.006	74.164
Measured Refl.	34329	19206	18899
Independent Refl.	7452	9323	8598
Reflections with I > 2(I)	7269	8156	7663
R_{int}	0.0286	0.0317	0.0325
Parameters	533	537	836
Restraints	16	12	217
Largest Peak	0.343	0.613	0.408
Deepest Hole	-0.310	-0.567	-0.346
GooF	1.050	1.025	1.153
wR_2 (all data)	0.0822	0.1020	0.1130
wR_2	0.0817	0.0973	0.1098
R_1 (all data)	0.0324	0.0454	0.0559
R_1	0.0317	0.0388	0.0492

Table S12 Crystallographic data for compounds **4a**, and **4b** and (*rac*)-**6**.

Compound	4a	4b	(*rac*)-6
Data set (internal naming)	**nf_512_tlc_1_cryst**	**Rx_249_Sol**	**nf_516_ml_BF3_2b _mP_abs_gaus**
Formula	$C_{29}H_{53}OPSSi$	$C_{29}H_{53}OPSSi$	$C_{19}H_{34}FPSSi$
$D_{calc.}$ / g · cm^{-3}	1.101	1.098	1.156
m/mm^{-1}	1.924	1.918	2.624
Formula Weight	508.83	508.83	372.58
Colour	clear colourless	clear colourless	clear colourless
Shape	block	block	needle
Size/mm^3	0.32×0.10×0.09	0.37×0.36×0.25	0.85×0.07×0.05
T/K	122.96(11)	123.01(10)	123(1)
Crystal System	monoclinic	orthorhombic	monoclinic
Flack Parameter	0.017(13)	-0.006(5)	
Hooft Parameter	-0.001(4)	-0.010(5)	
Space Group	$P2_1$	$P2_12_12_1$	$P2_1/c$
a/Å	11.60780(10)	9.08370(10)	15.6883(2)
b/Å	10.76190(10)	16.8632(2)	10.27550(10)
c/Å	12.29310(10)	20.1026(2)	13.2864(2)
α/°	90	90	90
β/°	91.6100(10)	90	91.2860(10)
γ/°	90	90	90
V/Å^3	1535.07(2)	3079.32(6)	2141.30(5)
Z	2	4	4
Z'	1	1	1
Wavelength/Å	1.54184	1.54184	1.54184
Radiation type	Cu K$_\alpha$	Cu K$_\alpha$	Cu K$_\alpha$
Q_{min}/°	3.597	4.399	5.146
Q_{max}/°	74.170	72.888	72.580
Measured Refl.	31282	23411	23977
Independent Refl.	6112	6029	4153
Reflections with I > 2(I)	6064	5921	3787
R_{int}	0.0297	0.0249	0.0389
Parameters	310	310	235
Restraints	1	0	0
Largest Peak	0.452	0.360	0.342
Deepest Hole	-0.168	-0.223	-0.189
GooF	1.027	1.058	1.036
wR_2 (all data)	0.0770	0.0709	0.0830
wR_2	0.0767	0.0705	0.0794
R_1 (all data)	0.0299	0.0281	0.0352
R_1	0.0297	0.0275	0.0313

3.7.1 Compound (*rac*)-1
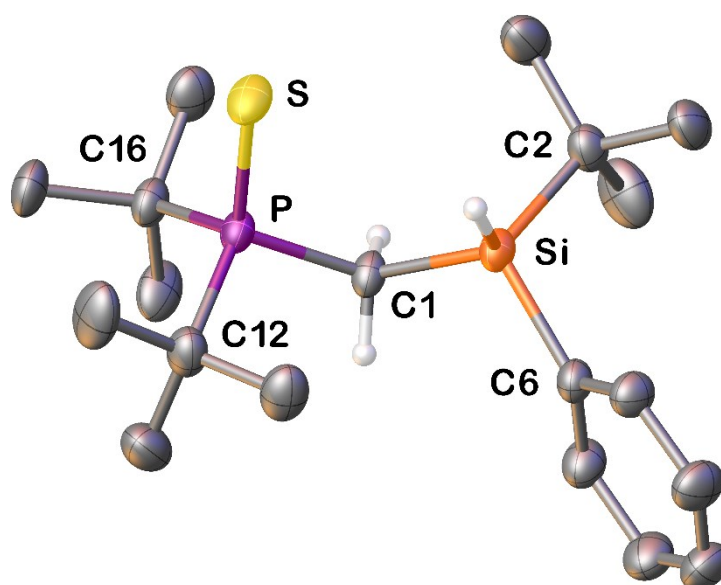
Selected Bond Lengths in Å		Selected Bond Angles in °	
P–S	1.9693(4)	S–P–C1	112.68(4)
P–C1	1.8173(12)	P–C1–Si	118.55(6)
C1–Si	1.9005(12)	C1–Si–C2	109.26(6)
Si–C2	1.8893(14)	C1–Si–C6	110.75(6)
Si–C6	1.8711(13)	C2–Si–C6	109.39(6)

3.7.2 Compound (^{Si}R)-1

Part 1 (83%)
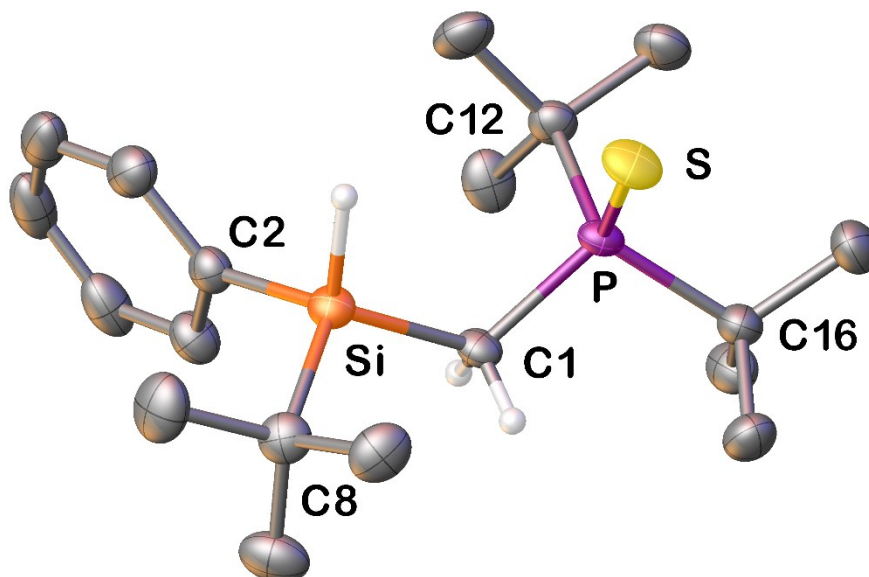
Part 2 (17%)
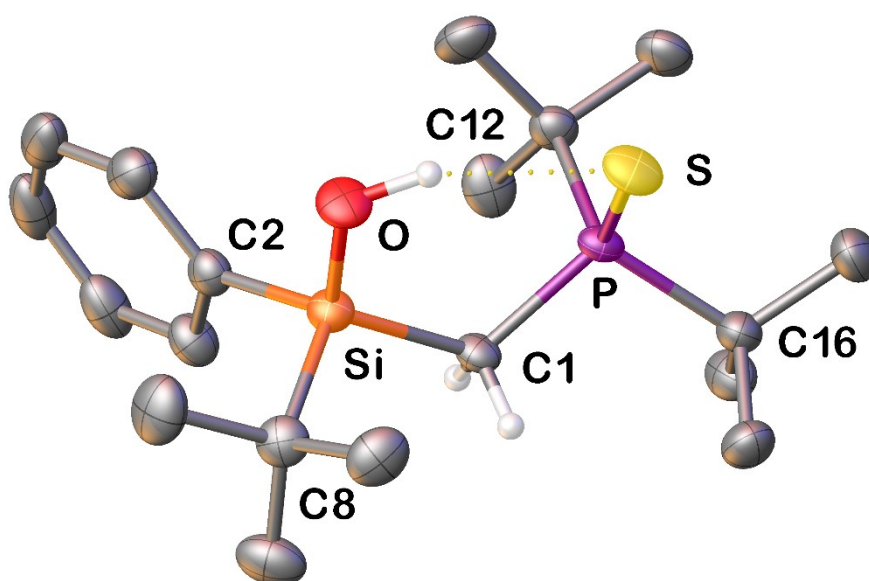
Selected Bond Lengths in Å		Selected Bond Angles in °	
P–S	1.9695(8)	S–P–C1	110.38(8)
P–C1	1.809(2)	P–C1–Si	120.19(12)
C1–Si	1.898(2)	C1–Si–O	113.8(7)
Si–O	1.569(10)	C1–Si–C2	110.75(11)
Si–C2	1.870(3)	C1–Si–C8	108.67(11)
Si–C8	1.894(3)		

3.7.3 Compound (*rac*)-1-Se
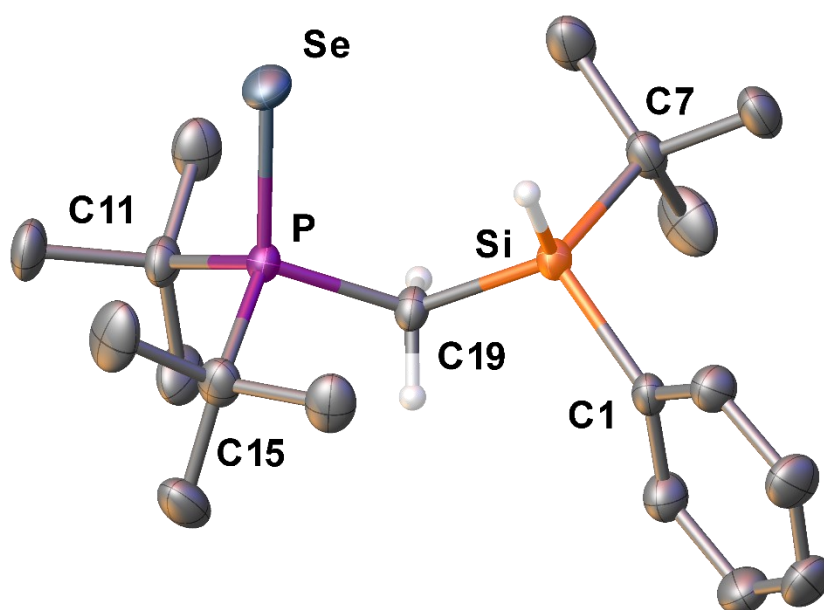
Selected Bond Lengths in Å		Selected Bond Angles in °	
P–Se	2.1262(6)	Se–P–C19	112.61(7)
P–C19	1.819(2)	P–C19–Si	119.11(11)
Si–C1	1.877(2)	C1–Si–C7	109.38(10)
Si–C7	1.892(2)	C19–Si–C7	109.14(10)
Si–C19	1.905(2)	C19–Si–C1	110.62(10)

3.7.4   Compound (*rac*)-2a
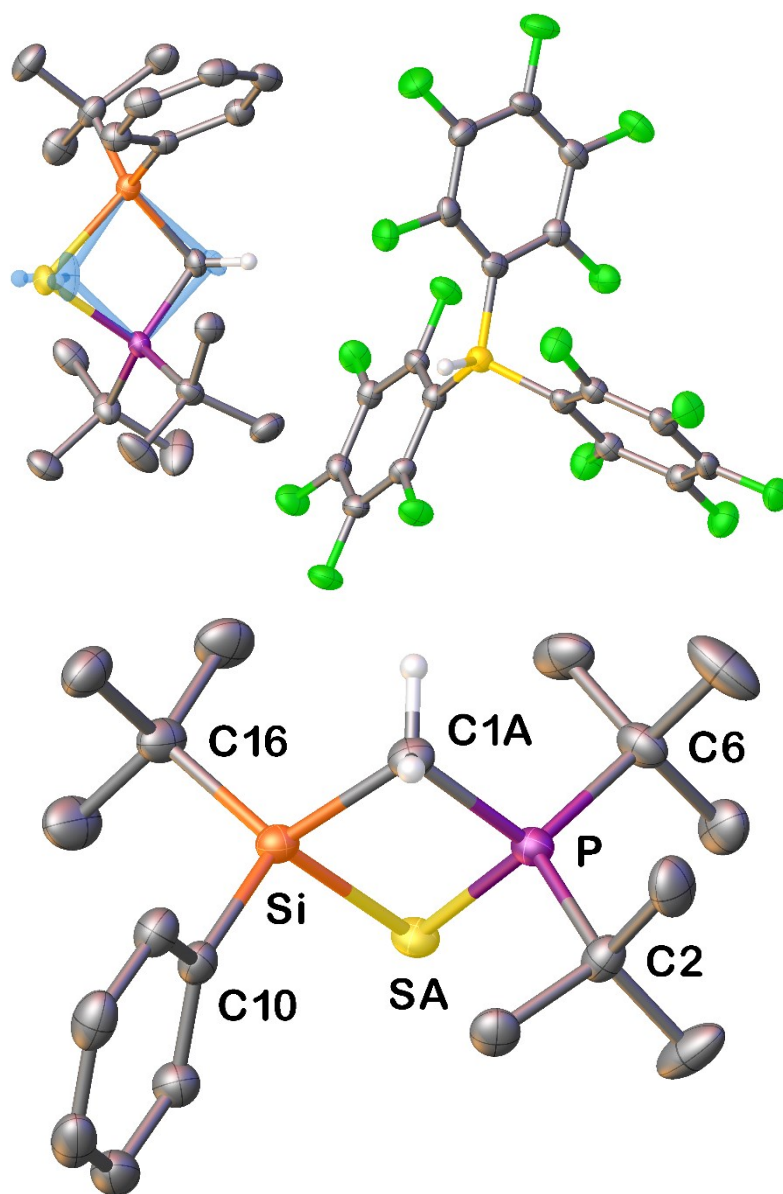
Selected Bond Lengths in Å		Selected Bond Angles in ˚	
P–SA	2.0755(6)	SA–P–C1A	96.21(13)
P–C1A	1.797(4)	P–C1A–Si	94.67(17)
C1A–Si	1.899(4)	C1A–Si–SA	89.14(12)
SA–Si	2.2059(6)	Si–SA–P	78.77(2)
Si–C10	1.8547(15)	C10–Si–C16	111.56(7)
Si–C16	1.8783(16)	C10–Si–SA	109.41(5)
		C16–Si–SA	115.06(5)
		C16–Si–C1A	115.13(19)

3.7.5   Compound (*rac*)-2a-Se
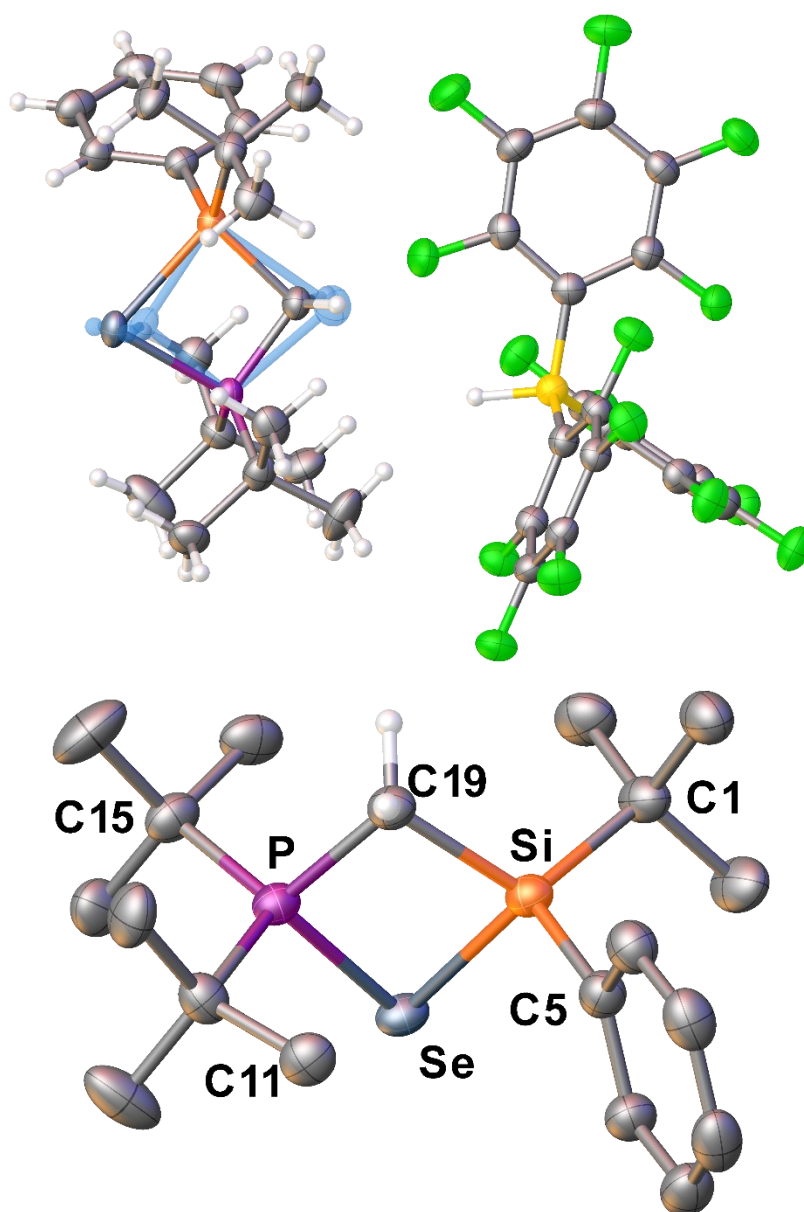
Selected Bond Lengths in Å		Selected Bond Angles in °	
P–Se	2.0755(6)	P–C19–Si	97.18(14)
P–C11	1.862(2)	P–Se–Si	74.818(19)
P–C15	1.861(2)	C19–Si–Se	90.15(9)
P–C19	1.803(3)	C19–P–Se	96.55(9)
Si–C1	1.884(2)	C19–Si–C1	114.36(10)
Si–C5	1.857(2)	Se–Si–C5	109.64(7)
Si–C19	1.894(3)	C1–Si–C5	111.83(10)
Si–Se	2.380(8)	C19–P–C11	109.13(11)

3.7.6   Compound (*rac*)-3
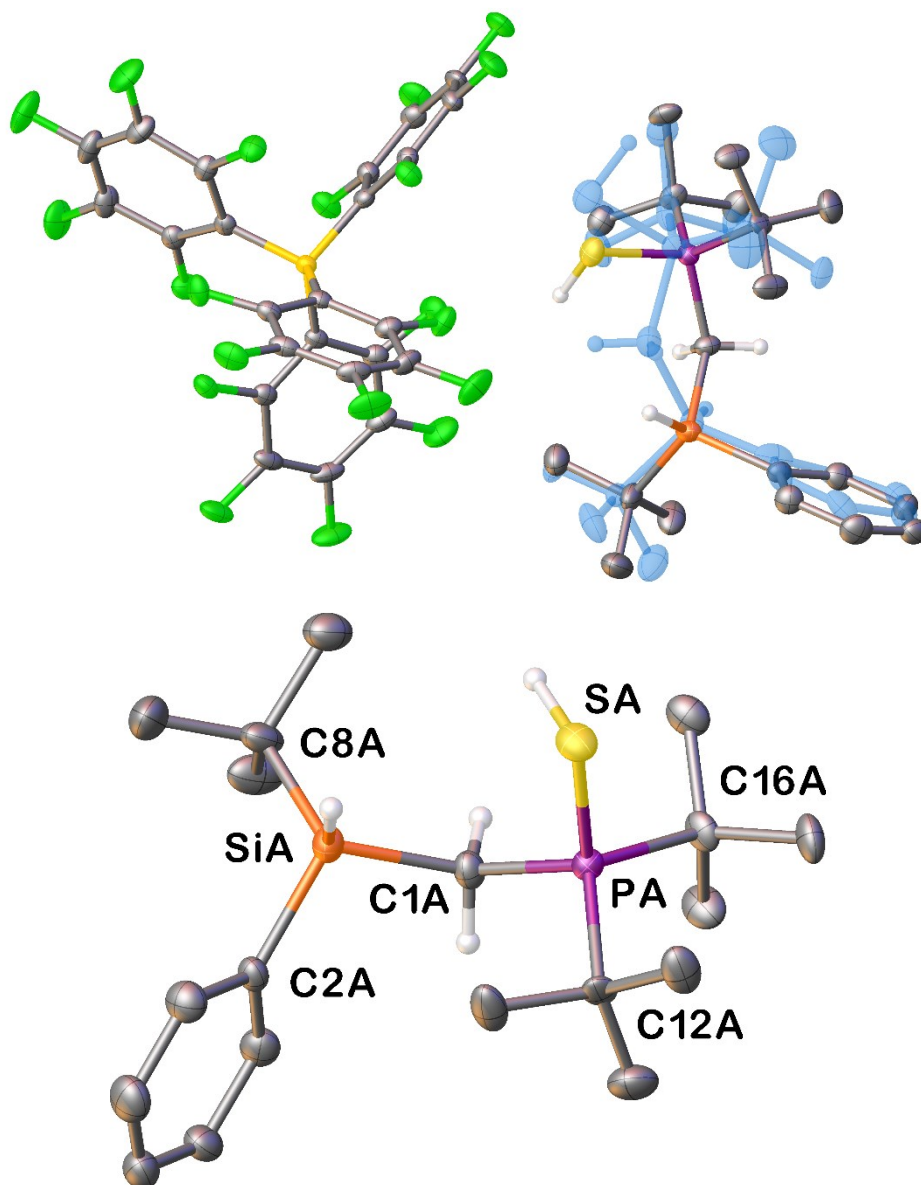
Selected Bond Lengths in Å		Selected Bond Angles in °	
PA–SA	2.0815(16)	SA–PA–C1A	110.94(14)
PA–C1A	1.785(3)	PA–C1A–SiA	123.24(18)
C1A–SiA	1.875(17)	C1A–SiA–C2A	107.6(2)
SiA–C2A	1.865(5)	C1A–SiA–C8A	108.8(5)
SiA–C8A	1.875(17)	C2A–SiA–C8A	111.9(4)

3.7.7   Compound 4a
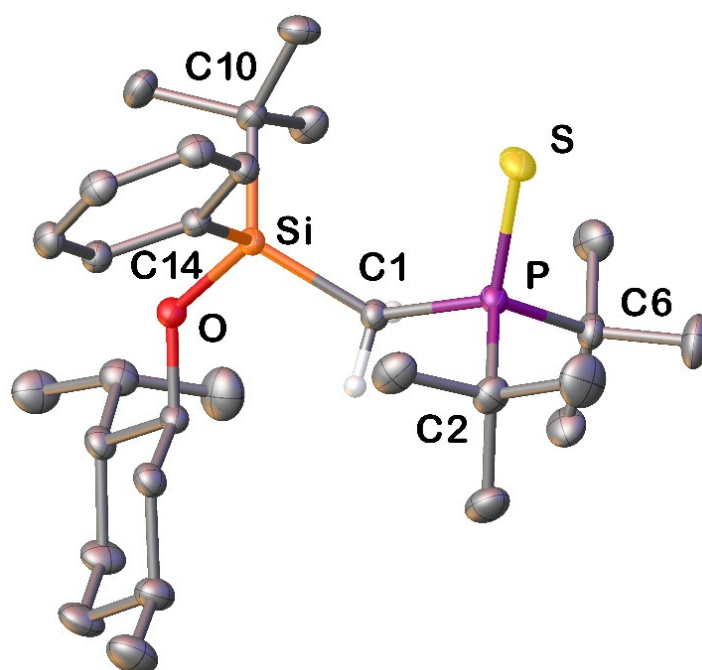
Selected Bond Lengths in Å		Selected Bond Angles in ˚	
P–S	1.9576(7)	**S–P–C1**	115.02(7)
P–C1	1.8218(19)	**P–C1–Si**	130.37(10)
C1–Si	1.899(2)	**C1–Si–O**	102.51(8)
Si–O	1.6589(13)	**C1–Si–C10**	114.49(9)
Si–C10	1.897(2)	**C1–Si–C14**	118.14(9)
Si–C14	1.8748(19)		

3.7.8   Compound 4b
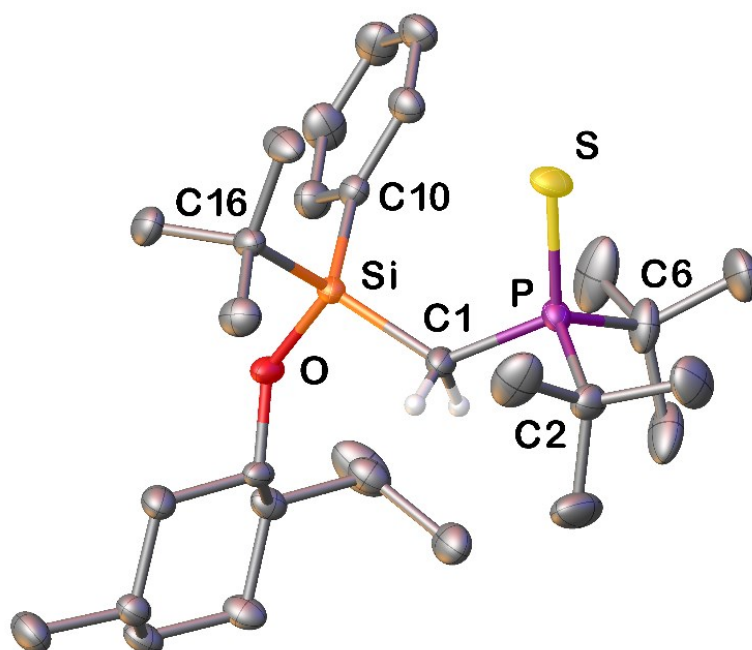
Selected Bond Lengths in Å		Selected Bond Angles in °	
P–S	1.9589(7)	S–P–C1	114.84(7)
P–C1	1.8221(19)	P–C1–Si	128.31(11)
C1–Si	1.903(2)	C1–Si–O	104.06(8)
Si–O	1.6355(13)	C1–Si–C10	117.72(9)
Si–C10	1.880(2)	C1–Si–C16	113.58(9)
Si–C16	1.903(2)		

3.7.9 Compound (*rac*)-6
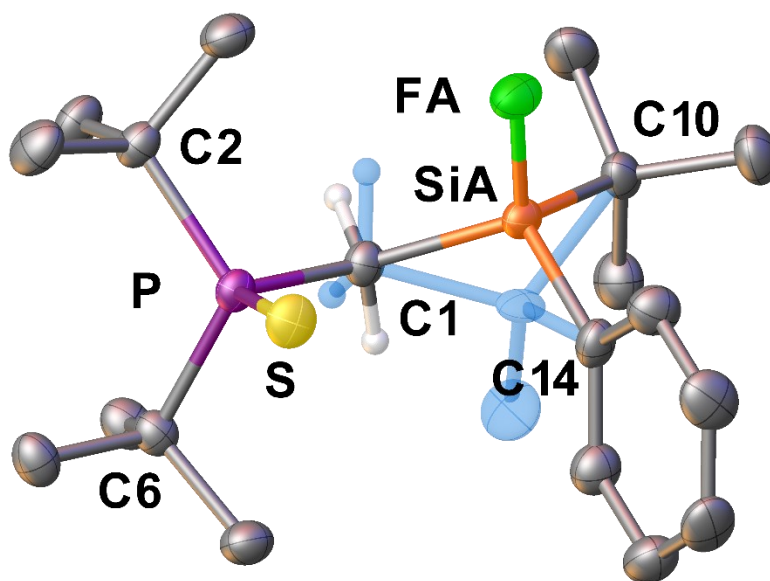
Selected Bond Lengths in Å		Selected Bond Angles in °	
P–S	1.9668(7)	S–P–C1	112.88(5)
P–C1	1.8185(15)	P–C1–Si	120.58(8)
C1–Si	1.8704(14)	C1–Si–F	111.80(6)
Si–F	1.6022(10)	C1–Si–C10	107.56(7)
Si–C10	1.8815(17)	C1–Si–C14	112.97(7)
Si–C14	1.8685(15)	C10–Si–C14	112.23(7)

3.8   References

[1]   M. Lehmann, A. Schulz, A. Villinger, *Angew. Chem. Int. Ed.* **2009**, *48*, 7444; *Angew. Chem.* **2009**, *121*, 7580.

[2]   S. F. Rach, E. Herdtweck, F. E. Kühn, *J. Organomet. Chem.* **2011**, *696*, 1817.

[3]   L. Fink, K. Samigullin, A. Bodach, E. Alig, M. Wagner, H.-W. Lerner, *Z. Anorg. Allg. Chem.* **2016**, *642*, 282.

[4]   K. Kuwabara. Y. Maekawa, M. Ebihara, T. Maruyama, T. Murai, *Heteroatom Chem.* **2018**, *29*, e21448.

[5]   G. Hägele, G. Tossing, W. Kückelhaus, J. Seega, *Z. Naturforsch.* **1984**, *B39*, 1574.

[6]   Gaussian 09 (Revision E.01): M. J. Frisch, G. W. Trucks, H. B. Schlegel, G. E. Scuseria, M. A. Robb, J. R. Cheeseman, G. Scalmani, V. Barone, B. Mennucci, G. A. Petersson, H. Nakatsuji, M. Caricato, X. Li, H. P. Hratchian, A. F. Izmaylov, J. Bloino, G. Zheng, J. L. Sonnenberg, M. Hada, M. Ehara, K. Toyota, R. Fukuda, J. Hasegawa, M. Ishida, T. Nakajima, Y. Honda, O. Kitao, H. Nakai, T. Vreven, J. A. Montgomery Jr., J. E. Peralta, F. Ogliaro, M. Bearpark, J. J. Heyd, E. Brothers, K. N. Kudin, V. N. Staroverov, T. Keith, R. Kobayashi, J. Normand, K. Raghavachari, A. Rendell, J. C. Burant, S. S. Iyengar, J. Tomasi, M. Cossi, N. Rega, J. M. Millam, M. Klene, J. E. Knox, J. B. Cross, V. Bakken, C. Adamo, J. Jaramillo, R. Gomperts, R. E. Stratmann, O. Yazyev, A. J. Austin, R. Cammi, C. Pomelli, J. W. Ochterski, R. L. Martin, K. Morokuma, V. G. Zakrzewski, G. A. Voth, P. Salvador, J. J. Dannenberg, S. Dapprich, A. D. Daniels, O. Farkas, J. B. Foresman, J. V. Ortiz, J. Cioslowski and D. J. Fox, Gaussian, Inc., Wallingford CT, 2013.

[7]   J. B. Foresman, A. Frisch, *Exploring Chemistry with Electronic Structure Methods*, 2nd Ed., Gaussian, Inc., Pittsburgh, PA (USA), 1996.

[8]   CrysAlisPro Software System, Rigaku Oxford Diffraction, **2020**.

[9]   O. V. Dolomanov, L. J. Bourhis, R. J. Gildea, J. A. K. Howard, H. Puschmann, *J. Appl. Crystallogr.* **2009**, *42*, 339.

[10] G. M. Sheldrick, *Acta Crystallogr.* **2015**, *A71*, 3.

[11] G. M. Sheldrick, *Acta Crystallogr.* **2015**, *C71*, 3.

Preface

The following chapter has already been published and is reprinted following author's rights.

"Hidden Silylium-Type Reactivity of a Siloxane-Based Phosphonium–Hydroborate Ion Pair"

Authors

N. Fontana, N. A. Espinosa-Jalapa, M. Seidl, J. O. Bauer, *Chem. Commun.*, **2022**, 58, 2144.

Author contribution

All the reported synthesis and characterizations (multinuclear NMR, MS, EA) in this work were performed by N. Fontana. Characterizations in the solid phase (single crystal X-ray diffraction) were performed by N. Fontana and the structures were refined by Dr. M. Seidl (Research group of Prof. M. Scheer) who also prepared the data for the SI. The reported characterization data and experimental procedures for the synthesis of *t*BuPhSi(H)Cl, *t*BuPhSi(H)OH and *t*BuPhSi(H)OLi were provided by Dr. N. A. Espinosa-Jalapa. In silico calculations were performed by Dr. J. O. Bauer. The supporting information were prepared by N. Fontana and revised by both Dr. N. A. Espinosa-Jalapa and Dr. J. O. Bauer. The original manuscript was prepared by N. Fontana and revised by Dr. J. O. Bauer.

Acknowledgements

4 Hidden Silylium-Type Reactivity of a Siloxane-Based Phosphonium–Hydroborate Ion Pair

Abstract: *A new class of siloxane-based cations with hidden silylium-type reactivity is provided, which, in combination with an arylborate counteranion, initiates an unexpected, highly selective para-C(sp^2)–F defuntionalisation of a perfluorinated aryl group. The hydrodefluorinated aryl borane is obtained as a crystalline solid via continuous sublimation during the reaction. The heterocyclic six-member-ed siloxysilyl phosphonium cation could be obtained single crystalline and fully characterized after dehydrogenative anion exchange. The para-defunctionalized borane was unambiguously identified and characterized by NMR spectroscopy, X-ray crystallography, mass spectrometry, and elemental analysis. Quantum chemical calculations gave insight into the bonding within the siloxane-based cation and the mechanism of the ion pair reaction.*

4.1 Introduction

Siloxanes with precisely defined structures and functionalities are of greatest interest for synthetic purposes and for technical processes, and are affecting numerous areas of current research.[1] The Si–O–Si motif offers a high degree of electronic flexibility, functional variability, and structural stability. It is therefore not only the subject of theoretical investigations into the nature of the Si–O bond,[2] but is still the focus of impressive synthetic achievements.[3–5] These include the targeted provision of functionalized disiloxane units,[3] the controlled build-up of oligosiloxanes,[4] or the construction of molecular silanolate model systems.[5] The provision and taming of strongly Lewis acidic silylium ions,[6] which is ensured by inter- or intramolecular electronic stabilization through interaction with a Lewis base,[7] has led to entirely new developments in the fields of main-group element-based catalysis and bond activation.[8] The activation of unreactive C–F bonds by main-group element compounds is still a demanding endeavor,[9] and new developments in this area have consistently attracted the attention.[10] The achievements in silylium ion chemistry in particular have given significant impetus to this field.[11] Especially the activation of C$_{aryl}$–F bonds has long been a fundamental challenge.[12] Heterolytic C(sp^2)–F bond cleavage of fluorobenzene by untamed highly reactive silylium ions was first described by Reed, Baldridge, and Siegel.[13] This has led to impressive catalytic coupling reactions with fluoroarenes.[14] However, despite the great importance of weakly coordinating anions (WCAs),[15] only little is known about the chemistry of C–F bonds in perfluorinated Lewis acidic arylboranes and weakly coordinating arylborates. These works are essentially limited to studies on the reactivity of [RB(C$_6$F$_5$)$_3$]$^-$ counterions towards zirconocenium catalysts, which are used in olefin polymerization,[16] and to studies on the nucleophilic attack of a perfluorinated ring of B(C$_6$F$_5$)$_3$ by a phosphorus ylide or phosphine.[17] We recently reported a methodology towards a new class of configurationally stable silicon-chiral heterocyclic cations, which is based on an anchimerically assisted cation formation by means of an incorporated phosphine sulfide function.[18] Herein, we draw an unexpected picture of silylium reactivity, which affects the common view on highly reactive silyl cations. Taking advantage of the intramolecular P$^+$–S$^-$ stabilization of a silicon cationic center in combination with the chemical robustness and electronic flexibility of the Si–O–Si framework, we introduced a previously unknown concept of ion pair reactivity. We report on a new class of six-membered heterocyclic siloxane-based phosphonium cations exhibiting hidden

silylium-type reactivity. The cation initiates a highly selective *para*-C(sp^2)–F defunctionalization of a perfluorinated aryl ring of the hydroborate counteranion in the ionic liquid phase. Different mechanistic proposals are discussed. In addition, a powerful anion exchange methodology was developed and DFT calculations provided deeper knowledge on the question how the silylium center is affected by the Si–O–Si bonding and the P$^+$–S$^-$ stabilization. In the light of the very interesting work on silylium-like species on oxidic[19] and AlCl$_x$F$_{3-x}$ surfaces,[20] our type of siloxane-based cations could serve as molecular model systems mimicking electrophilic surface sites.

4.2 Results and discussion

4.2.1 Synthesis of phosphine sulfide substituted disiloxane

We started our investigation by elaborating a synthetic route towards the phosphine sulfide functionalized disiloxane **6**, which features a hydrosiloxy unit active in the hydride abstraction reaction (Scheme 6). In the first step, we coupled dichlorosilane **1**[21] with lithium hydrosiloxide **2** that was specially produced for this purpose (for details on the synthesis of **2**, see the ESI). The phosphine sulfide moiety was then introduced by reacting disiloxane **3** with freshly prepared *t*Bu$_2$PCH$_2$Li (**4**) affording compound **5** as a colourless oil. Unfortunately, the isolation of this intermediate in the crystalline form kept eluding us. However, yellow crystals were obtained from cold pentane after reacting disiloxane **5** with the readily available THF complex [W(CO)$_5$(THF)]. With our delight, single crystal X-ray analysis identified them as complex [W(**5**)(CO)$_4$]. This complex crystallized in the monoclinic crystal system, *P*2$_1$/*n* space group, and features a distorted *pseudo* seven-membered ring in which a direct interaction between the silicon hydride and the tungsten centers can be observed. In the crystal structure, all the bond distances fit with the calculated covalent radii[33] except for the P–W bond which is elongated (2.6026(9) Å *vs* 2.48 Å) probably due to the high steric bulk around the phosphorus and tungsten centers. A strong interaction between the acidic metal and the hydride (1.916 Å *vs* 1.69 Å for a W–H single bond) is in accordance with ^{1}H NMR data which also show a broad signal in the hydridic region (-6.4 ppm). Moreover, in the ^{29}Si NMR spectrum, next to a sharp singlet for the Si-C-P silicon center, a very broad signal indicates the presence of a dynamic process involving the other silicon nucleus. The presence of the typical ^{183}W satellites ($^1J_{\text{P-W}}$ = 115.8 Hz) in the ^{31}P spectrum provides further evidence on the formation of a direct P–W bond. Although the chemical properties of this species have not yet been explored, a previous report from Gilges *et al.*[22] describes this kind of complexes as key intermediates in the study of the oxidative addition of SiH bonds. In fact, the possibility to activate relatively inert silicon-hydrogen bonds combining main group and transition metal chemistry will surely inspire future investigations.
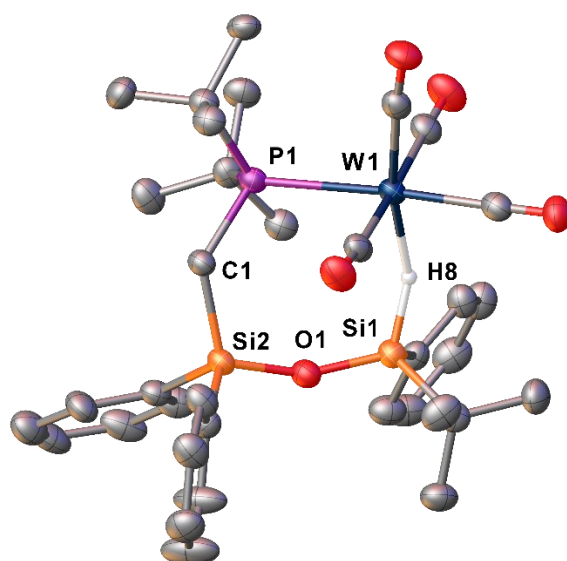
Figure 134 Crystal structure of [W(**5**)(CO)$_4$]. All hydrogens except the Si–H group are omitted for clarity.

Starting from intermediate **5**, direct oxidation of the phosphorus center using elemental sulfur afforded compound **6** which crystallized without addition of solvent in the monoclinic crystal system, space group *P*2$_1$/*n*, and was characterized by single-crystal X-ray diffraction analysis (Figure 135, left).The hydride abstraction supported by the neighboring group participation[23] of the P$^+$–S$^-$ unit, was easily accomplished using B(C$_6$F$_5$)$_3$ in dichloromethane with formation of the siloxysilyl phosphonium–hydroborate ion pair **7**[HB(C$_6$F$_5$)$_3$] (Scheme 6). Compound **7**[HB(C$_6$F$_5$)$_3$] was obtained as a solid, which could be stored for several months at room temperature under an inert atmosphere without noticeable decomposition. However, all attempts to get **7**[HB(C$_6$F$_5$)$_3$] in single-crystalline form suitable for X-ray diffraction analysis were unsuccessful.
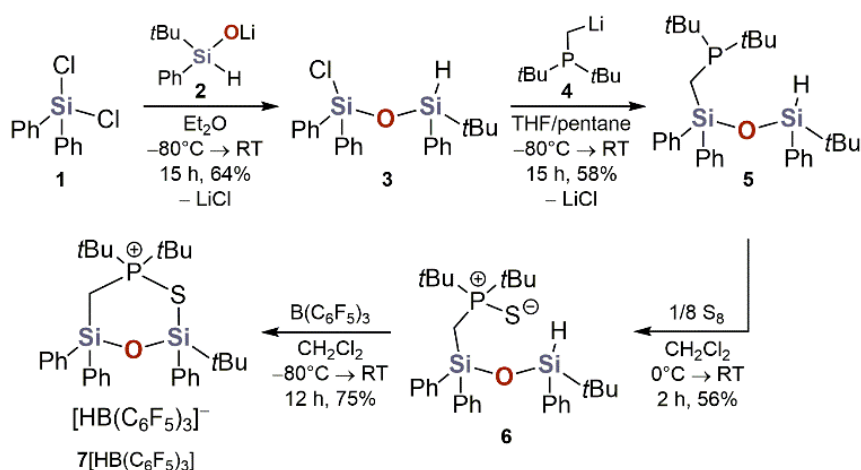
Scheme 6 Synthesis of the siloxysilylphosphonium–hydroborate ion pair **7**[HB(C$_6$F$_5$)$_3$].

4.2.2   Characterization of siloxysilylphosphonium ions

In order to make the cation accessible to a structural investigation, we tried to exchange the weakly coordinating hydroborate $[HB(C_6F_5)_3]^-$ for an anion with better crystallization tendencies and thus came across a new and elegant method that is also highly efficient. Since the exchange of WCAs is a demanding undertaking, the development of convenient methodologies is very desirable and would open up new possibilities for studying ion pairs. Our approach took advantage of a Brønsted acid-mediated dehydrogenation by reacting Jutzi's acid, $[H(OEt_2)_2]^+[B(C_6F_5)_4]^-$,[24] with ion pair **7**$[HB(C_6F_5)_3]$ achieving full conversion and excellent selectivity in short times (Scheme 7). The hydrogen release is responsible for the enormous driving force and irreversibility of the reaction and has the benefit that solely uncharged byproducts are formed, which can easily be separated from the product ion pair **7**$[B(C_6F_5)_4]$.[25] We consider this dehydrogenative approach to be a useful and elegant tool in order to meet future challenges of exchanging WCAs.[15] Species **7**$[B(C_6F_5)_4]$, that now contains $[B(C_6F_5)_4]^-$ instead of $[HB(C_6F_5)_3]^-$ as the counteranion, eventually gave single crystals suitable for X-ray crystallography (Figure 135, right). Ion pair **7**$[B(C_6F_5)_4]$ crystallized from toluene/pentane in the triclinic crystal system, space group $P\bar{1}$. The six-membered heterocyclic cation shows a boat-like conformation with the atoms C1 and Si2 sticking out of the plane. The Si2 atom exhibits an almost ideal tetrahedral coordination geometry. In comparison with the same bonds in siloxane **6**, the Si1–O1 bond in cation **7** is slightly elongated and the Si2–O1 bond slightly shortened. The Si–O–Si angle decreases from 156.83(16)° in **6** to 139.60(11)° in **7**, while the heterocyclic Si–S–P angle with 107.86(3)° is close to the tetrahedral angle.
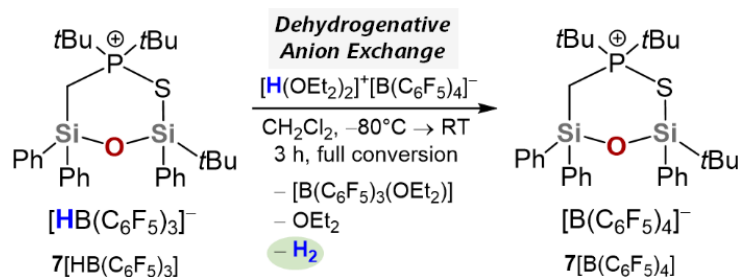
Scheme 7. Dehydrogenative anion exchange leading to compound **7**$[B(C_6F_5)_4]$.

The downfield-shifted ^{31}P NMR signal of δ = 87.2 ppm for cation **7** with respect to δ = 73.9 ppm for **6** matches with our previous findings.[18] ^{29}Si NMR spectroscopy of both compounds **7**$[HB(C_6F_5)_3]$ and **7**$[B(C_6F_5)_4]$ in CD$_2$Cl$_2$ each shows a chemical shift of δ = -2.7 ppm for the sulfur-stabilized silicon atom, which is only marginally downfield-shifted in comparison to the ^{29}Si NMR signal of the *Si*H group in disiloxane **6** [$\delta(^{29}Si)$ = -4.2 ppm]. The downfield shift of the ^{29}Si NMR signal upon hydride abstraction and intramolecular sulfur stabilization is much less pronounced here than in our previously described four membered silyl phosphonium sulfides.[18] However, it must be taken into account that the ^{29}Si NMR chemical shift can be strongly dependent on the ring size, which can

151

lead to significant deshielding in small ring systems compared to six membered rings.[26] This suggests a strong Si–S–P interaction within the heterocyclic cation **7**.
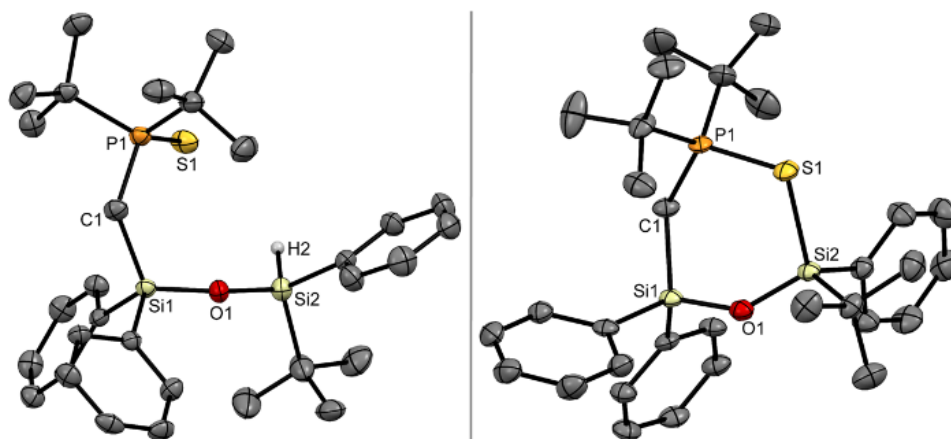
Figure 135. Molecular structures of **6** (left) and cation **7** (right) in the crystal (displacement ellipsoids set at the 50 % probability level). Hydrogen atoms, except for the Si–H group, are omitted for clarity.

The coupling between the silicon and the phosphorus nuclei ($^2J_{SiP}$ = 6.4 Hz for **7**[B(C$_6$F$_5$)$_4$]) of the Si–S–P structural unit also indicates a strong bond between the sulfur and the silicon atom. According to the NMR based Lewis acidity scale introduced by Müller,[7e] the diagnostic spectroscopic parameters show no interaction between cation **7** of hydroborate **7**[HB(C$_6$F$_5$)$_3$] and *para*-fluorobenzonitrile (FBN) indicating a Lewis acidity on the weakest end of the scale. We therefore tend to call our cations phosphonium rather than silylium ions and think that the bonding situation is best reflected using an electrovalent notation with single bonds and formal charges.[27] In this context, it seems interesting to examine how the Lewis acidity of the silicon center in cation **7** is affected by the P$^+$–S$^-$ stabilization and the Si–O–Si linkage. For this reason, we performed a thorough thermochemical and natural bond orbital (NBO) analysis[28] on the B3LYP/6-311+G(d,p) level of theory (for a detailed discussion, see the ESI). As expected, by far the greatest contribution to the stabilization of the Lewis acidic silicon center is provided by the intramolecular coordination through the P$^+$–S$^-$ group. Hyperconjugative $n_O \rightarrow \sigma^*_{vicinal}$ contributions only play a negligible role in the intramolecular Lewis base stabilized disiloxane based phosphonium cation. However, it appears that hyperconjugative effects become important in the open, trigonal planar form of the siloxy-substituted silylium ion by means of an out of plane interaction of an oxygen lone electron pair with the empty p-type acceptor orbital of the silicon atom.

4.2.3   The hidden silylium ion-type reactivity

In view of the spectroscopic and structural parameters of ion pair **7**[HB(C$_6$F$_5$)$_3$], it was all the more astonishing that the siloxane based phosphonium cation was sufficiently electrophilic to activate a C(sp^2)–F bond in the ionic liquid phase (Scheme 8). When the pure compound **7**[HB(C$_6$F$_5$)$_3$] is melted and heated at 120°C in a closed system, a heterolytic cleavage of a *para*-C(sp^2)–F bond of [HB(C$_6$F$_5$)$_3$]$^-$ occurs, while forming the fluorodisiloxane **8** (56% isolated yield after distillation) and the hydrodefluorinated aryl borane **9** (70% isolated yield). Although the conditions can still be optimized, the reaction can easily be carried out on a preparative scale with separation of the two products by continuous *in situ* sublimation of borane **9**, which condenses on the upper part of the reaction flask as thin needles. In order to obtain sharp NMR signals, compound **9** was fully characterized as the water/THF adduct **9**·H$_2$O·(THF)$_2$ and we were fortunate to even get single cocrystals suitable for X-ray crystallography, which unambiguously proved the *para*-defunctionalization (for details, see the ESI).[29] We assume that the ion pair reaction is initiated and assisted by the opening of the heterocycle. For this endothermic step an energy of 24.4 kcal mol^{-1} was calculated, which should be readily available under the thermal conditions in the reaction vessel. The formed encounter complex **Int-1** can be regarded as a siloxysilylium ion that is coordinated by the *para*-fluoro substituent of the hydroborate counteranion (Scheme 8). Based on this central intermediate, various mechanisms are conceivable, which are subjected to a detailed critical discussion in the ESI. Since the reaction takes place in the ionic liquid phase, intermolecular reaction pathways via S$_N$Ar mechanisms involving an additional hydroborate anion must also be taken into account. Such a reaction with the perfluorinated ring of a WCA was not to be expected. Apparently, the efficient stabilization of the Lewis acidic silicon center by the phosphine sulfide bridge can be abandoned in favor of the Si···F coordination upon heating. As a consequence, the heterocyclic phosphonium ion-looking cation hides a reactivity which, when heated, resembles that of highly reactive silylium ions. This creates a completely new picture for the character of a phosphine sulfide stabilized siloxysilylium unit.
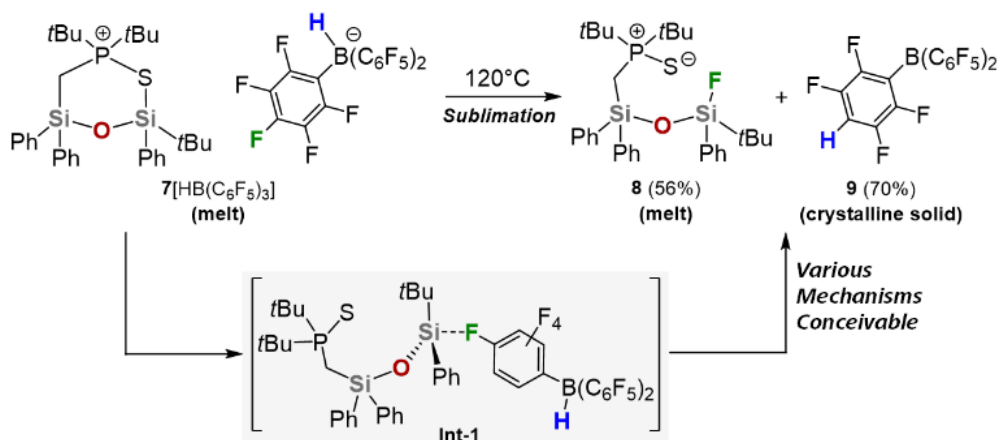
Scheme 8. Silylium-like reactivity of siloxane-based phosphonium ion **7**[HB(C$_6$F$_5$)$_3$] leading to *para*-C(sp^2)–F defunctionalisation of the perfluorinated hydroborate counteranion via a reactive encounter complex (**Int-1**).

4.2.1 The WCA exchange strategy

As previously mentioned (see chapters 1 and 3), weakly coordinating anions (WCAs) are ubiquitous in silylium ion chemistry. Their size and nature can deeply affect the chemical and physical properties of silicon-based ion pairs.[32] However, a precise, efficient, and versatile strategy to introduce these anions into previously obtained ion pairs has not yet been developed. In fact, the fragile nature of silylium ions, combined with the highly specific experimental conditions required to isolate them in pure form, make this approach an ongoing challenge. In order to increase the synthetic versatility of WCAs, and encouraged by the results obtained in the synthesis of **7**[B(C$_6$F$_5$)$_4$], we decided to develop a synthetic methodology that allows to perform a clean substitution of the counteranion in silylium ion pairs. As already described in section 4.2.2, the method is based on the direct reaction between the Brønsted acid of the desired WCA (*e.g.* [H(OEt$_2$)$_2$]$^+$[B(C$_6$F$_5$)$_4$]$^-$) and the preformed silylium ion featuring an hydridic counterion (*e.g.* **7**[HB(C$_6$F$_5$)$_3$]). The scope of this method was further explored by synthesizing borate counterions with the general formula [B(C$_6$F$_5$)$_3$R] (R = alkyl, aryl, allyl). A few examples of borates were readily available starting from BCF and introducing the fourth substituent *via* nucleophilic attack of the respective lithiated derivative. The most successful results were obtained for the synthesis, protonation, and subsequent exchange of [B(C$_6$F$_5$)$_3$Bn]. While attempts using BnK resulted in a violent and almost uncontrollable reaction, this anion was obtained in good yields *via* direct addition of BCF to a mixture containing toluene, butyllithium and TMEDA. [LiTMEDA][B(C$_6$F$_5$)$_3$Bn] crystallized in the orthorhombic crystal system (*Pna2$_1$* space group) featuring the expected tetrahedral geometry at the boron center and a η^6 interaction between the benzyl residue and the lithium atom. After treatment with anhydrous HCl, lithium chloride precipitate allowing the isolation of [HTMEDA][B(C$_6$F$_5$)$_3$Bn] which crystallized in the monoclinic crystal system (*P2$_1$/n* space group).
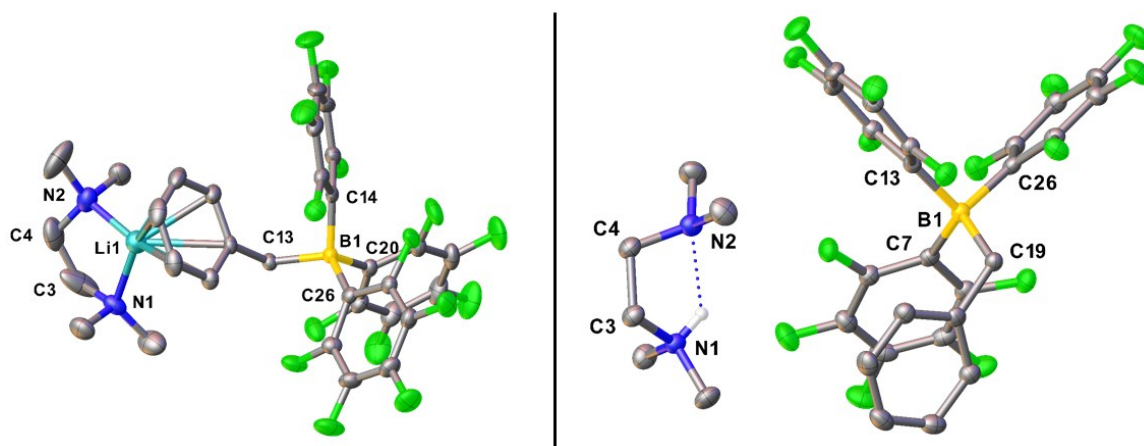
Figure 136. Crystal structures of [LiTMEDA][B(C$_6$F$_5$)$_3$Bn] and [HTMEDA][B(C$_6$F$_5$)$_3$Bn]. Hydrogen atoms, except for the N–H group, are omitted for clarity.

In this case, while the tetrahedral geometry at the boron center was not affected, no interaction between the benzyl residue and the protonated TMEDA could be observed. Although a full characterization of the desired exchange product has not yet been obtained and the reduced acidity of the

protonated diamine compared to the free proton in Jutzi's acid required higher temperatures (135°C), compound **7**[B(C$_6$F$_5$)$_3$Bn] was detected *via* NMR thus proving the efficacy of this strategy (for details see section 4.4.2). This approach, although in its infancy, will be thoroughly studied in the ongoing research since it could open up new synthetic routes towards a manifold of WCA containing ion pairs.

4.2.2 Conclusions

We have herein reported about the synthesis, isolation, and chemical properties of the first siloxysilylium ions (**7**[HB(C$_6$F$_5$)$_3$], and **7**[B(C$_6$F$_5$)$_4$]). These species have been thoroughly investigated experimentally (both in the solid state and in solution) and on a theoretical level exploiting the extraordinary resilience of the siloxane scaffold. A straightforward and reliable synthetic way has been introduced, assuring both availability and reproducibility for these compounds. Moreover, a new protocol for a clean and efficient anion exchange reaction has been developed and added to the synthetic toolbox. In conclusion, our work on robust heterocyclic siloxysilyl phosphonium ions opens up interesting perspectives for the provision of novel main group element-based cationic heterocycles [30] with hidden reactivity. Our findings on the controlled *para*-C(sp^2)–F hydrodefluorination shed new light on the nature of silylium type centers and about ion pair reactivity in ionic liquids. These results are closely related to fundamental questions concerning WCAs[15] and the chemistry of fluorinated arylboranes.[31] Furthermore, our siloxane-based cation may be regarded as a molecular model system for mimicking electrophilic silylium-type sites on oxide surfaces.[19]

4.3 References

[1]   a) M. A. Brook, *Silicon in Organic, Organometallic, and Polymer Chemistry*, John Wiley & Sons, New York, USA, 2000; b) U. Schubert, N. Hüsing, *Synthesis of Inorganic Materials* (4th Ed.), Wiley-VCH, Weinheim, Germany, 2019.

[2]   a) F. Weinhold, R. West, *Organometallics*, 2011, **30**, 5815; b) F. Weinhold, R. West, *J. Am. Chem. Soc.*, 2013, **135**, 5762; c) M. Fugel, M. F. Hesse, R. Pal, J. Beckmann, D. Jayatilaka, M. J. Turner, A. Karton, P. Bultinck, G. S. Chandler, S. Grabowsky, *Chem. Eur. J.*, 2018, **24**, 15275.

[3]   a) R. Pietschnig, K. Merz, *Organometallics*, 2004, **23**, 1373; b) J. O. Bauer, C. Strohmann, *Angew. Chem., Int. Ed.*, 2014, **53**, 720; c) K. M. Diemoz, S. O. Wilson, A. K. Franz, *Chem. Eur. J.*, 2016, **22**, 18349; d) P. Roesch, U. Warzok, M. Enke, R. Meller, C. Schattenberg, C. A. Schalley, M. Kaupp, T. Braun, P. Wittwer, *Chem. Eur. J.*, 2017, **23**, 13964; e) N. A. Espinosa-Jalapa, J. O. Bauer, *Z. Anorg. Allg. Chem.*, 2020, **646**, 828; f) J. Zhu, S. Chen, C. He, *J. Am. Chem. Soc.*, 2021, **143**, 5301.

[4]   a) N. Hurkes, C. Bruhn, F. Belaj, R. Pietschnig, *Organometallics*, 2014, **33**, 7299; b) N. Oguri, Y. Egawa, N. Takeda, M. Unno, *Angew. Chem., Int. Ed.*, 2016, **55**, 9336; c) K. Matsumoto, K. V. Sajna, Y. Satoh, K. Sato, S. Shimada, *Angew. Chem., Int. Ed.*, 2017, **56**, 3168; d) J. Yu, Y. Liu, *Angew. Chem., Int. Ed.*, 2017, **56**, 8706; e) M. Yoshikawa, Y. Tamura, R. Wakabayashi, M. Tamai, A. Shimojima, K. Kuroda,

Angew. Chem., Int. Ed., 2017, **56**, 13990; f) K. Matsumoto, Y. Oba, Y. Nakajima, S. Shimada, K. Sato, *Angew. Chem., Int. Ed.*, 2018, **57**, 4637.

[5]   a) C. Däschlein, J. O. Bauer, C. Strohmann, *Angew. Chem., Int. Ed.*, 2009, **48**, 8074; b) D. Čas, N. Hurkes, S. Spirk, F. Belaj, C. Bruhn, G. N. Rechberger, R. Pietschnig, *Dalton Trans.*, 2015, **44**, 12818; c) K. S. Lokare, N. Frank, B. Braun-Cula, I. Goikoetxea, J. Sauer, C. Limberg, *Angew. Chem., Int. Ed.*, 2016, **55**, 12325; d) C. Golz, P. Steffen, C. Strohmann, *Angew. Chem., Int. Ed.*, 2017, **56**, 8295; e) K. S. Lokare, B. Braun-Cula, C. Limberg, M. Jorewitz, J. T. Kelly, K. R. Asmis, S. Leach, C. Baldauf, I. Goikoetxea, J. Sauer, *Angew. Chem., Int. Ed.*, 2019, **58**, 902; f) R. F. Weitkamp, B. Neumann, H.-G. Stammler, B. Hoge, *Angew. Chem., Int. Ed.*, 2020, **59**, 5494; g) R. F. Weitkamp, B. Neumann, H.-G. Stammler, B. Hoge, *Chem. Eur. J.*, 2021, **27**, 915.

[6]   For some recent contributions in silylium chemistry, see: a) K. Müther, R. Fröhlich, C. Mück-Lichtenfeld, S. Grimme, M. Oestreich, *J. Am. Chem. Soc.*, 2011, **133**, 12442; b) A. Schäfer, M. Reißmann, A. Schäfer, W. Saak, D. Haase, T. Müller, *Angew. Chem., Int. Ed.*, 2011, **50**, 12636; c) A. Merk, H. Großekappenberg, M. Schmidtmann, M.-P. Luecke, C. Lorent, M. Driess, M. Oestreich, H. F. T. Klare, T. Müller, *Angew. Chem., Int. Ed.*, 2018, **57**, 15267; d) N. Kramer, H. Wadepohl, L. Greb, *Chem. Commun.*, 2019, **55**, 7764; e) Q. Wu, E. Irran, R. Müller, M. Kaupp, H. F. T. Klare, M. Oestreich, *Science*, 2019, **365**, 168; f) A. Fernandes, C. Laye, S. Pramanik, D. Palmeira, Ö. Ö. Pekel, S. Massip, M. Schmidtmann, T. Müller, F. Robert, Y. Landais, *J. Am. Chem. Soc.*, 2020, **142**, 564; g) Q. Wu, A. Roy, G. Wang, E. Irran, H. F. T. Klare, M. Oestreich, *Angew. Chem., Int. Ed.*, 2020, **59**, 10523.

[7]   a) D. Chen, V. Leich, F. Pan, J. Klankermayer, *Chem. Eur. J.*, 2012, **18**, 5184; b) M. Reißmann, A. Schäfer, S. Jung, T. Müller, *Organometallics*, 2013, **32**, 6736; c) V. H. G. Rohde, P. Pommerening, H. F. T. Klare, M. Oestreich, *Organometallics*, 2014, **33**, 3618; d) P. Ducos, V. Liautard, F. Robert, Y. Landais, *Chem. Eur. J.*, 2015, **21**, 11573; e) S. Künzler, S. Rathjen, A. Merk, M. Schmidtmann, T. Müller, *Chem. Eur. J.*, 2019, **25**, 15123; f) A. Denhof, M. Olaru, E. Lork, S. Mebs, L. Chęcińska, J. Beckmann, *Eur. J. Inorg. Chem.*, 2020, 4093; g) A. Dajnak, E. Maerten, N. Saffon-Merceron, A. Baceiredo, T. Kato, *Organometallics*, 2020, **39**, 3403; h) A. Merk, L. Bührmann, N. Kordts, K. Görtemaker, M. Schmidtmann, T. Müller, *Chem. Eur. J.*, 2021, **27**, 3496; i) N. Kumar, C. Laye, F. Robert, Y. Landais, *Eur. J. Org. Chem.*, 2021, 3613.

[8]   H. F. T. Klare, L. Albers, L. Süsse, S. Keess, T. Müller, M. Oestreich, *Chem. Rev.*, 2021, **121**, 5889.

[9]   For reviews, see: a) T. Stahl, H. F. T. Klare, M. Oestreich, *ACS Catal.*, 2013, **3**, 1578; b) S. S. Sen, H. W. Roesky, *Chem. Commun.*, 2018, **54**, 5046; c) L. Greb, *Chem. Eur. J.*, 2018, **24**, 17881.

[10]   For some recent contributions, see: a) V. S. V. S. N. Swamy, N. Parvin, K. V. Raj, K. Vanka, S. S. Sen, *Chem. Commun.*, 2017, **53**, 9850; b) R. Maskey, M. Schädler, C. Legler, L. Greb, *Angew. Chem., Int. Ed.*, 2018, **57**, 1717; c) C. Bakewell, A. J. P. White, M. R. Crimmin, *Angew. Chem., Int. Ed.*, 2018, **57**, 6638; d) O. Kysliak, H. Görls, R. Kretschmer, *Chem. Commun.* 2020, **56**, 7865; e) M. Talavera, G. Meißner, S. G. Rachor, T. Braun, *Chem. Commun.*, 2020, **56**, 4452; f) O. Kysliak, H. Görls, R. Kretschmer, *J. Am. Chem. Soc.*, 2021, **143**, 142; g) G. Kundu, V. S. Ajithkumar, M. K. Bisai, S. Tothadi, T. Das, K. Vanka, S. S. Sen, *Chem. Commun.*, 2021, **57**, 4428; h) M. K. Bisai, V. S. Ajithkumar, R. G. Gonnade, S. S. Sen, *Organometallics*, 2021, **40**, 2651.

[11]   For some selected contributions, see: a) V. J. Scott, R. Çelenligil-Çetin, O. V. Ozerov, *J. Am. Chem. Soc.*, 2005, **127**, 2852; b) R. Panisch, M. Bolte, T. Müller, *J. Am. Chem. Soc.*, 2006, **128**, 9676; c) C. Douvris, O. V. Ozerov, *Science*, 2008, **321**, 1188; d) C. Douvris, C. M. Nagaraja, C.-H. Chen, B. M. Foxman, O. V. Ozerov, *J. Am. Chem. Soc.*, 2010, **132**, 4946; e) D. G. Gusev, O. V. Ozerov, *Chem. Eur. J.*, 2011, **17**,

634; f) T. Stahl, H. F. T. Klare, M. Oestreich, *J. Am. Chem. Soc.*, 2013, **135**, 1248; g) N. Kordts, S. Künzler, S. Rathjen, T. Sieling, H. Großekappenberg, M. Schmidtmann, T. Müller, *Chem. Eur. J.,* 2017, **23**, 10068.

[12] a) M. Aizenberg, D. Milstein, *Science*, 1994, **265**, 359; b) H. H. Cornehl, G. Hornung, H. Schwarz, *J. Am. Chem. Soc.*, 1996, **118**, 9960; c) H. Torrens, *Coord. Chem. Rev.*, 2005, **249**, 1957; d) S. D. Pike, M. R. Crimmin, A. B. Chaplin, *Chem. Commun.*, 2017, **53**, 3615.

[13] S. Duttwyler, C. Douvris, N. L. P. Fackler, F. S. Tham, C. A. Reed, K. K. Baldridge, J. S. Siegel, *Angew. Chem., Int. Ed.*, 2010, **49**, 7519.

[14] a) O. Allemann, S. Duttwyler, P. Romanato, K. K. Baldridge, J. S. Siegel, *Science*, 2011, **332**, 574; b) O. Allemann, K. K. Baldridge, J. S. Siegel, *Org. Chem. Front.*, 2015, **2**, 1018; c) B. Shao, A. L. Bagdasarian, S. Popov, H. M. Nelson, *Science*, 2017, **355**, 1403; d) H. F. T. Klare, *ACS Catal.*, 2017, **7**, 6999.

[15] For reviews on WCAs, see: a) I. Krossing, I. Raabe, *Angew. Chem. Int. Ed.*, 2004, **43**, 2066; b) T. A. Engesser, M. R. Lichtenthaler, M. Schleep, I. Krossing, *Chem. Soc. Rev.*, 2016, **45**, 789; c) I. M. Riddlestone, A. Kraft, J. Schaefer, I. Krossing, *Angew. Chem., Int. Ed.*, 2018, **57**, 13982.

[16] a) X. Yang, C. L. Stern, T. J. Marks, *J. Am. Chem. Soc.*, 1994, **116**, 10015; b) P. Arndt, U. Jäger-Fiedler, M. Klahn, W. Baumann, A. Spannenberg, V. V. Burlakov, U. Rosenthal, *Angew. Chem., Int. Ed.*, 2006, **45**, 4195; c) J. Cano, M. Sudupe, P. Royo, M. E. G. Mosquera, *Angew. Chem., Int. Ed.*, 2006, **45**, 7572.

[17] a) S. Döring, G. Erker, R. Fröhlich, O. Meyer, K. Bergander, *Organometallics*, 1998, **17**, 2183; b) G. C. Welch, R. R. San Juan, J. D. Masuda, D. W. Stephan, *Science*, 2006, **314**, 1124; c) G. C. Welch, R. Prieto, M. A. Dureen, A. J. Lough, O. A. Labeodan, T. Höltrichter-Rössmann, D. W. Stephan, *Dalton Trans.*, 2009, 1559.

[18] N. Fontana, N. A. Espinosa-Jalapa, M. Seidl, J. O. Bauer, *Chem. Eur. J.*, 2021, **27**, 2649.

[19] a) D. B. Culver, M. P. Conley, *Angew. Chem., Int. Ed.*, 2018, **57**, 14902; b) D. B. Culver, A. Venkatesh, W. Huynh, A. J. Rossini, M. P. Conley, *Chem. Sci.*, 2020, **11**, 1510.

[20] M. Ahrens, G. Scholz, T. Braun, E. Kemnitz, *Angew. Chem., Int. Ed.*, 2013, **52**, 5328.

[21] a) N. A. Espinosa-Jalapa, N. Berg, M. Seidl, I. G. Shenderovich, R. M. Gschwind, J. O. Bauer, *Chem. Commun.*, 2020, **56**, 13335; b) J. O. Bauer, N. A. Espinosa-Jalapa, N. Fontana, T. Götz, A. Falk, *Eur. J. Inorg. Chem.*, 2021, 2636.

[22] U. Schubert, H. Gilges, *Organometallics*, 1996, **15**, 2373.

[23] B. Capon, *Q. Rev., Chem. Soc.*, 1964, **18**, 45.

[24] P. Jutzi, C. Müller, A. Stammler, H.-G. Stammler, *Organometallics*, 2000, **19**, 1442.

[25] Brønsted acids have also been used for direct dehydrogena-tive silylium ion formation, see: Q.-A. Chen, H. F. T. Klare, M. Oestreich, *J. Am. Chem. Soc.*, 2016, **138**, 7868. For a detailed mechanistic study on the dihydrogen release from a protonated hydrosilane intermediate, see Ref. 18.

[26] D. Seyferth, H. Friedrich, S. W. Krska, *Z. Naturforsch.*, 1994, **49b**, 1818.

[27] For a controversial discussion on dative bonds in main-group element compounds, see: a) D. Himmel, I. Krossing, A. Schnepf, *Angew. Chem., Int. Ed.*, 2014, **53**, 370; b) G. Frenking, *Angew. Chem. Int. Ed.*, 2014, **53**, 6040; c) D. Himmel, I. Krossing, A. Schnepf, *Angew. Chem., Int. Ed.*, 2014, **53**, 6047.

[28] F. Weinhold, C. R. Landis, *Valency and Bonding: A Natural Bond Orbital Donor-Acceptor Perspective*, Cambridge Univ. Press, Cambridge, UK, 2005.

[29] B(C_6F_5)$_3$·H_2O adducts have received considerable interest as strong Brønsted acids. For some examples, see: a) A. A. Danopoulos, J. R. Galsworthy, M. L. H. Green, S. Cafferkey, L. H. Doerrer, M. B. Hursthouse, *Chem. Commun.*, 1998, 2529; b) L. H. Doerrer, M. L. H. Green, *J. Chem. Soc., Dalton Trans.*, 1999, 4325; c) C. Bergquist, B. M. Bridgewater, C. J. Harlan, J. R. Norton, R. A. Friesner, G. Parkin, *J. Am.*

Chem. Soc., 2000, **122**, 10581; d) D. Neculai, H. W. Roesky, A. M. Neculai, J. Magull, B. Walfort, D. Stalke, *Angew. Chem., Int. Ed.*, 2002, **41**, 4294; e) X. Wang, P. P. Power, *Angew. Chem., Int. Ed.*, 2011, **50**, 10965.

[30] a) S. S. Sen, J. Hey, M. Eckhardt, R. Herbst-Irmer, E. Maedl, R. A. Mata, H. W. Roesky, M. Scheer, D. Stalke, *Angew. Chem., Int. Ed.*, 2011, **50**, 12510; b) M. Lehmann, A. Schulz, A. Villinger, *Angew. Chem., Int. Ed.*, 2012, **51**, 8087; c) M. K. Bisai, V. Sharma, R. G. Gonnade, S. S. Sen, *Organometallics*, **2021**, *40*, 2133.

[31] H. L. D. Hayes, R. Wei, M. Assante, K. J. Geogheghan, N. Jin, S. Tomasi, G. Noonan, A. G. Leach, G. C. Lloyd-Jones, *J. Am. Chem. Soc.*, 2021, **143**, 14814.

[32] H. F. T. Klare, L. Albers, L. Süsse, S. Keess, T. Müller, M. Oestreich, *Chem. Rev.* **2021**, *121*, 5889-5985.

[33] P. Pyykkö, M. Atsumi, *Chem. Eur. J.* **2009**, *15*, 12770.

4.4   Synthesis and characterizations

4.4.1   General Remarks

All experiments were performed in an inert atmosphere of purified nitrogen by using standard Schlenk techniques or an MBraun Unilab 1200/780 glovebox. Glassware was heated at 140°C prior to use. Diethyl ether (Et$_2$O), dichloromethane (DCM), hexane, pentane, tetrahydrofuran (THF), and toluene were dried and degassed with an MBraun SP800 solvent purification system. n-Butyllithium (2.5 M or 1.6 M solution in hexane, Merck KGaA), dichlorophenylsilane (97 %, Merck KGaA), di-$tert$-butyl(methyl)phosphine (97%, Merck KGaA), $tert$-butyllithium (1.9 M solution in pentane, Merck KGaA), sulfur (99%, Merck KGaA) and hydrogen chloride (2.0 M solution in diethyl ether, Merck KGaA), 4-fluorobenzonitrile (99%, Merck KGaA) were used as received without any further purification. Tris(pentafluorophenyl)borane [BCF, B(C$_6$F$_5$)$_3$][1] and [H(OEt$_2$)$_2$]$^+$[B(C$_6$F$_5$)$_4$]$^-$ [2] were synthesized following reported procedures. C$_6$D$_6$ and CD$_2$Cl$_2$ used for NMR spectroscopy were dried over Na/K amalgam and CaH$_2$, respectively. NMR spectra were either recorded using a Bruker Avance 400 (400.13 MHz) or a Bruker Avance III HD 400 (400.13 MHz) at 25 °C. Chemical shifts (δ) are reported in parts per million (ppm). ^{1}H and ^{13}C{^{1}H} NMR spectra are referenced to tetramethylsilane (SiMe$_4$, δ = 0.0 ppm) as external standard, with the deuterium signal of the solvent serving as internal lock and the residual solvent signal as an additional reference. ^{11}B{^{1}H}, ^{19}F{^{1}H}, ^{29}Si{^{1}H}, and ^{31}P{^{1}H} NMR spectra are referenced to BF$_3$·OEt$_2$, CFCl$_3$, SiMe$_4$, and H$_3$PO$_4$, respectively. For the assignment of the multiplicities, the following abbreviations are used: s = singlet, d = doublet, t = triplet m = multiplet. For simplicity, multiplets of order higher than one are described approximating them to the closest first-order type. High-resolution mass spectrometry was carried out on a Jeol AccuTOF GCX and an Agilent Q-TOF 6540 UHD spectrometer. Elemental analyses were performed on a Vario MICRO cube apparatus.

4.4.2 Synthesis of *t*Bu₂PCH₂Li (4)

$$tBu_2PCH_2Li \text{ (4)}$$

Me
|
P
tBu tBu

1.1 equiv. *t*BuLi

neat conditions
65°C
68%

Li
|
CH₂
|
P
tBu tBu
4
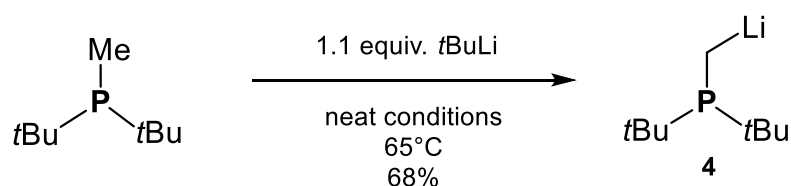
Compound **4** was synthesized according to a procedure by Lerner *et al.*[3] In a glovebox, a Schlenk flask was loaded with pure di-*tert*-butylmethylphosphine (2.0 g, 12.5 mmol, 1.0 equiv.). After connecting the flask to a Schlenk line, *tert*-butyllithium (7.3 ml of a 1.9 M solution in pentane, 13.8 mmol, 1.1 equiv.) was added carefully. The resulting clear solution was stirred during 15 min at room temperature. Afterwards, a distillation bridge with a receiving Schlenk flask was connected and the Schlenk containing the mixture was gradually heated up to 65°C while gently stirring. The system was allowed to react under these conditions for 16 h during which the solvent was slowly distilled off and the oily residue turned into a pale-yellow solid. The distillation bridge with the receiving Schlenk flask was removed while flowing nitrogen from both ends to prevent possible flames. The solid was washed with dry pentane (3 x 5 ml) and carefully dried in vacuum giving pure compound **4** as a white solid (1.41 g, 8.5 mmol, 68%). Spectroscopic data were in accordance with those reported in the literature.[3]

4.4.3 Synthesis of *t*BuPhSi(H)Cl

Cl
|
Cl—Si—H
|
Ph

1.0 equiv. *t*BuLi

pentane
-68°C to RT
88%

Cl
|
tBu—Si—H
|
Ph
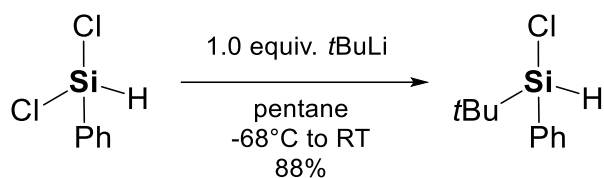
A two-necked Schlenk flask featuring a dropping funnel was filled with pentane (80 mL) and PhHSiCl₂ (4.57 g, 25.8 mmol, 1.0 equiv.). The whole mixture was cooled down to -68°C. *tert*-butyllithium (15.2 mL of a 1.7 M solution in pentane, 25.8 mmol, 1.0 equiv.) was loaded in the dropping funnel and diluted with additional pentane (35 mL). The diluted *tert*-butyllithium solution was added dropwise to the solution of PhHSiCl₂ in pentane at -68°C over a period of 1h under vigorous stirring. The clear solution was then allowed to slowly warm up to room temperature and stirred overnight at room temperature. The obtained white suspension was transferred by means of PTFE tubing to a fritted column layered with Celite®, filtered and the remaining solids washed with more pentane (2 x 20 mL). The clear colorless filtrates were collected, and all volatiles removed under vacuum yielding pure *t*BuPhSi(H)Cl as a clear colourless oil (4.84 g, 24.3 mmol, 88%).

¹H NMR (400.13 MHz, C$_6$D$_6$, 298 K): δ= 0.92 [s, 9H, C(CH_3)$_3$], 5.01 [s with ^{29}Si satellites, $^1J_{\text{H-Si}}$ = 223.6, 1H, SiH], 7.08–7.14 [m, 3H, H_{Ph}], 7.51–7.54 [m, 2H, H_{Ph}]. **¹³C{¹H} NMR** (100.62 MHz, C$_6$D$_6$, 298 K): δ= 19.4 [s, C(CH$_3$)$_3$], 25.4 [s, C(CH$_3$)$_3$], 128.3 [s, C_{Ph}], 131.0 [s, C_{Ph}], 131.7 [s, C_{Ph}], 134.8 [s, C_{Ph}]. **²⁹Si{¹H} NMR** (79.49 MHz, C$_6$D$_6$, 298 K): δ 11.5. **HR-MS (EI+)**, calculated m/z for C$_{10}$H$_{15}$SiCl [M]$^+$: 198.06261; found: 198.06276.
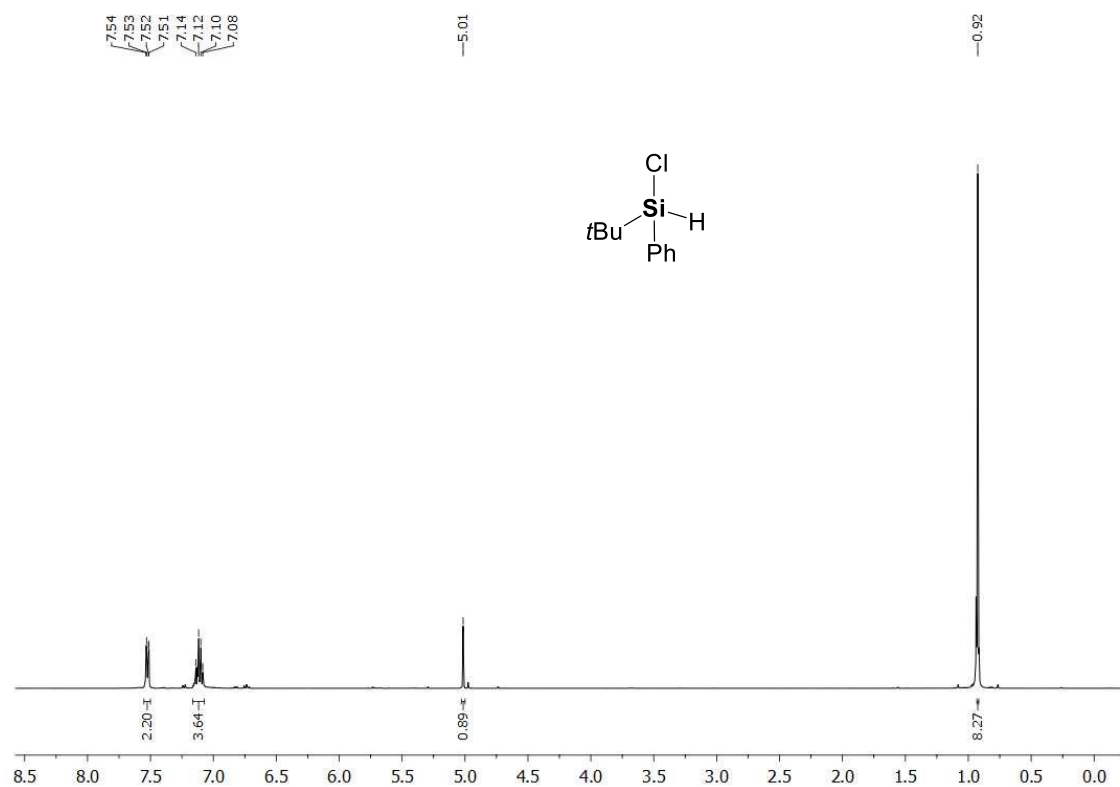
Figure S137. ¹H NMR spectrum (C$_6$D$_6$, 298 K) of tBuPhSi(H)Cl.
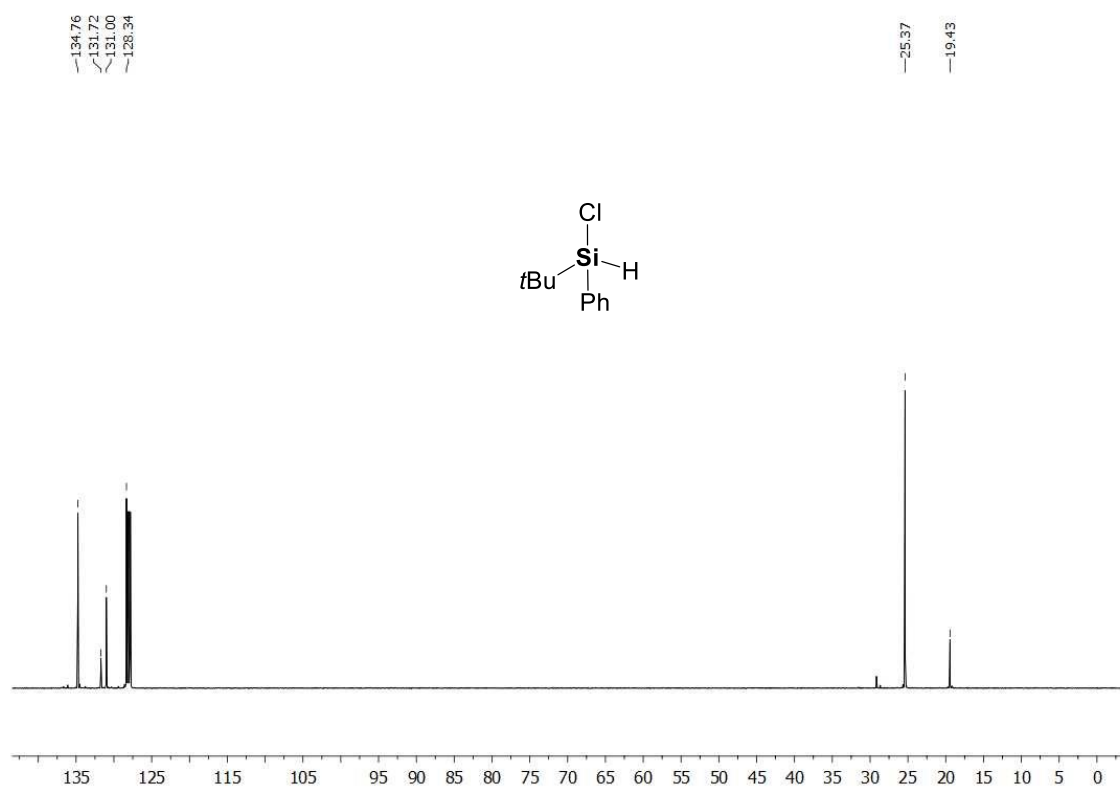
Figure S138. ^{13}C{^{1}H} NMR spectrum (C$_6$D$_6$, 298 K) of tBuPhSi(H)Cl.
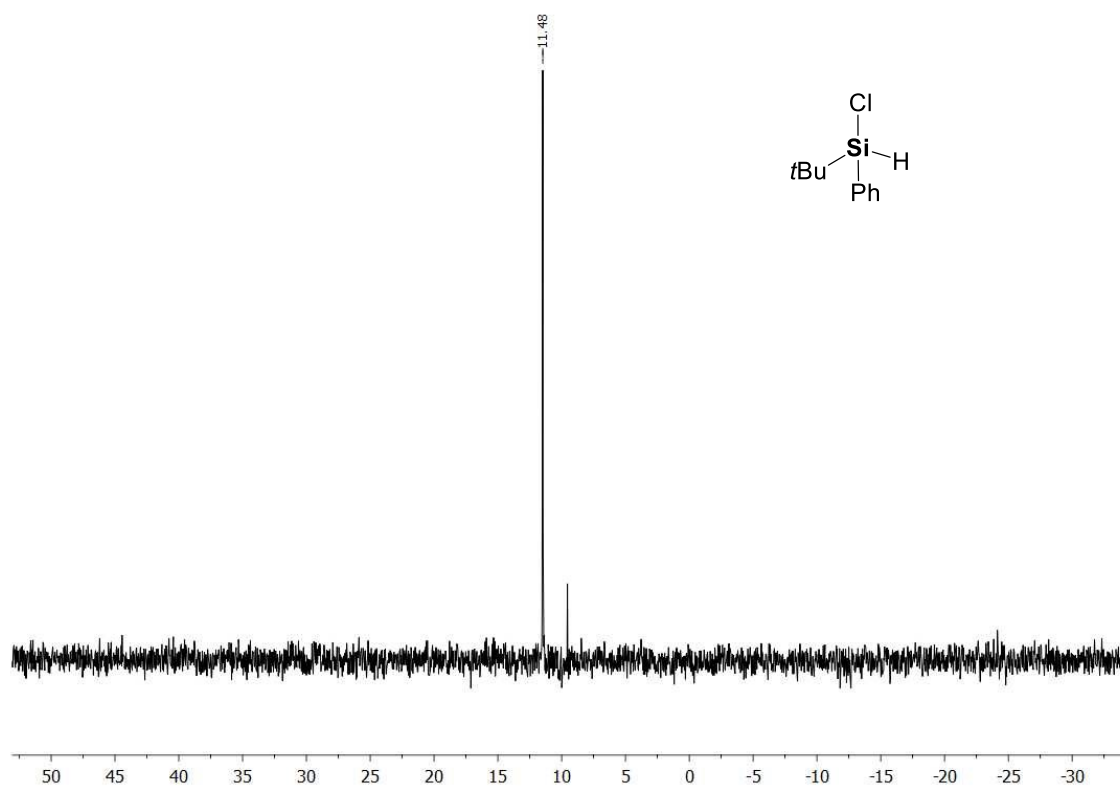
Figure S139. ^{29}Si{^{1}H} NMR spectrum (C$_6$D$_6$, 298 K) of tBuPhSi(H)Cl.

4.4.4   Synthesis of *t*BuPhSi(H)OH
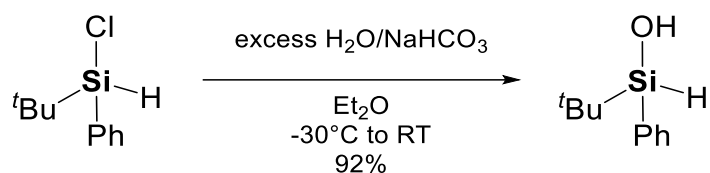
To a stirred solution of *t*BuPhSi(H)Cl (3.68 g, 18.55 mmol) in diethyl ether (60 ml) at -30°C, H_2O (2 ml, 111.11 mmol) was added followed by an excess of $NaHCO_3$. The resulting suspension was then allowed to slowly warm up to room temperature and reacted overnight under vigorous stirring. Afterwards, the reaction mixture was dried with $MgSO_4$, the white suspension filtered, and the remaining solids washed with diethyl ether (2 x 20 ml). The clear colorless filtrates were collected and all the volatiles were gently removed under vacuum, without an external source of heating, to yield pure *t*BuPhSi(H)OH as a clear colorless oil (3.08 g, 17.08 mmol, 92%). Batches of freshly prepared silanol, dissolved in hexane and stored at -30°C are stable over a period of months, otherwise the neat isolated silanol slowly converts to the respective siloxane at room temperature.

¹H NMR (400.13 MHz, C_6D_6, 298 K): δ= 0.97 [s, 9H, C(C*H₃*)₃], 2.59 [s, 1H, O*H*], 5.05 [s with ²⁹Si satellites, $^1J_{HSi}$ = 204.6, 1H, Si*H*], 7.17–7.18 [m, 3H, *H*$_{Ph}$], 7.56–7.57 [m, 2H, *H*$_{Ph}$]. **¹³C{¹H} NMR** (100.62 MHz, C_6D_6, 298 K): δ= 17.7 [s, *C*(CH₃)₃], 25.2 [s, C(*C*H₃)₃], 127.7 [s, *C*$_{Ph}$], 129.9 [s, *C*$_{Ph}$], 134.1 [s, *C*$_{Ph}$], 135.0 [s, *C*$_{Ph}$]. **²⁹Si{¹H} NMR** (79.49 MHz, C_6D_6, 298 K): δ= 0.9. **HR-MS (EI+)**, calculated. m/z for $C_{10}H_{16}OSi$ [M]⁺: 180.09649; found: 180.09652. **CHN Analysis** $C_{10}H_{16}OSi$; calculated: C 66.61%; H 8.94%; found: C 65.34%; H 8.31%.
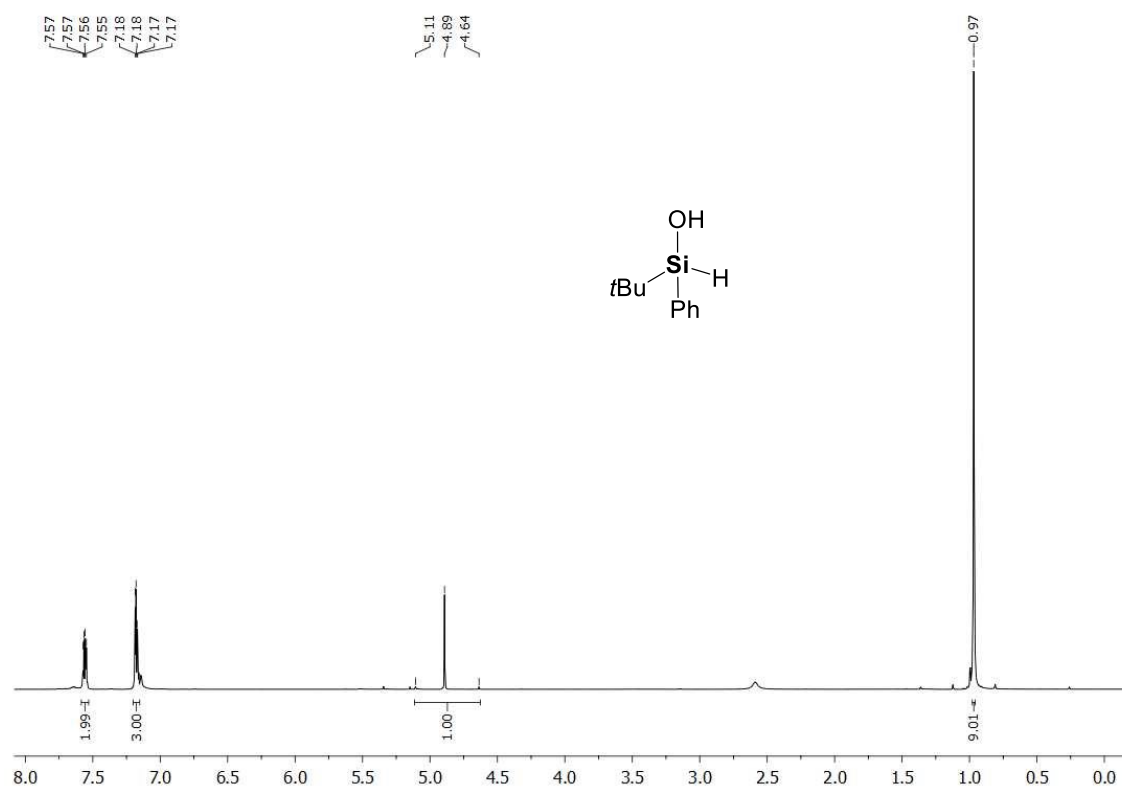
Figure S140. ^{1}H NMR spectrum (C$_6$D$_6$, 298 K) of tBuPhSi(H)OH.
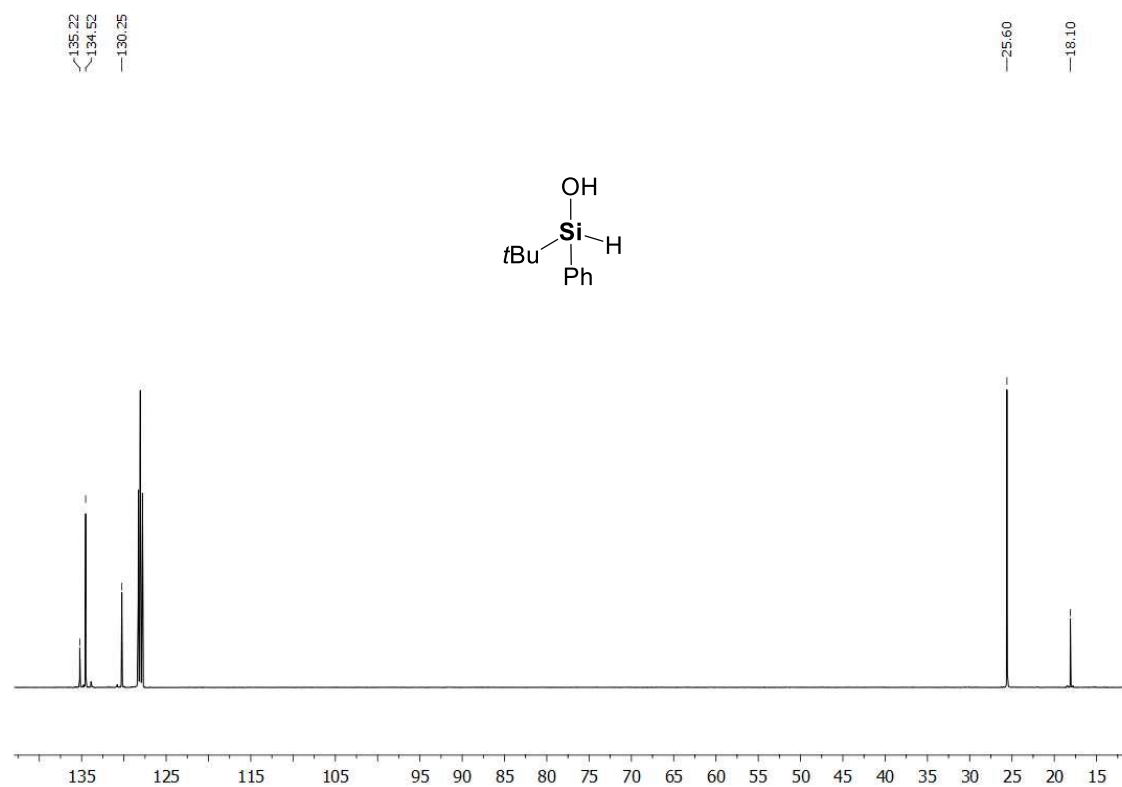
Figure S141. ^{13}C{^{1}H} NMR spectrum (C$_6$D$_6$, 298 K) of tBuPhSi(H)OH.

164
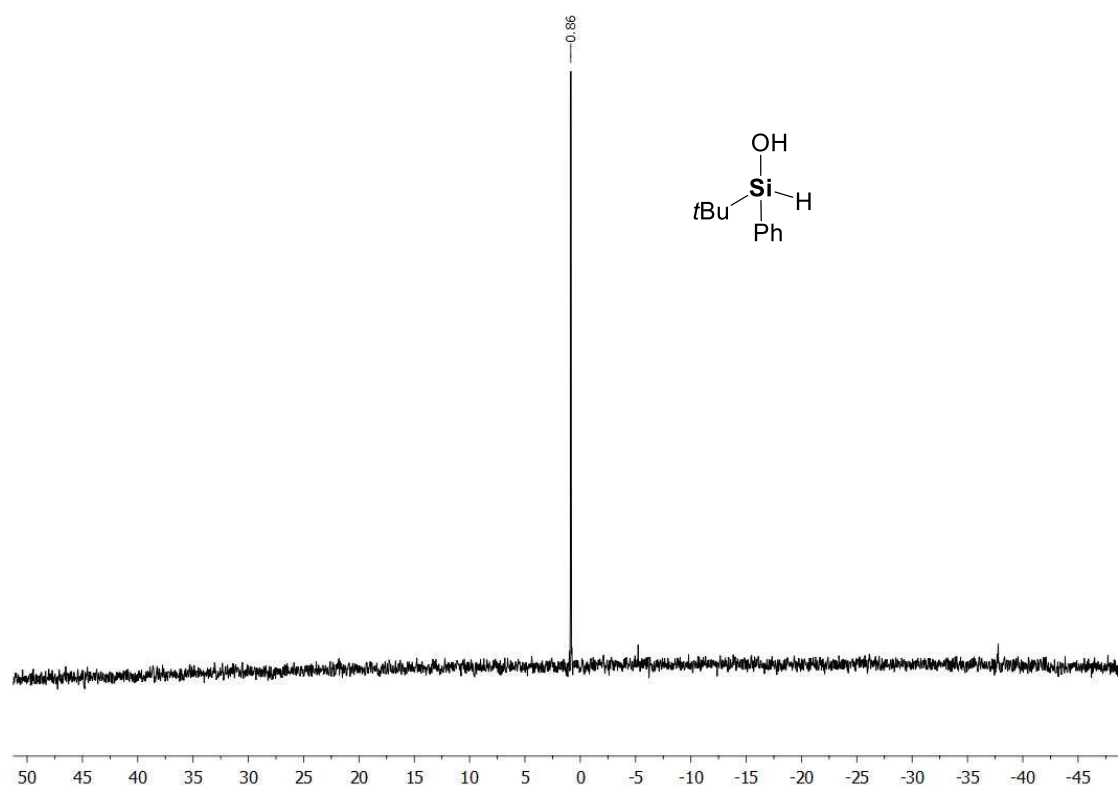
Figure S142. ^{29}Si$\{^1$H$\}$ NMR spectrum (C$_6$D$_6$, 298 K) of *t*BuPhSi(H)OH.

4.4.5   Synthesis of *t*BuPhSi(H)(OLi) (2)
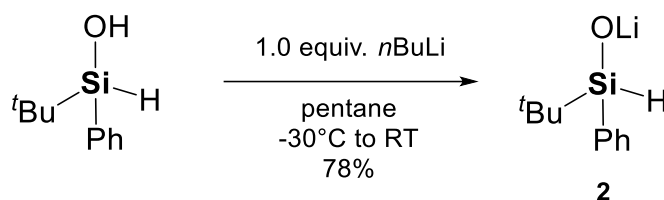
n-Butyllithium (6.8 ml, 2.5 M in hexane, 17.08 mmol, 1.0 equiv.) was added dropwise to a solution of *t*BuPhSiH(OH) (3.08 g, 17.08 mmol, 1.0 equiv.) in pentane (40 ml) at -30°C. The resulting clear pale-yellow solution was then allowed to slowly warm up to room temperature under vigorous stirring. After additional 2 h of stirring at room temperature, the Schlenk flask containing the whole mixture was sealed and stored at -30°C leading to the precipitation of the lithiated silanolate **2** as a clear colorless crystalline solid over a period of three days. Afterwards, the cold mother-liquor (-30°C) was removed *via* suction filtration and the solid dried under vacuum affording pure silanolate **2** as a white solid (2.48 g, 13.32 mmol, 78%).

^{1}H NMR (400.13 MHz, THF-d_8, 298 K): δ= 0.82 [s, 9H, C(C*H*$_3$)$_3$], 4.83 [s with ^{29}Si satellites, $^1J_{HSi}$ = 180.4, 1H, Si*H*], 7.17 [m, 3H, *H*$_{Ph}$], 7.56 [m, 2H, *H*$_{Ph}$]. **^{7}Li$\{^1$H$\}$ NMR** (155.50 MHz, THF-d_8, 298 K): δ= 0.3. **^{13}C$\{^1$H$\}$ NMR** (100.62 MHz, THF-d_8, 298 K): δ= 18.9 [s, *C*(CH$_3$)$_3$], 26.2 [s, C(*C*H$_3$)$_3$], 126.2

[s, C_{Ph}], 127.1 [s, C_{Ph}], 134.1 [s, C_{Ph}], 144.6 [s, C_{Ph}]. **^{29}Si{^{1}H} NMR** (79.49 MHz, THF-d_8, 298 K): δ= -14.8. **HR-MS (ESI+)**, calculated. m/z for $C_{20}H_{30}O_2Si_2$ [2M + Li]$^+$: 379.2264; found: 379.2252. **CHN Analysis** $C_{10}H_{15}LiOSi$: calculated: C 64.49%, H 8.12%; found: C 64.36%; H 8.08%.
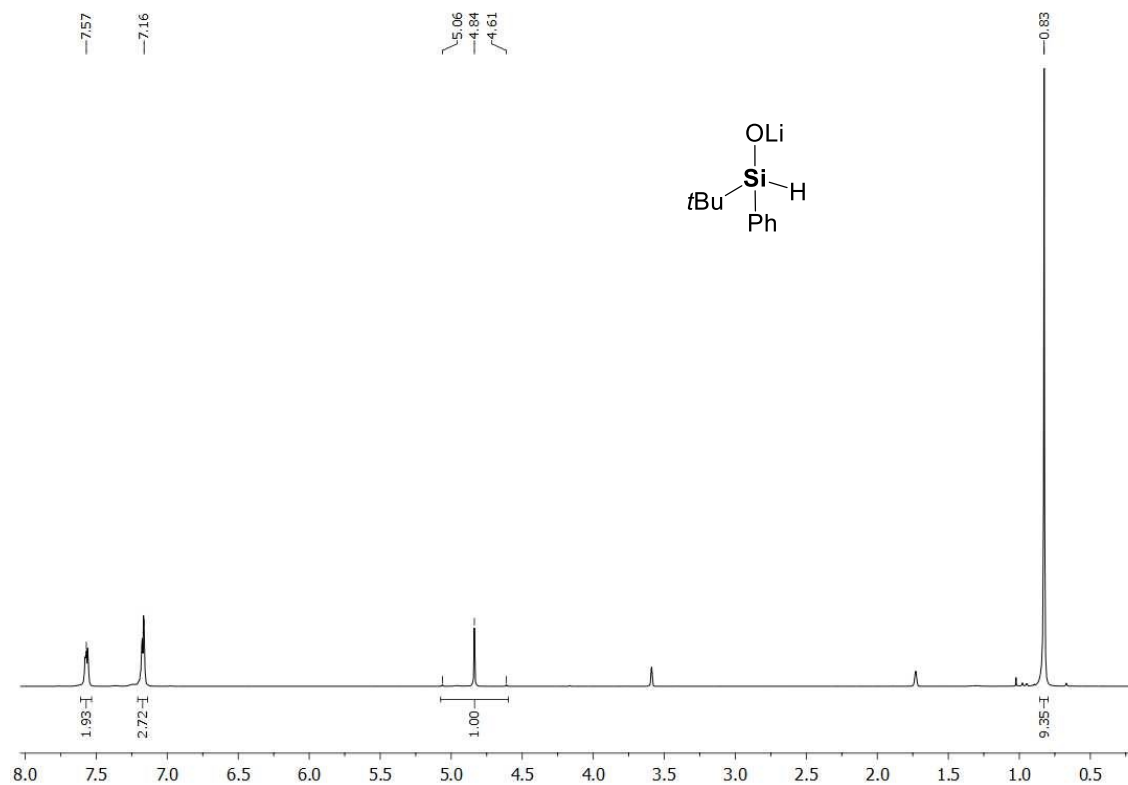
Figure S143. ^{1}H NMR spectrum (THF-d_8, 298 K) of compound **2**.
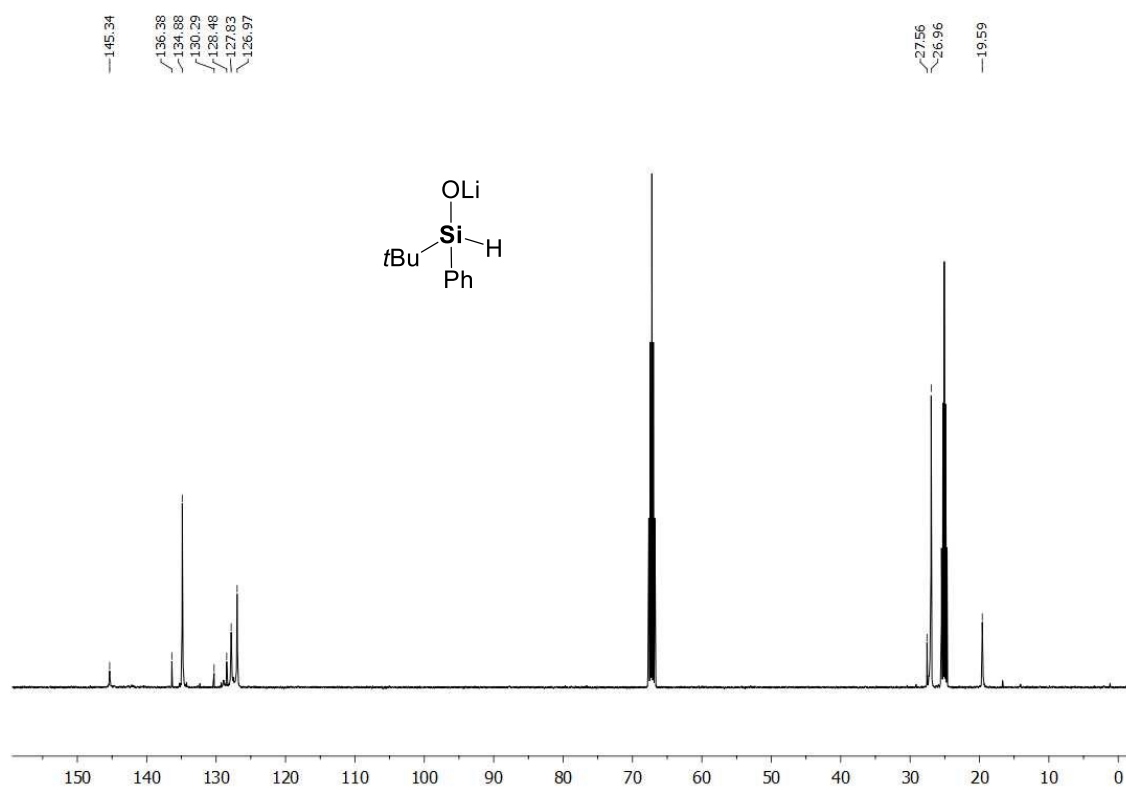
Figure S144. $^{13}C\{^1H\}$ NMR spectrum (THF-d_8, 298 K) of compound **2**.
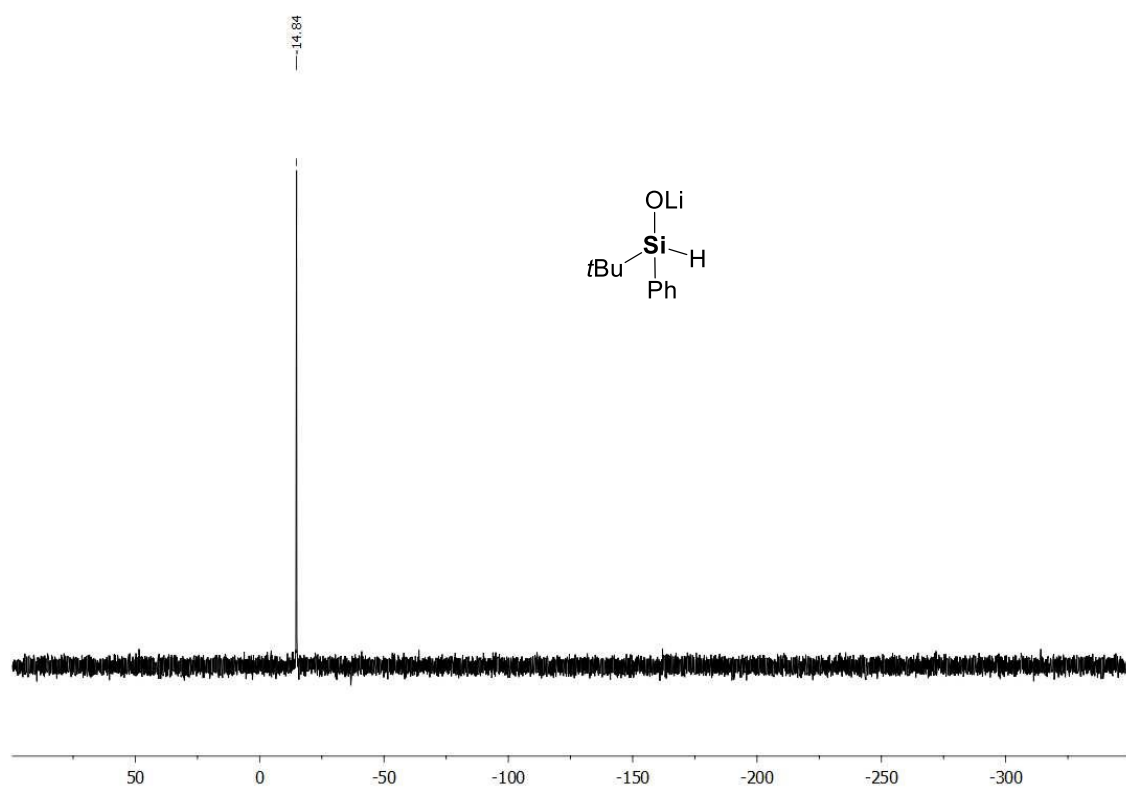
Figure S145. $^{29}Si\{^1H\}$ NMR spectrum (THF-d_8, 298 K) of compound **2**.
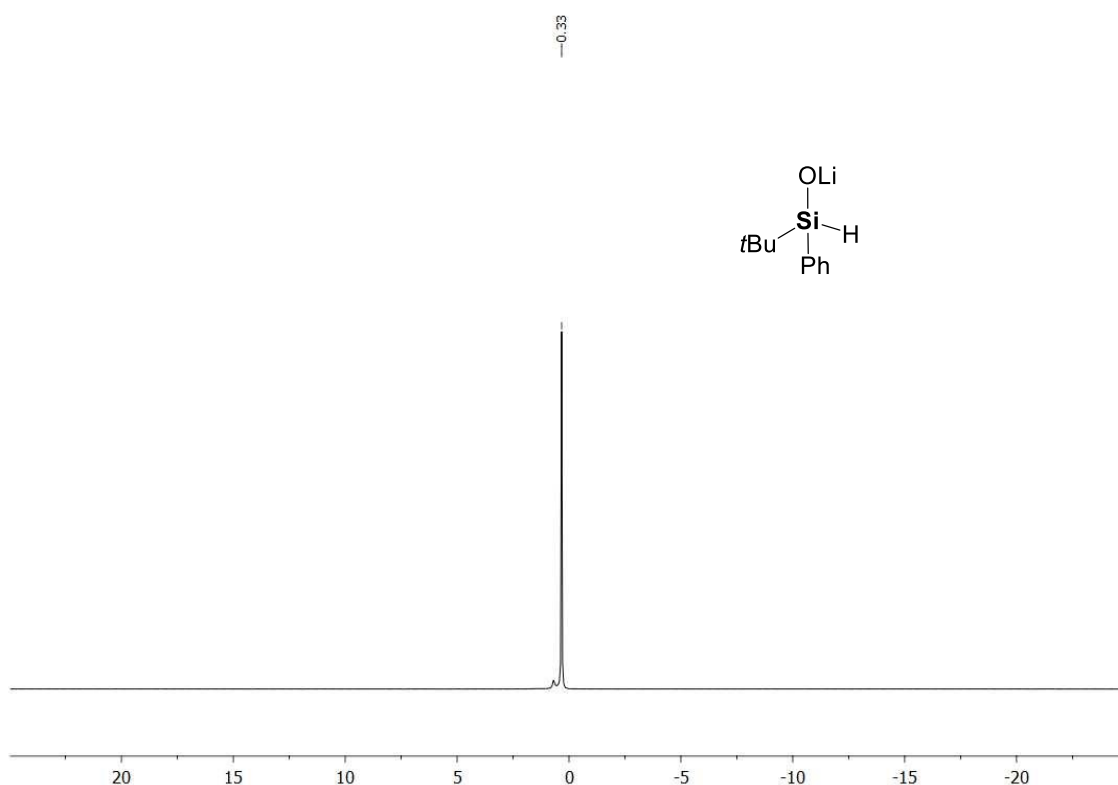
Figure S146. ^{7}Li{^{1}H} NMR spectrum (THF-d_8, 298 K) of compound **2**.

4.4.6   Synthesis of Ph$_2$Si(Cl)OSiPh(H)tBu (3)
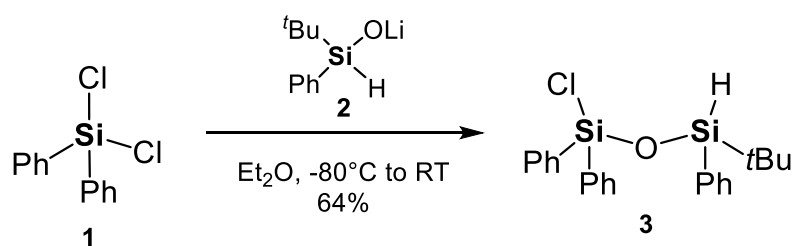
Lithium silanolate **2** (9.68 g, 52.0 mmol, 1.0 equiv.) was suspended in diethyl ether (100 ml) and the solution was cooled down to -80°C. Ph$_2$SiCl$_2$ **1** (13.2 g, 52.0 mmol, 1.0 equiv.) was added *via* syringe in one portion. The reaction mixture was stirred vigorously without further cooling for 15 h during which a white precipitate was formed. The solids were filtered off and rinsed three times with pentane (3 x 30 ml). All volatiles were removed under reduced pressure. The crude mixture was purified *via* Kugelrohr distillation (165 °C oven temperature, 1.0 x 10^{-3} mbar) affording pure product **3** as a colourless oil (13.2 g, 33.3 mmol, 64%).

^{1}H NMR (400.13 MHz, C$_6$D$_6$, 298 K): δ =1.00 [s, 9H, SiC(CH_3)$_3$], 5.18 [s, 1H, SiH], 7.08–7.14 [m, 9H, H_{Ph}], 7.60–7.62 [m, 2H, H_{Ph}], 7.74–7.76 [m, 4H, H_{Ph}]. **^{13}C{^{1}H} NMR** (100.61 MHz, C$_6$D$_6$, 298 K): δ = 18.5 [s, SiCH$_2$(CH$_3$)$_3$], 25.5 [s, SiCH$_2$(CH$_3$)$_3$], 128.2 [s, C$_{Ph}$], 128.4 [s, C$_{Ph}$], 130.5 [s, C$_{Ph}$], 131.2

[s, C$_{Ph}$], 134.0 [s, C$_{Ph}$], 134.1 [s, C$_{Ph}$], 134.6 [s, C$_{Ph}$]. **^{29}Si{^{1}H} NMR** (79.49 MHz, C$_6$D$_6$, 298 K): δ = -19.1 [s, ClSiO*Si*H], -3.3 [s, Cl*Si*OSiH]. **CHN Analysis** C$_{22}$H$_{25}$ClOSi$_2$: calculated: C 66.55%, H 6.35%; found C 69.90%, H 6.45%. **HR-MS (ESI+)**, calculated. m/z for C$_{18}$H$_{16}$ClOSi$_2^+$ [M-C$_4$H$_9$]$^+$: 339.0428; found: 339.0426.
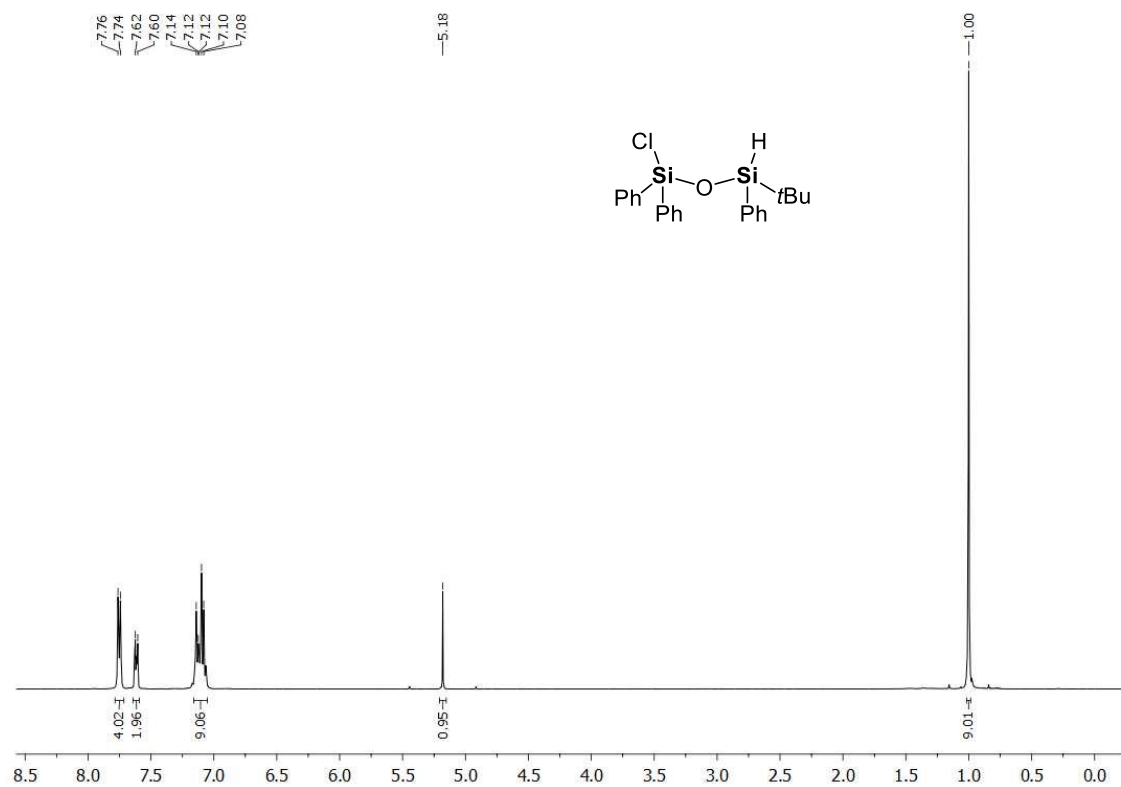
Figure S147. ^{1}H NMR spectrum (C$_6$D$_6$, 298 K) of compound **3**.
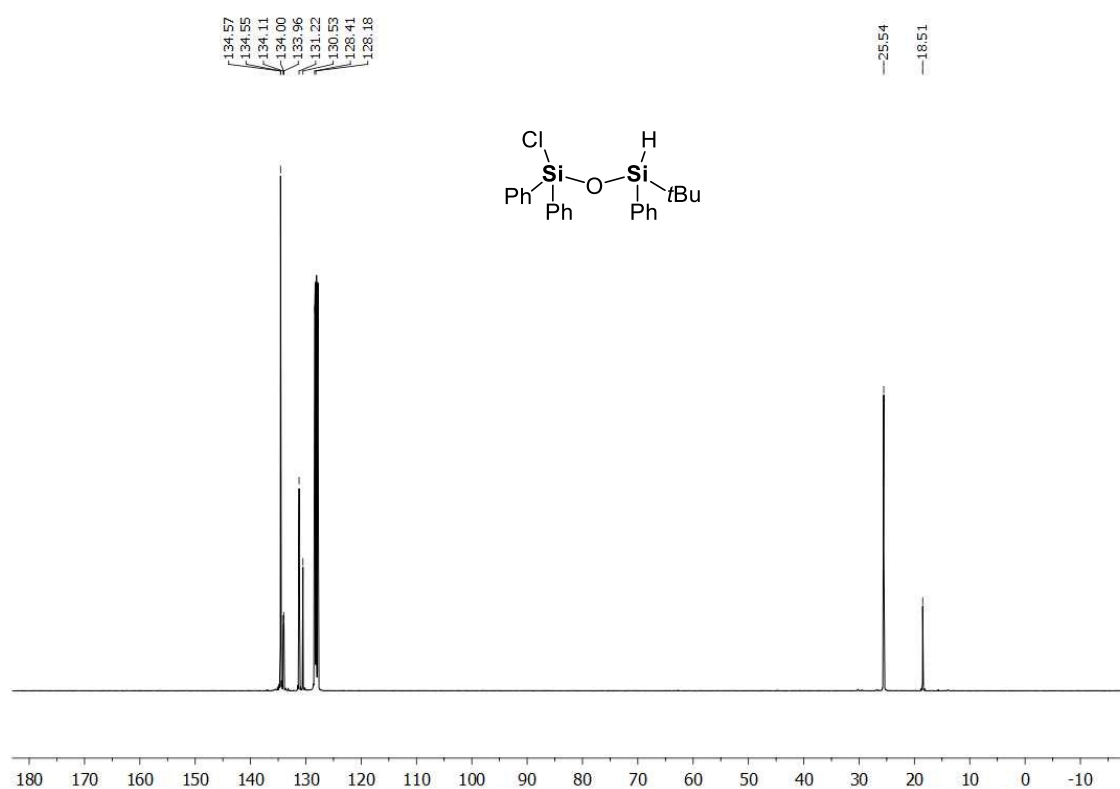
Figure S148. $^{13}C\{^1H\}$ NMR spectrum (C_6D_6, 298 K) of compound **3**.
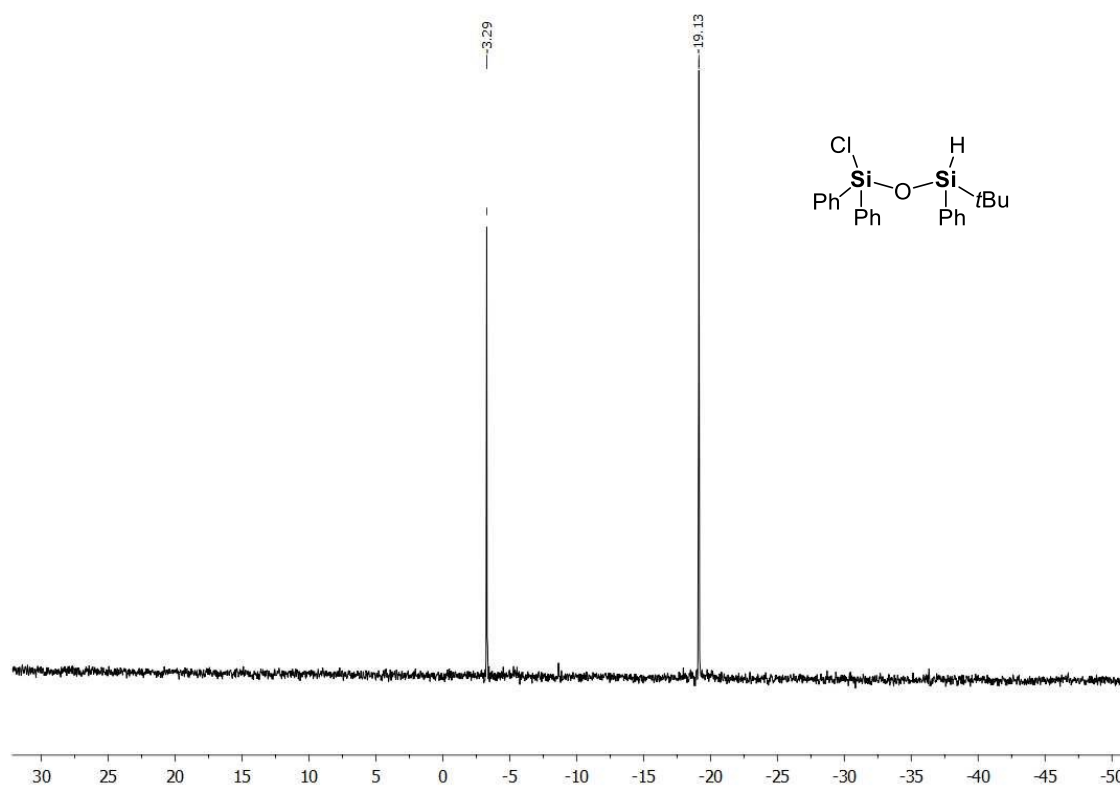
Figure S149. $^{29}Si\{^1H\}$ NMR spectrum (C_6D_6, 298 K) of compound **3**.

4.4.7 Synthesis of (*t*Bu)₂PCH₂SiPh₂OSiPh(H)*t*Bu (5)
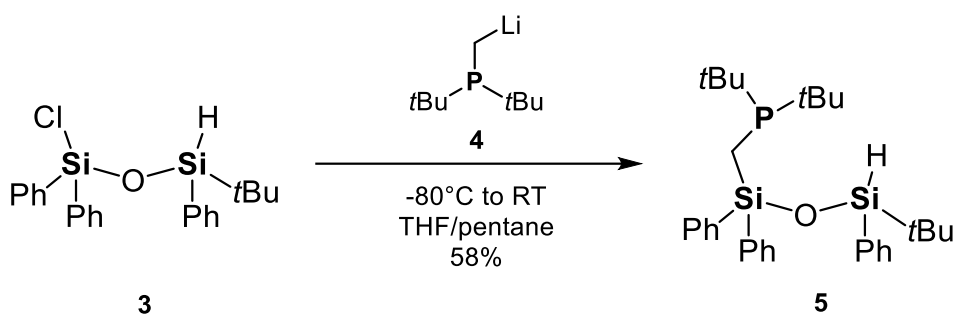
Siloxane **3** (3.85 g, 9.7 mmol, 1.0 equiv.) was dissolved in pentane (20 ml) and the solution was cooled down to -80 °C. Freshly prepared *t*Bu₂PCH₂Li (**4**) (1.61 g, 9.7 mmol, 1.0 equiv.) was added by the means of a PTFE cannula as a THF solution (10 ml). The reaction mixture was stirred for 15 h without further cooling. Afterwards, all volatiles were removed in vacuum yielding a colourless solid which was extracted with DCM (3 x 5 ml). The solids were filtered off by cannula filtration and the clear filtrates collected and dried under vacuum. The crude mixture was purified *via* Kugelrohr distillation (190°C oven temperature, 1.0×10^{-3} mbar) affording the desired compound **5** as a colourless oil (2.92 g, 5.6 mmol 58%).

¹H NMR (400.30 MHz, CD₂Cl₂, 298 K): δ =0.90 [s, 9H, SiC(C*H*₃)₃], 0.96 [d, $^3J_{\text{P-H}}$= 2.4 Hz, 9H, PC(C*H*₃)₃], 0.98 [d, $^3J_{\text{P-H}}$= 2.4 Hz, 9H, PC(C*H*₃)₃], 1.25 [b, 2H, SiC*H*₂P], 4.92 [s,1H, Si*H*], 7.28–7.39 [m, 9H, *H*Ph], 7.60–7.63 [m, 2H, *H*Ph], 7.66 [m, 2H, *H*Ph], 7.68 [m, 2H, *H*Ph]. **¹³C{¹H} NMR** (100.66 MHz, C₆D₆, 298 K): δ = 6.8 [d, $^1J_{\text{P-C}}$= 44.5 Hz, SiCH₂P], 18.8 [s, SiCH₂(CH₃)₃], 25.9 [s, SiCH₂(*C*H₃)₃], 29.6 [d, $^2J_{\text{P-C}}$= 2.2 Hz, PC(*C*H₃)₃], 29.7 [d, $^2J_{\text{P-C}}$= 2.3 Hz, PC(*C*H₃)₃], 31.7 [d, $^1J_{\text{P-C}}$= 2.9 Hz, P*C*(CH₃)₃], 31.9 [d, $^1J_{\text{P-C}}$= 3.0 Hz, P*C*(CH₃)₃], 127.8 [s, *C*Ph], 127.9 [s, *C*Ph], 127.9 [s, *C*Ph], 130.0 [s, *C*Ph], 130.0 [s, *C*Ph], 130.1 [s, *C*Ph], 134.9 [s, *C*Ph], 135.4 [m, *C*Ph], 135.6 [s, *C*Ph], 137.4 [dd, $J_{\text{P-C}}$= 1.8 Hz, $J_{\text{P-C}}$= 7.0 Hz, *C*Ph]. **²⁹Si{¹H} NMR** (79.49 MHz, CD₂Cl₂, 298 K): δ = -12.6 [d, $^2J_{\text{Si-P}}$= 23.9 Hz, PC*Si*OSiH], -5.6 [s, PCSiO*Si*H]. **³¹P{¹H} NMR** (162.04 MHz, CD₂Cl₂, 298 K): δ = 15.3 [s]. **CHN Analysis** C₃₁H₄₅OPSi₂: calculated: C 71.49%, H 8.71%; found C 71.96%, H 8.81%. **HR-MS (ESI+)**, calculated. m/z for C₃₁H₄₅OPSi₂⁺ [M+H]⁺: 521.2819; found: 521.2777.
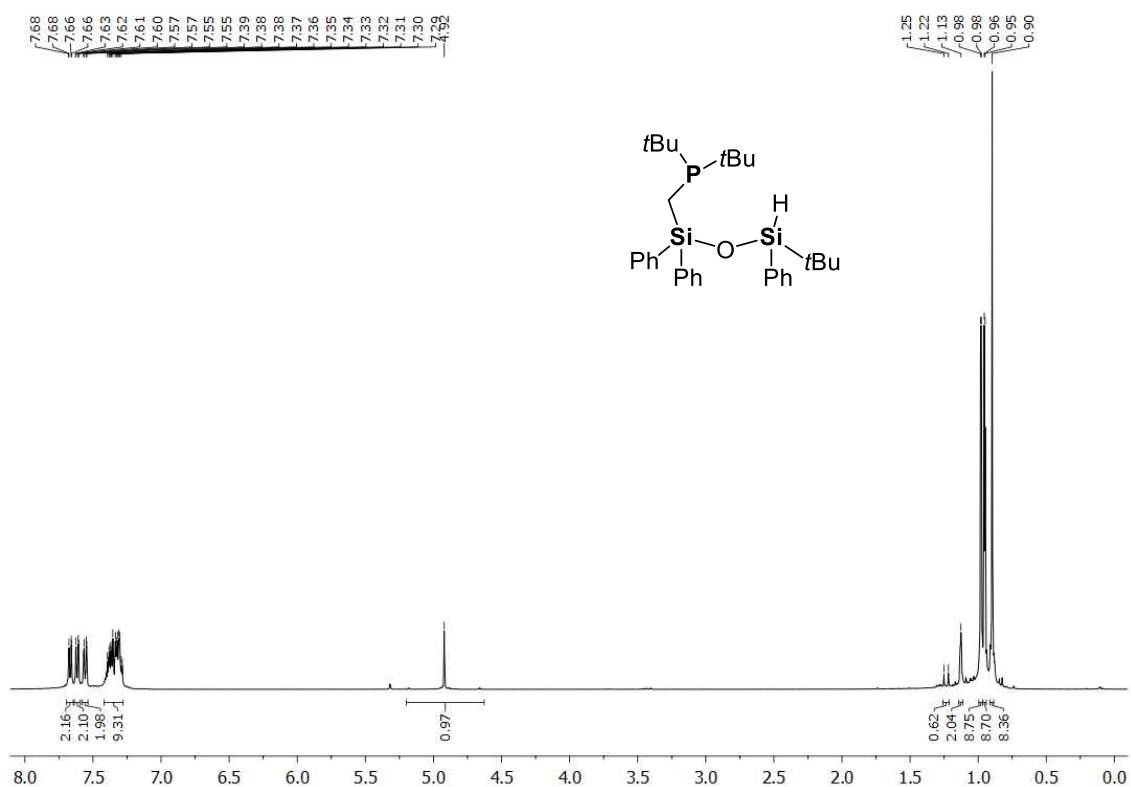
Figure S150. ^{1}H NMR spectrum (CD$_2$Cl$_2$, 298 K) of compound **5**.
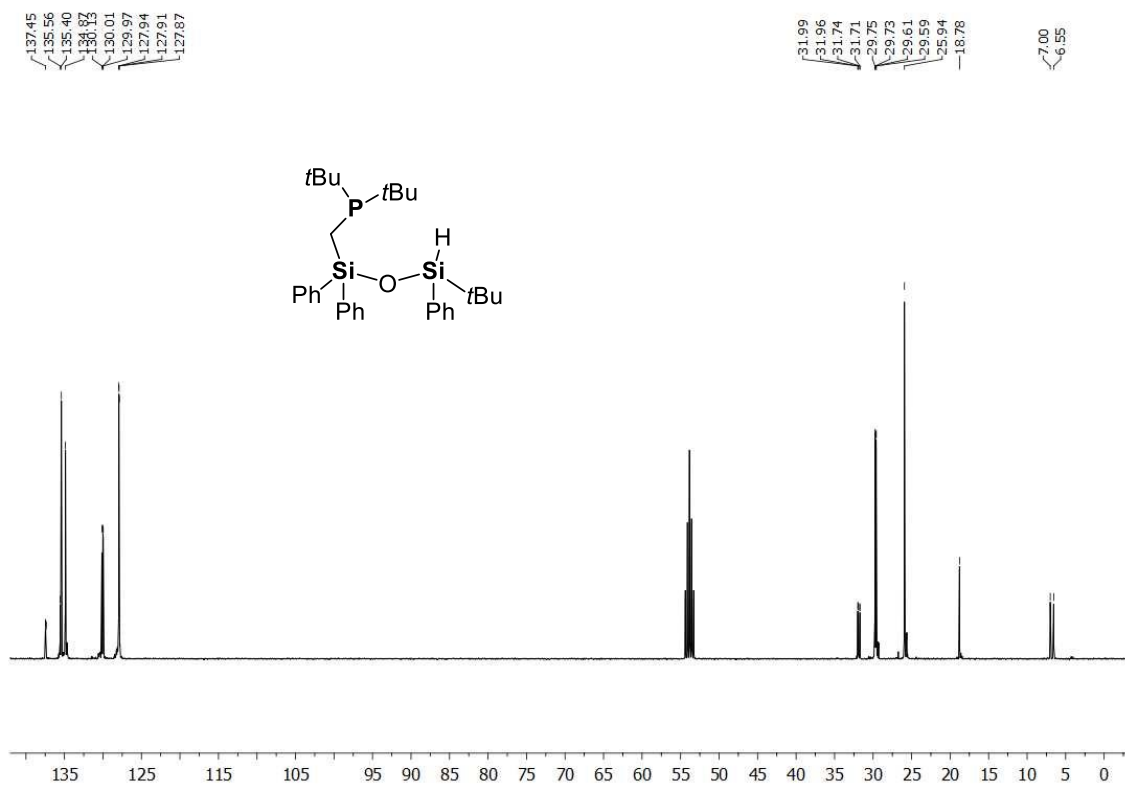
Figure S151. ^{13}C{^{1}H} NMR spectrum (C$_6$D$_6$, 298 K) of compound **5**.
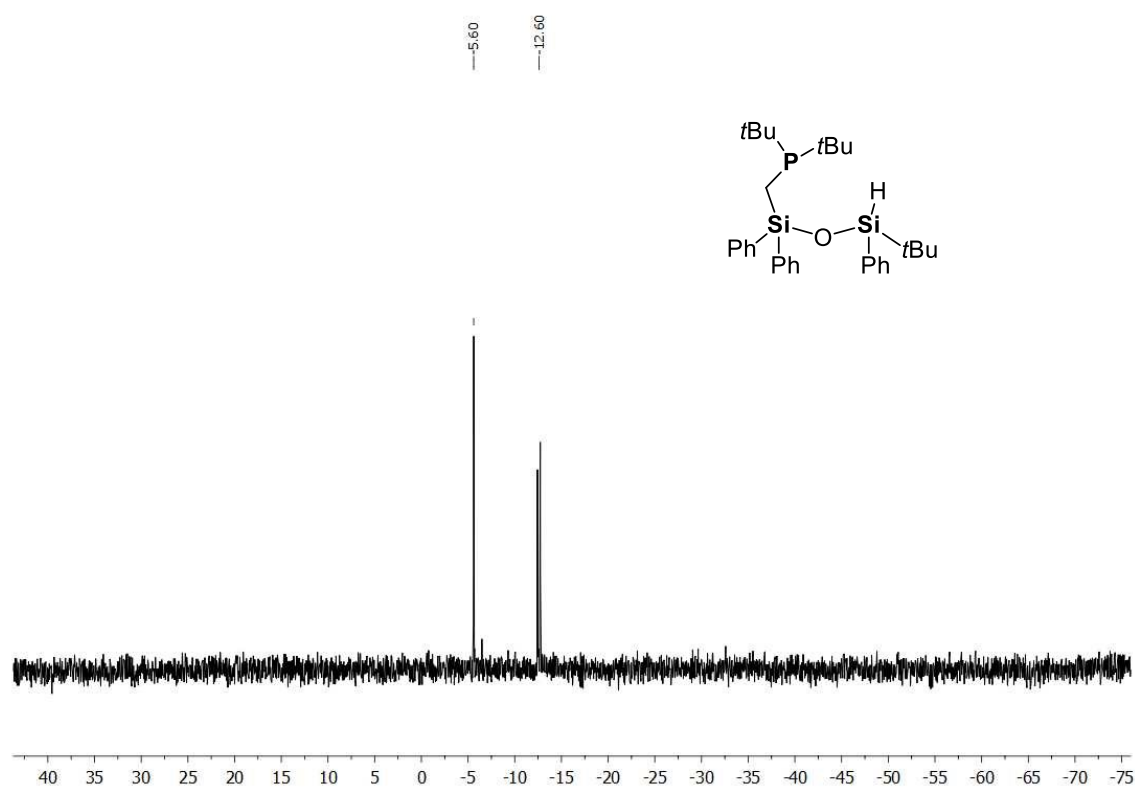
Figure S152. $^{29}Si\{^1H\}$ NMR spectrum (C_6D_6, 298 K) of compound **5**.
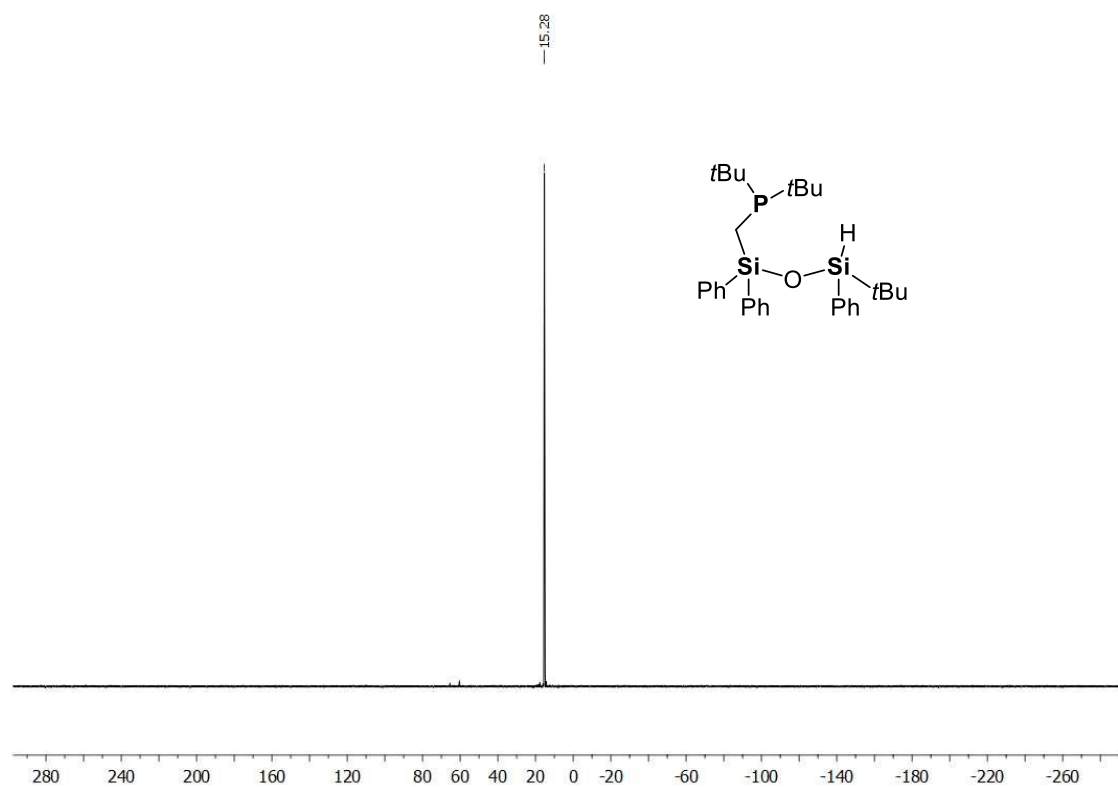
Figure S153. $^{31}P\{^1H\}$ NMR spectrum (CD_2Cl_2, 298 K) of compound **5**.

4.4.1   Synthesis of [W(CO)$_4$(5)]
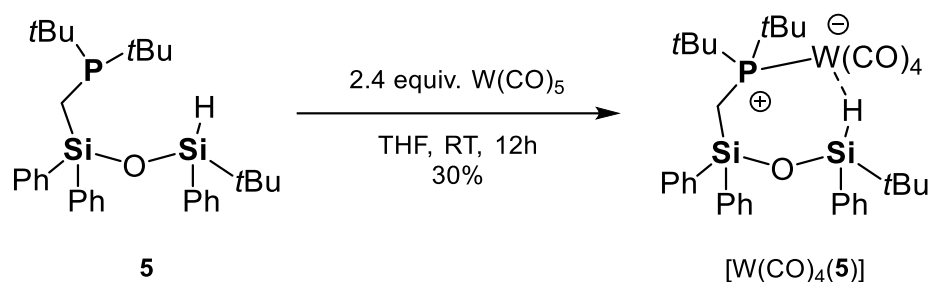
A reaction vessel featuring a cooler and a UV lamp was loaded with W(CO)$_6$ (324 mg, 0.92 mmol, 2.4 eq.) in THF (40 ml). The solution was irradiated for 3 hours during which the colour turned intense yellow. This solution was directly added to a previously prepared oven dried Schlenk flask containing a THF (5 ml) solution of compound **5** (200 mg, 0.384 mmol, 1.0 eq.). The yellow solution was stirred at room temperature for 12 hours. Afterwards, the volatiles were removed in vacuum and the residue recrystallized from cold pentane. From this solution the unreacted W(CO)$_6$ crystallized and was immediately separated. By further cooling down the liquid phase for one week, the desired complex [W(CO)$_4$(**5**)] was obtained as yellow crystals (98 mg, 0.12 mmol, 30%). These crystals were also suitable for X-ray diffraction.

^{1}H NMR (400.30 MHz, CD$_2$Cl$_2$, 298 K): δ = -6.34 [bs, 1H, SiHW], 1.04 [s, 9H, SiC(CH_3)$_3$], 1.25 [t, $^3J_{\text{P-H}}$= 13.9 Hz, 18H, PC(CH_3)$_3$], 1.98 [d, $^2J_{\text{P-H}}$= 10.0 Hz, 2H, SiCH_2P], 7.22–7.25 [m, 2H, H_{Ph}], 7.35–7.39 [m, 3H, H_{Ph}], 7.46–7.50 [m, 4H, H_{Ph}], 7.52–7.55 [m, 4H, H_{Ph}], 7.71–7.73 [m, 2H, H_{Ph}]. **^{13}C{^{1}H} NMR** (100.66 MHz, CD$_2$Cl$_2$, 298 K): δ = 7.8 [bs, SiCH$_2$P], 22.2 [bs, SiC(CH$_3$)$_3$], 25.8 [s, SiC(CH$_3$)$_3$], 30.2 [d, $^2J_{\text{C-P}}$= 5.4 Hz PC(CH$_3$)$_3$], 30.6 [d, $^2J_{\text{C-P}}$= 5.8 Hz PC(CH$_3$)$_3$], 36.6 [d, $^1J_{\text{C-P}}$= 13.0 Hz PC(CH$_3$)$_3$], 38.0 [d, $^1J_{\text{C-P}}$= 13.5 Hz PC(CH$_3$)$_3$], 127.8 [s, C_{Ph}], 128.5 [d, $J_{\text{C-P}}$= 5.9 Hz, C_{Ph}], 130.8 [s, C_{Ph}], 130.8 [s, C_{Ph}], 130.9 [s, C_{Ph}] 133.7 [s, C_{Ph}], 134.6 [s, C_{Ph}], 135.0 [s, C_{Ph}], 204.1 [s, W(CO)$_4$]. **^{29}Si{^{1}H} NMR** (79.49 MHz, CD$_2$Cl$_2$, 298 K): δ = -13.1 [s, PCSiOSiH], -11.5 [b, PCSiOSiHW]. **^{31}P{^{1}H} NMR** (162.04 MHz, CD$_2$Cl$_2$, 298 K): δ = 56.3 [s with satellites, $^1J_{\text{P-W}}$= 115.8 Hz]. **HR-MS (FD-MS)**, calculated. m/z for C$_{35}$H$_{45}$O$_5$PSi$_2$W$^+$ [M]$^+$: 816.2052; found: 816.2479.
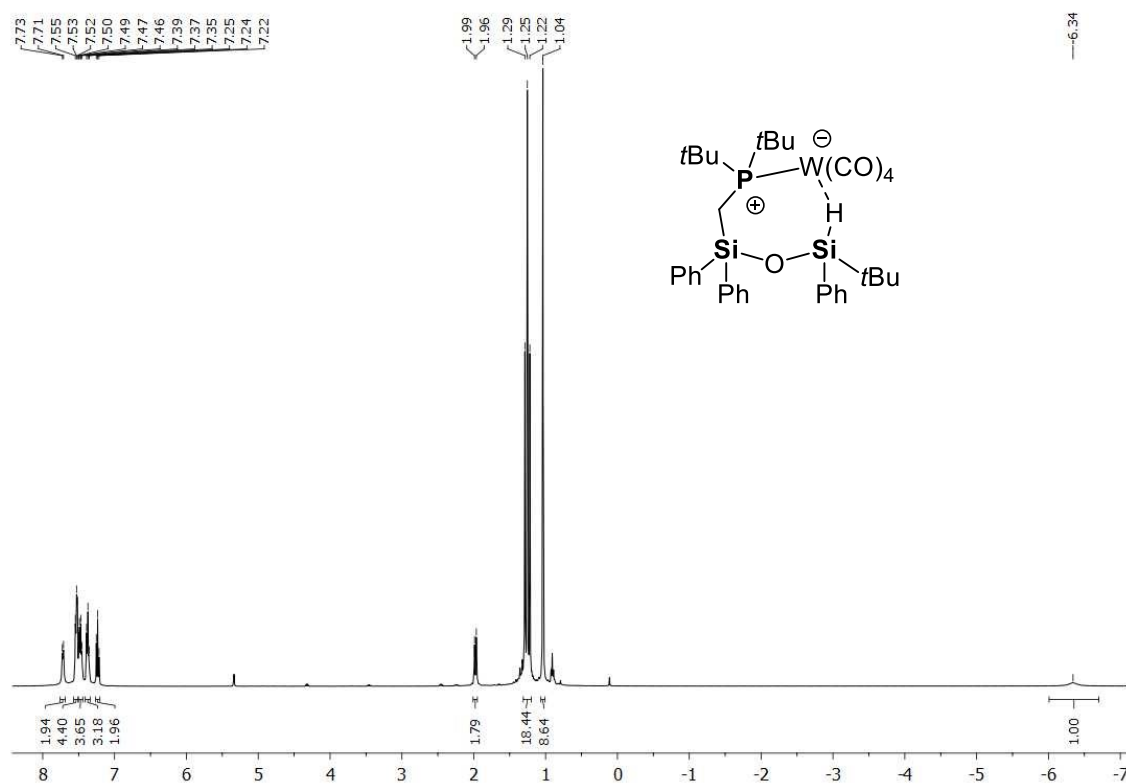
Figure S154. ^{1}H NMR spectrum (CD$_2$Cl$_2$, 298 K) of compound [W(CO)$_4$(**5**)].
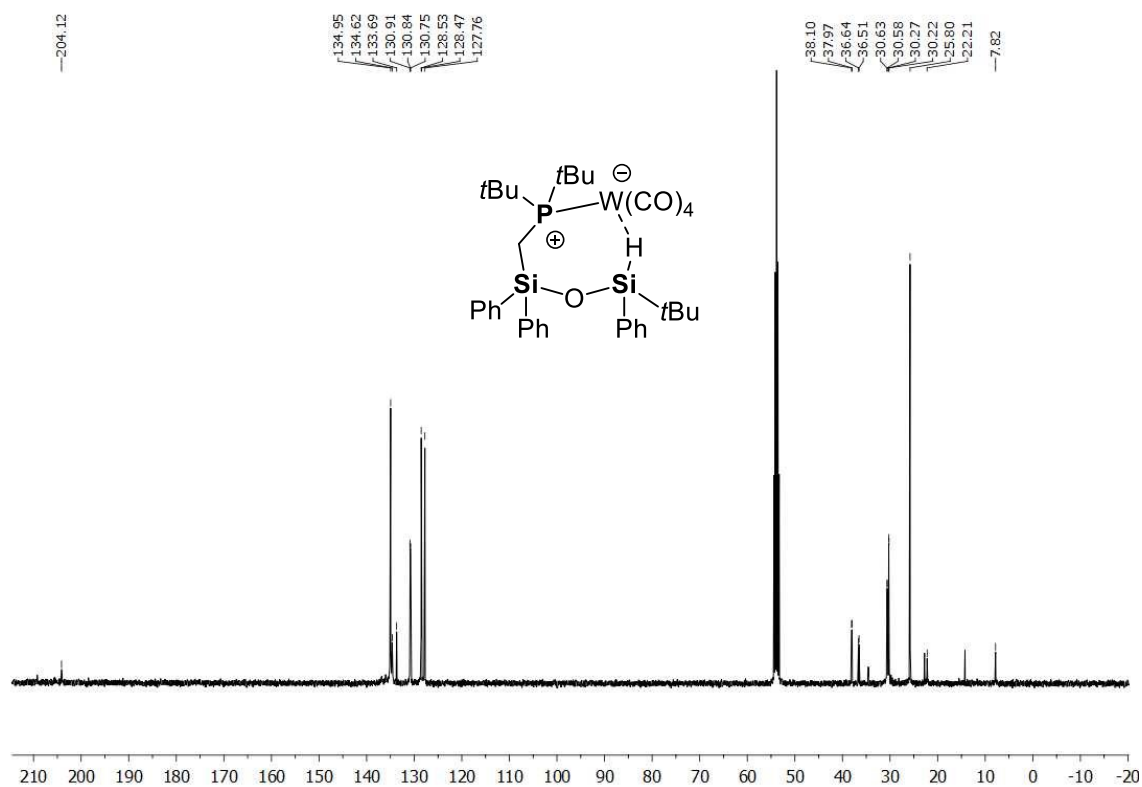
Figure S155. ^{13}C{^{1}H} NMR spectrum (CD$_2$Cl$_2$, 298 K) of compound [W(CO)$_4$(**5**)].

175
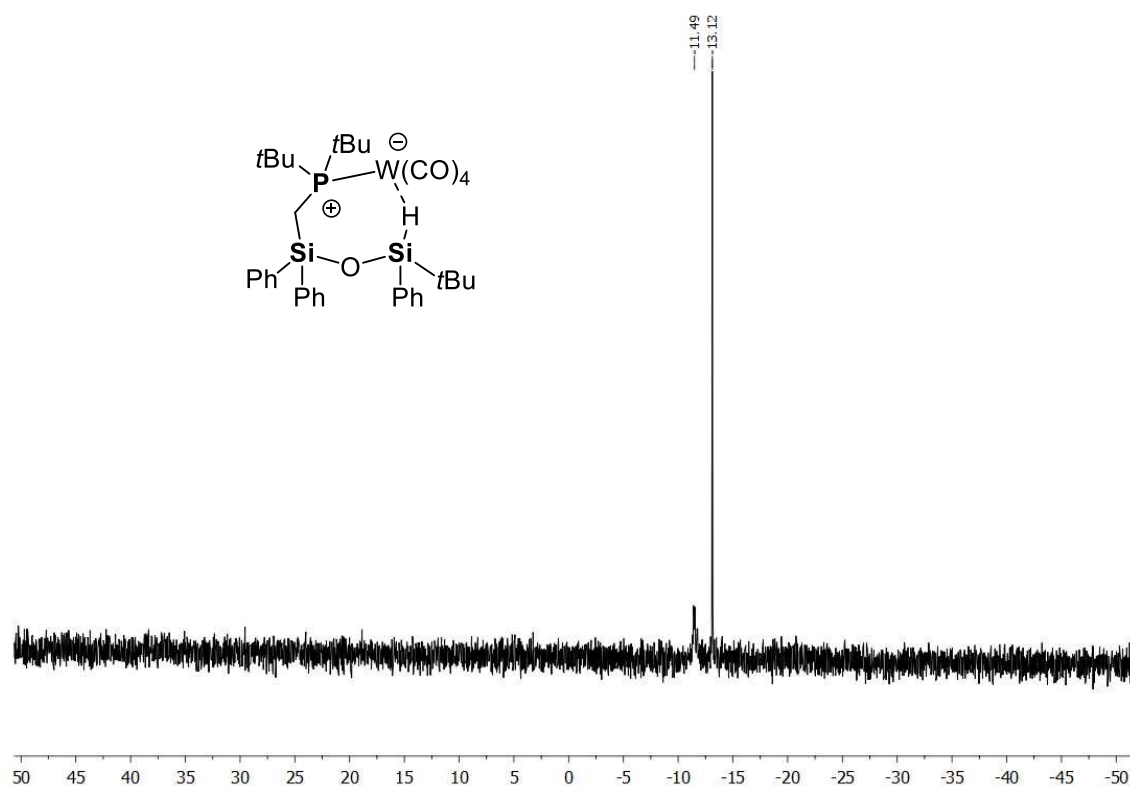
Figure S156. $^{29}Si\{^{1}H\}$ NMR spectrum (CD$_2$Cl$_2$, 298 K) of compound [W(CO)$_4$(**5**)].
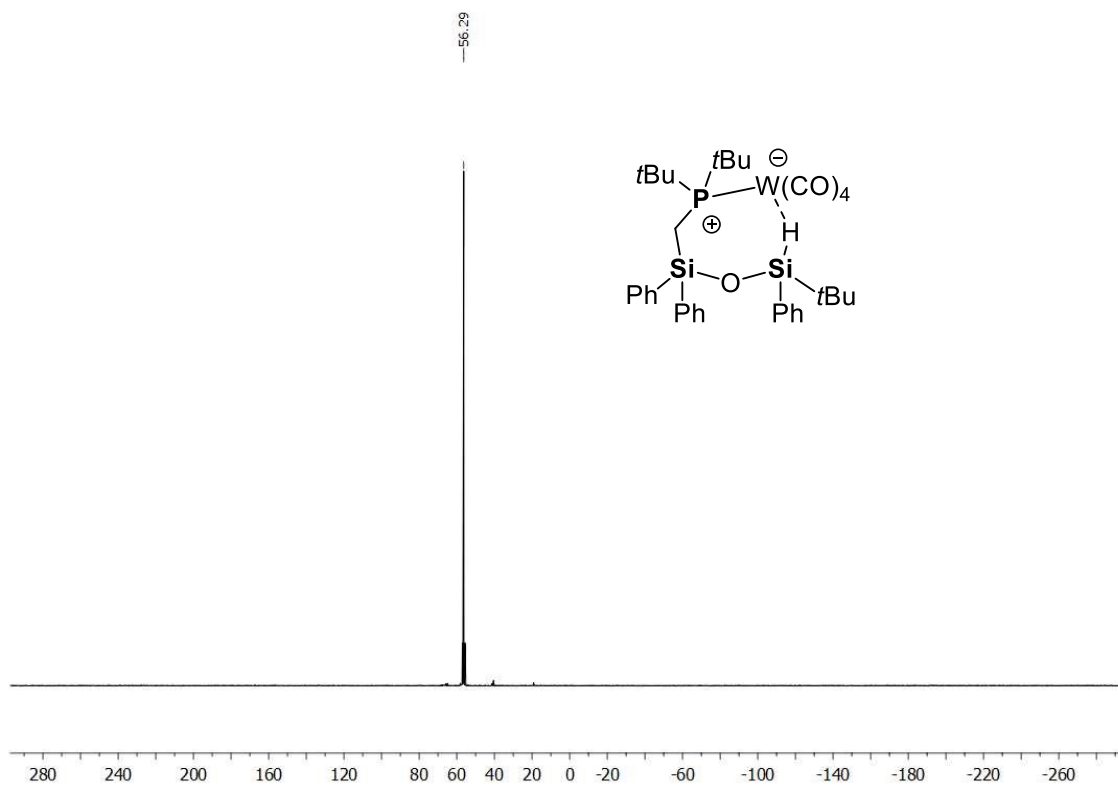
Figure S157. $^{31}P\{^{1}H\}$ NMR spectrum (CD$_2$Cl$_2$, 298 K) of compound [W(CO)$_4$(**5**)].

4.4.2 Synthesis of (*t*Bu)₂P(S)CH₂SiPh₂OSiPh(H)*t*Bu (6)
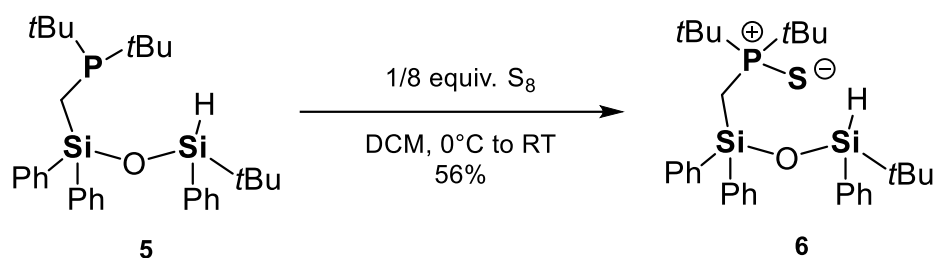
Siloxane **5** (3.27 g, 6.3 mmol, 1.0 equiv.) was dissolved in DCM (20 ml) and the solution was cooled down to 0°C. Pre-dried elemental sulfur (201 mg, 6.3 mmol, 1.0 equiv.) was added as a solid in one portion. The mixture was stirred without further cooling for 2 h during which the proceeding of the reaction could also be monitored by the disappearing of the solids. The solvent was removed in vacuum and the oily residue purified *via* Kugelrohr distillation (190°C oven temperature, 1.0×10^{-3} mbar). Compound **6** was obtained as a colourless oil (1.9 g, 3.5 mmol, 56 %). After two weeks, the oil spontaneously crystallized affording crystals suitable for single-crystal X-ray diffraction analysis.

¹H NMR (400.30 MHz, CD₂Cl₂, 298 K): δ =0.90 [s, 9H, SiC(C*H*₃)₃], 1.12 [d, $^3J_{P-H}$= 4.5 Hz, 9H, PC(C*H*₃)₃], 1.16 [d, $^3J_{P-H}$= 4.6 Hz, 9H, PC(C*H*₃)₃], 1.86 [d, 2H, $^1J_{P-H}$= 12.8 Hz, SiC*H*₂P], 4.96 [s, 1H, Si*H*], 7.29–7.40 [m, 10H, *H*ₚₕ], 7.55–7.57 [m, 2H, *H*ₚₕ], 7.75–7.76 [m, 3H, *H*ₚₕ]. **¹³C{¹H} NMR** (100.66 MHz, CD₂Cl₂, 298 K): δ = 13.1 [d, $^1J_{C-P}$= 37.2 Hz Si*C*(CH₃)₃], 25.8 [s, SiC(*C*H₃)₃], 27.6 [dd, $^2J_{C-P}$= 1.8 Hz, $^2J_{C-P}$= 1.8 Hz PC(*C*H₃)₃], 38.6 [d, $^1J_{C-P}$= 42.1 Hz P*C*(CH₃)₃],18.7 [s, Si*C*H₂(CH₃)₃], 127.7 [d, J_{C-P}= 3.3 Hz, *C*ₚₕ], 128.0 [s, *C*ₚₕ], 130.2 [s, *C*ₚₕ], 134.6 [s, *C*ₚₕ], 134.9 [s, *C*ₚₕ], 135.9 [s, *C*ₚₕ], 135.9 [s, *C*ₚₕ], 136.0 [s, *C*ₚₕ], 136.3 [s, *C*ₚₕ], 136.4 [s, *C*ₚₕ]. **²⁹Si{¹H} NMR** (79.49 MHz, CD₂Cl₂, 298 K): δ = -15.2 [d, $^2J_{Si-P}$= 5.6 Hz PC*Si*OSiH], -4.2 [s, PCSiO*Si*H]. **³¹P{¹H} NMR** (162.04 MHz, CD₂Cl₂, 298 K): δ = 73.9 [s]. **CHN Analysis** C₃₁H₄₅OPSSi₂: calculated: C 67.3%, H 8.2%; found C 67.73%, H 7.33%. **HR-MS (ESI+)**, calculated. m/z for C₃₁H₄₆OPSSi₂⁺ [M+H]⁺: 553.2540; found: 553.2541.
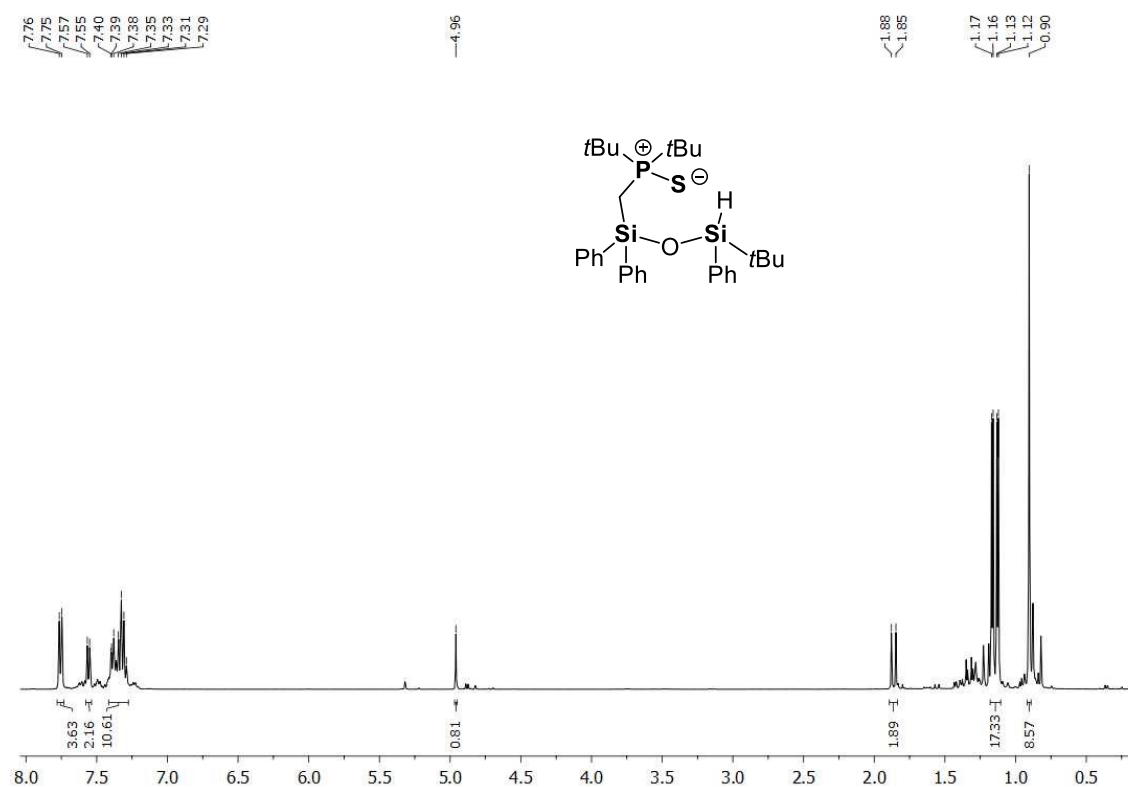
Figure S158. ^{1}H NMR spectrum (CD$_2$Cl$_2$, 298 K) of compound **6**.
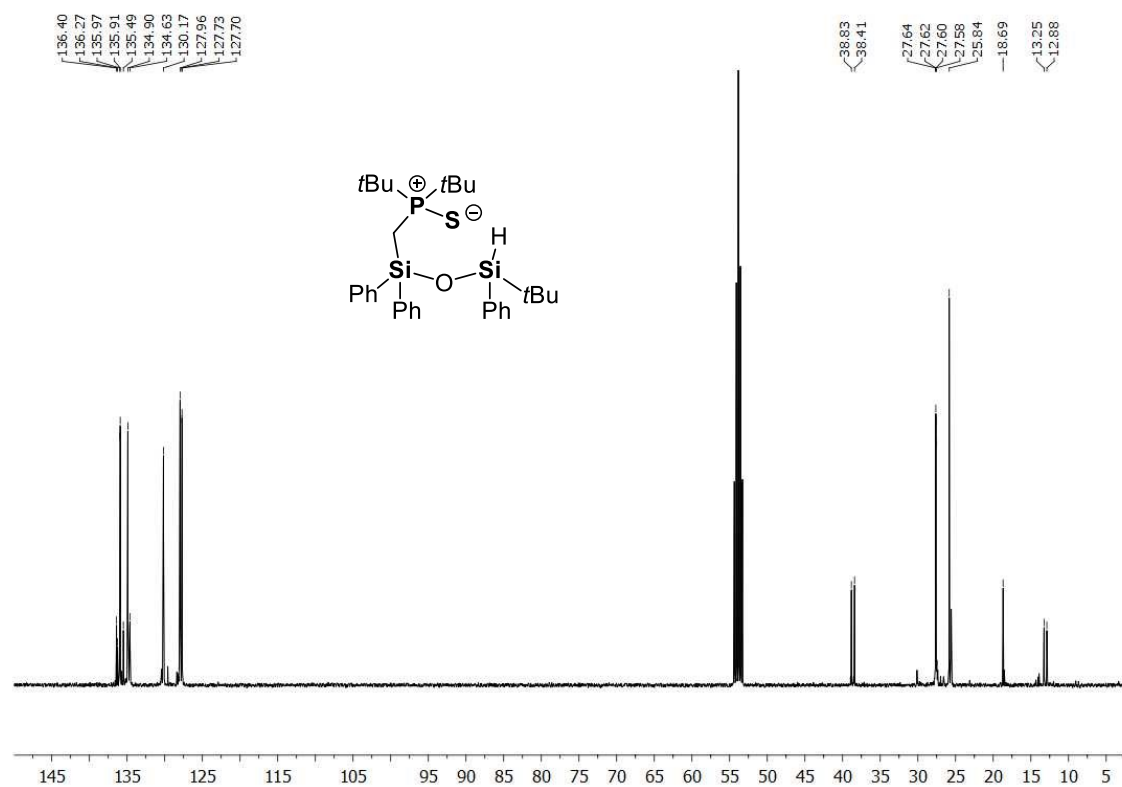
Figure S159. ^{13}C{^{1}H} NMR spectrum (C$_6$D$_6$, 298 K) of compound **6**.
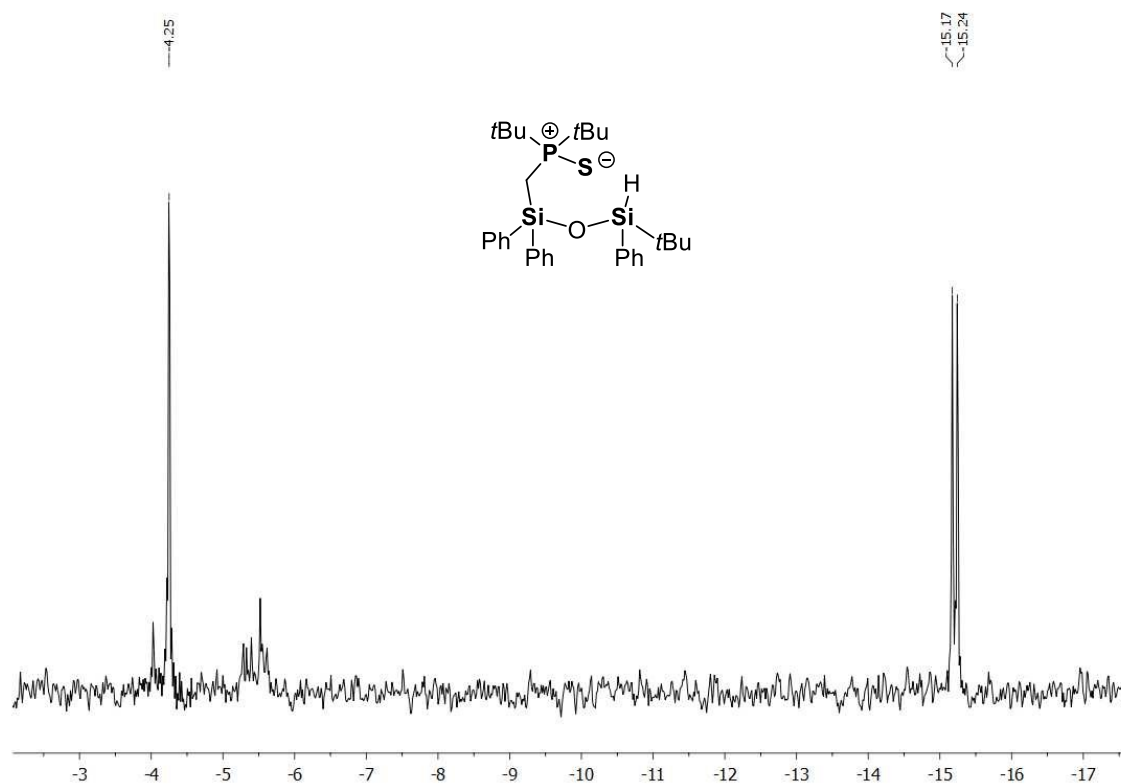
Figure S160. $^{29}Si\{^1H\}$ NMR spectrum (C$_6$D$_6$, 298 K) of compound **6**.
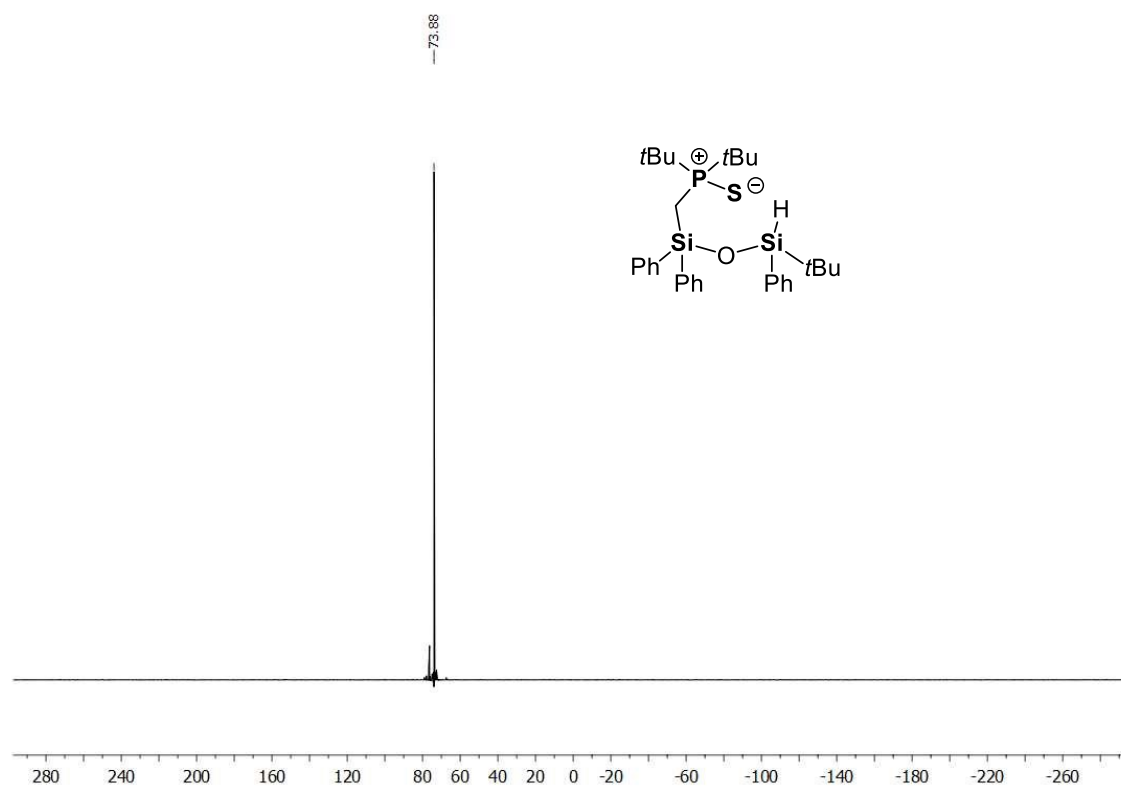
Figure S161. $^{31}P\{^1H\}$ NMR spectrum (CD$_2$Cl$_2$, 298 K) of compound **6**.

4.4.3 Synthesis of [(*t*Bu)₂P(S)CH₂SiPh₂OSiPh*t*Bu][HB(C₆F₅)₃] (7[HB(C₆F₅)₃])

6   **7**[HB(C₆F₅)₃]
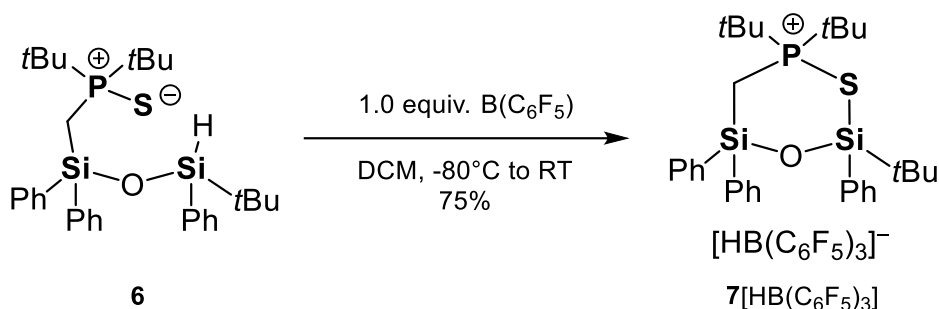
Siloxane **6** (757 mg, 1.37 mmol, 1.0 equiv.) was dissolved in DCM (5 ml) and the solution was cooled down to -80°C. BCF (701 mg, 1.37 mmol, 1.0 equiv.) was added as a DCM solution (~5 ml). The mixture was stirred without further cooling for 12 h. The solvent was concentrated down to 1 ml and the compound was precipitated adding pentane (~10 ml). The upper liquid phase was removed using a PTFE cannula and the cloudy oil was further rinsed with pentane (2 ml). After removing all the volatiles in vacuum, the desired product **7**[HB(C₆F₅)₃] was obtained as a foamy solid (1.1 g, 1.0 mmol, 75%).

^{1}H NMR (400.30 MHz, CD₂Cl₂, 298 K): δ =1.06 [s, 9H, SiC(CH_3)₃], 1.22 [d, $^3J_{\text{P-H}}$= 17.6 Hz, 9H, PC(CH_3)₃], 1.5 [d, $^3J_{\text{P-H}}$= 17.7 Hz, 9H, PC(CH_3)₃], 2.08 [ddd(ABX), J_1= 13.2 Hz, J_2= 14.8 Hz, J_3= 57,1 Hz, 2H, SiCH_2P], 3.66 [bq, $^1J_{\text{B-H}}$= 80.3 Hz 1H, BH], 7.41–7.60 [m, 11H, H_{Ph}], 7.69–7.70 [m, 4H, H_{Ph}]. **^{11}B{^{1}H} NMR** (128.43 MHz, CD₂Cl₂, 298 K): δ = 25.56 [s, BH]. **^{13}C{^{1}H} NMR** (100.66 MHz, CD₂Cl₂, 298 K): δ = 0.9 [d, $^1J_{\text{C-P}}$= 24.5 Hz, SiCH₂P], 23.2 [s, SiC(CH₃)₃], 24.9 [s, SiC(CH_3)₃], 26.7 [s], 26.8 [s], 27.9 [s], 27.1 [s], 41.2 [dd, $^1J_{\text{C-P}}$= 30.6 Hz, $^1J_{\text{C-P}}$= 30.6 Hz, PC(CH₃)₃], 129.1 [s, C$_{Ph}$], 129.2 [s, C$_{Ph}$], 129.4 [s, C$_{Ph}$], 129.6 [s, C$_{Ph}$], 129.8 [s, C$_{Ph}$], 132.5 [t, J= 9.5 Hz C$_{Ph}$], 134.3 [s, C$_{Ph}$], 134.4 [s,C$_{Ph}$], 134.8 [s, C$_{Ph}$], 137.1 [bd, $^1J_{\text{C-F}}$= 250.0 Hz, C$_{Ar\text{-}borate}$], 140.0 [bd, $^1J_{\text{C-F}}$= 243.0 Hz, C$_{Ar\text{-}borate}$], 148.1 [bd, $^1J_{\text{C-F}}$= 247.1 Hz, C$_{Ar\text{-}borate}$]. **^{19}F{^{1}H} NMR** (376.66 MHz, CD₂Cl₂, 298 K): δ = -167.6 [t, $^3J_{\text{F-F}}$= 20.2 Hz, 6F], -164.9 [t, $^3J_{\text{F-F}}$= 20.3 Hz, 3F], -133.5 [bd, 6F]. **^{29}Si{^{1}H} NMR** (79.49 MHz, CD₂Cl₂, 298 K): δ = -16.6 [d, $^2J_{\text{Si-P}}$= 8.8 Hz, PCSiOSiS], -2.7 [d, $^2J_{\text{Si-P}}$= 5.6 Hz, PCSiOSiS]. **^{31}P{^{1}H} NMR** (162.04 MHz, CD₂Cl₂, 298 K): δ = 87.2 [s]. **CHN Analysis** C₄₉H₄₅BF₁₅OPSSi₂: calculated: C, 55.27%; H, 4.26%; found C 54.51%, H 4.26%. **HR-MS (LIFDI+)**, calculated. m/z for C₃₁H₄₄OPSSi₂⁺ [M]⁺: 551.2384; found: 551.2405.

The Lewis acidity of this compound was tested using FBN as probe.[4] Solid **7**[HB(C₆F₅)₃] (70 mg, 0.066 mmol, 1.0 equiv.) was loaded into a Young-type NMR tube and dissolved into a CD₂Cl₂ solution (0.5 ml) containing FBN (8.0 mg, 0.066 mmol, 1.0 equiv.). The reagents were allowed to react for 2 hours before measuring the spectra. The low Lewis acidity of this compound was demonstrated by the following results:

^{13}C{^{1}H} NMR (100.66 MHz, CD₂Cl₂, 298 K): δ = 165.5 [d, $^1J_{\text{C-F}}$ = 257.9 Hz].
^{19}F{^{1}H} NMR (376.66 MHz, CD₂Cl₂, 298 K): δ = -103.38 [s].

Figure S162. ^{1}H NMR spectrum (CD$_2$Cl$_2$, 298 K) of compound **7**[HB(C$_6$F$_5$)$_3$].

Figure S163. ^{13}C{^{1}H} NMR spectrum (CD$_2$Cl$_2$, 298 K) of compound **7**[HB(C$_6$F$_5$)$_3$].
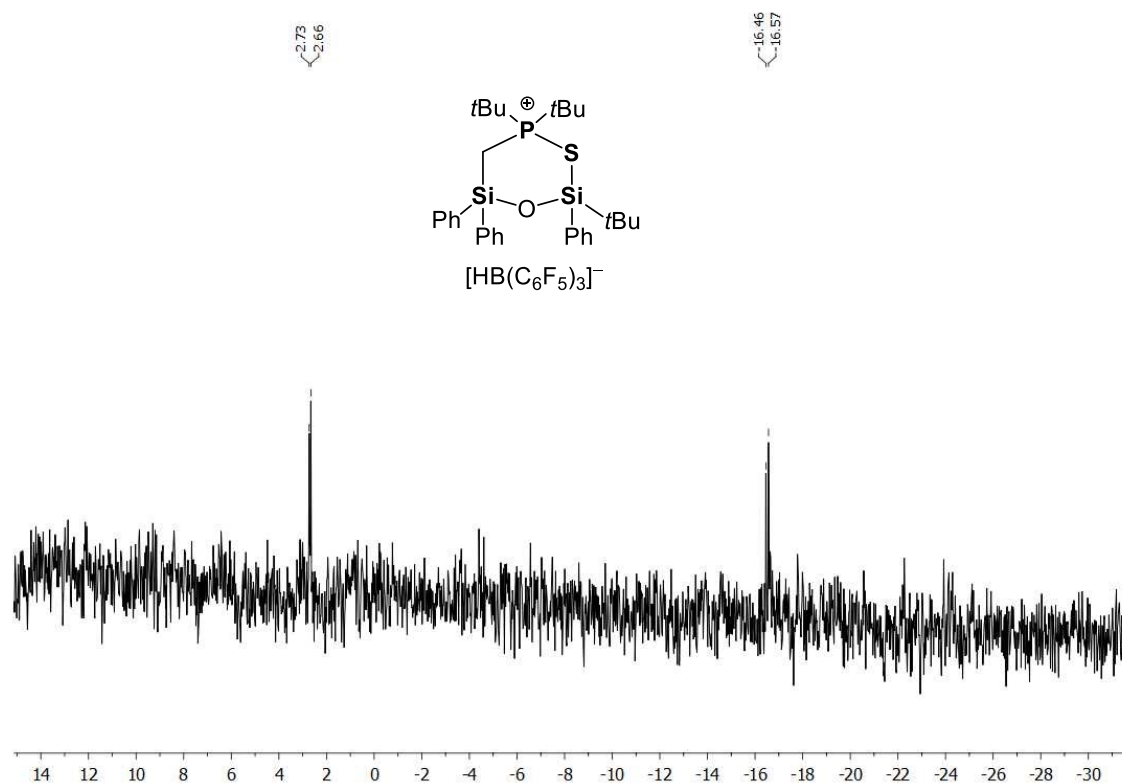
Figure S164. ^{29}Si{^{1}H} NMR spectrum (CD$_2$Cl$_2$, 298 K) of compound **7**[HB(C$_6$F$_5$)$_3$].
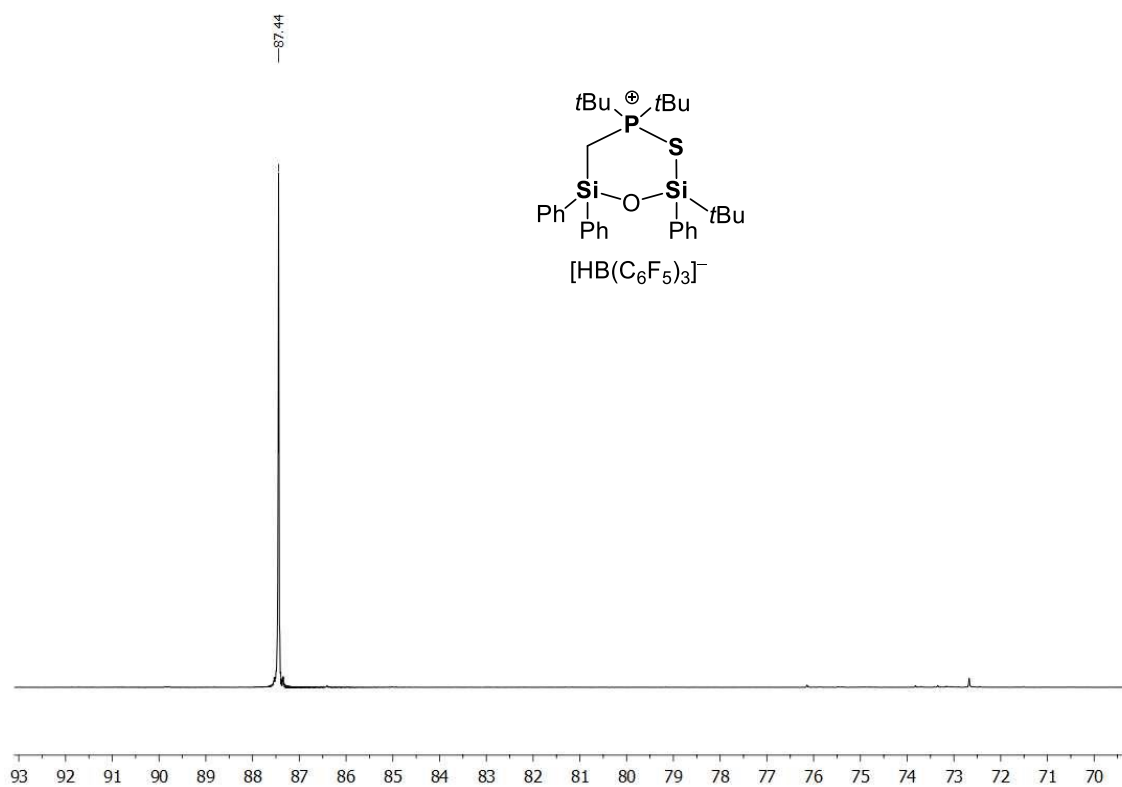
Figure S165. ^{31}P{^{1}H} NMR spectrum (CD$_2$Cl$_2$, 298 K) of compound **7**[HB(C$_6$F$_5$)$_3$].
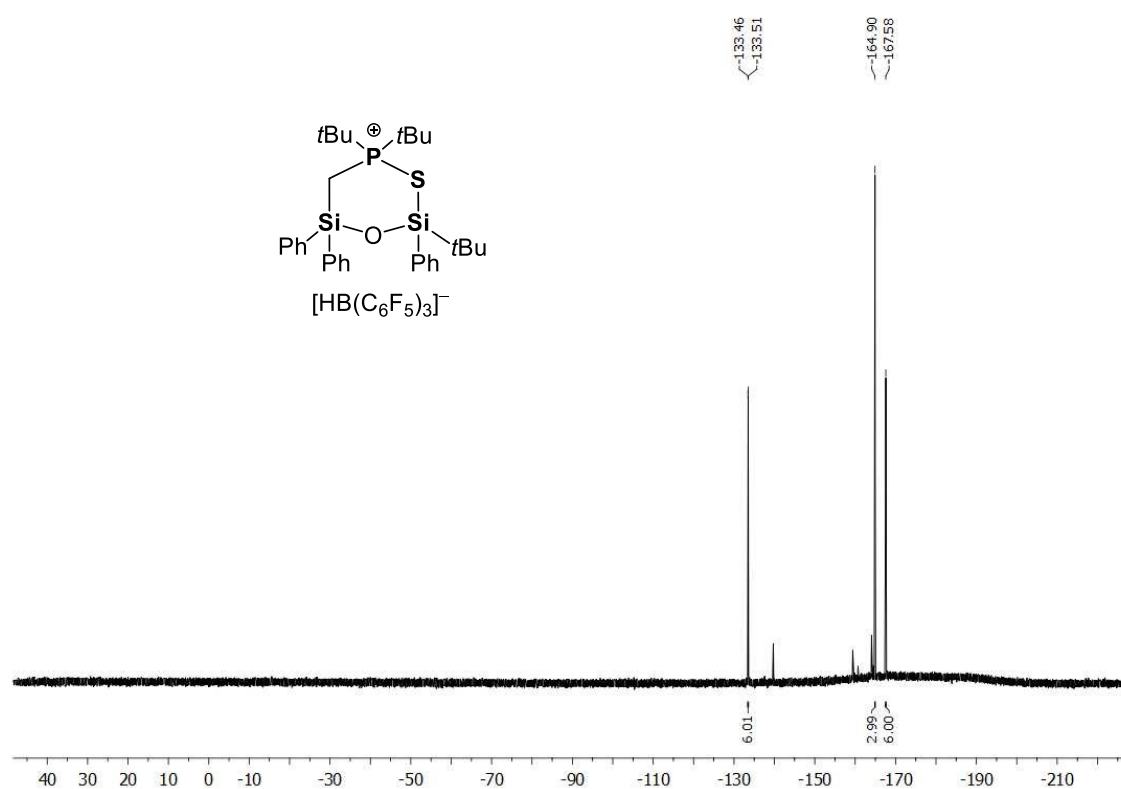
Figure S166. $^{19}F\{^1H\}$ NMR spectrum (CD$_2$Cl$_2$, 298 K) of compound **7**[HB(C$_6$F$_5$)$_3$].
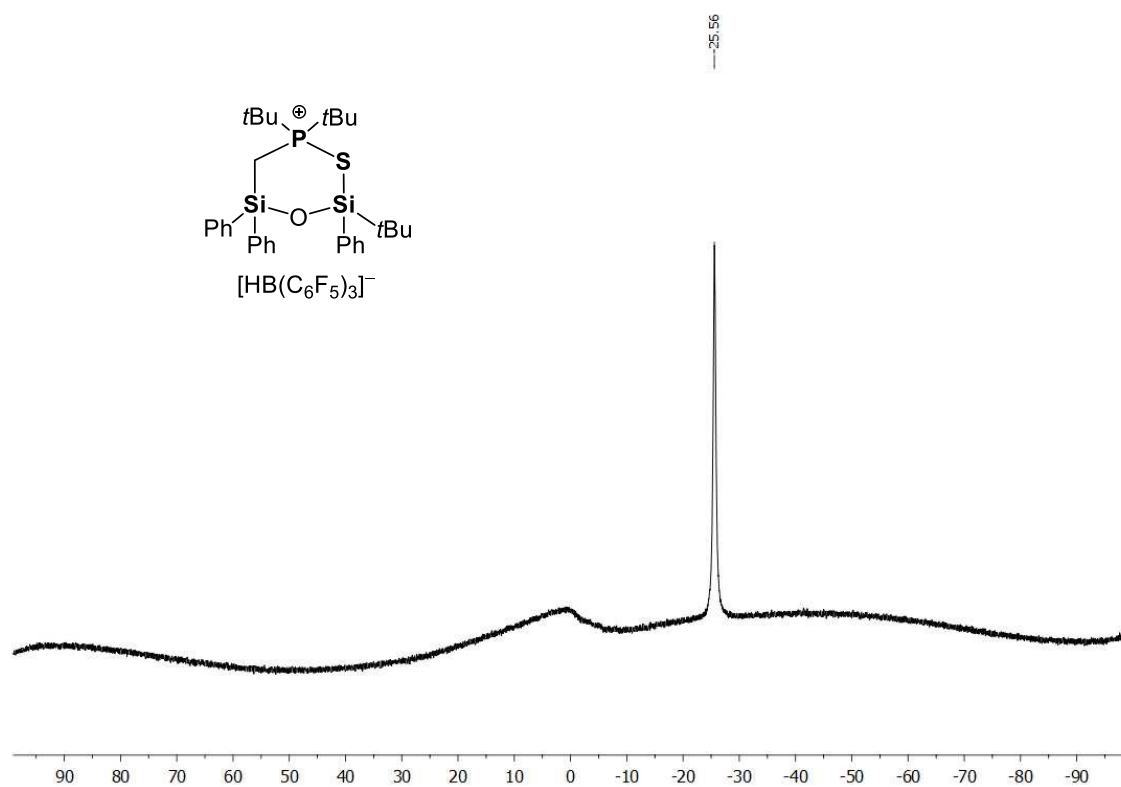
Figure S167. $^{11}B\{^1H\}$ NMR spectrum (CD$_2$Cl$_2$, 298 K) of compound **7**[HB(C$_6$F$_5$)$_3$].

4.4.4 Synthesis of [(*t*Bu)₂P(S)CH₂SiPh₂OSiPh*t*Bu][B(C₆F₅)₄] (7[B(C₆F₅)₄])
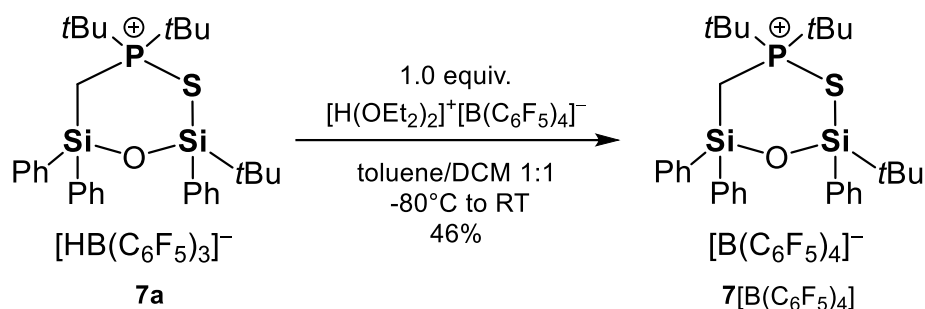
Compound **7**[HB(C₆F₅)₃] (100 mg, 0.094 mmol, 1.0 equiv.) was dissolved in toluene (5 ml) and the solution was cooled down to -80 °C. [H(OEt₂)₂]⁺[B(C₆F₅)₄]⁻ (77.8 mg, 0.094 mmol, 1.0 equiv.) was added dropwise as a DCM solution (~5 ml). The solution was stirred without further cooling for 3 h during which gas evolution was observed. An aliquot was dried directly in a Young-type NMR tube and the foamy solid was dissolved in CD₂Cl₂. Multinuclear NMR showed full conversion and complete selectivity towards the desired product. The solvent was concentrated down to ~1 ml and the compound was precipitated adding pentane (~10 ml). The upper liquid phase was removed using a PTFE cannula and the cloudy oil was further rinsed with pentane (2 ml). After removing all the volatiles in vacuum, the desired product **7**[B(C₆F₅)₄] was obtained as a foamy solid (52 mg, 0.043 mmol, 46%). Crystals suitable for X-ray diffraction analysis were obtained by vapor diffusion of pentane into a toluene solution of compound **7**[B(C₆F₅)₄].

¹H NMR (400.30 MHz, CD₂Cl₂, 298 K): δ =1.05 [s, 9H, SiC(CH_3)₃], 1.20 [d, $^3J_{\text{P-H}}$= 18.3 Hz, 9H, PC(CH_3)₃], 1.45 [d, $^3J_{\text{P-H}}$= 17.8 Hz, 9H, PC(CH_3)₃], 2.02 [ddd(ABX), J_1= 12.9 Hz, J_2= 14.8 Hz, J_3= 58,9 Hz, 2H, SiCH_2P], 7.41–7.49 [m, 6H, H_{Ph}], 7.51–7.62 [m, 5H, H_{Ph}], 7.64–7.68 [m, 4H, H_{Ph}]. **¹¹B{¹H} NMR** (128.43 MHz, CD₂Cl₂, 298 K): δ = -16.9 [s]. **¹³C{¹H} NMR** (100.66 MHz, CD₂Cl₂, 298 K): δ = 0.8 [d, $^1J_{\text{C-P}}$= 24.5 Hz, SiCH_2P], 23.1 [s, SiC(CH₃)₃], 24.9 [s, SiC(CH₃)₃], 27.1 [dd, $^2J_{\text{C-P}}$= 0.8 Hz, $^2J_{\text{C-P}}$= 5.5 Hz, PC(CH₃)₃], 41.1 [dd, $^1J_{\text{C-P}}$= 30.3 Hz, $^1J_{\text{C-P}}$= 32.2 Hz, PC(CH₃)₃], 128.6 [s, C$_{Ph}$], 129.0 [s, C$_{Ph}$], 129.2 [s, C$_{Ph}$], 129.4 [s, C$_{Ph}$], 132.2 [s, C$_{Ph}$], 132.5 [t, J= 9.8 Hz C$_{Ph}$], 134.3 [d, $J_{\text{C-P}}$= 4.8 Hz, C$_{Ph}$], 134.8 [s, C$_{Ph}$], 135.5 [bs, C$_{Ar\text{-}borate}$], 137.4 [bs, C$_{Ar\text{-}borate}$], 137.9 [bs, C$_{Ar\text{-}borate}$], 147.4 [bs, C$_{Ar\text{-}borate}$], 149.8 [bs, C$_{Ar\text{-}borate}$]. **¹⁹F{¹H} NMR** (376.66 MHz, CD₂Cl₂, 298 K): δ = -167.4 [t, $^3J_{\text{F-F}}$= 17.9 Hz, 8F], -163.6 [t, $^3J_{\text{F-F}}$= 19.4 Hz, 4F], -133.0 [bs, 8F]. **²⁹Si{¹H} NMR** (79.49 MHz, CD₂Cl₂, 298 K): δ = -16.5 [d, $^2J_{\text{Si-P}}$= 8.8 Hz PCSiOSiS], -2.7 [d, $^2J_{\text{Si-P}}$= 6.4 Hz PCSiOSiS]. **³¹P{¹H} NMR** (162.04 MHz, CD₂Cl₂, 298 K): δ = 87.2 [s]. **HR-MS (FD+)**, calculated. m/z for C₃₁H₄₄OPSSi₂⁺ [M]⁺: 551.2384; found: 551.2407.
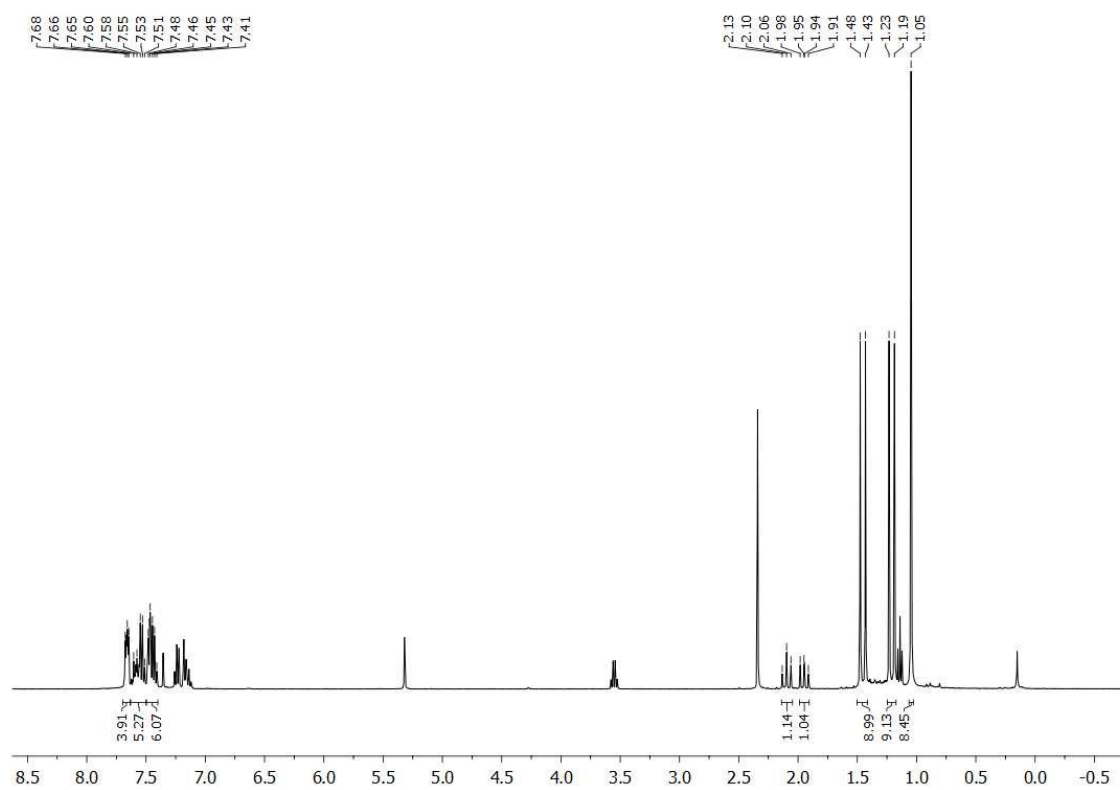
Figure S168. ^{1}H NMR spectrum (CD$_2$Cl$_2$, 298 K) of the crude reaction mixture.
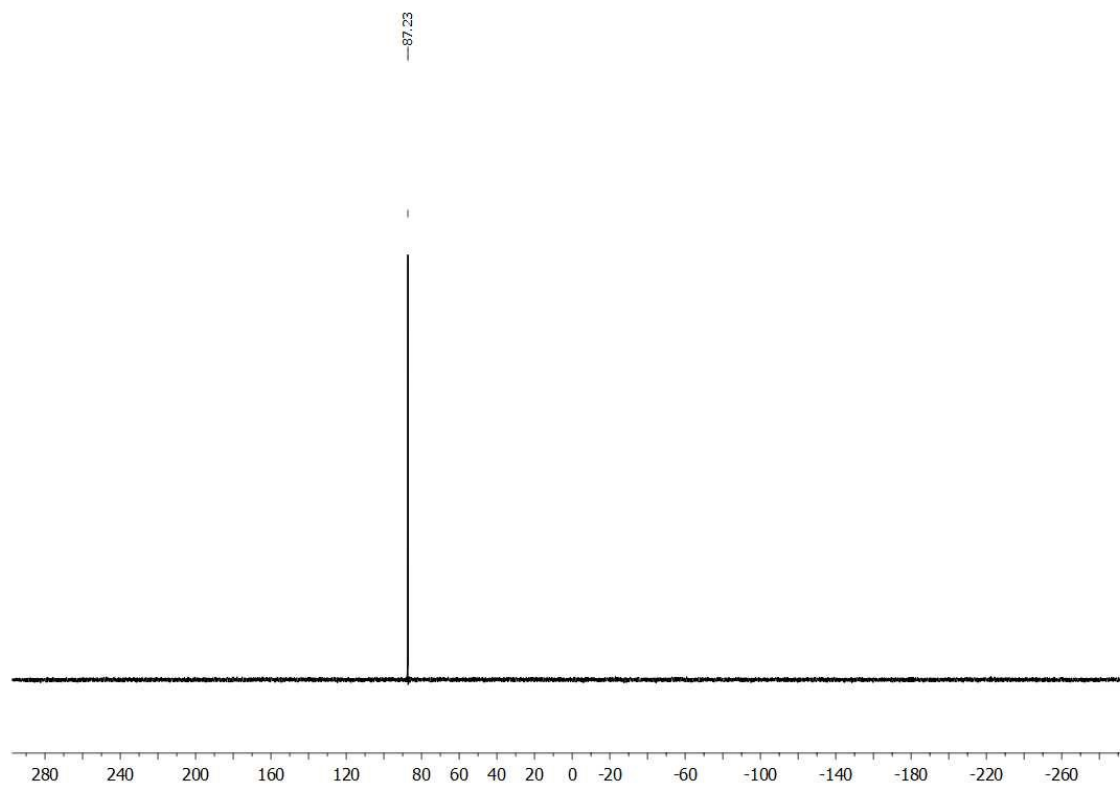
Figure S169. ^{31}P{^{1}H} NMR spectrum (CD$_2$Cl$_2$, 298 K) of the crude reaction mixture.
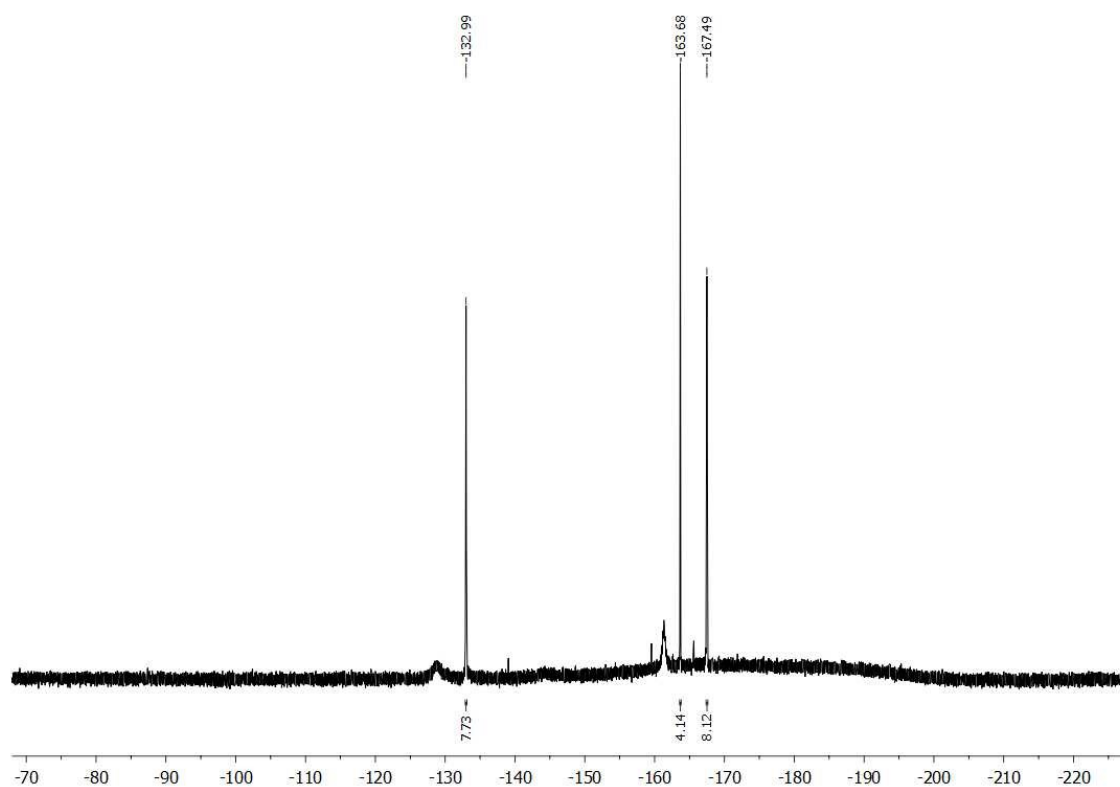
Figure S170. $^{19}F\{^1H\}$ NMR spectrum (CD$_2$Cl$_2$, 298 K) of the crude reaction mixture.
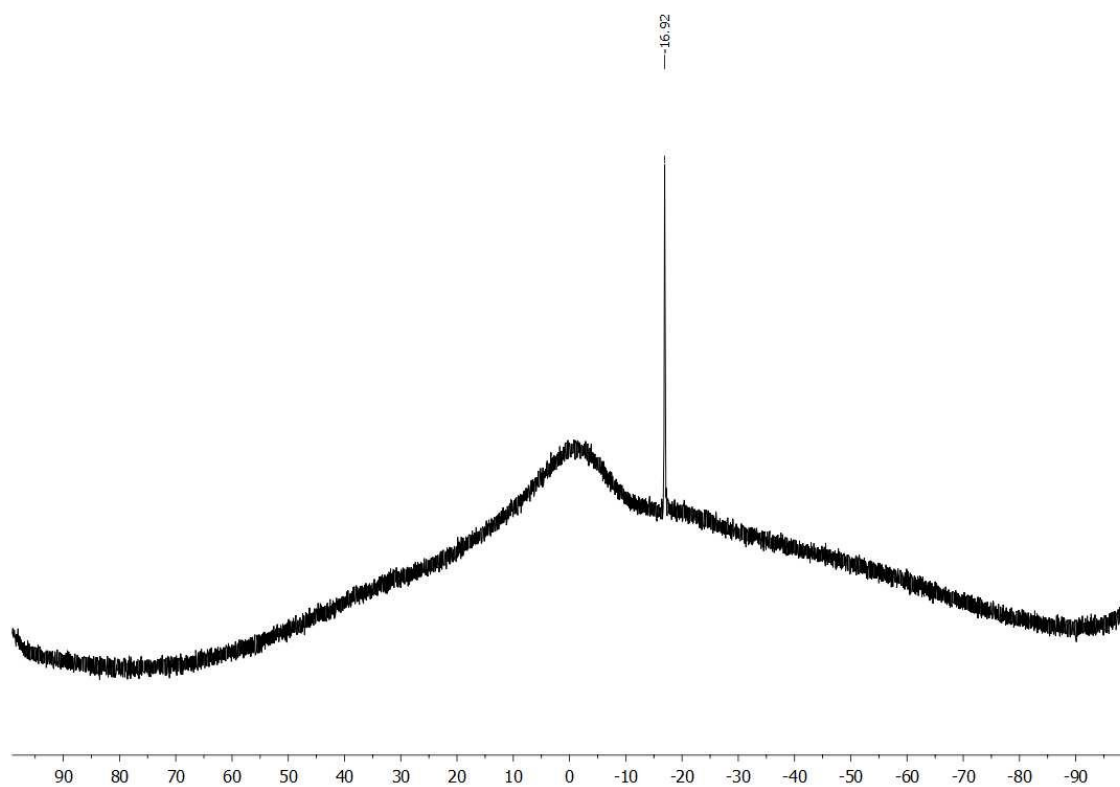
Figure S171. $^{11}B\{^1H\}$ NMR spectrum (CD$_2$Cl$_2$, 298 K) of the crude reaction mixture.
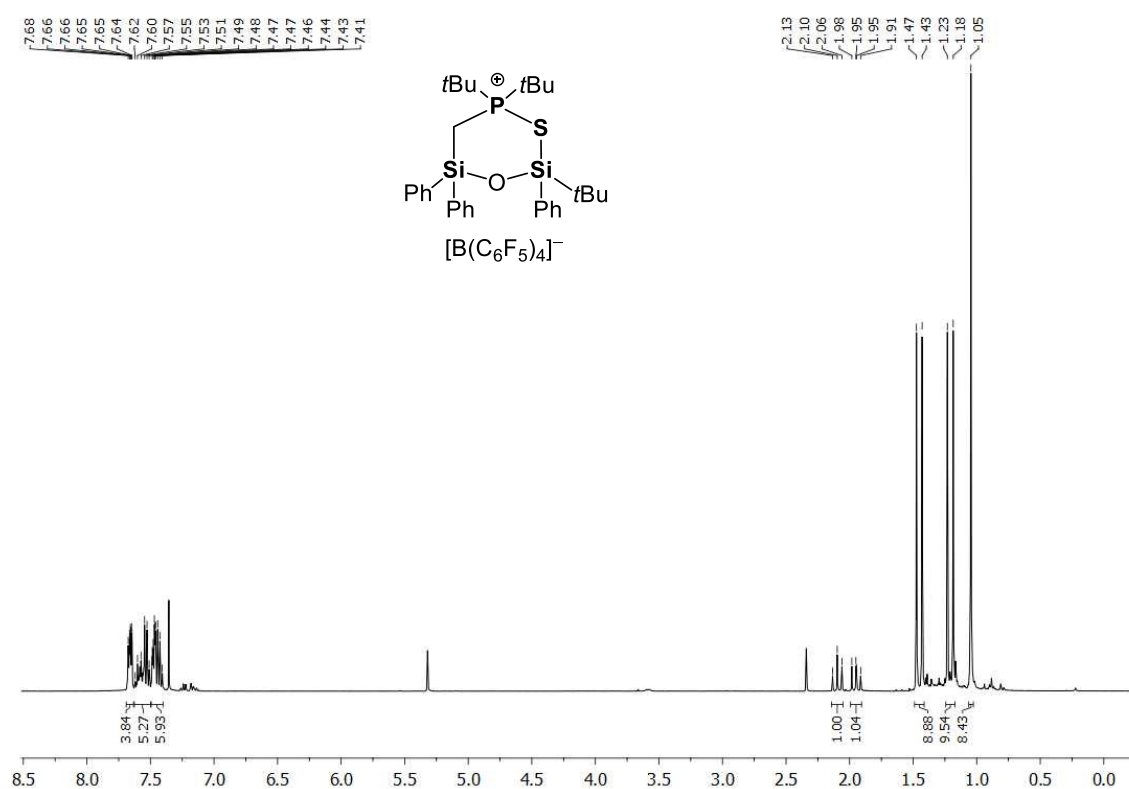
Figure S172. ^{1}H NMR spectrum (CD$_2$Cl$_2$, 298 K) of isolated compound **7**[B(C$_6$F$_5$)$_4$].
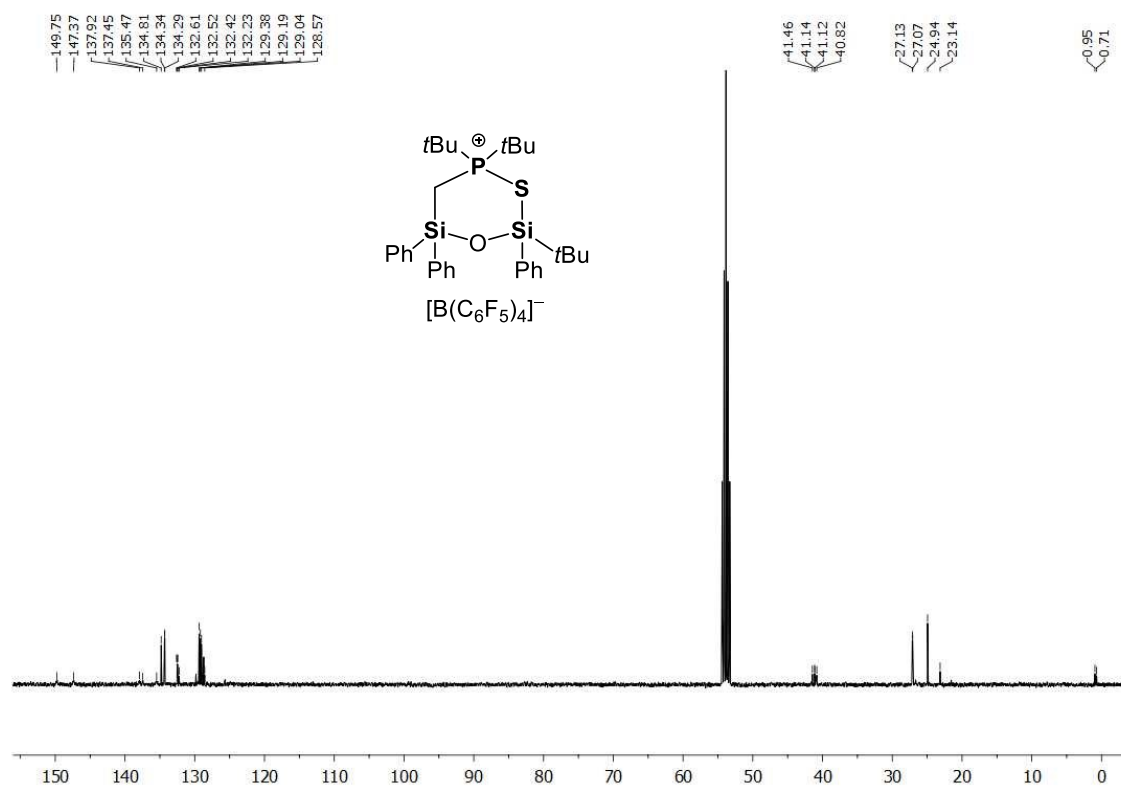
Figure S173. ^{13}C{^{1}H} NMR spectrum (CD$_2$Cl$_2$, 298 K) of isolated compound **7**[B(C$_6$F$_5$)$_4$].
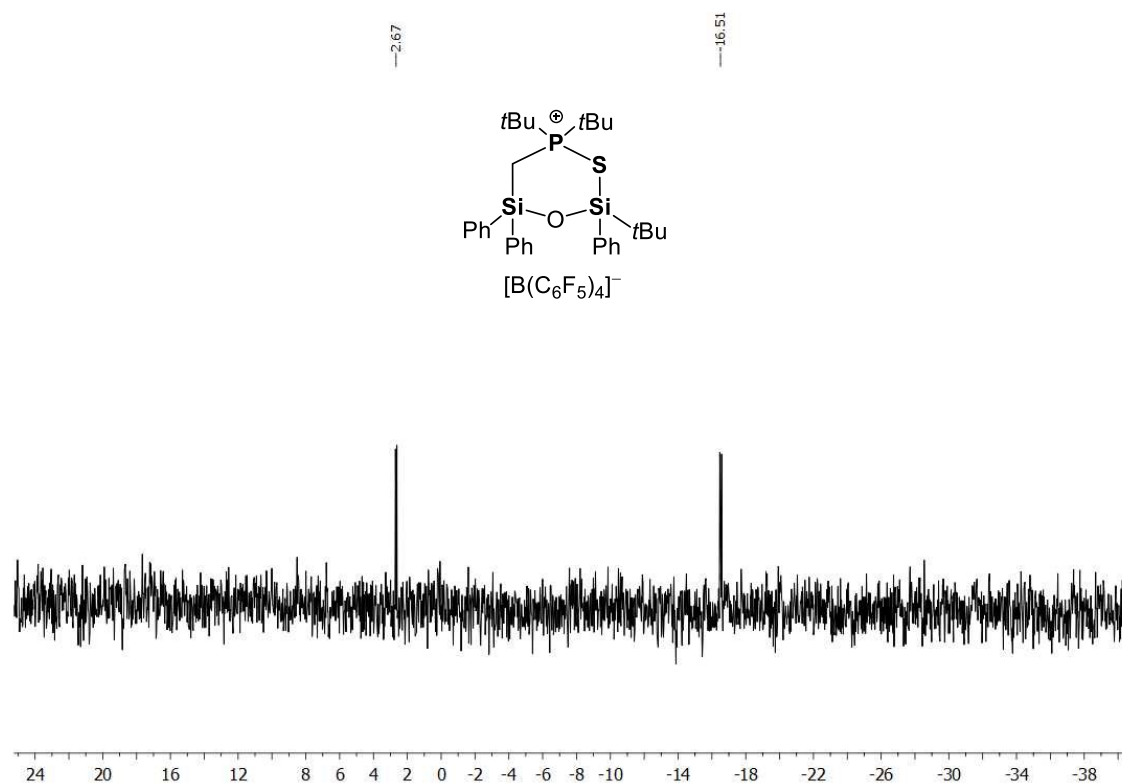
Figure S174. ^{29}Si{^{1}H} NMR spectrum (CD$_2$Cl$_2$, 298 K) of isolated compound **7**[B(C$_6$F$_5$)$_4$].
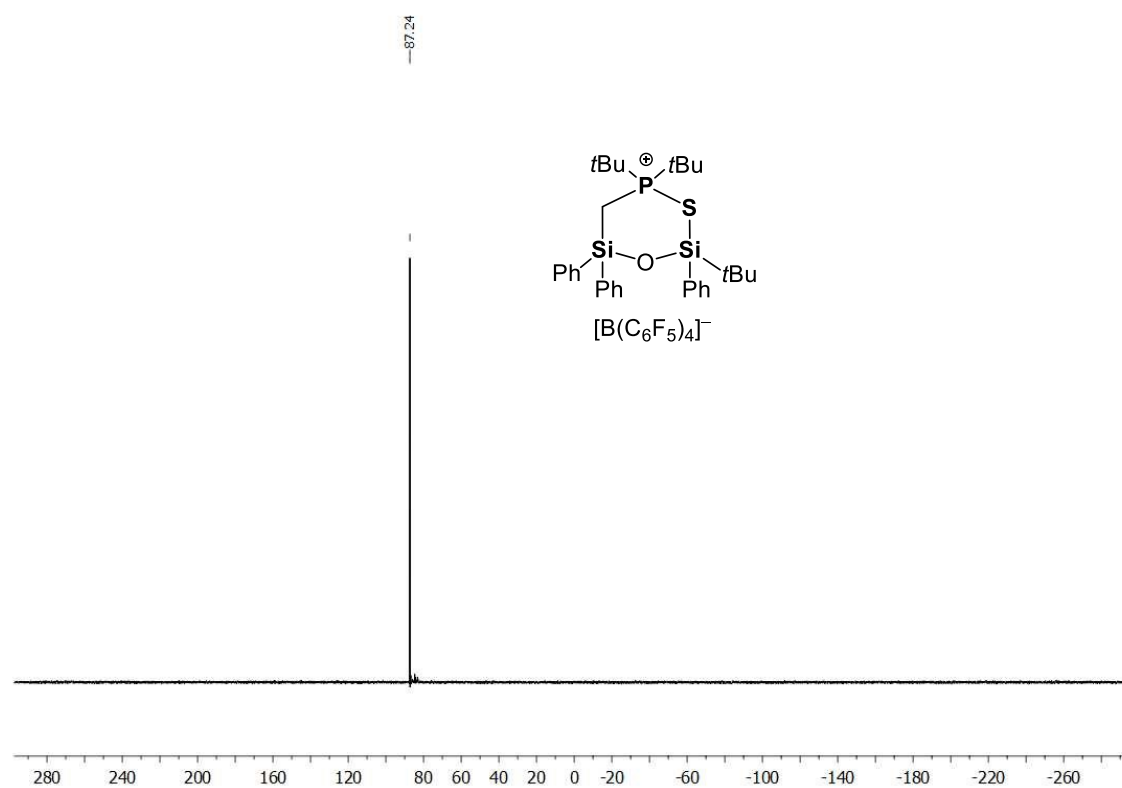
Figure S175. ^{31}P{^{1}H} NMR spectrum (CD$_2$Cl$_2$, 298 K) of isolated compound **7**[B(C$_6$F$_5$)$_4$].
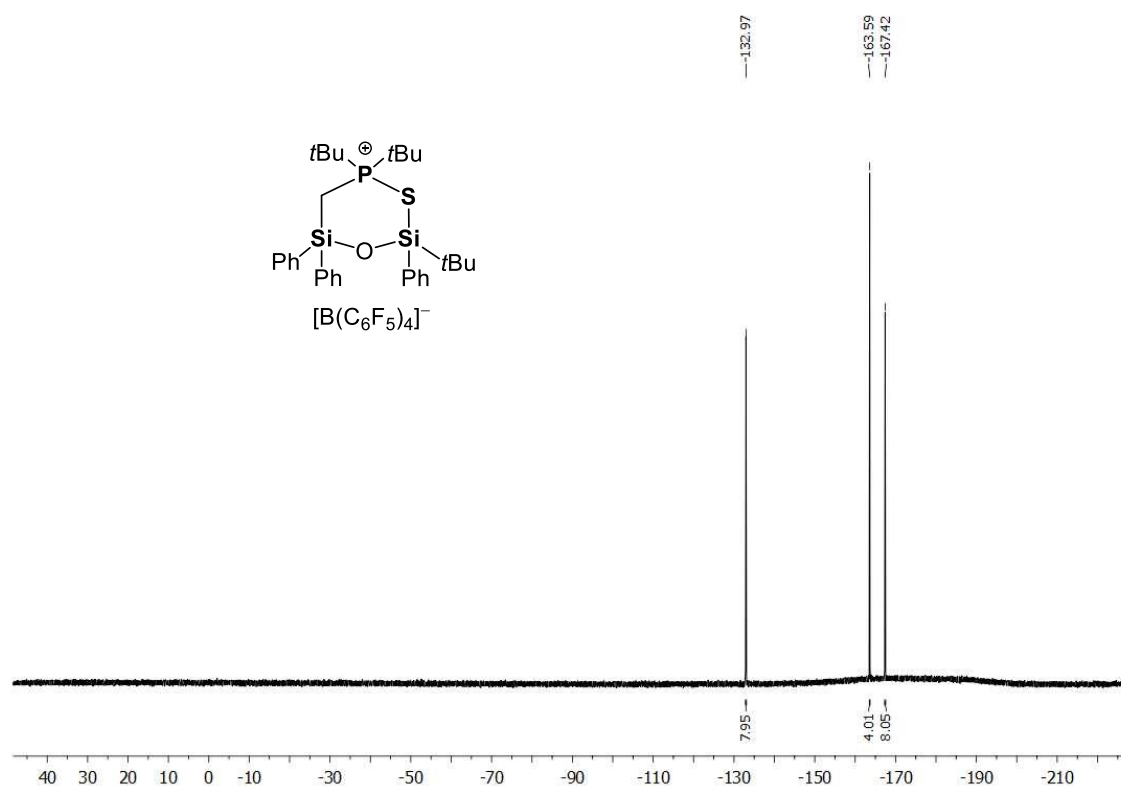
Figure S176. $^{19}F\{^{1}H\}$ NMR spectrum (CD_2Cl_2, 298 K) of isolated compound **7**[B(C_6F_5)$_4$].
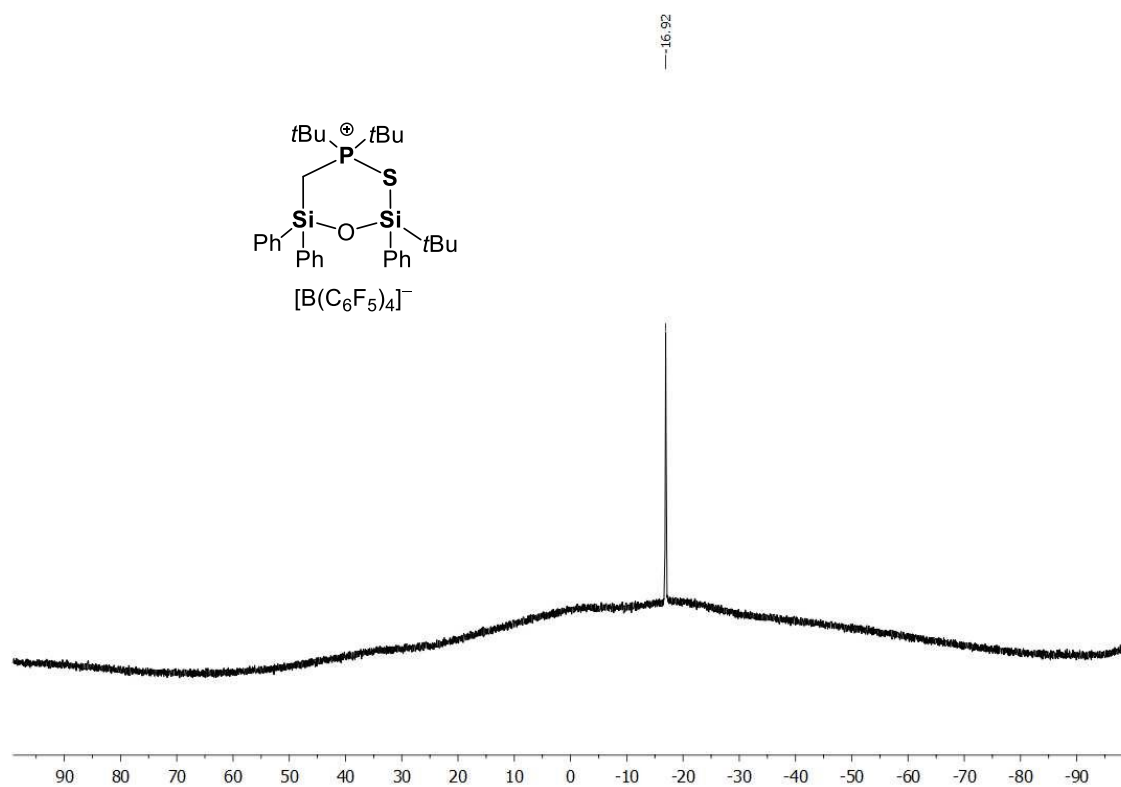
Figure S177. $^{11}B\{^{1}H\}$ NMR spectrum (CD_2Cl_2, 298 K) of isolated compound **7**[B(C_6F_5)$_4$].

4.4.1 Synthesis of [(C$_6$F$_5$)$_3$BBn][LiTMEDA]

1) 1.0 equiv. *n*-BuLi,
1.0 equiv. TMEDA

2) 1.0 equiv.B(C$_6$F$_5$)$_3$
-80°C to RT

[(C$_6$F$_5$)$_3$BBn][LiTMEDA]

Neat
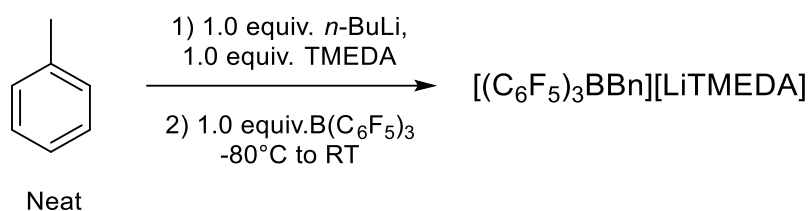
An oven dried Schlenk flask was loaded with toluene (5 ml) and TMEDA (227 mg, 1.95 mmol, 1.0 eq.). *n*-Butyllithium (1.6 M, 1.22 ml, 1.95 mmol, 1.0 eq.) was carefully added over 2 minutes while stirring vigorously. The solution turned almost immediately deep orange and it was further stirred for 30 minutes. Afterwards, the solution was transferred by the means of a PTFE tube into a Schlenk flask containing a cold suspension of BCF (1 g, 1.95 mmol, 1.0 eq.) in toluene (5 ml) at -80°C. The mixture was vigorously stirred without further cooling until the orange colour disappeared (roughly three hours) and dried in vacuum. The white residue was rinsed with pentane (3x10 ml) and dried to give the desired product as colourless dusty solid (950 mg, 1.31 mmol, 67%). Crystals suitable for X-ray diffraction were obtained by cooling down a DCM/pentane solution to -35°C.

^{1}H NMR (400.13 MHz, CD$_2$Cl$_2$, 298 K): δ = 2.11 [s, 12H, N(CH_3)$_4$], 2.30 [s, 4H, NCH_2CH_2N], 2.91 [bs, 2H, BCH_2Ph], 6.96-6.98 [m, 2H, H_{Ph}], 7.01-7.04 [m, 1H, H_{Ph}], 7.10-7.14 [m, 2H, H_{Ph}]. **^{11}B{^{1}H} NMR** (128.43 MHz, CD$_2$Cl$_2$, 298 K): δ = -13.1 [s]. **^{19}F{^{1}H} NMR** (376.50 MHz, CD$_2$Cl$_2$, 298 K): δ = -166.60 [bt, J_{F-F}= 20.2 Hz], -163.20 [t, J_{F-F}= 19.4 Hz], -132.9 [d, J_{F-F}= 22.1 Hz].
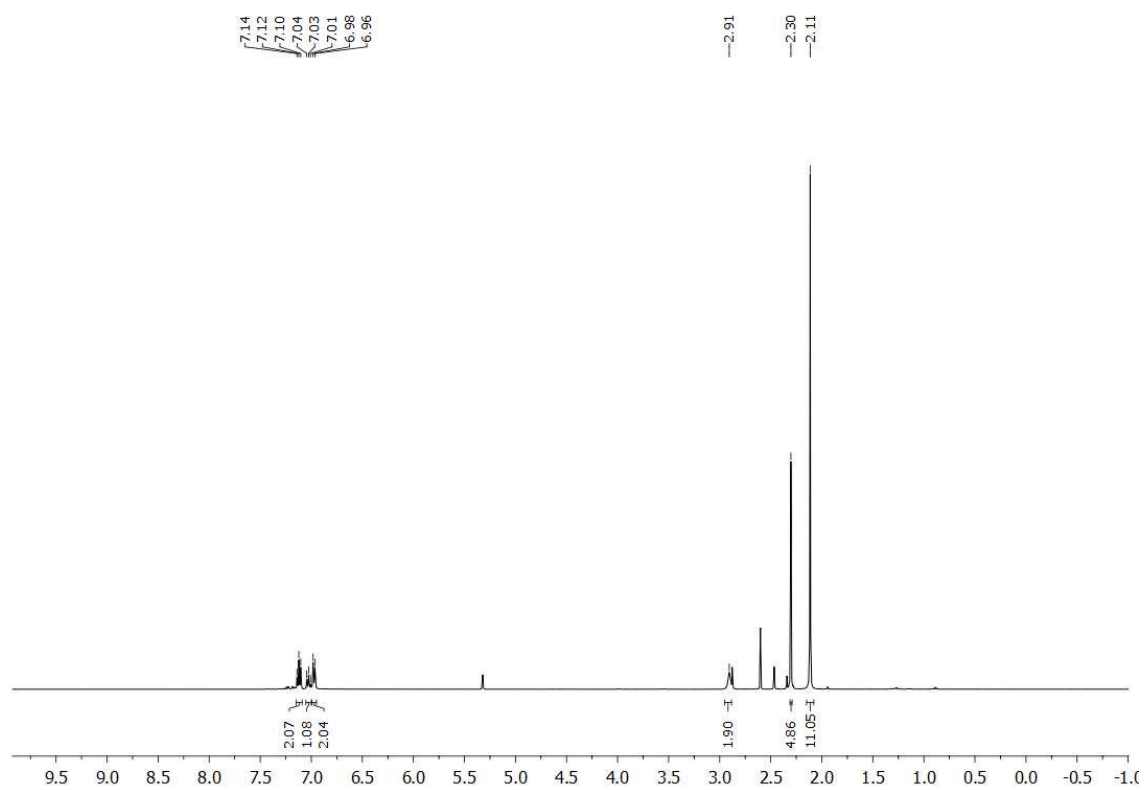
Figure S178. ^{1}H NMR spectrum (CD$_2$Cl$_2$, 298 K) of [(C$_6$F$_5$)$_3$BBn][LiTMEDA].
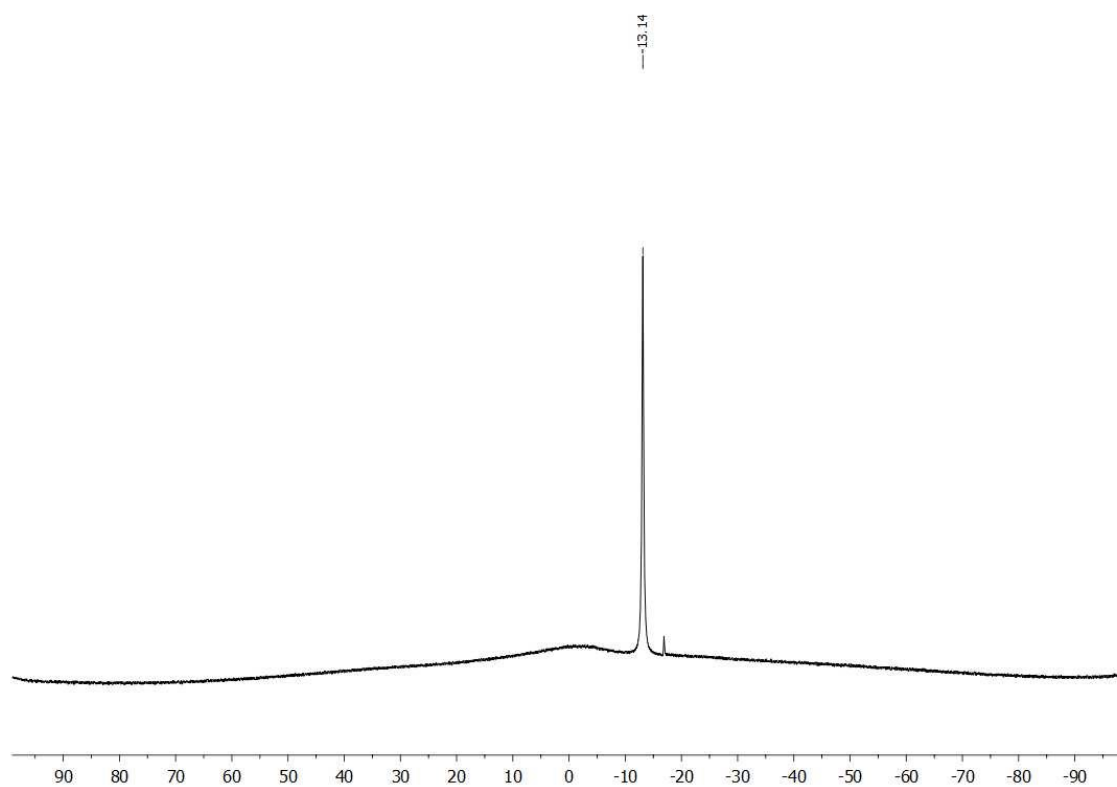
Figure S179. ^{11}B{^{1}H} NMR spectrum (CD$_2$Cl$_2$, 298 K) of [(C$_6$F$_5$)$_3$BBn][LiTMEDA].
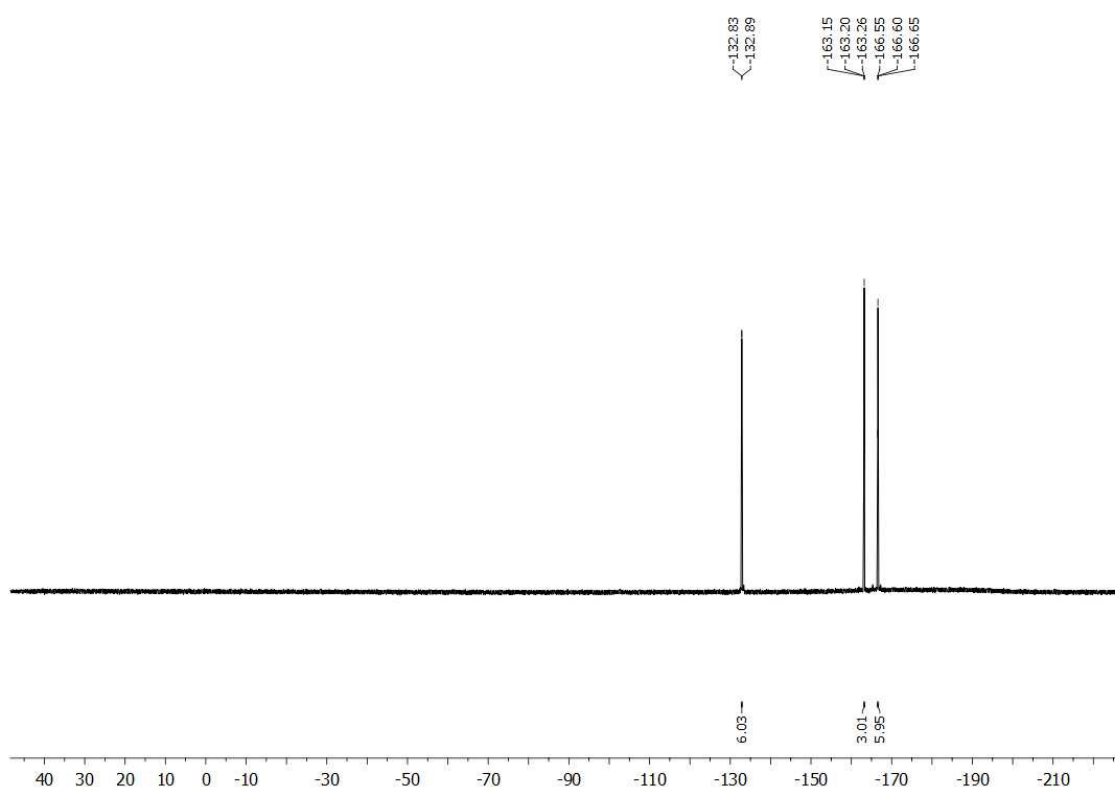
Figure S180. $^{19}F\{^1H\}$ NMR spectrum (CD$_2$Cl$_2$, 298 K) of [(C$_6$F$_5$)$_3$BBn][LiTMEDA].

4.4.2 Synthesis of [(C$_6$F$_5$)$_3$BBn][HTMEDA] and reaction with 7[HB(C$_6$F$_5$)$_3$]

$$[(C_6F_5)_3BBn][LiTMEDA] \xrightarrow[\substack{DCM, 12h \\ 0°C \text{ to } RT \\ 73\%}]{1.0 \text{ equiv. HCl}} [(C_6F_5)_3BBn][HTMEDA]$$
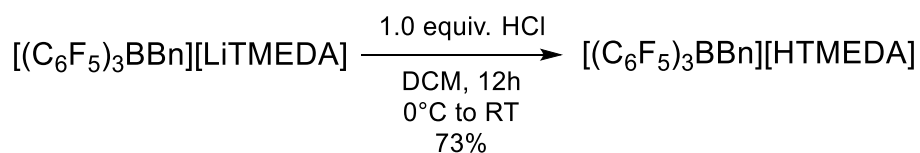
An oven dried Schlenk flask was loaded with [(C$_6$F$_5$)$_3$BBn][LiTMEDA] (610 mg, 0.84 mmol, 1.0 eq.) and DCM (5 ml). After cooling the mixture down to 0°C, HCl (2.0 M in Et$_2$O, 0.42 ml, 0.84 mmol, 1.0 eq.) was added directly *via* syringe in one portion. The mixture was stirred without further cooling for 12h during which the suspended solid disappeared and a new white solid reformed. The product was directly precipitated from the reaction mixture by adding pentane. After removing the liquid phase, the white solids were rinsed with pentane (2x5 ml) and subsequently with small amounts of Et$_2$O (2x2 ml) affording the desired product as a white dusty solid (441 mg, 0.61 mmol, 73%). Crystals suitable for X-ray diffraction were obtained by layering a DCM solution of the product with pentane. In a separate experiment, a Schlenk flask suitable for high pressure reactions was loaded with [(C$_6$F$_5$)$_3$BBn][HTMEDA] (271 mg, 0.38 mmol, 1.0 eq.), **7**[HB(C$_6$F$_5$)$_3$] (400 mg, 0.38 mmol, 1.0 eq.) and toluene (5 ml). After sealing, the vessel was heated up to 135°C for one hour. The colourless solution was cooled down to room temperature, an aliquot of the solution was analyzed showing formation of the desired product. Afterwards, the clear solution was transferred by the means

of a PTFE tube into a Schlenk flask containing pentane (30 ml). The mixture was stirred vigorously for 20 minutes and the resulting solids isolated. During the workup the cationic species polymerized affording no desirable product.

Characterization of $[(C_6F_5)_3BBn][HTMEDA]$

^{1}H NMR (400.30 MHz, CD_2Cl_2, 298 K): δ = 2.57 [s, 12H, $N(CH_3)_4$], 2.81 [bs, 2H, BCH_2Ph], 2.84 [s, 4H, NCH_2CH_2N], 6.75-6.76 [m, 2H, H_{Ph}], 6.79-6.83 [m, 1H, H_{Ph}], 6.88-6.92 [m, 2H, H_{Ph}], 7.39 [b, 1H, H_{Ph}]. **^{11}B{^{1}H} NMR** (128.43 MHz, CD_2Cl_2, 298 K): δ = -13.0 [s]. **^{13}C{^{1}H} NMR** (100.66 MHz, CD_2Cl_2, 298 K): δ = 32.1 [b, BCH_2Ph], 44.8 [s, $N(CH_3)_4$], 54.3 [s, NCH_2CH_2N], 122.9 [s, C_{Ph}], 127.3 [s, C_{Ph}], 129.1 [s, C_{Ph}], 136.8 [bd, $^1J_{C-F}$= 236.7 Hz, $C_{Ar-borate}$], 137.9 [bd, $^1J_{C-F}$= 241.2 Hz, $C_{Ar-borate}$], 148.6 [bd, $^1J_{C-F}$= 230.4 Hz, $C_{Ar-borate}$], 149.0 [s, C_{Ph}]. **^{19}F{^{1}H} NMR** (376.66 MHz, CD_2Cl_2, 298 K): δ = -167.5 [bt, J_{F-F}= 19.2 Hz], -164.5 [t, J_{F-F}= 20.7 Hz], -131.4 [d, J_{F-F}= 23.5 Hz].
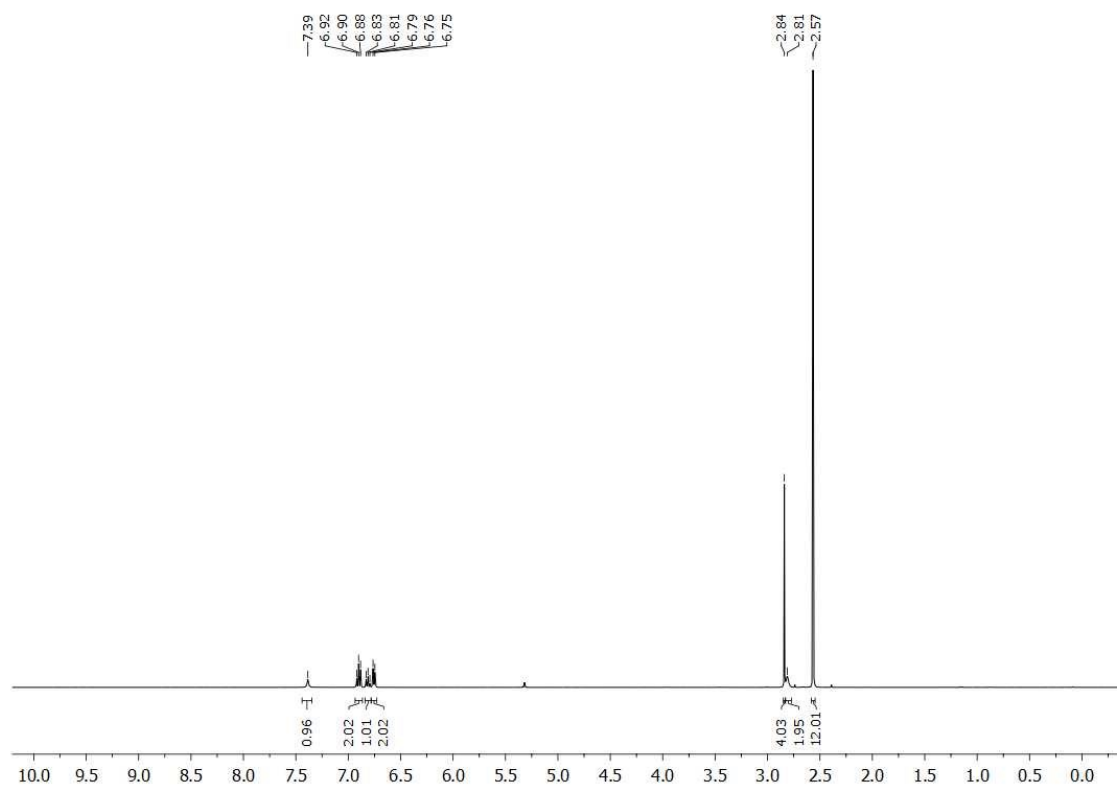
Figure S181. ^{1}H NMR spectrum (CD_2Cl_2, 298 K) of $[(C_6F_5)_3BBn][HTMEDA]$.
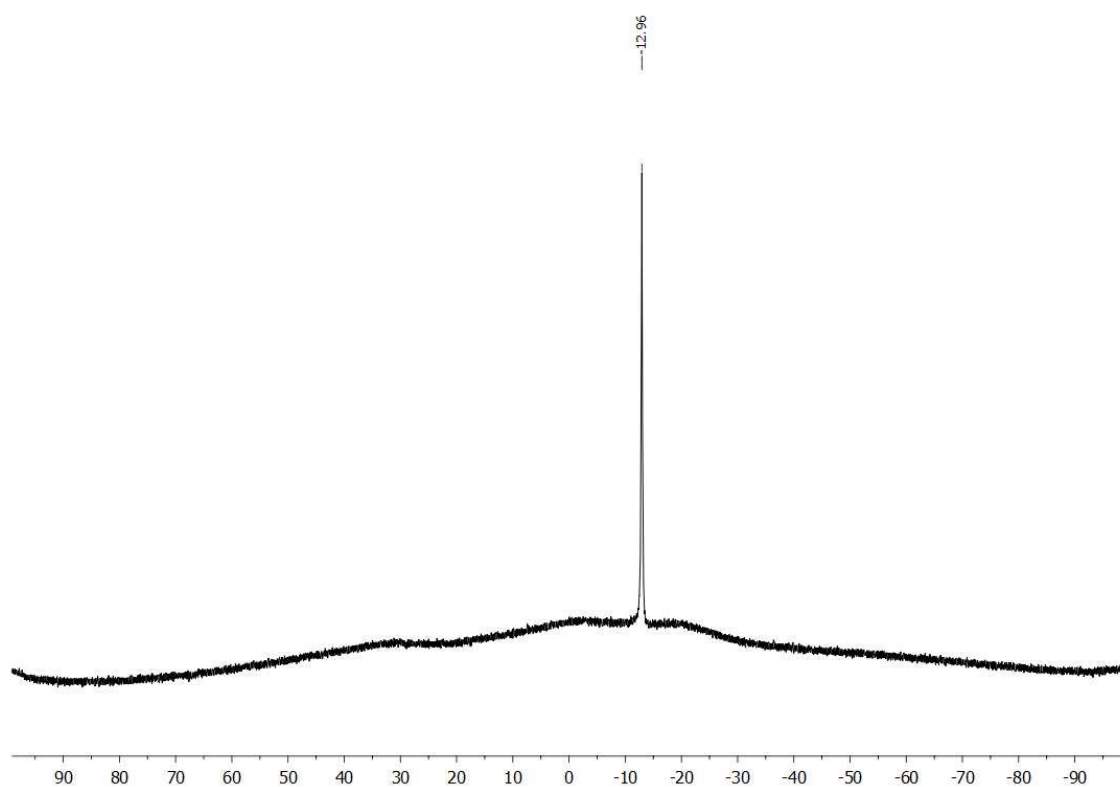
Figure S182. $^{11}B\{^1H\}$ NMR spectrum (CD$_2$Cl$_2$, 298 K) of [(C$_6$F$_5$)$_3$BBn][HTMEDA].
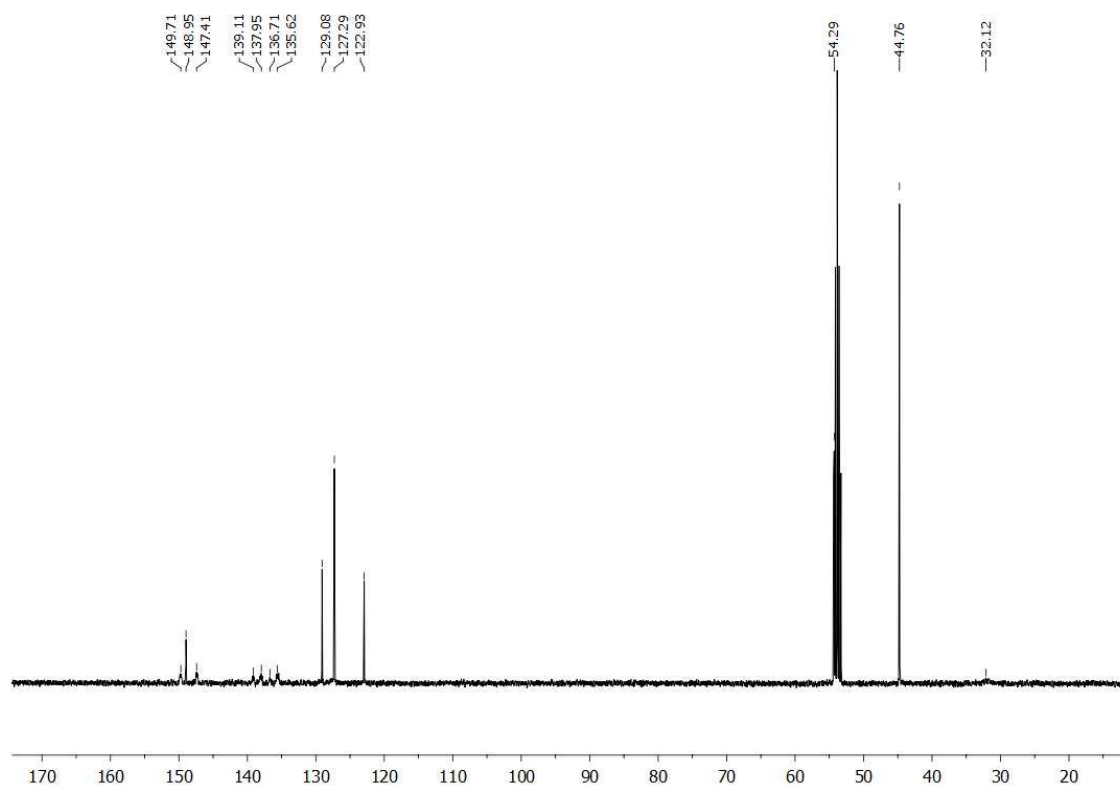
Figure S183. $^{13}C\{^1H\}$ NMR spectrum (CD$_2$Cl$_2$, 298 K) of [(C$_6$F$_5$)$_3$BBn][HTMEDA].
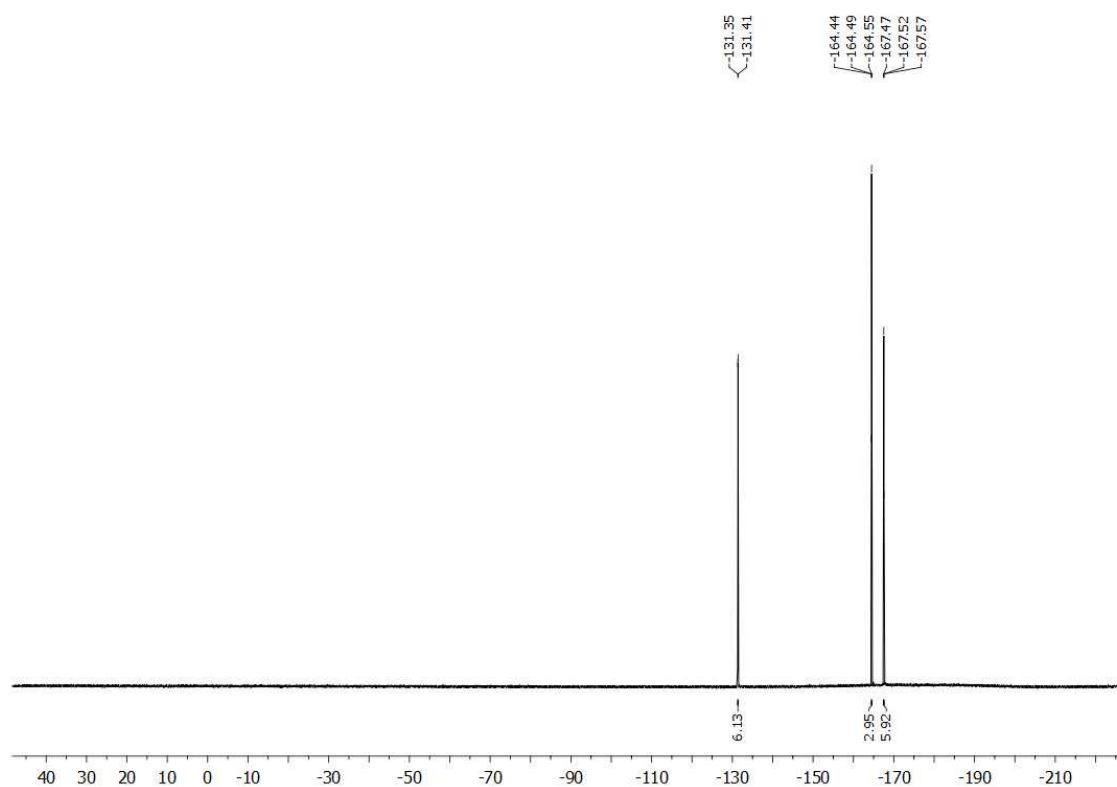
Figure S184. $^{19}F\{^1H\}$ NMR spectrum (CD$_2$Cl$_2$, 298 K) of [(C$_6$F$_5$)$_3$BBn][HTMEDA].
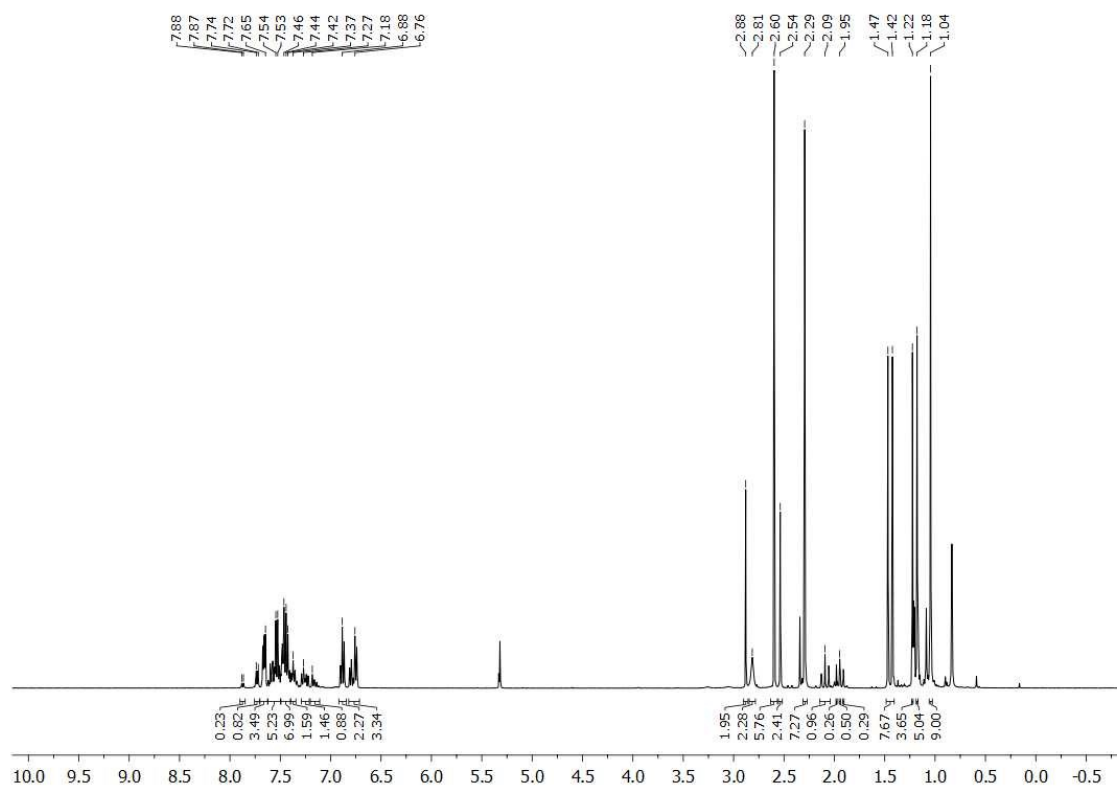
Figure S185. ^1H NMR spectrum (CD$_2$Cl$_2$, 298 K) of the crude mixture after the anion exchange reaction.
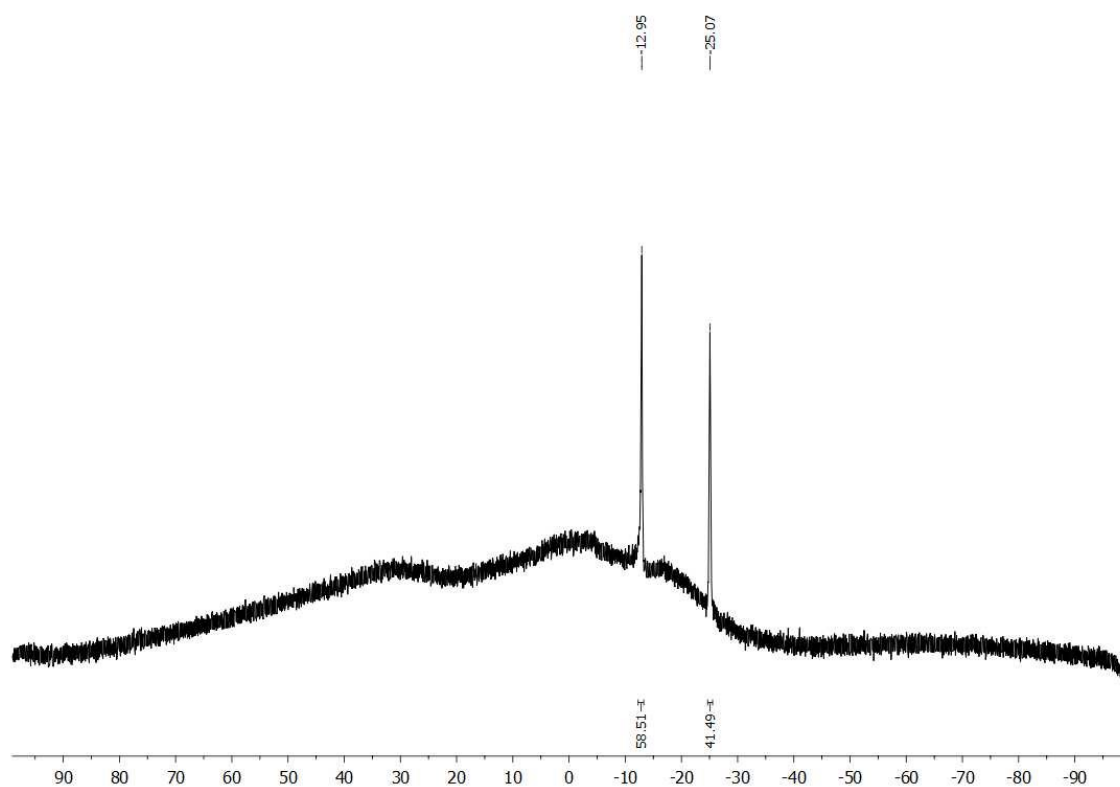
Figure S186. $^{11}B\{^1H\}$ NMR spectrum (CD$_2$Cl$_2$, 298 K) of the crude mixture after the anion exchange reaction.
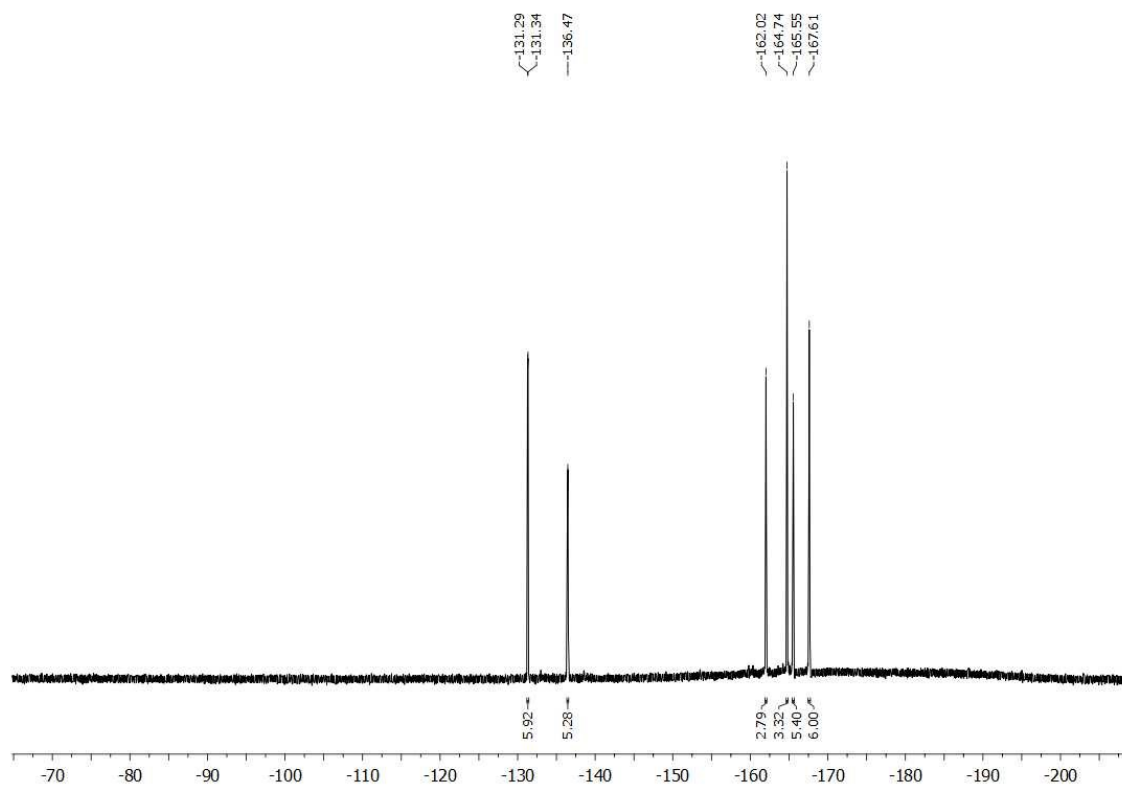
Figure S187. $^{19}F\{^1H\}$ NMR spectrum (CD$_2$Cl$_2$, 298 K) of the crude mixture after the anion exchange reaction.
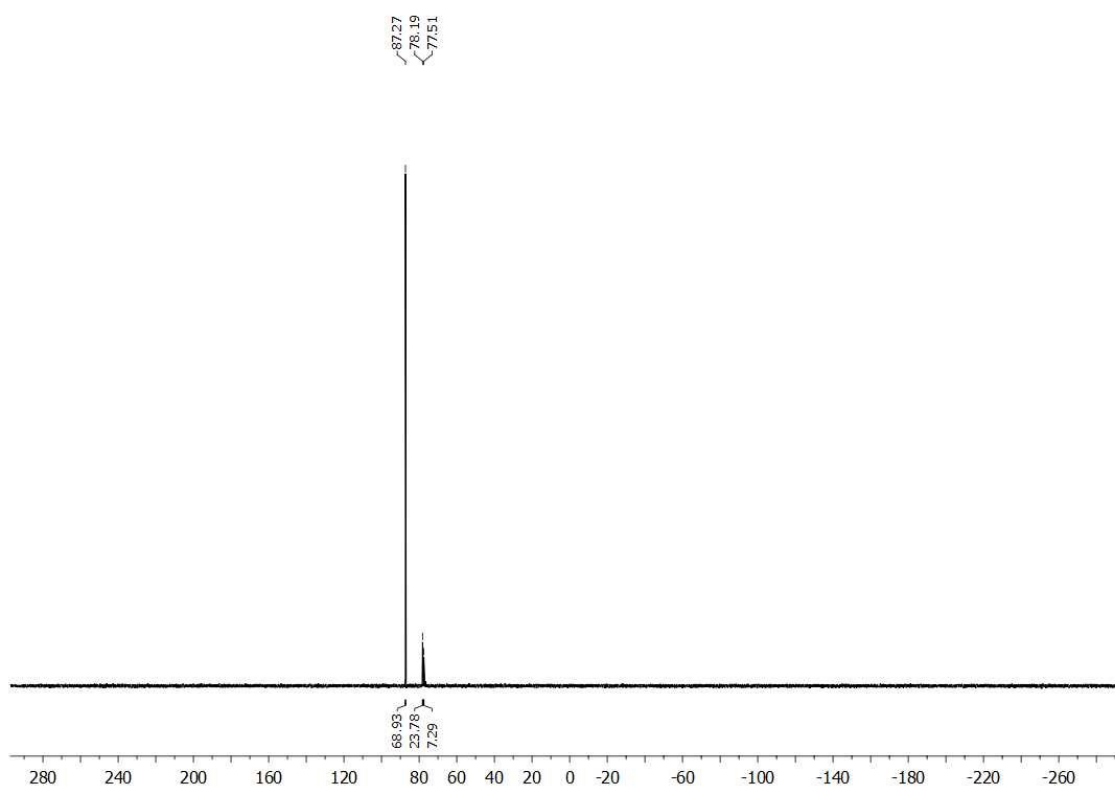
Figure S188. $^{31}P\{^1H\}$ NMR spectrum (CD$_2$Cl$_2$, 298 K) of the crude mixture after the anion exchange reaction.

4.4.3 Synthesis of (*t*Bu)₂P(S)CH₂SiPh₂OSi(F)Ph*t*Bu (8) and (C₆F₅)₂(C₆F₄H)B(OH₂) (9)
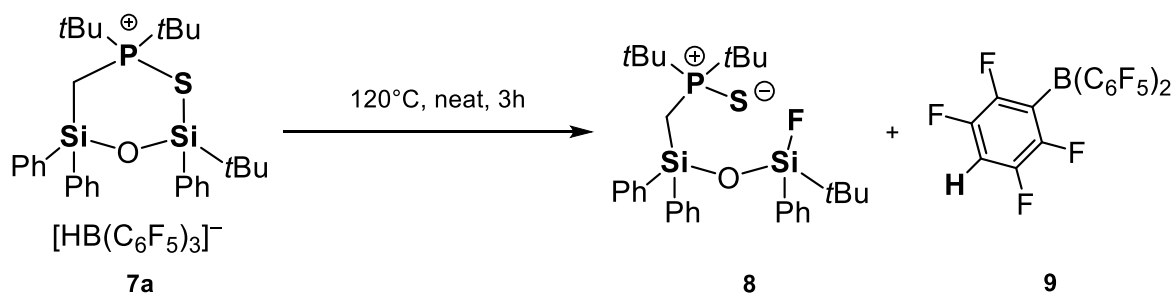
Compound **7**[HB(C₆F₅)₃] (200 mg, 0.188 mmol) was loaded in a Schlenk flask suitable for high pressure reactions (50 ml volume) and sealed under nitrogen atmosphere. The flask was heated up to 120°C for 3 h using an oil bath during which the solid melted while bubbling and turning into a yellow liquid. During the process, thin needles crystallized on the upper part of the flask in a web-like motif (see Figure S38). After 3 h, the vessel was cooled down to room temperature and two thin PTFE cannulas were carefully inserted all the way through the upper layer of the flask, which was covered with the delicate white crystals, to reach the lower half of the flask. Following, DCM was used to extract the yellow residue at the bottom of the flask. After three washings (~10 ml) of the lower part, the organic fractions were collected, dried, and the residue was distilled *via* Kugelrohr distillation (190-200°C oven temperature, 1.0×10^{-3} mbar) to yield fluorodisiloxane **8** as a pale-yellow oil (62 mg, 0.109 mmol, 56%). The crystalline compound on the upper part, free of the yellow residue, was extracted with DCM (3 x 5 ml), the extracts were collected and fully dried under vacuum yielding compound **9** as a white solid (86 mg, 0.132 mmol, 70%). Then, the solid was dissolved in the minimum amount of THF, a few drops of water were added and the mixture was stirred for 10 min. After removing all volatiles, the solid residue was suspended in pentane and brought into solution with a few drops of THF. The mixture was stirred over 30 min, then the reaction vessel was sealed and stored overnight at -30°C affording a few co-crystals of **9**·H₂O·(THF)₂/BCF (1:1) suitable for single-crystal X-ray diffraction analysis (6 mg, 9.14×10^{-3} mmol, 4%).

Figure S189. Spontaneous separation of the two product species **8** and **9** under the reaction conditions: Hydrodefluorinated borane **9** (white crystalline solid on the upper part of the vessel) and fluorodisiloxane **8** (yellow oily residue on the bottom part of the vessel).

Characterization of **8**

^{1}H NMR (400.30 MHz, CD$_2$Cl$_2$, 298 K): δ =0.95 [d, $^4J_{H\text{-}F}$= 0.9 Hz 9H, SiC(CH_3)$_3$], 2.22 [d, $^3J_{P\text{-}H}$= 12.2 Hz, 9H, PC(CH_3)$_3$], 1.14 [d, $^3J_{P\text{-}H}$= 12.2 Hz, 9H, PC(CH_3)$_3$], 1.87 [dd, J_1= 4.2 Hz, J_2= 12.8 Hz, 2H, SiCH_2P], 7.31–7.34 [m, 6H, H_{Ph}], 7.38–7.42 [m, 3H, H_{Ph}], 7.58 [m, 2H, H_{Ph}], 7.77–7.80 [m, 4H, H_{Ph}].

^{13}C{^{1}H} NMR (100.66 MHz, CD$_2$Cl$_2$, 298 K): δ = 13.4 [d, $^1J_{C\text{-}P}$= 37.8 Hz, SiCH$_2$P], 18.6 [d, $^2J_{C\text{-}F}$= 16.5 Hz, SiC(CH$_3$)$_3$], 25.6 [s, SiC(CH$_3$)$_3$], 27.6 [m, PC(CH$_3$)$_3$], 38.6 [d, $^1J_{C\text{-}P}$= 43.2 Hz PC(CH$_3$)$_3$], 127.7 [d, $^4J_{C\text{-}F}$= 3.7 Hz, C_{Ph}], 128.17 [s, C_{Ph}], 130.4 [d, $^5J_{C\text{-}F}$= 0.9 Hz, C_{Ph}], 130.9 [s, C_{Ph}], 131.8 [d, $^2J_{C\text{-}F}$= 19.5 Hz, C_{Ph}], 134.8 [d, $^5J_{C\text{-}F}$= 2.6 Hz, C_{Ph}], 135.6 [d, $^4J_{C\text{-}F}$= 3.4 Hz, C_{Ph}], 136.0 [d, $^3J_{C\text{-}F}$= 5.6 Hz, C_{Ph}]. **^{19}F{^{1}H} NMR** (376.66 MHz, CD$_2$Cl$_2$, 298 K): δ = -151.0 [s with satellites, $^1J_{F\text{-}Si}$= 298.5 Hz]. **^{29}Si{^{1}H} NMR** (79.49 MHz, CD$_2$Cl$_2$, 298 K): δ = -25.2 [d, $^2J_{Si\text{-}F}$= 298.4 Hz, PCSiOSiF], -14.9 [s, PCSiOSiF]. **^{31}P{^{1}H} NMR** (162.04 MHz, CD$_2$Cl$_2$, 298 K): δ = 73.4 [s]. **CHN Analysis** C$_{31}$H$_{44}$FOPSSi$_2$: calculated: C 65.22%; H 7.77%; found C 64.42%, H 7.45%. **HR-MS (ESI+)**, calculated. m/z for C$_{32}$H$_{44}$FOPSSi$_2$$^+$ [M+H]$^+$: 571.2451; found: 571.2469.

Figure S190. ^{1}H NMR spectrum (CD$_2$Cl$_2$, 298 K) of compound **8**.

Figure S191. ^{13}C{^{1}H} NMR spectrum (CD$_2$Cl$_2$, 298 K) of compound **8**.

Figure S192. ^{19}F{^{1}H} NMR spectrum (CD$_2$Cl$_2$, 298 K) of compound **8**.

Figure S193. ^{29}Si{^{1}H} NMR spectrum (CD$_2$Cl$_2$, 298 K) of compound **8**.

Figure S194. ^{31}P{^{1}H} NMR spectrum (CD$_2$Cl$_2$, 298 K) of compound **8**.

Characterization of **9**·H$_2$O·(THF)$_2$

^{1}H NMR (400.30 MHz, CD$_2$Cl$_2$, 298 K): δ =2.06 [s, 8H, OCH$_2$CH_2], 4.15 [s, 8H, OCH_2CH$_2$], 7.02 [m, 1H, B(C$_6$F$_4$$H$)], 10.24 [bs, 1H BO$H_2$]. **^{11}B{^{1}H} NMR** (128.43 MHz, CD$_2$Cl$_2$, 298 K): δ = -2.4 [bs]. **^{13}C{^{1}H} NMR** (100.66 MHz, CD$_2$Cl$_2$, 298 K): δ = 25.2 [s, OCH$_2$CH_2], 75.2 [s, OCH_2CH$_2$], 105.6 [bs, B(C$_5$F$_4$CH)], 137.6 [bd, $^1J_{\text{C-F}}$ = 237.7 Hz, $C_{Ar\text{-}borate}$], 139.6 [bs, $C_{Ar\text{-}borate}$], 143.6 [bd, $^1J_{\text{C-F}}$ = 290.8 Hz, $C_{Ar\text{-}borate}$], 148.2 [d, $^1J_{\text{C-F}}$= 250.0 Hz $C_{Ar\text{-}borate}$]. **^{19}F{^{1}H} NMR** (376.66 MHz, CD$_2$Cl$_2$, 298 K): δ = -164.5 [bm, 6F], -157.9 [bm, 1F], -157.7 [bm, 2F], -141.6 [bm, 1F], -135.1 [bm, 1F], -135.1 [bm, 6F]. **CHN Analysis** C$_{26}$H$_{19}$BF$_{14}$O$_3$: calculated: C 47.59; H 2.92; found C 47.19, H 2.79. **HR-MS (ESI-)**, calculated. m/z for C$_{18}$HBF$_{14}$O [M, -H]$^-$: 510.9981; found: 510.9993.
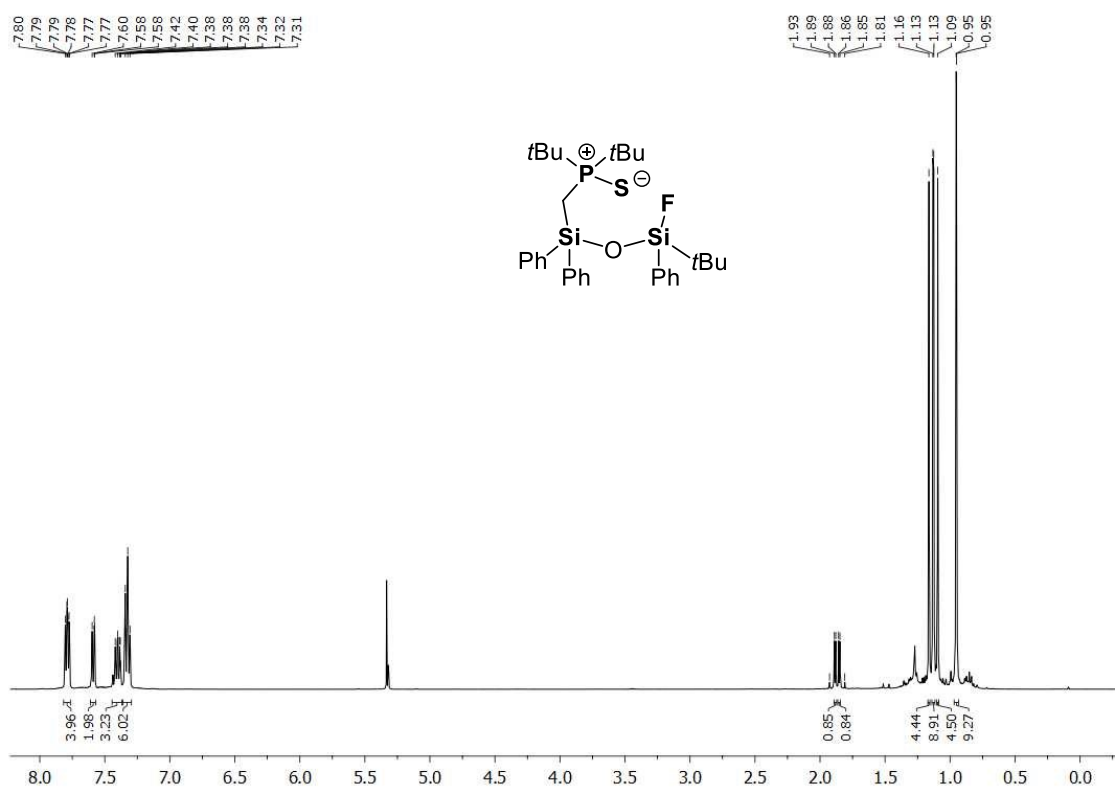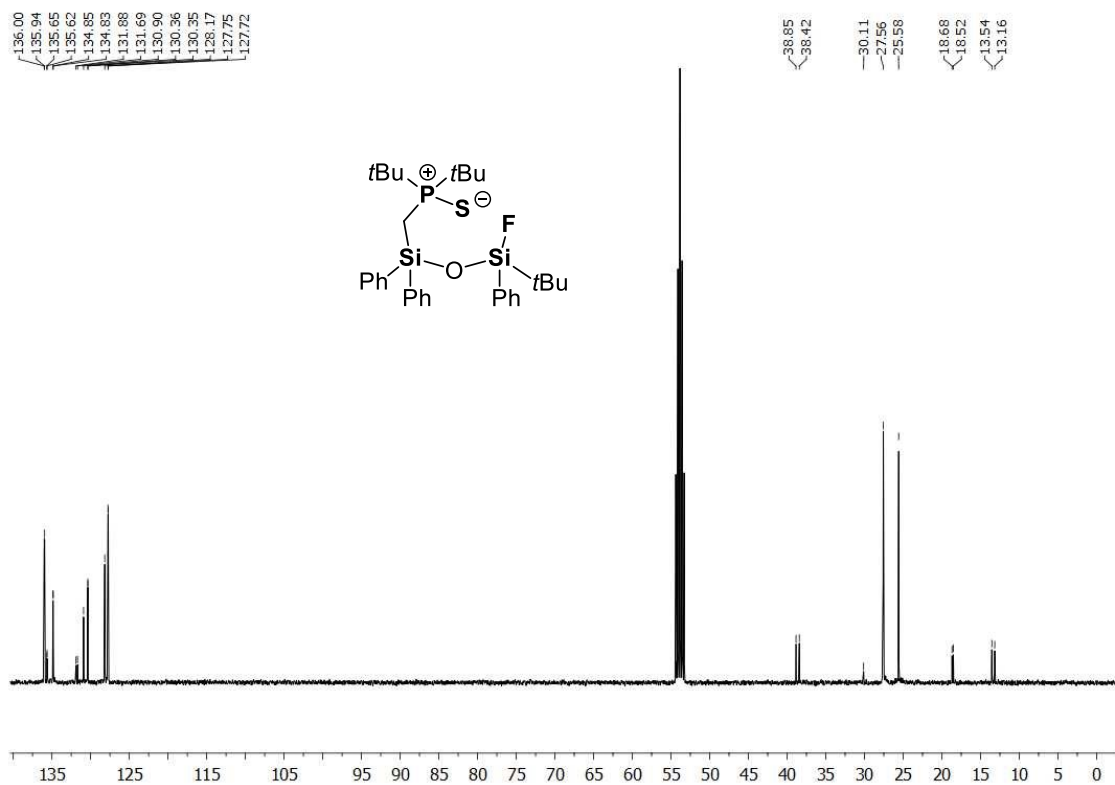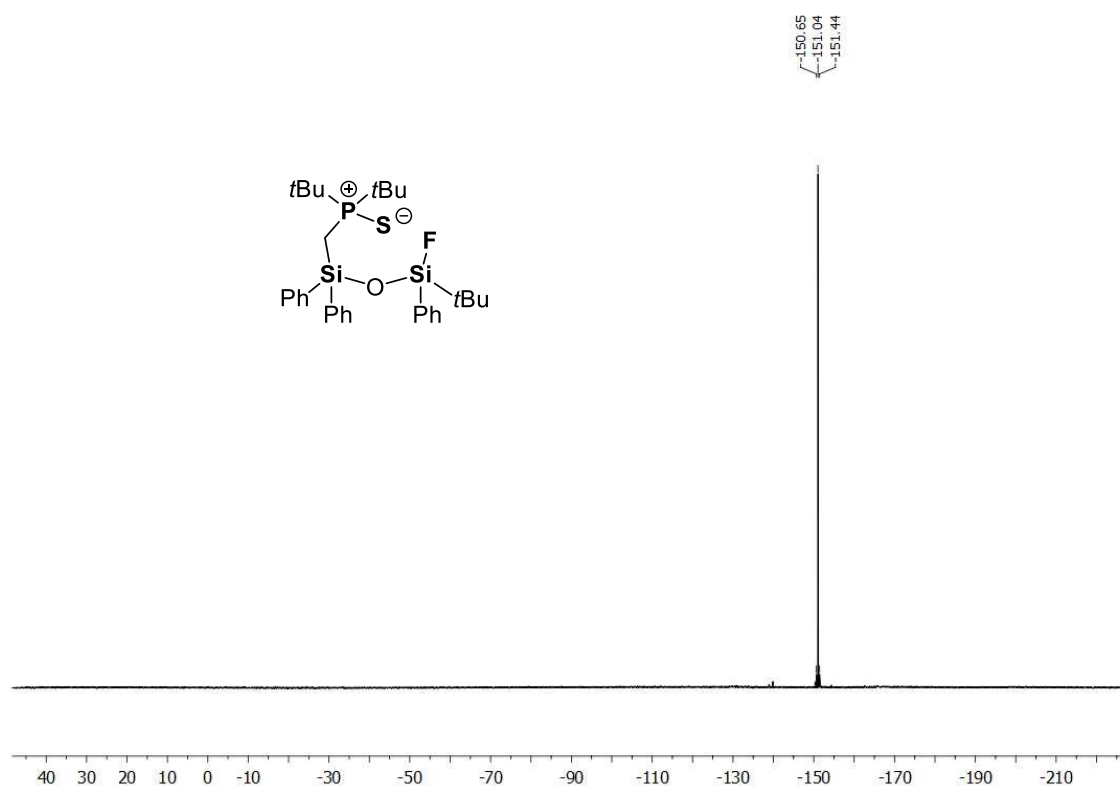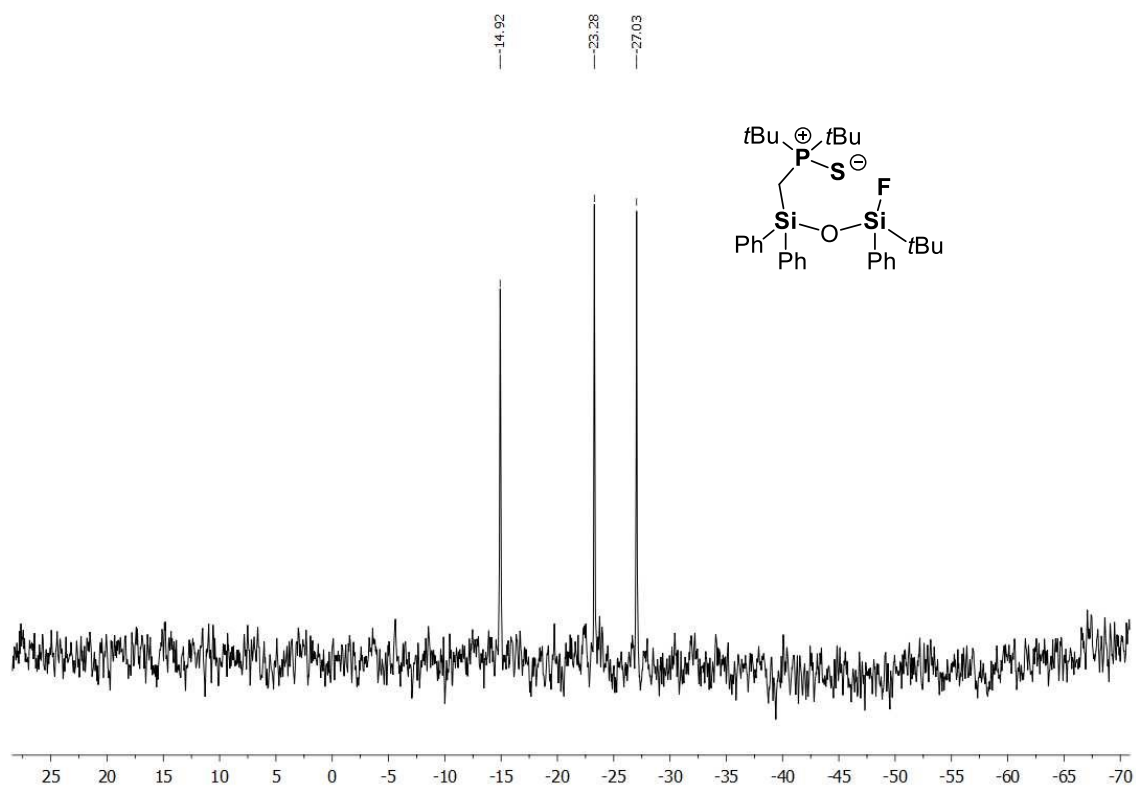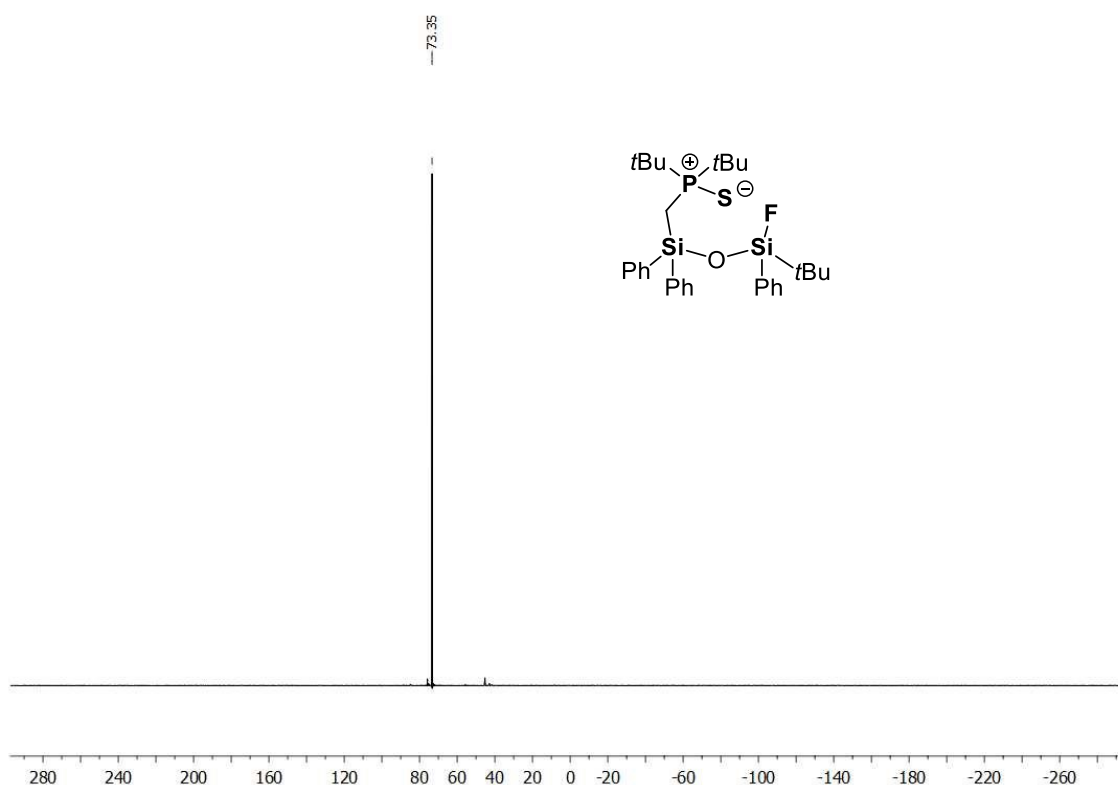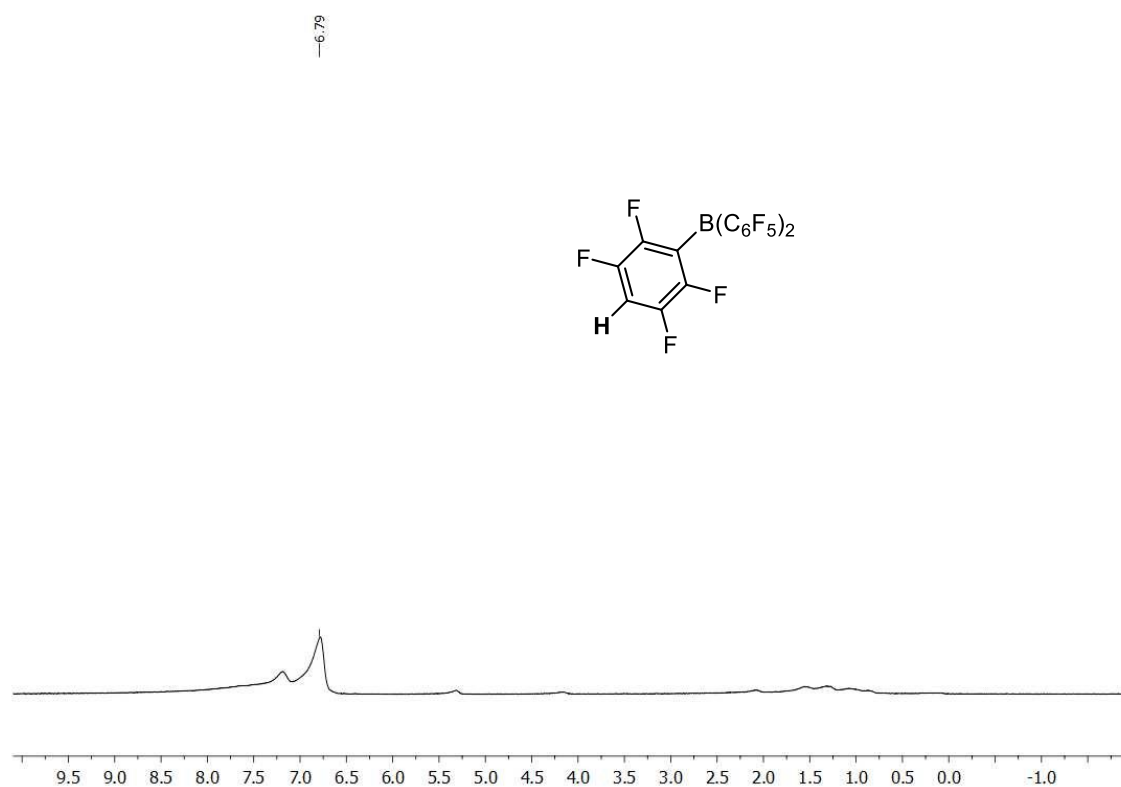
Figure S195. ^{1}H NMR spectrum (CD$_2$Cl$_2$, 298 K) of the isolated crystalline sublimate.
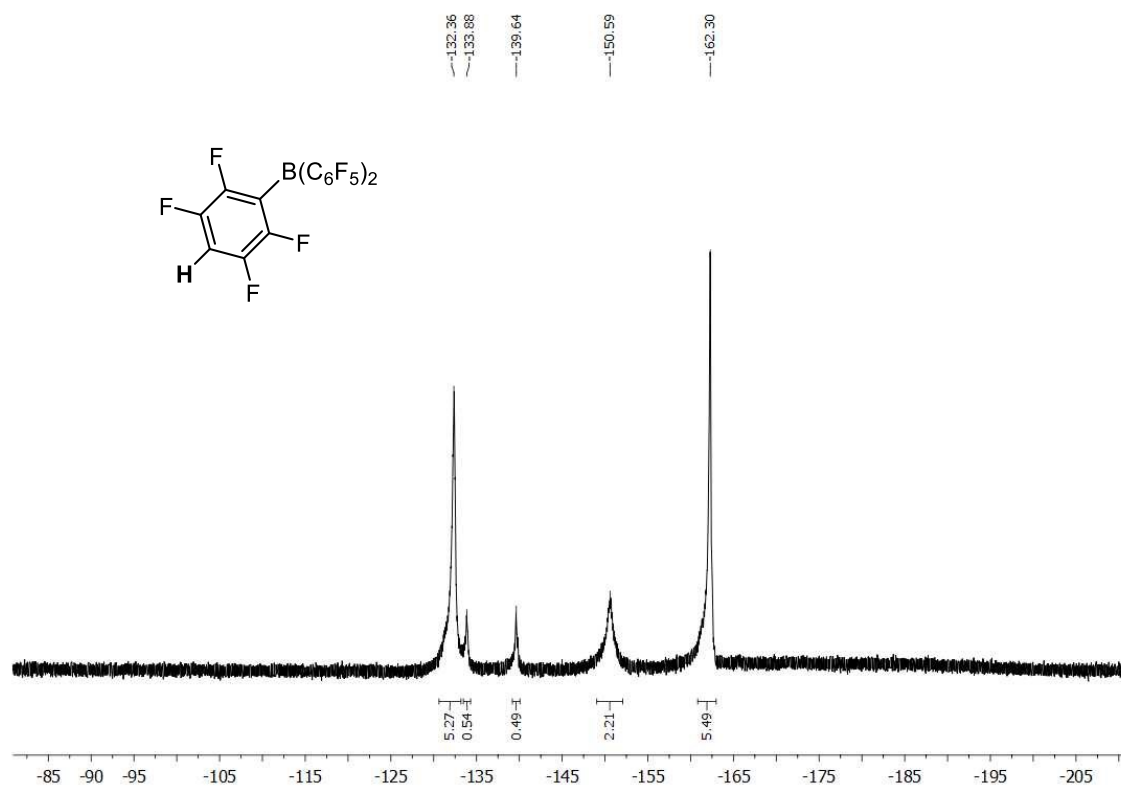
Figure S196. ^{19}F{^{1}H} NMR spectrum (CD$_2$Cl$_2$, 298 K) of the isolated crystalline sublimate.
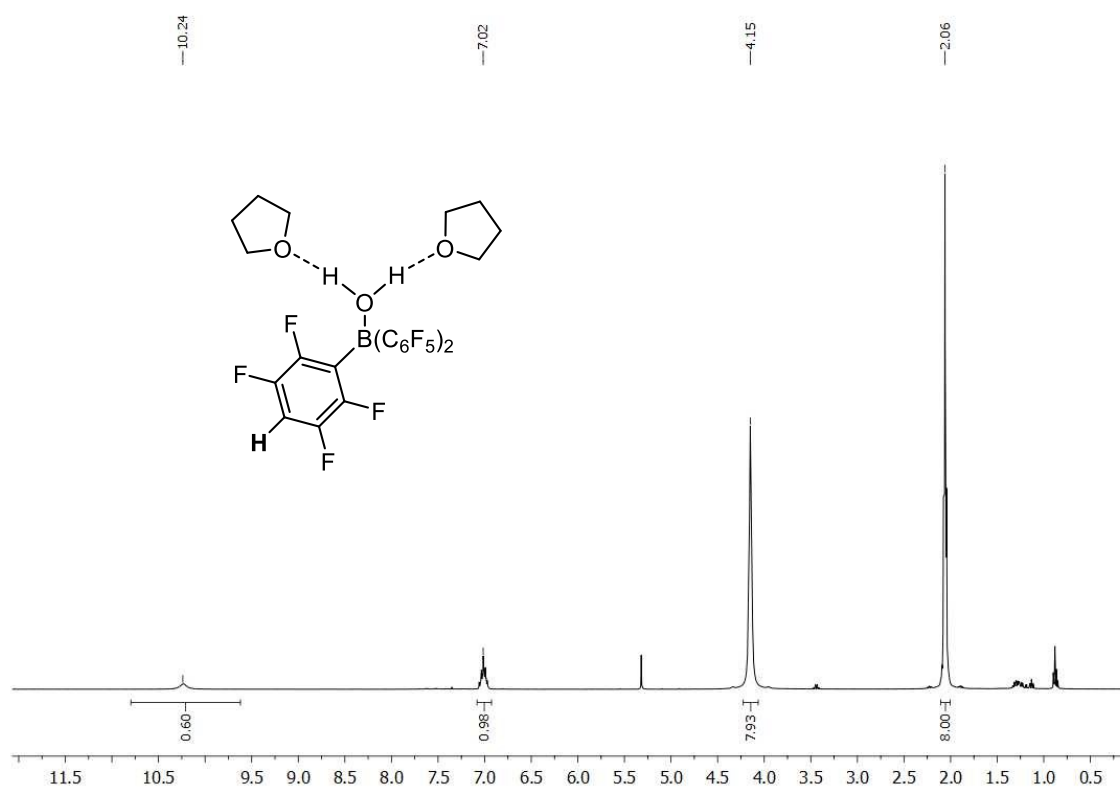
Figure S197. ^{1}H NMR spectrum (CD$_2$Cl$_2$, 298 K) of compound **9**·H$_2$O·(THF)$_2$.
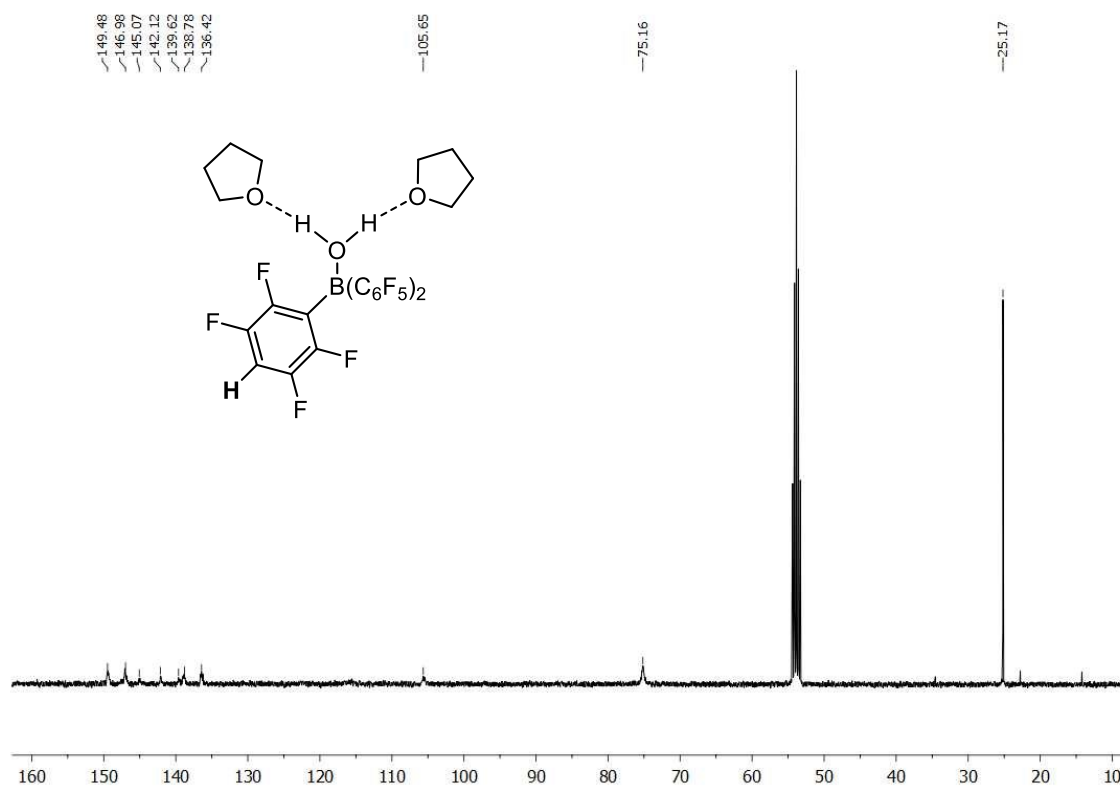
Figure S198. ^{13}C{^{1}H} NMR spectrum (CD$_2$Cl$_2$, 298 K) of compound **9**·H$_2$O·(THF)$_2$.
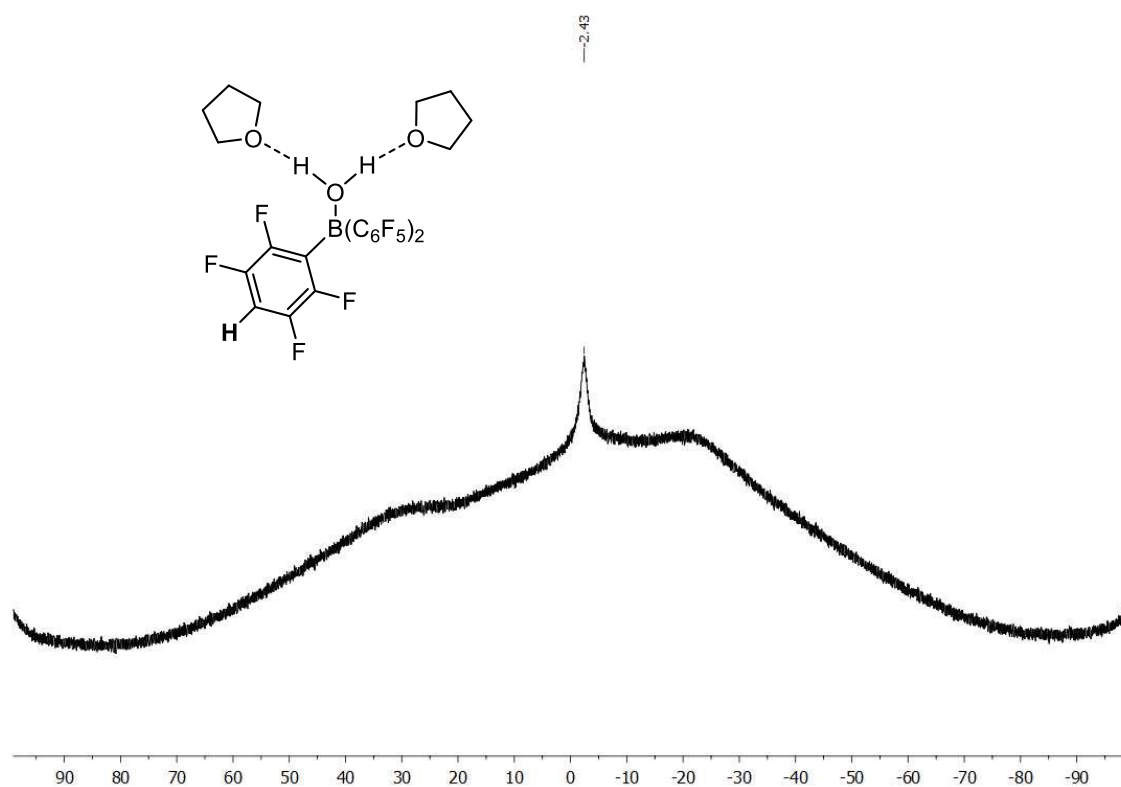
Figure S199. $^{11}B\{^1H\}$ NMR spectrum (CD$_2$Cl$_2$, 298 K) of compound **9**·H$_2$O·(THF)$_2$.
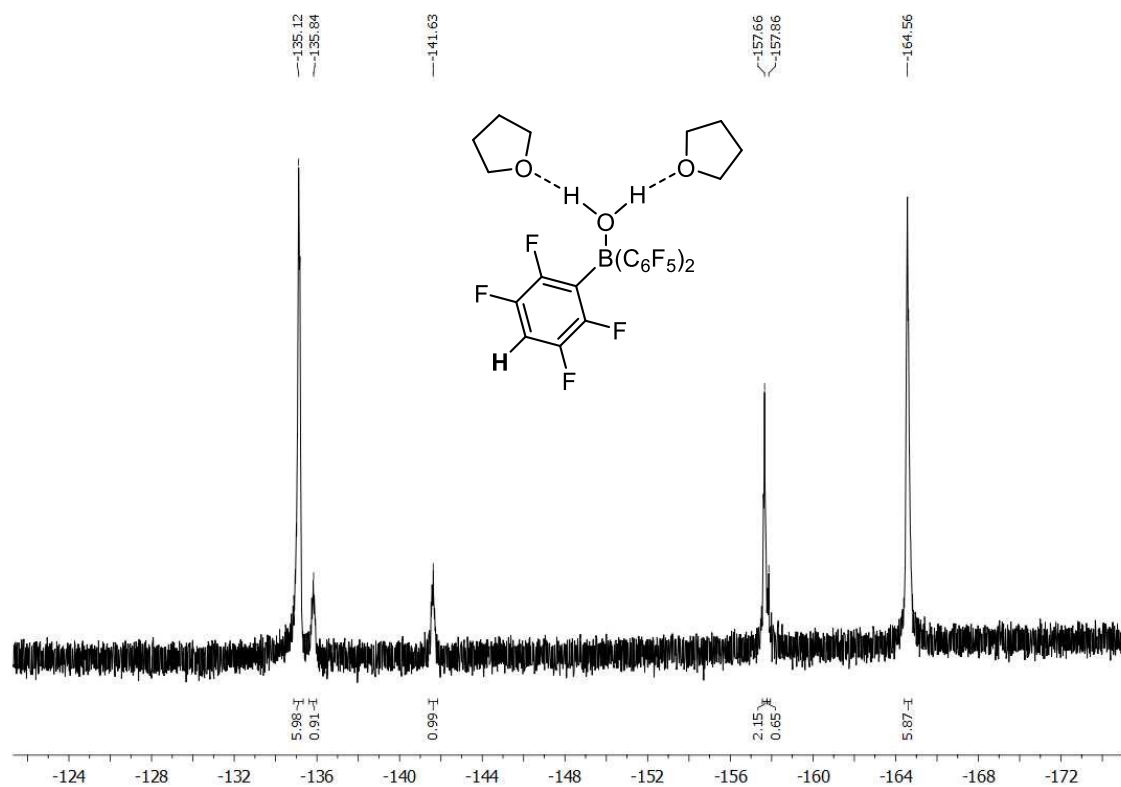
Figure S200. $^{19}F\{^1H\}$ NMR spectrum (CD$_2$Cl$_2$, 298 K) of compound **9**·H$_2$O·(THF)$_2$.

4.5   Quantum Chemical Calculations

Optimization and additional harmonic vibrational frequency analyses were performed with the software package Gaussian 09 (Revision E.01) either on the B3LYP/6-311+G(d,p) or the HF/3-21G level of theory without symmetry restrictions.[12] The GJF input files and the figures of the optimized structures were created with the program GaussView 5.0.9. For the ground state structures, vibrational frequency analysis showed no imaginary frequency in the harmonical approximation. Natural bond orbital (NBO) analysis has been performed on the B3LYP/6-311+G(d,p) level of theory with the Gaussian NBO Version 3.1. The total (SCF) and zero-point-corrected (ZPE) energies of the calculated systems can be found in Table S13. The results of the NBO analysis can be found in Table S14. The optimized structures can be found in Figures S200–S214. A mechanistic proposal is given in Figure S199. The calculated standard orientations of the optimized structures can be found in Tables S15–S29. The Hartree units can be converted as follows:[13]

1 Hartree = 2625.4995 kJ·mol^{-1}, 1 cal = 4.184 J.

Table S13. Total (SCF) and zero-point-corrected (ZPE) energies of the optimized structures.

Optimized structure	Method/Basis	SCF [Hartree]	ZPE [Hartree]
6	B3LYP/6-311+G(d,p)	–2602.77036406	–2602.087217
7-Cat-S	B3LYP/6-311+G(d,p)	–2601.98833969	–2601.311959
7-Cat-Ar	B3LYP/6-311+G(d,p)	–2601.92295396	–2601.246927
7-Cat-free	B3LYP/6-311+G(d,p)	–2601.92048049	–2601.245066
6-C	B3LYP/6-311+G(d,p)	–2566.76138254	–2566.055163
7-C-Cat-S	B3LYP/6-311+G(d,p)	–2565.98204034	–2565.282543
7-C-Cat-Ar	B3LYP/6-311+G(d,p)	–2565.92074226	–2565.221776
7[HB(C$_6$F$_5$)$_3$]	HF/3-21G	–4763.38969851	–4762.472467
Int-1	HF/3-21G	–4763.35063149	–4762.433706
Int-2	HF/3-21G	–2087.27448944	–2087.102606
Int-2	B3LYP/6-311+G(d,p)	–2109.48067241	–2109.325350
Int-3	HF/3-21G	–4763.37140144	–4762.455420
8	HF/3-21G	–2675.94366839	–2675.207020
9	HF/3-21G	–2087.54716625	–2087.367394
9	B3LYP/6-311+G(d,p)	–2109.67379911	–2109.512775

Table S14. Results of the natural bond orbital (NBO) calculations [B3LYP/6-311+G(d,p)].

Property	6	7-Cat-S	7-Cat-Ar	7-Cat-free	6-C	7-C-Cat-S	7-C-Cat-Ar
i_{Si2S}[a]	—	0.506	—	—	—	0.496	—
i_{SP}[a]	0.026	0.128	0.039	0.034	0.030	0.129	0.036
i_{PC1}[a]	0.256	0.221	0.271	0.277	0.251	0.226	0.271
i_{C1Si1}[a]	0.500	0.527	0.489	0.496	0.493	0.520	0.471
i_{Si1C2}[a]	—	—	—	—	0.455	0.469	0.491
i_{C2Si2}[a]	—	—	—	—	0.459	0.491	0.497
Q_{Si1}[b]	2.004	1.999	2.020	2.020	1.768	1.765	1.783
Q_{O}[b]	−1.266	−1.280	−1.296	−1.286	—	—	—
Q_{Si2}[b]	1.759	1.978	2.226	2.256	1.483	1.747	2.003
Q_{S}[b]	−0.629	−0.451	−0.611	−0.604	−0.632	−0.431	−0.597
Q_{P}[b]	1.421	1.519	1.439	1.434	1.426	1.526	1.429
Q_{C1}[b]	−1.275	−1.271	−1.288	−1.288	−1.252	−1.258	−1.260
Q_{C2}[b]	—	—	—	—	−1.410	−1.444	−1.451
h_{O} (% s)[c]	$sp^{0.08}$ (92.5)	$sp^{0.14}$ (87.7)	$sp^{0.25}$ (80.1)	$sp^{0.14}$ (87.3)	—	—	—
h_{Si2} (% s)[c]	$sp^{8.39}$ (10.6)	$sp^{9.17}$ (9.7)	$sp^{10.0}$ (9.0)	$sp^{7.57}$ (11.5)	$sp^{2.85}$ (25.8)	$sp^{2.57}$ (27.8)	$sp^{2.18}$ (31.2)
h_{C2} (% s)[c]	—	—	—	—	$sp^{2.49}$ (28.7)	$sp^{2.35}$ (29.9)	$sp^{2.47}$ (28.8)
occ. n_{O}'[d]	1.916	1.914	1.923	1.930	—	—	—
occ. n_{O}''[d]	1.907	1.904	1.900	1.841	—	—	—
hc loss n_{O}[e]	0.177	0.182	0.177	0.229	—	—	—
rel. hc loss n_{O}[f]	0 %	2.8 %	0 %	29.4 %	—	—	—
$E^{(2)}$ ($n_{O}'' \rightarrow p_{Si2}$)[g]	—	—	—	−29.98	—	—	—

[a] Bond ionicities (i_{AB}) of the A–B bonds ($i_{AB} = |c_A^2 - c_B^2|$ with c_A and c_B being NBO polarization coefficients). [b] Natural atomic charges (Q_A) at atoms A. [c] Natural hybrid types (h_O, h_{Si2}, h_{C2}) and their % s character at atoms O, Si2, and C2 in the O–Si2 and C2–Si2 bonds, respectively (h_O corresponds to the lone electron pair-like natural hybrid at oxygen that makes the greatest contribution to the O–Si2 bond). [d] Oxygen lone electron pair occupancies (occ. n_O', occ. n_O''). [e] Net hyperconjugative electronic loss of oxygen lone electron pairs (hc loss n_O). [f] hc loss n_O relative to compound **6** (rel. hc loss n_O). [g] Hyperconjugative stabilization energy ($E^{(2)}$) from the second order perturbation theory analysis for the $n_O'' \rightarrow p_{Si2}$ interaction.

Details on the thermochemistry and NBO calculations:

By far the greatest contribution to the stabilization of the Lewis acidic silylium center is provided by the intramolecular coordination through the P^+–S^- group. The ring opening of the heterocyclic sulfur-coordinated cation **7-Cat-S** with formation of the free, trigonal planar cation **7-Cat-free** requires an energy of 42.1 kcal mol^{-1}. Apparently, hyperconjugative $n_O \rightarrow \sigma^*_{vicinal}$ contributions only play a negligible role for the intramolecular Lewis base-stabilized siloxysilylium ions; the net hyperconjugative loss of oxygen lone electron pairs (hc loss n_O) of 0.182 in cation **7-Cat-S** is only 2.8 % larger than in disiloxane **6** (hc loss n_O = 0.177). A silylium ion (**7-Cat-Ar**) stabilized by an intramolecular aryl(π)–Si interaction was also found (sum of angles around Si2: 345.2°), which is 40.9 kcal mol^{-1} higher in energy than **7-Cat-S** and which shows no changes in the net hyperconjugative loss of oxygen lone electron pairs (hc loss n_O = 0.177) compared to compound **6**. It appears that hyperconjugative effects only play a role in the open, trigonal planar siloxysilylium ion **7-Cat-free** (sum of angles around Si2: 360.0°). Here, the $n_O \rightarrow \sigma^*_{vicinal}$ hyperconjugation increases by 29.4 % (with respect to disiloxane **6**) and the Si2–O bond length is shortened from 1.647 Å in **7-Cat-S** to 1.582 Å in **7-Cat-free**. Second order perturbation theory analysis gives an estimate for the hyperconjugative stabilization energy. In **7-Cat-free**, the out-of-plane interaction between n_O'' and the empty p-type orbital p_{Si2} ($n_O'' \rightarrow p_{Si2}$) of −29.98 kcal mol^{-1} provides the major contribution, while in **7-Cat-Ar**, the hyperconjugative interaction is largely abandoned in favor of the Lewis acid/base aryl(π)–Si interaction. However, this $n_O'' \rightarrow p_{Si2}$ interaction in the trigonal planar form could facilitate the ring opening required for the silylium-like reactivity. The cation **7-Cat-free** is only 1.2 kcal mol^{-1} higher in energy than **7-Cat-Ar**. The O–Si2 σ-bonds of all calculated disiloxane species can be regarded as strongly ionic with high electron occupancies at the oxygen atom. This is also reflected by the high s character of the involved lone electron pair-like natural hybrids at oxygen (h_O) and the high p character of h_{Si2} in the O–Si2 bonds in accordance with Bent's rule (Table S14).[14]

The formal exchange of the siloxane oxygen atom by a CH_2 group led to the analogous cations **7-C-Cat-S** and **7-C-Cat-Ar**, the latter being 38.2 kcal mol^{-1} higher in energy. It can be stated that the open forms of the disiloxane-based cation have a higher Lewis acidity than the open form of the methylene-bridged analog, although the differences between the Si–O–Si and the Si–CH_2–Si systems are not too pronounced. The consistently higher positive charge on the Si2 atom of the disiloxane-based cations (**7-Cat-S**: Q_{Si2} = 1.978; **7-Cat-Ar**: Q_{Si2} = 2.226; **7-Cat-free**: Q_{Si2} = 2.256) compared to the respective methylene-bridged analogs (**7-C-Cat-S**: Q_{Si2} = 1.747; **7-C-Cat-Ar**: Q_{Si2} = 2.003) points in the same direction (Table S14). The C2–Si2 bonds can be classified as polar covalent σ-bonds.
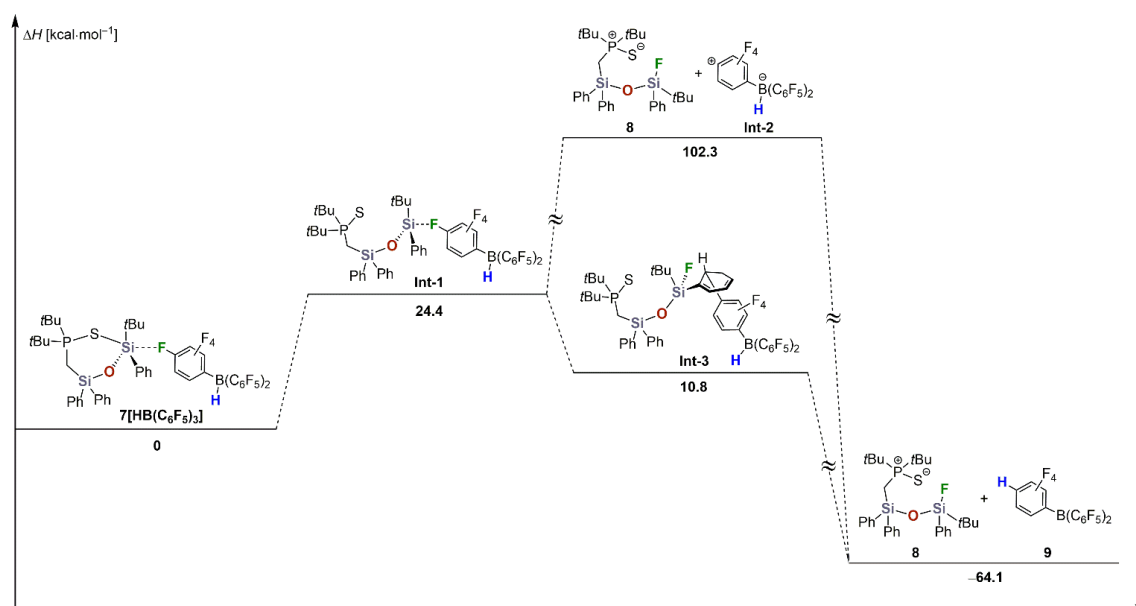
Figure S201. Mechanistic proposal for the *para*-C(sp^2)–F hydrodefluorination calculated on the HF/3-21G level of theory. Formal charges, except for product **8** and intermediate **Int-2**, are omitted for clarity.

Mechanistic details on the ion pair reaction:

A plausible reaction path for the *para*-C(sp^2)–F defunctionalization was calculated on the HF/3-21G level of theory, which is shown in Figure S201. The overall reaction from ion pair **7**[HB(C$_6$F$_5$)$_3$] to products **8** and **9** is an exothermic process (ΔH = −64.1 kcal mol^{-1}). The endothermic contribution in the ion pair reaction results mainly from the energy required to open the heterocyclic cation (**7a** → **Int-1**). For this step, 24.4 kcal mol^{-1} must be applied to create the reactive silylium–hydroborate encounter complex **Int-1** with the *para*-fluoro substituent of the anion coordinating to the siloxysilylium center. Given the reaction temperature of 120°C in the experiment, this should be thermodynamically achievable. From there, a route via fluoride abstraction with formation of the product fluorodisiloxane **8** and an extremely unstable zwitterionic intermediate (**Int-2**) appears unlikely in view of the considerably high energy of 77.9 kcal mol^{-1} required for this step. The zwitterion **Int-2** is 166.4 kcal mol^{-1} higher in energy than borane **9** [this energy difference was calculated to be 117.6 kcal mol^{-1} based on the structures optimized on the B3LYP/6-311+G(d,p) level of theory]. Since the reaction takes place in the ionic liquid phase, more plausible alternative reaction paths starting from **Int-1** should be considered. One possibility could be an exothermic fluoride abstraction with simultaneous participation of an aryl substituent leading to a covalently bound zwitterionic intermediate (**Int-3**). The latter could then decompose intramolecularly by hydride transfer from boron to the *para* position of the tetrafluorophenyl ring in a strongly exothermic process (ΔH = −74.9 kcal mol^{-1}) with concomitant rearomatization of the silicon-bound phenyl ring to give products **8** and **9**. However, direct intermolecular hydrodefluorination starting from the encounter complex **Int-1** via an S$_N$Ar mechanism is a plausible alternative that could easily take place in the highly concentrated ionic liquid phase. In this case the attacking hydride could come from a second hydroborate anion. In a similar way, intermediate **Int-3** could also react in an S$_N$Ar process with participation of a second

hydroborate anion. The *para*-defunctionalized hydroborate anion generated in these constellations would then be further converted to product borane **9** in the course of the reaction. Such intermolecular mechanisms can explain the traces of tris(pentafluorophenyl)borane (BCF) found in the co-crystals of compound **9**. It should be noted that electrostatically-driven, attractive σ-hole-type C(phenyl)–H⋯F–C(aryl) interactions between the phenyl groups of the cation and the perfluorinated aryl groups of the counterion could play an important role for the formation of a reactive encounter complex.[15] This is strongly suggested by the optimized structures **7**[HB(C₆F₅)₃] (Figure S207), **Int-1** (Figure S208), and **Int-3** (Figure S211).
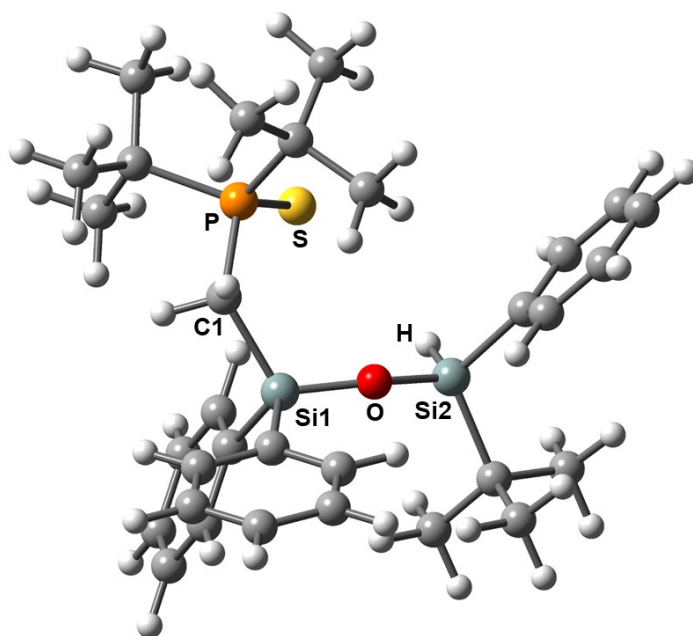
Figure S202. Optimized structure of compound **6** [B3LYP/6-311+G(d,p)]. Selected bond lengths [Å] and angles [°]: P–S 1.996, Si1–O 1.649, Si2–O 1.669, Si1–O–Si2 152.9.

Table S15. Standard orientation of **6** [B3LYP/6-311+G(d,p)].

Atomic symbol	x	y	z
C	−0.69870100	3.18636900	4.58302800
C	0.45819600	3.52036700	3.87927000
C	−1.60631200	2.28678800	4.02853900
C	0.70045600	2.95523500	2.62882600
C	−1.35794400	1.72594100	2.77540000
C	−0.20276000	2.04780400	2.04732900
C	3.08394100	−2.55619300	2.21621600
C	−3.41971300	−3.56542700	1.51219300
C	−3.02380200	−2.31699100	1.03616700
C	−3.50612400	−4.64984100	0.63930300
C	0.70301400	−2.54251800	1.42733900
C	5.02935100	−0.22512100	0.71910000
C	2.17524000	−2.61138900	0.97498000
C	1.82309500	0.33583800	0.66929300
C	2.38928300	−3.94721400	0.23836800

C	0.06966100	3.90339900	–0.70867000
C	–2.70583000	–2.11973200	–0.31793400
C	–3.18993300	–4.47896200	–0.70697300
C	4.30428700	–0.76360100	–0.53030900
C	0.38291700	2.55614000	–0.95701700
C	0.20677700	4.87293000	–1.70185200
C	–2.79285200	–3.22711300	–1.17645000
C	5.02149800	–2.02473700	–1.04509500
C	–3.76394100	0.68404900	–1.25218000
C	4.36439200	0.31594100	–1.63166200
C	0.83711900	2.21415700	–2.24379000
C	0.65891300	4.51325600	–2.96960500
C	–4.74719000	–0.06615900	–2.17817800
C	0.97218600	3.18134400	–3.23823600
H	–0.89023900	3.62503400	5.55617300
H	1.16904500	4.22131700	4.30353900
H	–2.50835200	2.02238000	4.57000700
H	1.60652700	3.23684000	2.09995300
H	–3.65914500	–3.69379400	2.56253800
H	2.75333200	–3.32548500	2.92215800
H	3.03456700	–1.59807000	2.73966400
H	–2.07135600	1.02703700	2.35447400
H	4.12680100	–2.76759100	1.97544000
H	–2.95129000	–1.48991600	1.73503500
H	1.87863300	0.11160300	1.73802400
H	–3.81370400	–5.62251200	1.00773500
H	0.47897700	–3.43599300	2.01881700
H	5.07556200	–0.94754700	1.53207700
H	0.49804000	–1.67570100	2.05881800
H	4.57860300	0.69211200	1.10376000
H	6.06049200	0.01790900	0.44102400
H	–0.28949400	4.20443400	0.26954600
H	2.55879700	1.12752700	0.49912600
H	2.12989300	–4.76466200	0.91931400
H	0.01742100	–2.52298500	0.58096100
H	3.42335000	–4.09238100	–0.07587600
H	5.14403400	–2.77814000	–0.26457600
H	–0.04198100	5.90643900	–1.48560800
H	–3.24583200	–5.32005300	–1.38964300
H	1.75269500	–4.01747300	–0.64392200
H	3.85994600	1.24143500	–1.34176000
H	6.02289600	–1.74821100	–1.39135100
H	5.41497700	0.55978200	–1.82211300
H	4.48602000	–2.47243800	–1.88470900
H	–2.53515700	–3.11597100	–2.22514600
H	–5.11146100	–0.99305000	–1.72628500
H	3.91476000	–0.03708100	–2.55953600

H	–1.61572500	–0.63883800	–2.34804500
H	1.08161400	1.18114100	–2.47245800
H	–5.61919700	0.56611800	–2.38691200
H	0.76481900	5.26534700	–3.74405000
H	–4.29183600	–0.31800400	–3.14181200
H	1.32116000	2.89344600	–4.22419700
O	–1.13450700	0.26904300	0.03324600
P	2.44377100	–1.15166000	–0.24013000
S	1.53331400	–1.51509400	–1.97922300
Si	0.15594600	1.23778200	0.37540400
Si	–2.22884800	–0.43378200	–1.01326500
C	–3.34276100	2.00149900	–1.93600800
C	–4.46943700	1.00454100	0.07986900
H	–3.81809900	1.55769900	0.76229400
H	–5.35308500	1.62925300	–0.10386700
H	–4.81184400	0.09959200	0.59065000
H	–2.84924600	1.82383100	–2.89634700
H	–4.22727300	2.62169500	–2.12974300
H	–2.65969700	2.58839900	–1.31713200
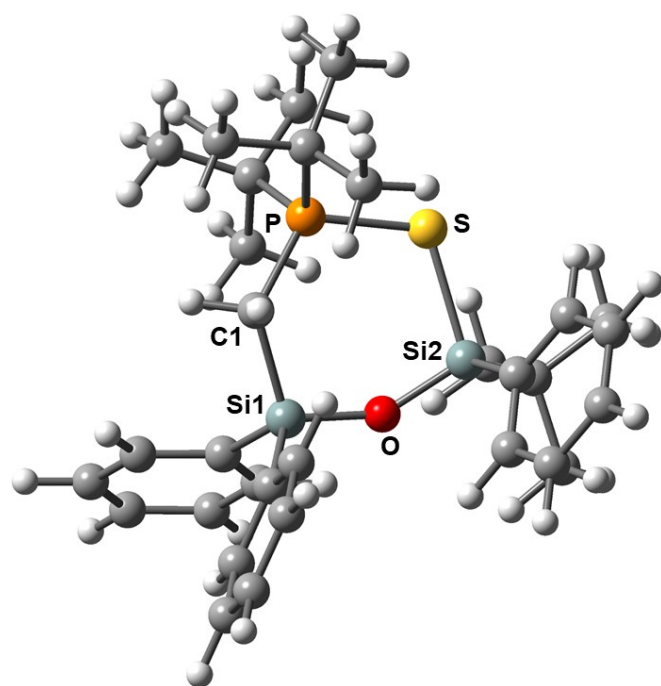
Figure S203. Optimized structure of compound **7-Cat-S** [B3LYP/6-311+G(d,p)]. Selected bond lengths [Å] and angles [°]: P–S 2.108, Si1–O 1.663, Si2–O 1.647, Si1–O–Si2 144.5, Si2–S 2.259.

Table S16. Standard orientation of **7-Cat-S** [B3LYP/6-311+G(d,p)].

Atomic symbol	x	y	z
Si	–1.04309400	1.12388600	–0.21645900
O	0.08144400	0.84073500	0.97601000
Si	1.38221900	–0.07576000	1.40185400

C	–1.01843700	–0.42487400	–1.37261000
C	–2.71859100	1.37230500	0.57318800
P	–0.45501200	–2.10197500	–0.89541400
C	–0.57798200	2.59138500	–1.28541800
C	1.53590000	–0.24143700	3.28812400
C	2.93065900	0.53455400	0.55142700
S	0.93841900	–2.17104500	0.68459500
C	–1.95406500	–3.09028100	–0.25987600
C	0.43981400	–2.81506200	–2.42213000
C	–1.51200900	–4.42232700	0.37682800
C	–2.62631400	–2.22248400	0.82236200
C	–2.95514900	–3.36699200	–1.39929700
C	1.73309600	–1.99873300	–2.62969900
C	–0.44538500	–2.68115100	–3.67890100
C	0.81015600	–4.29135100	–2.19037000
C	–3.87401600	1.47774100	–0.22181900
C	–5.12572800	1.68240400	0.35348900
C	–5.24489800	1.79498500	1.73877300
C	–4.11033100	1.70592300	2.54258200
C	–2.85941300	1.49574100	1.96387200
C	0.46958000	2.53272900	–2.22222200
C	0.81769900	3.64223600	–2.98729500
C	0.12358900	4.84170200	–2.82959500
C	–0.91348900	4.92570200	–1.90352400
C	–1.26061800	3.81189100	–1.14059600
C	3.05758200	1.90050700	0.24447500
C	4.23775600	2.40443700	–0.29972600
C	5.31227800	1.55268200	–0.54705300
C	5.20457100	0.19418100	–0.25047200
C	4.02555000	–0.30880800	0.29378900
C	0.23118100	–0.76294800	3.92181600
C	1.84503900	1.17382700	3.83589300
C	2.70008600	–1.19123200	3.64556500
H	–0.40216600	–0.14647700	–2.22962200
H	–2.40367400	–4.91135800	0.77892700
H	–1.05892200	–5.10787300	–0.33781000
H	–0.81908800	–4.26973900	1.20439000
H	–3.44947100	–2.79897800	1.25331400
H	–3.04818900	–1.29911100	0.42629200
H	–1.93880200	–1.97440200	1.63261500
H	–2.58100500	–4.10317400	–2.11134600
H	–3.86375700	–3.78160400	–0.95404300
H	–3.25077900	–2.46803100	–1.94512800
H	2.22846300	–2.37955000	–3.52701000
H	2.42515600	–2.10010400	–1.79455900
H	1.54603800	–0.93557500	–2.79570800
H	0.12295300	–3.06574400	–4.53040400

H	−1.36564100	−3.25996700	−3.61756100
H	−0.70133400	−1.64502100	−3.90739800
H	1.36296400	−4.43926800	−1.26040100
H	−0.06378800	−4.94329900	−2.19167800
H	1.45679400	−4.61570900	−3.01039000
H	−3.80470700	1.41448600	−1.30449600
H	−6.00480400	1.76245800	−0.27577100
H	−6.21774800	1.95855100	2.18795400
H	−4.19891500	1.80227100	3.61874600
H	−1.98370600	1.43276300	2.59943300
H	1.04170000	1.61930100	−2.35346800
H	1.62856600	3.57363900	−3.70356900
H	0.39121300	5.70610600	−3.42646000
H	−1.45425400	5.85641600	−1.77590100
H	−2.07463700	3.89649900	−0.42935500
H	2.23200100	2.57917900	0.42741400
H	4.31722200	3.46114700	−0.52803300
H	6.23133900	1.94503100	−0.96714900
H	6.03906300	−0.47114100	−0.44066200
H	3.96446500	−1.36932400	0.51593700
H	0.33632700	−0.77973400	5.01204900
H	−0.00223800	−1.78104500	3.60027800
H	−0.62426200	−0.12572100	3.68545700
H	1.95867700	1.12206000	4.92421500
H	2.77475000	1.58074400	3.42954100
H	1.04002400	1.88288500	3.62338800
H	2.52631300	−2.21280800	3.29300300
H	3.65495600	−0.84594500	3.24131500
H	2.80655900	−1.24138700	4.73457400
H	−2.03114800	−0.55825000	−1.76632900
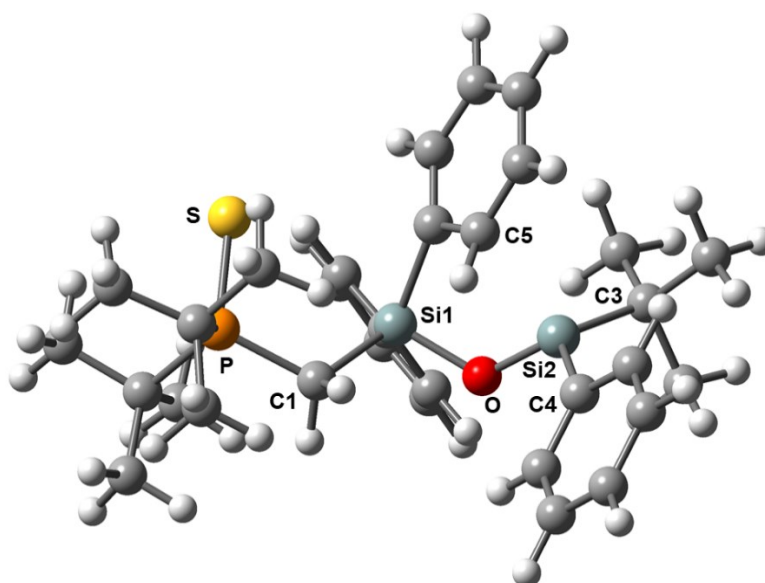
Figure S204. Optimized structure of compound **7-Cat-Ar** [B3LYP/6-311+G(d,p)]. Selected bond lengths [Å] and angles [°]: P–S 2.012, Si1–O 1.721, Si2–O 1.638, Si1–O–Si2 124.3, Si2–C5 2.285, O–Si2–C3 116.2, O–Si2–C4 110.6, C3–Si2–C4 118.4 (Σ angles around Si2: 345.2°).

Table S17. Standard orientation of **7-Cat-Ar** [B3LYP/6-311+G(d,p)].

Atomic symbol	x	y	z
C	−1.37590900	5.09961900	−1.48368600
C	−1.94295900	4.57391300	−0.32369200
C	−0.49863700	4.32356700	−2.23831900
C	−1.63952200	3.27573000	0.08011200
C	−0.18232000	3.03026900	−1.82710600
C	−0.74838800	2.48130500	−0.66139300
C	−2.68086400	−3.73618400	−0.53381700
C	3.13001600	−3.35904000	−2.53692600
C	2.67661700	−2.14539000	−2.02543100
C	4.18180700	−4.02952800	−1.91514700
C	−1.70206400	−2.96605900	1.64008900
C	−4.49128600	−1.41066100	−2.20055000
C	−2.88077100	−2.78342000	0.66108200
C	−1.33973900	−0.68550000	−0.80626400
C	−4.18801200	−3.12915400	1.39804300
C	0.43168400	1.43998700	2.59492800
C	3.28148000	−1.57472700	−0.89000000
C	4.78413200	−3.48443500	−0.78145300
C	−4.34639300	−0.45597500	−1.00195700
C	0.53781000	0.54083700	1.53457600
C	1.25129000	1.32417100	3.71840700
C	4.34128200	−2.26591100	−0.27506300
C	−5.65836000	−0.41358800	−0.19521400
C	3.87231100	1.48822000	−0.06342900
C	−4.05443600	0.96761000	−1.51914100

C	1.53299300	–0.48592700	1.63560000
C	2.21008900	0.30768300	3.82336000
C	5.09035100	1.08996600	0.79352500
C	2.33615800	–0.61286600	2.79895300
H	–1.61910900	6.10774200	–1.79939300
H	–2.63025200	5.17241700	0.26345400
H	–0.05869300	4.72458000	–3.14441200
H	–2.12022400	2.86846900	0.96149500
H	2.66417800	–3.78001000	–3.42045100
H	–2.56644900	–4.75352100	–0.14672100
H	–1.78066000	–3.51190000	–1.11136200
H	0.51146000	2.44393100	–2.41940000
H	–3.52850600	–3.74658600	–1.21642400
H	1.85672300	–1.63156200	–2.51442700
H	–0.74380200	–1.60014200	–0.75825200
H	4.53226000	–4.97509100	–2.31243700
H	–1.70174800	–4.00313400	1.98814900
H	–4.88303500	–2.38497000	–1.90866500
H	–0.73412400	–2.78788300	1.16342300
H	–3.55532700	–1.56058300	–2.74544700
H	–5.20653900	–0.97563800	–2.90519400
H	–0.29520000	2.24100700	2.55269400
H	–1.55610300	–0.52033500	–1.86549700
H	–4.08330200	–4.11671400	1.85709100
H	–1.78968700	–2.31007600	2.50588600
H	–5.04096300	–3.17703000	0.72009300
H	–5.98287400	–1.40053200	0.13311400
H	1.14561500	2.03933000	4.52690000
H	5.60025400	–4.00654900	–0.29579600
H	–4.40803300	–2.41295600	2.19225000
H	–3.16877500	1.01824700	–2.15578300
H	–6.44535000	–0.00578600	–0.83657600
H	–4.90575800	1.29134000	–2.12492500
H	–5.56840400	0.23063000	0.68062600
H	4.82884700	–1.86155600	0.60482300
H	5.65060400	0.25865500	0.36054200
H	–3.93529400	1.67818800	–0.70150700
H	1.40016700	–1.39699000	1.05013100
H	5.77547200	1.94213700	0.85213300
H	2.82384500	0.22901400	4.71248700
H	4.80995300	0.82943000	1.81760300
H	3.02140800	–1.44845500	2.88864300
P	–2.90061000	–0.93635100	0.15286000
S	–2.84599700	0.25736900	1.77176700
Si	–0.24950900	0.74235500	–0.19583900
Si	2.64071300	0.06237200	–0.28580600
C	3.20519100	2.74557000	0.52495100

C	4.34175700	1.78337300	−1.51598700
H	3.52101400	2.11640400	−2.15660300
H	5.08147900	2.59048900	−1.48517400
H	4.82047800	0.91992500	−1.98598400
H	2.90521900	2.59941200	1.56381200
H	3.92375300	3.57193900	0.50312100
H	2.32935600	3.06108200	−0.04600900
O	1.22781600	0.43676200	−1.02431200
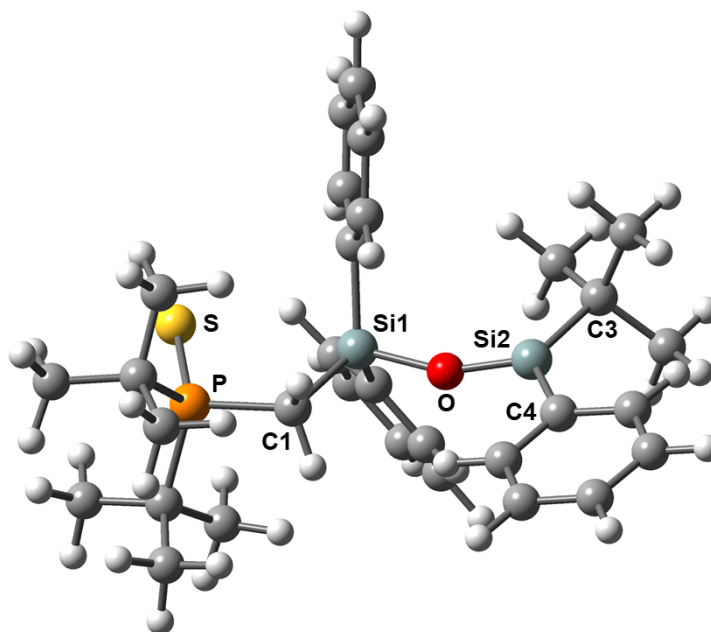
Figure S205. Optimized structure of compound **7-Cat-free** [B3LYP/6-311+G(d,p)]. Selected bond lengths [Å] and angles [°]: P–S 2.001, Si1–O 1.767, Si2–O 1.582, Si1–O–Si2 157.0, O–Si2–C3 122.1, O–Si2–C4 113.5, C3–Si2–C4 124.4 (Σ angles around Si2: 360.0°).

Table S18. Standard orientation of **7-Cat-free** [B3LYP/6-311+G(d,p)].

Atomic symbol	x	y	z
C	0.34765400	−3.86822200	−3.35071400
C	1.08151800	−4.06009200	−2.18194600
C	−0.41407600	−2.71148900	−3.50279600
C	1.05552400	−3.10301200	−1.16958100
C	−0.45031600	−1.76366700	−2.48203200
C	0.27876700	−1.93877300	−1.29117100
C	3.06785800	3.43929100	0.94747200
C	−3.07990100	4.21620700	−1.04253200
C	−2.66274900	2.91373900	−0.80163100
C	−4.43861900	4.53225300	−0.99594900
C	2.97148200	1.61027100	2.65806900
C	3.72804300	2.37329100	−2.21639200
C	3.56923900	2.02464100	1.29733700
C	1.20373000	0.94965400	−0.19059500

C	5.10452600	2.02573500	1.41799600
C	0.13705900	−2.47666700	2.27588100
C	−3.60540400	1.90320600	−0.51253300
C	−5.38432200	3.54657200	−0.71043900
C	3.81458100	0.92521500	−1.70433800
C	−0.07062800	−1.16274100	1.83050700
C	−0.10910100	−2.83431400	3.59968200
C	−4.97491800	2.24078100	−0.47159800
C	5.28431900	0.46448400	−1.66347300
C	−4.11500500	−1.27833600	0.12634500
C	3.05129300	−0.00310200	−2.67084500
C	−0.53783100	−0.22006200	2.76388200
C	−0.56734400	−1.88390600	4.51049400
C	−4.91702900	−1.01192500	1.42761200
C	−0.78192400	−0.57255600	4.09049400
H	0.37604600	−4.60977200	−4.14082400
H	1.68669400	−4.95124100	−2.06079600
H	−0.97500500	−2.54531300	−4.41577800
H	1.67386500	−3.25096500	−0.29432000
H	−2.35097500	4.98590200	−1.26631500
H	3.36642300	4.11829300	1.75232000
H	1.97882800	3.49475400	0.87435800
H	−1.04619700	−0.86911000	−2.63204500
H	3.49218700	3.82846400	0.02370000
H	−1.60770300	2.67080300	−0.83870500
H	0.86146600	1.67806100	0.54905200
H	−4.76197200	5.54969600	−1.18321000
H	3.27715600	2.34762500	3.40668700
H	4.40029700	3.04329000	−1.67956200
H	1.87884700	1.58713000	2.64914400
H	2.71525800	2.78289000	−2.16588600
H	4.03045000	2.39037700	−3.26816200
H	0.49882000	−3.23298000	1.59099200
H	0.99240700	1.37993100	−1.17324700
H	5.38895000	2.63013100	2.28465600
H	3.32625400	0.62883800	2.97157700
H	5.58853700	2.46485900	0.54425100
H	5.91211000	1.11161400	−1.05193800
H	0.06341700	−3.85492700	3.92167200
H	−6.43755200	3.79760600	−0.67555000
H	5.49824900	1.01884100	1.57167500
H	2.01732700	0.30910300	−2.83208400
H	5.68224500	0.48676300	−2.68270600
H	3.55170100	0.02687500	−3.64330100
H	5.37073400	−0.55555200	−1.28672100
H	−5.72470000	1.49061900	−0.25291200
H	−5.55464000	−0.12713500	1.36697100

H	3.05279700	−1.03642300	−2.32279600
H	−0.70354600	0.81238500	2.46695500
H	−5.56929700	−1.87194000	1.61090200
H	−0.75091700	−2.16202500	5.54191800
H	−4.26524100	−0.90713300	2.29910400
H	−1.12884600	0.17504300	4.79515700
O	−1.42504300	0.07483800	−0.27832400
P	3.02897000	0.69700500	0.02786200
S	3.35231900	−1.15204100	0.72213700
Si	0.16543300	−0.62409200	0.04681800
Si	−3.00044200	0.20590100	−0.20605100
C	−3.26608000	−2.55578000	0.29276500
C	−5.08208300	−1.44993900	−1.07483900
H	−4.55012100	−1.66432400	−2.00584700
H	−5.73378600	−2.30538800	−0.86998800
H	−5.72461800	−0.58258800	−1.23997900
H	−2.58414800	−2.49087600	1.14215900
H	−3.94234900	−3.39776100	0.47210900
H	−2.68021300	−2.78542900	−0.59975300
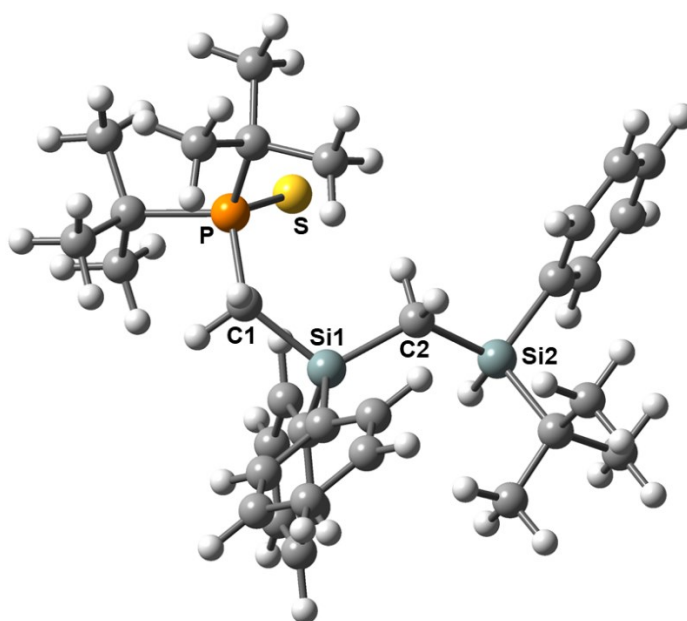
Figure S206. Optimized structure of compound **6-C** [B3LYP/6-311+G(d,p)]. Selected bond lengths [Å] and angles [°]: P–S 1.999, Si1–C2 1.886, Si2–C2 1.902, Si1–C2–Si2 123.4.

Table S19. Standard orientation of **6-C** [B3LYP/6-311+G(d,p)].

Atomic symbol	x	y	z
C	−0.33336400	4.79838200	−2.98942500
C	−1.04211000	4.83558500	−1.78918000
C	0.42804600	3.67492800	−3.30168800
C	−0.98420600	3.75551100	−0.91063700
C	0.48057200	2.59800000	−2.41604400

C	–0.21838800	2.61086900	–1.19888700
C	–3.99383000	–1.27888100	–2.65892200
C	3.79555200	–4.03523600	–1.24965100
C	3.30707000	–2.73669500	–1.11566500
C	4.37652700	–4.67814100	–0.15750900
C	–1.55723700	–1.84755900	–2.47156800
C	–5.29577100	0.18655300	0.12541500
C	–2.93367600	–1.97546600	–1.78683700
C	–2.09169600	0.50085400	–0.32661300
C	–3.26639900	–3.47510800	–1.66935900
C	0.43655800	2.92904400	2.08636800
C	3.38724500	–2.04477600	0.10456700
C	4.46250200	–4.01544500	1.06508600
C	–4.44806700	–0.89993000	0.81607900
C	–0.10544800	1.67483500	1.75836000
C	0.59464600	3.32683300	3.41390300
C	3.97259100	–2.71575300	1.19074900
C	–5.24517900	–2.21488100	0.88335600
C	4.05722400	0.97242200	–0.37971200
C	–4.14012700	–0.44085200	2.25652100
C	–0.47501200	0.82789900	2.81869400
C	0.21505700	2.47439800	4.44841400
C	5.39385700	0.70155100	0.34508600
C	–0.31792000	1.22239700	4.14631800
H	–0.37485500	5.63802100	–3.67447000
H	–1.63813100	5.70610700	–1.53676200
H	0.98385100	3.63630800	–4.23239900
H	–1.54297600	3.81191200	0.01843800
H	3.71946300	–4.54689700	–2.20329600
H	–3.91807300	–1.66910600	–3.67953000
H	–3.85635300	–0.19634900	–2.71771000
H	1.08276000	1.73743100	–2.68600800
H	–5.00868700	–1.48078700	–2.31376600
H	2.85102800	–2.26265100	–1.97958900
H	–2.35163200	0.77718200	–1.35227900
H	4.75363000	–5.69005300	–0.25781000
H	–1.60220400	–2.35607300	–3.44023400
H	–5.58257300	–0.07745600	–0.89127800
H	–1.27850000	–0.80911800	–2.66240000
H	–4.79534000	1.15645400	0.09752800
H	–6.21903800	0.31887000	0.69960100
H	0.74428600	3.60960900	1.30051900
H	–2.68000500	1.16852900	0.30826500
H	–3.22453400	–3.92084700	–2.66885200
H	–0.77277300	–2.31946500	–1.87883300
H	–4.26559000	–3.65382600	–1.27149700
H	–5.63106300	–2.51297400	–0.09340200

H	1.01498200	4.30147300	3.63832200
H	4.90523200	–4.51167000	1.92214900
H	–2.54767500	–3.99039600	–1.03117500
H	–3.55775000	0.48345400	2.28964300
H	–6.10657900	–2.07395100	1.54458600
H	–5.08818900	–0.25063000	2.77047400
H	–4.64041500	–3.02918500	1.28740200
H	4.04068100	–2.22016200	2.15425800
H	5.76881500	–0.30674900	0.15084600
H	–3.59265100	–1.20507400	2.80820400
H	2.63835400	–0.02578600	1.76786500
H	–0.87618900	–0.15853500	2.60781600
H	6.15668300	1.41211900	0.00176800
H	0.33711100	2.78173000	5.48147100
H	5.29916400	0.82265500	1.42893100
H	–0.60821300	0.54786500	4.94480400
P	–2.75053700	–1.20494400	–0.03669600
S	–1.59595400	–2.37721500	1.09857100
Si	–0.27263700	1.09921600	–0.04131600
Si	2.74967500	–0.26902400	0.30408800
C	3.62727700	2.42402500	–0.08680600
C	4.26894300	0.79209600	–1.89570900
H	3.35585500	0.98693200	–2.46634600
H	5.03139900	1.49396000	–2.25735100
H	4.61158400	–0.21733200	–2.14079200
H	3.46596300	2.59066700	0.98235600
H	4.41090400	3.12010200	–0.41363600
H	2.71053300	2.70139600	–0.61280700
C	1.02687900	–0.18925800	–0.49761300
H	1.12760300	–0.23591500	–1.58788100
H	0.57217000	–1.14410400	–0.20318100
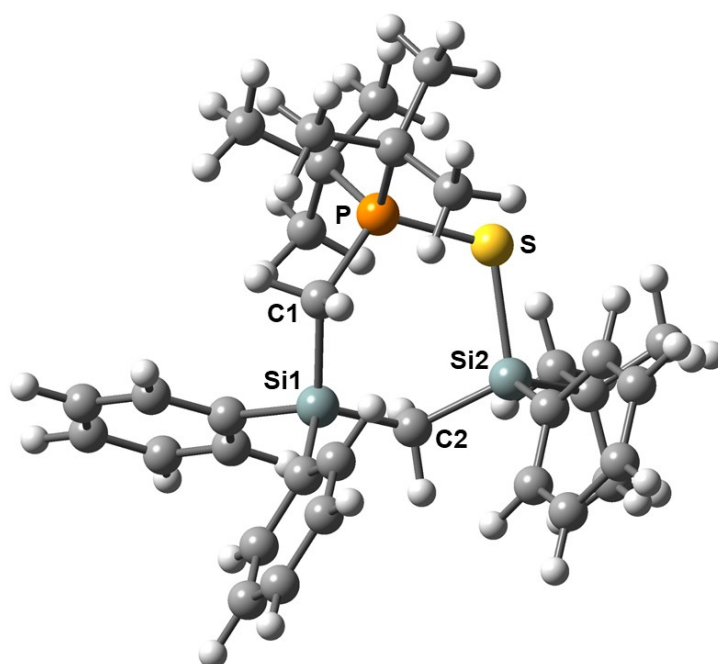
Figure S207. Optimized structure of compound **7-C-Cat-S** [B3LYP/6-311+G(d,p)]. Selected bond lengths [Å] and angles [°]: P–S 2.104, Si1–C2 1.890, Si2–C2 1.880, Si1–C2–Si2 121.6, Si2–S 2.257.

Table S20. Standard orientation of **7-C-Cat-S** [B3LYP/6-311+G(d,p)].

Atomic symbol	x	y	z
Si	−1.20929000	1.02389100	0.14401600
Si	1.65108700	−0.07633900	1.34580300
C	−1.00193500	−0.37951800	−1.17575700
C	−2.99181100	1.02768700	0.76621400
P	−0.33669300	−2.05635400	−0.90177900
C	−0.91831200	2.63580300	−0.79706200
C	2.47163300	−0.53729400	3.02172400
C	2.82957400	0.85983500	0.22197300
S	1.25533800	−2.11974800	0.47183900
C	−1.68076100	−3.18877100	−0.16832400
C	0.37143900	−2.61557100	−2.58656400
C	−1.08426900	−4.53942200	0.27632000
C	−2.25293400	−2.47652500	1.07292300
C	−2.81236200	−3.42457600	−1.18792500
C	1.62259000	−1.76250800	−2.88161500
C	−0.66433600	−2.38339300	−3.70765800
C	0.78412300	−4.09827500	−2.54600400
C	−4.04831900	1.06972400	−0.16215100
C	−5.37697100	1.10537800	0.25291300
C	−5.68145600	1.11041200	1.61413900
C	−4.65230000	1.08417500	2.55202400
C	−3.32310600	1.04290600	2.13029600
C	−0.00818400	2.76791000	−1.85900900
C	0.17658100	3.98631300	−2.50922600

C	–0.54250200	5.10906400	–2.10422100
C	–1.44476500	5.00612300	–1.04736500
C	–1.63267000	3.78323000	–0.40633400
C	2.78677300	2.26410200	0.17411800
C	3.73328400	2.98958100	–0.54749200
C	4.74208300	2.32487200	–1.24063700
C	4.80186100	0.93182100	–1.20938900
C	3.85748600	0.20995000	–0.48413000
C	1.49081600	–1.28945600	3.94446200
C	2.88215200	0.79324500	3.69809600
C	3.73395200	–1.39867300	2.80584200
H	–0.36194900	0.04187800	–1.95403200
H	–1.88304300	–5.11363800	0.75406900
H	–0.70680900	–5.13561400	–0.55219400
H	–0.28628600	–4.41366800	1.00901100
H	–2.97501500	–3.14997600	1.54293000
H	–2.78198700	–1.55649000	0.82740200
H	–1.48034100	–2.26104300	1.81329500
H	–2.49847400	–4.05322900	–2.02120900
H	–3.62247500	–3.95052700	–0.67515300
H	–3.23523300	–2.49764300	–1.58167400
H	1.99120300	–2.04171100	–3.87247000
H	2.41932300	–1.94321600	–2.16185400
H	1.41781700	–0.69022100	–2.90691500
H	–0.21099300	–2.70027300	–4.65113200
H	–1.57659800	–2.96384000	–3.57809100
H	–0.93332400	–1.33165100	–3.81921400
H	1.44476900	–4.32317500	–1.70599700
H	–0.07446200	–4.76917300	–2.51288700
H	1.33473400	–4.32499600	–3.46322200
H	–3.83948900	1.09495800	–1.22818700
H	–6.17322200	1.13885700	–0.48209300
H	–6.71466700	1.14231300	1.94022400
H	–4.88225400	1.09884100	3.61136300
H	–2.54321300	1.02739300	2.88418500
H	0.58585700	1.92186100	–2.18867000
H	0.88189700	4.05890600	–3.32933900
H	–0.40210800	6.05725500	–2.61045700
H	–2.00914700	5.87459600	–0.72733100
H	–2.35565200	3.72366800	0.40010800
H	2.01004000	2.80933800	0.69875600
H	3.67996000	4.07196900	–0.56806500
H	5.48010300	2.88824800	–1.80010000
H	5.58715100	0.40979600	–1.74440600
H	3.92743100	–0.87231600	–0.46722000
H	1.98738200	–1.52122400	4.89303400
H	1.15725200	–2.23612100	3.51145100

H	0.60699100	–0.69189200	4.18492600
H	3.35450700	0.57694400	4.66268000
H	3.60294000	1.35695000	3.10058700
H	2.02304800	1.44060200	3.89979800
H	3.50269100	–2.37340700	2.36599200
H	4.46909900	–0.90084600	2.16881800
H	4.21547500	–1.58827000	3.77162000
H	–1.98026300	–0.52624900	–1.64476700
C	–0.00656500	0.77860500	1.58171000
H	0.18739600	1.76625000	2.01786700
H	–0.52496500	0.20481900	2.35701200
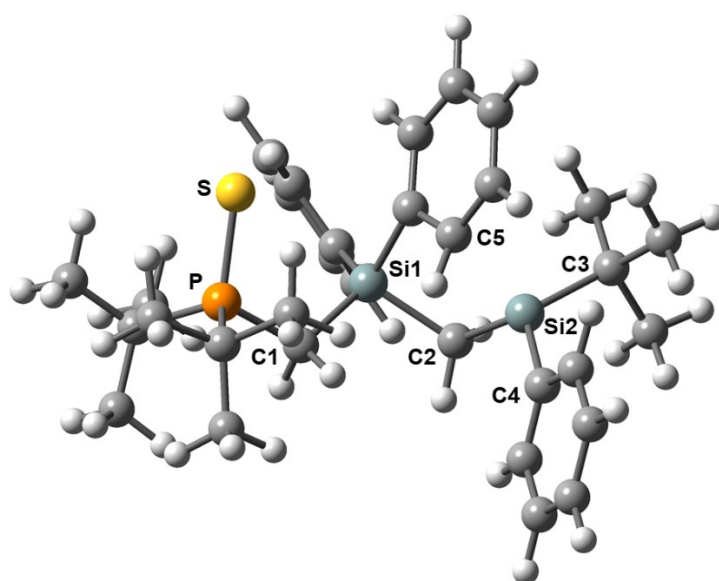
Figure S208. Optimized structure of compound **7-C-Cat-Ar** [B3LYP/6-311+G(d,p)]. Selected bond lengths [Å] and angles [°]: P–S 2.007, Si1–C2 1.915, Si2–C2 1.882, Si1–C2–Si2 109.9, Si2–C5 2.219, C2–Si2–C3 114.2, C2–Si2–C4 114.2, C3–Si2–C4 114.7 (Σ angles around Si2: 343.1°).

Table S21. Standard orientation of **7-C-Cat-Ar** [B3LYP/6-311+G(d,p)].

Atomic symbol	x	y	z
C	–2.66061000	4.99794700	–1.25060200
C	–2.90661900	4.28615000	–0.07744600
C	–1.75588700	4.49867800	–2.18465700
C	–2.25092000	3.08080200	0.16201300
C	–1.09064300	3.29890800	–1.93780800
C	–1.32162800	2.56558800	–0.76055300
C	–1.99121400	–3.89825800	–0.82098300
C	3.64422400	–3.11250900	–2.47472900
C	3.10803700	–1.88034400	–2.10401000
C	4.41868700	–3.83680200	–1.57216900
C	–0.90479000	–3.17930800	1.31382000
C	–4.47318200	–1.90228800	–1.90257800
C	–2.20943400	–3.12309600	0.49347000

C	–1.30004900	–0.65158300	–0.91828000
C	–3.33153300	–3.78433200	1.31523900
C	0.33276200	1.87713700	2.25857700
C	3.34321500	–1.33935200	–0.82677000
C	4.66148200	–3.32225300	–0.29898500
C	–4.30098100	–0.99580500	–0.67093700
C	0.43918000	0.90478200	1.26237100
C	1.12501700	1.81948900	3.40333200
C	4.13332900	–2.08741200	0.06635600
C	–5.45687800	–1.22767200	0.32151900
C	3.98772200	1.69581800	–0.07739900
C	–4.34336700	0.47850600	–1.11775600
C	1.45658400	–0.09829100	1.41993100
C	2.06282900	0.79333000	3.59835600
C	5.06740900	1.25750300	0.92999700
C	2.21413700	–0.17393700	2.62723900
H	–3.17430500	5.93401900	–1.43743600
H	–3.61628200	4.66571500	0.64907400
H	–1.56564800	5.04253700	–3.10289500
H	–2.48461100	2.52209100	1.06150400
H	3.45682500	–3.50402800	–3.46792800
H	–1.66338800	–4.91214500	–0.57086200
H	–1.21234800	–3.45804000	–1.44842600
H	–0.38907900	2.93683500	–2.68231600
H	–2.89598700	–3.99184400	–1.41799200
H	2.51296500	–1.33905100	–2.83095400
H	–0.54272900	–1.43635600	–0.99894600
H	4.83394500	–4.79594700	–1.85875900
H	–0.69003600	–4.22550200	1.55043700
H	–4.64504600	–2.94365400	–1.62958500
H	–0.04702700	–2.80053100	0.75024500
H	–3.62470700	–1.85788400	–2.59051600
H	–5.35429400	–1.56730700	–2.45841400
H	–0.38742900	2.67873300	2.15643500
H	–1.70270300	–0.52982000	–1.92906400
H	–3.00115700	–4.77937400	1.62817300
H	–0.98792600	–2.62256700	2.24728600
H	–4.24377000	–3.91605300	0.73233900
H	–5.54579400	–2.26847400	0.63118600
H	1.00726900	2.58063100	4.16725300
H	5.26647000	–3.88039700	0.40618800
H	–3.56732100	–3.21157200	2.21439200
H	–3.59194800	0.71933600	–1.87234400
H	–6.39397800	–0.94933800	–0.16993300
H	–5.32284700	0.67257900	–1.56466800
H	–5.34508200	–0.61176900	1.21486900
H	4.35079200	–1.70792100	1.05835600

H	5.57790300	0.34431800	0.61625400
H	–4.21981800	1.15947600	–0.27640200
H	1.29928900	–1.05186200	0.91308400
H	5.82780300	2.04218400	1.00737700
H	2.64189900	0.75252900	4.51280800
H	4.66068400	1.10259400	1.93210900
H	2.88904300	–1.00745000	2.78321200
P	–2.62850600	–1.26885200	0.22217200
S	–2.56051500	–0.25503500	1.95345800
Si	–0.38630500	0.96500700	–0.46299900
Si	2.65984200	0.35367100	–0.38947100
C	3.36382100	3.03089800	0.37421800
C	4.65136500	1.88524600	–1.46894500
H	3.94453600	2.22823600	–2.23000300
H	5.43025500	2.65090300	–1.38594800
H	5.13002300	0.97120700	–1.83056300
H	2.92297200	2.96010900	1.36955600
H	4.14436700	3.79847000	0.41359500
H	2.59421300	3.39323500	–0.31285900
C	1.23452500	0.91606500	–1.48223100
H	1.47041100	1.92824200	–1.82375100
H	1.14038700	0.29510700	–2.37609000
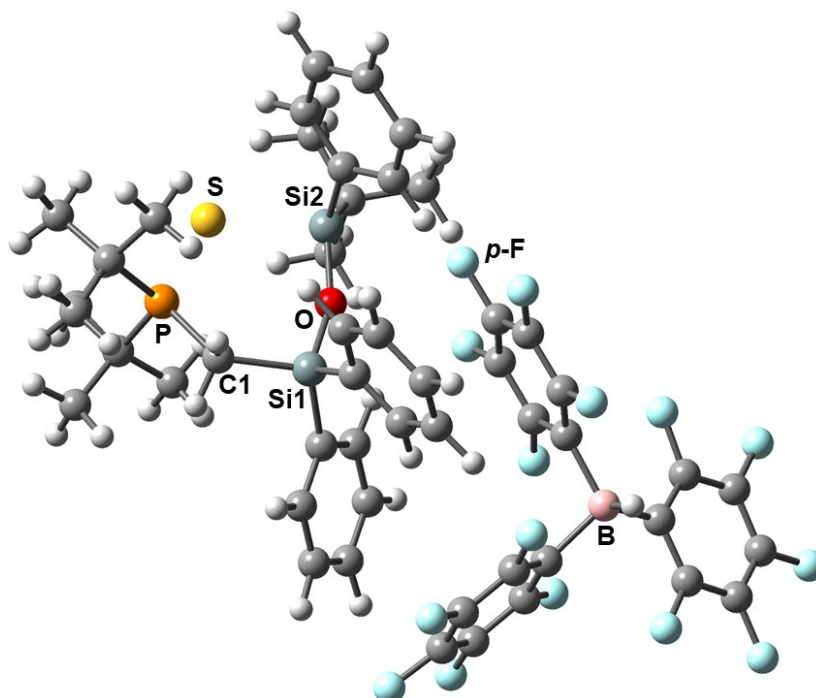
Figure S209. Optimized structure of compound **7**[HB(C$_6$F$_5$)$_3$] [HF/3-21G]. Selected bond lengths [Å]: Si1–O 1.665, Si2–O 1.639, Si2–S 2.435, Si2–(*p*-F) 2.913.

Table S22. Standard orientation of **7**[HB(C_6F_5)$_3$] [HF/3-21G].

Atomic symbol	x	y	z
Si	2.09023100	0.87740100	0.33003600
O	2.40753000	−0.56123300	−0.44641500
Si	3.34622400	−1.84049100	−0.86026100
C	3.78598800	1.81410500	0.45964200
C	0.84190600	1.88974500	−0.64859200
P	5.25545600	1.44529900	−0.62264600
C	1.51647300	0.61670700	2.10825000
C	3.04152300	−2.74898700	−2.51442000
C	3.96668800	−2.85289000	0.61183200
S	5.32800000	−0.57770700	−1.49654400
C	5.18949900	2.62271000	−2.13662000
C	6.79661400	1.53001500	0.51811200
C	6.28738400	2.26961100	−3.15580500
C	3.80937500	2.40709300	−2.79021400
C	5.33157300	4.09194500	−1.69842500
C	6.65870700	0.38699200	1.54683600
C	6.85673700	2.87857300	1.26123200
C	8.08028800	1.31612800	−0.30155700
C	0.52239800	3.18781800	−0.24524100
C	−0.47057500	3.90393800	−0.88517700
C	−1.15830400	3.33351300	−1.94564000
C	−0.84696900	2.05339600	−2.36243700
C	0.14822400	1.33683900	−1.71845300
C	2.37233000	0.12011200	3.09189200
C	1.92366100	−0.09014100	4.38105800
C	0.60528800	0.18707800	4.70812700
C	−0.26033000	0.67317100	3.74741000
C	0.19848600	0.88992700	2.45858500
C	3.14520400	−3.15867800	1.69724500
C	3.62811900	−3.91882400	2.75009800
C	4.92569800	−4.39274700	2.73382700
C	5.75177200	−4.10275000	1.66109800
C	5.27682100	−3.33750800	0.61352300
C	2.58460500	−1.75723500	−3.60595900
C	1.96329400	−3.85481600	−2.37078100
C	4.36013500	−3.43577900	−2.95596100
H	4.12326700	1.69179800	1.47982700
H	6.12049400	2.86950600	−4.04399700
H	7.27633800	2.49671300	−2.78546900
H	6.24558400	1.22669000	−3.43590400
H	3.74827100	3.04336900	−3.66634700
H	2.99420100	2.67166100	−2.13267700
H	3.68338600	1.38207100	−3.11078200
H	6.32205100	4.30721900	−1.32329800

H	5.16724600	4.71600100	–2.57013000
H	4.59988300	4.37707600	–0.95291100
H	7.54081200	0.39576600	2.17775200
H	6.59086000	–0.57699700	1.06460700
H	5.79806100	0.51729800	2.19047500
H	7.69110500	2.84072800	1.95364000
H	7.02519300	3.70791500	0.59026300
H	5.96068500	3.06964500	1.83774300
H	8.02532900	0.41334300	–0.89538600
H	8.28702400	2.15669500	–0.94902300
H	8.91159700	1.22000800	0.38847300
H	1.01650700	3.62756200	0.60222800
H	–0.75761600	4.87173200	–0.52658800
H	–1.97439600	3.86142300	–2.39403000
H	–1.40291000	1.59528300	–3.15548400
H	0.33802600	0.32933900	–2.01880200
H	3.38907500	–0.12862400	2.85155200
H	2.59194500	–0.47763100	5.12443800
H	0.25311000	0.01437200	5.70542800
H	–1.28702200	0.86781800	3.96937700
H	–0.48287300	1.26595900	1.72271000
H	2.13023800	–2.83188800	1.73453200
H	2.98140200	–4.14163000	3.57486000
H	5.29182800	–4.98562800	3.54837900
H	6.75887900	–4.46913800	1.64080600
H	5.93572600	–3.10578100	–0.19910900
H	2.45658600	–2.29755200	–4.53901900
H	3.31602300	–0.97475000	–3.76748000
H	1.63370100	–1.31019300	–3.34733000
H	1.94988600	–4.43054200	–3.29067400
H	2.18282300	–4.52903700	–1.55119000
H	0.98643300	–3.42902900	–2.22261300
H	5.16300400	–2.72518500	–3.11132200
H	4.68003400	–4.18116500	–2.23604000
H	4.18000700	–3.94270900	–3.89840300
H	3.57382100	2.87129700	0.33414200
F	0.73816900	–2.80290100	0.01112100
C	–0.49022000	–2.25047900	0.23757400
C	–1.00326300	–2.24395900	1.49847900
C	–1.18516300	–1.69621500	–0.80062500
C	–2.24118200	–1.67966900	1.71922400
C	–2.40430700	–1.12937200	–0.55532600
C	–2.97473400	–1.11161200	0.70165600
B	–4.42063100	–0.37158400	0.96863900
H	–4.74644900	–0.57743100	2.09990500
C	–5.64732000	–0.91112100	0.03700100
C	–6.84742300	–0.23071300	0.07712300

C	–5.64292100	–2.05896800	–0.71916000
C	–7.96524500	–0.64443500	–0.59447900
C	–6.74915600	–2.50030700	–1.40622200
C	–7.91341900	–1.78992400	–1.34537900
C	–4.13060700	1.24136400	0.82303800
C	–3.54864800	1.90715800	1.87887900
C	–4.36325500	1.99624200	–0.30665700
C	–3.19598900	3.23242400	1.82758300
C	–4.02007600	3.32195900	–0.38510200
C	–3.42905400	3.93946300	0.68144600
F	–0.62952300	–1.70645300	–2.04463700
F	–3.05510800	–0.56293800	–1.59757000
F	–2.69331600	–1.69798200	2.99165000
F	–0.26615800	–2.77534100	2.50256400
F	–4.53102300	–2.83532100	–0.81903400
F	–6.69277100	–3.63520500	–2.13956300
F	–9.00832400	–2.21318100	–2.01527300
F	–6.95172400	0.90144700	0.81850500
F	–9.11761300	0.05835500	–0.52618700
F	–4.20640700	4.02194600	–1.53161900
F	–4.92960300	1.44759400	–1.40614800
F	–3.26298100	1.24608400	3.03543400
F	–2.59779600	3.83412000	2.88115500
F	–3.02918400	5.23045600	0.58108300
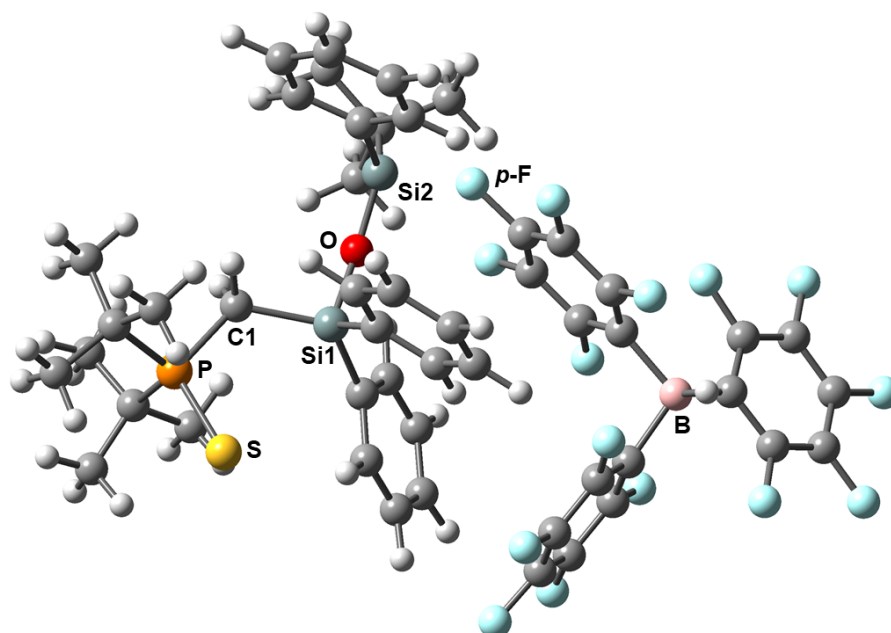
Figure S210. Optimized structure of compound **Int-1** [HF/3-21G]. Selected bond lengths [Å]: Si1–O 1.715, Si2–O 1.616, Si2–(*p*-F) 1.875.

229

Table S23. Standard orientation of **Int-1** [HF/3-21G].

Atomic symbol	x	y	z
Si	–2.47787900	–0.27449000	–0.27084100
O	–2.15104200	1.27878700	–0.92047500
Si	–2.07336600	2.89286300	–0.90607800
C	–4.35915400	–0.36575000	–0.65548600
C	–1.27980200	–1.44772200	–1.13867800
P	–5.34639400	–1.93080200	–0.38668000
C	–2.05185800	–0.13570400	1.56780600
C	–1.85783500	3.76223000	–2.57882400
C	–3.05773200	3.73646000	0.44998700
C	–6.99132900	–1.34674700	0.40910900
C	–5.53517300	–2.75632300	–2.10613600
C	–7.95570100	–2.54106600	0.52410200
C	–6.65102900	–0.85787900	1.83325700
C	–7.66471100	–0.19693200	–0.36247000
C	–4.11648500	–2.87962500	–2.69758900
C	–6.42056400	–1.94641900	–3.06739900
C	–6.10285400	–4.17949500	–1.93966400
C	–1.01205900	–2.71426700	–0.61502700
C	–0.02476200	–3.51034800	–1.16508100
C	0.70607400	–3.06111600	–2.25318700
C	0.43279100	–1.82181800	–2.80179200
C	–0.55117700	–1.02160700	–2.24540500
C	–2.90475400	0.44821600	2.50042600
C	–2.52002800	0.59816800	3.82014800
C	–1.26947800	0.16846500	4.23162800
C	–0.40431900	–0.41136200	3.32184500
C	–0.79901000	–0.56197200	2.00401200
C	–2.48759200	4.07339300	1.67540300
C	–3.25321000	4.66392100	2.66519700
C	–4.59484400	4.91708200	2.45085200
C	–5.17990500	4.57515500	1.24326100
C	–4.41670000	3.99102500	0.25155800
C	–1.72220200	2.73047200	–3.72218300
C	–0.59865200	4.66868100	–2.56346700
C	–3.09544000	4.65404200	–2.85808400
H	–4.48550100	–0.05302900	–1.68711600
H	–8.80749300	–2.24185900	1.12617400
H	–8.32824100	–2.84959100	–0.44335400
H	–7.47519000	–3.38337300	1.00556400
H	–7.57786700	–0.60559100	2.33843300
H	–6.03349600	0.03133000	1.81569900
H	–6.13673800	–1.62310800	2.39638200
H	–7.99814700	–0.49836700	–1.34377400
H	–8.53700400	0.12273200	0.19944200

H	–7.00975300	0.65968400	–0.46610700
H	–4.18685200	–3.40692900	–3.64328900
H	–3.46608500	–3.43975800	–2.04136000
H	–3.66404400	–1.91592000	–2.88851800
H	–6.36554600	–2.40460400	–4.04971700
H	–7.45722700	–1.95424800	–2.76094500
H	–6.09085800	–0.91810100	–3.16494300
H	–5.51643500	–4.74538100	–1.22930400
H	–7.13298100	–4.17317600	–1.61395700
H	–6.06017000	–4.67685900	–2.90339500
H	–1.56722500	–3.07119200	0.22836600
H	0.21202800	–4.45365400	–0.71700200
H	1.50945700	–3.65909900	–2.63316400
H	1.00274900	–1.46598900	–3.63688000
H	–0.72167800	–0.04813400	–2.65164200
H	–3.87631000	0.79126000	2.20525900
H	–3.19338700	1.04474400	4.52478100
H	–0.97144100	0.28350700	5.25470700
H	0.56981600	–0.74312000	3.61449500
H	–0.12411200	–1.02466000	1.31315900
H	–1.45985700	3.86546800	1.87872000
H	–2.79952600	4.91725800	3.60184200
H	–5.18396500	5.37441600	3.22030700
H	–6.22089000	4.76510300	1.07495400
H	–4.88827800	3.73757300	–0.67843700
H	–1.64797900	3.26412600	–4.66392000
H	–2.58268200	2.07292100	–3.77398900
H	–0.83472000	2.12779300	–3.60389200
H	–0.54885300	5.20081900	–3.50681900
H	–0.63718200	5.40464300	–1.76701700
H	0.30279300	4.08157800	–2.46363200
H	–4.00567600	4.06838400	–2.94297900
H	–3.23501900	5.40686200	–2.09211500
H	–2.94369600	5.15880200	–3.80566900
H	–4.81622100	0.40709200	–0.04634500
F	–0.38760400	3.10711800	–0.11467700
C	0.80596800	2.39363500	0.20692600
C	1.26492800	2.41946200	1.48556400
C	1.41817700	1.70823000	–0.80259900
C	2.41039300	1.69986200	1.75982400
C	2.54296600	1.00133900	–0.49088600
C	3.06637200	0.97574500	0.78944800
B	4.36368400	0.01671700	1.13611500
H	4.65766100	0.18764700	2.28047100
C	5.69013600	0.34723000	0.25348600
C	6.77111800	–0.50415600	0.35432600
C	5.88445500	1.46570900	–0.51910000

C	7.96336300	–0.27260500	–0.27503300
C	7.06928400	1.72667200	–1.16541700
C	8.11164400	0.85348500	–1.04360200
C	3.78915900	–1.51238900	0.98346700
C	2.99244100	–2.01541100	1.98792100
C	3.97284200	–2.33292500	–0.10794900
C	2.40332600	–3.25285600	1.92924700
C	3.38648500	–3.56964700	–0.19918600
C	2.60249400	–4.03017600	0.82184600
F	0.88480100	1.77170500	–2.04625800
F	3.14669700	0.31322000	–1.47995200
F	2.84896600	1.74483200	3.03212800
F	0.60801600	3.12705900	2.42660600
F	4.89727000	2.39090700	–0.67802700
F	7.20814400	2.84184400	–1.91720500
F	9.28238600	1.09691900	–1.67161900
F	6.66937800	–1.62267200	1.11380500
F	8.99483200	–1.13502100	–0.14906100
F	3.53286000	–4.32505400	–1.31358300
F	4.72749900	–1.93399300	–1.15778600
F	2.72065100	–1.25783600	3.08818400
F	1.61396600	–3.69184100	2.93307100
F	1.98335400	–5.22877000	0.70796000
S	–4.33626400	–3.27543600	0.95375800
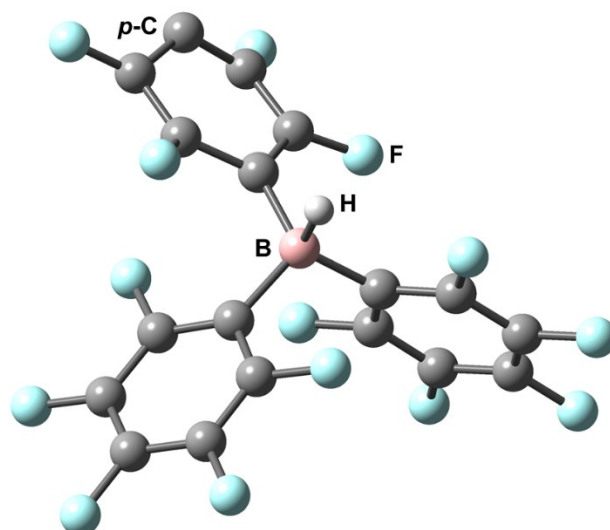
Figure S211. Optimized structure of compound **Int-2** [HF/3-21G].

Table S24. Standard orientation of **Int-2** [HF/3-21G].

Atomic symbol	x	y	z
C	–3.05523800	0.20672600	1.43430500
C	–4.07421000	–0.01852600	0.54251200
C	–1.77817700	0.31631400	0.95889900

C	2.39519100	–2.26929700	1.07757900
C	–3.80647500	–0.12548600	–0.79505400
C	1.81435100	–1.11040700	0.63124300
C	1.98401400	–3.46320300	0.54966100
C	–1.46896900	0.21056700	–0.37611600
C	–2.51091500	–0.00933500	–1.24235700
C	0.83631500	–1.08675900	–0.32932200
C	1.00806100	–3.48532700	–0.41365100
C	0.28576200	2.79999500	–0.12000700
C	1.14525100	3.86007300	0.16656500
C	0.45086400	–2.30684200	–0.83784200
C	0.84797400	1.62060100	–0.50798300
C	2.39965800	3.84113900	–0.40520800
C	2.28298400	1.66420600	–0.82455400
C	3.13700900	2.72651200	–0.60622300
B	0.06919500	0.24205000	–0.85146600
F	–3.32369700	0.32074600	2.75130000
F	–5.34083600	–0.12931900	0.98829600
F	3.35913600	–2.23991800	2.01944000
F	–0.76611900	0.55406400	1.83604400
F	2.26061800	0.06791700	1.16136000
F	–4.81580500	–0.34092300	–1.66333000
F	–1.00049300	2.94109000	0.23656100
F	0.81519800	4.79457600	1.03691400
F	0.60902800	–4.66319400	–0.93155100
F	–2.29109400	–0.11105900	–2.57055000
F	–0.51291400	–2.35773100	–1.78559100
F	2.75129500	0.68275500	–1.57505400
F	4.39884000	2.68263200	–1.04255300
H	0.14107500	0.28227700	–2.06101500
F	2.54042700	–4.61477200	0.97245600
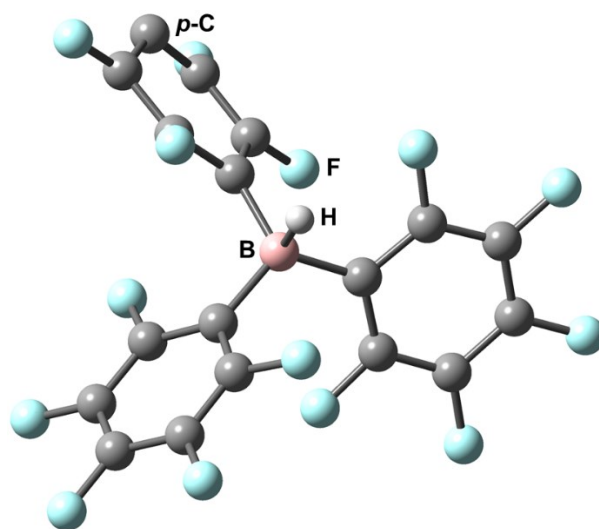
Figure 212. Optimized structure of compound **Int-2** [B3LYP/6-311+G(d,p)].

Table S25. Standard orientation of **Int-2** [B3LYP/6-311+G(d,p)].

Atomic symbol	x	y	z
C	–3.25343900	–1.21060700	–1.06387900
C	–3.56291800	–2.27591500	–0.22593100
C	–2.13380000	–0.43741700	–0.78991400
C	0.34945000	3.83927900	–0.88875800
C	–2.74488700	–2.55200000	0.86504300
C	0.71545200	2.50652100	–0.57859700
C	–0.60004700	4.51697300	–0.14970000
C	–1.27990100	–0.67489600	0.28722100
C	–1.63342600	–1.75510800	1.09932600
C	–0.11148300	1.75521300	0.22719700
C	–1.56107400	3.85077500	0.50675100
C	1.66558600	–1.57145900	–0.57502000
C	2.90897100	–2.14604800	–0.79502700
C	–1.17814500	2.50802400	0.82364300
C	1.46813300	–0.46667400	0.26204700
C	4.03071700	–1.61890800	–0.15976900
C	2.63276700	0.02606700	0.87093200
C	3.89174900	–0.51969800	0.68131900
B	0.04435100	0.19629200	0.60513200
F	–4.03104700	–0.94742900	–2.12012000
F	–4.63654400	–3.02836300	–0.46658800
F	0.79899000	4.35130900	–2.02039500
F	–1.86825300	0.56997400	–1.65547200
F	1.68778600	1.96240300	–1.31098100
F	–3.04139200	–3.57588200	1.67199600
F	0.63003300	–2.11934300	–1.23543400
F	3.04758000	–3.19283600	–1.61303400
F	–2.53456500	4.39863700	1.22950200
F	–0.87025100	–2.06771700	2.16243200
F	5.22914100	–2.15988400	–0.36249100
F	–1.69763700	2.05607800	1.94286400
F	2.55235300	1.09553800	1.68600300
F	4.96705400	–0.00667000	1.28737600
H	0.05676900	0.35145700	1.83211500
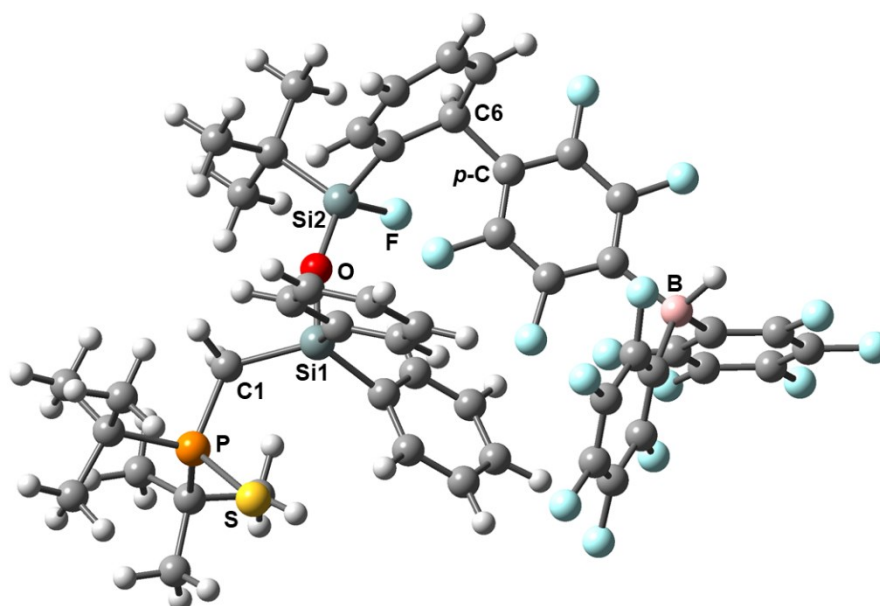
Figure S213. Optimized structure of compound **Int-3** [HF/3-21G]. Selected bond lengths [Å]: Si1–O 1.699, Si2–O 1.615, Si2–F 1.628, C6–(*p*-C) 1.552.

Table S26. Standard orientation of **Int-3** [HF/3-21G].

Atomic symbol	x	y	z
Si	–2.75798500	0.02738500	–0.13515500
O	–2.50254000	1.60885900	–0.69964200
Si	–1.76879600	2.99862000	–1.07266600
C	–4.56814600	–0.19038500	–0.75415700
C	–1.39820100	–1.06055300	–0.87449100
P	–5.47975600	–1.81910900	–0.67168400
C	–2.62115700	0.05486300	1.76247200
C	–2.92728900	4.23863900	–1.88051800
C	–0.91025300	3.82018000	0.46261800
C	–7.25636400	–1.35972900	–0.10844600
C	–5.37793500	–2.59103300	–2.42394800
C	–8.15294700	–2.60950900	–0.16652300
C	–7.15537100	–0.90423500	1.36313200
C	–7.88291900	–0.22264800	–0.93649900
C	–3.88600700	–2.61206200	–2.81274900
C	–6.16728300	–1.79644000	–3.47739800
C	–5.87576000	–4.04880800	–2.38258300
C	–1.12680400	–2.32535400	–0.34994400
C	–0.00630000	–3.03231800	–0.75071600
C	0.85518300	–2.49366000	–1.68962700
C	0.57392300	–1.26437500	–2.25670900
C	–0.54192300	–0.55533400	–1.85130600
C	–3.63277900	0.55361000	2.57708000
C	–3.49253800	0.58597000	3.95459400
C	–2.33458700	0.10720800	4.54347700

C	–1.31297300	–0.39001500	3.75275700
C	–1.45638800	–0.40684200	2.37657600
C	0.52065100	4.28844000	0.39488100
C	0.97679000	5.06716800	1.58664600
C	0.23156300	5.19494700	2.70173600
C	–1.05146100	4.62376400	2.72295700
C	–1.61669900	3.98712600	1.61640700
C	–4.17262700	4.49219400	–1.00302500
C	–3.38430600	3.63689300	–3.23478400
C	–2.19942500	5.57591400	–2.14442500
H	–4.58261100	0.15759300	–1.78177500
H	–9.09868400	–2.38119200	0.31453500
H	–8.36429600	–2.90290500	–1.18590500
H	–7.69433400	–3.44022000	0.35470500
H	–8.15895600	–0.72434400	1.73552300
H	–6.59774700	0.01901000	1.45891000
H	–6.67910000	–1.65834200	1.97280800
H	–8.05918500	–0.50923800	–1.96199700
H	–8.84196100	0.03051800	–0.49452000
H	–7.27071400	0.67081800	–0.92740600
H	–3.79183500	–3.10459300	–3.77509700
H	–3.29993400	–3.15982400	–2.08912800
H	–3.47002500	–1.61839200	–2.90603100
H	–5.94518700	–2.21257200	–4.45493300
H	–7.23443400	–1.87543200	–3.32335500
H	–5.89141400	–0.74815300	–3.49551300
H	–5.36209200	–4.60688200	–1.61234300
H	–6.94006500	–4.11282600	–2.20762800
H	–5.66694000	–4.50610200	–3.34458800
H	–1.77969000	–2.74867900	0.38632200
H	0.22911900	–3.97493000	–0.29888200
H	1.76506800	–3.00182200	–1.93644600
H	1.25502400	–0.83781300	–2.96298700
H	–0.69958000	0.41929500	–2.26364800
H	–4.54978900	0.90481600	2.14431300
H	–4.29122000	0.95974300	4.56564600
H	–2.23351400	0.11208100	5.61101700
H	–0.41256000	–0.77299800	4.19389800
H	–0.64667900	–0.76753400	1.78005100
H	0.68527800	4.85905800	–0.51679900
H	1.96470300	5.47128400	1.52458900
H	0.60634800	5.70177400	3.56544800
H	–1.63097000	4.69136400	3.62359400
H	–2.60614400	3.58987200	1.70784500
H	–4.85255000	5.15605800	–1.52742300
H	–3.91160400	4.96450000	–0.06108800
H	–4.69731100	3.56650000	–0.79354300

H	–4.05861600	4.32940000	–3.72819500
H	–2.53915100	3.45738000	–3.89031800
H	–3.90697900	2.69873800	–3.08421500
H	–1.88800700	6.05176900	–1.21834100
H	–1.32737700	5.43528700	–2.77506200
H	–2.87183000	6.25886000	–2.65324200
H	–5.15185600	0.52817400	–0.18951500
C	1.51204000	3.09495300	0.36734600
C	2.86471300	3.31928600	0.21675900
C	1.12639700	1.79620700	0.53367100
C	3.76842700	2.29077300	0.30015800
C	2.02475400	0.76840500	0.58179400
C	3.38267700	0.97860200	0.51532200
B	4.52768500	–0.18148100	0.80475300
H	5.25211900	0.30869600	1.61736700
C	5.39701600	–0.50832400	–0.52715400
C	6.76476300	–0.64584300	–0.46284800
C	4.82973200	–0.65008000	–1.77178600
C	7.52937900	–0.89041000	–1.57882700
C	5.56440500	–0.89186100	–2.90142700
C	6.92567600	–1.00986100	–2.80047000
C	3.77985400	–1.46261800	1.50172900
C	3.24418900	–1.27039400	2.75923500
C	3.47396400	–2.65972800	0.90016700
C	2.42792900	–2.18272300	3.37033400
C	2.67373100	–3.60267700	1.49944100
C	2.14817600	–3.36527600	2.73769900
F	–0.19800000	1.50398500	0.63946600
F	1.47887100	–0.46059000	0.73202600
F	5.07942000	2.60291100	0.19083500
F	3.28096700	4.60517700	0.03735900
F	3.48008400	–0.55685000	–1.90836900
F	4.96513100	–1.01598600	–4.10759600
F	7.66683100	–1.24630200	–3.90453800
F	7.41479600	–0.54711800	0.71974900
F	8.87183300	–1.01323400	–1.48294300
F	2.34653200	–4.74236600	0.84479000
F	3.88829900	–2.94224700	–0.36213700
F	3.43496000	–0.08780100	3.40216600
F	1.84249000	–1.90375500	4.56290700
F	1.33708600	–4.27270700	3.32159200
S	–4.61091600	–3.16848700	0.76152000
F	–0.50595000	2.75963800	–2.07137600
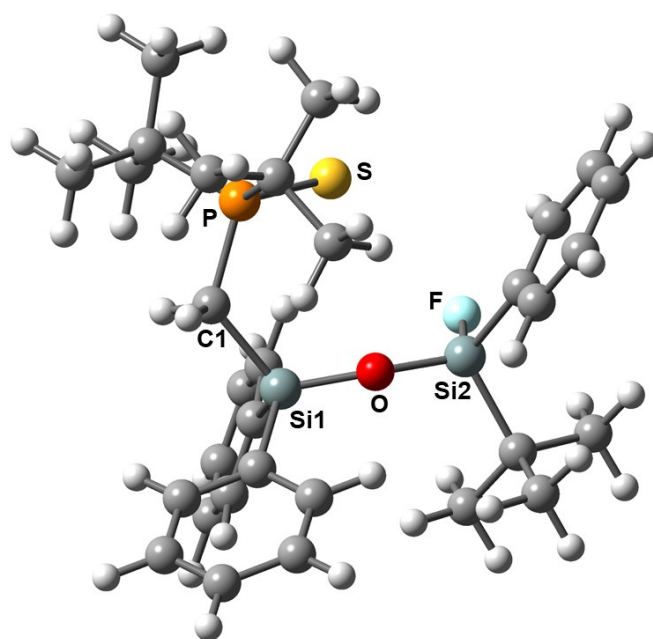
Figure S214. Optimized structure of compound **8** [HF/3-21G]. Selected bond lengths [Å] and angles [°]: P–S 2.151, Si1–O 1.656, Si2–O 1.648, Si1–O–Si2 157.2, Si2–F 1.631.

Table S27. Standard orientation of **8** [HF/3-21G].

Atomic symbol	x	y	z
C	0.78773300	–3.50531900	4.37945900
C	–0.26888800	–3.94005700	3.59614200
C	1.57556600	–2.45416700	3.94871200
C	–0.53154100	–3.32182700	2.38754800
C	1.30981600	–1.84114000	2.73516100
C	0.25659400	–2.26454400	1.93301300
C	–3.34617400	1.86315000	2.49031400
C	2.68762700	4.14253000	1.47844600
C	2.58505300	2.80831500	1.12855200
C	2.48978700	5.12332900	0.52145700
C	–0.90889000	1.89837200	1.89066800
C	–5.18133300	–0.18221900	0.42559300
C	–2.33945400	2.10549500	1.35383300
C	–1.94686800	–0.75822200	0.52002900
C	–2.45748700	3.55453000	0.84477100
C	0.23734300	–3.93205600	–1.00131300
C	2.28768700	2.43071800	–0.17824400
C	2.18371600	4.76661900	–0.77936100
C	–4.36507000	0.57604600	–0.63740100
C	–0.13132300	–2.59939400	–1.16240800
C	0.24170000	–4.80453700	–2.07674400
C	2.08160200	3.43050500	–1.12507700
C	–5.03805200	1.91960900	–0.96846700
C	3.86733400	–0.23771200	–0.67768300

C	–4.31378400	–0.27648400	–1.92425600
C	–0.48290400	–2.15692500	–2.43913300
C	–0.11600400	–4.35249700	–3.33368900
C	4.79162200	0.45574100	–1.70938500
C	–0.47407100	–3.02724600	–3.51437400
H	0.99290300	–3.98304700	5.31706100
H	–0.88255900	–4.75505800	3.92624700
H	2.39316500	–2.11331100	4.55299200
H	–1.35397400	–3.67090400	1.79116000
H	2.91888400	4.41590600	2.48920100
H	–3.07916600	2.50538400	3.32382000
H	–3.32653600	0.83896400	2.84446300
H	1.92244000	–1.02741000	2.40669800
H	–4.35556800	2.11329900	2.19377400
H	2.73202800	2.06000600	1.88372800
H	–2.18434600	–0.82165600	1.57608900
H	2.57005100	6.15833600	0.79014500
H	–0.71588500	2.65130900	2.64792200
H	–5.31017900	0.38899600	1.33256800
H	–0.78514900	0.92505700	2.34931000
H	–4.73019500	–1.13410500	0.67584400
H	–6.16734900	–0.38244100	0.01726500
H	0.52771700	–4.29276500	–0.03441900
H	–2.54482800	–1.51394600	0.02258600
H	–2.22715000	4.22507300	1.66680600
H	–0.17621800	2.01077700	1.10705500
H	–3.45513200	3.78246800	0.49506200
H	–5.19572400	2.51845100	–0.08080300
H	0.52812600	–5.82802500	–1.93393200
H	2.01984400	5.52377100	–1.52030800
H	–1.75899800	3.73449900	0.03995900
H	–3.86245200	–1.24660700	–1.75127100
H	–6.00861900	1.72332300	–1.41298700
H	–5.33073800	–0.43864000	–2.26755900
H	–4.44463600	2.48475000	–1.67631400
H	1.82742400	3.15529200	–2.12855500
H	4.93495400	1.50328900	–1.46364500
H	–3.75476000	0.22781200	–2.69871200
H	–0.74695000	–1.12832100	–2.59521700
H	5.76327800	–0.02988000	–1.71202300
H	–0.11013500	–5.02583700	–4.16832000
H	4.37361000	0.39343900	–2.70730800
H	–0.74011000	–2.66978400	–4.48943600
O	1.04053600	–0.23449300	0.07574700
P	–2.55018700	0.88672000	–0.10635200
S	–1.41952900	1.56773000	–1.80454400
Si	–0.13466300	–1.38042100	0.29465900

Si	2.18373100	0.63517200	−0.73263000
C	3.69968000	−1.72162100	−1.07740200
C	4.54339100	−0.16512700	0.70724400
H	3.94712400	−0.65249300	1.47097900
H	5.50259000	−0.67378000	0.66457700
H	4.72315300	0.86112100	1.00707600
H	3.23564400	−1.81756000	−2.05329300
H	4.67407100	−2.20103200	−1.11494400
H	3.08724800	−2.25702500	−0.36080300
F	1.79785400	0.68712300	−2.31610900
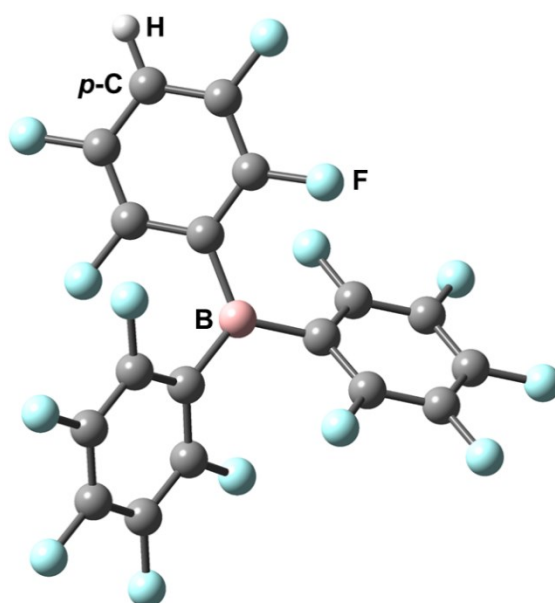
Figure S215. Optimized structure of compound **9** [HF/3-21G].

Table S28. Standard orientation of **9** [HF/3-21G].

Atomic symbol	x	y	z
C	−3.76945600	−1.96697300	0.00853600
C	−3.64950800	−0.79862500	0.71379100
C	−2.70313500	−2.46132700	−0.69618000
C	−2.45753300	−0.12517800	0.69927900
C	−1.51619400	−1.78040600	−0.68087100
C	−1.35904900	−0.59504200	0.00850000
C	−0.91849700	2.46994900	−0.73848600
C	0.00002300	1.75329900	0.00000700
C	−0.91670600	3.84076800	−0.74953000
C	1.35903000	−0.59508000	−0.00847800
C	0.91856700	2.46993500	0.73848600
C	1.51614000	−1.78046900	0.68085800
C	0.00006400	4.52989100	−0.00001700
C	2.45753100	−0.12522400	−0.69923700

C	0.91681500	3.84075400	0.74950800
C	2.70306200	–2.46142200	0.69615200
C	3.64948800	–0.79870400	–0.71376400
C	3.76940000	–1.96707700	–0.00854400
B	0.00000200	0.18551800	0.00001900
F	–4.93511600	–2.63036900	0.00820500
F	–4.69894500	–0.32316700	1.41002000
F	–2.83014800	–3.60689800	–1.39151500
F	–2.36995700	1.01718000	1.41203700
F	–0.48673700	–2.28930200	–1.39036700
F	–1.83164300	1.81333300	–1.49161100
F	–1.82049900	4.50727100	–1.49622200
F	0.48666700	–2.28935800	1.39033600
F	2.36999000	1.01716000	–1.41195600
F	1.83169600	1.81330500	1.49162000
F	1.82062800	4.50724500	1.49618500
F	2.83004200	–3.60701800	1.39145300
F	4.69894100	–0.32325300	–1.40997200
F	4.93504200	–2.63050400	–0.00822900
H	0.00008000	5.59736900	–0.00002600
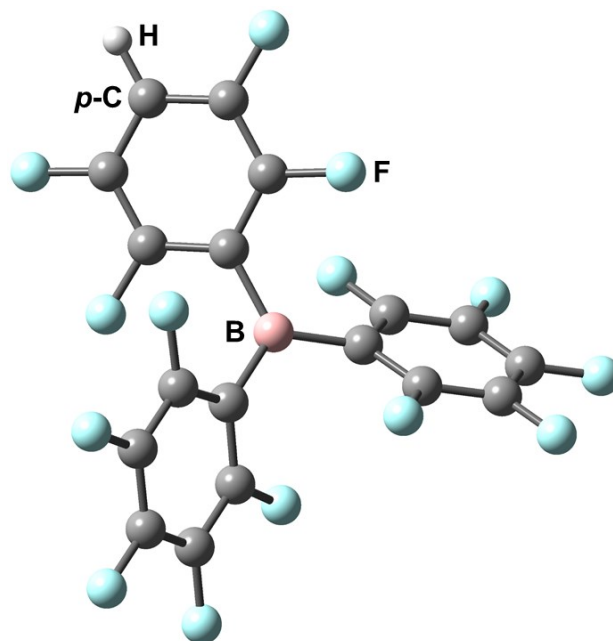
Figure S216. Optimized structure of compound **9** [B3LYP/6-311+G(d,p)].

Table S29. Standard orientation of **9** [B3LYP/6-311+G(d,p)].

Atomic symbol	x	y	z
C	–3.82494100	–1.98816600	0.00516500
C	–3.66882100	–0.84932700	0.78776600
C	–2.76744000	–2.44329800	–0.77506700
C	–2.45780400	–0.17357000	0.76786900

C	−1.56294300	−1.75654400	−0.75114600
C	−1.36038100	−0.59769700	0.00842200
C	−0.86330900	2.49400100	−0.81203100
C	0.00067900	1.75141800	−0.00002600
C	−0.85680000	3.88163200	−0.82378400
C	1.35979000	−0.59876100	−0.00850500
C	0.86538000	2.49317900	0.81196700
C	1.56124000	−1.75809300	0.75060700
C	0.00198800	4.59076600	0.00002000
C	2.45777100	−0.17508700	−0.76738300
C	0.86014000	3.88081600	0.82377800
C	2.76520900	−2.44577100	0.77458100
C	3.66828800	−0.85174500	−0.78721600
C	3.82329800	−1.99107900	−0.00511400
B	0.00001400	0.18123800	−0.00006600
F	−4.98303800	−2.64099700	0.00344000
F	−4.68095400	−0.42084500	1.54528900
F	−2.92207900	−3.53111400	−1.53309800
F	−2.35601400	0.91290000	1.55039100
F	−0.57735800	−2.23260300	−1.52981500
F	−1.71580600	1.86119600	−1.63967900
F	−1.69502800	4.53921100	−1.63976800
F	0.57503800	−2.23374900	1.52874400
F	2.35704200	0.91187900	−1.54935700
F	1.71733600	1.85955400	1.63954500
F	1.69899500	4.53759300	1.63976400
F	2.91879000	−3.53405100	1.53216000
F	4.68099100	−0.42365100	−1.54419700
F	4.98090400	−2.64478000	−0.00332200
H	0.00248500	5.67288400	0.00003700

4.6   X-Ray Crystallographic Details

The crystals were selected and measured on a SuperNova Dualflex diffractometer equipped with a TitanS2 detector ([B(C$_6$F$_5$)$_3$Bn][Li(TMEDA)], **6**, **7**[B(C$_6$F$_5$)$_4$]), on a XtaLAB Synergy R, DW system equipped with a HyPix-Arc 150 detector ([W(**5**)(CO)$_4$], **9**) or on a Xcalibur, AtlasS2, Gemini ultra diffractometer ([B(C$_6$F$_5$)$_3$Bn][Li(TMEDA)]). The crystals were kept at *T* = 123(1) K ([B(C$_6$F$_5$)$_3$Bn][Li(TMEDA)], [B(C$_6$F$_5$)$_3$Bn][H(TMEDA)], **6**, **7**[B(C$_6$F$_5$)$_4$], **9**) or T= 100.01(10) K ([W(**5**)(CO)$_4$]) during data collection. Data collection and reduction were performed with **CrysAlisPro** Version 1.171.41.89a ([B(C$_6$F$_5$)$_3$Bn][Li(TMEDA)], [B(C$_6$F$_5$)$_3$Bn][Li(TMEDA)]) or with **CrysAlisPro** Version 1.171.41.90a (**6**, **7**[B(C$_6$F$_5$)$_4$], **9**).[5] An analytical numeric absorption correction using a multifaceted crystal model based on expressions derived by R. C. Clark & J. S. Reid[6] and an empirical absorption correction using spherical harmonics, implemented in SCALE3 ABSPACK scaling algorithm, was applied for all compounds. Using **Olex2**,[7] the structures were solved with **ShelXT**[8] and a least-square refinement on *F*^{2} was carried out with **ShelXL**[9] or **olex2.refine**[10], respectively. All non-hydrogen atoms were refined anisotropically. Hydrogen atoms at the carbon atoms were located in idealized positions and refined isotropically according to the riding model. Figures were created with **Olex2**.[7]

Compound [W(5)(CO)$_4$]: The asymmetric unit contains one molecule of [W((*t*Bu)$_2$P(S)CH$_2$Si(Ph)$_2$OSi(H)Ph*t*Bu)(CO)$_4$]. The hydrogen atom on the Si atom was located from the difference Fourier map and refined without restraints.

Compound [B(C$_6$F$_5$)$_3$Bn][Li(TMEDA)]: The asymmetric unit contains one molecule of [B(C$_6$F$_5$)$_3$Bn][Li(Me$_2$CH$_2$CH$_2$NMe$_2$)]. Disorder of the diamine ligand was modelled without the use of any restrains. The structure was refined as a 2 component inversion twin.

Compound [B(C$_6$F$_5$)$_3$Bn][H(TMEDA)]: The asymmetric unit contains one molecule of [B(C$_6$F$_5$)$_3$Bn][H(Me$_2$CH$_2$CH$_2$NMe$_2$)].

Compound 6: The asymmetric unit contains one molecule of (*t*Bu)$_2$P(S)CH$_2$Si(Ph)$_2$OSi(H)Ph*t*Bu. The hydrogen atom on the Si atom was located from the difference Fourier map and refined without restraints. The *t*Bu group at the Si atom shows a disorder over two positions with an occupancy of 0.6 for the main part and 0.4 for the minor part. To describe this disorder the SIMU restraint was applied.

Compound 7[B(C$_6$F$_5$)$_4$]: The asymmetric unit contains one molecule of the cation [(*t*Bu)$_2$P(S)CH$_2$Si(Ph)$_2$OSiPh*t*Bu]$^+$ and one molecule of the anion [B(C$_6$F$_5$)$_4$]$^-$.

Compound 9·H$_2$O·(THF)$_2$: The asymmetric unit contains one molecule of B(C$_6$F$_5$)$_2$(C$_6$HF$_4$)·(H$_2$O) and two THF solvent molecules. The hydrogen atom located in para position at the C$_6$HF$_4$ substituent is only partly occupied (0.5) and distributed over the para positions of the three phenyl substituents (0.1:0.2:0.2). Consequently B(C$_6$F$_5$)$_2$(C$_6$HF$_4$)·(H$_2$O) co-crystalizes with B(C$_6$F$_5$)$_3$·(H$_2$O) in a 1:1 ratio. Additionally, the two THF molecules are disordered over two positions, which were described using the restraints SADI and SIMU.

CCDC-2107143 (**6**), CCDC-2107144 {**7**[B(C$_6$F$_5$)$_4$]}, and CCDC-2107145 [**9**·H$_2$O·(THF)$_2$] contain the supplementary crystallographic data for this paper. These data can be obtained free of charge at www.ccdc.cam.ac.uk/conts/retrieving.html (or from the Cambridge Crystallographic Data Center, 12 Union Road, Cambridge CB2 1EZ, UK; Fax: + 44-1223-336-033; E-mail: deposit@ccdc.cam.ac.uk).

Table 30 Crystallographic data for compounds [W(**5**)(CO)$_4$], [B(C$_6$F$_5$)$_3$Bn][Li(TMEDA)], [B(C$_6$F$_5$)$_3$Bn][H(TMEDA)].

Compound	[W(5)(CO)$_4$]	[B(C$_6$F$_5$)$_3$Bn] [Li(TMEDA)]	[B(C$_6$F$_5$)$_3$Bn] [H(TMEDA)]
Data set (internal naming)	**nf_670_l_l_1_m P_abs_gaus**	**nf_755_2_abs**	**nf_746_l_auto_abs**
Formula	C$_{35}$H$_{43}$O$_5$PSi$_2$W	C$_{31}$H$_{23}$BF$_{15}$LiN$_2$	C$_{31}$H$_{24}$BF$_{15}$N$_2$
Dcalc	1.515	1.581	1.589
μ/mm^{-1}	7.373	1.399	1.416
Formula Weight	814.69	726.26	720.33
Colour	clear yellow	clear colourless	clear colourless
Shape	block-shaped	block-shaped	block-shaped
Size/mm^3	0.24×0.12×0.11	0.80×0.59×0.48	0.33×0.28×0.16
T/K	100.01(10)	123.01(10)	122.97(14)
Crystal System	monoclinic	orthorhombic 0.26(12) 0.23(6)	monoclinic
Space Group	$P2_1/n$	$Pna2_1$	$P2_1/n$
a/Å	9.93090(10)	17.2502(12)	13.61170(10)
b/Å	18.1624(2)	12.8903(10)	12.78080(10)
c/Å	20.1325(3)	13.7184(10)	18.45210(10)
α/°	90	90	90
β/°	100.4830(10)	90	110.2970(10)
γ/°	90	90	90
V/Å^3	3570.67(8)	3050.4(4)	3010.76(4)
Z	4	4	4
Z'	1	1	1
Wavelength/Å	1.54184	1.54184	1.54184
Radiation type	Cu K$_\square$	Cu K$_a$	Cu K$_\square$
θ_{min}/°	3.302	4.282	3.518
θ_{max}/°	73.191	67.044	66.858
Measured Refl's.	17843	15562	36294
Indep't Refl's	6707	4829	5324
Refl's I≥2 σ(I)	6391	4664	5173
R_{int}	0.0244	0.0476	0.0331
Parameters	410	516	450
Restraints	0	1	0
Largest Peak	1.180	0.223	0.225
Deepest Hole	-1.685	-0.246	-0.247
GooF	1.100	1.040	1.075
wR_2 (all data)	0.0851	0.1020	0.0883
wR_2	0.0842	0.1006	0.0877
R_1 (all data)	0.0336	0.0420	0.0328
R_1	0.0318	0.0391	0.0322

Table 31 Crystallographic data for compounds **6**, **7**[B(C_6F_5)$_4$], and **9**·H_2O·(THF)$_2$.

Compound	6	7[B(C$_6$F$_5$)$_4$]	9·H$_2$O·(THF)$_2$
Data set (internal naming)	**nf_719_2b_GV**	**nf_693_1**	**nf_771_subl_thf_2**
CCDC number	2107143	2107144	2107145
Formula	C$_{31}$H$_{45}$OPSSi$_2$	C$_{55}$H$_{44}$BF$_{20}$OPSSi$_2$	C$_{26}$H$_{18.5}$BF$_{14.5}$O$_3$
Dcalc	1.167	1.528	1.666
μ/mm^{-1}	2.276	2.247	0.175
Formula Weight	552.913	1230.92	665.236
Colour	colourless	colourless	colourless
Shape	block-shaped	block-shaped	plate-shaped
Size/mm^3	0.12×0.10×0.08	0.35×0.24×0.21	0.44×0.12×0.08
T/K	123.0(1)	123.0(1)	123.01(10)
Crystal System	monoclinic	triclinic	monoclinic
Space Group	$P2_1/n$	$P\bar{1}$	$P2_1/c$
a/Å	8.3897(2)	9.9141(2)	9.2436(3)
b/Å	35.0632(6)	14.3805(2)	29.8297(7)
c/Å	11.2062(2)	19.1892(3)	9.9706(3)
α/°	90	101.2990(10)	90
β/°	107.304(2)	90.3210(10)	105.288(3)
γ/°	90	93.8460(10)	90
V/Å^3	3147.32(11)	2676.24(8)	2651.94(14)
Z	4	2	4
Z′	1	1	1
Wavelength/Å	1.54184	1.54184	0.71073
Radiation type	Cu K$_\alpha$	Cu K$_\alpha$	Mo K$_\alpha$
θ_{min}/°	4.32	4.278	2.22
θ_{max}/°	66.60	66.647	32.62
Measured Refl's.	35994	41863	44425
Indep't Refl's	5524	9402	9629
Refl's I≥2 σ(I)	5124	8248	7025
R_{int}	0.0563	0.0812	0.0289
Parameters	359	739	436
Restraints	42	0	59
Largest Peak	0.5996	0.640	0.6516
Deepest Hole	-0.4918	-0.605	-0.5345
GooF	1.0223	1.024	1.0261
wR_2 (all data)	0.1286	0.1342	0.1263
wR_2	0.1267	0.1286	0.1156
R_1 (all data)	0.0623	0.0561	0.0690
R_1	0.0588	0.0491	0.0463

4.6.1 Compound [W(5)(CO)₄]
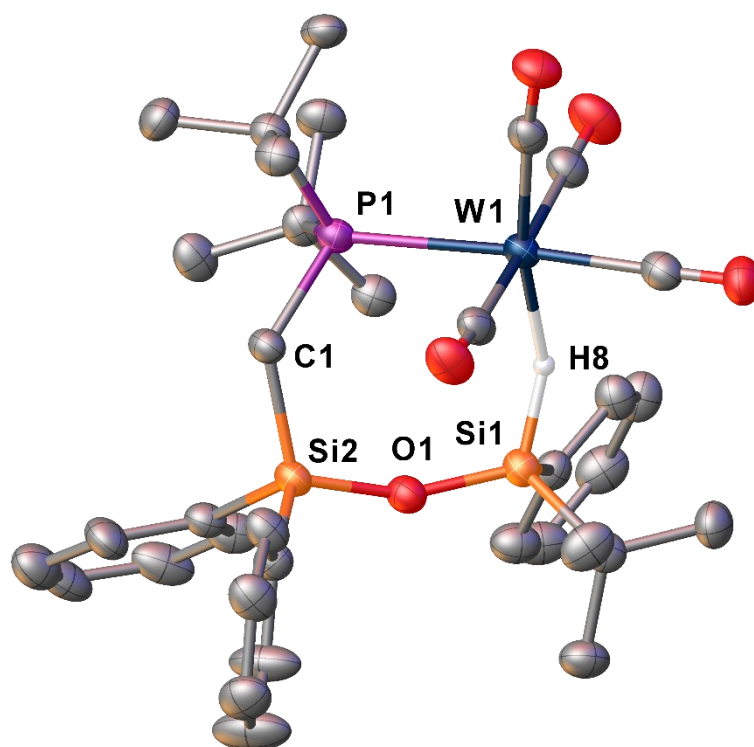
Selected Bond Lengths in Å		Selected Bond Angles in °	
P1–W1	2.6027(9)	**P1–W1–C1**	109.86(12)
P1–C1	1.847(4)	**Si1–O1–Si2**	157.16(18)
C1–Si2	1.884(4)	**Si2–C1–P1**	126.3(2)
O1–Si2	1.641(3)		
O1–Si1	1.614(3)		

4.6.1 Compound [B(C₆F₅)₄Bn][LiTMEDA]
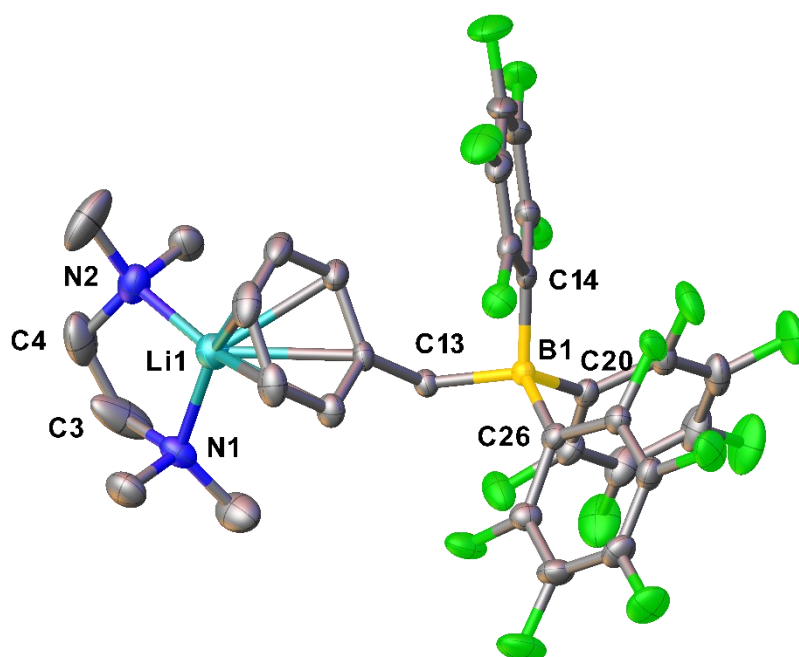
4.6.1 Compound [B(C₆F₅)₄Bn][HTMEDA]
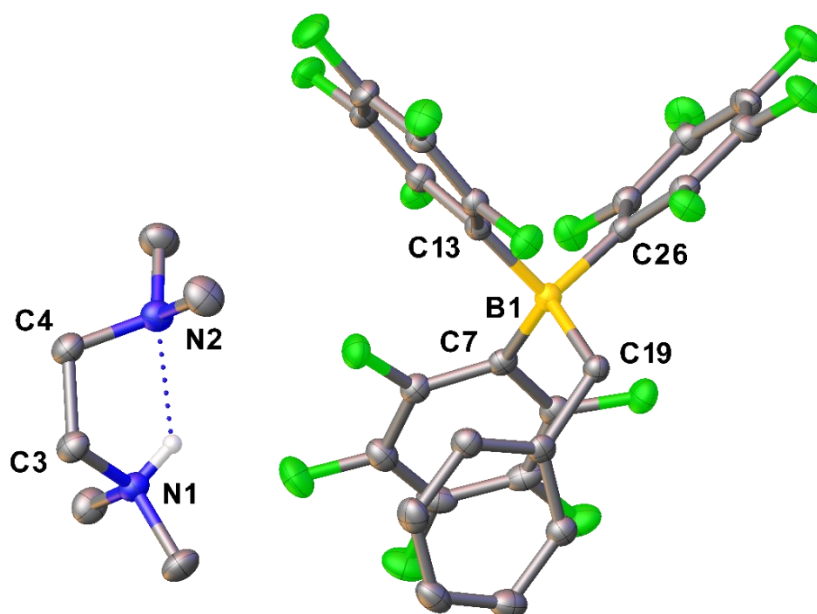
4.6.2   Compound 6
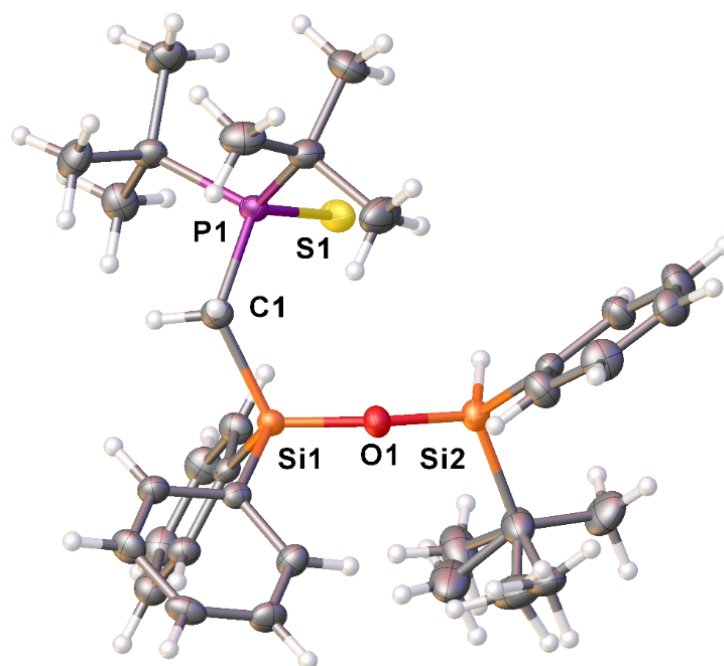
Selected Bond Lengths in Å		Selected Bond Angles in °	
P1–S1	1.9671(12)	S1–P1–C1	114.38(11)
P1–C1	1.818(3)	P1–C1–Si1	125.15(18)
C1–Si1	1.891(3)	C1–Si1–O1	115.52(14)
Si1–O1	1.614(2)	Si1–O1–Si2	156.83(16)
Si2–O1	1.644(2)		

4.6.3 Compound 7[B(C₆F₅)₄]
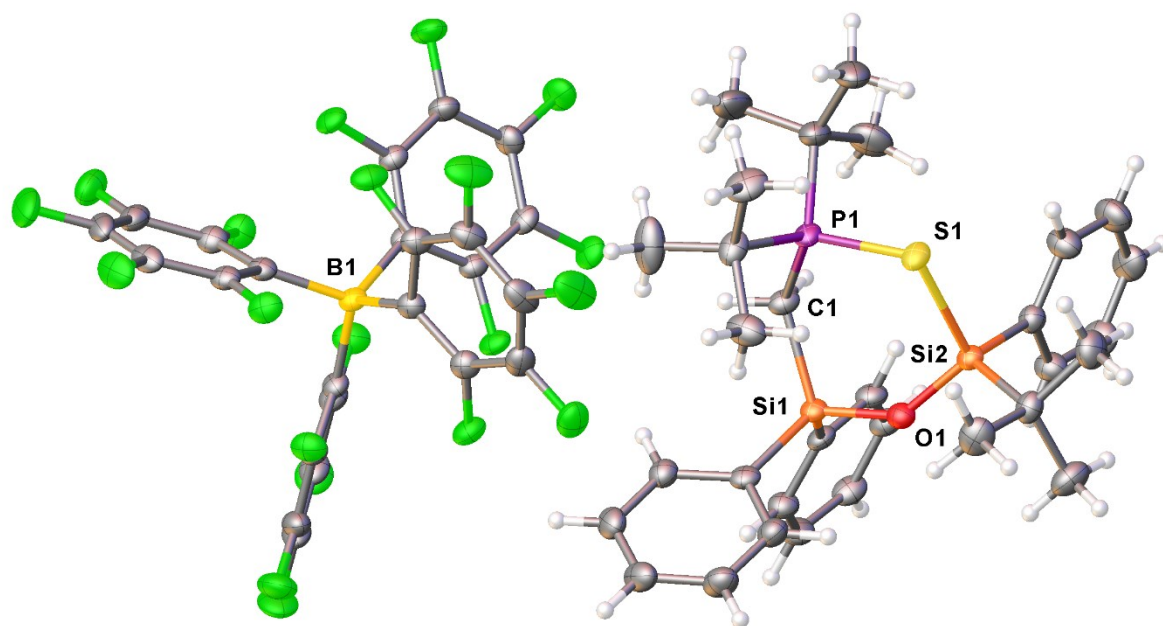
Selected Bond Lengths in Å		Selected Bond Angles in °	
P1–S1	2.0678(9)	S1–P1–C1	114.11(9)
P1–C1	1.803(2)	P1–C1–Si1	124.60(13)
C1–Si1	1.899(2)	C1–Si1–O1	106.42(10)
Si1–O1	1.6381(18)	Si1–O1–Si2	139.60(11)
O1–Si2	1.6265(18)	O1–Si2–S1	109.26(7)
Si2–S1	2.1940(8)	Si2–S1–P1	107.86(3)

4.6.4   Compound 9·H₂O·(THF)₂
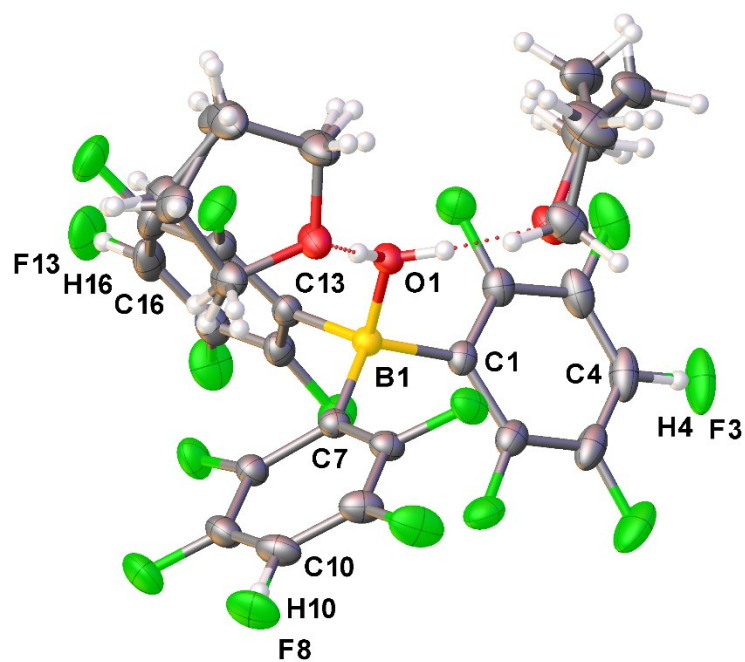
Selected Bond Lengths in Å		Selected Bond Angles in °	
B1−O1	1.5502(15)	**O1−B1−C1**	104.01(9)
B1−C1	1.6365(17)	**O1−B1−C7**	106.18(9)
B1−C7	1.6383(18)	**O1−B1−C13**	107.70(9)
B1−C13	1.6359(17)	**C1−B1−C7**	116.35(10)
		C1−B1−C13	109.74(9)
		C7−B1−C13	112.14(9)

4.7   References

[1]   Lehmann, M.; Schulz, A.; Villinger, A. *Angew. Chem., Int. Ed.*, 2009, **48**, 7444.

[2]   Rach, S. F.; Herdtweck, E.; Kühn, F. E. *J. Organomet. Chem.*, 2011, **696**, 1817.

[3]   Fink, L.; Samigullin, K.; Bodach, A.; Alig, E.; Wagner, M.; Lerner, H.-W. *Z. Anorg. Allg. Chem.*, 2016, **642**, 282.

[4]   S. Künzler, S. Rathjen, A. Merk, M. Schmidtmann, T. Müller, *Chem. Eur. J.* **2019**, *25*, 15123.

[5]   CrysAlisPro Software System, Rigaku Oxford Diffraction, 2020.

[6]   Clark, R. C.; Reid, J. S. *Acta Crystallogr.*, 1995, **A51**, 887.

[7]   Dolomanov, O. V.; Bourhis, L. J.; Gildea, R. J.; Howard, J. A. K.; Puschmann, H. *OLEX2*: a complete structure solution, refinement and analysis program, *J. Appl. Crystallogr.*, 2009, **42**, 339.

[8]   Sheldrick, G. M. *SHELXT* – Integrated space-group and crystal-structure determination, *Acta Crystallogr.*, 2015, **A71**, 3.

[9]   Sheldrick, G. M. Crystal structure refinement with *SHELXL*, *Acta Crystallogr.*, 2015, **C71**, 3.

[10]   Bourhis, L. J.; Dolomanov, O. V.; Gildea, R. J.; Howard, J. A. K.; Puschmann, H. The anatomy of a comprehensive constrained, restrained refinement program for the modern computing environment – *Olex2* dissected, *Acta Crystallogr.*, 2015, **A71**, 59.

[11]   Macrae, C. F.; Edgington, P. R.; McCabe, P.; Pidcock, E.; Shields, G. P.; Taylor, R.; Towler, M.; van de Streek, J. *Mercury*: visualization and analysis of crystal structures, *J. Appl. Crystallogr.*, 2006, **39**, 453.

[12]   Gaussian 09 (Revision E.01): M. J. Frisch, G. W. Trucks, H. B. Schlegel, G. E. Scuseria, M. A. Robb, J. R. Cheeseman, G. Scalmani, V. Barone, B. Mennucci, G. A. Petersson, H. Nakatsuji, M. Caricato, X. Li, H. P. Hratchian, A. F. Izmaylov, J. Bloino, G. Zheng, J. L. Sonnenberg, M. Hada, M. Ehara, K. Toyota, R. Fukuda, J. Hasegawa, M. Ishida, T. Nakajima, Y. Honda, O. Kitao, H. Nakai, T. Vreven, J. A. Montgomery Jr., J. E. Peralta, F. Ogliaro, M. Bearpark, J. J. Heyd, E. Brothers, K. N. Kudin, V. N. Staroverov, T. Keith, R. Kobayashi, J. Normand, K. Raghavachari, A. Rendell, J. C. Burant, S. S. Iyengar, J. Tomasi, M. Cossi, N. Rega, J. M. Millam, M. Klene, J. E. Knox, J. B. Cross, V. Bakken, C. Adamo, J. Jaramillo, R. Gomperts, R. E. Stratmann, O. Yazyev, A. J. Austin, R. Cammi, C. Pomelli, J. W. Ochterski, R. L. Martin, K. Morokuma, V. G. Zakrzewski, G. A. Voth, P. Salvador, J. J. Dannenberg, S. Dapprich, A. D. Daniels, O. Farkas, J. B. Foresman, J. V. Ortiz, J. Cioslowski and D. J. Fox, Gaussian, Inc., Wallingford CT, 2013.

[13]   a) Weinhold, F.; Landis, C. R. Valency and Bonding: A Natural Bond Orbital Donor-Acceptor Perspective, Cambridge Univ. Press, Cambridge, UK, 2005; b) Glendening, E. D.; Badenhoop, J. K.; Reed, A. E.; Carpenter, J. E.; Bohmann, J. A.; Morales, C. M.; Landis, C. R.; Weinhold, F. NBO 6.0, Theoretical Chemistry Institute, University of Wisconsin, Madison, WI, 2013.

[14]   Foresman, J. B.; Frisch, A. Exploring Chemistry with Electronic Structure Methods, 2nd Ed., Gaussian, Inc., Pittsburgh, PA, USA, 1996.

Preface

The following treasury contains unpublished results obtained between February 2018 and September 2021. The compounds presented in this section were obtained while investigating ideas related to the topics reported in the previous chapters. A brief overview and a short discussion on the ideas behind these syntheses and the related findings is provided. The collected procedures and analytics are available for further use by the working group of Dr. Jonathan O. Bauer.

Authors

N. Fontana, T. Huber, Dr. M. Seidl, Dr. J. O. Bauer.

Author contribution

All the reported synthesis and characterizations (multinuclear NMR) in this work were performed for the first time by N. Fontana. Elemental analysis and mass spectrometry samples were provided by T. Huber together with NMR pictures and optimization of the reaction conditions. Characterizations in the solid phase (single crystal X-ray diffraction) were performed by N. Fontana and the structures were refined by Dr. M. Seidl (AK Scheer). The commentary and the supporting information were prepared by N. Fontana and revised by Dr. J. O. Bauer.

Acknowledgements

5 Synthesis of Phosphonamides and Their Salts

5.1 Introduction

As seen so far (see Chapters 3 and 4), the use of anchimerically assisting groups, based on the –CH$_2$P(Chalc)tBu$_2$ structural motif to form and tame the reactivity of silylium ions, offers not only an unprecedented stability of the final products but also remarkable insights about the electronic properties of these species. Encouraged by these results, we have decided to investigate the possible changes in the structure and reactivity when the carbon bridging atom is replaced by a nitrogen. After preparing tBu$_2$PNH$_2$ using a reported procedure[1] and subsequently oxidizing it with elemental sulfur, compound **T1** was obtained and fully characterized. Although not included in this work, compounds **T2** and **T3** were synthesized shortly after, using the same approach reported previously for the carbon homologue (lithiation followed by nucleophilic substitution). Interestingly, while trying to obtain the relative silylium ions, we have isolated crystals of the precursor **T1** after proton induced desilylation (**T4**).
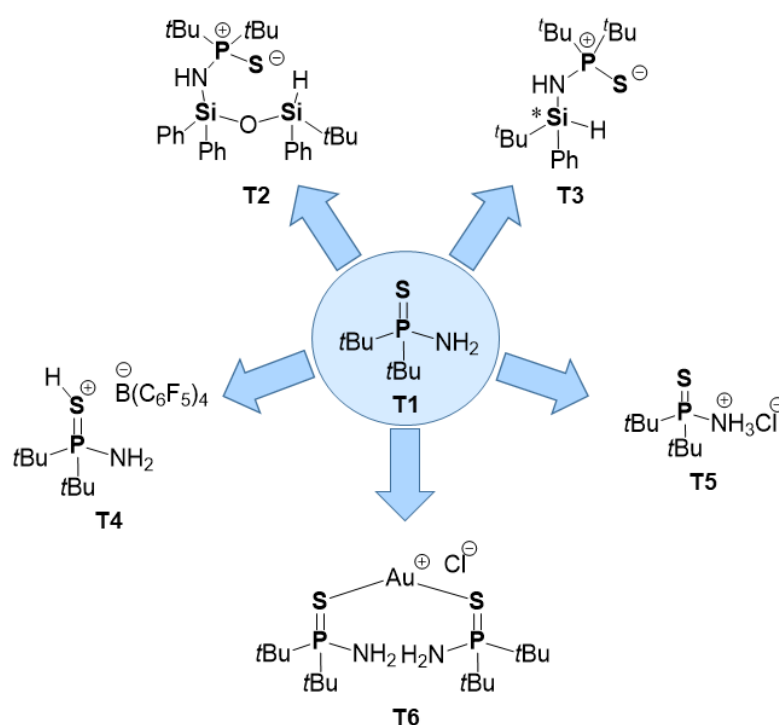
Figure 217. Thiosphosphonamide **T1** and its derivatives. On top, target precursor for new anchimerically stabilized silylium ions (**T2** and **T3**; not included in this work). On bottom, examples of different reactivity for compound **T1** towards Brønsted (**T4** and **T5**) and Lewis (**T6**) acids.

---

[1]   M. Köster, A. Kreher, C. von Hänisch, *Dalton Trans.* **2018**, *47*, 7875–7878.

Even though a direct synthesis for this compound has eluded us so far, we were lucky enough to obtain a crystal structure which undeniably features a protonated sulfur center together with a weakly coordinating anion. Intrigued by this unexpected basicity of the chalcogen atom and the total lack of reports regarding this phenomenon in the literature, we decided to fully exploit the differences between the two Lewis basic centers in this molecule and the possible presence of a tautomeric process. Herein we report about some interesting molecular structures, that were obtained during this preliminary study, either by using hydrogen chloride (**T5**) or by coordinating Gold(I) species (**T6**).

5.2 Results and discussion

5.2.1 Synthesis of $tBu_2P(S)NH_2$ (T1)
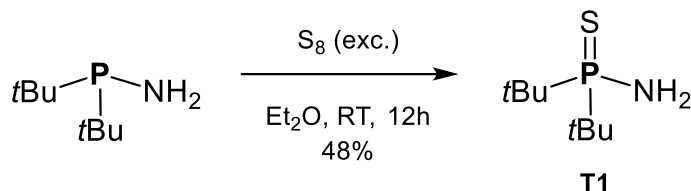
An oven dried Schlenk flask was loaded with sulfur (1 g, 31.24 mmol, exc) and Et_2O (10 ml). tBu_2PNH_2 (0.7 g, 4.34 mmol, 1.0 eq.) was added directly to the suspension *via* syringe. The mixture was stirred for 12 hours and afterwards dried in vacuum. The crude residue was purified *via* sublimation using a Kugelrohr ($1*10^{-3}$ mbar oven temperature, 100°C) to afford the pure product **T1** as a white solid (400 mg, 2.07 mmol, 48%). Crystals suitable for X-ray diffraction were grown from cold pentane. The compound crystallizes in the tetragonal space group $I\bar{4}$ and shows the expected tetrahedral geometry. All bond lengths match with the calculated ones.[2]

¹H NMR (400.13 MHz, C_6D_6, 298 K): δ = 1.12 [s, 9H, $PC(CH_3)_3$], 1.16 [s, 9H, $PC(CH_3)_3$], 1.63 [b, 2H, PNH_2]. **¹³C{¹H} NMR** (100.61 MHz, C_6D_6, 298 K): δ = 27.3 [d, $^2J_{C-P}$= 1.58 Hz, $PC(CH_3)_3$], 38.5 [d, $^1J_{C-P}$= 55.5 Hz, $PC(CH_3)_3$]. **³¹P NMR** (161.98 MHz, C_6D_6, 298 K): δ = 92.9 [s]. **Elemental analysis**: $C_8H_{20}NPS$: calcd. C 49.71%, H 10.43%, N 7.25%; found: C 49.92%, H 10.15%, N 7.29%. **HR-MS (EI)**: calcd. m/z for $C_8H_{20}NPS$ [M+]: 193.1049, found: 193.1054.

---

[2]   P. Pyykkö, M. Atsumi, *Chem. Eur. J.* **2009**, *15*, 12770.
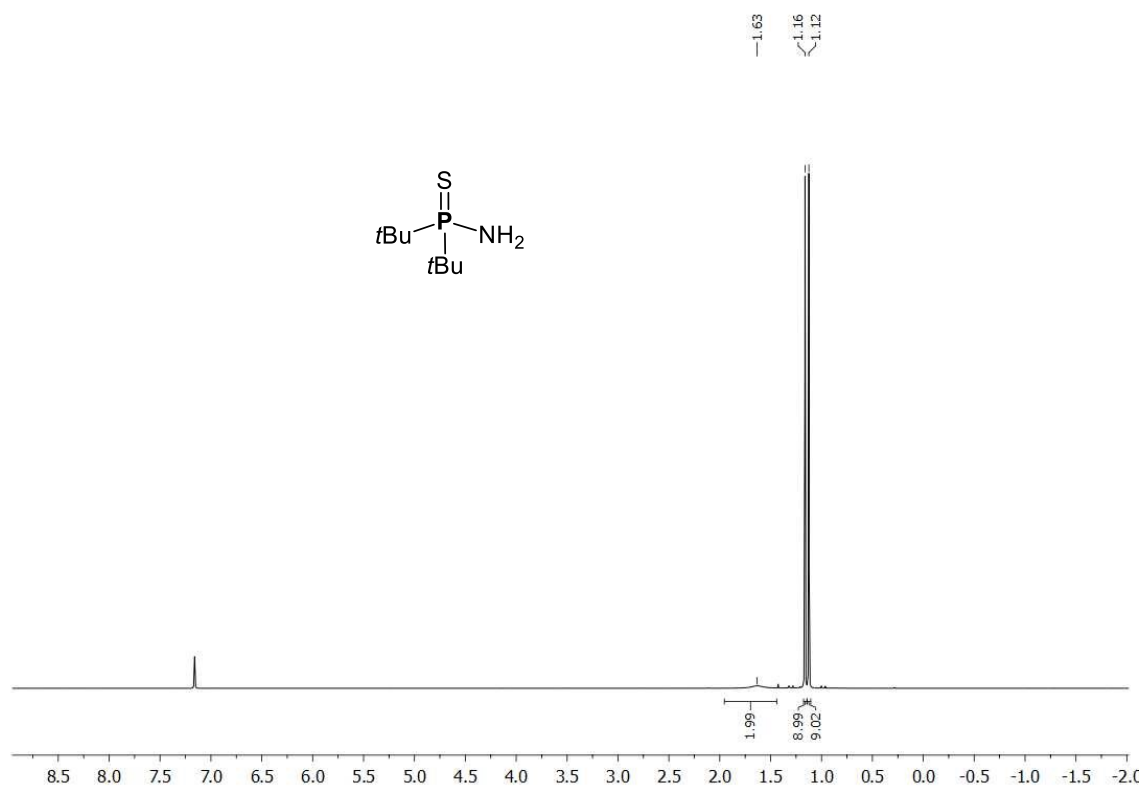
Figure S218. ^{1}H NMR (CD$_2$Cl$_2$, 298 K) of compound **T1**.
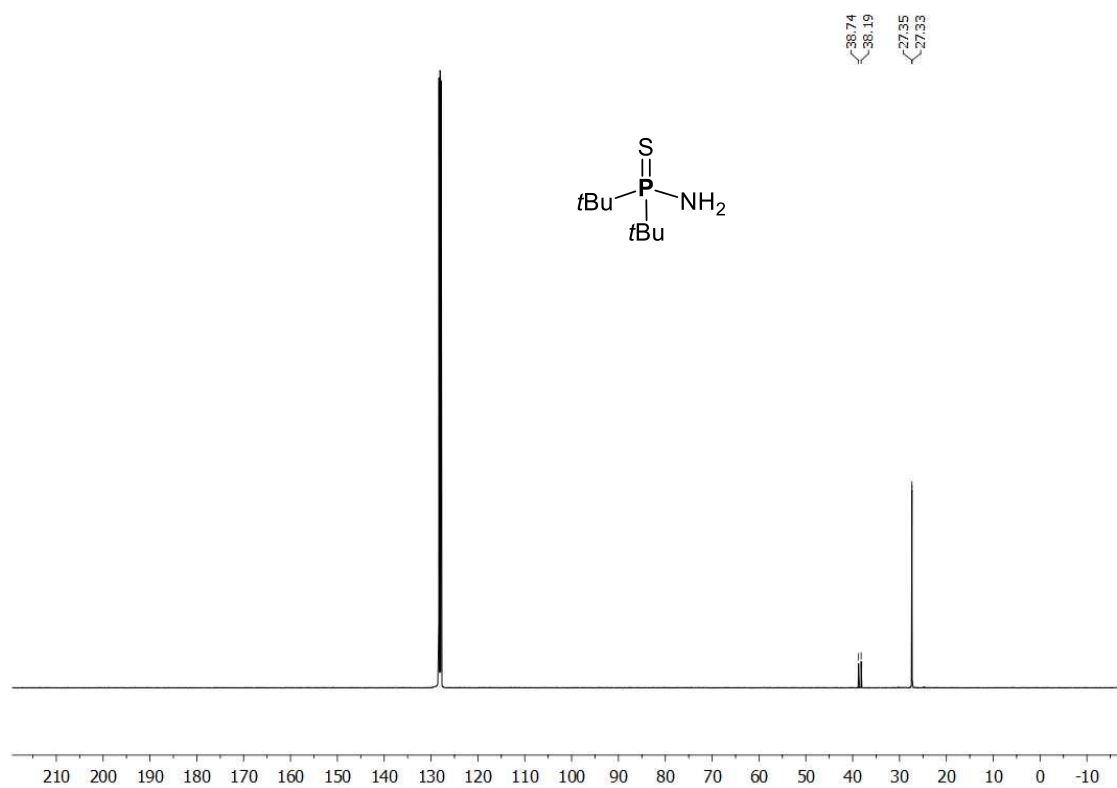
Figure S219. ^{13}C{^{1}H} NMR (CD$_2$Cl$_2$, 298 K) of compound **T1**.
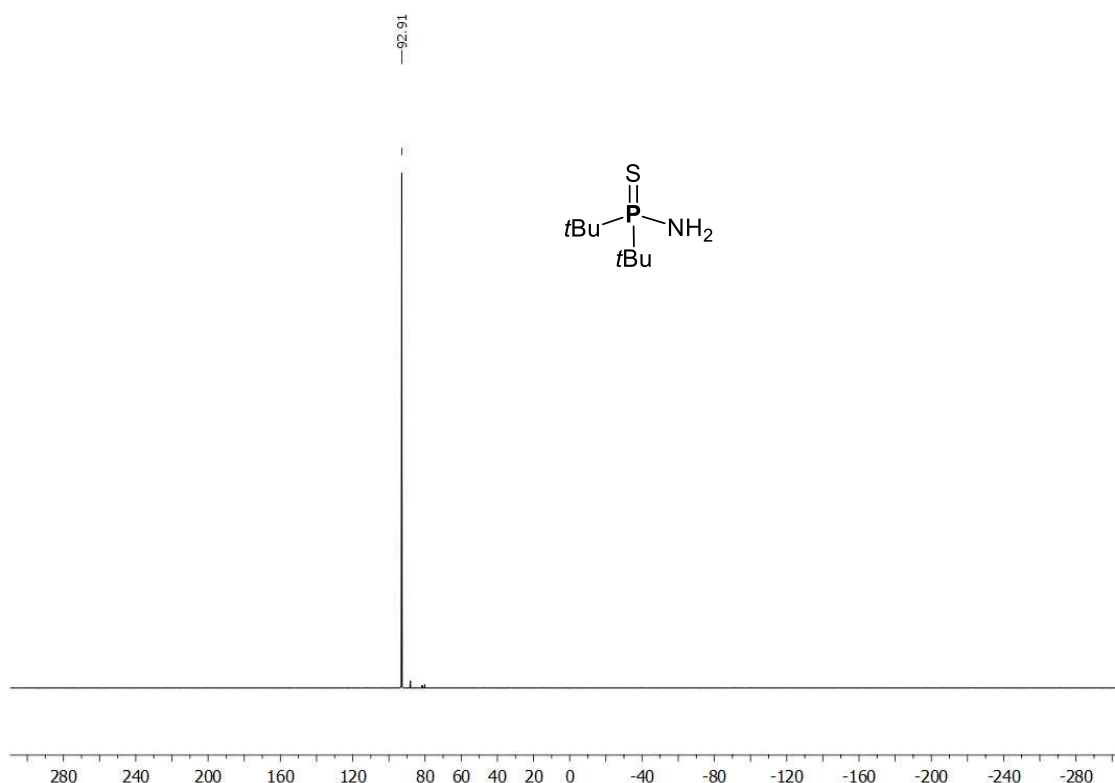
Figure S220. $^{31}P\{^1H\}$ NMR (CD$_2$Cl$_2$, 298 K) of compound **T1**.

5.2.2 Synthesis of tBu$_2$P(S)NH$_3$Cl (T5)
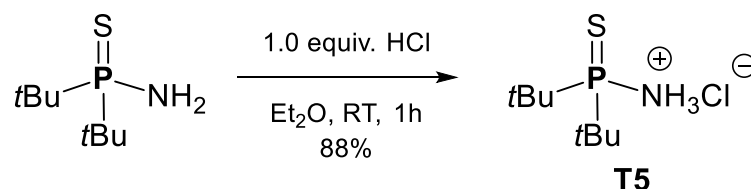
In an oven dried Schlenk flask tBu$_2$P(S)NH$_2$ (0.60 g, 3.10 mmol, 1.0 equiv.) was dissolved in diethyl ether (20 mL). HCl (1.55 mL, 3.10 mmol, 1.0 equiv., 2.0 M in diethyl ether) was added dropwise at room temperature resulting in a colorless suspension after a few minutes. After stirring for 1 h, the solvent was removed in vacuum and the solid further dried affording compound **T5** as a colorless solid (0.63 g, 2.74 mmol, 88%). Crystals suitable for single crystal X-ray diffraction were grown from Et$_2$O at −35°C.

The compound crystallizes in the triclinic space group P$\bar{1}$ and presents a cubical tetrameric structure where the chloride anions and the protons at the nitrogen atom are bound by hydrogen interactions (average Cl-H distance = 2.287 Å). In comparison with its precursor (**T1**), an elongation of the P-N bond (from 1.659(4) Å to 1.7819(13) Å) together with a shortening of the P=S double bond (from 1.9668(11) Å to 1.9315(6) Å) are observed. At the same time, the S-P-N angle is narrower (from 110.75(12)° to 108.90(5)°) while the S-P-C angle is wider (from 110.51(11)° to 114.34(6)°).

^{1}H NMR (400.13 MHz, CD$_2$Cl$_2$, 298 K): δ = 1.50 (d, $^3J_{P-H}$ = 17.4 Hz, 18H, PC(CH_3)), 9.32 (br, 3H, NH_3). **^{31}P{^{1}H} NMR** (162.04 MHz, CD$_2$Cl$_2$, 298 K): δ = 111.5. **^{13}C{^{1}H} NMR** (100.61 MHz, CD$_2$Cl$_2$, 298 K): δ = 27.5 (d, $^2J_{P-C}$ = 2.0 Hz, PC(CH$_3$)$_3$), 40.8 (d, $^1J_{P-C}$ = 43.2 Hz, PC(CH$_3$)$_3$). **Elemental analysis**: C$_8$H$_{21}$ClNPS: calcd.: C 41.82%, H 9.21%, N 6.10%; found: C 41.90%, H 8.81%, N 6.06%.
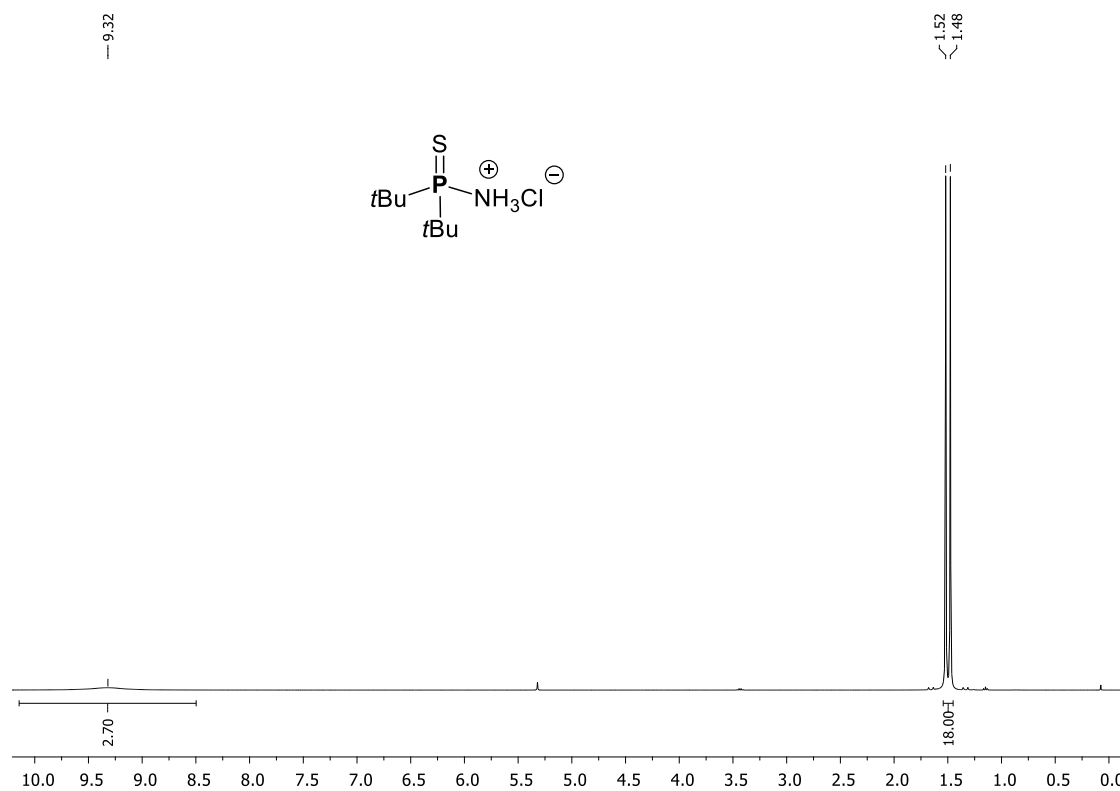
Figure S221. ^{1}H NMR (CD$_2$Cl$_2$, 298 K) of compound **T5**.
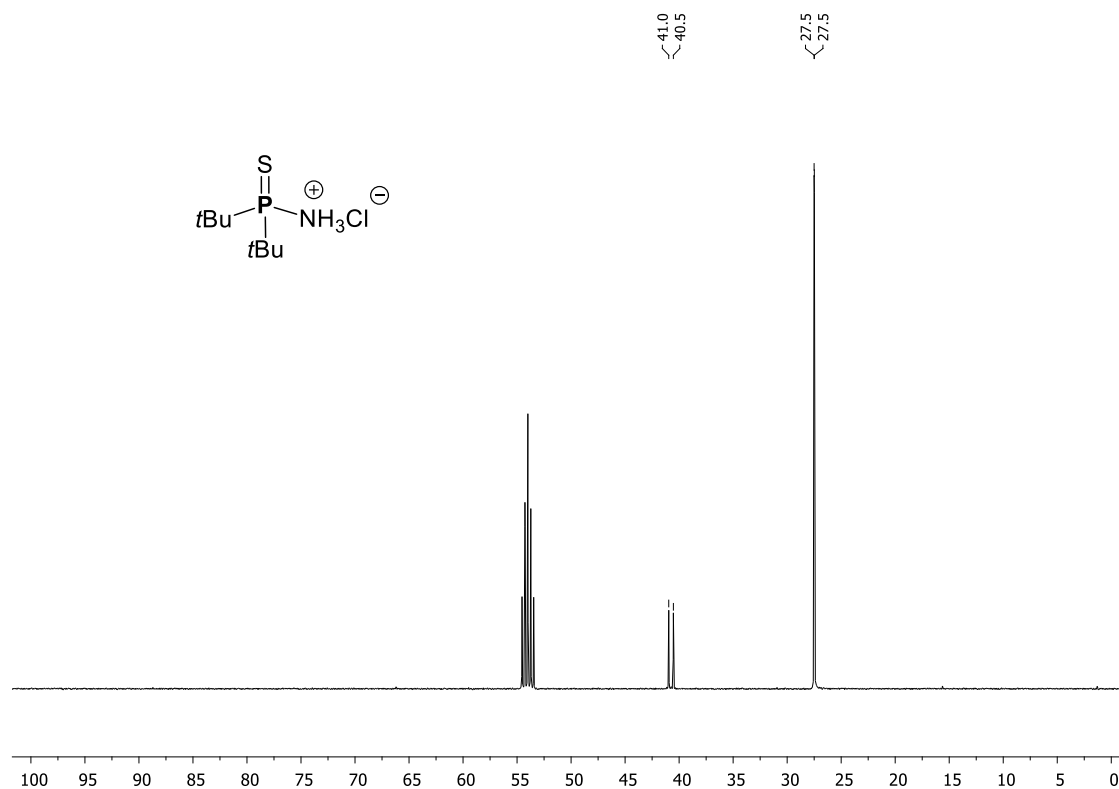
Figure S222. ^{13}C{^{1}H} NMR (CD$_2$Cl$_2$, 298 K) of compound **T5**.
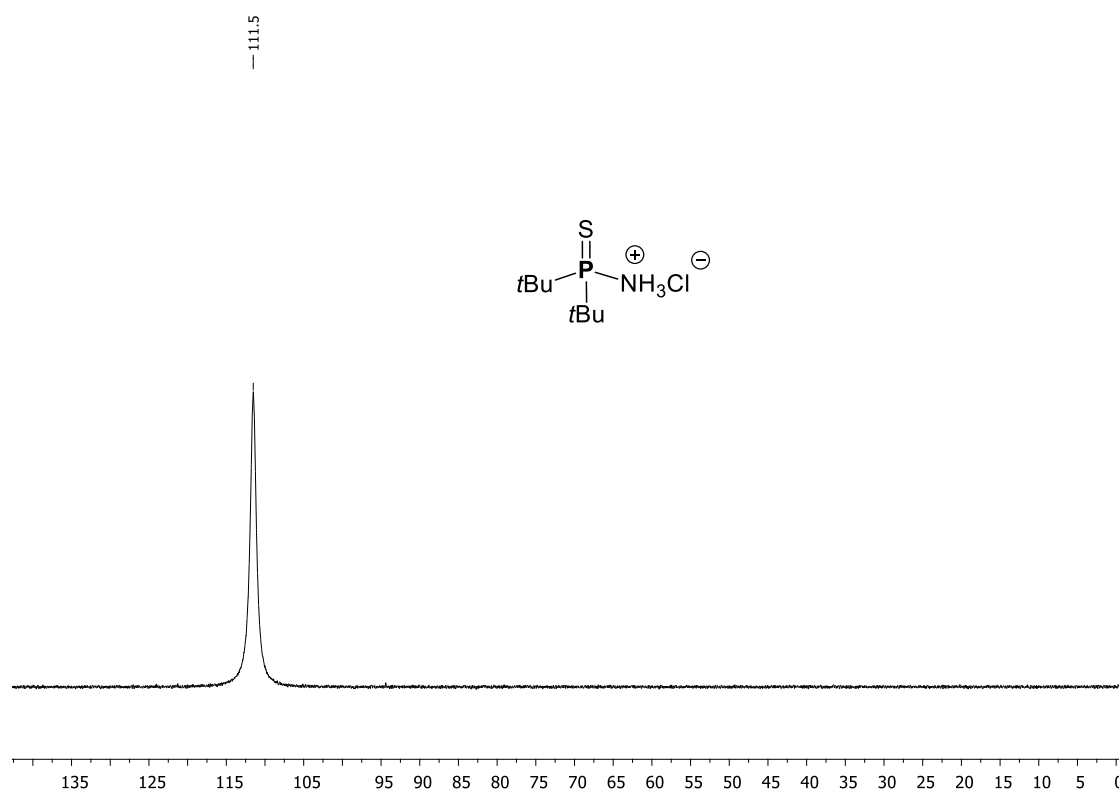
Figure S223. ^{31}P{^{1}H} NMR (CD$_2$Cl$_2$, 298 K) of compound **T5**.

5.2.3 Synthesis of [(*t*Bu₂P(S)NH₂)₂Au]Cl (T6)

T6
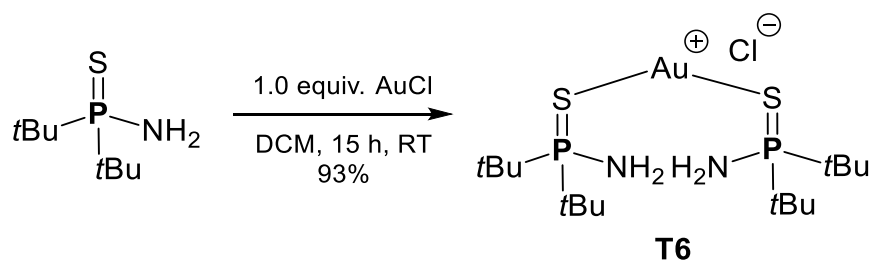
An oven dried Schlenk flask was loaded with *t*Bu₂P(S)NH₂ (50 mg, 0.258 mmol, 2.0 equiv.) and AuCl (30 mg, 0.129 mmol, 1.0 equiv.). The solids were dissolved in DCM (2 mL) and stirred at room temperature for 15 h during which a shiny precipitate formed. The light-yellow solution was filtered *via* cannula filtration and the solvent was removed in vacuum affording the desired gold complex **T6** as a colorless solid (74 mg, 0.120 mmol, 93%). Crystals suitable for single crystal X-ray diffraction were grown from DCM/pentane at −35°C.

The compound crystallizes in the tetragonal space group *I*4₁22 and presents a dimeric structure with four sulfur centers connected to two gold atoms (P-Au distance = 2.2842(7) Å, Au-Au distance 3.0234(3) Å). While the former interaction can be described as a single bond (calculated length value for a S-Au single bond = 2.27 Å), the latter is better represented by an interaction between the two metallic centers (calculated length value for a Au-Au single bond = 2.48 Å).[2] In comparison with its precursor (**T1**), the only bonds affected by the coordination of the transition metal are the elongated P=S double bond (from 1.9668(11) Å to 2.0357(10) Å) and the slightly shortened P-N single bond (from 1.659(4) Å to 1.640(3) Å). The tetrahedral geometry around the phosphorus atom is not affected.

¹H NMR (400.13 MHz, CD₂Cl₂, 298 K): δ = 1.43 (d, $^3J_{\text{P-H}}$ = 16.2 Hz, 18H, PC(C*H*₃)₃), 3.65 (br, 2H, N*H*₂). **³¹P{¹H} NMR** (162.04 MHz, CD₂Cl₂, 298 K): δ = 94.9. **¹³C{¹H} NMR** (100.61 MHz, CD₂Cl₂, 298 K): δ = 27.7 (d, $^2J_{\text{P-C}}$ = 1.2 Hz, PC(CH₃)₃), 38.9 (d, $^1J_{\text{P-C}}$ = 52.7 Hz, P*C*(CH₃)₃). **Elemental analysis**: C₁₆H₄₀AuClN₂P₂S₂: calcd.: C 31.05%, H 6.51%, N 4.53%; found: C 31.47%, H 6.28%, N 4.56%. **HR-MS (+ESI)**: calcd. m/z for [C₁₆H₄₀AuN₂P₂S₂]⁺: 583.1768, found: 583.1789.
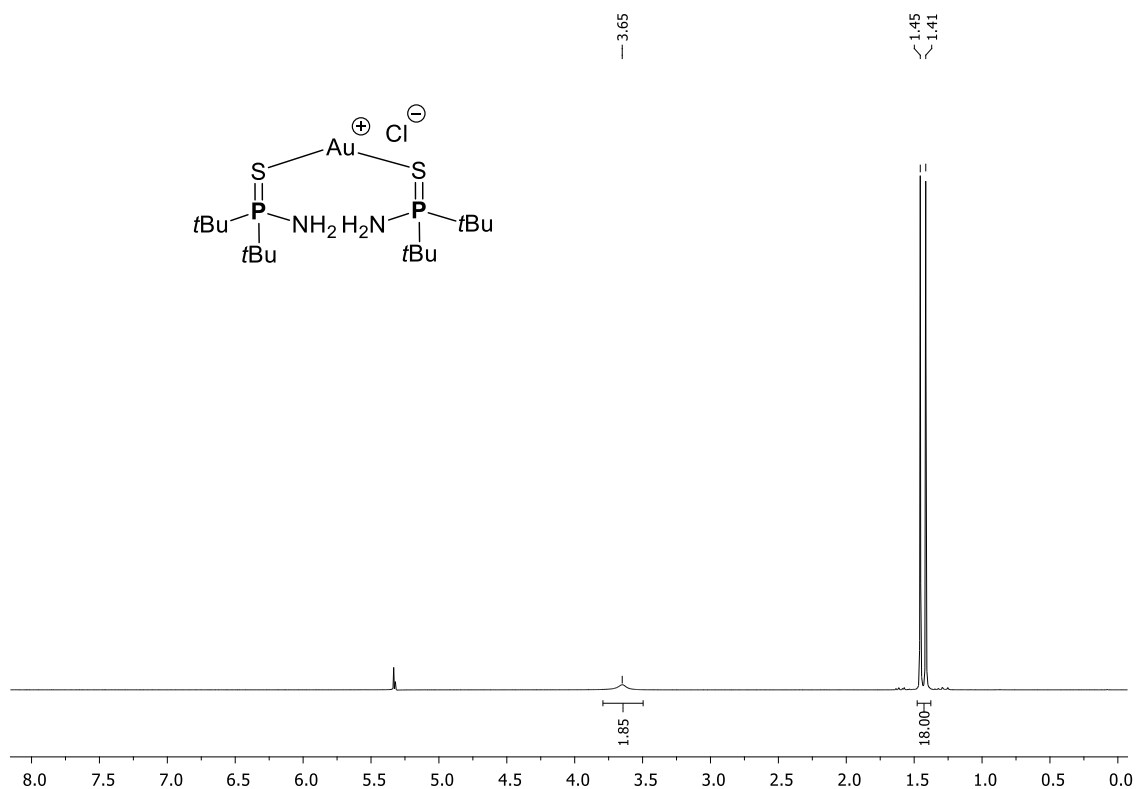
Figure S224. ¹H NMR (CD₂Cl₂, 298 K) of compound **T6**.
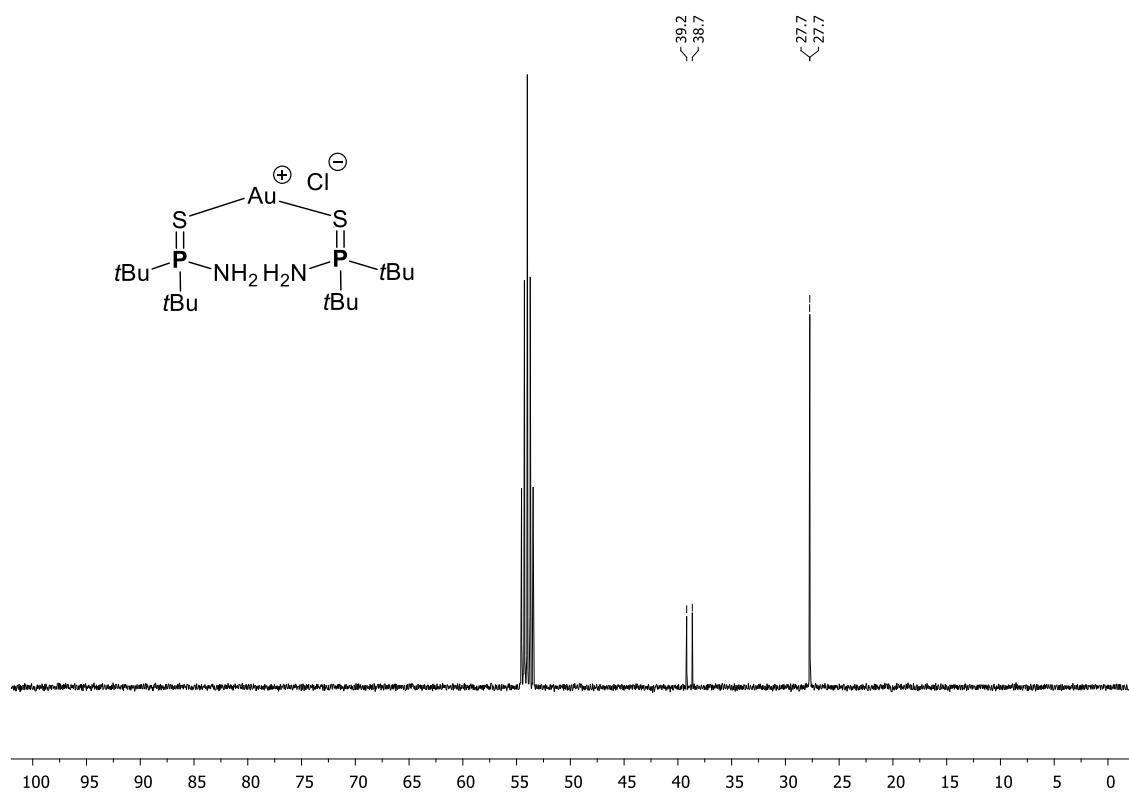
Figure S225. ¹³C{¹H} NMR (CD₂Cl₂, 298 K) of compound **T6**.
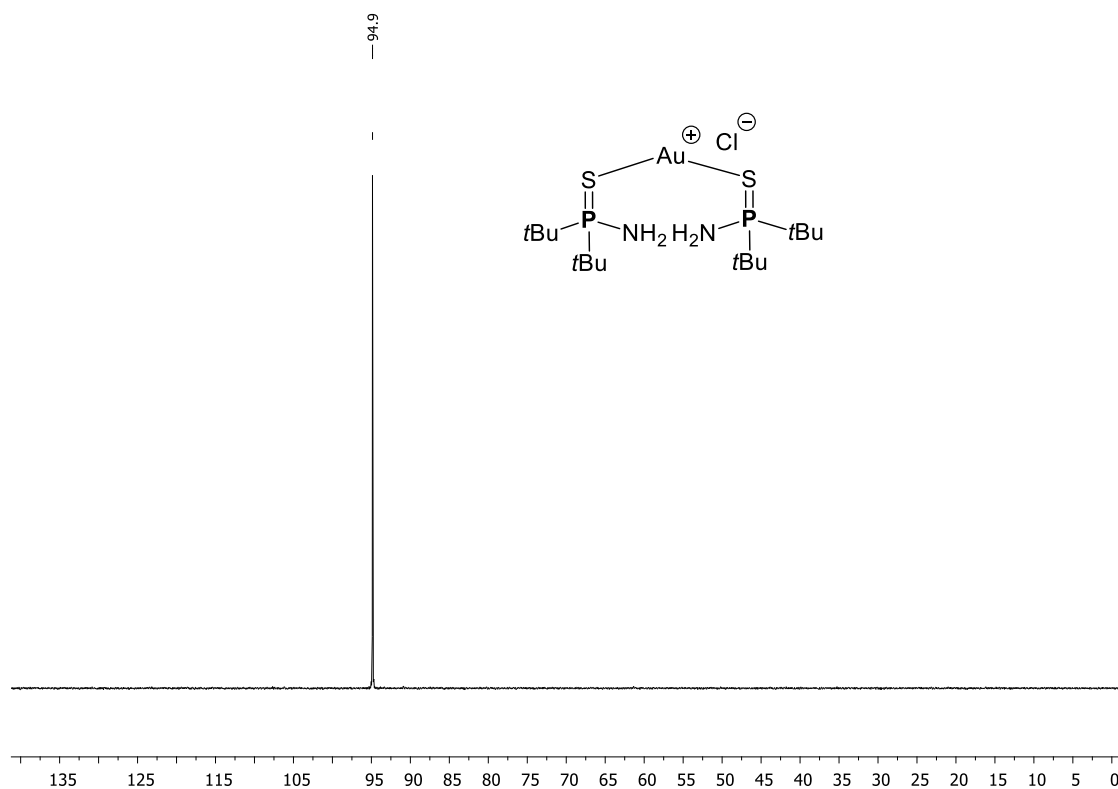
Figure S226. $^{31}P\{^1H\}$ NMR (CD$_2$Cl$_2$, 298 K) of compound **T6**.

5.3   X-Ray Crystallographic Details

The crystals were selected and measured on a GV1000 diffractometer equipped with a TitanS2 detector (**T4**, **T6**), on a SuperNova diffractometer equipped with an Atlas detector (**T1**) or on an Xcalibur, AtlasS2, Gemini ultra diffractometer (**T5**). The crystals were kept at T = 123(1) K during data collection. Data collection and reduction were performed with **CrysAlisPro** [Version 1.171.39.46 (**T1**, **T5**, **T6**) or 1.171.41.89a (**T4**)].[3] For the compounds a numerical absorption correction based on gaussian integration over a multifaceted crystal model and an empirical absorption correction using spherical harmonics as implemented in SCALE3 ABSPACK was applied. Using **Olex2**,[4] the structures were solved with **ShelXT**[5] and a least-square refinement on F^2 was carried out with **ShelXL**[6] for all structures. All non-hydrogen atoms were refined anisotropically. Hydrogen atoms at the carbon atoms were located in idealized positions and refined isotropically according to the riding model. Figures were created with **Olex2**.[4]

Compound T1: The asymmetric unit contains one molecule of $(t\mathrm{Bu})_2\mathrm{P(S)CH_2NH_2}$. Disorder on one of the *tert*-butyl groups was modelled and a DFIX restrain to 1.5 was subsequently added Å.

Compound T4: The asymmetric unit contains one molecule of $[(t\mathrm{Bu})_2\mathrm{P(SH)CH_2NH_2}][\mathrm{B(C_6F_5)_4}]$.

Compound T5: The asymmetric unit contains four molecules of $(t\mathrm{Bu})_2\mathrm{P(S)CH_2NH_3Cl}$.

Compound T6: The asymmetric unit contains half molecule of $((t\mathrm{Bu})_2\mathrm{P(S)CH_2})_2\mathrm{Au}$ and half molecule of $\mathrm{CH_2Cl_2}$.

[3]   CrysAlisPro Software System, Rigaku Oxford Diffraction, 2020.

[4]   Dolomanov, O. V.; Bourhis, L. J.; Gildea, R. J.; Howard, J. A. K.; Puschmann, H. *OLEX2*: a complete structure solution, refinement and analysis program, *J. Appl. Crystallogr.*, 2009, **42**, 339.

[5]   Sheldrick, G. M. *SHELXT* – Integrated space-group and crystal-structure determination, *Acta Crystallogr.*, 2015, **A71**, 3.

[6]   Sheldrick, G. M. Crystal structure refinement with *SHELXL*, *Acta Crystallogr.*, 2015, **C71**, 3.

Table 32 Crystallographic data for compounds **T1**, **T4**, **T5** and **T6**.

Compound	T1	T4	T5	T6
Data set (internal naming)	**nf-341_cryst**	**nf_268**	**nf-349_2**	**nf_441_l_exp**
Formula	$C_8H_{20}NPS$	$C_{32}H_{21}BF_{20}NPS$	$C_{32}H_{84}Cl_4N_4P_4S_4$	$C_{17}H_{42}AuCl_3N_2P_2S_2$
$D_{calc.}$ / g · cm^{-3}	1.125	1.733	1.189	1.696
m/mm^{-1}	3.421	1.889	0.544	11.668
Formula Weight	193.28	873.34	918.95	703.90
Colour	clear colourless	yellow	clear colourless	clear colourless
Shape	needle-shaped	block-shaped	block-shaped	block-shaped
Size/mm^3	0.23×0.05×0.05	0.24×0.12×0.07	0.29×0.17×0.11	0.29×0.23×0.12
T/K	123.00(10)	123.01(13)	123.00(1)	123.01(10)
Crystal System	tetragonal	triclinic	triclinic	tetragonal
Flack Parameter	-0.003(13)			0.001(4)
Hooft Parameter	-0.016(9)			-0.002(4)
Space Group	I-4	P-1	P-1	$I4_122$
a/Å	16.6872(2)	10.5990(5)	13.2428(3)	16.29530(10)
b/Å	16.6872(2)	12.7851(5)	13.8454(4)	16.29530(10)
c/Å	8.1934(2)	13.9954(6)	14.2309(5)	20.7595(3)
α/°	90	73.712(3)	81.036(3)	90
β/°	90	72.122(4)	88.007(2)	90
γ/°	90	71.222(4)	84.808(2)	90
V/Å^3	2281.56(8)	1673.78(14)	2566.25(13)	5512.41(10)
Z	8	2	2	8
Z'	1	1	1	0.5
Wavelength/Å	1.54184	1.39222	0.71073	1.39222
Radiation type	Cu K$_\alpha$	Cu K	Mo K$_\alpha$	Cu K
Q_{min}/°	3.746	3.059	3.314	3.113
Q_{max}/°	76.319	65.995	32.052	72.191
Measured Refl.	5804	21932	23459	15348
Independent Refl.	2312	7738	15503	3641
Reflections with I > 2(I)	2269	6913	12488	3634
R_{int}	0.0185	0.0343	0.0216	0.0276
Parameters	128	523	471	136
Restraints	2	0	0	0
Largest Peak	0.376	0.501	0.465	0.723
Deepest Hole	-0.323	-0.409	-0.312	-0.687
GooF	1.044	1.034	1.085	1.118
wR_2 (all data)	0.0919	0.1050	0.0888	0.0406
wR_2	0.0910	0.1004	0.0822	0.0406
R_1 (all data)	0.0376	0.0405	0.0591	0.0160
R_1	0.0368	0.0366	0.0422	0.0159

5.3.1 Compound T1
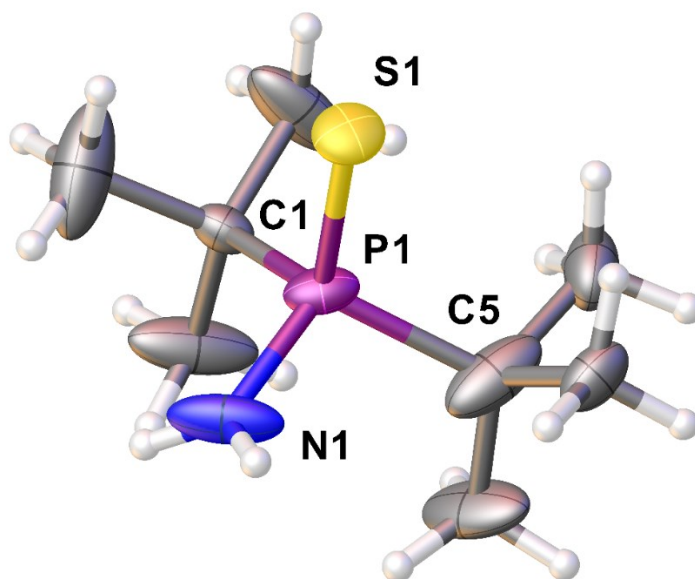
Selected Bond Lengths in Å		Selected Bond Angles in ˚	
P–S	1.9668(11)	N–P–S	110.75(12)
P–N	1.659(4)	N–P–C1	106.8(2)
P–C1	1.855(3)	N–P–C5	104.3(2)
P–C5	1.858(5)	C1–P–C5	110.51(11)

5.3.1 Compound T4
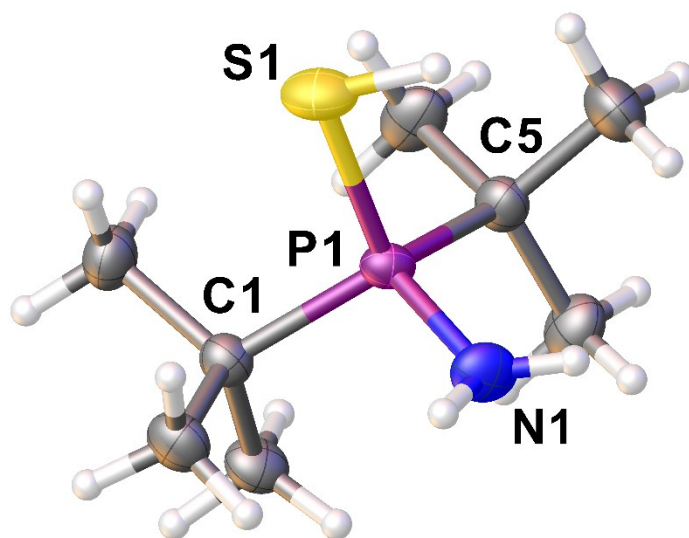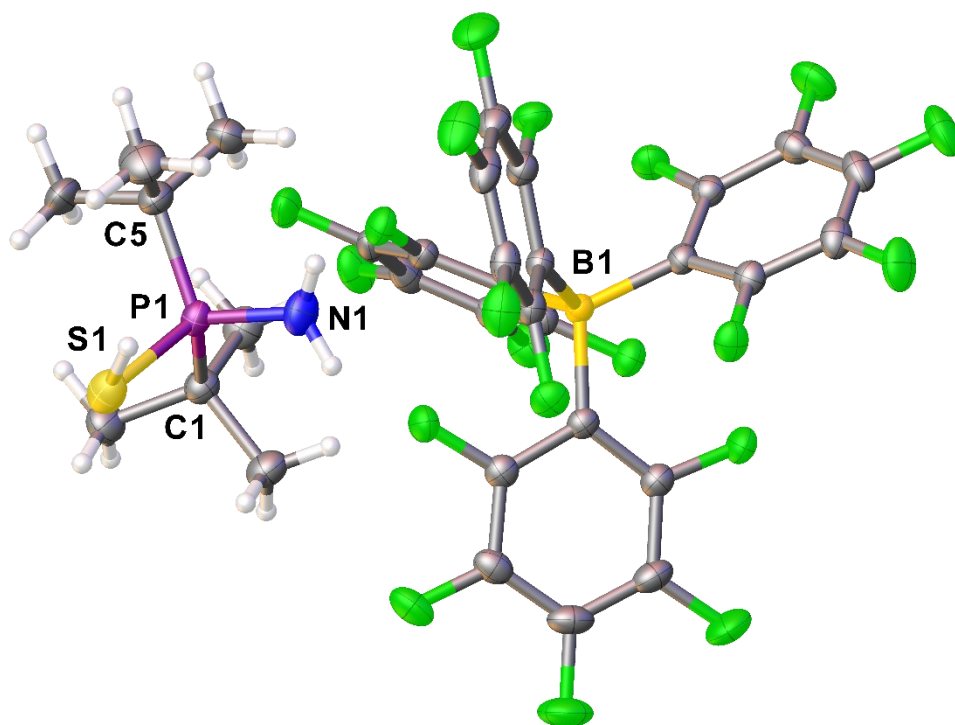
Selected Bond Lengths in Å		Selected Bond Angles in °	
P–S	2.0704(6)	**N–P–S**	112.54(6)
P–N	1.6358(15)	**N–P–C1**	107.51(8)
P–C1	1.8398(16)	**N–P–C5**	105.63(9)
P–C5	1.8385(16)	**C1–P–C5**	118.24(8)

5.3.1   Compound T5
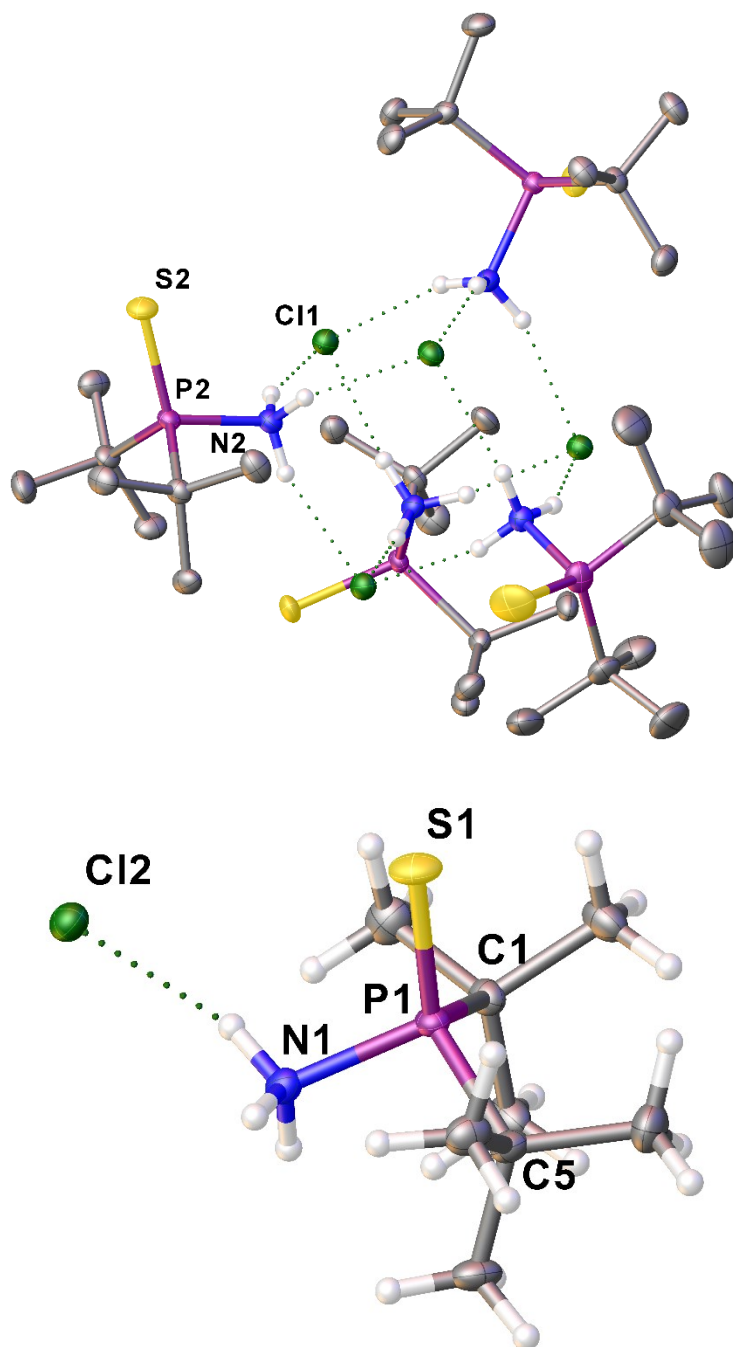
Selected Bond Lengths in Å		Selected Bond Angles in ˚	
P–S	1.9293(6)	**N–P–S**	109.01(5)
P–N	1.7790(13)	**N–P–C1**	102.33(7)
P–C1	1.8526(16)	**N–P–C5**	101.31(7)
P–C5	1.8562(16)	**C1–P–S**	111.99(5)

5.3.1 Compound T6
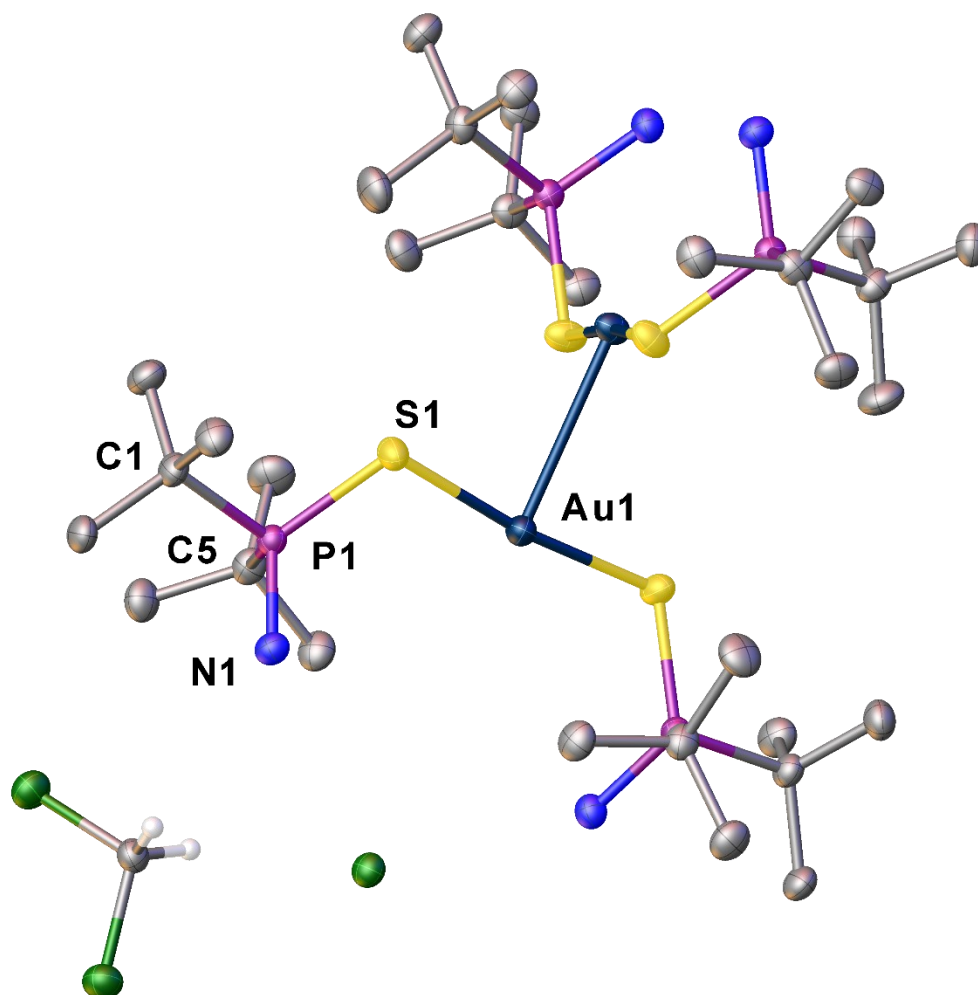
Selected Bond Lengths in Å		Selected Bond Angles in °	
Au–Au	3.0234(3)	P–S–Au	106.99(4)
P–N	1.640(3)	N–P–S	117.41(10)
P–C1	1.859(3)	N–P–C1	104.97(13)
P–C5	1.863(3)	N–P–C5	104.61(13)
P–S	2.0357(10)	C1–P–S	102.91(10)
S–Au	2.2842(7)	C1–P–C5	115.60

6 Conclusions

In this work, the chemistry of main group-element based heterocycles has been elucidated. Starting from a general overview on the current state of the art (see chapter 1) and including silane- and siloxane-based silylium ions (chapter 3 and 4 respectively), different species and their properties have been described. In these studies, we have introduced for the first time the phosphine sulfide and selenide fragments as stabilizing functional groups to tame the extreme Lewis acidity of silylium ions. After developing a relatively mild and efficient hydride transfer protocol to obtain the targeted silicon-based cationic species (Chapter 3, compounds **2a**, **2a-Se**), we have thoroughly characterized them using state of the art methods. The remarkable stability of the obtained cations allowed us to further investigate different stereochemical properties of these compounds such as chiral memory and the matched/mismatched case of dihydrogen evolution. By introducing for the first time the brand new four membered heterocyclic silylphosphonium ions (chapter 3, (*rac*)-**2**), we have paved the way to the synthesis and understanding of a completely unexplored family of compounds. The many "adjusting screws" present on both the phosphorus and the silicon centers allow a fine tuning of the electronic and steric properties, opening up new applications while maintaining a robust structure at the same time. Full characterization of these new compounds showed unprecedented bonding motifs and a highly pacified silicon center.
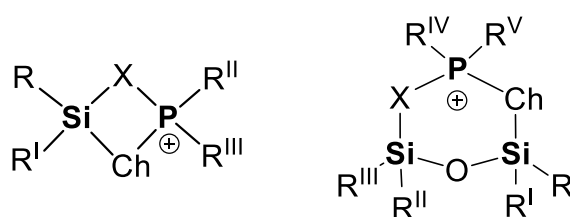
Figure 227. General schemes for four and six membered silylphosphonium ions, highlighting their synthetic flexibility.

The nature of the S-Si stabilizing interaction could be further studied by both reacting the substrates with FBN and by synthesizing the selenium homologue (Chapter 3, **1-Se** and **2-Se**). Subsequently, using the ^{19}F and ^{77}Se nuclei as probes in NMR experiments, we have demonstrated that, due to the extent of electron density drawn from the phosphorus atom in order to stabilize the silicon center, these species are better defined as silyl phosphonium ions than silylium ions. Seeking to separate the single enantiomers of silane from the racemic mixture of (*rac*)-**1**, a new process, based on (+)-menthol as chiral auxiliary, was developed leading to the isolation of enantiomerically pure crystals of a silyl phosphine sulfide (Chapter 3, (^{Si}R)-**1**). The stability of the respective four-membered heterocyclic cation (Chapter 3, compound **2a**) was investigated from a stereochemical point of view, demonstrating how a process including a first hydride abstraction reaction and a subsequent hydridic quenching yielded the starting material with no racemization (a phenomenon described as "chiral memory"). The spontaneous, or heat induced, dihydrogen release observed after protonation of the phosphine sulfide moiety of a neutral precursor (Chapter 3, compounds **3**) provided

evidence on the presence of a matched/mismatched case, together with an elegant way to obtain the four-membered cationic ring with a different counterion (Chapter 3, compound **2b**). Moreover, deuterium labelling experiments, in combination with a thorough kinetic investigation accompanied by quantum chemical calculations regarding the spontaneous dihydrogen release at room temperature supported the presence of a preferred intermolecular mechanism involving two molecules of opposite configuration. Having exploited the properties and potential of these monomeric silylphosphonium ions, we have ventured further by studying the related disiloxane homologue. After introducing a reliable synthetic methodology to obtain the target molecule and its sulfur derivative (Chapter 4, **5** and **6**), a full characterization of the first siloxane-based silylium ion was provided (Chapter 4, **7**[HB(C_6F_5)$_3$]). This study demonstrated how such a stable structure not only could withstand temperatures up to 100°C without sensible degradation, but also how the enhanced stability of the siloxane backbone would allow for a temperature-driven disruption of the Si-S interaction before breaking. The result of this "hidden reactivity" could be directly observed by heating the six-membered heterocyclic silyl phosphonium borate salt (Chapter 4, compound **7**[HB(C_6F_5)$_3$]) above 120°C in a closed vessel. After melting into an ionic liquid around 105°C, a para-hydrodefluorinated borane (Chapter 4, compound **9**) continuously sublimated on the upper walls of the flask leaving the relative fluorodisiloxane as residue (Chapter 4, compound **8**). This process demonstrated the presence of a remarkable silylium ion-mediated C(sp^2)-F activation. Calculated mechanisms for this transformation describe the activation of the C-F bond *via* direct fluoride abstraction leading to a zwitterionic intermediate as highly disfavored (Chapter 4 SI, structure **Int-2**). However, due to the high concentration of the species in the ionic liquid, a S_NAr activation followed by an intermolecular hydride attack proved energetically more feasible, explaining at the same time the traces of residual BCF found in the crystals. Taking advantage of the remarkable stability of the heterocyclic products in inert atmosphere, we have also developed a very elegant and facile way to perform a counterion exchange reaction on **7**[HB(C_6F_5)$_3$]. By using a "naked" proton source ([H(OEt$_2$)$_2$B(C_6F_5)$_4$]) and obtaining only dihydrogen and BCF as byproducts, we selectively formed the desired product, which could even be characterized in the solid phase by X-ray diffraction analysis (Chapter 4, compound **7**[B(C_6F_5)$_4$]. The reliability and easiness of this approach have been demonstrated and first attempts to investigate the substrate scope of this reaction have been carried out. Calculations about the electronic properties of compound **7**[B(C_6F_5)$_4$] revealed that, only in the absence of the intramolecular stabilization, an unneglectable participation of the siloxane bond in stabilizing the positive charge can be registered. Remarkably, in the presence of the phosphine sulfide stabilizing group, no relevant electron density is drawn from the neighboring Si-O-Si motif towards the silylium center.
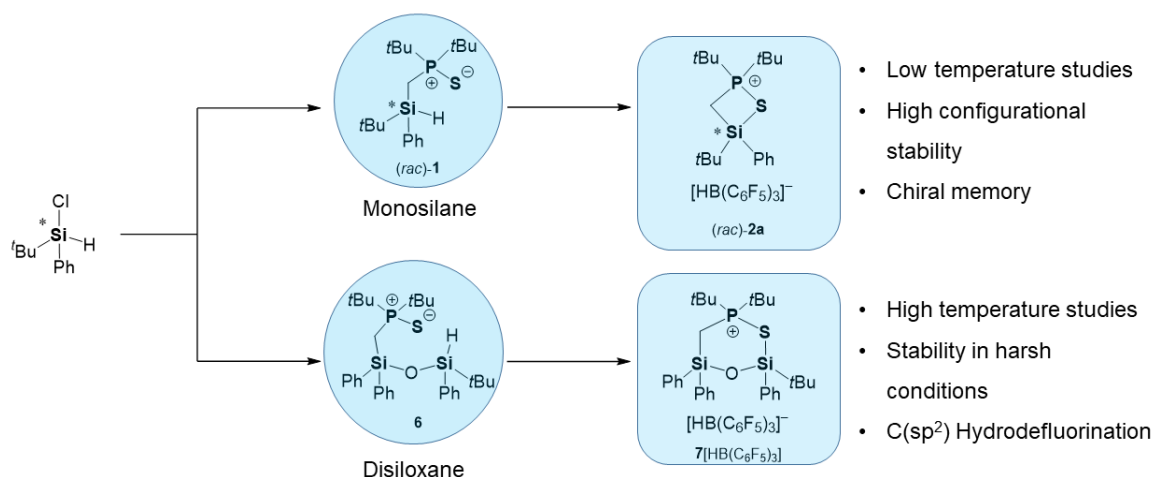
Figure 228. Comparison between the silane and the disiloxane silylphosphonium ions and their study in this work.

Although we could report about the aforementioned hydrodefluorination reaction, the development of a true catalytic process based on the use of these ionic species has, so far, eluded us. Future projects will concern the synthesis of species with enhanced reactivity either by reducing the electron density at the phosphorus or at the silicon centers. Furthermore, the introduction of a second stereogenic center on phosphorus might open up new ways for stereochemical investigations. In conclusion, in this work new main group element-based cationic heterocycles are reported, emphasizing the interaction between the phosphine sulfide/selenide functionality and the cationic silylium center. The species have been synthesized, characterized and applied as stereochemical probes or in C-F activation opening up a manifold of new possibilities and research directions in the field of silylium ion chemistry.

7 Acknowledgments